Using cryptotephra layers to understand volcanic ash clouds

Elizabeth Jane Watson

Submitted in accordance with the requirements for the degree of
Doctor of Philosophy

The University of Leeds

Faculty of Earth and Environment

School of Geography

April 2016

The candidate confirms that the work submitted is his/her own, except where work which has formed part of jointly-authored publications has been included. The contribution of the candidate and the other authors to this work has been explicitly indicated below. The candidate confirms that appropriate credit has been given within the thesis where reference has been made to the work of others.

The following results chapters contain jointly authored manuscripts where E.J.W. is the lead author:

Chapter 3: Spatial variability of tephra and carbon accumulation in a Holocene peatland.

Watson, E.J., Swindles, G.T., Lawson, I.T. & Savov, I.P. Spatial variability of tephra and carbon accumulation in a Holocene peatland. *Quaternary Science Reviews* 124, 248-264.

Contributions: E.J.W. planned the study, conducted fieldwork, lab analysis, tephra extraction, geochemical analysis, data analysis, wrote the paper and prepared all Figures. G.T.S. assisted with fieldwork. G.T.S., I.T.L. and I.P.S. supervised E.J.W. and commented on the manuscript.

Chapter 4: First discovery of Holocene cryptotephra in Amazonia

Watson, E.J., Swindles, G.T., Savov, I.P., Bacon, K.L. 2015. First discovery of Holocene cryptotephra in Amazonia. *Scientific Reports* 5, 15579. DOI:10.1038/srep15579

Contributions: E.J.W. wrote the first draft of the paper, conducted tephra extraction and geochemical analysis, data analysis, assignment to source eruption, discussion and prepared Figures 1, 4 and 5. G.T.S. conducted fieldwork, contributed age depth model, manuscript text, and contributed Figures 2 and 3. IS aided identification of source eruption and contributed manuscript text, K.L.B. contributed expertise on the impacts of volcanism on plants. All authors reviewed the final manuscript.

Chapter 5: Do peatlands or lakes provide the most comprehensive tephra records?

Watson, E.J., Swindles, G.T., Lawson, I.T. & Savov, I.P. 2016. Do peatlands or lakes provide the most comprehensive tephra records? *Quaternary Science Reviews* 139, 110-128.

Contributions: E.J.W. planned the study, conducted fieldwork, lab analysis, tephra extraction, geochemical analysis, data analysis and wrote the paper and prepared all Figures. I.T.L, G.T.S., and I.PS. assisted with fieldwork. G.T.S., I.T.L. and I.P.S. supervised E.J.W. and commented on the manuscript.

Chapter 6: The transport of Icelandic volcanic ash: insights from European tephra records.

Contributions: E.J.W. planned the study, conducted fieldwork, lab analysis, tephra extraction, geochemical analysis, data analysis and wrote the paper and prepared all Figures. I.T.L, G.T.S., and I.PS. assisted with fieldwork. G.T.S., I.T.L. and I.P.S. supervised E.J.W. and commented on the manuscript. J.S. checked and assisted with Python coding. M.L. contributed peat cores from Polish peatlands.

Chapter 7: Climatic control on explosive Icelandic volcanism during the Holocene

E.J.W. wrote the first draft of the paper, conducted data analysis and prepared all Figures. G.T.S., I.P.S., I.T.L., A.S., contributed expertise on cryptotephra layers, volcanic ash and Icelandic volcanism, A.H. advised on links between surface loading and rates of mantle melting, J.C. contributed expertise on Icelandic glaciers during the Holocene. All authors contributed to and reviewed the final manuscript.

Chapter 8: Estimating the frequency of volcanic ash cloud events over northern Europe

E.J.W. wrote the first draft of the paper, conducted data analysis and prepared all Figures. G.T.S., I.T.L. and I.P.S. supervised E.J.W. and commented on the manuscript. C.C. and J.W. helped with statistical analysis and commented on the manuscript. M.L. contributed peat cores from Polish peatlands.

Acknowledgements

I have immensely enjoyed my time as a PhD student and the many exciting experiences during this time. I would like to offer my sincere thanks to a number of people who have shared the highs and helped to smooth the lows. Principally my main supervisor Graeme Swindles whose endless enthusiasm has lifted my sprits when the workload feels insurmountable. For treating me as an equal, engaging in healthy debate and persevering with my occasional bouts of pessimism. For encouraging me to publish my work and helping me to experience one of the best parts of academia – an accepted manuscript! I hope that this PhD will not be the end of our work together.

Thanks also to my co-supervisors Ivan Savov and Ian Lawson who trudged enthusiastically across many a mosquito ridden bog in Arctic Sweden without complaint, and for providing valuable guidance and inspiration along the way. Many thanks to John Stevenson for his guidance on tephra particle size modelling; Chris Hayward for technical assistance on the EPMA at Edinburgh; and to Chuck and Laura Connor for introducing me to statistical modelling and for hosting me at the University of South Florida.

Many thanks to my Husband Tim who is the most optimistic and positive person I know and whose smile and humour have been an unwavering support over the last 3 years. Thanks also to my family, in particular my Dad, Stuart Watson, whose advice on programming was greatly appreciated.

Last but not least thanks to the PhD community at Leeds and in particular to Gemma Dooling, Kathryn Smith and Carol White who have smoothed the lows (usually with cocktails!) and celebrated the highs. To Tom Kelly for hours spent chatting while staring down a microscope (usually at a slide containing no tephra!) and coring Irish peatlands. To Dylan Young, the only person with whom I have continually shared an office for bike and dog related chatter. To Ed Turner for getting me into this mess in the first place (thanks Ed!) and for the nickname which has well and truly stuck. Finally, thanks to the members of peat club for allowing my frequent diversions from peatlands toward volcanoes and tephra.

Abstract

The aim of this thesis is to evaluate the use of microscopic volcanic ash ('cryptotephra') layers for providing information on the timing, characteristics and spatial extent of past volcanic ash clouds. The fine ash produced by explosive eruptions can travel long distances and even in low concentrations represents a hazard for aviation. Understanding the frequency and nature of ash clouds is important if economic and social losses are to be mitigated.

This thesis is split into two research compartments. Compartment 1 focusses on understanding the limits of tephrochronology and investigates cryptotephra preservation and reworking bias in lakes and peatlands. Compartment 2 focusses on applying cryptotephras as records of ash cloud events. In addition to the objectives which fit into the two research compartments, two overarching objectives were outlined. These objectives focus on conducting new field campaigns in order to fill spatial gaps in existing cryptotephra records through the development of new, high quality tephrostratigraphies.

I examine tephra layers from 13 new sites and contribute toward filling spatial gaps in northern European tephra records in northern Sweden, Poland, Wales and Southern England. Three new tephra layers are identified as part of this study, two in northern Europe: a basaltic tephra, CLA-L1 most likely derived from an eruption of the Iceland's Grímsvötn volcano and SN-1, from the Icelandic Snæfellsjökull volcano - identified for the first time in mainland Europe. Finally, the AUC-1 tephra traced to a probable Ecuadorian source, represents the first discovery of a Holocene cryptotephra in the Amazon basin and highlights the opportunities for extending tephrochronology to tropical peatlands.

In this study I present a number of methodological advances which are important for the design of future tephra studies, including: the replicability of tephrostratigraphies from a mid-latitude peatland; differences in lake and peatland records even at sites in close proximity; and the robustness of tephra glass shard geochemistry to acidic conditions and acid extraction. Beyond methodological advances, this study demonstrates how cryptotephra records can be utilised in new ways to compliment proximal records of

volcanism; includes the first comprehensive analysis of distal tephra shard size (9500 shards); and presents a new recurrence estimate for the frequency of ash cloud events over northern Europe (44 ± 7 years).

Contents

List of Figures

Chapter 7: Climatic control on Icelandic volcanic activity during the Holocene

Chapter 8: Estimating the frequency of volcanic ash clouds over northern Europe

List of Tables

Chapter 1: Introduction

n/a

Chapter 2: Literature review

Chapter 3: Spatial variability of tephra and carbon accumulation in a Holocene peatland

n/a

Chapter 4: First discovery of Holocene cryptotephra in Amazonia

n/a

Chapter 5: Do peatlands or lakes provide the most comprehensive distal tephra records?

Chapter 6: The transport of Icelandic volcanic ash: information from European tephra records

Chapter 7: Climatic control on Icelandic volcanic activity during the Holocene

n/a

Chapter 8: Estimating the frequency of volcanic ash clouds over northern Europe

Abbreviations

ATCA	Apparent total carbon accumulation
LA-ICP-MS	Laser Ablation Inductively Coupled Plasma Mass Spectrometry
LARCA	Long-term apparent rate of carbon accumulation
LIA	Little ice age
EDS	Energy Dispersive Spectroscopy
EPMA	Electron Probe Micro-Analysis
SCP	Spheroidal carbonaceous particle
SIMS	Secondary ion mass spectrometry
TSC	Total shard count per unit area, the total number of tephra shards relating to a given eruption per unit area.
VAAC	Volcanic Ash Advisory Centre
VSWIR	Visible to shortwave infrared spectroscopy
WDS	Wavelength Dispersive Spectroscopy
XRF	X-ray fluorescence

Chapter 1: Introduction

1.1 Introduction

This thesis will examine microscopic volcanic ash ('cryptotephra') layers with particular reference to their use as records of the source, frequency and nature of volcanic eruptions and the resulting ash clouds. This work represents a key step toward using cryptotephra layers, not only as a tool for the correlation of sedimentary sequences, but also as a record of volcanic eruptions which occurred in the past. Understanding past volcanic ash deposition may help in predicting the frequency and characteristics of future volcanic eruptions.

1.2 Context of research and rationale

The invention of passenger jet aircraft has led to a large increase in global air transport of both people and freight over the last 70 years. The global economy is increasingly dependent on reliable air transportation; any disruption to air traffic can result in large economic losses. Thankfully, modern aircraft can operate in the majority of meteorological conditions and widespread disruption to flights is rare. However, despite technological advances, the passage of modern jet aircraft through volcanic ash can result in substantial damage to the fuselage and even complete engine failure (Folch, 2012). Given the safety risk of engine failure when flying through volcanic ash, and in line with recommendations from the International Civil Aviation Organisation, the British Civil Aviation Authority began implementing no fly zones where volcanic ash was present. This policy was subsequently reviewed, during the eruption of Eyjafjallajökull, 2010, allowing flights to continue where the ash concentration is below 0.2 mg m^{-3} (Marks, 2010). Any decision regarding the closure of airspace by the Civil Aviation Authority is based on information provided by the relevant Volcanic Ash Advisory Centre (VAAC). There are nine VAACs, each responsible for a different geographic area. The London VAAC covers Iceland, and the north-east sector of the north Atlantic. The centre provides information on volcanic ash presence/absence and concentration during a volcanic eruption based on forecasts from dispersion models, satellite data and aircraft observation data.

The impact of volcanic ash clouds on aviation is a problem of global relevance. The fine ash produced during explosive volcanic eruptions can be transported long distances (1000s of km) from the volcanic source and cause flight disruption across a wide area. The first reported encounter between a modern jet aircraft and volcanic ash was during the eruption of Mount St Helens, USA in 1980. Since then, similar events have occurred in Indonesia, Alaska and the Philippines (Miller and Casadevall, 2000). Australia, which itself has no active volcanoes, was affected by ash from the eruption of the Chilean volcano, Cordón del Caulle, which grounded flights from Melbourne (>10,000 km distant) in 2011 (Pistolesi *et al*., 2015).

Evidence of past ash clouds is recorded by fine volcanic ash particles. These microscopic shards have been identified thousands of kilometres from their volcanic source, where they form invisible ('cryptotephra') layers in records such as peatlands, ice cores and marine and lake sediments (Jensen *et al*., 2014; Pyne-O'Donnell *et al*., 2012). These cryptotephra layers can often be traced to a volcanic source and eruption based on the uniqueness of the particle chemistry linked back to the magmatic source (Swindles *et al*., 2011). They can also be assigned an age, either through correlation with an eruption of a known age, or through dating the host material (e.g. peat or lake sediment). As cryptotephra layers are spatially widespread and deposited over a short space of time, they are predominantly used in the dating and correlation of sedimentary sequences ('tephrochronology') (Lowe, 2011).

The majority of cryptotephra research has been conducted in northern Europe, where the main source of cryptotephra is Icelandic volcanism. Iceland's position in the north Atlantic puts it in a prime location for causing disruption to trans-Atlantic and European air traffic. Iceland is also one of the most active volcanic regions in the world, with the last 10 ka recording an average of 20 eruptions per century (Thordarson and Hoskuldsson, 2008). However, prior to AD 2010 there had been no significant explosive eruptions since that of Hekla in AD 1947, at a time when there were no passenger jet aircraft. Therefore it came as a surprise to many European governments, insurers and the general public when the ash cloud produced during the eruption of the Icelandic volcano Eyjafjallajökull in 2010 triggered two months of intermittent travel disruption (Gudmundsson *et al*., 2012). The estimated cost to airlines for the first six days of disruption was in excess of €900 million (Hooper, 2012). In order to mitigate

such economic losses and inconvenience to the travelling public in the future, understanding the frequency and nature of ash dispersal events from Icelandic eruptions is vital.

Swindles *et al*. (2011) identified an opportunity to use cryptotephra layers in a novel way to estimate the reoccurrence of ash clouds. Cryptotephra layers and details of observations in historical records provide information on the frequency of ash clouds reaching northern Europe in the past. Assuming that the rate of ash clouds is stationary, and does not change significantly over time, information on past volcanic ash cloud frequency can be used to understand and model the frequency of future Icelandic eruptions. The reoccurrence model of Swindles *et al*. (2011) is based on a new database of tephra records in northern Europe, compiled from online databases and published literature and represents the first attempt to estimate ash cloud reoccurrence based on observed ash fall and cryptotephra records.

In addition to recording volcanic ash cloud frequency, cryptotephra layers may offer additional insights into the volcanic eruption from which they are derived. The geochemistry of the glass shards in cryptotephra layers reflects the magma composition at the time of eruption (Ponomareva *et al*., 2015). Furthermore, cryptotephra shard morphology reflects the magma properties, the degree of magma vesiculation (degassing state), fragmentation and explosivity of the eruption (Liu *et al*., 2015). Tephra transport distance is influenced by meteorology (mostly wind direction), plume heights and particle morphology (Carey and Sparks, 1986; Stevenson *et al*., 2015).

Growing interest in volcanic ash clouds globally, and in northern Europe in particular, has led to increased collaboration between atmospheric scientists and tephrochronologists (Stevenson *et al*., 2015). The value of cryptotephra layers, not only as dating isochrons, but also as records of the frequency and nature of volcanic activity is being recognised (Ponomareva *et al*., 2015). This research project will examine the extent to which cryptotephra layers in northern Europe and further afield can be applied as records of the frequency and nature of volcanic ash falls, and the extent to which they are confounded the issues of re-deposition, preservation and reworking in terrestrial environments. The results are likely to be of interest to a wide range of scientists including tephrochronologists, paleo-environmental scientists and atmospheric and

climate modellers. Furthermore, the findings of this thesis have the potential to impact on the model of ash cloud reoccurrence over northern Europe, which is of relevance to the travelling public, as well as to the insurance and aviation industries.

1.3 Research aim

The aim of this thesis is to evaluate the use of microscopic volcanic ash ('cryptotephra') layers for providing information on the timing, characteristics and spatial extent of past volcanic ash clouds.

1.4 Objectives

The main aim outlined above (Section 1.2) will be met through the following research objectives. The objectives of this research project are in two main compartments:

Compartment 1: The limits of tephrochronology

1. To examine the spatial complexity of tephra shard concentrations in a single peatland, in order to evaluate the level of sampling bias in studies which analyse a single core from a site (Chapter 3).
2. To evaluate the preservation of cryptotephra shards in extreme conditions and assess the opportunities for extending the spatial coverage of tephrochronology by carrying out the first tephra investigation in a South American tropical peatland (Chapter 4).
3. To identify possible preservation bias in lake and peatland records by investigating the tephrostratigraphies recorded in lake and peatland sites in close proximity to one another (Chapter 5).
4. Using the above objectives, to assess the level of bias in models of volcanic ash reoccurrence over northern Europe such as that developed by Swindles *et al*. (2011) (Chapter 8).

Compartment 2: The application of tephra layers as records of volcanic ash

5. To report tephra shard size and characteristics (colour and morphology) at all sites and to evaluate the extent to which these properties can further understanding of volcanic ash clouds (Chapter 6).
6. To compare distal ash cloud records with records of Icelandic volcanism over the last 7000 years (Chapter 7, Chapter 8).
7. To develop a new model for ash cloud reoccurrence over northern Europe using new modelling techniques and including additional data based on new tephra layers (Chapter 8).

General

8. To conduct field campaigns in order to assess whether spatial and temporal gaps in tephra records in northern Europe reflect the true margins of the spatial distribution of Icelandic volcanic ash, or whether they are an artefact of research intensity (Chapters 1, 2, 3, 4).
9. To produce new high quality tephra profiles, prepared and geochemically characterised following standard protocols (Chapters 1, 2, 3, 4).

1.5 Thesis structure

This thesis is structured in nine Chapters. Chapter one provides an introduction to the research context and rationale for this project. Chapter two contains a literature review which offers a critical analysis of existing literature and methods relevant to this research project. During the literature review I identify and highlight key gaps in the existing body of literature which form the basis for the aims and objectives outlined in Chapter one.

This thesis is presented in an ‘alternative format’, following the guidelines outlined by the University of Leeds, whereby each results chapter is in the form of a manuscript for publication. There are six results chapters, each with its own abstract, introduction, methods, results and discussion and conclusion section. Each is accompanied by a reference list. At the time of submission results chapters 3, 4 and 5 are published.

The results chapters fit into two main compartments, in line with those outlined in the objectives in Chapter 1 (Fig. 1). Chapters three, four and five fit into Compartment 1: The limits of tephrochronology. These chapters examine the robustness of tephrochronology, specifically the use of cryptotephra layers in lakes and peatlands as a technique for understanding past ash clouds (Objectives 1-4, 8-9). During these chapters I critically examine the influence of deposition, redistribution and reworking processes on tephra records in peatlands and lakes. Chapters six, seven and eight fit into Compartment 2: The application of tephra layers as records of volcanic ash, and focus on identifying opportunities for the application of cryptotephra layers as records of volcanic ash clouds (Objectives 5-9).

Finally, Chapter 9 offers a synthesis of the preceding results chapters bringing together the two research compartments and offering overall conclusions. The implications of the findings of this research project are discussed, together with limitations and ideas for future directions.

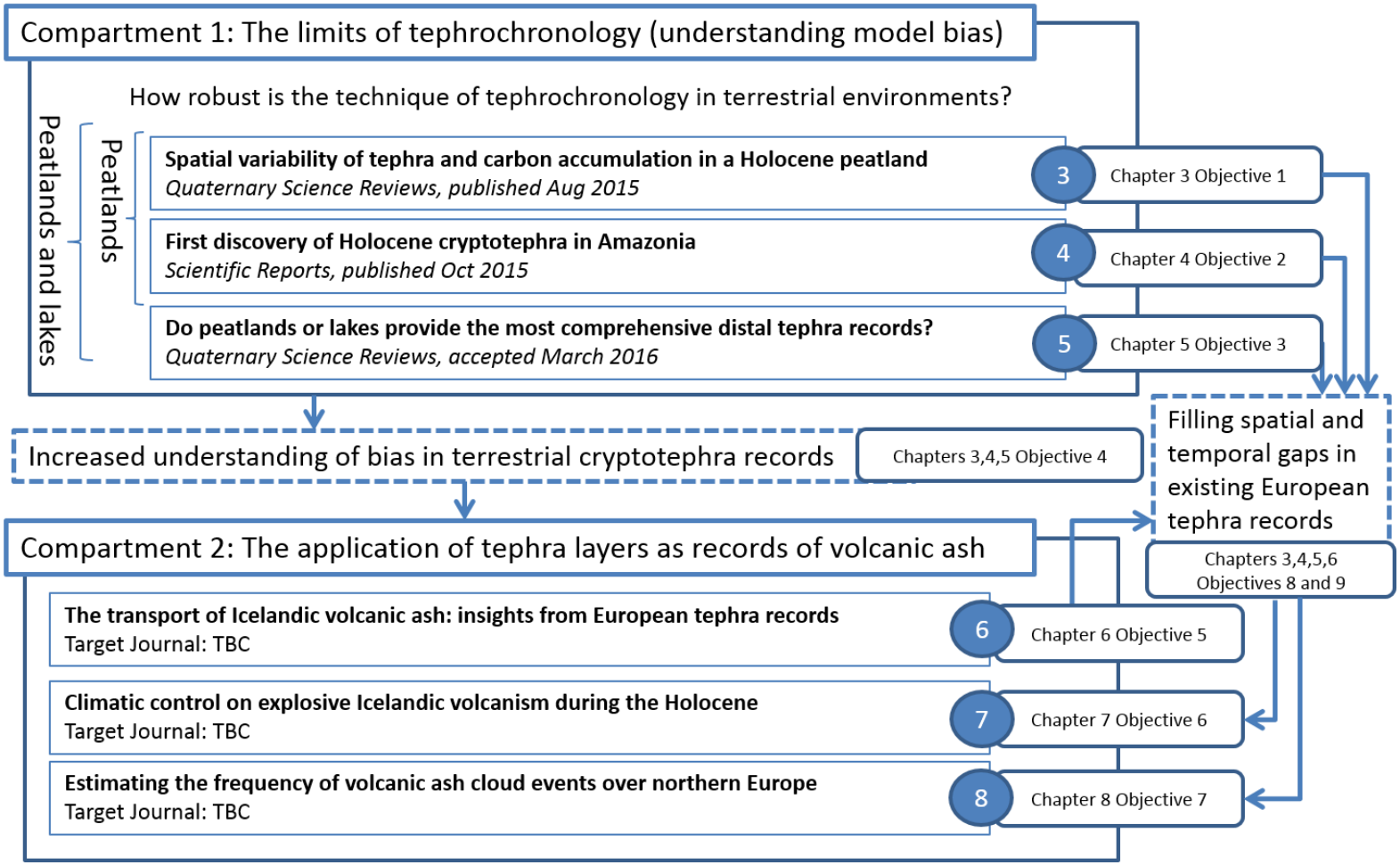

Figure 1. Conceptual model of this research project. Research is split into two main compartments. Blue circles indicate Chapter numbers for results chapters, each results chapter is related to one main objective.

Chapter 2: Literature review

2.1 Introduction

This review is focussed on cryptotephra layers with particular reference to their use as records of ash-cloud distribution and frequency. I critically examine existing literature and methods relevant to this research project and highlight key questions and gaps in existing research.

2.1.1 Tephra

The word ‘tephra’ is used to describe a wide range of pyroclastic debris released during volcanic eruptions (Thorarinsson, 1944). This review will focus on volcanic ash (tephra) which has been transported in the atmosphere and deposited in areas far (>500 km) from the volcanic source. These distal tephra layers are often referred to as cryptotephras or ‘hidden tephras’ as they are not visible to the naked eye. Cryptotephras contain low concentrations of small shards (typically <125 μm) (Lowe, 2011).

During a tephra-producing volcanic eruption, shards of tephra are ejected from the vent into the atmosphere. The direction and distance of transport are affected by the height of the eruption column, wind speed and direction, as well as particle terminal velocity (Fig. 11). As the terminal velocity of a tephra shard or aggregate is reached, it will fall-out and be deposited. Eruption style and shard characteristics are predominantly controlled by magma composition and volatile content. The height of the eruption column, which can be maintained or variable, exerts a strong control on tephra transport distance. Plume height is controlled in part by the gas content of the magma, where higher gas content results in a higher plume (Wilson *et al.*, 1978). Plinian eruptions which are characterised by high plumes (> 20 km) (Mader, 2006) can produce widely dispersed tephra isochrones.

Tephra shard characteristics include the shape, size and density of shards, all of which impact on settling velocity. Larger, more dense shards are deposited closer to the vent than smaller less dense shards (Folch, 2012). Generally basaltic tephra shards have a

higher density (c. 2400-3200 kg m^{-3}) than rhyolitic shards (c.2150-2600 kg m^{-3}) (Schön, 2011). Models suggest that basaltic tephra shards fall out more rapidly than rhyolitic shards due to their higher density (Stevenson *et al*., 2015). Shard shape, size and density characteristics are controlled partly by magma type and volatile content (Mader, 2006) which affect bubble formation and brittle fragmentation (Cashman, 2000).

2.1.2 Tephrochronology

Tephrochronology is the use of tephra layers as a dating and correlation method. The technique was developed using visible tephra layers in Iceland (Thorarinsson, 1944; Thórarinsson, 1981). Tephrochronology is based on two fundamental assumptions:

1) That tephra deposition (from a single eruption) over a wide area can be considered to be simultaneous in geological time. This claim is supported by the short duration of most explosive eruptive phases (Lowe, 2011) and the rapid fallout of tephra even when transported long distances (Stevenson *et al*., 2012);

2) That the geochemistry of tephra shards reflects magma geochemistry during a given eruption and therefore, tephra layers from different eruptions can have different geochemistries (Baker, 1983).

The assumption of simultaneous deposition allows for the use of tephra records as isochrones. If a tephra layer can be assigned a date, using stratigraphy, and either historical or radiometric dating methods, that age can be inferred at other sites where an identical tephra layer is present (Fig. 1). As I discuss in detail later, recently, it has become increasingly apparent that the assumption of an individual geochemical fingerprint for each eruption is a simplification and event stratigraphy and independent dating are important when assigning tephra layers to an eruptive event.

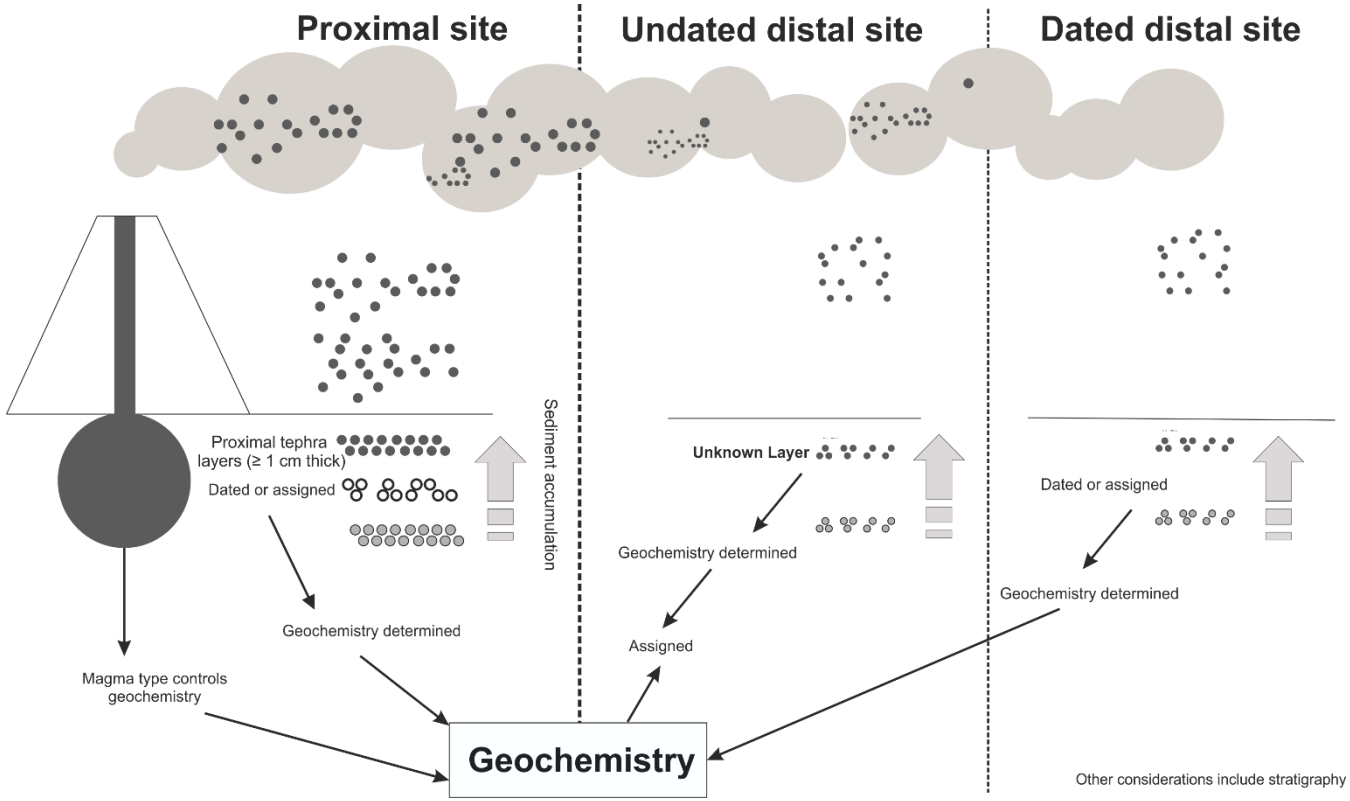

Figure 1. Diagram illustrating the theory behind tephrochronology, based on the assumptions of simultaneous deposition and geochemical 'fingerprinting' tephra layers can be used as a precise method of dating and correlation for proximal and distal sequences in lakes, marine cores, ice cores and peatlands.

The discovery of Icelandic tephra layers in the Faroe islands and Scandinavia provided an opportunity to extend tephrochronology into regions further from their volcanic sources (Persson, 1966, 1968, 1971). The promise of distal tephrochronology was further advanced by the discovery of cryptotephra layers in peatlands (e.g. Hall and Pilcher, 2002; Plunkett, 2006), lakes (e.g. Davies *et al*., 2007; Stanton *et al*., 2010), ice (e.g. Gronvold *et al*., 1995) and marine (e.g. Gudmundsdóttir *et al*., 2011) cores. The first cryptotephra found on the UK mainland, at Altnabreac in Caithness, Scotland, was geochemically correlated to the eruption of Hekla 4 (4287 BP) (Dugmore, 1989). Since these early discoveries, numerous cryptotephras from many volcanic source regions have been identified across northern Europe and in other regions of the world including Russia (Wastegård *et al*., 2000), New Zealand (Gehrels *et al*., 2006a), Africa (Lane *et al*., 2013b), South America (Wastegård *et al*., 2013) and China (Zhao and Hall, 2015). Cryptotephras which transcend continental or even hemispheric boundaries are particularly useful for the dating and correlation of palaeoenvironmental records from different regions in different depositional environments (Jensen *et al*., 2014; Lane *et al*., 2013a; Pyne-O'Donnell *et al*., 2012).

Tephrochronology is now widely applied as a dating and correlation method in palaeoenvironmental studies (e.g. Cole and Mitchell, 2003; Lawson *et al*., 2008). Where adequate tephra layers allow, tephrochronology provides a cost-effective, accurate and precise technique to complement other dating methods. Accurately dated tephra layers can provide tie points in radiocarbon-based age-depth models, which can be particularly important during plateaux in the radiocarbon calibration curve (Plunkett, 2006). Tephras are also of particular value in dating records where radiocarbon or other dating methods are confounded by errors (Lowe *et al*., 2007). More recently deposited tephras such as Hekla 1947 are likely to become increasingly important as ^{210}Pb dating which has a half-life of just 22 years becomes less effective (Rea *et al*., 2012). Cryptotephra layers, being deposited far from the volcano are also valuable for the reconstruction of volcanic activity in regions where there has been abundant Quaternary volcanism. Proximal deposits are often confounded by reworking or buried by new deposits, whereas cryptotephra layers are typically far away enough from the volcanic source not to be subject to these complications. Therefore, in some instances cryptotephra layers present a more complete record of volcanic activity than proximal records.

Despite the advantages offered by tephrochronology there are a number of complications which must be considered when applying this technique. Cryptotephra layer identification to a source volcano, or another cryptotephra layer is often based on analysis of major element data. Major elements form a major component (>0.1%) of the material, in this instance glass and the following species are typically analysed: SiO_2, FeO, TiO_2, K_2O, Al_2O_3, Na_2O, CaO, MgO and MnO. The analysis of major elemental composition is routinely conducted in the majority of tephra studies. Trace elements are present at concentrations of below 1000 ppm and in tephra samples must be analysed separately to major elements, the analysis of trace elements is not yet routine in tephra studies.

One of the principals of tephrochronology is the assumption that a tephra layer has a distinctive geochemical fingerprint. However, magma and thus tephra geochemistry can be heterogeneous (Hunt and Hill, 1993). Therefore tephra erupted during the early stages of an eruption can be different in geochemical composition to the main bulk of tephra, due to contamination with (pre-existing) material from previous eruptions (Larsen and Eiriksson, 2008b). Some volcanoes show indications of magma mixing and evolving tephra geochemistry throughout an eruption, meaning tephra from one eruption can have a range of different geochemistries. These complex geochemical signatures are caused by magma chamber zonation (Hodder *et al*., 1991) or alternatively by the fluctuation of the composition of deeply sourced magmas feeding the magma storage region under the volcanic source. Conversely, multiple tephra layers from different eruptions have been identified with overlapping geochemistry, demonstrating that the assumption that every tephra has a unique geochemical fingerprint is not always valid.

A recent focus on late-glacial European tephra layers has led to the discovery of multiple tephra layers attributed to the Katla volcano with very similar major element geochemistry (MacLeod *et al*., 2015): the Vedde ash (c. 12 cal ka BP), Dimna Ash (c. 15 cal ka BP), Suđurøy (c. 8 cal ka BP), AF555 (c.11.5 cal ka BP) and Abernethy (11.7-11.2 cal ka BP). There are approaches to mitigate issues where tephra layers have overlapping geochemistry. The analysis of trace elements can be used to try and aid discrimination. However, trace elemental composition can also be similar between eruptions, and the Dimna ash and Vedde ash have geochemically indistinguishable

major and trace element geochemistry (Lane *et al*., 2012). Other methods such as Raman spectroscopy are being developed and show early promise for distinguishing between tephras of similar major elemental composition (Surtees et al., 2016). Stratigraphy, independent dating (e.g. ^{14}C or varve counting) and stratigraphic markers such as spheroidal carbonaceous particles can also be used to discriminate between geochemically indistinguishable tephra layers, for example the tephras of Hekla 1510 and 1947 (Swindles and Roe, 2006).

Although tephra layers can be a useful dating tool, they are only as good as the date assigned to the eruption (or tephra layer). Where tephra layers can be historically dated and the geochemistry of a tephra is well known, the dates can be assumed to be well defined, providing that documents are reliable. For pre-historic tephras where no written record exists, assigning a date is more complex. Due to the poor preservation of volcanic ash on some surfaces, and the active geology of volcanic regions, it is sometimes not possible to obtain a date for a tephra from the region proximal to the volcano. Instead, tephras can be dated with respect to their position in the distal stratigraphy (Lowe, 2011). The detection of tephra in high-resolution records such as ice-cores and varved lake sediments provides the most precise means for dating a tephra, sometimes to sub-annual (seasonal) resolution (Coulter *et al*., 2012; Lane *et al*., 2013a; Zolitschka *et al*., 2015). However, not all tephras are present in high resolution records, and the detailed examination of annually accumulated ice or sediment for cryptotephra layers is time consuming. Current research focusses on specific core sections, and scanning for cryptotephra has not been conducted continuously in many records (e.g. Greenland ice cores). Therefore, the majority of pre-historic tephras have been assigned dates based on a ^{14}C derived chronology (Fig. 2). This may be achieved through interpolation from an age-depth model, direct radiocarbon dating or, more recently, wiggle-match dating (Plunkett *et al*., 2004).

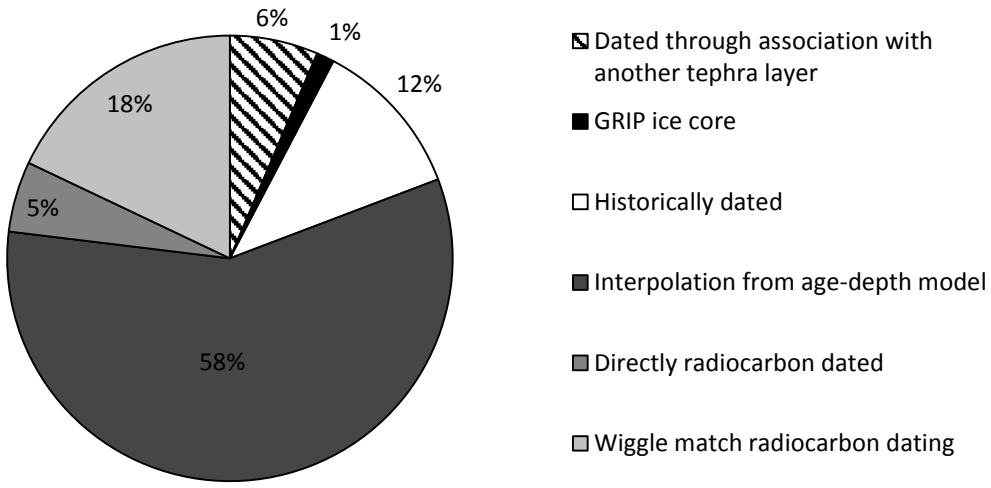

Figure 2. Pie chart indicating the dating methods for cryptotephras identified in northern Europe. The majority of tephras have been dated using radiocarbon dating on surrounding organic material. Tephras dated by association with another tephra layer have been identified alongside (mixed with) tephras of a known age. Data source: European cryptotephra database of Swindles *et al*. (2011) and references therein.

2.2 Cryptotephra research: a global view

The first cryptotephra layers were identified in northern Europe and were of Icelandic source (Dugmore, 1989; Hall and Pilcher, 2002). The majority of cryptotephra research is focused on northern Europe and the north Atlantic where multiple well dated and widespread tephra layers have been identified. However, increasingly there are a number of studies which explore visible tephra records and cryptotephra records from other regions (Davies, 2015) (Table 1). Expanding cryptotephra research into new regions, including the tropics, may offer opportunities to further our understanding of the preservation of cryptotephra layers in different environments and to understand the past dynamics of nearby active volcanic systems as well as offering a chronological tool for palaeoenvironmental reconstructions. However, as the majority of cryptotephra research has so far been conducted in the cooler northern latitudes the preservation of cryptotephra shards in tropical environments has not been studied. Understanding the potential for the preservation of cryptotephras in tropical environments is important in establishing whether cryptotephra studies in these regions could aid our understanding of past volcanism and potential impacts on ecosystems.

Country or region	Example References
Greenland ice cores	Davies *et al*. (2002); Davies *et al*. (2004); Fiacco *et al*. (1993); Mortensen *et al*. (2005); Zielinski *et al*. (1995)
North Atlantic and adjacent seas	Andrews *et al*. (2006); Austin *et al*. (2004); Bond *et al*. (2001); Haflidason *et al*. (2000); Jennings *et al*. (2002); Lacasse *et al*. (1998); Sjøholm *et al*. (1991)
Faroe Islands, Iceland	Dugmore and Newton (1998); Gehrels et al. (2006b); Larsen et al. (2001); Rasmussen et al. (2003); Wastegård (2002); Wastegård et al. (2001)
Great Britain and Ireland	Barber *et al*. (2008); Dugmore (1989); Dugmore *et al*. (1995); Dugmore *et al*. (1996); Hall and Pilcher (2002); Langdon and Barber (2001); Pilcher and Hall (1992); Pilcher and Hall (1996); Pilcher *et al*. (1995); Wastegard *et al*. (2000)
Norway, Sweden, Svalbard (Finland), Russia	Bergman *et al*. (2004); Boygle (2004); Davies *et al*. (2007); Oldfield *et al*. (1997); Persson (1971); Pilcher *et al*. (2005); Wastegård (2005); Wastegard *et al*. (2000) Ponomareva *et al*. (2013); Vorren *et al*. (2007)
Denmark, The Netherlands	Blockley *et al*. (2007); Davies *et al*. (2005); Turney *et al*. (2006)
Germany, Austria, Poland	Housley *et al*. (2013); Juvigne *et al*. (1995); Merkt *et al*. (1993); Schmidt *et al*. (2002); Van Den Bogaard and Schmincke (2002)
Estonia, Albania, Macedonia, Adriatic Sea, central Mediterranean area	Bescoby *et al*. (2008); Calanchi and Dinelli (2008); Hang *et al*. (2006); Siani *et al*. (2004); Wagner *et al*. (2008)
British Columbia, Alaska, North America	Payne and Blackford (2008); Pyne-O'Donnell *et al*. (2012)
China, Japan	Eden *et al*. (1996); Lim *et al*. (2008); Suzuki *et al*. (2005); Takemura and Danhara (1994); Zhao and Hall (2015)
Chile, Patagonia, Falkland Islands (Islas Malvinas), Peru	Haberle and Lumley (1998); Holmes *et al*. (1999); Wastegård *et al*. (2013); Watson *et al*. (2015)
New Zealand	Gehrels *et al*. (2006a); Gehrels *et al*. (2008)
Antarctica	de Angelis *et al*. (1985); Dunbar (2005); Kurbatov *et al*. (2006)
East Africa	Lane *et al*. (2013b)

Table 1. Table indicating the locations of tephra studies, updated from Pyne-O'Donnell *et al*. (2008). The majority of cryptotephra research has focused on northern Europe and the north Atlantic where multiple well dated and widespread tephra layers have been identified. However, increasingly there are a number of studies which explore visible tephra records and cryptotephra records from other regions (Davies, 2015).

2.2.1 Cryptotephra records in northern Europe

As afore mentioned the majority of cryptotephra studies have focused on northern Europe. This makes northern Europe the ideal location for using cryptotephra layers as records of volcanic ash clouds as there are numerous studies across different depositional environments which have examined cryptotephra layers primarily for the purpose of chronological control on paleoenvironmental reconstructions.

2.2.1.1 Icelandic volcanism

The majority of cryptotephra layers in northern Europe are of Icelandic source. Iceland is one of the most volcanically active regions in the world (Thordarson and Hoskuldsson, 2008). The island is located on the Mid-Atlantic Ridge, along which the North American and Eurasian plates are diverging at an average rate of 1.8 cm yr^{-1} (Gudmundsson, 2000). Iceland also sits above a mantle plume, leading to frequent effusive and explosive volcanism (Wolfe *et al*., 1997). There have been an estimated 2400 volcanic eruptions on Iceland during the Holocene; mafic (effusive) volcanism dominates (Thordarson and Hoskuldsson, 2008).

Volcanoes in Iceland exhibit a wide range of magma compositions. Magma composition is a key control on explosivity and thus the propensity for the production of fine ash. Eruptions of rhyolitic and mixed geochemical compositions are often associated with the production of large quantities of fine tephra. Silicic magmas are more viscous and contain a higher volatile content than their mafic counterparts. As a result, eruptions of silicic magmas are often more explosive with increased magma fragmentation and the production of more tephra, when compared to eruptions of mafic compositions which are less viscous and escape the vent as lava. A recent example of effusive activity was the eruption of the Bárðarbunga-Veiðivötn volcanic system between August 2014 and February 2015 which produced approximately 1.5 km^3 of lava (Schmidt *et al*., 2015). Effusive eruptions pose hazards such as the emission of toxic gases and physical damage to property. However, the interaction of magma with ice/water from glaciers during sub-glacial eruptions frequently results in explosive phreatomagmatic phases (Gudmundsson *et al*., 2008). The fragmentation of magma during explosive phreatomagmatic phases can result in the production of large volumes

of fine tephra. Eruptions of silicic magma are less common on Iceland than mafic eruptions, although still more frequent than in many other volcanic regions (Thordarson and Hoskuldsson, 2008). The Hekla volcano has been the most prolific producer of silicic tephra in Iceland during the Holocene, depositing 50 proximal tephra layers in the last ~8000 years (Larsen and Eiriksson, 2008a) (Fig. 3).

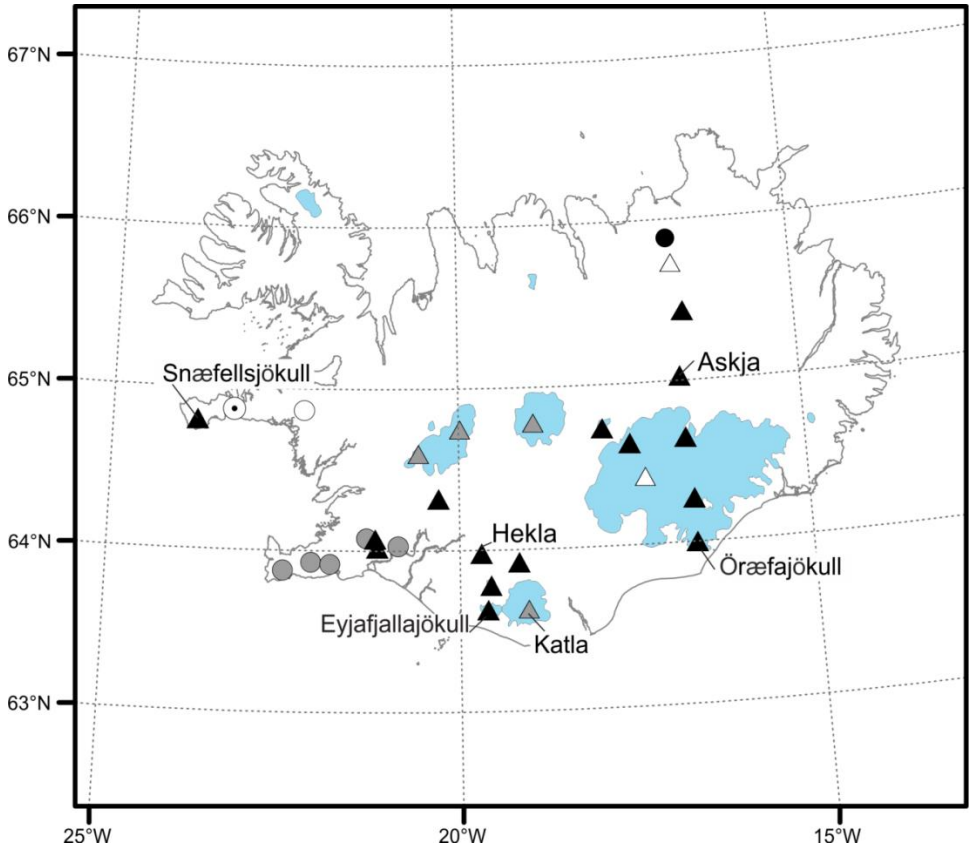

Figure 3. Map of Iceland indicating volcanoes which have been active during the Holocene and approximate boundaries of large ice masses (blue shading). Data on Holocene volcanoes from the Smithsonian Database (Global Volcanism Program, 2013). Volcanoes are indicated as follows: white triangle = Caldera, white circle = Fissure vent, white circle with point = Pyroclastic cone, black circle = Shield volcano, black triangle = Stratovolcano, grey triangle = sub-glacial, grey circle = Crater.

2.2.1.2 Icelandic volcanism and climate

Icelandic volcanism is controlled not only by internal factors such as the rate of plate boundary rifting and pulses of the magma plume, but also by external factors such as climate. The position of Iceland at 64º latitude results in a cold climate capable of sustaining glaciers throughout much of the mid- to late- Holocene and a large ice cap during the last glacial maximum. In addition to increasing the explosivity of eruptions through ice/water interaction, there is evidence that the degree of ice overlying Icelandic volcanoes has effected the frequency of volcanism in the past (Sigvaldason *et al*., 1992). A 30% increase in eruption frequency during the period 10-8 ka BP has been attributed to rapid glacial unloading at the start of the Holocene which led to depressurisation, increased melt production and a subsequent increase in volcanism (Jull and McKenzie, 1996; Maclennan *et al*., 2002). Ice caps on Iceland are currently retreating, but current glacial unloading is on a much smaller scale than during the last glacial-interglacial transition and appears to be resulting, at least in the short term, in increased intrusive activity and thus increased magma storage capacity, as opposed to increasing the risk of an eruption (Hooper *et al*., 2011).

Modelling and observations suggest that even small seasonal changes in ice volume can increase the probability of, or even trigger volcanic eruptions (Albino *et al*., 2010). There has been a limited amount of research, focussed on modelling increases in melt generation due to the relatively small (compared to glacial-interglacial unloading) declines in ice volume since the Little Ice Age (~AD 1890), these studies suggest that reducing ice volume is resulting in significant increases in melt generation rates (Pagli and Sigmundsson, 2008; Schmidt *et al*., 2013). However, there are no observational studies which indicate an increase or decrease in volcanic frequency during the current interglacial with changes in ice volume, with which to support models. Proximal records of past volcanic frequency are often confounded by the erosion of deposits in areas proximal to volcanoes. Some distal cryptotephra records are not confounded by the same reworking issues. Therefore, examining the past record of ash clouds (cryptotephra) alongside proximal records can aid confidence in the identification of periods of change in the frequency of Icelandic volcanism in the past. When used alongside climate records such as study may allow for further assessment of a potential link between the frequency of Icelandic volcanism and climate (Thesis Objective 6).

2.2.1.3 Spatial distribution of existing Holocene tephra records

This section will focus on records of tephra in peatlands and lakes across northern Europe and is limited to the last 7000 years, the period for which climatic conditions have been largely similar to the modern era. This temporal limitation has been applied because of the increase in frequency of Icelandic volcanism prior to 7000 years BP during the transition from the last glacial period to the Holocene (Section 2.2.1.2). This review was conducted prior to the commencement of fieldwork for this PhD project and was updated last in autumn 2012. Tephra has also been identified in ice cores (e.g. Gronvold *et al*., 1995) and marine sediments (e.g. Gudmundsdóttir *et al*., 2011) in the north Atlantic. However, here we are primarily concerned with ash clouds which travelled toward northern Europe. Ice core evidence from Greenland is therefore beyond the spatial remit of this study. Furthermore, no complete records of tephra fall from Greenland are currently available. Due to the high resolution of the Greenland record, only small sections of ice cores have been examined, usually targeted at identifying a particular tephra or time interval (Coulter *et al*., 2012).

The current database of cryptotephras referred to in this section was compiled and reported by Swindles *et al*. (2011) and updated by the author of this review. The number of tephra layers recorded in northern European peatlands and lakes is 84, of which the majority, 44 have been identified at only one site (Fig. 4, Fig. 5) The database contains data from cryptotephras in the geological record (n = 77) and those observed to fall-out over northern Europe in historical times (n = 7). A thorough analysis of the spatial distribution of northern European cryptotephras was conducted by Lawson *et al*. (2012).

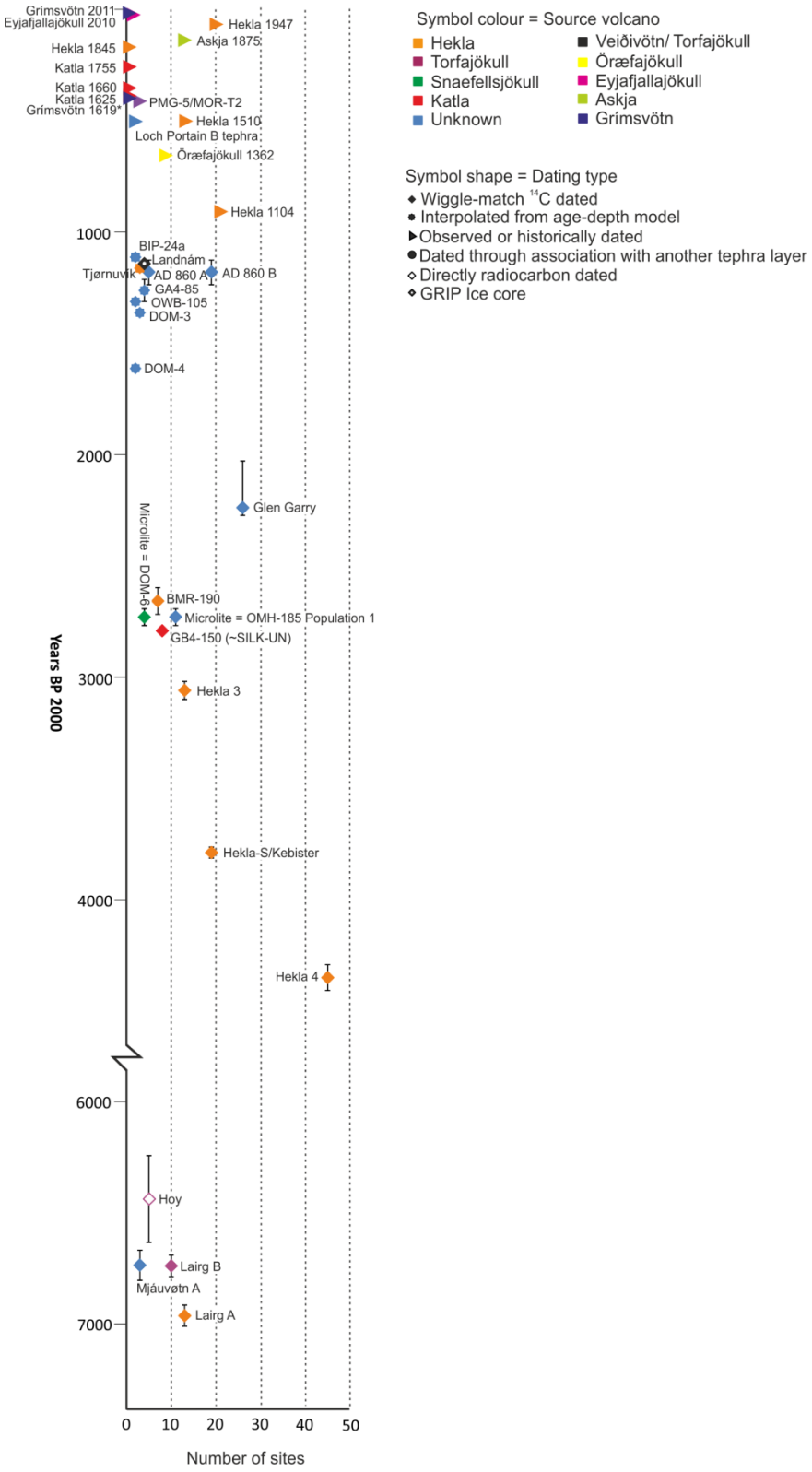

Figure 4. Diagram indicating the outline tephrostratigraphy for northern Europe. The diagram includes only tephras which have been identified at more than one site. Error bars indicate uncertainty in age estimate. *Suggested to be from the eruption of Grímsvötn in 1619

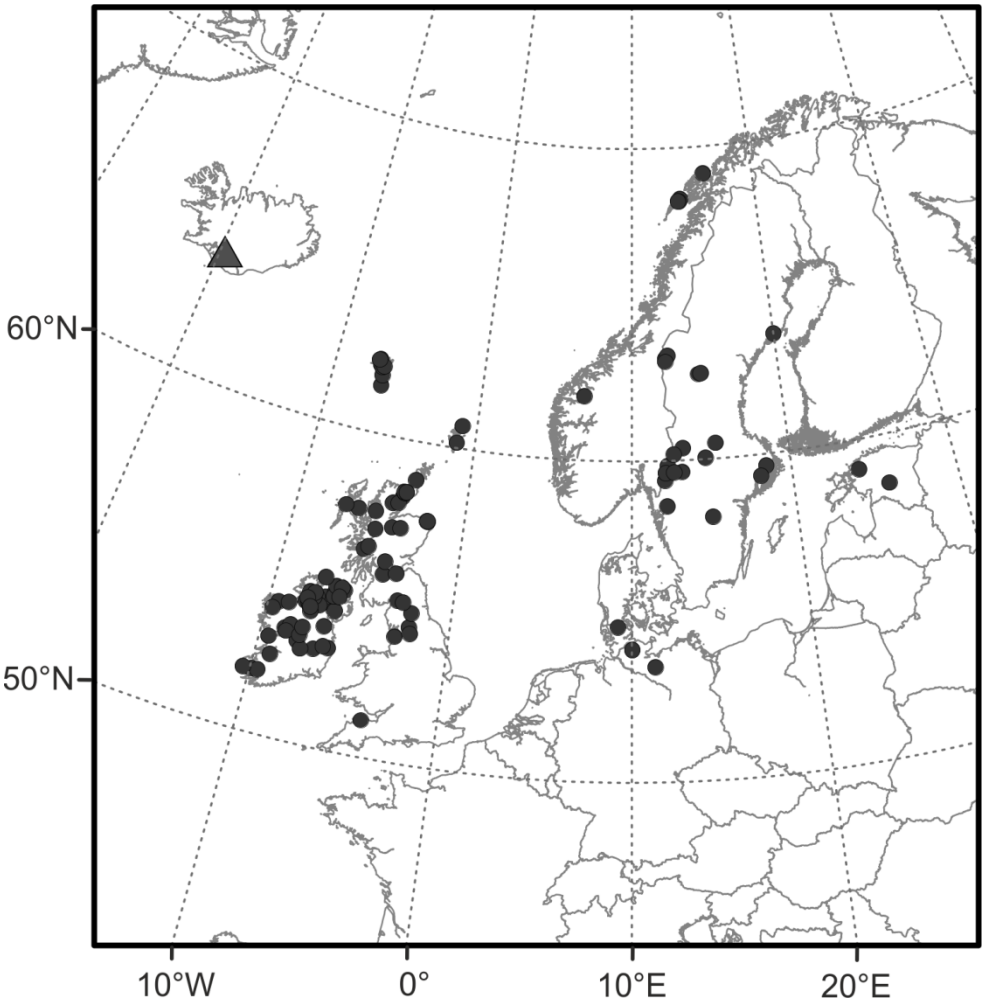

Figure 5. Map showing the distribution of sites where Holocene cryptotephras have been identified, based on the Holocene cryptotephra database of Swindles *et al*. (2011) (updated as of Autumn 2012). Filled circles indicate lake and peatland sites where cryptotephras have been geochemically analysed. The grey triangle shows the location of the Hekla volcano. The source of the majority of Holocene tephra layers in Northern Europe.

The database contains tephra records from 100 peatlands and 20 lakes. The dominance of peatland sites is most likely related to a combination of: firstly, the abundance of peatlands in northern Europe, some of which date to the early Holocene and secondly, the ease of extracting tephra from peat when compared to lake sediments, which contain more mineral material necessitating the use of additional extraction steps. No site has a complete record containing every tephra layer; this is due to differences in topography and meteorological conditions which affect tephra transport and fallout. Meteorological conditions, particularly wind strength and direction are a major control on tephra distribution. As evidenced by infrared satellite images, discrete air masses often

maintain their integrity rather than mixing, resulting in a patchy distribution of tephra rather than a uniform dusting (Cooke *et al*., 2014). Furthermore, radionuclides fall out preferentially during periods of rainfall (Mattsson and Vesanen, 1988). Langdon and Barber (2004) suggest that a similar wash-out effect may affect tephra deposition, depositing more tephra from the atmosphere during rainfall events and resulting in patchy tephra distributions.

Tephra layers from Hekla volcano dominate the geological record of cryptotephra layers for Northern Europe in the mid- to late- Holocene. Hekla is the source for just under half of the cryptotephra layers found at five or more sites (Fig. 6, Table 2). The most spatially widespread tephra layer is Hekla 4 which has been identified at 45 sites spanning much of Europe and which provides a valuable isochron for dating the period c. 4287 BP (Pilcher *et al*., 1995) (Fig. 7). In contrast, the Glen Garry tephra c. 2176 BP (Dugmore et al., 1995), although identified at 26 sites (Fig. 8) has a narrower spatial distribution toward South and East Europe and has not been identified in Scandinavia.

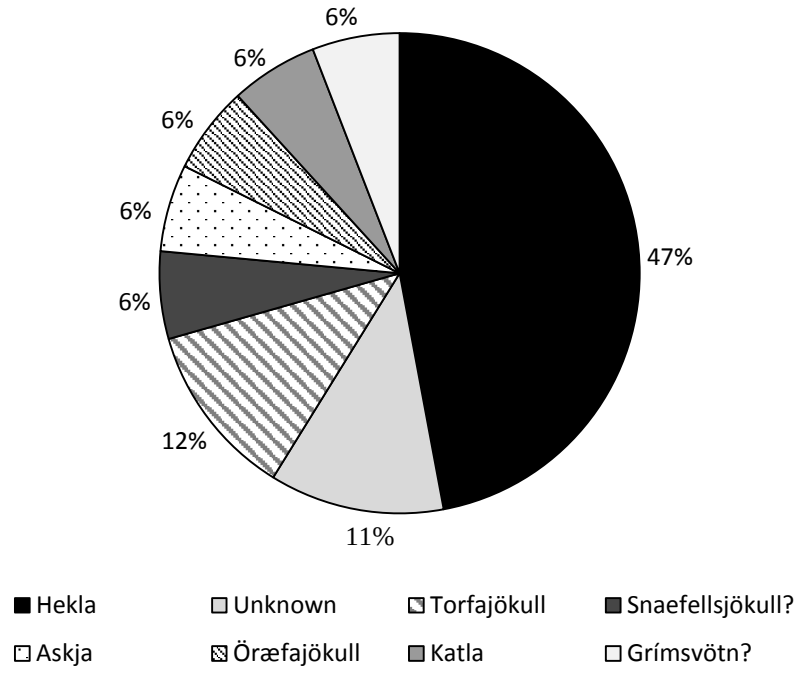

Figure 6. The distribution of eruptions among volcanic systems. A total of 17 explosive eruptions over the last 7000 years have resulted in tephra found at ≥5 European sites. Question marks indicate eruptions where attribution to source volcano is tentative.

Name	Sites (n)	Source	Date	Geochemistry	Dating Method
Hekla 4	45	Hekla	2395-2279 BC	Rhyolitic	Wiggle-match ^{14}C
Glen Garry	26	Unknown	16-260 BC	Dacitic-Rhyolitic	Wiggle-match ^{14}C
Hekla 1104	21	Hekla	AD 1104	Rhyolitic	Historical
Hekla 1947	20	Hekla	AD 1947	Dacitic-Andesitic	Historical
AD 860 B	19	Alaska	AD 776-887	Rhyolitic	Wiggle-match ^{14}C
Hekla-S/Kebister	19	Hekla	1800-1750 BC	Dacitic-Rhyolitic	Wiggle-match ^{14}C
Microlite	15	Snaefellsjökull?	755-680 BC	Rhyolitic	Wiggle-match ^{14}C
Askja 1875	13	Askja	AD 1875	Rhyolitic	Historical
Hekla 1510	13	Hekla	AD 1510	Dacitic-Andesitic	Historical
Hekla 3	13	Hekla	1087-1006 BC	Dacitic-Rhyolitic	Wiggle-match ^{14}C
Lairg A/Hekla 5	13	Hekla	4997-4902 BC	Rhyolitic	Wiggle-match ^{14}C
Lairg B	10	Torfajökull	4774-4677 BC	Rhyolitic	Wiggle-match ^{14}C
Öræfajökull 1362	9	Öræfajökull	AD 1362	Rhyolitic	Historical
GB4-150 (~SILK-UN)	8	Katla	800-758 BC	Dacitic-Trachydacitic	Wiggle-match ^{14}C
BMR-190	7	Hekla	705-585 BC	Dacitic	Wiggle-match ^{14}C
AD 860 A	5	Grímsvötn?	AD 776-887	Rhyolitic	Wiggle-match ^{14}C
Hoy	5	Torfajökull	4620-4230 BC	Rhyolitic	Directly ^{14}C dated

Table 2. Characteristics of cryptotephra layers which occur at ≥5 sites in northern Europe. The majority of widespread tephra layers in northern Europe have been dated using either historical records or Wiggle-match ^{14}C. Data from this study (thesis) is not included.

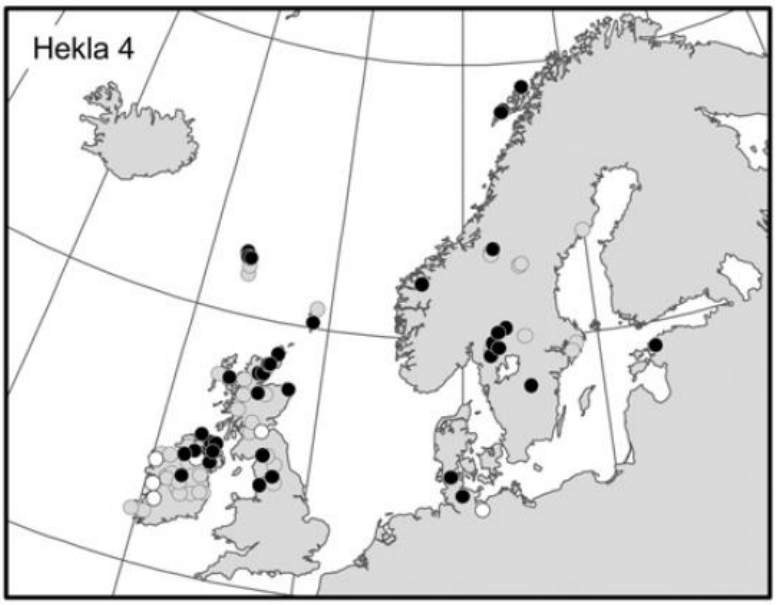

Figure 7. Diagram from Lawson *et al*. (2012) indicating widespread nature of Hekla 4, black dots indicate sites where the Hekla 4 tephra has been identified, white dots indicate sites where tephra has been investigated and Hekla 4 has not been found, grey dots indicate all sites in the European tephra database.

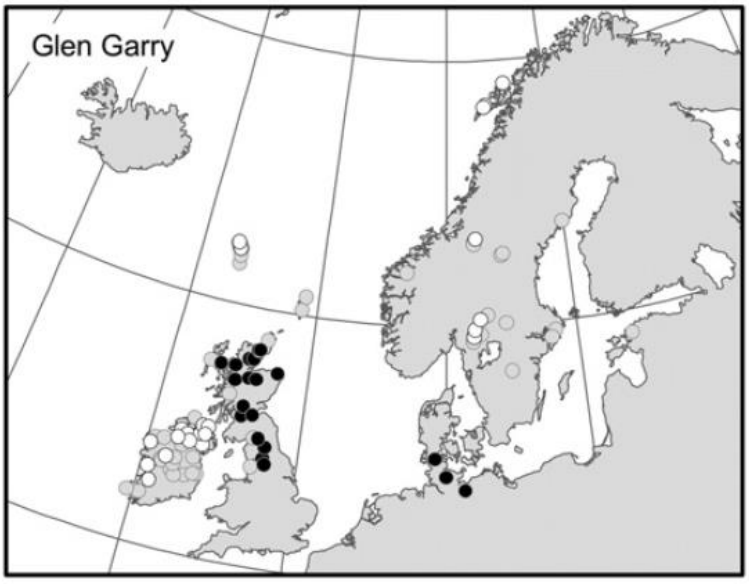

Figure 8. Diagram from Lawson *et al*. (2012) indicating the distribution of Glen Garry tephra, black dots indicate sites where the Glen Garry tephra has been identified, white dots indicate sites where tephra has been investigated and Glen Garry has not been found, grey dots indicate all sites in the European tephra database.

2.2.1.4 Geochemistry of existing Holocene tephra records

Fig. 9 indicates the geochemistry of tephras found at more than five sites in northern Europe. The record is dominated by tephra layers of silicic composition. Despite the dominance of basaltic volcanism in Iceland and the potential for explosive phreatomagmatic eruptions which have been shown to distribute fine ash over long distances (Stevenson *et al*., 2012; Thordarson and Hoskuldsson, 2008), only five basaltic cryptotephra layers have been identified in Holocene records in northern Europe: the Landnám (1079 ± 2 BP) tephra thought to be from either the Veiðivötn or Torfajökull volcanic system (Cage *et al*., 2011; Hannon *et al*., 2001; Wastegård, 2002), the Mjáuvøtn A (6668-6533 BP) tephra of unknown source (Olsen *et al*., 2010; Wastegård *et al*., 2001), Veiðivötn 473 BP (Chambers *et al*., 2004; Davies *et al*., 2007), and the Hov (6190-5720 BP) and BRACSH-1 (222-70 BP) tephra layers thought to be from Grímsvötn (Reilly and Mitchell, 2015; Wastegård, 2002).

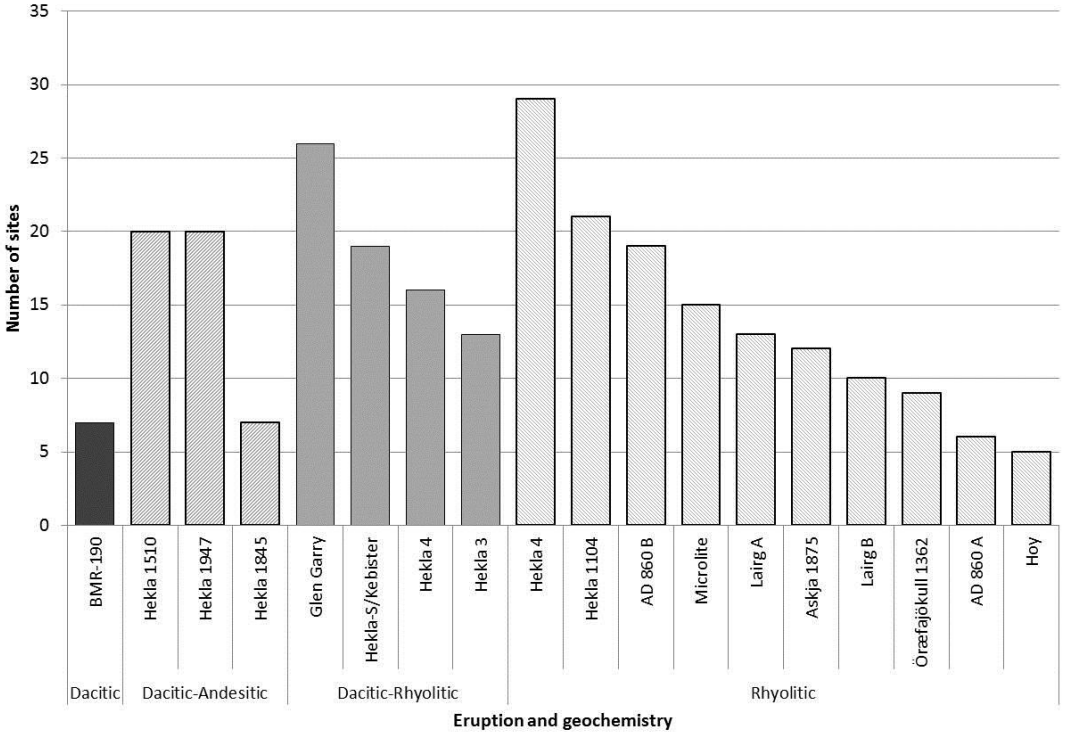

Figure 9. The number of sites where a tephra layer is found in Northern Europe. Tephra layers found at fewer than five sites are excluded (n = 267). More information on the characteristics these eruptions are given in Table 2.

The majority of basaltic cryptotephras have been identified in sites on the Faroe Islands, although basaltic tephras have also been identified in Ireland (Chambers *et al*., 2004; Reilly and Mitchell, 2015) and Scandinavia (Davies *et al*., 2007). A number of possible reasons for the lack of basaltic cryptotephras in Holocene European cryptotephra records have been suggested:

1) There is experimental evidence that basaltic glass is more prone to hydration, alteration and even completely dissolving in acidic environments (pH 4), than rhyolitic glass (Pollard *et al*., 2003; Wolff-Boenisch *et al*., 2004). Prolonged exposure to the acidic and wet environments in peatlands may result in the dissolution of glasses of mafic composition.

2) Basaltic tephra shards have a higher density than silicic shards (2.5-3.0 and 2.3 g cm^{-3} respectively). Models suggest that basaltic tephra shards fallout of the atmosphere earlier than silicic shards of the same size and arrive over northern Europe in lower concentrations in the air (Stevenson *et al*., 2015).

3) Density separation extraction methods might result in the under-detection of basaltic tephra layers, especially in lake sediments (density separation is rarely required in peats).

The work of Swindles *et al*. (2011) and Lawson *et al*. (2012) has gathered data from many cryptotephra studies in northern Europe and highlighted the low number of basaltic tephras in the distal record. However, although many theories have been put forward to explain these observations these rely on experimental or modelled evidence. More research is required in order to assess the possible reasons for the underrepresentation of basaltic tephras in the distal cryptotephra record. An examination of naturally deposited tephra layers, in order to better understand the reason or reasons for the underrepresentation of basaltic tephras in the distal tephra record is an objective of this thesis (Thesis Objective 3).

2.3 Spatial gaps in European tephra records

Satellite monitoring of the ash clouds produced during recent Icelandic eruptions indicate that volcanic ash does not travel evenly across northern Europe and fall as a blanket across all sites (Folch *et al*., 2012). Therefore a full spatial coverage of sites across the continent is important if all cryptotephra layers and to be recorded. Spatial analysis of cryptotephra distribution by Lawson *et al*. (2012) indicates a number of gaps in the spatial distribution of terrestrial tephra records (Fig. 10). Lawson *et al*. (2012) strive to include an analysis of sites where a tephra has been looked for, but not found in order to map the margins of tephra distribution. However, this is often not possible as searches for tephra with a negative outcome are not routinely reported. Therefore, the spatial gaps in European cryptotephra distribution maps may be considered to represent either: the ‘true’ margins of the spatial distribution of a tephra or, they may be an artefact of sampling. Establishing the presence or absence of tephra horizons in these ‘gap’ regions will allow for the assessment of the extent to which current distribution maps are confounded by sampling bias. Identification of tephra in these regions would suggest that, rather than reflecting areas of no tephra fallout, these regions are areas where cryptotephra have not been sought. Should they be an artefact of sampling bias, these ‘gap’ regions also offer the most promise for identifying new, previously undiscovered tephra layers.

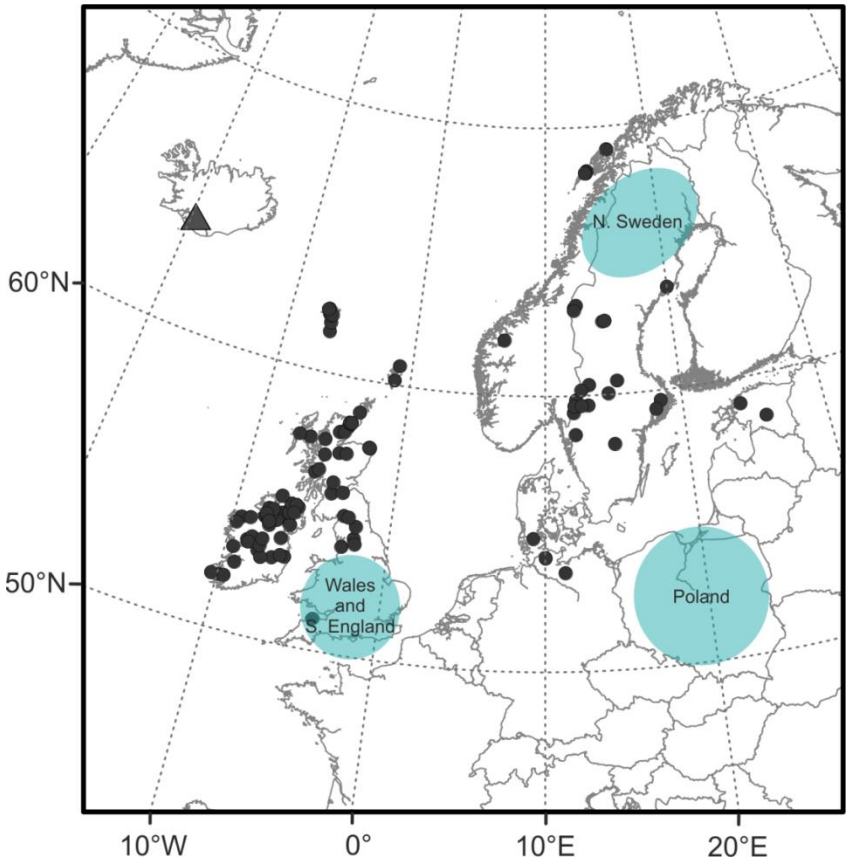

Figure 10. A map of all European cryptotephra sites (autumn 2012) (filled circles). Spatial gaps in tephra records referred to in the text have been shaded blue. Triangle indicates the location of the Hekla volcano.

I focus on three spatial gaps in tephra records which offer the most promise for identifying previously undiscovered cryptotephras. These regions contain peatlands and/or lakes, some of which have not been subject to anthropogenic disturbance and should provide records for the mid- to late- Holocene.

2.3.1 Poland

A recent investigation has identified two Late Glacial tephras thought to be of Icelandic origin in the South West of Poland (Housley *et al*., 2013), this suggests that there is no reason why Holocene Icelandic tephras should not also have reached Poland. Prior to the commencement of this research project there were no published records of Holocene Icelandic tephras in Poland. More recently, Wulf *et al*. (2016) identified a number of tephra layers including Askja 1875, and two other tephra layers of suggested Icelandic origin in a varved lake sequence in central northern Poland. Low shard concentrations suggest that some of the tephras identified were close to the edge of their detectable

range. Further research in this region might identify the margins for the spatial distribution of these tephras.

2.3.2 Northern Scandinavia

Scandinavia, lies in the path of the dominant lower stratospheric winds from Iceland (Wastegård, 2005). A number of tephra isochrones including: Hekla 4, Hekla 3, Hekla-Selsund and Askja 1875 have been identified in Holocene records (Wastegård, 2005). However, records are clustered toward southern and central areas, which are closer to major population centres, and contain ombrotrophic peatlands. There has been a limited amount of work in the northern regions, including the examination of a site on the Lofoten Islands (northern Norway) which identified a number of previously unrecognised cryptotephra layers (Pilcher *et al*., 2005). There is only one published tephra record from the north-east coast of Sweden, which has a temporal extent of 700 years and where the Askja 1875 tephra has been identified (Oldfield *et al*., 1997). This leaves a major spatial and temporal gap in tephra records from northern Sweden prior to AD 1875.

2.3.3 Wales and southern England

Multiple cryptotephra layers have been identified across northern Britain (Lawson *et al*., 2012). However, only one tephrostratigraphy exists for the South of Britain, from Exmoor (Matthews, 2008). The data which is published in a technical report for English Heritage, spans only the last 2700 years. Cryptotephras have been observed in cores from peatlands in Wales (Buckley and Walker, 2002; Hall and Pilcher, 2002), but the lack of geochemical data prevents their use as chronological markers.

2.3.4 Addressing spatial gaps

Spatial gaps in current tephra records may reflect regions where no tephra has fallen, and thus be useful for mapping the margins of tephra fallout. However, they may also represent regions where research intensity has been low and therefore cryptotephras have not been identified. An examination of the literature, suggests that the latter is

more likely. The identification of late-glacial Icelandic tephra layers in Poland, and reports of tephra layers in Wales, suggests that these regions are within the distal fallout range of Holocene Icelandic tephra and therefore the lack of cryptotephras in these regions in the Swindles *et al*. (2011) database is an artefact of research intensity rather than a reflection of the distribution of tephras. During this research project we will test this hypothesis further by examining material from sites in areas identified above as 'spatial gaps' for cryptotephra layers (Thesis Objectives 8 and 9).

2.4 Cryptotephras as records of volcanic ash

Until recently cryptotephras were predominantly used as dating isochrons. However, they also represent a record of fall-out from ash clouds and can be used to understand the frequency of ash cloud events and other details, such as geochemistry, of the eruptions from which they are derived.

2.4.1 Statistical modelling of the recurrence intervals of volcanic ash cloud events

Given the social and economic cost of disruption caused by volcanic ash cloud events, understanding the frequency of future events is important, particularly for the insurance and aviation industries. The probabilistic assessment of volcanic hazards typically involves estimating the number of events (eruptions or in this case ash cloud coverage) that have occurred in a given time interval in the past. With the assumption that the volcanic system will continue to behave in a similar way, this information can be used to forecast a recurrence rate for future events (Kiyosugi, 2012). Probabilistic modelling allows for the quantification of uncertainties associated with hazard assessments (Rymer *et al*., 2009; Sandri *et al*., 2012).

Owing to the popularity of tephra for chronological control in northern Europe a large amount of data on past Icelandic ash events is available. Swindles *et al*. (2011) compiled tephra records from northern Europe into a database spanning the last 7000 years. For the period with the best records (the last 1000 years) they calculated the average recurrence interval of ash clouds over Northern Europe to be 56 ± 9 yr. Repose intervals ranged from 6 to 115 years. In a given 10 year period there is a 16% chance of an ash cloud occurring.

Swindles *et al*. (2011) calculated the chance of future eruptions in a given time period using survival analysis. Survival analysis focuses on a failure point (Cox and Oakes, 1984). In the case of medical research this may be a patient fatality; in the case of volcanology this would be an ash cloud producing eruption. The time between a specific starting point and the failure event is termed 'survival time', in this instance the survival time is the repose interval between events (Banerjee, 2003). The empirical survivor function is calculated and analysed using the observed repose intervals, where the repose interval is taken as the time between the start times of two successive ash clouds. In this instance the survivor function S(t) gives the probability that T (repose interval) exceeds a given time interval (t) (Cox and Oakes, 1984):

$$S_T(t) = P[T > t]$$

The use of non-parametric methods is necessitated as distribution for the repose intervals is not assumed (Connor *et al*., 2006). The survivor function at each repose (time between eruption) is calculated as below (where *ti* is a given repose interval from 1…N and N is the total number of events):

$$S(t_i) = \frac{N - i}{N}$$

An appropriate model for survival time for which parameters have been assessed will assist the precision of prediction of survival. This is commonly and easily achieved using graphical comparison whereby a parametric survival function is chosen which best aligns with the empirical survival time data (Lee, 1992). Examples of commonly utilised distributions for natural hazard modelling include the exponential (Swindles *et al*., 2011); Weibull (Dzierma and Wehrmann, 2012) and log logistic distributions (Connor *et al*., 2006). The exponential distribution suggests the rate of eruptions is constant over time and approximates toward a Poisson distribution. Weibull distributions allow for a change in the rate of a hazard over time, for example an increase in the rate of eruptions (or clustering). Finally, log logistic distributions allow competing factors to be taken into account (Dzierma and Wehrmann, 2012).

There are a number of assumptions which must be considered when utilising survival analysis to forecast the probability of future events. These are:

1) The forecast will always represent a minimum probability because there is the possibility that some events have not been preserved, or yet identified in the geological record and are therefore not included in the calculations.
2) The geological record probably contains some (unquantified) noise due to, for example, incorrect tephra source identifications or unreliable dating.
3) The rate of volcanism can change over time, therefore the input parameters of start time and end time for a given period of past activity are important and must be justified (Connor *et al*., 2015) .
4) Changes in the rate of volcanism are also complicated by an increase in the reporting of volcanic events over the last 1000 years. This is due to: the expansion of the human population and an increase in the quantity and quality of written records; as well as better preservation of more recent events in the geological record.
5) One major source of error in many estimates of volcanic hazard recurrence is errors in the date assigned to individual events/eruptions. Although some events can be dated historically with a negligible temporal uncertainty, events in the geological record may be dated by other methods with various degrees of accuracy. The recurrence model for northern Europe used by Swindles *et al*. (2011) uses the midpoint of each age estimate as the date for each interpolated event and therefore does not account for uncertainties in the estimated ages of these units.

Assessing the reoccurrence of volcanic ash clouds over northern Europe using geological and observed records represents the only available means of estimating future hazard. However, there are a number of assumptions and limitations involved when applying this sort of model. The unpredictability of volcanic eruptions means that even models based on an idealised (complete) history of past volcanic ash cloud data can only offer an estimate of reoccurrence. The extent to which geological records are incomplete is unknown, but bias in the geological record makes any estimate of reoccurrence a minimum estimate. The reoccurrence estimate of Swindles *et al*. (2011) was 56 ± 9 yr. Repose intervals ranged from 6 to 115 years. In 2011, just one year after the eruption of Eyjafjallajökull, Grímsvötn erupted, the explosive eruption resulted in transport of volcanic ash over northern Europe (Stevenson *et al*., 2013). The repose

interval between these two events (1 year) was much less than any previously identified in the geological record and underlines the extent to which estimates of volcanic ash reoccurrence based on past eruption frequency are complex.

Despite the challenges and limitations of modelling the reoccurrence of ash cloud events, the past is often the only way to establish what might occur in the future. In this thesis I will aim to further assess the bias in the northern European tephra database on which the Swindles *et al*. (2011) model is based (Thesis Objectives 1-4). I will also assess spatial gaps in northern European tephra records, with the aim of identifying new tephras and thus increasing the completeness of the northern European tephra database (Thesis Objectives 8-9). Finally I will use the new database to outline a new reoccurrence estimate for volcanic ash over northern Europe and compare this with the reoccurrence of Icelandic eruptions (Thesis Objective 7).

2.4.2 Beyond frequency: Other information about past ash cloud events

In addition to information on the frequency of past ash cloud events, cryptotephra layers may offer further insights into previous ash cloud characteristics. For example, variation in the geochemistry of cryptotephra from the Hekla 4 eruption has been suggested to reflect changes in magmatic SiO_2 content during the eruption (Langdon and Barber, 2004). It has been suggested that the examination of the geochemistry of distal tephra, can inform understanding of the physiochemical conditions under which the melt was formed (Ponomareva *et al*., 2015).

Shard concentrations (total numbers of shards or ‘tephra loading’) have also been examined at a large scale for Glen Garry and Hekla tephras at sites in Scotland and for the Hekla 1947 tephra across northern Ireland (Langdon and Barber, 2004; Rea *et al*., 2012). Both studies identify differences in tephra loading at different sites on a regional scale. Hypotheses to explain the regional variation in shard concentrations include: periods of wet and dry deposition; differences in site altitude; and the location of a site with reference to the position of the ash cloud. However, both of these studies are based on one or two cores at a peatland. As of the commencement of this thesis, no research has been conducted regarding the degree of within site variation in tephra concentrations. This thesis will examine multiple peat cores within one site (Thesis

Objective 1). Such research is of methodological interest (are multiple cores needed to identify all the tephra layers in one site?). Furthermore, if tephra is being redistributed at a site scale, any regional scale inferences based on shard counts from one or two cores may be invalid.

Although tephra shard count totals are often reported, the shard size and morphology of distal cryptotephras is rarely described. However, there are a small number of studies which have begun to report distal tephra shard size and morphology data. Information on shard characteristics, in particular particle size distributions, has proved useful in evaluating current methods for monitoring ash clouds using satellites (Stevenson *et al*., 2015). Furthermore, although scanning electron microscope observations indicate the irregular (non-spherical) shape of cryptotephra, which is often characterised by fractured bubble walls, models of tephra fallout predominantly simplify tephra shards to spheres (Carey and Sigurdsson, 1982; Sparks *et al*., 1992). Increasingly it is being recognised that particle shape has a significant impact on predicted transport distances in tephra fallout models (Beckett *et al*., 2015). Dellino *et al*. (2012) identified a 400% difference in the settling velocities of spherical and irregularly shaped shards of equal mass, with irregularly shaped shards travelling further. There is a need to build on this pioneering work with a comprehensive analysis of cryptotephra shard sizes from multiple sites across northern Europe (Thesis Objective 5). Further work is required to understand the extent to which cryptotephra shard size and morphology can inform understanding of source eruption parameters and to establish standard protocols for the reporting for cryptotephra size and morphology. Information on the shard size and shape of cryptotephras will be of interest to modellers, satellite monitoring specialists and tephrochronologists.

2.5 To what extent do tephra records represent past ash cloud events?

In order to use cryptotephra records as records of ash cloud events it is necessary to understand the extent to which they might be confounded by issues of preservation and reworking following deposition. Following the deposition of tephra onto peat or a lake/lake catchment, a number of factors can affect preservation and thus the tephrostratigraphy at any given point (or coring location). Reworking is here defined as the movement of tephra following initial deposition. The degree of reworking is

affected by: meteorological conditions such as wind and rain; vegetation; human impact; and hydrological factors (e.g. peatland water-table movements) (Fig. 11). Identifying reworking presents a key challenge in tephrochronology (Dugmore *et al*., 2011). In this section we discuss the reworking of tephras in peatlands, and then in lakes.

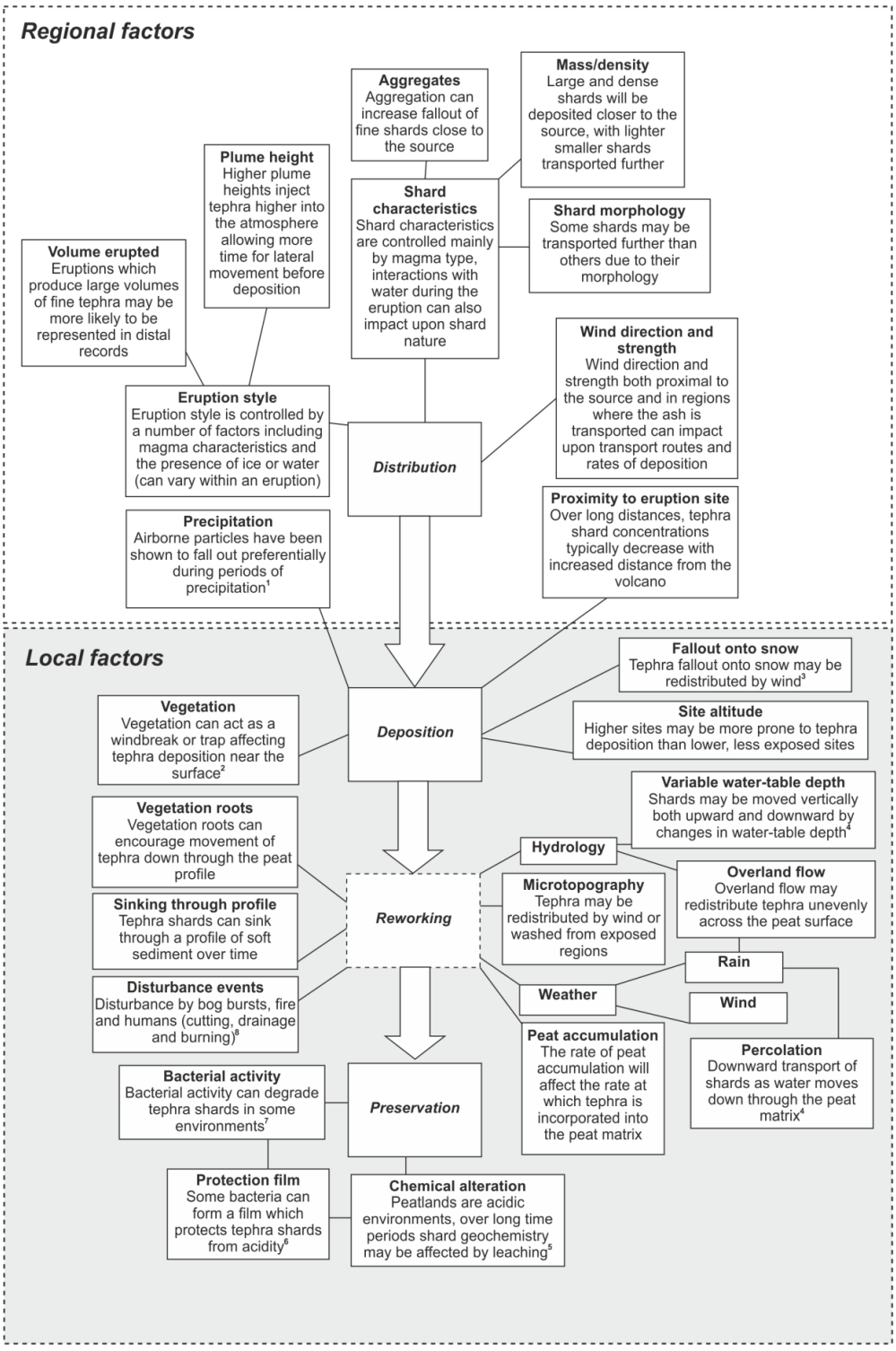

Figure 11. A summary diagram of the factors influencing tephra deposition. Key references (1) Mattsson and Vesanen (1988); (2) Pouget *et al*. (2014b); (3) Bergman *et al*. (2004); (4) Payne and Gehrels (2010); (5) Hodder *et al*. (1991); (6) Techer *et al*. (2001); (7) Thorseth *et al*. (1995) (8) Swindles *et al*. (2013). Published in Watson *et al*., (2015).

The movement of tephra laterally, across the surface of a peatland is important, as the degree of lateral movement will determine the extent to which tephra is above/ below levels of detection. Tephra fallout onto snow and subsequent reworking has been invoked as a cause of fragmented or 'patchy' tephra deposits in northern peatlands (Bergman *et al*., 2004). Tephra that has been deposited onto snow may be trapped until a subsequent melt, causing a lag which might be seasonal or cover many years, between deposition and incorporation into lake sediments (Davies *et al*., 2007). Whether tephra is deposited onto snow or directly onto the peat or lake catchment, localised aeolian redistribution can also occur. The type and coverage of vegetation have been identified as important factors in determining the impact of aeolian redistribution processes on proximal tephra layers (Boygle, 1999). Peatlands and lakes are often particularly exposed, with few trees to reduce the reworking of tephra shards by wind (Bergman *et al*., 2004).

There is limited experimental evidence for the redistribution of thin (1 mm) tephra layers on peatlands during overland flow generated by precipitation. Such redistribution of shards across the peatland surface may cause tephra layers to become spatially patchy or to be washed from the peatland entirely (Payne and Gehrels, 2010). A study of the tephrostratigraphy of proximal upland and lowland sites on the Shetland islands concluded that landscape scale changes, in this instance an increase in burning, can result in the remobilisation and redistribution of already deposited cryptotephra layers (Swindles *et al*., 2013).

As well as moving across the surface of the landscape, tephra can also move vertically through the peat profile or lake sediment. It is common to identify a peak in the shard concentration within a stratigraphic record, with lower shard concentrations above and below. There has been some debate regarding the horizon which should be identified as representing the event date (Davies *et al*., 2007). This is particularly a problem in lake sediments, where shards can continue to wash in from the catchment for a number of years following the initial event. Experimental work on peatlands indicates that the majority of shards remain at the palaeo-surface and the peak in tephra shard concentration can be considered to represent the timing of the eruption or dating isochron (Payne and Gehrels, 2010).

Tephra may be reworked in a number of ways in lake sediments including: downward migration through soft sediment (Davies *et al*., 2007); bioturbation; within-basin focussing; and movement by plant roots (Davies *et al*., 2007; Davies *et al*., 2005). Pyne-O'Donnell (2011) investigated tephra layers in small Scottish lakes and identified catchment size and the number of stream inlets as having a significant impact on the within-basin concentrations and locations of microscopic tephra layers.

Alongside physical redistribution and reworking, there is evidence that tephra might be subject to chemical attack in some depositional environments. Tephrochronology is dependent on matching the geochemistry of a cryptotephra with a well dated tephra. However, distal tephra layers recorded in lake and especially peat sediments have potentially been subject to extended periods of exposure to low pH (bogs are typically < pH 4: (Holden *et al*., 2004)) and microbial activity. Distal tephra layers are especially vulnerable to geochemical attack given their large surface area (Pollard *et al*., 2003). At low pH conditions rhyolitic tephras, which contain more silica, appear to be more stable than basaltic tephras (Pollard *et al*., 2003; Wolff-Boenisch *et al*., 2004). There is some visual evidence for damage to tephra shards in peatlands (Hodder *et al*. (1991), examination of tephra shards in a range of depositional environments in Iceland and Scotland has indicated that the chemical integrity of shards is maintained for at least 4000 years (Dugmore *et al*., 1992). However, the rate of chemical attack is governed by temperature (Wolff-Boenisch *et al*., 2004), research into the preservation of tephra shards in warm tropical environments, where lab based experiments suggest the rate of chemical attack will be highest, may offer observational evidence to build on previous lab based experiments (Thesis Objective 2).

In this section I have discussed previous research on tephra reworking and redistribution in lakes and peatlands. Although there have been a number of studies which look at lakes and peatlands in isolation, there have been no studies which look at the tephrostratigraphy in a lake and peatland which are proximal to one another and therefore would have been expected to receive the same air fall tephras and to record the same tephrostratigraphy. A study of this type would allow for the assessment of whether peatland or lake sites contain the most complete tephrostratigraphy (Thesis Objective 3).

2.6 Methods

In this section we critically examine the methods used to detect, extract and geochemically analyse cryptotephra layers in lake sediments and peat as these are the two terrestrial environments which form the focus of this thesis. Samples are usually extracted from peatlands and lakes as sediment/peat cores. Coring protocols for peatlands are reviewed by De Vleeschouwer *et al*. (2011). The limitations of extracting single cores to represent tephra fallout from peatland and lake sites has been discussed previously (Section 2.5)

2.6.1 Detection/ Extraction

Various methods have been developed in order to determine the presence and/or geochemistry of cryptotephra in peat and lake sediments. Some methods of detection are destructive, leading to the loss of the peat or sediment matrix, while others are non-destructive and allow for the detection of tephra layers 'in-situ'. The tephra identification process is typically conducted in two phases:

1) Initial scans: Contiguous samples are extracted along the length of a core and tephra shards are counted under a high power microscope to identify the depth of peak tephra shard concentration. Typically the number of shards is reported per cm^3 of substrate (Gehrels *et al*., 2008). Shards can be characterised based on morphology and colour during the microscopy process (Heiken, 1972; Schmid, 1981). This step is often conducted at a coarse resolution (5-10 cm continuous samples) and then core depths found to contain tephra are re-sampled at a finer resolution (typically 1 cm) (Swindles *et al*., 2010).
2) Geochemical analysis: New samples are extracted from the core at the depths containing the peak in tephra shard concentration. These samples are subject to geochemical analysis.

2.6.1.1 The 'quick burn' method

The most established method for conducting initial scans on peat samples is the "quick burn method" (Hall and Pilcher, 2002). Samples are ashed in a furnace at 600°C before being washed in 10% HCl to remove carbonates (Pilcher and Hall, 1992). Where diatoms or quartz (SiO_2) are present- additional treatment with dilute sodium hydroxide (NaOH) may be required; this is particularly common for lake sediments (Hall and Pilcher, 2002). Samples are then mounted onto slides and shards are counted at 100-400x magnification (Swindles *et al*., 2010). Tephra shards extracted using this method are not suitable for geochemical analysis as chemical alteration of alkalis occurs at temperatures in excess of 350°C (Dugmore *et al*., 1995).

2.6.1.2 Density separation

Density separation using heavy liquids was originally developed for lake samples. This method is particularly valuable for samples which contain large amounts of mineral material or biogenic silica (Lowe and Turney, 1997; Turney, 1998). Density separation for initial identification can be conducted as an additional step to the 'quick burn method' following the ashing and HCl treatment steps thus avoiding the use of NaOH, which has been shown to reduce the shard count numbers for rhyolitic tephra (Blockley *et al*., 2005). Density separation (without ashing) can also be used to extract samples for geochemical analysis and is discussed further below.

2.6.1.3 Extraction for geochemistry: acid digestion and density separation

There are two main methods of extraction for tephra suitable for geochemical analysis: acid digestion and density separation. Acid digestion is the most established method (Lawson *et al*., 2012). Samples are subject to treatment with concentrated HNO_3 and H_2SO_4 to digest the peat substrate before washing through a fine Teflon sieve (typically between 6-10 µm) and rinsing thoroughly with water to remove any remaining acid (Dugmore *et al*., 1992; Hall and Pilcher, 2002). Samples containing biogenic silica may require further washing with dilute NaOH (Rose *et al*., 1996).

There is experimental evidence that exposure to acids and especially alkalis can result in the leaching of cations from the surface of the tephra shards (Blockley *et al*., 2005). However, there is some debate as to whether tephra geochemistry is altered significantly during acid extraction, especially when alkali treatment, which has been shown to be more damaging, is not necessary (e.g. in ombrotrophic peatlands). Roland *et al*. (2015) identify no difference in the major element geochemistry of rhyolitic tephra extracted using density separation and acid extraction. The majority of data in geochemical databases (e.g. Tephrabase) has been obtained from shards extracted by acid digestion.

Density separation offers an alternative to acid digestion for the extraction of tephra from the surrounding substrate and was advocated by Blockley *et al*. (2005) following their critique of the acid digestion method. Density separation involves using a medium of controlled density, usually a solution of sodium polytungstate (aka SPT and with chemical formula $Na_6[H_2W_{12}O_{40}]$). Various contaminants are removed in a stepwise process by varying the specific gravity of the liquid. Although density separation is often necessary for samples containing biogenic silica or mineral material, the process is time consuming and care must be taken to monitor the density of float to avoid shard loss. Basaltic shards do not always float at the commonly used recovery float density of 2.5 g cm^{-3} and are often only detected through magnetic separation (Davies *et al*., 2001; Mackie *et al*., 2002). Furthermore, the process of density separation can be challenging when working on organic-rich samples (e.g. peat) where shards become trapped in organic material, and extra steps must be applied to prevent the loss of shards in cleaning floats (Pyne-O'Donnell *et al*., 2012).

2.6.1.4 Non-destructive tephra detection methods

A number of tephra identification (and geochemical analysis) methods which do not destroy the peat or lake sediment have been developed. Methods include: X-ray fluorescence; magnetic susceptibility; X-ray photography; and spectrophotometry.

Although non-destructive methods provide continuous data without the need to damage the matrix, they work best on visible tephras where layers are more dense. These methods are, however, not always reliable when detecting cryptotephra layers (Gehrels *et al*., 2008). For example, X-ray fluorescence does not detect tephra layers with low shard concentrations (<850 shards cm^{-3}) and has difficulty detecting lighter elements

such as silica, a major component of felsic tephras (Kylander *et al*., 2012). Similarly, magnetic susceptibility is only sensitive to ferromagnetic materials, which do not represent a major constituent of felsic (rhyolitic) tephra shards (McCanta *et al*., 2015). Combining a number of different tephra detection methods (e.g. magnetic susceptibility, visible to short wave infrared spectroscopy (VSWIR) and XRF core scanning or reflectance and luminescence) increases the possibility of detecting cryptotephra layers. However, this is expensive and time consuming and necessitates access to multiple pieces of equipment (Caseldine *et al*., 1999; McCanta *et al*., 2015). More recently, hyperspectral imaging has shown promise in detecting macro- and potentially cryptotephra layers, although the analysis of cores for cryptotephra layers was not compared to an analysis conducted by traditional methods, so it is difficult to assess whether all cryptotephra layers were detected by hyperspectral imagining (Aymerich *et al*., 2016). Due to inconsistencies in these different methods and the need for access to equipment, at present the majority of cryptotephra studies utilise the destructive detection methods outlined in sections 2.6.1.1 and 2.6.1.2.

2.6.2 Major elements

Electron Probe Micro-Analysis (EPMA) is the most widely used procedure for determining the major element geochemistry of cryptotephra glass shards. There are two types of EPMA analysis: Wavelength Dispersive Spectroscopy (WDS) and Energy Dispersive Spectroscopy (EDS). EDS allows the analysis of exceptionally small grains present in low concentrations, such as those found in ice cores. However, due to limited use of standards and potential influence of grain morphology, EDS is semi-quantitative and thus not widely used (Haflidason *et al*., 2000).

The process of WDS involves firing an electron beam at the sample (an individual glass shard), which has been mounted in a hard-setting resin, exposed and polished (c.f. Dugmore *et al*., 1992; Hall and Hayward, 2014), and measuring the intensity and wavelength of resulting X-rays. The electron bombardment of each element results in the emission of a different X-ray wavelength. The abundance of each element is related to the intensity of the resulting X-ray (Hunt and Hill, 1996). The EPMA contains crystals of precisely known composition which are used for internal calibrations

allowing for the quantification of X-rays emitted from unknown samples. ZAF, PAP or X-PHI algorithms are usually applied automatically by probe software to convert the intensity of the X-ray into the concentration for a given element (Merlet, 1994). Percentage abundances by mass (wt %) of around ten species (typically $FeO_{(total)}$, TiO_2, SiO_2, K_2O, Al_2O_3, Na_2O, CaO, MgO and MnO) are determined by the analysis (Lowe, 2011).

EPMA offers the ability to analyse small shards (beam sizes down to 3 µm), a necessity for cryptotephra work where shard sizes are commonly <100 µm (Hunt and Hill, 2001). Although there is no universally agreed standard for the number of shards to be analysed from one tephra layer, typically around 15 shards is considered a suitable minimum (Lowe, 2011; Shane, 2000; Swindles *et al*., 2010). Where layers are particularly sparse an analysis based on fewer shards may be necessary, although larger sample sizes are preferable to help reduce the impact of heterogeneity due to chemical variation of the magmas during the eruption, hydration, and shard surface roughness (Hunt and Hill, 2001)

Alkali migration (loss of mobile elements presumably deeper into the material during exposure to the electron beam) can lead to certain chemical species being under or over represented in the % total oxides (Haflidason *et al*., 2000; Nielsen and Sigurdsson, 1981). Alkali migration is related to the intensity, duration and diameter of the electron beam. Altering the focus of the beam or 'rastering' to beam coverage of 10-20 µm reduces the intensity of the bombardment and thus alkali migration (Hunt and Hill, 2001). However, wider beams, which cover a larger area of the sample provide less precise analysis (Coulter *et al*., 2010) and are not practical for smaller vesicular shards. Hayward (2012) proposed and tested an analysis set up using low beam currents for alkalis (<0.1 nA/ μm^2) to minimise Na mobilisation while using a beam size as small as 3 µm. The beam current is then increased to analyse the remaining elements. This method avoids the need for corrections post analysis and requires no hardware or software modification.

It should also be noted that following EPMA the analytical total is nearly always below 100%. This can be a result of the inability of the probe to detect hydrogen and thus water dissolved in the glass (Hunt and Hill, 1993). The range of H_2O contents for felsic

glasses can reach 5-6% (Wallace, 2005). Tephras can become hydrated during the eruption, if magmatic water is not sufficiently outgassed from the magma before an eruption, or in the post-depositional environment (Pearce *et al*., 2004; Pollard *et al*., 2006; Shane, 2000). Although the level at which an EPMA analysis is accepted is debated, generally sums of all oxides in excess of 95% are considered acceptable (Pearce *et al*., 2007; Swindles *et al*., 2010).

2.6.3 Trace elements

The major element composition of magma (and thus tephra) can be similar for different eruptions, especially those from the same volcanic system. This can lead to false correlation and incorrect stratigraphy (Pearce *et al*., 2007; Tomlinson *et al*., 2012). Trace elements are present in minute amounts in the glass samples. Trace elements can enable the user to distinguish between magmas of similar major element composition, particularly useful trace elements in tephrochronology include: Rb, Sr, Zr and Nb (Lowe, 2011). Trace elements differ from major elements in that they are controlled not only by the major magma evolution processes (such as fractional crystallization), but also by details in the composition of the source region of each individual eruption. Therefore some magmas with a similar major elemental composition can contain differences in trace elemental composition (Allan *et al*., 2008). Processes such as fractional crystallisation can alter the trace elemental composition of magma so that even magmas with highly similar major element compositions may be distinguished through the application of trace element analysis (Allan *et al*., 2008).

Analysis of trace elements is a relatively new development in distal tephrochronology. Only in the past 15 years have instruments been developed with the capacity to analyse shards in the distal tephra size range (Pearce *et al*., 2011). Developments in hardware are increasingly enabling the analysis of smaller shards. Analysis of shards with beam diameters of between 10-20 μm using Laser Ablation Inductively Coupled Plasma Mass Spectrometry (LA-ICP-MS) is now possible (Pearce *et al*., 2007; Tomlinson *et al*., 2010). Fractionation effects caused by the formation of a thin melt film increase with decreasing beam diameters (Pearce *et al*., 2011).

An alternative technique for the analysis of the trace elemental composition of glass shards is secondary ion mass spectrometry (SIMS) analysis. Although more expensive, slower, and less widely available than LA-ICP-MS (Pearce *et al*., 2011), rather than ablation, SIMS uses 'sputtering' to remove sample material. The process of sputtering is less damaging to small and thin shards (5-10 μm) which are too small or thin to undergo analysis using LA-ICP-MS (Lowe, 2011).

The utility of trace elements to provide information which would allow two tephras with similar major element glass geochemistry to be distinguished has been questioned as the substitution of major elements for trace elements can follow systematic pathways (Pollard *et al*., 2006). However, trace elements have been successfully employed to discriminate between eruptions of similar major elemental composition such as those from the Yellowstone Caldera tephras (Pearce *et al*., 2008) and Mexican tephras (Luhr *et al*., 2010). Despite the promise of trace elemental analysis, there is little work on the trace elements of Holocene Icelandic tephras, the majority of which can be distinguished based on major element glass geochemistry. As a result there is a lack of trace element comparison data from dated eruptions (Hall and Pilcher, 2002).

Further work on the trace elemental composition might allow cryptotephra layers containing glass shards with a very similar major elemental composition e.g. those from Hekla 1947 and Hekla 1510 to be differentiated based on geochemistry. However, the value of trace elemental analysis is limited for distal Icelandic Holocene cryptotephra layers in northern Europe, the majority of which can be distinguished based on the analysis of major elements.

2.6.4 Statistical analysis of tephra geochemistry

The standard method for comparing the geochemistry of a known and unknown tephra is through the use of bi-plots/tri-plots of major elements. Bi-variate oxide plots such as FeO vs.TiO_2 and TAS plots (SiO_2 vs Na_2O+K_2O) allow for an informed but ultimately subjective decision on the similarity of a known and unknown tephra (Charman and Grattan, 1999; Stokes *et al*., 1992). Another simple means of assessing the similarity between two sets of geochemical data is the use of similarity coefficients and the coefficient of variation (Froggatt, 1992).

Although these numerical manipulations can allow for a more informed decision on the similarity of two sets of data, the decision to attribute an unknown tephra to a source eruption is still ultimately subjective (Stokes *et al*., 1992). Similarity coefficient (SC) analysis will produce a 'score' of similarity, whereby a score of 1.00 indicates that two samples are identical across all elements (Lowe, 2011). However, the point at which two samples are considered to be 'dissimilar' is debated with cut off points varying from 0.92 (e.g. Froggatt, 1992) to 0.96 (Lowe, 2011). As with the use of bi-plots, the number of elements included in coefficients of variation (CV) and similarity coefficients can affect the outcome (Charman and Grattan, 1999). No consensus exists on the best combination of element oxide concentrations for these analyses (Lowe, 2011).

Cluster analysis works by grouping entities which are similar. Although cluster analysis takes account of the entire dataset and can be more objective than SC and CV calculations (Froggatt, 1992), uncertainties are not always stated (Pouget *et al*., 2014b). One method of assessing the uncertainties associated with the clustering of objects is the use of bootstrap resampling (Suzuki and Shimodaira, 2006). This allows for a quantitative estimation of the error associated with any particular cluster and thus a decision can be made to accept only clusters which are statistically significant, removing some of the subjectivity of assignments. More recent developments in the statistical analysis of tephra data have centred on ordination. Both principal components analysis and discriminant analysis have been applied with some success to assess underlying trends in tephra geochemical data (Pouget *et al*., 2014a; Tryon *et al*., 2010).

2.6.5 Radiocarbon dating

Radiocarbon dating is the most common means by which a date is assigned to pre-historic cryptotephra layers. Therefore it is reviewed (only briefly) here, and in particular with reference to tephrochronology and the dating of cryptotephra layers. The expense and time involved in ^{14}C sample preparation and analysis necessitates the development of age-depth models, whereby a number of radiocarbon dates are dispersed within a profile and the ages between these points are inferred (Blaauw and Christen, 2005). Many age depth models for peat and lake sequences are based on the mid-point

ages of individually calibrated radiocarbon dates. Between midpoints interpolation, either linear, polynomial and/or spline interpolation (considering not only the two adjoining dates but also other information in order to obtain a smooth overall curve) is usually conducted (Bennett, 1994). Ages for cryptotephra layers derived from these traditional age-depth models may have large uncertainty depending on the spacing of ^{14}C dates above and below the tephra.

Wiggle-match dating can go some way to addressing the problems with traditional age-depth models, especially where they are confounded by plateau in the calibration curve. Wiggle-matching takes advantage of the 'wiggles' in the ^{14}C curve due to short term atmospheric ^{14}C fluctuations (Kilian *et al*., 1995). Therefore wiggle match dating is most effective where there are excursions in the ^{14}C curve and when many closely spaced ^{14}C measurements are available (Blaauw *et al*., 2003). All wiggle-matching variations consider un-calibrated radiocarbon dates (Blaauw *et al*., 2003). Using a Monte Carlo process, the depth (or age) axis is then stretched or compressed in order to align best with the ^{14}C calibration curve (Blaauw *et al*., 2004). Developments on these models have drawn upon Bayes theorem. By incorporating information from past evidence e.g. accumulation rates (not the radiocarbon data) (the *prior*) with the information from our radiocarbon data (the *likelihood*) we can assess the probability of a particular set of parameters (the *posterior*) (Blaauw and Christen, 2011; Ramsey, 2009). Given the errors associated with radiocarbon measurements, and the non-monotonic nature of the ^{14}C calibration curve, it is possible that models whereby age does not increase with depth could be computed. Incorporating information about accumulation rate (the prior) allows for the dismissal of age-depth models which appear to be ecologically unlikely, thus reducing the model uncertainty (Blaauw and Christen, 2011).

2.6.5.1 Examples of wiggle-matching in tephra studies

Wiggle-match dating has been used to refine the accuracy of dating for the Hekla 4 eruption in distal peat records. Although radiocarbon dated samples were precise (replicated across laboratories), assigning a calendar date was made difficult by a hiatus at this time in the radiocarbon calibration curve. Using wiggle-match techniques Pilcher *et al*. (1995) refined the date of the Hekla 4 eruption from 4230-4450 BP to 4260 +/- 10

BP. Similar research has refined the dates of the first millennium BC tephras in Ireland (Plunkett *et al*., 2004) and the Glen Garry tephra in Scotland (Barber *et al*., 2008).

2.7 Conclusion

In this chapter, I have reviewed the use of cryptotephra layers, not only for tephrochronology but with a focus on their usefulness as records of volcanic ash cloud events. I have also reviewed methods relevant to cryptotephra research.

Our increasing economic and social dependence on aviation makes understanding the threat from volcanic ash cloud events desirable, around the world and in the congested airspace of northern Europe. There are a number of questions which remain, surrounding the use of tephra layers as records of volcanic ash fall events, these include:

1) How robust is tephrochronology in terrestrial environments?
    i. There is currently a lack of cryptotephra studies in tropical peatlands. Further research is required as to whether cryptotephra studies in tropical peatlands can offer opportunities to further understand past volcanic ash clouds and the potential impacts of these events (Section 2.2).
    ii. There is experimental and (limited) field evidence for the remobilisation and reworking of tephra in both peatlands and lakes. These findings have led to calls for multiple core studies and concerns about the ‘patchiness’ of cryptotephra records (Section 2.5). However, there has been no comprehensive study of naturally deposited tephra layers across multiple cores from the same site.
    iii. Despite research which suggests that tephra layers in lakes and peatlands are subject to different preservation conditions and processes of reworking, there has been no comprehensive study looking at peatland and lake sites in close proximity. Such a study might identify whether peatlands or lakes preserve the most detailed tephrostratigraphy. Furthermore, despite experimental and visual evidence for tephra geochemical damage in peatlands a study comparing the geochemistry of the same tephra in different environments has not been conducted (Section 2.5).

Although cryptotephra layers are commonly used as dating isochrons, the use of cryptotephras as records of volcanic ash cloud fallout is relatively new and therefore very little literature is available. There are also a number of spatial and temporal gaps in northern European tephra records. Spatial gaps in northern European tephra records may reflect the true margins of Icelandic ash cloud distribution in northern Europe, or may be an artefact of bias in regional research focus. Examining sites in these spatial and temporal gaps, may confirm the extent of cryptotephra deposits from Iceland, or lead to the development of new tephrostratigraphies possibly extending the known distribution of existing cryptotephra layers, and leading to the discovery of cryptotephra layers representing ash clouds from eruptions which were not previously identified in northern Europe.

2) Can distal cryptotephra records be used to support proximal records of volcanism
    i. The frequency of Icelandic volcanism increased at the end of the last glacial period due to the unloading of ice from the lithosphere (Section 2.2.1.2). However, there has been no research into the potential impact of smaller magnitude changes in surface loading (ice mass), such as those which have occurred during the Holocene, on the frequency of volcanic eruptions. One problem with examining past records of eruption frequency is that the proximal geological record can be confounded by the erosion of deposits by subsequent events. No previous research has utilised both distal records of ash clouds and proximal records of Icelandic volcanism to examine eruption frequency.

3) Can cryptotephra shard size inform our understanding of past volcanic events?
    i. There is a need for a comprehensive analysis of cryptotephra shard sizes from multiple sites across northern Europe. Information on the shard size of cryptotephras is of interest to atmospheric modellers, satellite monitoring specialists and tephrochronologists (Section 2.4.2). Current research on cryptotephra shard size is based on the analysis of a small number of shards from a handful of sites across northern Europe.

Chapter 3: Spatial variability of tephra and carbon accumulation in a Holocene peatland

Watson, E.J.*[1], Swindles, G.T.[1], Lawson, I.T.[2], Savov, I.P.[3]

[1]School of Geography, University of Leeds, Leeds, LS2 9JT, UK
[2]Department of Geography and Sustainable Development, University of St Andrews, St Andrews, KY16 9AL, UK
[3]School of Earth and Environment, University of Leeds, Leeds, LS2 9JT, UK
**Corresponding author: Elizabeth Watson (gy08ejw@leeds.ac.uk)*
Manuscript for: Quaternary Science Reviews

Keywords: Tephrostratigraphy, Volcanic ash, Peatlands, Geochronology, Spheroidal Carbonaceous Particles, Ireland

Abstract

Microscopic tephra layers (‘cryptotephras’) represent important age-equivalent stratigraphic markers utilised in many palaeoenvironmental reconstructions. When used in conjunction with proximal records of volcanic activity they can also provide information about volcanic ash cloud fallout and frequency. However, the spatial distributions of tephra layers can be discontinuous even within the same region. Understanding the deposition and post-depositional redistribution of tephra is vital if we are to use cryptotephras as records of ash cloud occurrence and chronostratigraphic markers. The discrete nature of tephra layers also allows for detailed study into processes of deposition and reworking which affect many palaeoenvironmental proxy records.

We undertook a multi-core study in order to examine the historical tephrostratigraphy of a raised peatland in Northern Ireland. Three tephra layers originating from Iceland (Hekla 1947, Hekla 1845 and Hekla 1510) are present in 14 of the 15 cores analysed. This suggests that in areas not influenced by snowfall or anthropogenic disturbance at the time of tephra delivery, the presence or absence of a tephra layer is generally consistent across a peatland of this type. However, tephra shard counts (per unit area) vary by an order of magnitude between cores. These intra-site differences may confound the interpretation of shard counts from single cores as records of regional ash

cloud mass/density. Bootstrap resampling analysis suggests that total shard counts from multiple cores are required in order to make a reliable estimate of median shard counts for a site. The presence of three historical tephras in 14 cores enables a spatio-temporal analysis of the long-term apparent rate of carbon accumulation (LARCA) in the peatland. Substantial spatial and temporal variations in LARCA are identified over the last ~450 years. This high variability needs to be taken into account when designing studies of peatland carbon accumulation.

Highlights

- Three tephra layers were detected in 14 out of 15 cores from the same peatland
- Tephra shard counts (per unit area) varied by an order of magnitude between cores
- Several cores are required to reliably estimate the shard concentrations at a given site
- Tephra shard counts differed significantly between the three ash fallout events
- Carbon accumulation rates within the peatland varied spatially and temporally

3.1 Introduction

Tephra layers preserved in European peatlands provide both a valuable geochronological tool (e.g. Davies, 2015; Dugmore *et al*., 1995; Lane *et al*., 2013) and a record of past volcanic activity and ash dispersal events (Swindles *et al*., 2011b). Tephra deposited onto a peat surface far from the volcanic source is typically fine-grained (<125 μm in size) and accordingly called 'cryptotephra'. It is mostly considered to be primary air fall material (Davies *et al*., 2007; *contra* Swindles *et al*., 2013a) and is not thought to be subject to the vigorous reworking processes in the water column and/or the soft sediment which may distort tephra records in lacustrine and marine sediments (Davies *et al*., 2007; Griggs *et al*., 2014; Pyne-O'Donnell, 2011). Although tephra layers in peatlands can occasionally span a depth of a few centimetres, the peak is most often confined to a narrow horizon in thickness (Swindles and Plunkett, 2011). These factors suggest that peatlands should act as an excellent archive of past volcanic ash fallout, and that peat records can be used to map the spatial distribution of past fallout events on a continental scale (Swindles *et al*., 2011; Lawson *et al*., 2012).

One major issue with this approach is that cryptotephra layers in peatlands can be discontinuous even over small distances (hundreds of metres to kilometres: (Bergman *et al*., 2004; Langdon and Barber, 2004)), which requires an explanation. At a regional scale some spatial variation in tephra horizons can be attributed to fluctuation of the volcanic plume heights during the eruption, wind speed and direction variability, atmospheric processes (e.g. clouds and ice) and precipitation (Fig. 1), which can influence ash cloud density (Schumann *et al*., 2011), alter ash cloud trajectory and in the case of rainfall, increase the fallout of particles (Mattsson and Vesanen, 1988). At a local scale, the interaction of wind and vegetation may produce localised airflow patterns which result in the uneven delivery of tephra to the ground surface (Boygle, 1999; Pouget *et al*., 2014).

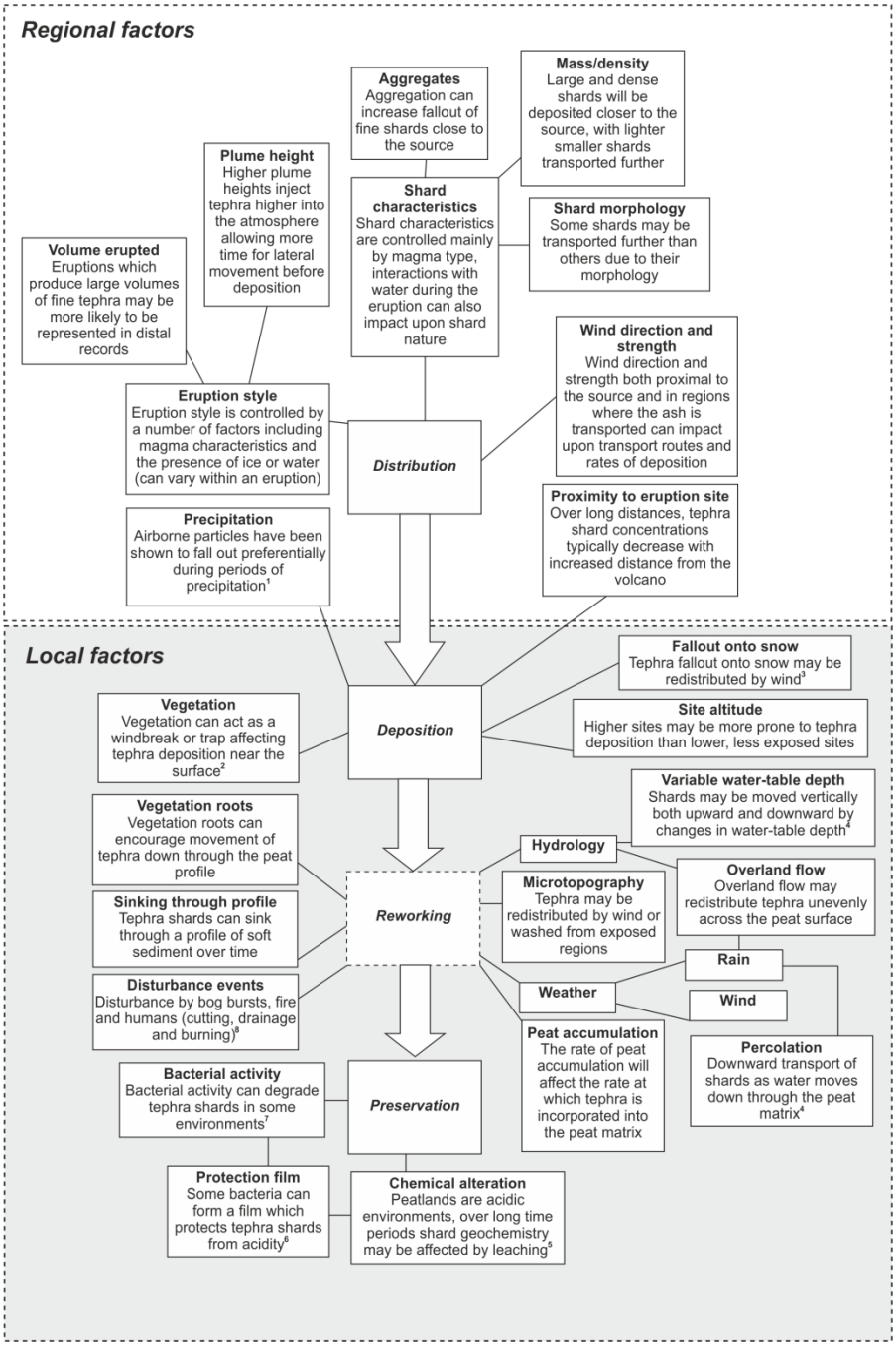

Fig. 1. Flow chart indicating the main factors which might be expected to (or have been shown to) have an effect on tephra distribution, deposition, reworking and preservation in peatland environments. This study will focus on the influence of local factors. Key references (1) Mattsson *et al*., 1988; (2) Pouget *et al*., 2014; (3) Bergman *et al*., 2004; (4) Payne and Gehrels, 2010; (5) Hodder *et al*., 1991; (6) Techer *et al*., 2001; (7) Thorseth *et al*., 1995; (8) Swindles *et al*., 2013a.

Even once the tephra has been deposited on the peat surface, the peat is unlikely to act as a straightforward, passive archive. Peatlands are complex ecosystems with dynamic topography, hydrological regimes, accumulation rate and vegetation composition (Swindles *et al*., 2012). Therefore peatland processes are likely to exert some control over the redistribution of tephra (and other paleoenvironmental proxies) both vertically and laterally, across the peatland surface (Fig. 1) – albeit probably to a lesser extent than in lacustrine or marine environments.

Previous studies of regional tephra occurrence have focused predominantly on single cores from different sites (Langdon and Barber, 2004). Inconsistent tephra records in two cores from Klocka bog, Sweden, suggest that tephra occurrence may vary at much smaller scales. In this instance tephra fell onto a prolonged snowpack (ca. 7 months) and was subsequently re-dispersed by wind and meltwater, leading to intra-site variation (Bergman *et al*., 2004). The majority of Holocene European tephra studies have been carried out in mid-latitude peatlands (Lawson *et al*., 2012), which are less likely to have been affected by prolonged snow cover. A study of two cores from Fallahogy bog in Northern Ireland comparable to the study by Bergman *et al*. (2004) found much less within-site dissimilarity, raising the possibility that, where prolonged snow cover is rare, tephra stratigraphies may be more consistent (Rea *et al*., 2012).

Tephra shards are commonly counted in order to determine the depth of peak shard concentration in the vertical profile. Recently, these counts have been used to infer ash cloud fallout over a region (Rea *et al*., 2012). Understanding the spatial variation in tephra shard concentrations in peatlands is important if it is to be assumed that they represent a record of ash density during an eruption event (Davies *et al*., 2010). The assumption that reworking has a negligible impact on total tephra shard counts within a given layer, and therefore that tephra shard counts represent a record of ash cloud density, is fundamental when attempting to use counts from one core per site to compare ash cloud fallout across many sites in a region (e.g. Langdon and Barber, 2004; Rea *et al*., 2012).

The main aim of this study is to assess the spatial variability in the total number of tephra shards relating to a given eruption and carbon accumulation across multiple cores from one site and to consider the implications for the interpretation of results from single core studies.

3.1.1 Tephra preservation in peatlands

Much of our current understanding of tephra preservation in peatlands is based on experimental evidence rather than detailed study of naturally-deposited tephra. Laboratory and artificial field experiments indicate that although the majority of tephra shards remain at the palaeo-surface during incorporation into the peat matrix, some migrate vertically (both upward and downward) (Payne and Gehrels, 2010; Payne *et al*., 2005). This would support the common assumption that the peak in tephra shard concentrations, rather than the first occurrence of shards, coincides with the timing of the ash fall event.

Shards are also likely to move laterally across a peatland on a variety of scales. Tephra shards may be deposited differently and/or moved to such an extent that the number of shards in some areas of the peatland becomes too low to be detected and analysed using current methods (Payne and Gehrels, 2010). Our understanding of cryptotephra redistribution on peatlands extends only to the lateral movement of tephra by wind at microtopographical scales. Experiments suggest that only a small proportion of tephra is transported over the short distance (<3 m) from hummock to hollow (Payne and Gehrels, 2010). There is evidence that tephra may move at even smaller scales (a few centimetres or less). Simulated rainfall onto thin (1 mm) tephra layers has been shown to generate patches of high and low tephra concentration across a peat surface (Payne and Gehrels, 2010). These experiments suggest that reworking does occur at small scales, but they do not address the possibility of tephra shard movement at larger scales (metres, to hundreds of metres).

Although these studies offer valuable information on the reworking on tephra in peatlands, they are experimental and represent both a simplification of reality and a compression of time. Evidence from naturally-deposited tephras which have been subject to peatland processes over a period of hundreds of years is needed to understand

the interaction and overall impact of these processes on tephra redistribution in 'real world' scenarios.

Research into the spatial variation of other palaeoenvironmental proxies found in peatlands, specifically pollen and charcoal, suggests that two or more cores taken in close proximity usually display the same general trends in reconstructions but show minor differences which might affect detailed interpretation (cf. Edwards, 1983; Innes *et al*., 2004; Lawson *et al*., 2005; Turner *et al*., 1989). The resolution of these studies is restricted by the dating methods available. In a more recent study, Blaauw and Mauquoy (2012) used wiggle-match radiocarbon dating, which offers a more precise chronological framework, and identified variation in arboreal pollen records from four cores across the same peatland over centennial timescales, although trends were more consistent over millennial timescales. Within-site variation in peatland proxy records over centennial timescales may limit the temporal resolution of palaeoenvironmental studies.

Unlike palaeoecological proxies, historical tephra layers are unique in representing a discrete depositional event rather than a continuous influx, allowing for easier identification of reworking processes (Housley *et al*., 2013). By improving our understanding of the deposition and redistribution of tephra layers, we will also gain insights into how other palaeoenvironmental proxies may be reworked as they enter the stratigraphic record (cf. Irwin, 1989; Turner *et al*., 1989).

3.1.2 Carbon storage in European peatlands

Peatlands represent an important global carbon store and as such the accumulation of carbon in peat has been the focus of large-scale studies (e.g. Charman *et al*., 2013; Turunen *et al*., 2004; van der Linden *et al*., 2014). Although regional climate is often the major control on carbon accumulation rates (Magnan and Garneau, 2014), internal peatland processes can also exert an influence. Spatial differences in carbon accumulation within a peatland could lead to unrepresentative estimates based on one core being extrapolated over a large area.

There has been only limited investigation into variation in long-term apparent rate of carbon accumulation (LARCA) within one peatland site, the majority of studies focusing on high-latitude peatlands (e.g. Belyea and Clymo, 2001; Ohlson and Økland, 1998; Turunen *et al*., 2004). For example, Turunen *et al*. (2004) identified spatial variation in carbon accumulation within Canadian peatlands dated using ^{210}Pb and ^{14}C: hummocks had significantly higher carbon accumulation rates than hollows over the last 150 years. However, the large uncertainty in radiometric age estimates, and their cost, is a limitation to this approach. Another line of research has used the 'pine method' of Ohlson and Dahlberg (1991) to estimate peat LARCA: young pine trees growing on a peatland are removed, their age is calculated by counting annual rings, and the original growing point (depth at which the stem meets the root) and the thickness of peat subsequently accumulated are determined. Peat LARCA estimated using this approach varied by a factor of five (over 125 years of peat growth) in 151 different cores from the same 20 m^2 area of a boreal bog (Ohlson and Økland, 1998). However, this technique can only be used on forested peatlands. The presence of three historical tephra layers at our study site (see below for description) offers the opportunity to examine spatial variation in carbon accumulation rates in a mid-latitude, unforested peatland within a secure chronological framework. The same approach could be applied at many other peatlands where there is a well-resolved cryptotephra record.

3.1.3 Hypotheses

Using data from 15 cores from an ombrotrophic bog, we tested the following null hypotheses:

- Tephra layers show no spatial variation within the peatland in terms of:
    - Presence/absence
    - Total shard counts relating to a given eruption (TSCs, defined as the total number of shards > 10 μm associated with each tephra layer in a column of peat with surface area 1 cm^2)
- Tephra layers from different eruptions recorded in the same peatland do not have significantly different TSCs.
- LARCA shows no spatial variation.

3.2 Study site

Fallahogy peatland is an ombrotrophic lowland raised bog located north of Portglenone, Northern Ireland (54. 912°N, 6.562°W). The peatland is located in the Lower Bann valley, a low-lying area with a mean annual rainfall of ~1000 mm (average from 1941 to 1970) (MetOffice, 1976). The main dome of the peatland is intact, although there has been a limited amount of cutting on the lagg. Plant communities range from *Sphagnum magellanicum* and *Sphagnum rubellum* dominated hollows, to hummocks dominated by Ericaceae and *Eriophorum* sp. The site has been the focus of several palaeoecological studies (e.g.Barber *et al*., 2000; Rea *et al*., 2012; Roland *et al*., 2014).

3.3 Methods

3.3.1 Field sampling

A Russian-type corer (Jowsey, 1966) with a 50 cm-long barrel was used to retrieve 15 short cores. Random sampling locations were selected using a random number generator, entered into a handheld GPS, and located in the field (Fig. 2). Samples were taken as close to the pre-selected point as possible (maximum 5 m distant), whilst accounting for the need to extract from areas of similar micro-topography; in this instance *Sphagnum* lawns were sampled (De Vleeschouwer *et al*., 2011).

To investigate movement of shards on a microtopographical scale three transects from hummock to hollow were investigated. Each transect was surveyed, the dominant vegetation was described and three 50 cm-long cores were extracted from different microtopographical zones. Only the FAL_1 tephra (later identified as Hekla 1947 tephra see section *4.3*) was investigated in these cores.

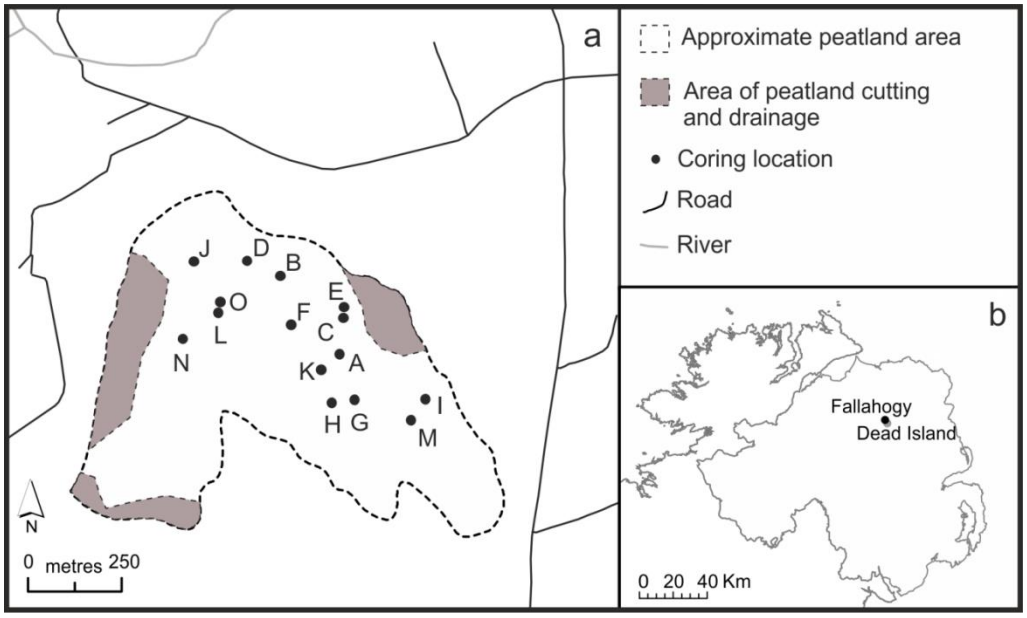

Fig. 2. Map indicating a) the location of the 15 core sampling sites in Fallahogy peatland b) the location of Fallahogy and Dead Island peatlands within Northern Ireland. Some evidence of peat cutting and drainage is evident around the edges of Fallahogy peatland as illustrated.

3.3.2 Tephra analysis

In the laboratory, samples were prepared using the 'quick burn' method (Pilcher and Hall, 1992; Swindles *et al*., 2011a). 1 cm^3 contiguous samples were ashed at 550°C and treated with 10% HCl. To aid shard identification, samples were gently sieved at 6 µm to remove finer silt and clay fractions, and the coarse fraction mounted onto slides. Absolute tephra counts (shards >10 µm cm^{-3}) were conducted at 200x magnification on a standard Leica binocular microscope. Spheroidal carbonaceous particles (SCPs) were counted in the tephra slides and are reported as counts cm^{-3}. Total shard counts (TSCs) for each tephra layer cm^{-2} (total deposition per square centimetre of peatland surface) were calculated by summing the absolute tephra counts for all the depth samples within that layer.

Samples for geochemical analysis were extracted from core A which showed three distinct peaks of tephra (Fig. 3). An additional sample was extracted from FAL_3 in core K in order to confirm the high accumulation rate which was later identified in this core (see section *4.9.1.*). Due to the abundance of roots in the top of the peat profile and low shard concentration in the second peak (14-15 cm), density separation following the

method of Blockley *et al*. (2005) was unsuccessful. Instead, extraction for geochemical analysis for all samples followed the acid digestion method (Dugmore *et al*., 1992). Samples were treated with hot conc. HNO_3 and H_2SO_4 acids, diluted with water and sieved at 10 µm. The coarse residue was rinsed thoroughly with clean water. There is experimental evidence that exposure to acidic and particularly alkaline treatments for the removal of diatoms can alter tephra geochemistry (Blockley *et al*., 2005). In this instance the risk of geochemical alteration was reduced as alkaline treatment was not necessary and acid treatment was short (<2 hours). Recent work has shown that rhyolitic shards extracted using the acid digestion method and then analysed using Electron probe micro analysis (EPMA) are geochemically indistinguishable from shards extracted using density separation (Roland *et al*., 2015). This suggests that chemical alteration during the acid digestion method is minor and unlikely to affect the assignment of a tephra to an eruption event.

Samples were mounted onto glass slides using EpoThin resin, ground to expose the shards (cf. Dugmore *et al*., 1992) and polished to a 0.25 µm finish. EPMA was conducted at the Tephra Analytical Unit, University of Edinburgh. All analyses were conducted with a beam diameter of 5 µm, 15 kV and beam currents of 2 nÅ (Na, Mg, Al, Si, K, Ca, Fe) or 80 nÅ (P, Ti, Mn) (Hayward, 2012). Secondary glass standards, basalt (BCR-2G) and rhyolite (Lipari) were analysed before and after EPMA runs of unknown glass shard analyses.

3.3.3 Carbon accumulation

It was assumed that the peak of each tephra layer represented the year of the eruption (cf. Payne and Gehrels, 2010). Bulk density was calculated on 1 cm^3 samples taken contiguously between the tephra peaks of layers which were subsequently identified as those from the eruptions of Hekla in 1510 and 1947 (see section *4.3*). Samples were oven dried at 105°C and dry weight was divided by volume to determine bulk density.

Carbon content was estimated using loss-on-ignition (LOI) which offers an approximation of organic matter content. The equation of Bol *et al*. (1999) was used to convert LOI into % Carbon. This equation was developed from UK moorland soils and has been successfully applied in studies of carbon content on blanket peatlands in the

UK (Garnett *et al*., 2001; Parry and Charman, 2013). Furthermore, % Carbon results obtained for Fallahogy using this equation were in line with typical organic carbon contents in northern peatlands (Charman *et al*., 2013). LARCA (g C m^{-2} y^{-1}) was calculated by dividing the cumulative carbon mass over a given period by the number of years (Clymo *et al*., 1998). Apparent total carbon accumulated (ATCA) was calculated as the sum of the total carbon accumulated in each 1 cm^3 interval between the peak shard concentrations of the FAL_1 and FAL_3 tephras.

3.3.4 Plant macrofossils

In order to reconstruct the microtopography at the coring location at the time of tephra deposition, plant macrofossil analysis was conducted on samples corresponding to peak tephra shard concentrations for the 1510 and 1947 eruptions of Hekla (see section *4.3*). Samples of c. 3 cm^3 of peat were sieved at 125 µm, floated in a petri-dish and examined at 10-50x magnification using a standard binocular microscope. Volume percentages were assigned using a modified version of the quadrat leaf count method of Barber *et al*. (1994). Moss leaves and epidermal tissues were picked and mounted onto slides for identification at higher magnification. *Sphagnum* was identified to section or species when possible.

3.3.5 Statistical methods

Cluster analysis with bootstrap resampling (Suzuki and Shimodaira, 2006) and PCA were applied, but did not help greatly to discriminate between the three tephras (supplementary file, Fig.S1, S2).

3.4 Results and Discussion

3.4.1 Stratigraphy

The tephrostratigraphic and SCP profiles for 15 cores (named A-O) are displayed in Fig. 3. Although there is some variation in the depth of the tephra layers, all but one of the cores contain three peaks in tephra abundance. The three tephra layers are more distinct in some cores than others. This is most likely due to differences in local accumulation rate and vegetation composition. In some instances the FAL_1 and FAL_2 tephras show a degree of merging toward the tails of their vertical distribution. This suggests that the time between these two events may represent the minimum temporal resolution of eruption events which can be recorded, at least in areas of this peatland where peat accumulation is slower.

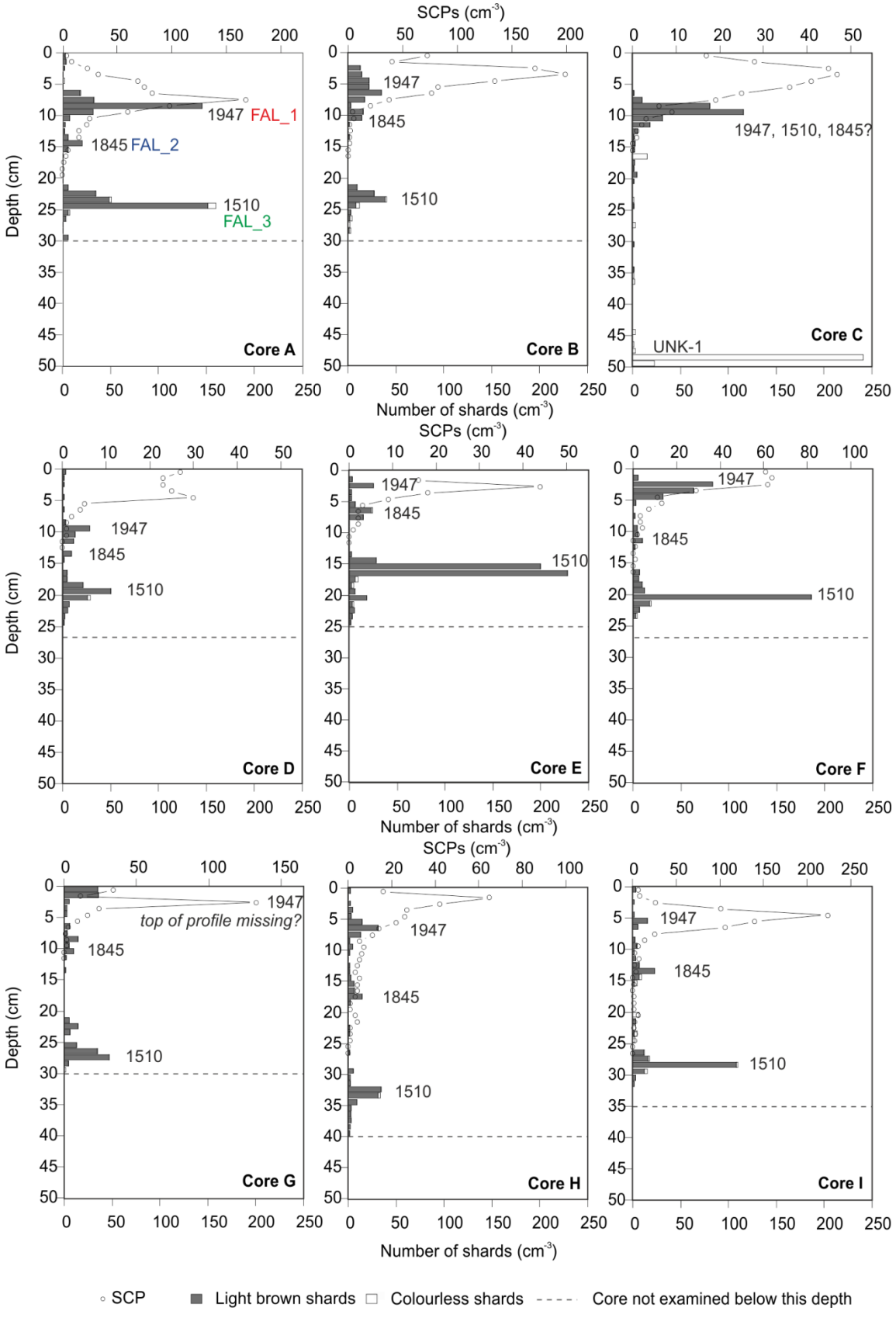
SCPs (cm-3)
Depth (cm)
Number of shards (cm-3)
1947
FAL_1
1845
FAL_2
1510
FAL_3
Core A
Core B
1947, 1510, 1845?
UNK-1
Core C
Core D
Core E
Core F
top of profile missing?
Core G
Core H
Core I
SCP
Light brown shards
Colourless shards
Core not examined below this depth

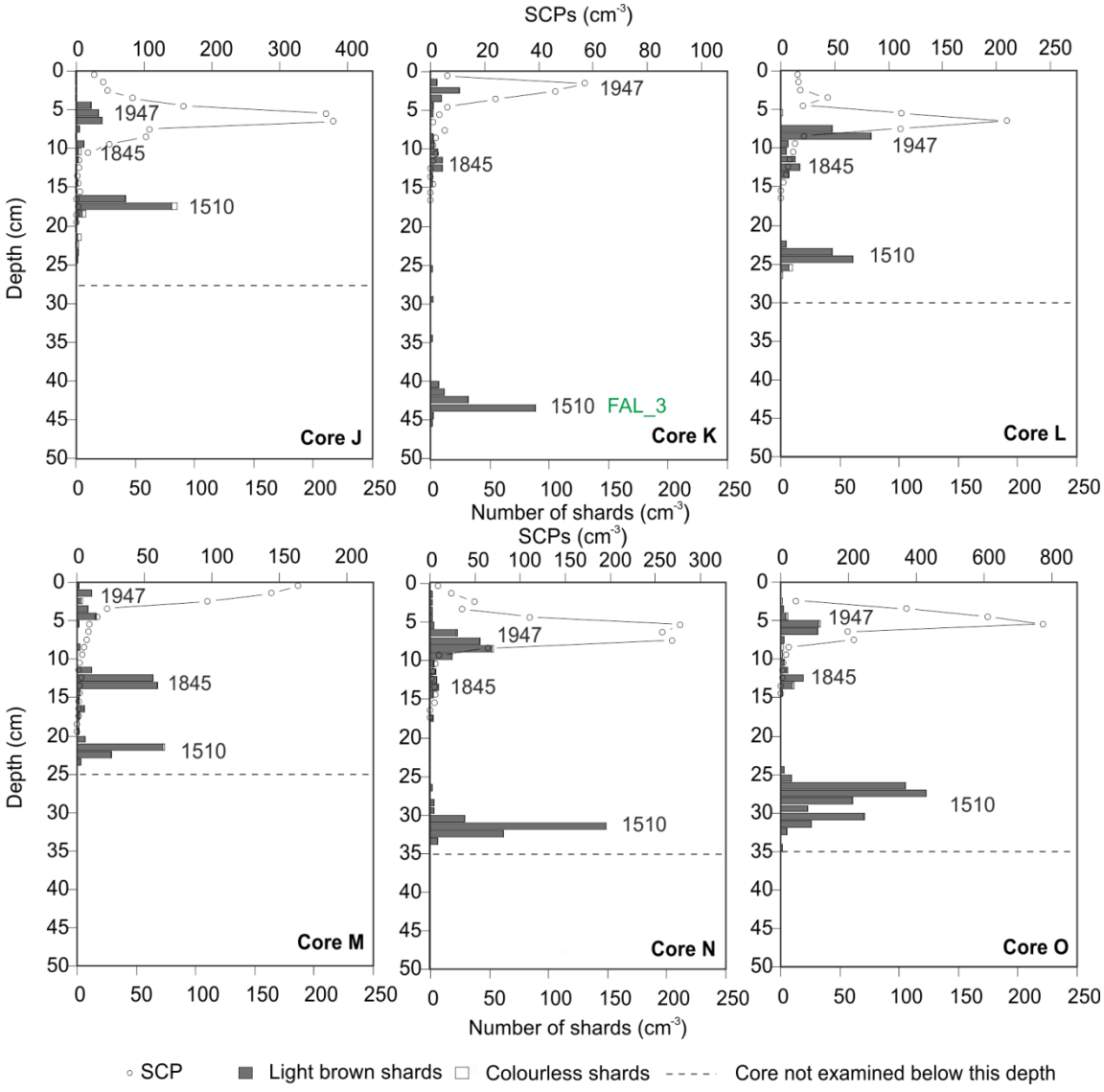

Fig. 3. (2 Panels) Diagrams showing tephrostratigraphy and Spheroidal Carbonaceous Particle (SCP) profiles for the 15 peat profiles. Note horizontal scales for SCP profiles vary. Labels indicating the source event (Hekla 1947, Hekla 1845 and Hekla 1510) have been placed next to peaks in tephra shard concentration. Core C contains a peak of colourless tephra shards which have not been geochemically analysed (UNK-1). Geochemical samples were obtained from tephra peaks in Cores A and K (labelled FAL_1, FAL_2 and FAL_3).

Some cores (D and G) show slight deviations from the majority of profiles. In core G, the top of the FAL_1 tephra peak was not recovered, and there is also a rise in SCPs in the uppermost sample indicating that the true SCP peak in this profile may be missing. Therefore we suggest that the top of core G is absent; this is taken into account in subsequent analyses.

Core D appears to have experienced a high rate of accumulation between FAL_1 and the present surface when compared to other cores. However, the assignment of the FAL_1 tephra is supported by its position in line with the rapid increase in SCPs c. 1950 and the FAL_1 and FAL_2 are separated by a sample containing no tephra shards. Plant macrofossil analysis indicates that core D may have been a pool or low hollow in the past. There is abundant *Menyanthes trifoliata* 'bog bean' epidermis corresponding with the FAL_3 tephra layer and Sphagnum section Cuspidata corresponding with the FAL_1 tephra. All cores were extracted from lawn microforms at the time of coring, therefore a transition between pool or low hollow and lawn microform appears to have occurred in this core between the FAL_1 tephra and the time of coring. The high accumulation rate post FAL_1 in this core might be attributed to a rapid increase in the rate of peat accumulation related to the temperature rise during the twentieth century.

Unlike the majority of cores, core C shows only two peaks in tephra shard concentration. Furthermore, the tephra in core C at a depth of 48-50 cm is distinct from those detected in other cores both in terms of colour and morphology. The anomalous tephrostratigraphy of core C might be attributed to a post-depositional disturbance in peat accumulation. Disturbance events, such as fire and bog bursts, can occur naturally (e.g. Caseldine and Gearey, 2005). However, core C is in close proximity to an area of drainage and peat extraction (Fig. 2). This is likely to be the cause of the anomaly in peat accumulation. For this reason core C was excluded from subsequent analyses.

3.4.2 Shard morphology

Shards from all three tephras are predominantly light brown and morphologically similar (Fig. 4). Shard size ranges from 15 to 155 μm indicating that relatively large shards can be transported long distances, particularly if shard terminal velocity is low due to a high degree of vesicularity (Stevenson *et al*., 2015).

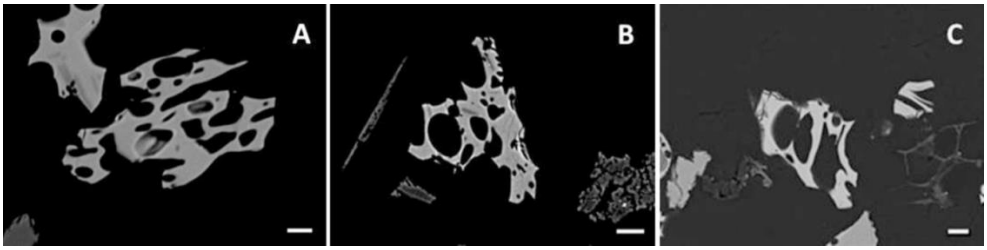

Fig. 4. Scanning electron microscope images of typical tephra shards exposed for geochemical analysis (a) Hekla 1510 (b) Hekla 1845 (c) Hekla 1947. White scale bars are 10 μm.

3.4.3 Shard geochemistry and assignment to eruptive event

The major element geochemistry of the three tephra layers detected at Fallahogy is similar. They have bimodal character and include a minor rhyolitic component, as well as dominance of the dacite-andesite composition (Fig. 5; full geochemical dataset is provided in the supplementary file, table S1). The geochemistries closely resemble those of tephra from the Hekla (H) eruptions in 1510 and 1947 (Dugmore *et al*., 1995; Hall and Pilcher, 2002; Larsen *et al*., 1999; Pilcher *et al*., 1996; Swindles, 2006). There is good evidence, supported by ^{14}C dating, as well as geochemistry, that the tephras of H1510 and H1947 reached the UK and have been found in many peatlands in Northern Ireland (Lawson *et al*., 2012). Distinguishing between FAL_1 and FAL_3 based on co-variation major element diagrams proved difficult (Fig. 6), although some discrimination can be observed between the geochemistry of FAL_2 and the other tephras (Fig. 6c, d). FAL_2 also has a generally higher TiO_2, FeO_t and P_2O_5 content than FAL_1 and FAL_3.

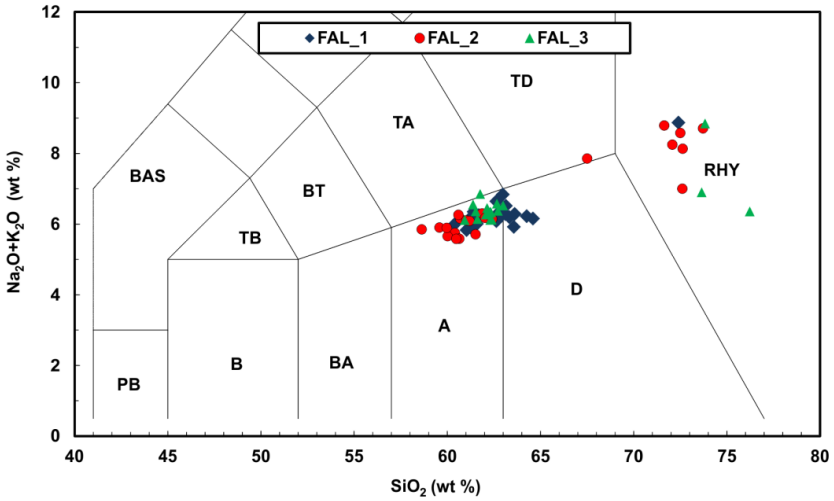

Fig. 5. Total Alkali Silica (TAS) Diagram showing the three tephras detected in core A at Fallahogy (raw data). Shards are mainly of andesitic-dacitic geochemistry. Annotations follow standard terminology e.g. RHY = Rhyolite, D = Dacite, A = Andesite (Le Maitre *et al*., 1989).

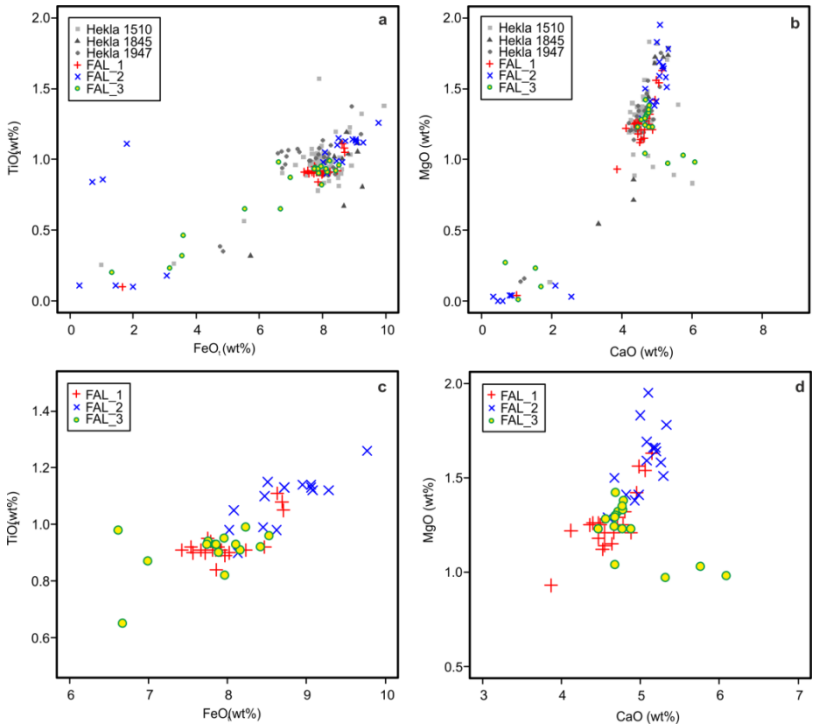

Fig. 6. Tephra geochemistry co-variation diagrams for (a-b) full range of FeO_t(wt%), TiO_2(wt%), CaO(wt%), MgO(wt%) values for the three tephra horizons in core A at Fallahogy plotted against type data for the Hekla eruptions of 1510, 1845 and 1947 from Tephrabase (Newton *et al*., 2007). (c-d) a restricted range of FeO_t(wt%), TiO_2(wt%), CaO(wt%), MgO(wt%) values for the three tephra horizons in core A at Fallahogy to show in more detail the overlap between the geochemical distributions, all values are normalised.

3.4.4 SCPs as a method of distinguishing between historically-deposited tephras

Where shards from different tephras are not easily distinguished by their geochemistry, in some instances SCP profiles can be used to complement geochemical data (Swindles and Roe, 2006). SCPs provide a chronological marker for the last ~150 years (Renberg and Wik, 1984), appearing in this region c. AD 1850 and reaching peak abundance AD 1978 ± 6 years (Rose and Appleby, 2005). The FAL_3 tephra occurs before SCPs appear in the profiles at Fallahogy suggesting a date prior to 1850. The increase in abundance of SCPs corresponding with the FAL_1 tephra in the majority of cores suggests a date around AD 1950. In the majority cores from Fallahogy, FAL_2 occurs just after the appearance of SCPs in the peat profile, suggesting a date around the time of the first appearance of SCPs in this region (c. 1850 AD).

Although SCP profiles offer further information for the dating on peat profiles, they must be interpreted with caution because SCPs are themselves subject to movement in the peat matrix. In some instances it appears that the peak in SCPs (AD 1978 ± 6 years) coincides with the peak in tephra concentration for the FAL_1 event. Given that there were no large eruptions of silicic tephra in Iceland in the 1970s or 1980s (Larsen *et al*., 1999) and given that no claims of cryptotephra layers in Irish peatlands later than Hekla 1947 tephra have ever been made in the literature, we infer that the apparent coincidence of the SCP and tephra peaks is an artefact of either: i) slow rates of peat accumulation between 1947 and c. 1978, or ii) the differential vertical movement of tephra and SCPs. Such differential movement might result from differences in the deposition (continuous vs. one event), morphology, density or size of SCPs and tephra.

3.4.5 Possible sources for FAL_2

Although FAL_2 has a slightly different major element geochemistry (e.g. slightly higher TiO_2 and FeO_t) to FAL_1 and FAL_3, it shows some similarity and therefore may be derived from the same volcanic system. Furthermore, the Hekla volcano has produced the majority of widespread mid to late Holocene cryptotephras, many of which are of a bi-modal composition. There were five recorded eruptions from Hekla between 1510 and 1947 which produced silicic tephra. Many eruptions produced low tephra volumes or had dominant fallout pathways toward the north of Iceland (Larsen *et*

al., 1999; Larsen *et al*., 2014). Apart from H1845 there is no solid documentary or geochemical evidence that any of these tephras reached northwest Europe. However, there is documentary evidence for the fallout of tephra on the Faroe Islands during AD 1845, suggesting that tephra from the H1845 eruption travelled some distance in a south-easterly direction (Connell, 1846). A report of tephra on the Orkney Islands, dated by interpolation to ca. AD 1800 and with a similar geochemistry to that of H1947 and H1510, has been tentatively linked to the eruption of H1845 (Wastegård, 2002). To further support assignment to H1845, FAL_2 was plotted against the major element geochemistry of all tephras dated to between 1510 and 1947 AD in the Tephrabase geochemical database (supplementary file, Fig. S3). There was no clear match with any of these tephras. We therefore correlate the FAL_2 tephra to the eruption of Hekla 1845.

It appears that H1845 may be an under-recognized tephra in N. Ireland. The shard count totals for this tephra at Fallahogy are generally low (<40 shards cm^{-3}). Low shard concentration and a similar geochemistry to other historical Hekla tephras may have prevented detection in some previous research, particularly in peatlands with lower accumulation rates where the tephra peaks for H1947 and H1845 may be challenging to distinguish. The H1845 tephra corresponds to, and provides a dating isochron for palaeoenvironmental studies concerned with the end of the Little Ice Age as well as the Irish famine of 1845-1849, which was a period of great hardship, economic and social importance in Irish history (O'Rourke, 1994).

Based on the SCP profiles, information about tephras previously identified in this region and geochemical data the tephra layers are assigned to the Hekla eruptions of 1947 (FAL_1), 1845 (FAL_2) and 1510 (FAL_3). We suggest that SCP stratigraphies may be valuable for distinguishing tephra shards from the eruption of H1845 (FAL_2) which occur at the beginning of the SCP profile in this region.

3.4.6 Do cryptotephra layers in peatlands reflect fallout concentrations?

3.4.6.1 Within-site variation

The same sequence of three tephras was found in 14 of the 15 cores at Fallahogy (Fig. 3). The presence of three peaks indicates three distinct historical ash fallout events. This suggests that in small, unforested, undisturbed peatlands like Fallahogy, where there is a low chance of snow cover at the time of tephra deposition, the presence or absence of tephra from a given eruption can be highly consistent from one core site to another. The extraction of almost any single core from an undisturbed area of the Fallahogy peatland would have been sufficient to determine the presence or absence of all three tephras. However, total shard counts for each tephra layer differ between the cores. The total number of shards for H1510 (total deposition per square centimetre of peatland surface) ranges from 97 to 508 shards cm^{-2} (median 143). Shard counts for H1947 and H1845 also show an order-of-magnitude variation in different cores, with counts of 21–236 cm^{-2} and 10–156 shards cm^{-2} respectively (Fig. 7). Some small variation in TSCs might be expected as a result of analytical uncertainty. However, differences of this magnitude between cores are most likely due to real spatial variation. A Mantel test of the null hypothesis that there is no spatial autocorrelation in the TSCs for the H1510 tephra indicated that, over scales of tens to hundreds of metres, there is no spatial autocorrelation in shard counts (p=0.82). This suggests that any systematic sorting of shards is predominantly occurring at smaller or larger scales. Variation in the total number of tephra shards relating to a given eruption across different cores in a peatland may plausibly be due to three sets of processes: i) uneven deposition from the atmosphere; ii) lateral movement of tephra over the surface of the peatland prior to its incorporation in the peat; iii) loss of tephra through processes such as hydrolysis and dissolution to different extents in different places.

Fig. 7. Maps showing the spatial distribution of cores alongside total shard counts (cm^{-2}) for Hekla 1510, 1845 and 1947 eruptions. Apparent total carbon accumulated between 1510 and 1947 is also shown. Circle sizes are proportional to total shard counts per unit area or apparent total carbon accumulated.

The latter appears unlikely, as although it has been suggested that tephra may dissolve in acidic environments, dissolution is slow, and based on the results of laboratory experiments, rhyolitic shards are predicted to survive for more than 4500 years at a pH of 4 (conversely, mafic tephras deteriorate more rapidly) (Wolff-Boenisch *et al*., 2004). The tephras detected at Fallahogy are of intermediate composition and have been deposited in the last 450 years, therefore although loss of shards due to dissolution cannot be ruled out, it is unlikely. No visible signs of damage to tephra (e.g. silica gel layer formation or pitting: cf. Blockley *et al*., 2005) were identified during microscope analysis.

Following deposition, any lateral transport of tephra is likely to occur relatively quickly because there is evidence that tephra is rapidly incorporated into the peat matrix. Experiments indicate that tephra deposited onto a peatland can percolate downward by up to 6 cm in less than 2 years (Payne *et al*., 2005). Even allowing for subsequent decomposition, long term peat accumulation at Fallahogy over the last c. 5000 years has been relatively rapid in comparison to northern peatlands in general (11 years cm^{-1};

(Roland *et al*., 2014)). Therefore tephra is likely to be incorporated into the peat more quickly than in peatlands where accumulation rates are lower, which is typically the case at higher latitudes. Variation in TSC across the peat surface at the peatland (macro) scale might be facilitated during periods when the water-table is at or above the surface, resulting in surface flow and therefore the transport of shards from higher to lower areas of the peatland by water, or by preferential deposition of tephra on areas of higher ground, where the dominance of relatively tall vascular plants might encourage interception of airborne shards. However, there is no correlation between the elevation of the core location (at time of coring) and the total number of shards for any of the three eruptions.

Similarly, there is no relationship between total shard count for the H1510 and H1845 tephras and distance from the edge of the peatland (Spearman's rank correlation (SRC) supplementary file, Table S2). However, for the most recent eruption (H1947) there is a weak relationship between TSC and distance from the edge of the peatland (SRC r = 0.65, p = 0.016). Shard counts are higher toward the centre of the peatland, suggesting that tephra was either preferentially deposited onto the cupola or preferentially lost from the rand slope.

Either a change in peatland topography or in the processes operating at the macro scale over time might explain why the most recent tephra layer shows a weak non-random pattern of distribution, whilst the earlier two tephras do not. There is no evidence at Fallahogy that the peatland topography at the macro-scale has changed substantially over the last 500 years. However, there is some evidence of a change in water-table depth. Fig. 8b shows the reconstructed water-table depth at Dead Island bog, just 1.2 km south of Fallahogy (Swindles *et al*., 2010). During the Little Ice Age (LIA, c. 1400 – 1850 AD), a period characterised by wet and cold conditions which has been identified across multiple sites in Europe (Blundell and Barber, 2005; De Vleeschouwer *et al*., 2009; Turner *et al*., 2014) and Ireland (Swindles *et al*., 2013b), the Dead Island Bog reconstruction suggests the water-table was at or above the peat surface (Swindles *et al*., 2010). Between 1845 and 1947 the water-table dropped considerably, which could have reduced the potential for redistribution of tephra from the middle of the peatland towards the edges by surface flow.

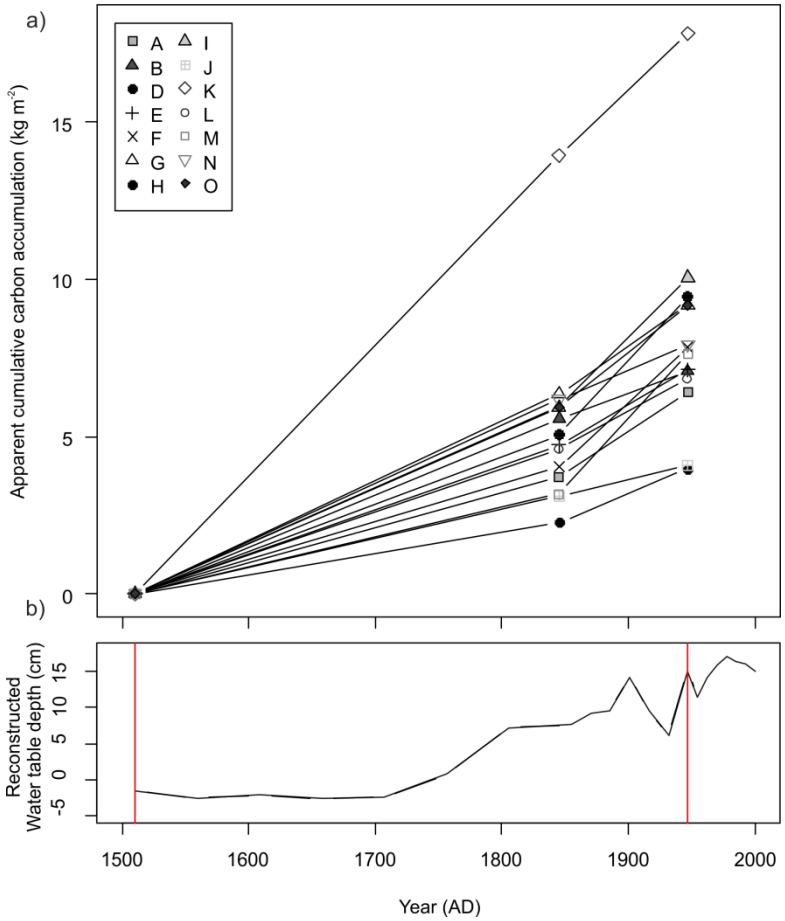

Fig. 8. (a) Graph showing the apparent cumulative carbon accumulation between AD 1510 and AD 1947 in 14 cores at Fallahogy. The peak shard concentrations for tephra from the eruptions of Hekla 1510, Hekla 1845 and Hekla 1947 are used as chronological tie points. (b) Water-table depth reconstruction data from Dead Island bog (~1.2km from Fallahogy) (Swindles *et al*., 2010) based on the transfer function of Charman *et al*., (2006). Red lines indicate tephra horizons identified in both sites and used as chronological tie points.

Given that systematic differences in the total shard count per unit area only appear for one tephra layer, evidence for movement of tephra at a macro scale is inconclusive. Our results also indicate that the movement of tephra shards over the peat surface is variable between events. There are no cores which consistently show higher or lower than average counts for each event. This may reflect the differences in water-table (at or below the peatland surface) during each tephra fall, or the complex interactions of different reworking processes under slightly different environmental conditions.

Hummock and hollow microforms are common on many peatlands. Fallahogy has a well-defined hummock, hollow and lawn microtopography (see section *2*). Hummocks

represent raised features where vascular vegetation types dominate and might therefore be expected to preferentially trap airborne particles; however, tephra might also be delivered to hollows during periods of surface water flow. Previous research into pollen concentrations across hummock and hollow microforms identified higher pollen concentrations in hollows (Irwin, 1989). However, the continuous deposition of pollen can make it difficult to decipher whether the differences in concentration are attributable to differential deposition, post-depositional redistribution or dissimilarities in accumulation rates.

All cores in this study were extracted from lawn microforms. However, peatland microforms have been shown to migrate or alter over time (Kettridge *et al*., 2012). A different microtopography at the coring location at the time of tephra deposition might explain the differences in shard counts. It was initially suggested that the cyclic regeneration of hollows into hummocks was self-regulating, driven by faster rates of peat accumulation in hollows (Osvald, 1923; Von Post, 1910). Following increasing evidence that hummocks are long-term features controlled mainly by changes in bog surface wetness, the theory of cyclic regeneration has largely been disregarded (Barber, 1981; Svensson, 1988; Walker and Walker, 1961). Hummocks are now considered long-term features linked to climate, rather than the product of autogenic peatland processes. However, there is no simple sequential or transitional relationship of hummock to hollow microforms with time (Ohlson and Økland, 1998).

Plant macrofossil analysis was conducted on the 14 randomly distributed cores at depths corresponding to the peak shard concentration in the FAL_1, FAL_2 and FAL_3 tephra layers to assess whether the microtopography at each coring location had changed significantly since the FAL_3 tephra layer. The results suggest that the majority of cores had been extracted from areas where the microtopography had not changed dramatically (from a lawn community) in the last 450 years. Core D contained some unambiguous indicators of very wet conditions corresponding with the H1510 tephra layer (see section *4.1*). However, there does not seem to be an exceptionally large or small TSC for the H1510 tephra in this core.

On the three hummock-to-hollow transects (labelled HH 1, 2 and 3), tephra was more abundant in cores where the surface vegetation type at the time of coring was at least

partly composed of *Sphagnum* (Fig. 9). The vegetation appears to be more important than the downslope movement, in that, where S*phagnum* appears in the vegetation community on the mid-slope (e.g. HH3), the presence of *Sphagnum* deters further downslope movement. Our results are in agreement with those of an experimental study into the trapping of SCPs in *Sphagnum* peat (Punning and Alliksaar (1997), which found that the majority (>99%) of SCPs were trapped by the *Sphagnum*.

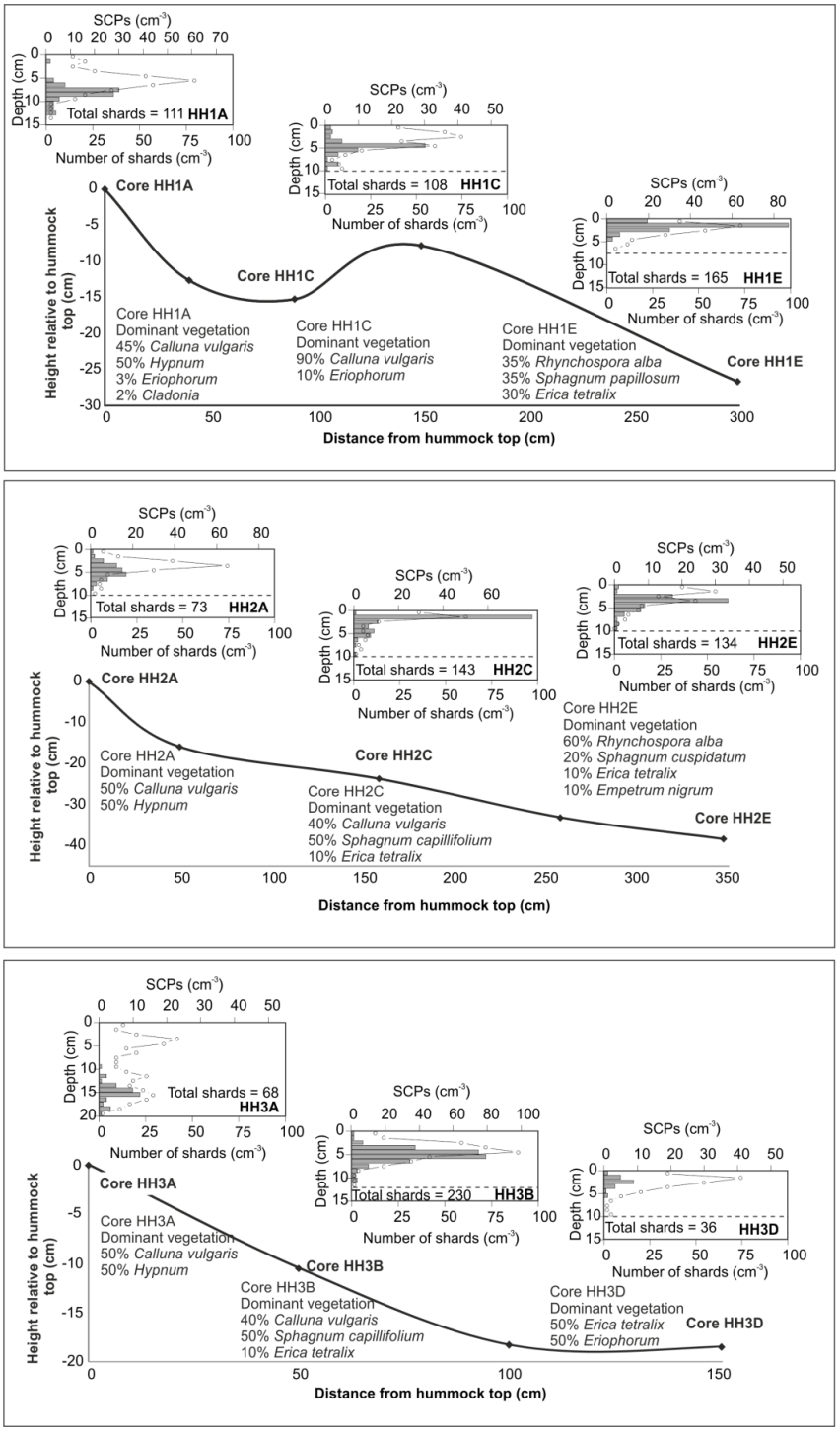

Fig. 9. Diagram indicating shard counts and surface vegetation at time of coring at various points along three transects taken from hummock to hollow on Fallahogy peatland.

The redistribution of tephra shards may also be occurring at even smaller scales (sub-micro-topographical). Surface water flow is likely to be affected at these scales by the interplay between vegetation composition and small changes in gradient.

3.4.6.2 Within site vs. between site variation

In order to make valid inferences about regional ash cloud fallout based on TSC measurements in single cores, the variation in the total number of tephra shards relating to a given eruption within a site must be lower than the variation between sites. Tephra from the eruption of H1947 has been identified in 12 peatlands across Northern Ireland (Rea *et al*., 2012), with TSCs appearing to vary along a West to East gradient. Higher concentrations in western sites were interpreted as reflecting higher ash fallout in this region (Rea *et al*., 2012). The range of TSCs was smaller in the 15 cores at Fallahogy than the range of TSCs across the 12 different peatlands in Northern Ireland (Fig. 10). This suggests that, in this instance, regional-scale factors such as precipitation and ash cloud density had a greater influence on the spatial distribution of TSCs than local (within-site) processes.

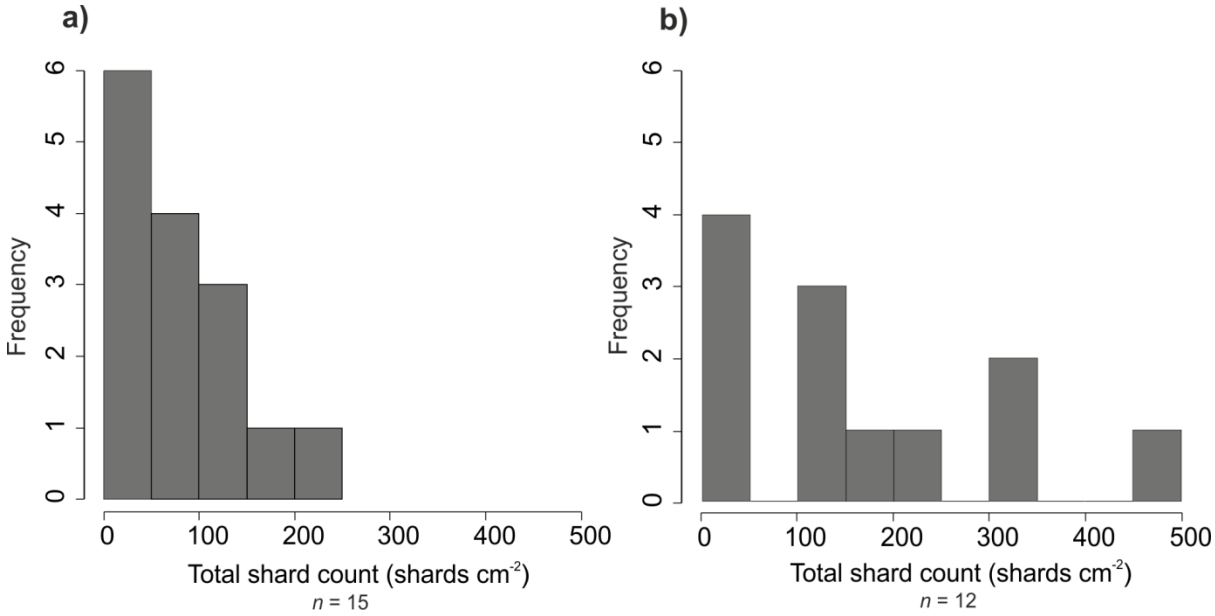

Fig. 10. Histograms showing the total shard counts for the a) Hekla 1947 eruption in 15 cores at Fallahogy (13 cores from this study and 2 cores examined by (Rea *et al*., 2012)) and b) at 12 other sites across Northern Ireland (Rea *et al*., 2012).

Nevertheless, using the TSCs from one core to infer ash fallout concentration over the entire peatland is not advisable due to a large degree of internal variation in TSCs within a site. In order to estimate how many cores would be required to establish a reliable median value we conducted a bootstrap analysis (10,000 iterations, random sampling with replacement) of shard counts for each of the tephra layers (Fig. 11). The

number of cores required to estimate the median value adequately is subjective. However, multiple cores would have been advisable for any of the three tephra layers detected at Fallahogy peatland.

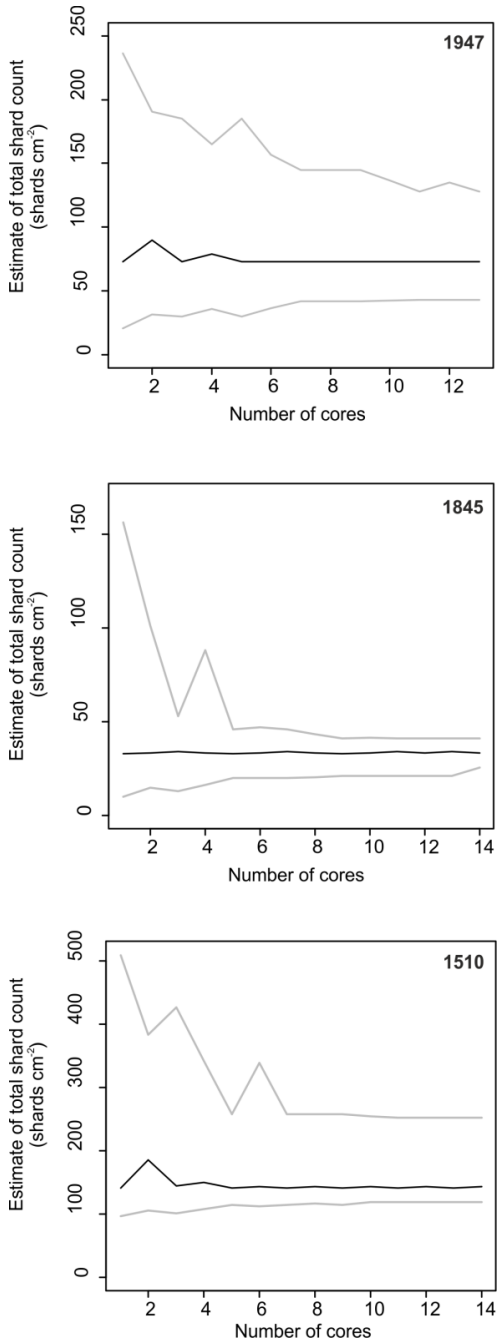

Fig. 11. Results of a bootstrap analysis (10,000 simulations) estimating median shard concentration with different amounts of cores for the three Hekla eruptions. The 0.025 and 0.975 boundaries are indicated by light grey lines. Although the number of cores required for a robust estimate of median shard concentration is subjective, this analysis suggests that multiple cores are required to adequately assess median total shard counts for these three events.

3.4.7 Variation in shard counts for different events

Shard counts vary in different tephra layers within a single core as well as the same event from multiple cores. Mann-Whitney tests indicated a significant difference between each pair of events ($p < 0.05$, n=14 [n =13 for H1947]). H1510 has the highest shard counts, followed by H1947 and H1845 (Fig. 12). The same pattern of relative abundance has been found in many other Northern Irish peatlands (Rea *et al*., 2012; Swindles, 2006).

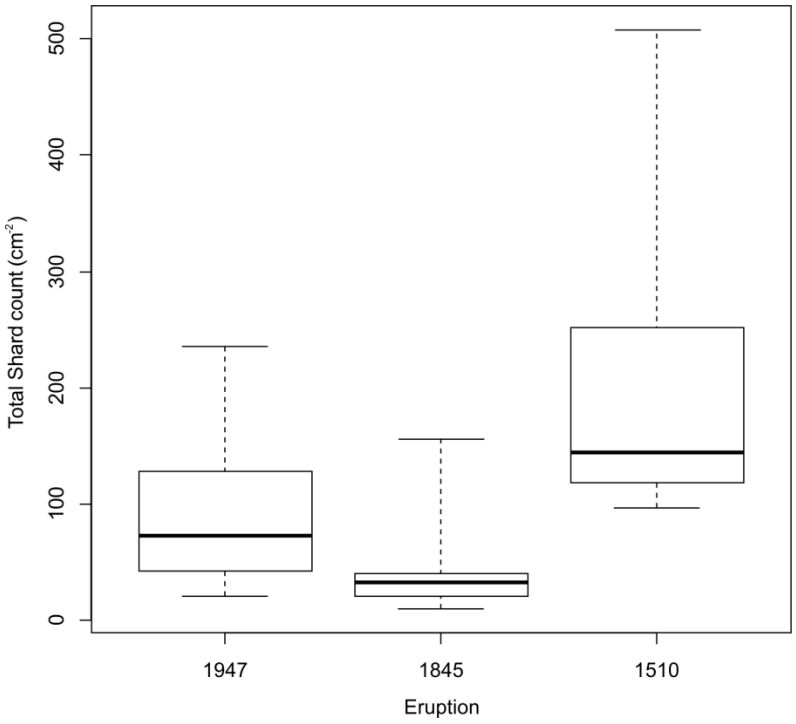

Fig. 12. Boxplots showing the total shard counts for Hekla 1947, Hekla 1845 and Hekla 1510 eruptions in 13 cores at Fallahogy. Boxplot convention is as follows: boxes indicate the interquartile range; the central line through each box indicates the median. The far extent of the upper and lower lines from each quartile indicate the maximum and minimum.

The higher TSCs for H1510 may reflect the nature of the eruption which had a much larger recorded tephra volume (0.32 km^3) when compared with H1947 (0.18 km^3) and H1845 (0.23 km^3) (Larsen *et al*., 1999; Larsen *et al*., 2014). The eruption of H1510 is also inferred (on the basis of its deposits in Iceland) to have had a more intense Plinian phase than H1947 (Larsen *et al*., 2014), perhaps resulting in more distal tephra transport. Less information is available about the nature of the eruption of Hekla in 1845, although it is described as having wide tephra dispersal within Iceland (Larsen *et*

al., 2014). The estimated tephra volume for H1845 is similar to (within error) that of H1947, which is not reflected in the TSC for these eruptions at the Fallahogy site. This suggests that there is no simple relationship between tephra volume and the total number of tephra shards relating to a given eruption in cores from distal peatlands.

3.4.8 Spatial trends in spheroidal carbonaceous particle (SCP) concentration

Tephra is not the only palaeoenvironmental proxy to be deposited onto a peatland from the atmosphere. SCPs, which are a product of the combustion of fossil fuels, are often used as a proxy for atmospheric pollution, with an assumption that the concentration or accumulation rate of SCPs is related to the magnitude of pollution (i.e. the concentration of SCPs in the atmosphere) at the time of deposition. For example, the concentrations of SCPs in lakes have been used to infer differences in the degree of atmospheric pollution in different regions (Rose and Harlock, 1998; Rose *et al*., 1999). Our results suggest that SCP concentrations within a peatland can be highly spatially variable (the total number of SCPs in our cores range from 97 to 2268 (summing all samples containing SCPs)). Therefore any inference of pollution levels based on SCP counts from one core in a peatland should be undertaken with caution.

To determine whether different microparticles are reworked in the same way we tested the hypothesis: Tephra shard concentrations are positively correlated with SCP concentrations across a peatland. If the two different types of microparticle are deposited and reworked in the same way, we might expect cores with higher than average tephra shard concentrations to also contain higher than average SCP concentrations. Two tests for correlation were conducted: i) between total tephra shard counts and total SCP counts in the whole core; ii) between total shard counts at one point in the core and total SCP counts at the same depth (1947 tephra peak). In both cases there was no significant relationship between the counts of SCPs and tephra shards at the 5% level.

Although this suggests that tephra shards and SCPs are reworked differently on a peatland it is not conclusive. It is difficult to compare microparticles which have been continuously deposited (SCPs) with microparticles which are the result of a single event and have been deposited over a number of days or weeks (tephra). However, it is

possible that the microparticles are reworked differently due to differences in their morphology, density or size. Different weather conditions and water table depth at the time of deposition may also affect reworking.

3.4.9 Implications for studies of carbon accumulation

3.4.9.1 Spatial trends in apparent carbon accumulation

Carbon accumulation in peatlands is controlled by the balance between organic matter production and decay (Clymo, 1984). Rates of production and decay vary according to peatland microtopography due to differences in vegetation community and water-table position (Belyea and Clymo, 2001).

The average peat accumulation rate at Fallahogy between 1510 and 1947 (20 years cm^{-1}) was in the range of 10–40 years cm^{-1}, which is typical for peatlands in Northern Ireland (Swindles and Plunkett, 2010). Peat accumulation rate and apparent total carbon accumulation (ATCA) varied spatially (Fig. 7). The ATCA between 1947 and 1510 ranged from 4.0 to 17.8 kg C m^{-2}, although ATCA in the majority of cores was around the average of 8.6 kg C m^{-2}.

These results indicate that ATCA in this peatland is spatially variable over scales of tens to hundreds of metres. There is no spatial autocorrelation in ATCA at these scales, suggesting that any spatial trends are occurring over larger or smaller scales (Mantel test, *p*-value 0.60). There is also no relationship between ATCA and elevation or distance from the peatland edge (SRC, supplementary file, Table S2). Instead, differences in accumulation might be occurring on a microform scale.

Plant macrofossil analysis suggests that there has been no significant change in the microform (lawn) at the majority of the core locations over the last 450 years. However, core D contains indicators of wet conditions, symptomatic of the LIA, corresponding with the H1510 tephra (see section *4.1*). Core D has the lowest ATCA of all the cores between 1510 and 1947 (4.0 kg C m^{-2}), although the accumulation rate increases post 1947. The low ATCA in Core D in the period between 1510 and 1845 might be attributed at least in part to localised very wet conditions during the LIA.

Core K is of particular interest as it shows a much higher LARCA than the other cores. As a check, the FAL_3 tephra in core K was analysed to exclude the possibility that the shards are from a different tephra. Geochemical analysis and SCP chronology confirm assignment to H1510 eruption (supplementary file, Fig. S4) and therefore we can be confident in the high rate of peat accumulation between 1510 and 1845 (0.094 cm year^{-1}). It would appear the cause is localised as other cores located nearby do not show elevated peat accumulation rates. Large proportions of unidentifiable organic material in plant macrofossil samples from core K suggest high levels of decay. High rates of peat accumulation have been shown to occur where the balance between production and decay is optimal (Belyea and Clymo, 2001). We suggest that a high rate of litter productivity by vascular plants (*Calluna vulgaris* roots were abundant in plant macrofossil samples) has resulted in high peat accumulation at this coring location, despite a relatively high rate of decay.

3.4.9.2 Temporal trends in apparent carbon accumulation rate

When considering recent temporal changes in the rate of carbon accumulation, it is important to note that apparent carbon accumulation rates would be expected to increase towards the surface, because younger peats have undergone relatively less decomposition than older peats. Consideration must also be given to the position of the oxic zone (or active layer), where decay rates are higher than in the anoxic zone below. Although none of our cores display a clear boundary, recent carbon accumulation (between 1947 and present) is not included in our analysis as the peat is likely to be undergoing particularly rapid decomposition in the oxygenated zone.

As would be expected, the majority of cores (11 out of 14) show lower peat accumulation rates between 1510 and 1845 when contrasted against the period between 1845 and 1947, with average peat accumulation rates of 0.04 cm yr^{-1} and 0.06 cm year^{-1}, respectively (Fig. 8). The difference in peat accumulation is reflected in LARCA values of 16.6 (1510–1845) and 28.9 g C m^{-2} y^{-1} (1845-1947). The slower peat accumulation during the period 1510 to 1845 might be attributed to a reduction in primary productivity due to the LIA (Charman *et al*., 2013), however it is difficult to untangle the possible climatic link from the impact of increased time for decomposition to occur in the deeper peats. Three cores show (slightly) higher rates of accumulation during

1510–1845 than during 1845–1947, perhaps indicating some degree of autogenic variation in the balance of primary production and decay.

3.5 Conclusions

1. Using geochemistry and SCP profiles we have detected 3 tephra layers that correlate to the Hekla eruptions of 1510, 1845 and 1947 in 14 cores from the same peatland. Suggesting that in small, largely undisturbed, mid-latitude peatlands, the presence or absence of tephra from a given eruption can be determined, with a high degree of certainty, by analysing a single core.
2. Shard counts for a given eruption showed an order-of-magnitude variation between cores from the same site, suggesting differential deposition or lateral post-depositional movement of tephra. No spatial autocorrelation was identified over the scale investigated (tens to hundreds of metres), indicating that any differential deposition or reworking occurs at different scales.
3. Studies comparing tephra shard concentration across multiple sites must consider the differences in shard concentration within a single site. Bootstrap analysis suggests that multiple cores are required in order to ascertain a reasonably reliable median shard count for a site.
4. There was a significant difference in the TSCs for the tephras from the 3 Hekla eruptions, suggesting that in some cases shard counts might be a useful proxy for ash cloud density. However, owing to the influence of meteorological conditions, results must be interpreted with caution.
5. The three historical tephra layers detected in the 14 cores at Fallahogy allowed us to establish a chronological framework within which to examine spatial differences in carbon accumulation within a site. We find differences in the apparent total carbon accumulation between 1510 and 1947 AD.
6. Further work is required on (i) the impact of microtopography on tephra distribution, and (ii) tephra dissolution processes and rates in acidic low pH environments.

Acknowledgements

This research was undertaken while Elizabeth Watson was in possession of a NERC funded Doctoral Training Grant NE/K500847/1. We thank Thomas Kelly for help in the field, Chris Hayward for help with tephra geochemical analysis and Anthony Blundell for guidance on plant macrofossil analysis.

References

Barber, K., 1981. Peat stratigraphy and climatic change: a palaeoecological test of the theory of cyclic peat bog regeneration. Balkema, Rotterdam.

Barber, K.E., Chambers, F.M., Maddy, D., Stoneman, R., Brew, J.S., 1994. A sensitive high-resolution record of late Holocene climatic change from a raised bog in northern England. The Holocene 4, 198-205.

Barber, K.E., Maddy, D., Rose, N., Stevenson, A.C., Stoneman, R., Thompson, R., 2000. Replicated proxy-climate signals over the last 2000 yr from two distant UK peat bogs: new evidence for regional palaeoclimate teleconnections. Quat. Sci. Rev. 19, 481-487.

Belyea, L.R., Clymo, R., 2001. Feedback control of the rate of peat formation. Proc. R. Soc Lond. B 268, 1315-1321.

Bergman, J., Wastegård, S., Hammarlund, D., Wohlfarth, B., Roberts, S.J., 2004. Holocene tephra horizons at Klocka Bog, west-central Sweden: aspects of reproducibility in subarctic peat deposits. J. Quat. Sci. 19, 241-249.

Blaauw, M., Mauquoy, D., 2012. Signal and variability within a Holocene peat bog — Chronological uncertainties of pollen, macrofossil and fungal proxies. Rev. Palaeobot. Palynol. 186, 5-15.

Blockley, S.P.E., Pyne-O'Donnell, S.D.F., Lowe, J.J., Matthews, I.P., Stone, A., Pollard, A.M., Turney, C.S.M., Molyneux, E.G., 2005. A new and less destructive laboratory procedure for the physical separation of distal glass tephra shards from sediments. Quat. Sci. Rev. 24, 1952-1960.

Blundell, A., Barber, K., 2005. A 2800-year palaeoclimatic record from Tore Hill Moss, Strathspey, Scotland: the need for a multi-proxy approach to peat-based climate reconstructions. Quat. Sci. Rev. 24, 1261-1277.

Bol, R., Harkness, D., Huang, Y., Howard, D., 1999. The influence of soil processes on carbon isotope distribution and turnover in the British uplands. Eur. J. Soil Sci. 50, 41-51.

Boygle, J., 1999. Variability of tephra in lake and catchment sediments, Svínavatn, Iceland. Glob. Planet. Change 21, 129-149.

Caseldine, C., Gearey, B., 2005. A multiproxy approach to reconstructing surface wetness changes and prehistoric bog bursts in a raised mire system at Derryville Bog, Co. Tipperary, Ireland. The Holocene 15, 585-601.

Charman, D.J., Beilman, D.W., Blaauw, M., Booth, R.K., Brewer, S., Chambers, F.M., Christen, J.A., Gallego-Sala, A., Harrison, S.P., Hughes, P.D.M., Jackson, S.T., Korhola, A., Mauquoy, D., Mitchell, F.J.G., Prentice, I.C., van der Linden, M., De Vleeschouwer, F., Yu, Z.C., Alm, J., Bauer, I.E., Corish, Y.M.C., Garneau, M., Hohl, V., Huang, Y., Karofeld, E., Le Roux, G., Loisel, J., Moschen, R., Nichols, J.E., Nieminen, T.M., MacDonald, G.M., Phadtare, N.R., Rausch, N., Sillasoo, U., Swindles, G.T., Tuittila, E.S., Ukonmaanaho, L., Valiranta, M., van Bellen, S., van Geel, B., Vitt, D.H., Zhao, Y., 2013. Climate-related changes in peatland carbon accumulation during the last millennium. Biogeosciences 10, 929-944.

Charman, D.J., Blundell, A., Chiverrell, R.C., Hendon, D., Langdon, P.G., 2006. Compilation of non-annually resolved Holocene proxy climate records: stacked Holocene peatland palaeo-water table reconstructions from northern Britain. Quat. Sci. Rev. 25, 336-350.

Clymo, R., 1984. The limits to peat bog growth. Philos.Trans. of the R. Soc. Lond. B. 303, 605-654.

Clymo, R., Turunen, J., Tolonen, K., 1998. Carbon accumulation in peatland. Oikos. 81, 368-388.

Connell, A., 1846. Analysis of the volcanic dust which fell on the Orkney Islands on 2nd September 1845. New Edinb. Philos. J. 40, 217-219.

Davies, S.M., 2015. Cryptotephras: the revolution in correlation and precision dating. J. Quat. Sci. 30, 114-130.

Davies, S.M., Elmquist, M., Bergman, J., Wohlfarth, B., Hammarlund, D., 2007. Cryptotephra sedimentation processes within two lacustrine sequences from west central Sweden. The Holocene 17, 319-330.

Davies, S.M., Larsen, G., Wastegård, S., Turney, C.S.M., Hall, V.A., Coyle, L., Thordarson, T., 2010. Widespread dispersal of Icelandic tephra: how does the Eyjafjöll eruption of 2010 compare to past Icelandic events? J. Quat. Sci. 25, 605-611.

De Vleeschouwer, F., Chambers, F.M., Swindles, G.T., 2011. Coring and sub-sampling of peatlands for palaeoenvironmental research. Mires and Peat 7 1-10.

De Vleeschouwer, F., Piotrowska, N., Sikorski, J., Pawlyta, J., Cheburkin, A., Le Roux, G., Lamentowicz, M., Fagel, N., Mauquoy, D., 2009. Multiproxy evidence of 'Little Ice Age' palaeoenvironmental changes in a peat bog from northern Poland. The Holocene. 19, 625-637.

Dugmore, A.J., Larsen, G., Newton, A.J., 1995. 7 Tephra isochrones in Scotland. The Holocene 5, 257-266.

Dugmore, A.J., Newton, A.J., Sugden, D.E., Larsen, G., 1992. Geochemical stability of fine-grained silicic Holocene tephra in Iceland and Scotland. J. Quat. Sci. 7, 173-183.

Edwards, K.J., 1983. Quaternary palynology: multiple profile studies and pollen variability. Prog. Phys. Geogr. 7, 587-609.

Garnett, M., Ineson, P., Stevenson, A.C., Howard, D.C., 2001. Terrestrial organic carbon storage in a British moorland. Glob. Change Biol. 7, 375-388.

Griggs, A.J., Davies, S.M., Abbott, P.M., Rasmussen, T.L., Palmer, A.P., 2014. Optimising the use of marine tephrochronology in the North Atlantic: a detailed

investigation of the Faroe Marine Ash Zones II, III and IV. Quat. Sci. Rev. 106, 122-139.

Hall, V.A. and Pilcher, J.R., 2002. Late-Quaternary Icelandic tephras in Ireland and Great Britain: detection, characterization and usefulness. The Holocene, 12 (2), 223-230.

Hayward, C., 2012. High spatial resolution electron probe microanalysis of tephras and melt inclusions without beam-induced chemical modification. The Holocene 22, 119-125.

Hodder, A. P. W., De Lange, P. J., Lowe, D. J. 1991. Dissolution and depletion of ferromagnesian minerals from Holocene tephra layers in an acid bog, New Zealand, and implications for tephra correlation. J. Quat. Sci., 6, 195-208.

Housley, R.A., MacLeod, A., Nalepka, D., Jurochnik, A., Masojć, M., Davies, L., Lincoln, P.C., Bronk Ramsey, C., Gamble, C.S., Lowe, J.J., 2013. Tephrostratigraphy of a Lateglacial lake sediment sequence at Węgliny, southwest Poland. Quat. Sci. Rev. 77, 4-18.

Innes, J.B., Blackford, J., Simmons, I.G., 2004. Testing the integrity of fine spatial resolution palaeoecological records: microcharcoal data from near-duplicate peat profiles from the North York Moors, UK. Palaeogeogr. Palaeoclimatol., Palaeoecol. 214, 295-307.

Irwin, T.E., 1989. Pollen percentage, concentration and influx to a mire hummock and hollow. Pollen et Spores 31, 317-328.

Jowsey, P., 1966. An improved peat sampler. New Phytol. 65, 245-248.

Kettridge, N., Binley, A., Comas, X., Cassidy, N.J., Baird, A.J., Harris, A., Kruk, J., Strack, M., Milner, A.M., Waddington, J.M., 2012. Do peatland microforms move through time? Examining the developmental history of a patterned peatland using ground-penetrating radar. J. Geophys. Res. Biogeosci., 117. DOI: 10.1029/2011JG001876

Lane, C.S., Brauer, A., Blockley, S.P.E., Dulski, P., 2013. Volcanic ash reveals time-transgressive abrupt climate change during the Younger Dryas. Geol. 41, 1251-1254.

Langdon, P.G., Barber, K.E., 2004. Snapshots in time: precise correlations of peat-based proxy climate records in Scotland using mid-Holocene tephras. The Holocene 14, 21-33.

Larsen, G., Dugmore, A., Newton, A., 1999. Geochemistry of historical-age silicic tephras in Iceland. The Holocene 9, 463-471.

Larsen, G., Eiríksson, J., Gudmundsdóttir, E.R., 2014. Last millennium dispersal of air-fall tephra and ocean-rafted pumice towards the north Icelandic shelf and the Nordic seas. Geol. Soc. Lond. Spec. Pub. 398, SP398. 394.

Lawson, I.T., Al-Omari, S., Tzedakis, P.C., Bryant, C.L., Christaniss, K., 2005. Lateglacial and Holocene vegetation history at Nisi Fen and the Boras mountains, northern Greece. The Holocene 15, 873-887.

Lawson, I.T., Swindles, G.T., Plunkett, G., Greenberg, D., 2012. The spatial distribution of Holocene cryptotephras in north-west Europe since 7 ka: implications for understanding ash fall events from Icelandic eruptions. Quat. Sci. Rev. 41, 57-66.

Le Maitre, R.W., Bateman, P., Dudek, A., Keller, J., Lameyre, J., Le Bas, M., Sabine, P., Schmid, R., Sorensen, H., Streckeisen, A., 1989. A classification of igneous rocks and glossary of terms: Recommendations of the International Union of Geological Sciences Subcommission on the Systematics of Igneous Rocks. Blackwell Oxford.

Magnan, G., Garneau, M., 2014. Climatic and autogenic control on Holocene carbon sequestration in ombrotrophic peatlands of maritime Quebec, eastern Canada. The Holocene. 24, 1054-1062.

Mattsson, S., Vesanen, R., 1988. Patterns of Chernobyl fallout in relation to local weather conditions. Env. Int. 14, 177-180.

MetOffice, 1976. Average Annual Rainfall (in mm), International Standard Period (1941-1970). Met. 0886 (NI). HMSO: London.

Newton, A.J., Dugmore, A.J., Gittings, B.M., 2007. Tephrabase: tephrochronology and the development of a centralised European database. J. Quat. Sci. 22, 737-743.

O'Rourke, K., 1994. The Economic Impact of the Famine in the Short and Long Run. Am. Econ. Rev. 84, 309-313.

Ohlson, M., Økland, R.H., 1998. Spatial variation in rates of carbon and nitrogen accumulation in a boreal bog. Ecology 79, 2745-2758.

Osvald, H., 1923. Die Vegetation des Hochmoores Komosse. Sven. Växtsociol. Sällsk. Handl. 1. Handl. 1., 266.

Parry, L.E., Charman, D.J., 2013. Modelling soil organic carbon distribution in blanket peatlands at a landscape scale. Geoderma 211, 75-84.

Payne, R., Gehrels, M., 2010. The formation of tephra layers in peatlands: An experimental approach. Catena 81, 12-23.

Payne, R.J., Kilfeather, A.A., Van der Meer, J.J.M., Blackford, J.J., 2005. Experiments on the taphonomy of tephra in peat. Suoseura Finn. Peatl. Soc. 56, 147-156.

Pilcher, J.R., Hall, V.A., 1992. Towards a tephrochronology for the Holocene in the north of Ireland The Holocene 2 255-259

Pilcher, J.R., Hall, V.A. and McCormac, F.G., 1996 An outline tephrochronology for the Holocene of the north of Ireland. J. Quat. Sci**. 11 (6),** 485-494

Pouget, S., Bursik, M., Rogova, G., 2014. Tephra redeposition and mixing in a Late-glacial hillside basin determined by fusion of clustering analyses of glass-shard geochemistry. J. Quat. Sci. 29, 789-802.

Punning, J.M., Alliksaar, T., 1997. The trapping of fly-ash particles in the surface layers of Sphagnum-dominated peat. Water, air, and soil pollut. 94, 59-69.

Pyne-O'Donnell, S., 2011. The taphonomy of Last Glacial-Interglacial Transition (LGIT) distal volcanic ash in small Scottish lakes. Boreas 40, 131-145.

Rea, H.A., Swindles, G.T., Roe, H.M., 2012. The Hekla 1947 tephra in the north of Ireland: regional distribution, concentration and geochemistry. J. Quat. Sci. 27, 425-431.

Renberg, I., Wik, M., 1984. Dating recent lake sediments by soot particle counting. Verh Internat Verein. Limnol. 22, 712-718.

Roland, T., Mackay, H., Hughes, P., 2015. Tephra analysis in ombrotrophic peatlands: A geochemical comparison of acid digestion and density separation techniques. J. Quat. Sci. 30, 3-8.

Roland, T.P., Caseldine, C.J., Charman, D.J., Turney, C.S.M., Amesbury, M.J., 2014. Was there a '4.2 ka event' in Great Britain and Ireland? Evidence from the peatland record. Quat. Sci. Rev. 83, 11-27.

Rose, N., Appleby, P., 2005. Regional applications of lake sediment dating by spheroidal carbonaceous particle analysis I: United Kingdom. J. Paleolimn. 34, 349-361.

Rose, N.L., Harlock, S., Appleby, P.G., 1999. The Spatial and Temporal Distributions of Spheroidal Carbonaceous Fly-Ash Particles (SCP) in the Sediment Records of European Mountain Lakes. Water, Air, and Soil Pollution 113, 1-32.

Rose, N.L., Harlock, S., 1998. The Spatial Distribution of Characterised Fly-Ash Particles and Trace Metals in Lake Sediments and Catchment Mosses in the United Kingdom. Water, Air, and Soil Pollution 106, 287-308.

Schumann, U., Weinzierl, B., Reitebuch, O., Schlager, H., Minikin, A., Forster, C., Baumann, R., Sailer, T., Graf, K., Mannstein, H., Voigt, C., Rahm, S., Simmet, R., Scheibe, M., Lichtenstern, M., Stock, P., Rüba, H., Schäuble, D., Tafferner, A., Rautenhaus, M., Gerz, T., Ziereis, H., Krautstrunk, M., Mallaun, C., Gayet, J.F., Lieke, K., Kandler, K., Ebert, M., Weinbruch, S., Stohl, A., Gasteiger, J., Groß, S., Freudenthaler, V., Wiegner, M., Ansmann, A., Tesche, M., Olafsson, H., Sturm, K., 2011. Airborne observations of the Eyjafjalla volcano ash cloud over Europe during air space closure in April and May 2010. Atmos. Chem. and Phys. 11, 2245-2279.

Stevenson, J., Millington, S., Beckett, F., Swindles, G., Thordarson, T., 2015. Big grains go far: reconciling tephrochronology with atmospheric measurements of volcanic ash. Atmos. Meas. Tech. Discuss., 8, 65-120.

Suzuki, R., Shimodaira, H., 2006. Pvclust: an R package for assessing the uncertainty in hierarchical clustering. Bioinformatics 22, 1540-1542.

Svensson, G., 1988. Fossil plant communities and regeneration patterns on a raised bog in South Sweden. J. of Ecol. 76, 41-59.

Swindles, G.T., 2006. Reconstruction of Holocene climate change from peatlands in the north of Ireland. Thesis for the degree of Doctor of Philosophy. Queens University Belfast.

Swindles, G.T., Blundell, A., Roe, H.M., Hall, V.A., 2010. A 4500-year proxy climate record from peatlands in the North of Ireland: the identification of widespread summer 'drought phases'? Quat. Sci. Rev. 29, 1577-1589.

Swindles, G.T., De Vleeschouwer, F., Plunkett, G., 2011a. Dating peat profiles using tephra: stratigraphy, geochemistry and chronology Mires and Peat 7, 1-9.

Swindles, G.T., Galloway, J., Outram, Z., Turner, K., Schofield, J.E., Newton, A.J., Dugmore, A.J., Church, M.J., Watson, E.J., Batt, C., Bond, J., Edwards, K.J., Turner, V., Bashford, D., 2013a. Re-deposited cryptotephra layers in Holocene peats linked to anthropogenic activity. The Holocene 23, 1493-1501.

Swindles, G.T., Lawson, I.T., Matthews, I.P., Blaauw, M., Daley, T.J., Charman, D.J., Roland, T.P., Plunkett, G., Schettler, G., Gearey, B.R., 2013b. Centennial-scale climate change in Ireland during the Holocene. Earth Sci. Rev. 126, 300-320.

Swindles, G.T., Morris, P.J., Baird, A.J., Blaauw, M., Plunkett, G., 2012. Ecohydrological feedbacks confound peat-based climate reconstructions. Geophys. Res. Lett. 39, L11401, doi:10.1029/2012GL051500.

Swindles, G.T., Lawson, I.T., Savov, I.P., Connor, C.B., Plunkett, G., 2011b. A 7000 yr perspective on volcanic ash clouds affecting northern Europe. Geol. 39, 887-890.

Swindles, G.T., Plunkett, G., 2011. 'The methodological basis for fine-resolution, multi-proxy reconstructions of ombrotrophic peat bog surface wetness': Comments. Boreas 40, 379-381.

Swindles, G.T., Roe, H.M., 2006. Constraining the age of spheroidal carbonaceous particle (SCP) stratigraphies in peats using tephrochronology. Quat. Newsl. 110, 2-9.

Techer, I., Advocat, T., Lancelot, J. & Liotard, J. M. 2001. Dissolution kinetics of basaltic glasses: control by solution chemistry and protective effect of the alteration film. Chem.Geol. 176, 235-263.

Thorseth, I. H., Fumes, H. & Tumyr, O. 1995. Textural and chemical effects of bacterial-activity on basaltic glass – an experimental approach. Chem.Geol. 119, 139-160.

Turner, J., Innes, J.B., Simmons, I.G., 1989. Two pollen diagrams from the same site. New Phytol. 113, 409-416.

Turner, T.E., Swindles, G.T., Roucoux, K.H., 2014. Late Holocene ecohydrological and carbon dynamics of a UK raised bog: impact of human activity and climate change. Quat. Sci. Rev. 84, 65-85.

Turunen, J., Roulet, N.T., Moore, T.R., Richard, P.J., 2004. Nitrogen deposition and increased carbon accumulation in ombrotrophic peatlands in eastern Canada. Glob. Biogeochem. Cycles 18. DOI: 10.1029/2003GB002154.

van der Linden, M., Heijmans, M.M., van Geel, B., 2014. Carbon accumulation in peat deposits from northern Sweden to northern Germany during the last millennium. The Holocene 24.

Von Post, L., 1910. Das Skagershultmoor, In: Von Post, L., Sernander, L. (Eds.), Pflanzen-physiognomische Studien auf Torfmoores in Narke, 1–24. Livretguide des exursions en Suede du XI Congres Geologique Internationale, Excursion A 7, No 14, Stockholm.

Walker, D., Walker, P.M., 1961. Stratigraphic Evidence of Regeneration in Some Irish Bogs. Journal of Ecol. 49, 169-185.

Wastegård, S., 2002. Early to middle Holocene silicic tephra horizons from the Katla volcanic system, Iceland: new results from the Faroe Islands. J. Quat. Sci. 17, 723-730.

Wolff-Boenisch, D., Gislason, S.R., Oelkers, E.H., Putnis, C.V., 2004. The dissolution rates of natural glasses as a function of their composition at pH 4 and 10.6, and temperatures from 25 to 74°C. Geochim. Cosmochim. Acta 68, 4843-4858.

Chapter 4: First discovery of Holocene cryptotephra in Amazonia

Elizabeth J. Watson*[1], Graeme T. Swindles[1], Ivan P. Savov[2], Karen L. Bacon[1]

[1]School of Geography, University of Leeds, Leeds, LS2 9JT, UK
[2]School of Earth and Environment, University of Leeds, Leeds, LS2 9JT, UK
**Corresponding author*
Manuscript for Nature Scientific Reports

Keywords: Tephra; Tropical Peatlands; Vegetation; South America;

Abstract

The use of volcanic ash layers for dating and correlation (tephrochronology) is widely applied in the study of past environmental changes. We describe the first cryptotephra (non-visible volcanic ash horizon) to be identified in the Amazon basin, which is tentatively attributed to a source in the Ecuadorian Eastern Cordillera (0–1°S, 78-79°W), some 500-600 km away from our field site in the Peruvian Amazon. Our discovery 1) indicates that the Amazon basin has been subject to volcanic ash fallout during the recent past; 2) highlights the opportunities for using cryptotephras to date palaeoenvironmental records in the Amazon basin and 3) indicates that cryptotephra layers are preserved in a dynamic Amazonian peatland, suggesting that similar layers are likely to be present in other peat sequences that are important for palaeoenvironmental reconstruction. The discovery of cryptotephra in an Amazonian peatland provides a baseline for further investigation of Amazonian tephrochronology and the potential impacts of volcanism on vegetation.

4.1 Introduction

Tephrochronology (dating sedimentary sequences using volcanic ash layers) is a particularly useful method for dating and correlating records of past environmental change [1-3]. Although the majority of volcanic ash (tephra) falls out close to the volcanic source, fine ash (<1 mm) can have an atmospheric residence time in the region of hours to months, during which tephra may be transported thousands of kilometres [4]. In high concentrations fine ash is a hazard for the health of humans and animals [5] and even far

from the volcanic source ash can be present in concentrations which can induce engine failure in modern jet aircraft [6].

Following the initial discovery of microscopic tephra shards from Icelandic volcanoes in distal lakes and peatlands of Ireland and Scotland [7,8], such invisible isochrons, commonly referred to as 'cryptotephras' have been identified in ice cores, terrestrial and marine sediments [9-11]. Cryptotephras can often be linked to a source region or even specific eruption(s) based on their glass geochemistry. Advances in geochemical analysis techniques, predominantly through Electron Probe Micro Analysis (EPMA) now allow for precise and accurate analysis with beam sizes as small as 3 μm [12]. Cryptotephra layers in distal archives are predominantly used as correlation and dating tools; however they can also provide insights into past volcanic activity otherwise buried by younger deposits or eroded in the proximal (near vent) area. Tephra layers which transgress continental boundaries [13,14] provide the opportunity for the correlation of palaeoenvironmental records over large distances. Cryptotephra studies have focussed predominantly on northern latitudes of Europe, although cryptotephras have also been identified in many other regions for example China [15], North America [16], New Zealand [17] and Far East Russia [18]. There have been several studies of macroscopic tephra layers in South America e.g. [19,20], but cryptotephra studies have been confined to the regions of Argentina and Patagonia [21,22]. To the authors' knowledge there have been no previous published studies of cryptotephra occurrence in the Amazon basin.

There has been much recent interest in tropical peatlands as they represent globally-important carbon sinks, support important ecosystems and are currently threatened by climate change and human activities [23]. It has been estimated that tropical peatlands contain approximately 88.6 Gt of carbon, equivalent to up to 19 % of the global peatland carbon pool [23,24] and can be found in both lowland and upland areas in SE Asia, Africa and Central and South America [25-27]. A variety of peatlands have recently been discovered in the subsiding Pastaza-Marañon basin in Western (Peruvian) Amazonia including minerotrophic palm swamps and ombrotrophic domed bogs [27-29]. The Pastaza-Marañon basin was recently identified as the most carbon-dense landscape in Amazonia, storing 892 ± 535 Mg C ha^{-1} [30]. There have been a small number of studies of the ecology and paleoecology of Amazonia peatlands owing to their potential as archives of past environmental change [28,31-33]. Such studies are rare and thus

important as they can provide a long-term baseline for recent climate changes in tropical Amazonia and globally. However, tropical peats are notoriously difficult to date due to the presence of large roots leading to deep biological alteration [32].

Here we present a new discovery of a historic cryptotephra layer from a domed peatland in the Peruvian Amazon. The presence of this tephra has important implications for dating and correlating very recent peats and lake sediments in western Amazonia, and provides unambiguous evidence that Amazonia has been affected by volcanic ash fall in the very recent past.

Aucayacu ("water of the natives" or "water of the warriors") is a domed peatland in western Peru that currently operates as an ombrotrophic 'raised bog' system [28]. It is situated on alluvial fan sediments between a stream of the Pastaza fan and the Tigre River (Figure 1). The peatland began as a nutrient rich minerotrophic system that gradually became an ombrotrophic raised bog through its developmental history [28]. Aucayacu represents the deepest and oldest peatland that has been discovered in the Amazon basin (~7.5 m thick) and peat initiation at the site has been dated to c. 8870 cal. yr BP [28]. The vegetation of Aucayacu is characterised by 'pole' and 'dwarf' forest communities [33].

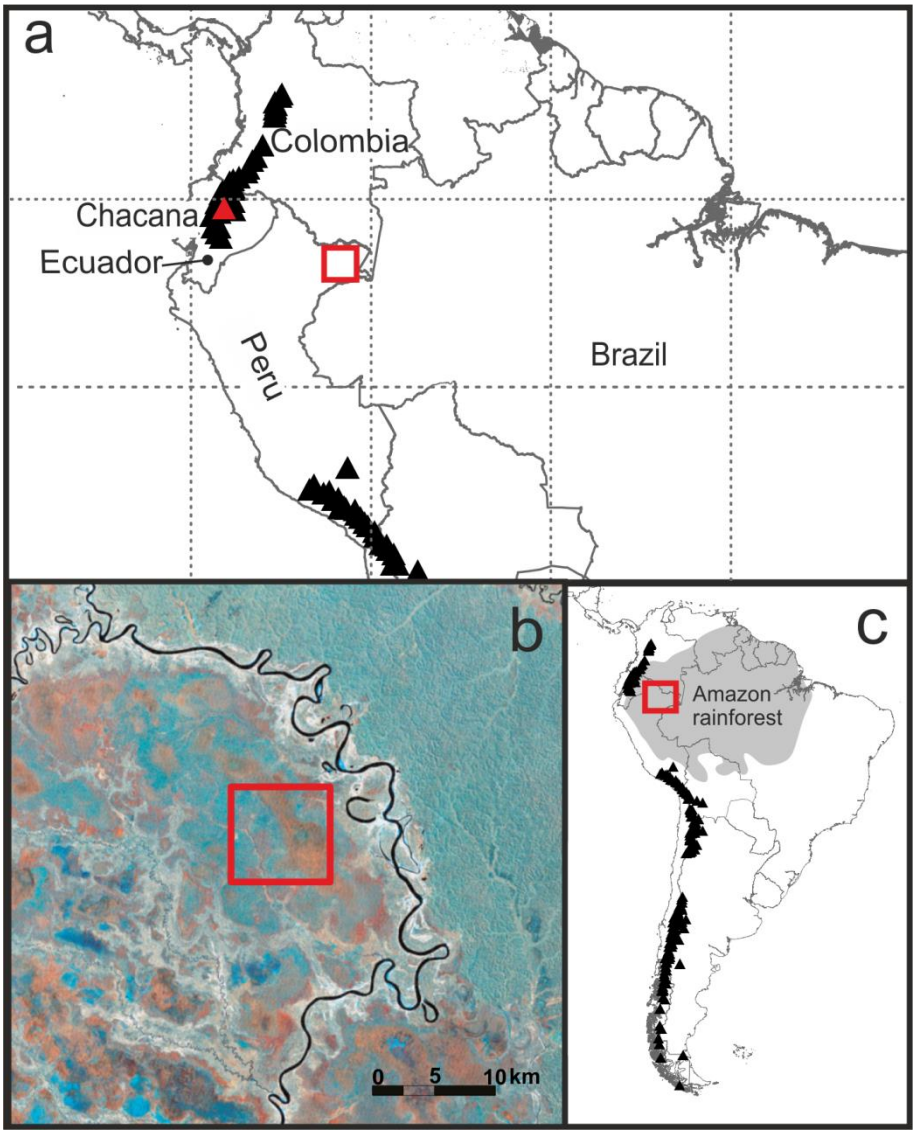

Fig 1. Maps showing the location of Aucayacu peatland, Loreto region, Peruvian Amazonia, a) overview map of the approximate location of Aucayacu (red box) and the locations of volcanoes with known Holocene eruptions, the Chacana volcano, which is within the Eastern Cordillera is indicated in red, gridlines are at 10° intervals, b) False colour Landsat TM RGB image (Orthorectified, WRS-2, Path 007, Row 063). Band 4 was assigned to red, band 5 was assigned to green and band 7 was assigned to blue. c) Map indicating location of the field site in South America, again Holocene volcanoes are shown, shaded region indicates approximate forest cover. Maps were constructed using Arc Map 10.2.2. Landsat Data are free to download and available from the U.S. Geological Survey. Locations of Holocene locations downloaded from the Smithsonian Global Volcanism Program (http://www.volcano.si.edu/list_volcano_holocene.cfm#)

4.2 Methods

A peat core of length 1 m was extracted from the interior of Aucayacu peatland using a Russian D-section corer with a 50-cm-long chamber [34,35]. Peat moisture content and loss-on-ignition were calculated at 2 cm intervals following [36] and peat humification was determined following [37]. The core was dated using AMS ^{14}C dating of extracted wood and macrofossils. ^{14}C dates were calibrated using IntCal13 [38] in Clam v.2.2 [39]. Age-depth models using linear interpolation were constructed.

The core was analysed for tephra using the quick-burn technique [1,3]. After burning, the residue was sieved at 15 µm in an ultrasonic bath for 20 minutes to remove fine siliceous material, rinsed with deionised water, and the coarse fraction mounted onto slides. Tephra shard counts were conducted at 200x magnification on a standard Leica binocular microscope. Following detection of the peak tephra shard concentration, tephra was extracted for geochemical analysis following the density separation method of [40]. The peat sample was sieved between 80 and 15 µm. Further extraction was conducted using various densities of LST heavy liquid. A cleaning float of 2.0 g cm^{-3} was used to remove organic material a further float at of 2.2 g cm^{-3} was also required to remove abundant phytoliths. Finally tephra was floated off at 2.5 g cm^{-3} and rinsed thoroughly with deionised water. Samples were mounted onto glass slides using EpoThin resin, ground to expose the shards c.f. [41] and polished to a 0.25 µm finish. Analysis was conducted by EPMA at the Tephra Analytical Unit, University of Edinburgh. Analysis setup followed the method of [12], beam diameter was 5 µm with 15 kV and variable beam current 2 nÅ (Na, Mg, Al, Si, K, Ca, Fe) to 80 nÅ (P, Ti, Mn). Secondary glass standards, rhyolite (Lipari) and basalt (BCR-2G) were analysed before and after the unknown samples. The tephra geochemical data was compared with the Smithsonian's Global Volcanism Program (2013) "Volcanoes of the World" database and the Large Magnitude Explosive Volcanic Eruptions (LaMEVE) database, which is part of VOGRIPA Project [42]. This resource and other published literature were searched for tephra geochemical data to identify a source volcano and/or eruption. Total Alkali-Silica (TAS) and geochemical bi-plots were constructed for comparison of the published tephra geochemical data with geochemical data from the AUC1 tephra.

4.3 Results

Figure 1 shows the location of Aucayacu peatland in Amazonia and volcanoes discussed in the text. In the 1-m core from Aucayacu there were no visible tephra layers; however, two microscopic tephra layers were encountered at 10-15 cm and 75-80 cm (Figure 2). No tephra shards were identified in samples outside of these depths. The tephra layer at 10-15 cm (AUC1) had a sufficient concentration for analysis (44 shards 5 cm^{-3}); however the lower layer only contained 2 shards and was not suitable for further analysis. The shards of AUC1 were all transparent and vesicular, with a mean size of 53 μm, median = 50 μm, maximum = 125 μm, and minimum 25 μm or less (n = 40). There is no clear event in the core properties (moisture content, loss-on-ignition or peat humification) that corresponds with the tephra layer. This (layer) is merely a trace of (volcanic) material and would not have been detected through visual means or analysis of basic core properties.

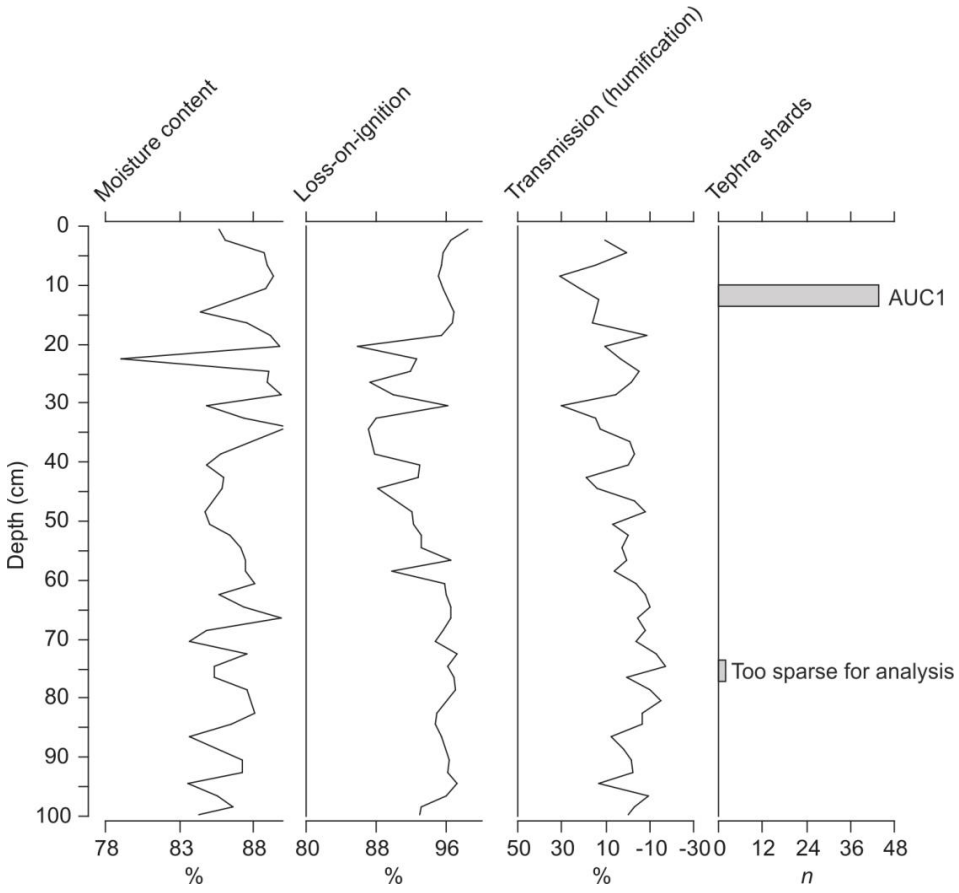

Fig 2. Core properties and tephrostratigraphy, *n* = number of tephra shards counted in the 5 cm^3 sample, AUC1 is the tephra layer described in this study, a second tephra layer was detected but was not suitable for geochemical analysis due to a sparse number of tephra shards.

Age modelling, based on linear interpolation between the current surface (date of sampling = 2012) and two ^{14}C dates, suggests a date range of AD 1769-1970 for the AUC1 tephra (Figure 3). We note that the date at 21 cm runs to the modern period; however, the ^{14}C date at 50 cm provides a solid constraint to the tephra being dated to within the last ~800 years.

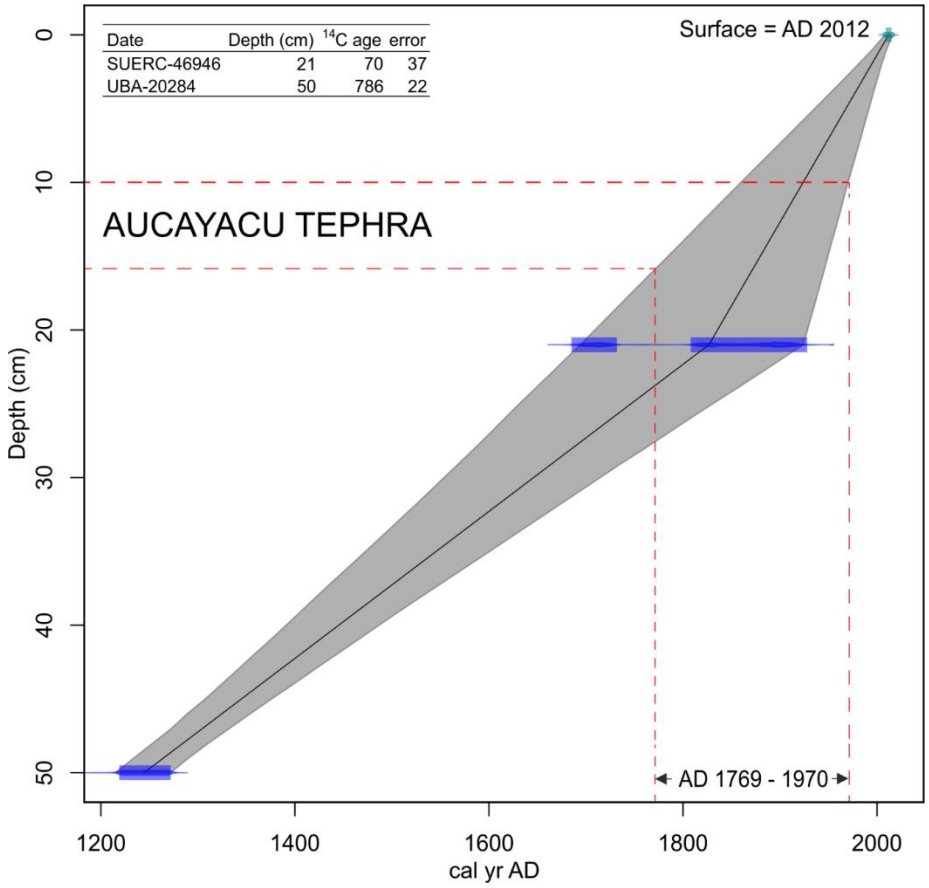

Fig 3. Age-depth model based on linear interpolation between the current surface and ^{14}C dates at 21 and 50 cm. Based on our age depth model the peat depth containing the tephra is dated to between AD 1769 and 1970.

4.4 Discussion

Our discovery represents the first report of cryptotephra layers from Amazonia. Based on the distances travelled by other cryptotephras [13,14] Aucayacu peatland is within cryptotephra fallout range for a moderate to large eruption from volcanoes in Peru, Ecuador and Colombia. The prevailing wind directions in the region of our study site are S/SE in the summer and N/NE in the winter [43]. However, there are no active Holocene volcanoes to the East of Aucayacu peatland. We therefore suggest that the tephra layers deposited at Aucayacu result from the eruptions of volcanoes along the Nazca and South American plate boundary which occurred during atypical (Westerly) wind conditions.

In an attempt to identify a source region and/or volcano for the AUC1 tephra we searched the Smithsonian Global Volcanism Database [44] for volcanoes in Colombia,

Ecuador or Peru, which had recorded eruptive activity around the time of the AUC1 tephra deposition. A total of 20 volcanoes have observed or dated eruptions during this time period (6 in Colombia, 9 in Ecuador and 5 in Peru). Geochemical analysis of the AUC1 tephra illustrates that it is rhyolitic with silica content >75%. Geochemical data is provided in supplementary table 1. Only one of these volcanoes, Chacana (Ecuador) is described as having a rhyolitic dominant rock type. However, there is evidence that volcanoes with a bulk rock geochemistry in the andesite range (as determined by XRF) can erupt rhyolitic glass which is the dominant constituent of distal cryptotephras[45].

We examined the magnitude of eruptions around the time of the AUC1 tephra deposition. 16 of the volcanoes had no eruptions which were estimated to be larger than VEI 3, of the remaining volcanoes, 1 was in Ecuador (Cotopaxi), 1 in South Peru (Tutupaca erupted between AD 1787 and 1802[46]) and 1 in Colombia (Doña Juana erupted AD 1897-1906). There is evidence of distal ash deposition from Tutupaca at multiple locations including Arica (165 km from the vent)[46] suggesting ash from this eruption was carried toward the South, the opposite direction to Aucayacu peatland. Although Doña Juana was active between 1897 and 1906 and activity peaked during 1899, contemporary reports do not indicate significant ash clouds [47].

Following this initial search we focussed on the volcanoes of Ecuadorian Eastern Cordillera as: 1) They are closer to Aucayacu peatland than Colombian and Peruvian volcanoes (c. 5-600km vs. 1500 km to Tutupaca and 700 km to Dona Juana); 2) Volcanoes in the Ecuadorian Eastern Cordillera have been highly active during the late Holocene, in particular Cotopaxi volcano which has three recorded eruptions with a magnitude of VEI 4 (AD 1744, 1768 and 1877[44]); 3) There is geochemical evidence to support the eruption of rhyolitic compositions from these volcanic systems in the past (Fig. 4).

Holocene Ecuadorian volcanism can be described by an East to West split with volcanoes in Eastern Cordillera generally more active than those in the West [48]. For this reason we focused our search to the East and specifically three large rhyolitic centres: Chalupas, Cotopaxi and Chacana (0–1°S, 78-79°W). Eruptions of Cotopaxi show characteristic rhyolitic and andesitic bimodal magmatism during the Holocene [48] and multiple effusive and explosive eruptions of the volcano have been recorded in

chronicles since 1534, with the largest historical event occurring in AD 1768 (VEI =4) [49]. These eruptions were of andesitic bulk rock geochemistry. Less information is available about historical eruptive activity at the Chalupas volcano, which is adjacent Cotopaxi. The Chacana caldera complex is an eroded caldera complex of Pliocene-Holocene age [44]. Chacana stratovolcano (0.37°S, 78.25°W, elev. 4643 m) has been the source of multiple lava flows during the 18th century [50].

Unfortunately only XRF bulk rock geochemical data is available for previous eruptions of Chalupas and Chacana [51]. Although XRF data indicates that these volcanoes have previously erupted bulk rock of rhyolite composition, due to the contamination of phenocrystals and microcrystals, the XRF data cannot be directly compared with the AUC 1 glass geochemistry (determined using EPMA), the data are plotted on Figures 4 and 5 for illustration only. There is an urgent need for the collection of representative proximal historical samples from Ecuador, Colombia and Peru which could be analysed via EPMA. There is some geochemical data based on EPMA of glass for Holocene and Late Pleistocene glasses from Cotopaxi [52] . Although this is similar to our AUC 1 data for some elements (Figure 5), Cotopaxi rhyolites typically have a lower K_2O value than the AUC 1 tephra (Figure 4).

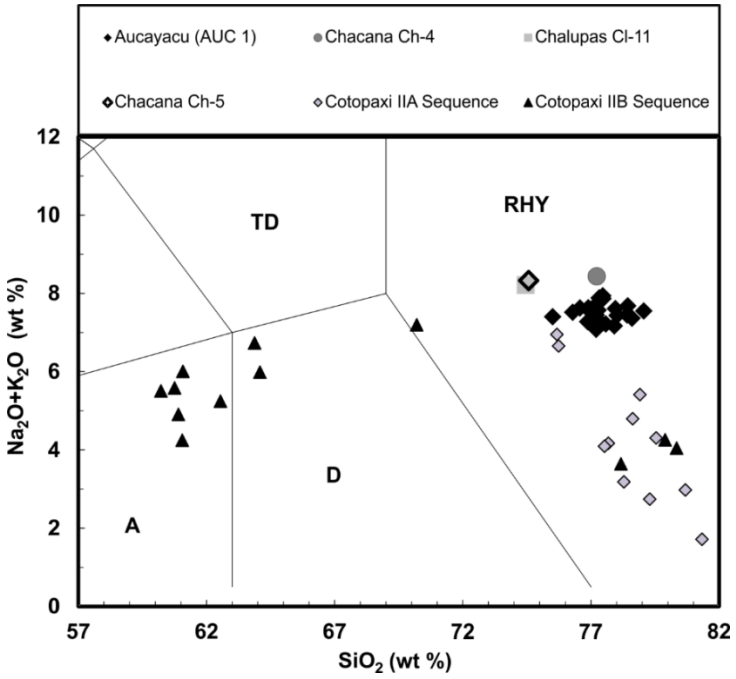

Fig 4. Total Alkali Silica (TAS) plot indicating the geochemistry of the Aucayacu tephra shards as determined by EPMA plotted against the whole rock geochemistry of volcanic rocks from the Chacana-Chalupas caldera region determined by XRF (X-ray fluorescence) [51] and glass geochemical data for Cotopaxi determined by EPMA (Cotopaxi IIA and IIB sequences from the Holocene and late Pleistocene) [52]. Major element totals are normalised to 100%. Annotations follow standard terminology e.g. RHY = Rhyolite, D = Dacite, TD = Trachydacite [53].

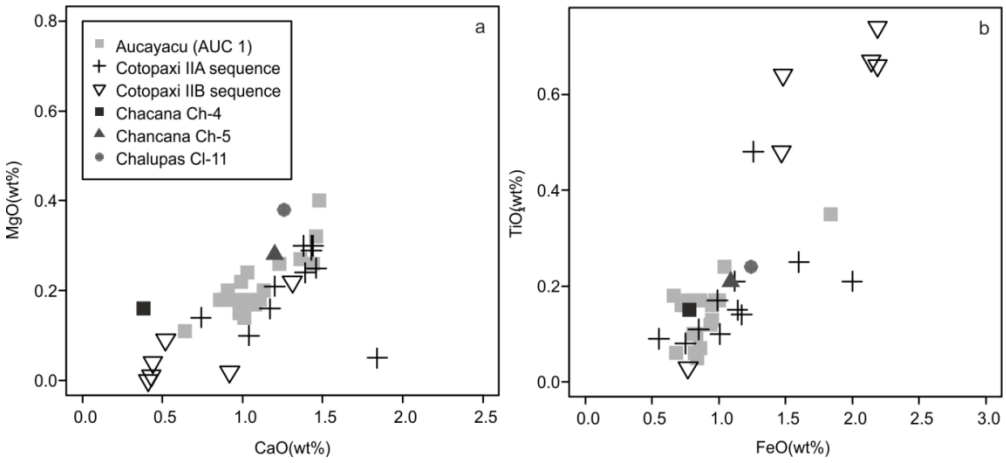

Fig 5. Co-variant plots of (a) CaO (%), MgO (%) (b) FeO (%), TiO_2 (%) values of the Aucayacu tephra glass shards as determined by EPMA plotted against the whole rock major values of volcanic rocks from the Chacana-Chalupas caldera region determined by X-ray fluorescence [51] and glass geochemical data for Cotopaxi determined by EPMA (Cotopaxi IIA and IIB sequences from the Holocene and late Pleistocene) [52]. Major element totals are normalised to 100%.

Our work shows that volcanic ash has been deposited more than once in Amazonia in the recent past. Given the close proximity of Amazonia to major volcanic chains of the Andes, the basin is likely to have been affected by volcanic ash fall throughout the Holocene. Analysis of the deeper peats (~7.5 m) at Aucayacu, for example, is likely to reveal a tephra record spanning a considerable proportion of the Holocene (peat initiation at c. 8870 cal. BP [28]). However, further work on a network of peatlands and lakes of Amazonia is needed to understand the long-term tephra record across the region. One problem is the current lack of a tephra geochemical database (e.g. Tephrabase for Europe [54]) for northern South America, making geochemical cross correlations difficult. Our work indicates that tephra glass shards are preserved for long periods of time and show no indication of either visible damage e.g. silica gel layer formation or pitting (cf.[40]) or geochemical changes (e.g. low total oxide values, fluctuation in alkaline elements) even in dynamic Amazonian peatlands with a pH of <4 and where the temperature (and thus rate of chemical and biological attack [55]) is likely to be higher than in northern peatlands.

Tephras may provide an important tool for correlating and dating palaeoenvironmental records from Amazonia and enable the determination of spatio-temporal variability in ecological dynamics and responses of ecosystems to changing climate. Furthermore, the AUC1 tephra may form an important isochron for dating and correlation of the recent part of tropical peatlands in western Amazonia which has implications for understanding recent changes, from the Little Ice Age to present. Tropical peatlands are highly dynamic in terms of biological activity (bioturbation) and hydrological regime. Amazonian peatlands are also affected by river flooding that is a significant factor for the reworking of microfossils. Tephra layers represent a discrete event in time; analysis of the structure of tephra layers in peat cores can offer a powerful tool to detect reworking with important implications for palaeoecological studies.

Tephra layers represent unequivocal evidence of deposition from ash clouds. As a result of the remote nature of much of Amazonia, written records of volcanic activity are unlikely to span more than a few centuries. In addition, proximal tephra records are often eroded or overlain by material from subsequent eruptions and therefore provide incomplete records of past volcanic activity. In these situations cryptotephras offer a complimentary approach to understanding the frequency of past explosive volcanic

eruptions and the spatial extents of ash clouds [9,56]. Further research into cryptotephra deposits in the Amazon basin may provide some information on volcanic activity in this region.

Ash fall from volcanic eruptions is known to have significant impacts on vegetation that vary from short- to long-term [57,58].The unequivocal evidence of ash clouds over Amazonia presented here highlights that the region has experienced the fallout products of volcanism. This raises the question of how much volcanic activity has impacted plant communities and plant function within this important ecosystem over time. Investigating the peat record could help to gain a further understanding of both the impact of volcanic activity on the plants of the Amazon basin and also of how wide-spread these impacts may be. When combined with palaeoecological records, cryptotephra layers offer the opportunity to consider plant community responses to volcanic events [59,60].

As well as highlighting the opportunities for the development of tephrochronology for the dating of peatlands and lakes in Amazonia, this first discovery of cryptotephra in Amazonia indicates that volcanism has deposited volcanic ash and possibly volcanic gases over Amazonia. We suggest that this paper highlights the potential for future research into the tephrochronology and past ecology of this important region.

4.5 Conclusions

We present information on the first microscopic tephra layer found in a peatland in western (Peruvian) Amazonia. Electron probe microanalysis provides geochemical data for the tephra that indicates a rhyolitic major element geochemistry. Radiocarbon dating suggests the AUC1 tephra fell between AD 1769 and 1970.

We suggest, based on the proximity to the Aucayacu peatland, geochemistry, and records of late Holocene volcanic activity that the most likely source for the AUC1 tephra is a volcano in the Ecuadorian Eastern Cordillera (0–1°S, 78-79°W).

This represents the first discovery of a historic microscopic tephra (cryptotephra) from Amazonia. The tephra layer may provide a new isochron for precise dating and

correlation of palaeoenvironmental records from peatlands and lakes in western Amazonia.

The discovery of two tephra layers in the top 1 m of peat at Aucayacu demonstrates that cryptotephra layers can be preserved in the aggressive environments of Amazonian peatlands (low pH and high temperatures) and presents an opportunity for further research into the tephrochronology of this region.

Distal tephra layers in Amazonia may also provide much needed information on the frequency of volcanic activity and the characteristics of ash clouds in this region.

Further research is required; the presence of cryptotephra layers in Amazonian peatlands has important implications for understanding the influence of volcanic activity on the functioning of Amazonian vegetation communities. The possible impact of volcanic ash and gas fallout on the functioning of these communities is yet to be assessed.

Acknowledgements

This research was undertaken while Elizabeth Watson was in possession of a NERC funded Doctoral Training Grant NE/K500847/1. Graeme Swindles was funded by a Royal Society research grant (grant no. 481831). We thank Outi Lähteenoja for advice on accessing the Aucayacu peatland and Ricardo Farroñay Peramas and Denis del Castillo Torres of the Instituto de Investigaciones de la Amazonía Peruana in Iquitos for assisting with fieldwork planning. Aristidis Vasques is acknowledged for piloting the boats and helping us run the field campaign. Many thanks to Lucho Freyre and David Huayaban (villagers from Bellavista and Malvinas), Ed Turner and Chris Williams for assistance in the field. Freddie Draper is thanked for providing the Landsat image in Figure 1b. Kimberley Goodall is acknowledged for her assistance in the laboratory and we thank Chris Hayward for help with tephra geochemical analysis. Jonathan Castro and Constanza Bonadonna provided valuable advice for the identification of the volcanic (vent) source of the cryptotephra.

References

1 Hall, V. A. & Pilcher, J. R. Late-Quaternary Icelandic tephras in Ireland and Great Britain: detection, characterization and usefulness. *Holocene* **12**, 223-230, doi:10.1191/0959683602h1538rr (2002).

2 Lowe, D. J. Tephrochronology and its application: A review. *Quaternary Geochronology* **6**, 107-153, doi:10.1016/j.quageo.2010.08.003 (2011).

3 Swindles, G. T., De Vleeschouwer, F. & Plunkett, G. Dating peat profiles using tephra: stratigraphy, geochemistry and chronology *Mires and Peat* **7**, 1-9 (2010).

4 Rose, W. I. & Durant, A. J. Fine ash content of explosive eruptions. *Journal of Volcanology and Geothermal Research* **186**, 32-39, doi:http://dx.doi.org/10.1016/j.jvolgeores.2009.01.010 (2009).

5 Horwell, C. & Baxter, P. The respiratory health hazards of volcanic ash: a review for volcanic risk mitigation. *Bulletin of Volcanology* **69**, 1-24, doi:10.1007/s00445-006-0052-y (2006).

6 Casadevall, T. J. Volcanic ash and aviation safety: proceedings of the first international symposium, Seattle, Washington, July 1991. *US Geological Survey Bulletin* **2047** (1994).

7 Dugmore, A. Icelandic volcanic ash in Scotland. *Scottish Geographical Magazine* **105**, 168-172, doi:10.1080/14702548908554430 (1989).

8 Pilcher, J. R. & Hall, V. A. Towards a tephrochronology for the Holocene in the north of Ireland *The Holocene* **2** 255-259 (1992).

9 Lawson, I. T., Swindles, G. T., Plunkett, G. & Greenberg, D. The spatial distribution of Holocene cryptotephras in north-west Europe since 7 ka: implications for understanding ash fall events from Icelandic eruptions. *Quaternary Science Reviews* **41**, 57-66, doi:10.1016/j.quascirev.2012.02.018 (2012).

10 Abbott, P. M. & Davies, S. M. Volcanism and the Greenland ice-cores: the tephra record. *Earth-Science Reviews* **115**, 173-191, doi:10.1016/j.earscirev.2012.09.001 (2012).

11 Satow, C. *et al.* A new contribution to the Late Quaternary tephrostratigraphy of the Mediterranean: Aegean Sea core LC21. *Quaternary Science Reviews* **117**, 96-112, doi:http://dx.doi.org/10.1016/j.quascirev.2015.04.005 (2015).

12 Hayward, C. High spatial resolution electron probe microanalysis of tephras and melt inclusions without beam-induced chemical modification. *Holocene* **22**, 119-125, doi:10.1177/0959683611409777 (2012).

13 Jensen, B. J. L. *et al.* Transatlantic distribution of the Alaskan White River Ash. *Geology* **42**, 875-878, doi:10.1130/g35945.1 (2014).

14 Lane, C. S., Chorn, B. T. & Johnson, T. C. Ash from the Toba supereruption in Lake Malawi shows no volcanic winter in East Africa at 75 ka. *Proceedings of the National Academy of Sciences* **110**, 8025-8029 (2013).

15 Zhao, H. & Hall, V. A. Assessing the potential for cryptotephra studies in Northeastern China. *The Holocene* **doi:10.1177/0959683615569320**, doi:10.1177/0959683615569320 (2015).

16 Pyne-O'Donnell, S. D. F. *et al.* High-precision ultra-distal Holocene tephrochronology in North America. *Quaternary Science Reviews* **52**, 6-11, doi:10.1016/j.quascirev.2012.07.024 (2012).

17 Gehrels, M. J., Lowe, D. J., Hazell, Z. J. & Newnham, R. M. A continuous 5300-yr Holocene cryptotephrostratigraphic record from northern New Zealand and implications for tephrochronology and volcanic hazard assessment. *Holocene* **16**, 173-187, doi:10.1191/0959683606hl1918rp (2006).

18 Ponomareva, V. *et al.* Identification of a widespread Kamchatkan tephra: A middle Pleistocene tie-point between Arctic and Pacific paleoclimatic records. *Geophysical Research Letters* **40**, 3538-3543, doi:10.1002/grl.50645 (2013).

19 de Silva, S. L. & Zielinski, G. A. Global influence of the AD 1600 eruption of Huaynaputina, Peru. *Nature* **393**, 455-458 (1998).

20 Juvigné, E. *et al.* Retombées volcaniques dans des tourbières et lacs autour du massif des Nevados Ampato et Sabancaya (Pérou méridional, Andes Centrales). *Quaternaire. Revue de l'Association française pour l'étude du Quaternaire* **19**, 157-173 (2008).

21 Wastegård, S. *et al.* Towards a late Quaternary tephrochronological framework for the southernmost part of South America – the Laguna Potrok Aike tephra record. *Quaternary Science Reviews* **71**, 81-90, doi:http://dx.doi.org/10.1016/j.quascirev.2012.10.019 (2013).

22 Roland, T. P. Holocene tephrochronology on southern Patagonia: Development and incorporation of cryptotephra framework. *Quaternary Newsletter* **135**, 48-52 (2015).

23 Page, S. E., Rieley, J. O. & Banks, C. J. Global and regional importance of the tropical peatland carbon pool. *Glob. Change Biol.* **17**, 798-818, doi:10.1111/j.1365-2486.2010.02279.x (2011).

24 Moore, S. *et al.* Deep instability of deforested tropical peatlands revealed by fluvial organic carbon fluxes. *Nature* **493**, 660-663, doi:http://www.nature.com/nature/journal/v493/n7434/abs/nature11818.html#supplementary-information (2013).

25 Anderson, J. The structure and development of the peat swamps of Sarawak and Brunei. *The Journal of Tropical Geography* **18**, 716 (1964).

26 Joosten, H. The global peatland CO2 picture. *Wetlands International, Ede* **33** (2009).

27 Lähteenoja, O., Ruokolainen, K., Schulman, L. & Oinonen, M. Amazonian peatlands: an ignored C sink and potential source. *Glob. Change Biol.* **15**, 2311-2320 (2009).

28 Lähteenoja, O. *et al.* The large Amazonian peatland carbon sink in the subsiding Pastaza‐Marañón foreland basin, Peru. *Glob. Change Biol.* **18**, 164-178 (2012).

29 Lähteenoja, O. & Page, S. High diversity of tropical peatland ecosystem types in the Pastaza-Marañón basin, Peruvian Amazonia. *Journal of Geophysical Research: Biogeosciences* **116**, G02025, doi:10.1029/2010JG001508 (2011).

30 Draper, F., C. *et al.* The distribution and amount of carbon in the largest peatland complex in Amazonia. *Environmental Research Letters* **9**, 124017 (2014).

31 Roucoux, K. H. *et al.* Vegetation development in an Amazonian peatland. *Palaeogeography, Palaeoclimatology, Palaeoecology* **374**, 242-255, doi:http://dx.doi.org/10.1016/j.palaeo.2013.01.023 (2013).

32 Lawson, I. T., Jones, T. D., Kelly, T. J., Coronado, E. N. H. & Roucoux, K. H. The geochemistry of Amazonian peats. *Wetlands* **34**, 905-915 (2014).

33 Swindles, G. T. *et al.* Ecology of testate amoebae in an Amazonian peatland and development of a transfer function for palaeohydrological reconstruction. *Microbial ecology* **68**, 284-298 (2014).

34 Jowsey, P. An improved peat sampler. *New Phytologist* **65**, 245-248 (1966).

35 De Vleeschouwer, F., Chambers, F. M. & Swindles, G. T. Coring and sub-sampling of peatlands for palaeoenvironmental research. *Mires and Peat* **7**, 1-10 (2011).

36 Chambers, F. M., Beilman, D. W. & Yu, Z. Methods for determining peat humification and for quanitifying peat bulk density, organic matter and carbon content for palaeostudies of climate and peatland carbon dynamics *Mires and Peat* **7**, 1-10 (2010).

37 Roos-Barraclough, F., Van Der Knaap, W., Van Leeuwen, J. & Shotyk, W. A Late-glacial and Holocene record of climatic change from a Swiss peat humification profile. *The Holocene* **14**, 7-19 (2004).

38 Reimer, P. J. *et al.* IntCal13 and Marine13 Radiocarbon Age Calibration Curves 0–50,000 Years cal BP. *Radiocarbon* **55**, 1869-1887 (2013).

39 Blaauw, M. Methods and code for 'classical' age-modelling of radiocarbon sequences. *Quaternary Geochronology* **5**, 512-518 (2010).

40 Blockley, S. P. E. *et al.* A new and less destructive laboratory procedure for the physical separation of distal glass tephra shards from sediments. *Quaternary Science Reviews* **24**, 1952-1960, doi:10.1016/j.quascirev.2004.12.008 (2005).

41 Dugmore, A. J., Newton, A. J., Sugden, D. E. & Larsen, G. Geochemical stability of fine-grained silicic Holocene tephra in Iceland and Scotland. *Journal of Quaternary Science* **7**, 173-183, doi:10.1002/jqs.3390070208 (1992).

42 Crosweller, H. *et al.* Global database on large magnitude explosive volcanic eruptions (LaMEVE). *Journal of Applied Volcanology* **1**, 1-13, doi:10.1186/2191-5040-1-4 (2012).

43 Fittkau, E. J. *Biogeography and Ecology in South-America*. Vol. 2 (Springer Science & Business Media, 1969).

44 Global Volcanism Program. *Volcanoes of the World, v. 4.3.4.* , <http://dx.doi.org/10.5479/si.GVP.VOTW4-2013> (2013).

45 Calvache V, M. L. & Williams, S. N. Geochemistry and petrology of the Galeras Volcanic Complex, Colombia. *Journal of Volcanology and Geothermal Research* **77**, 21-38, doi:http://dx.doi.org/10.1016/S0377-0273(96)00084-4 (1997).

46 Samaniego, P. *et al.* The historical (218 ± 14 aBP) explosive eruption of Tutupaca volcano (Southern Peru). *Bulletin of Volcanology* **77**, 1-18, doi:10.1007/s00445-015-0937-8 (2015).

47 Self, S., Rampino, M. R., Zhao, J. & Katz, M. G. Volcanic aerosol perturbations and strong El Niño events: No general correlation. *Geophysical Research Letters* **24**, 1247-1250, doi:10.1029/97GL01127 (1997).

48 Hall, M. & Mothes, P. The rhyolitic–andesitic eruptive history of Cotopaxi volcano, Ecuador. *Bulletin of Volcanology* **70**, 675-702, doi:10.1007/s00445-007-0161-2 (2008).

49 Pistolesi, M. *et al.* Physical volcanology of the post–twelfth-century activity at Cotopaxi volcano, Ecuador: Behavior of an andesitic central volcano. *Geological Society of America Bulletin* **doi:10.1130/B30301.1**, doi:10.1130/b30301.1 (2011).

50 Hall, M. L., Samaniego, P., Le Pennec, J. L. & Johnson, J. B. Ecuadorian Andes volcanism: A review of Late Pliocene to present activity. *Journal of Volcanology and Geothermal Research* **176**, 1-6, doi:http://dx.doi.org/10.1016/j.jvolgeores.2008.06.012 (2008).

51 Bryant, J., Yogodzinski, G., Hall, M., Lewicki, J. & Bailey, D. Geochemical constraints on the origin of volcanic rocks from the Andean Northern Volcanic Zone, Ecuador. *Journal of Petrology* **47**, 1147-1175 (2006).

52 Garrison, J. M., Davidson, J. P., Hall, M. & Mothes, P. Geochemistry and Petrology of the Most Recent Deposits from Cotopaxi Volcano, Northern

Volcanic Zone, Ecuador. *Journal of Petrology*, doi:10.1093/petrology/egr023 (2011).

53 Le Maitre, R. W. *et al. A classification of igneous rocks and glossary of terms: Recommendations of the International Union of Geological Sciences Subcommission on the Systematics of Igneous Rocks*. Vol. 193 (Blackwell Oxford, 1989).

54 Newton, A. J., Dugmore, A. J. & Gittings, B. M. Tephrabase: tephrochronology and the development of a centralised European database. *Journal of Quaternary Science* **22**, 737-743, doi:10.1002/jqs.1094 (2007).

55 Wolff-Boenisch, D., Gislason, S. R., Oelkers, E. H. & Putnis, C. V. The dissolution rates of natural glasses as a function of their composition at pH 4 and 10.6, and temperatures from 25 to 74°C. *Geochim. Cosmochim. Acta* **68**, 4843-4858, doi:10.1016/j.gca.2004.05.027 (2004).

56 Swindles, G. T., Lawson, I. T., Savov, I. P., Connor, C. B. & Plunkett, G. A 7000 yr perspective on volcanic ash clouds affecting northern Europe. *Geology* **39**, 887-890, doi:10.1130/g32146.1 (2011).

57 Antos, J. A. & Zobel, D. B. in *Ecological responses to the 1980 eruption of Mount St. Helens* (eds V. H. Dale., F.J. Swanson, & C.M. Crisafulli) 47-58 (Springer, 2005).

58 De Schutter, A. *et al.* Ash fall impact on vegetation: a remote sensing approach of the Oldoinyo Lengai 2007–08 eruption. *Journal of Applied Volcanology* **4**, 15 (2015).

59 Payne, R., Edwards, K. & Blackford, J. Volcanic impacts on the Holocene vegetation history of Britain and Ireland? A review and meta-analysis of the pollen evidence. *Vegetation History and Archaeobotany* **22**, 153-164, doi:10.1007/s00334-012-0359-x (2013).

60 Hall, V. A., Pilcher, J. R. & McCormac, F. G. Icelandic volcanic ash and the mid-Holocene Scots pine (Pinus sylvestris) decline in the north of Ireland: no correlation. *The Holocene* **4**, 79-83, doi:10.1177/095968369400400110 (1994).

Chapter 5: Do peatlands or lakes provide the most comprehensive distal tephra records?

Watson, E.J.*[1], Swindles, G.T.[1], Lawson, I.T.[2], Savov, I.P.[3]

[1]School of Geography, University of Leeds, Leeds, LS2 9JT, UK
[2]Department of Geography and Sustainable Development, University of St Andrews, St Andrews, KY16 9AL, UK
[3]School of Earth and Environment, University of Leeds, Leeds, LS2 9JT, UK
**Corresponding author: Elizabeth Watson (gy08ejw@leeds.ac.uk)*
Manuscript for: Quaternary Science Reviews

Keywords: Tephrochronology, cryptotephra, northern Europe, Holocene, basalt

Abstract

Despite the widespread application of tephra studies for dating and correlation of stratigraphic sequences ('tephrochronology'), questions remain over the reliability and replicability of tephra records from lake sediments and peats, particularly in sites >1000 km from source volcanoes. To address this, we examine the tephrostratigraphy of four pairs of lake and peatland sites in close proximity to one another (<10 km), and evaluate the extent to which the microscopic (crypto-) tephra records in lakes and peatlands differ. The peatlands typically record more cryptotephra layers than nearby lakes, but cryptotephra records from high-latitude peatlands can be incomplete, possibly due to tephra fallout onto snow and subsequent redistribution across the peatland surface by wind and during snowmelt. We find no evidence for chemical alteration of glass shards in peatland or lake environments over the time scale of this study (mid- to late-Holocene). Instead, the low number of basaltic cryptotephra layers identified in distal peatlands reflects the capture of only primary tephra-fall, whereas lakes concentrate tephra falling across their catchments which subsequently washes into the lake, adding to the primary tephra fallout received in the lake. A combination of records from both lakes and peatlands must be used to establish the most comprehensive and complete regional tephrostratigraphies. We also describe two previously unreported late Holocene cryptotephras and demonstrate, for the first time, that Holocene Icelandic ash clouds frequently reached Arctic Sweden.

5.1 Introduction

Tephrochronology can be defined as the use of tephra (volcanic ash) layers for the dating and correlation of stratigraphic profiles. The technique was initially developed using visible tephra layers in Iceland (Thorarinsson, 1944), but the discovery of Icelandic tephra layers on the Faroe Islands and in Scandinavia allowed the extension of tephrochronology into regions further away from source volcanoes (e.g. Persson, 1966; 1968). The potential of distal tephrochronology was further advanced by the discovery of microscopic layers of volcanic ash ('cryptotephras') in peatlands, lakes, ice and marine cores across the North Atlantic and northern Europe (Dugmore *et al*., 1995; Gudmundsdóttir *et al*., 2011). Widespread tephra and cryptotephra layers can now be used to correlate stratigraphic sequences in different depositional environments and provide tie points for climate reconstructions across regions (Davies *et al*., 2012; Lane *et al*., 2013).

Despite the widespread application of cryptotephras for the dating and correlation of stratigraphic sequences, and more recently as a record of ash cloud frequency (Swindles *et al*., 2011, 2013b), there remain a number of questions over the chronostratigraphic reliability of cryptotephra layers in terrestrial archives. There is evidence for the gradual in-washing, within-basin focussing and re-deposition of cryptotephra layers in lakes (Davies *et al*., 2007; Pyne-O'Donnell, 2011). In peatlands, which have been proposed to record primary tephra-fall material, patchy tephra distribution patterns can occur due to fallout onto snow (Bergman *et al*., 2004), and there is evidence for the movement of tephra-derived glass shards across the peat surface by wind or water (Payne and Gehrels, 2010; Swindles *et al*., 2013a; Watson *et al*., 2015). Furthermore, despite the dominance of basaltic over silicic volcanism in Iceland and the potential for phreatomagmatic eruptions which have been shown to distribute fine ash over long distances, only five cryptotephras of basaltic composition have been detected in N. European sites over the last 7000 years, mostly in lake sediments (Lawson *et al*., 2012). This is in contrast to ~80 silicic cryptotephras which have been widely identified in both peatlands and lakes (silicic > 63% SiO_2: Dugmore *et al*., (1995)).

In this paper we investigate Holocene tephra records from lakes and peatlands in close proximity to one another (<10 km apart). Based on the assumption that both lake and

peatland have received the same primary tephra-fall deposits, we aim to evaluate whether they record the same or different tephrostratigraphies. In addition, we evaluate the differential preservation of glass (tephra) shards in lakes versus peatlands.

5.2 Site description

Four pairs of sites in northern Europe (each comprised of one lake and one peatland) were identified using the following criteria: 1) close proximity (< 10 km apart); 2) coverage of a range of meteorological conditions (e.g. high-latitude sites where tephra might be more likely to fall out onto snow, see Fig. 1); and 3) coverage of a range of different peatland and lake types (spanning a range of preservation conditions including acidic peatlands and alkaline lakes). Sites were favoured if prior information on basal age or outline chronology was available. A brief description of each site is given below; sites are listed according to their location on a south-west to north-east transect. Detailed information on site characteristics can be found in Table 1 and photos of each site can be found in Fig. S1.

Site	Lake or peatland (L/P)	Location (decimal degrees)	Elevation (m a.s.l.)	Site type	pH (at time of sampling)	Mean annual precipitation (mm y^{-1})	Mean annual Temperature	Water depth (cm)	Length of core (cm)	Distance between lake and peatland
Claraghmore Lake	L	54.631°N, 7.450°W	78	Small lake	6.5	1000-1200[4]	4°C in January 15°C in July[4]	350	450	0.3 km Bearing of 310°
Claraghmore Bog	P	54.633°N, 7.454°W		Raised bog	N/A			NA	910	
Malham Tarn Lake	L	54.096°N, 2.165°W	380	Small marl lake	8.2	1502[2]	6.9°C[3]	250	310	0.5 km Bearing of 282°
Malham Tarn Moss	P	54.097°N, 2.173°W		Raised bog	N/A			NA	640	
Lake Svartkälsjärn	L	64.264°N, 19.552°E	260	Small lake	6.7	520	2°C with average temperatures of -12°C in January and 15°C in July[1]	312	203	~9 km Bearing of 176°
Degerö Stormyr	P	64.181°N, 19.564°E	270	Acid bog complex	4.3			NA	440	
Sammakovuoma Lake	L	66.992°N, 21.500°E	237	Small lake	7.0	480[5]	-2 to -3 °C[6] -1.5 °C[5]	350	240	1.9 km Bearing of 280°
Sammakovuoma Bog	P	66.995°N, 21.457°E		Acid bog complex	5.9			NA	440	

Table 1. Location and characteristics of each of the lake and peatland sites included in this study. Shading indicates the pairing of peatland and lake sites. The climatic data refer to the following periods and sources: 1 = 1951-1980 (Sweeney, 1997); 2 = 1961-2000 (Burt and Horton, 2003); 3 = 1959-2000 (Burt and Horton, 2003); 4 = 1961-1990 (Alexandersson *et al*., 1991); 5 = (1961-1990) (Norwegian Meteorological Institute, 2015) 6 = 1961-1990 (Tveito *et al*., 2000).

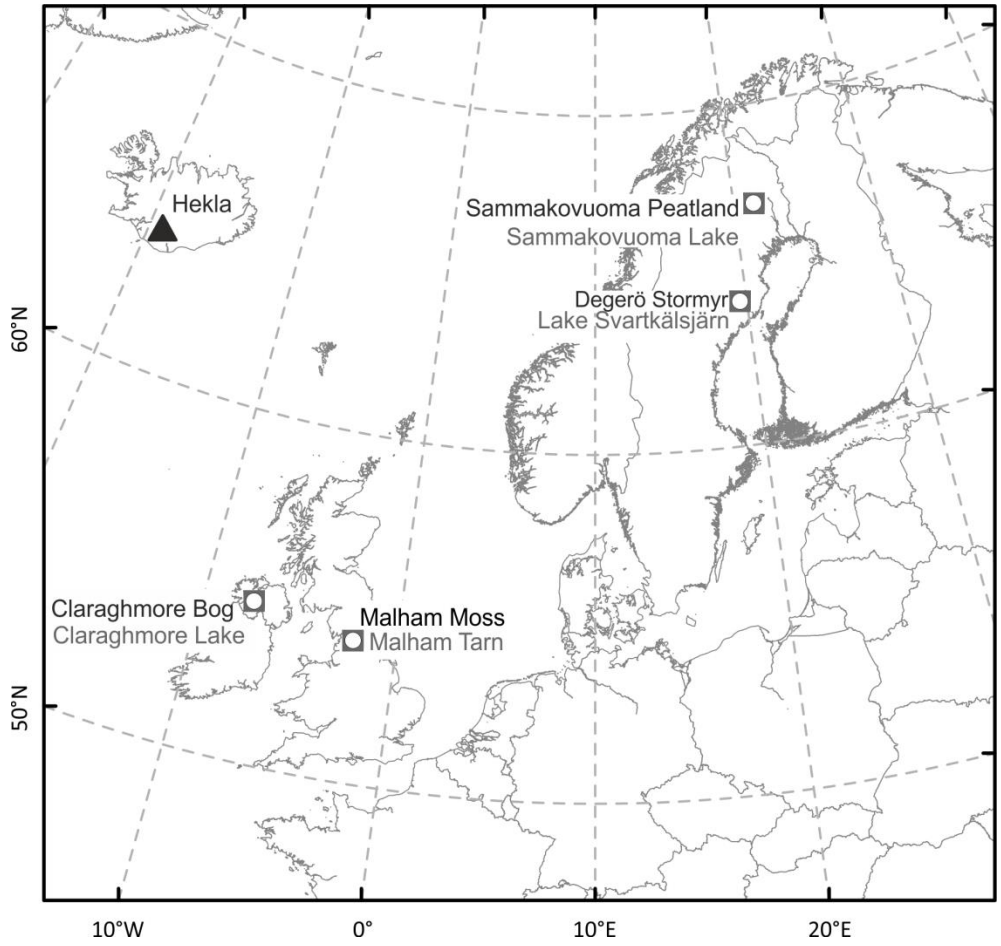

Fig. 1. Map showing the location of lake (grey square) and peatland (white circle) sites sampled in this study. The black triangle indicates the location of the Hekla volcano, the source for the majority of widespread late Holocene tephras in northern Europe.

5.2.1 Site 1: Claraghmore, Northern Ireland

Claraghmore bog is an intact raised bog. Previous palaeoecological studies suggest the site contains a peat record spanning much of the Holocene (Plunkett, 2006; 2009). Claraghmore Lake is one of two small lakes which lie at the bottom of a shallow slope immediately adjacent to the peatland. The lake is approximately 100 metres in length, with a maximum water depth of 3.5 m at the time of sampling, and is bordered by *Quercus* and *Corylus* woodland. The lake margins are characterised by fens containing *Cyperaceae* and *Poaceae*. Lake sediments are composed of gyttja. To the best of our knowledge this study represents the first palaeoenvironmental investigation of this lake.

5.2.2 Site 2: Malham, England

Malham Moss is an ombrotrophic raised bog adjacent to Malham Tarn (lake). Over the last c. 8000 years *Sphagnum* peat has accumulated in Malham Moss up to a depth of up to 6 m (Pigott and Pigott, 1963). Malham Tarn is ~600 meters in length and the lake sediments, which span more than 6 m, are composed mainly of *Chara* marls. The average water depth is ~2.5 m. The lake is fed by springs and its waters are alkaline (pH = 8.2: Pentecost, (2009)). Previous palaeoecological research suggests a basal age for the lake sediments of c.12 000 cal yr BP (Nuñez *et al*., 2002).

5.2.3 Site 3: Lake Svartkälsjärn and Degerö Stormyr, Sweden

Degerö Stormyr and Lake Svartkälsjärn are located in the Västerbotten region of northern Sweden. Degerö Stormyr is an acid peatland complex with an area of 6.5 km^2 and peat depth of 3–8 m. The deepest peat has an age of c. 8000 cal yr BP (Nilsson *et al*., 2008). Lake Svartkälsjärn is a small lake with a total area of c. 0.05 km^2, catchment area of c. 2.5 km^2 and a water depth of 3.1 m at the time of sampling. Lake sediments are composed mainly of gyttja. Previous paleoecological research suggests the lacustrine sediment record (2.2 m) spans the period from 10,000 cal yr BP to present (Barnekow *et al*., 2008).

5.2.4 Site 4: Sammakovuoma, Sweden

The Sammakovuoma sites in northern Sweden represent the most northerly locations in this study. Radiocarbon dating suggests a peatland age of 9260 cal yr BP (depth 4.6 m) (Matts Nilsson, personal comm.). Lake Sammakovuoma is a small lake (c. 400 m in length) with a water depth of 3.5 m at the time of sampling. Lake sediments are composed mainly of gyttja. The catchment vegetation comprises forest dominated by *Pinus.* The lake catchment also contains areas of bog and fen. To the best of our knowledge this study represents the first palaeoenvironmental investigation of this lake.

5.3 Methods

5.3.1 Field sampling

Where possible, cores from peatlands were extracted from areas containing the deepest peat. Lake cores were extracted from the middle of each lake in an attempt to minimise the risk of obtaining sediments exposed to reworking during previous lake level fluctuations. Samples were taken either from the peatland surface or from a small boat using a Russian D-section corer with either a 50 or 100 cm barrel length (sample diameter 5 cm and 9 cm respectively) following the parallel hole method (De Vleeschouwer *et al*., 2011).

5.3.2 Organic matter content

Organic matter content was determined through loss-on-ignition (LOI) which was conducted on adjacent 5-10 cm intervals on all cores. Samples were oven dried at 105°C for 24 hours, weighed and combusted in a furnace at 550°C for 4 hours following procedures described in detail in Chambers *et al*. (2010).

5.3.3 Tephra analysis

All cores were sub-sampled at 5–10 cm intervals, then combusted at 550°C and treated with 10% HCl (Hall and Pilcher, 2002; Swindles *et al*., 2010). Samples containing mineralogical material or biogenic silica required sieving at 10 µm in an ultrasonic bath (no coarse sieving e.g. 125 µm required) and, in some instances (all lake sites and the Swedish peatlands), separation using heavy liquid floatation (Blockley *et al*., 2005). All residues (including heavy fractions) were examined to ensure extraction had been successful. Residues were rinsed thoroughly in deionised water, mounted onto glass slides using Histomount and examined on a Leica binocular microscope at x200 and x400 magnification. Where glass shards were identified, subsampling was repeated at 1 cm intervals. Comparing the number of shards (n shards g^{-1}) in the peak sample identified in a lake and peatland is not possible due to the difference in dry bulk density between peat and lake sediments. However, in order to give some indication of the

relative concentrations of glass shards in peatlands and lakes, the total shard counts for each cryptotephra layer per cm^2 (total tephra deposited per square centimetre of peatland/sediment surface) were calculated by summing the numerical glass shard counts for all the depth samples within that layer (Table 2).

Tephra shards from peatlands with low minerogenic content were extracted for geochemical analysis using the acid digestion method (Dugmore *et al*., 1992). Samples were treated with conc. HNO_3 and H_2SO_4 before sieving the residue at 10 µm and rinsing with deionised water. Samples containing minerogenic material were extracted using heavy density liquids (cleaning float 2.25 g cm^{-3}, retaining float 2.50 g cm^{-3}) (Blockley *et al*., 2005). Information on the extraction method and ID code for each tephra sample is given in Table 2.

Site	Depth in sediment/ peat (cm)	Sample ID	Tephra(s)	Age	Geochemical composition	Total shards (cm^{-2})	Total shards analysed (*n*)	References
Claraghmore bog	44-48	CLA-B1†	Öræfajökull 1362 Hekla 1510?	c. AD 1362	Rhyolitic 1 Basaltic shard	30	7	Dugmore *et al*., (1995); Hall and Pilcher,(2002); Larsen *et al*., (1999); Pilcher *et al*., (2005); Pilcher *et al*., (1995, 1996)
	58-61	CLA-B2†	Unknown #4 Mix?	*721-726 cal yr BP (724 BP)*	Mixed composition	75	20	n/a
	73-77	CLA-B2a†	Hekla 1104	AD 1104	Rhyolitic	21	4	Hall and Pilcher, (2002); Larsen *et al*., (1999); Pilcher *et al*., (2005); Pilcher *et al*., (1995, 1996)
	87-90	CLA-B3†	MOR-T4	c. AD 1000	Rhyolitic-Dacitic	20	20	Chambers *et al*., (2004)
	108-110	CLA-B4†	AD860B	AD 846-848	Rhyolitic	51	12	Hall and Pilcher, (2002); Pilcher *et al*., (1995); Swindles, (2006)
	241-244	CLA-B5†	Microlite GB4-150	2705 - 2630 cal yr BP 2750 - 2708 cal yr BP	Rhyolitic Dacitic-Trachydacitic	13	17	Hall and Pilcher, (2002); Swindles, (2006)
	415-418	CLA-B6-B7†	Hekla 4 Silk N2	4345 - 4229 cal yr BP 4345 - 4229 cal yr BP	Rhyolitic-Dacitic Dacitic-Trachydacitic	73	29	Dugmore and Newton, (1992); Pilcher *et al*., (2005); Pilcher and Hall, (1996); Plunkett *et al*., (2004); Zillen *et al*., (2002)
	868-870	CLA-B8†	Lairg A	6947- 6852 cal yr BP	Rhyolitic	79	4	Dugmore *et al*., (1995); Hall and Pilcher, (2002); Pilcher *et al*., (2005); Pilcher *et al*., (1996)
Claraghmore lake	110-113	CLA-L1	Unknown #3	Post AD 1000	Basaltic	141	19	n/a
	145-149	CLA-L2	MOR-T4	c. AD 1000	Rhyolitic-Dacitic	42	2	Chambers *et al*., (2004)
	206-208	CLA-L3	Hekla 4	4345 - 4229 cal yr BP	Rhyolitic-Dacitic	26	1	Dugmore and Newton, (1992); Pilcher *et al*., (2005); Pilcher and Hall, (1996); Zillen *et al*., (2002)
	328-331	CLA-L4	Lairg B	6724 - 6627 cal yr BP	Rhyolitic	275	21	Dugmore *et al*., (1995); Pilcher *et al*., (1996)
	332-338	CLA-L5	Lairg A	6947 - 6852 cal yr BP	Rhyolitic	723	20	Dugmore *et al*., (1995); Hall and Pilcher, (2002); Pilcher *et al*., (1996)
Malham Moss	123-125	MM-1†	Glen Garry	2210 - 1966 cal yr BP	Dacitic-Rhyolitic	131	12	Dugmore *et al*., (1995); Dugmore and Newton, (1992); Pilcher and Hall, (1996)
	323-328	MM-2†	Hekla 4	4345 - 4229 cal yr BP	Rhyolitic-Dacitic	221	10	Dugmore and Newton, (1992); Pilcher *et al*., (2005); Pilcher and Hall, (1996); Zillen *et al*., (2002)
	577-580	MM-3†	Lairg B	6724 - 6627 cal yr BP	Rhyolitic	23	4	Dugmore *et al*., (1995); Pilcher *et al*., (1996)
	595-598	MM-4†	Lairg A	6947- 6852 cal yr BP	Rhyolitic	152	10	Dugmore *et al*., (1995); Hall and Pilcher, (2002); Pilcher *et al*., (1996)
Malham Tarn	135-145	MT-1	Glen Garry	2210 - 1966 cal yr BP	Dacitic-Rhyolitic	85	15	Dugmore *et al*., (1995); Dugmore and Newton, (1992); Pilcher and Hall, (1996)
Degerö Stormyr	42-44	SV-B1†	Askja 1875	AD 1875	Rhyolitic	103	16	Larsen *et al*., (1999); Oldfield *et al*., (1997); Pilcher *et al*., (2005)

	71-74	SV-B2†	Hekla 1158 Hekla 1104	AD 1158 AD 1104	Dacitic Rhyolitic	186	15	Hall and Pilcher, (2002); Larsen *et al*., (1999); Pilcher *et al*., (2005); Pilcher *et al*., (1995, 1996)
	152-154	SV-B3†	Hekla 3	3037 - 2956 cal yr BP	Dacitic-Rhyolitic	51	21	Lawson *et al*., (2007); Zillen *et al*., (2002)
	180-183	SV-B4†	Hekla-S/Kebister	*4053 – 3886 cal yr BP (3968 BP)*	Dacitic-Rhyolitic	42	5	Dugmore *et al*., (1992); Wastegård *et al*., (2001); Zillen *et al*., (2002)
	190-193	SV-B5†	Hekla 4	4345 - 4229 cal yr BP	Rhyolitic-Dacitic	35	16	Dugmore and Newton, (1992); Pilcher *et al*., (2005); Pilcher and Hall, (1996); Zillen *et al*., (2002)
	237-240	SV-B6†	Lairg A	6947- 6852 cal yr BP	Rhyolitic	50	23	Dugmore *et al*., (1995); Hall and Pilcher, (2002); Pilcher *et al*., (2005); Pilcher *et al*., (1996)
Svartkälsjärn lake	11-18	SV-L1	Hekla 1104 Hekla 1158	AD 1104 AD 1158	Rhyolitic Dacitic	246	21	Hall and Pilcher, (2002); Larsen *et al*., (1999); Pilcher *et al*., (2005); Pilcher *et al*., (1995, 1996)
	41-44	SV-L2	QUB 570 Group 2 (c. AD 650)? (Unknown #2)	c. 2500- 2000cal yr BP*	Dacite-Andesite	147	20	Pilcher *et al*., (2005)
	79-82	SV-L3	Hekla 4	4345 - 4229 cal yr BP	Rhyolitic-Dacitic	303	21	Dugmore and Newton, (1992); Pilcher *et al*., (2005); Pilcher and Hall, (1996); Zillen *et al*., (2002)
	108-113	SV-L4	Unknown #5	c. 6000-5000 cal yr BP*	Rhyolitic-Dacitic	16	7	n/a
	123-128	SV-L5	Lairg A?	c. 6500-6000 cal yr BP*	Rhyolitic	40	10	Dugmore *et al*., (1995); Hall and Pilcher, (2002); Pilcher *et al*., (2005); Pilcher *et al*., (1996)
Sammakovuoma peatland	46-49	SB-1†	Hekla 1104	AD 1104	Rhyolitic	109	20	Hall and Pilcher, (2002); Larsen *et al*., (1999); Pilcher *et al*., (2005); Pilcher *et al*., (1995, 1996)
	67-70	SB-2†	SN-1 (Unknown #1)	1232-1226 *cal yr BP (1229 BP)*	Trachydacite	193	26	Larsen *et al*., (2002); Holmes *et al*., (2016)
Sammakovuoma lake	15-17	SL-1	Hekla 1104	AD 1104	Rhyolitic	539	8	Hall and Pilcher, (2002); Larsen *et al*., (1999); Pilcher *et al*., (2005); Pilcher *et al*., (1995, 1996)
	39-42	SL-2	SN-1 (Unknown #1)	*1781-1721 cal yr BP (1752 BP)*	Trachydacite	285	19	Larsen *et al*., (2002); Holmes *et al*., (2016)
	109-113	SL-3	Hekla 4	4345 - 4229 cal yr BP	Rhyolitic-Dacitic	828	35	Dugmore and Newton, (1992); Pilcher *et al*., (2005); Pilcher and Hall, (1996); Zillen *et al*., (2002)

Table 2. Cryptotephra layers detected in peatland and lake sites as part of this study. *= based on the age-depth model of Barnekow *et al*. (2008). Ages shown in Italics are based on age depth model (linear interpolation) from other dated tephras, median probability age given in brackets. †= Tephras extracted for geochemical analysis by the acid extraction method alone (c.f. Dugmore *et al*., 1992), or acid extraction followed by density separation. All other tephras were extracted using density separation only, following Blockley *et al*., (2005).

Glass shards were mounted onto glass slides (Dugmore *et al*., 1992) or into blocks (Hall and Hayward, 2014). All samples were polished to a 0.25 µm finish. Major element geochemistry for all samples excluding those from Malham Moss was analysed using a Cameca SX100 electron probe micro analyser (EPMA) at the University of Edinburgh. Small shard sizes necessitated the use of narrow beam sizes (3-5 µm) and the beam current was varied during each analysis to limit volatile element (Na and K) loss (Hayward, 2012). Glass shards from cryptotephra layers identified in Malham Moss were analysed using a 10 µm beam on the JEOL JXA8230 EPMA housed at the University of Leeds. In both locations, analyses were conducted at 15 kV (full analytical conditions are listed in Table S1). Secondary glass standards (Lipari obsidian and BCR-2G: Jochum *et al*., (2005)) were analysed before and after EPMA runs of unknown glass shard analyses. Assignments to specific eruptions were based on stratigraphy and visual comparison of tephra geochemistry with the Tephrabase database (Newton *et al*., 2007) and published literature using bi-plots of oxides.

5.3.4 Radiocarbon dates

Five radiocarbon dates were obtained for peatland sites on above-ground vegetation macrofossils which were picked from sieved samples (>125 µm) under a low power microscope. One radiocarbon date was obtained for Claraghmore lake. In this instance the lack of plant macrofossils in the lake sediment necessitated the extraction of a bulk sample. Samples of lake sediment and peat were pre-treated using the standard acid-alkali-acid treatment, digested in hot (80˚C) 1M HCl for 2 hours, hot (80˚C) 0.5M KOH for a further 2 hours and then re-treated with 1M HCl. Samples were rinsed thoroughly with de-ionised water between each acid/alkali stage and were submitted to Direct AMS, Seattle, USA for ^{14}C dating. All dates were calibrated using Calib 7.1 (Stuiver and Reimer, 1993) and the IntCal13 atmospheric curve (Reimer *et al*., 2013).

5.4 Results and discussion

5.4.1 Tephra correlations

Site 1: Claraghmore

Claraghmore bog contains tephra from nine eruptions in the form of eight cryptotephra layers (CLA-B6-B7 contains tephra from two eruptions) (Figs. 2 and 3). The majority of the cryptotephra layers identified at Claraghmore bog are silicic, of Icelandic provenance, and have previously been documented at other sites across Ireland. A small number of light brown shards in the top few centimetres of peat at Claraghmore bog were too sparse for geochemical analysis (3 shards cm^{-3}). These shards are similar in morphology and colour to shards from the eruption of Hekla 1947, which have previously been identified at multiple sites across Northern Ireland (Rea *et al*., 2012). Spheroidal carbonaceous particles (SCPs) were identified alongside these shards, suggesting that they were deposited after the Industrial Revolution which supports tentative assignment to the AD 1947 eruption of the Hekla volcano (Swindles and Roe, 2006; Swindles *et al*., 2015).

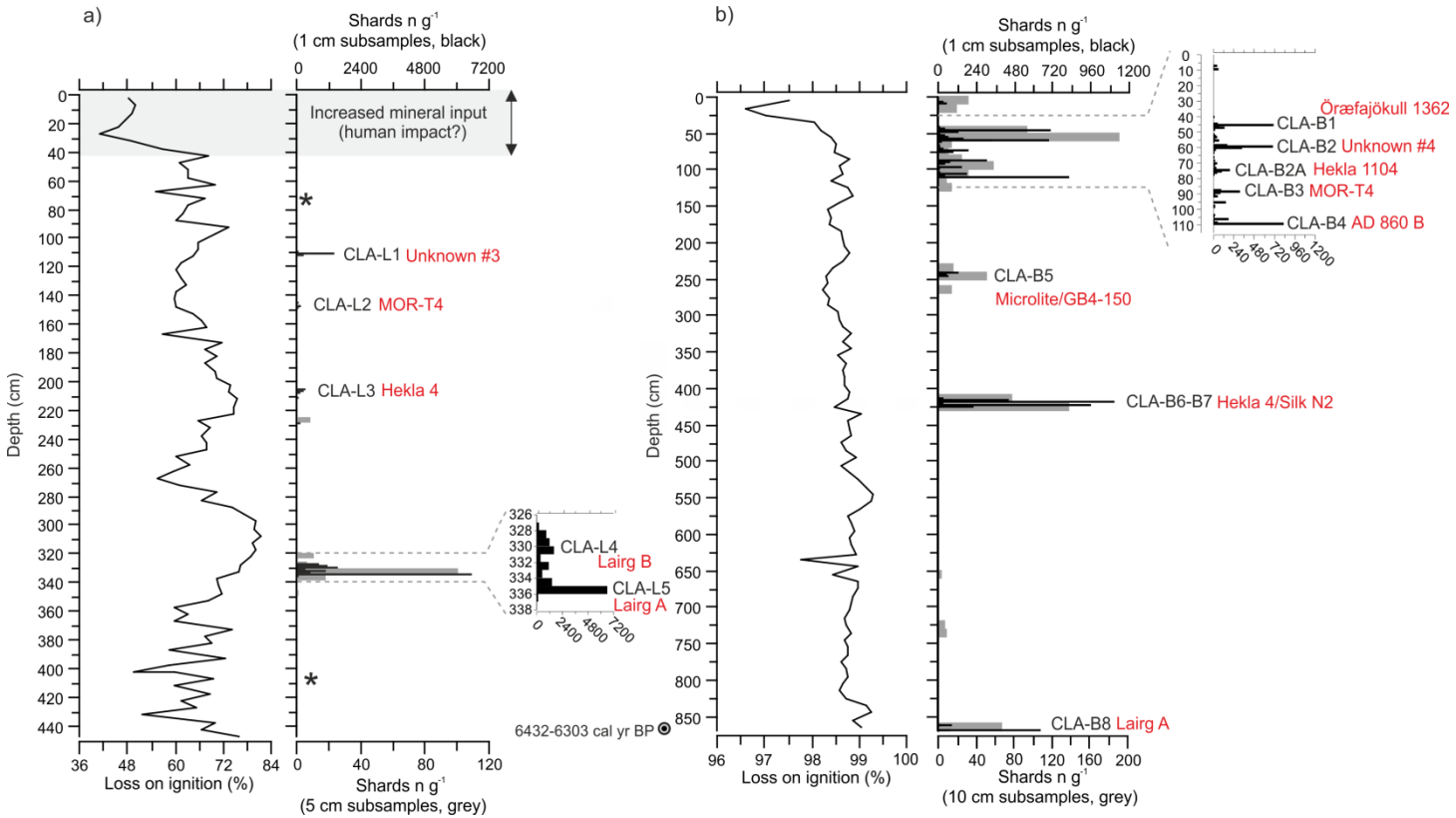

Fig. 2. Diagram showing the tephrostratigraphy and loss-on-ignition values at Claraghmore a) lake and b) bog. Tephra codes are indicated in black. Where assignments to a known tephra isochron have been made based on glass geochemistry and stratigraphy, these are indicated in red beside the tephra code. Tephras which could not be assigned to a known tephra isochron are marked as 'Unknown' and numbered. Samples containing traces of shards (<5 shards) are indicated by an asterisk. An area of increased mineral input has been highlighted at the top of the lake profile. Radiocarbon dates are reported as the calibrated 2σ range.

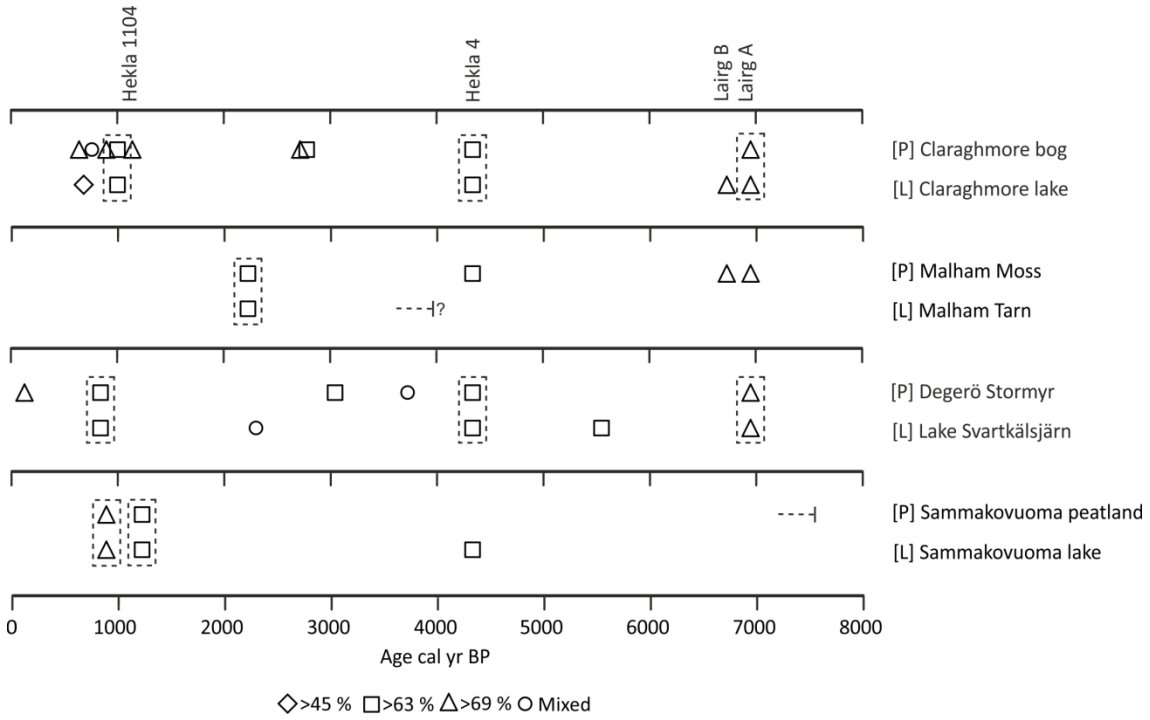

Fig. 3. Diagram summarising the tephras identified at each lake and peatland pair. [P] and [L] mark peatland and lake sites, respectively. Tephras identified in both the lake and the peatland are enclosed in dashed lines. The style of the point reflects the SiO_2 content (wt %). Ages plotted are midpoint ages. Where the basal age of the core has been ascertained using ^{14}C dating this has been marked by a dashed line. One basal date was estimated using less secure methods (sedimentation rate/pollen analysis) and is indicated with a question mark. The most common tephra deposits in this study have been named.

CLA-B1 contains glass shards which show geochemical similarity to those from a mixture of different Icelandic eruptions including Öræfajökull 1362 and Hekla 1510. CLA-B2 could not be matched to previously recognised cryptotephra layers based on glass geochemistry. The age of CLA-B2 (~720 cal yr BP) is constrained by bracketing cryptotephra layers CLA-B1 and CLA-B2A (=Hekla 1104) to between AD 1104 and AD 1362. The glass major element analyses for CLA-B2 are not a complete geochemical match to any of the five northern European cryptotephras identified during this period, although some individual analyses show similar geochemistry to the analyses of shards from Hekla 1158, BGMT1, GB4-57 and QUB-385 (Fig. 4 (a-b)). It is possible that CLA-B2 is a previously undiscovered tephra; however, given the diversity in glass geochemistry and the low resolution of the peatland record, CLA-B2 may represent a mixture of shards from two or more of the tephras listed above.

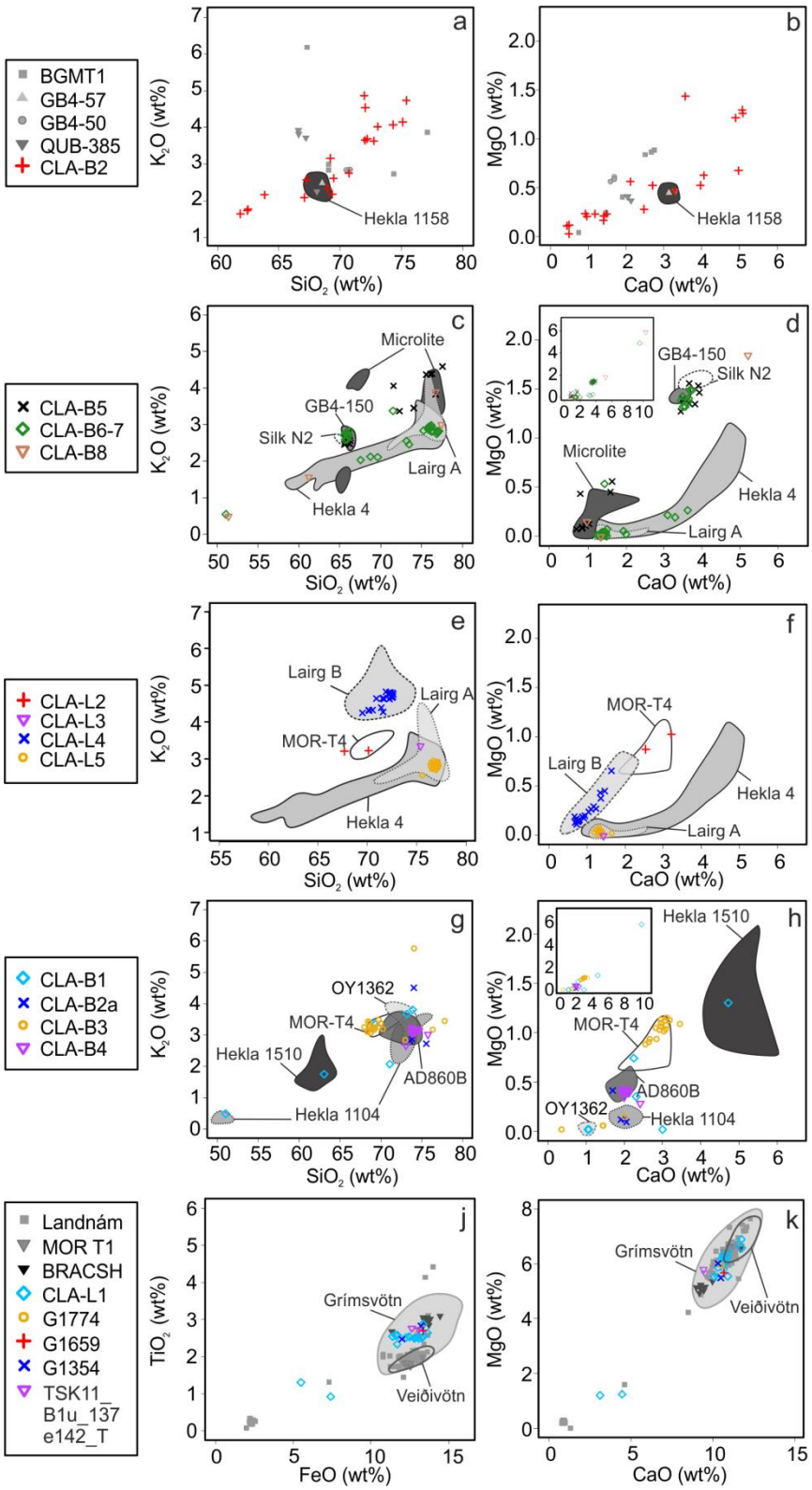

Fig. 4. Geochemical bi-plots of major elements of glass from Claraghmore sites plotted against envelopes for the glass geochemistry of known tephras based on type data from the Tephrabase database (type data references in Table 2). All data have been normalised. (a-b) Claraghmore bog sample CLA-B2 is an unidentified tephra or mix of tephras dating between AD 1104 and AD 1362 plotted against northern

European cryptotephras from this period. (c-d) Claraghmore bog cryptotephra layers prior to AD 860; inset plots show the full range of the data. (e-f) Claraghmore lake cryptotephra layers and suggested sources. (g-h) Claraghmore bog cryptotephra layers from AD 860 to present. The main plots illustrate the geochemical variation among silicic to intermediate shards; inset plots show the full range of the data, including basaltic shards. (j-k) Claraghmore lake tephra ClA-L1, which contains glass shards of a basaltic composition; also shown are geochemical envelopes of glass data for eruptives from the Veiðivötn (dark grey) and Grímsvötn (light grey) volcanoes. Envelopes are based on geochemical data from Streeter and Dugmore, (2014); Lawson *et al*., (2007); Chambers *et al*., (2004); Wastegård, (2002); Wastegård *et al*., (2001); Haflidason *et al*., (2000); Dugmore and Newton, (1998); Thordarson *et al*., (1996); Mangerud *et al*., (1986) and references therein. TSK11_B1u_137_e142_T tephra data from Wulf *et al*., (2016).

Analyses of glass shards in sample CLA-B3 indicate a rhyolitic-dacitic major element geochemistry similar to that of glass shards from the MOR-T4 tephra layer (c. AD 1000) previously identified at one site in Ireland (Chambers *et al*., 2004). The position of CLA-B3 above CLA-B4 (=AD 860 B) supports correlation to the MOR-T4 tephra. CLA-B4 contains shards matching the geochemistry of glass shards from the AD 860 B tephra, recently correlated to a volcano in Alaska (Jensen *et al*., 2014). The 17 analyses on glass shards from the CLA-B5 tephra indicate that this cryptotephra layer contains shards with major element glass geochemistry matching analyses on glass from both the Microlite and GB4-150 tephras.

The CLA-B6-B7 tephra is correlated to Hekla 4 (4345-4229 cal yr BP), as the majority of shards show geochemical similarity to those of tephra from this eruption. However, the CLA-B6-B7 cryptotephra layer contains a number of glass shards which do not match the geochemistry of glass shards from the Hekla 4 eruption (Table 2) (Fig. 4 (c-d)). These shards show geochemical similarity to glass shards most likely from an eruption of Katla volcano in Iceland (Silk-N2) which occurred at around the same time as Hekla 4 (Larsen *et al*., 2001, Plunkett *et al*., 2004).

Only a small number of geochemical analyses were possible on glass shards from the CLA-B8 tephra. These analyses show some similarities to the glass geochemistry of the Lairg A tephra (6947-6852 cal yr BP). Assignment to the Lairg A tephra, a product of the Hekla volcano, is supported by a ^{14}C age of 6432-6303 cal yr BP above the CLA-B8 tephra. Previous research has also identified the Hekla 3 (3037-2956 cal yr BP) and

BMR 190 (2655-2535 cal yr BP) tephras in Claraghmore bog (Plunkett, 2009). We find no evidence for the presence of these cryptotephras in our core. Conversely, we identify cryptotephras in the Claraghmore bog that correlate with MOR-T4 (CLA-B3), Öræfajökull 1362 (CLA-B1) and Hekla 1104 (CLA-B2A), cryptotephra layers which were not identified in the previous study (Plunkett, 2009).

The Claraghmore lake core contains five cryptotephra layers (Table 2, Fig. 4 (e-f)); most have previously been recorded in Ireland. Three of the cryptotephra layers (MOR-T4 (=CLA-L2), Hekla 4 (=CLA-L3) and Lairg A (=CLA-L5)) are present in both the lake and peatland (Fig. 5). MOR-T4 and Hekla 4 form sparse glass shard horizons in the lake and therefore correlation is based on a small number of glass geochemical analyses combined with stratigraphic position. CLA-L4, correlated to the eruption of Lairg B (Torfajökull volcano) is present in the lake, but not in the peatland. CLA-L1 predominantly contains glass shards of a basaltic geochemical composition, which do not match the geochemical composition of glass from any previously identified cryptotephra deposits (Table 3). Glass shards from this tephra are of a different geochemical composition to glass shards from two basaltic tephras identified in western Ireland: the Veiðivötn 1477 tephra found at An Loch Mór (Chambers *et al*., 2004) and the BRACSH-1 (c. AD 1800) tephra identified at Brackloon (Reilly and Mitchell, 2015). They are also not a geochemical match with glass shards from the 'Unknown Basaltic' tephra (1060-1094 ± 75 cal yr BP) identified at Lake Tiefer See, Germany (Wulf *et al*., 2016) (Fig. 4j-k). CLA-L1 represents the third Holocene basaltic tephra horizon to be identified in Ireland and most closely matches the geochemistry of glass derived from the pyroclastic eruptives of the Grímsvötn volcano. Given the highly similar geochemistry of glass from cryptotephra layers from the Grímsvötn volcanic system, which can make attributing tephra to a specific eruption based on geochemistry difficult, 14C dating was conducted on a bulk lake sediment sample from below CLA-L1. Analysis suggested that CLA-L1 is younger than 2517-2750 cal yr BP. However, there are no widespread tephra layers from the Grímsvötn volcanic system between 6000 cal yr BP and 1800 cal yr BP. Furthermore, tephra from the eruption of Grímsvötn in AD 150 (1800 cal yr BP) has been found in only one lake in the north of Iceland, suggesting it was not widely distributed toward Europe (Haflidason *et al*., 2000). The ^{14}C age obtained also suggests an age reversal as it lies above the CLA-L2 cryptotephra

layer which has been geochemically assigned to the MOR-T4 tephra (c. AD 1000, 950 cal yr BP). MOR-T4 was also identified in Claraghmore bog (CLA-B3) and contains glass with a distinct geochemical signature, not easily confused with other European cryptotephras. Given the problems with bulk sediment samples in lakes (e.g. carbonate contamination - Barnekow *et al*., 1998), and possible contamination of the lake with older carbon eroded from the catchment and washed into the lake, we suggest that the ^{14}C age below CLA-L1 is unreliable and indicates an age which is too old for the CLA-L1 cryptotephra. For this reason it is not possible to assign CLA-L1 to a specific eruption, but this cryptotephra is most likely the product of an eruption of the Grímsvötn volcanic system after AD 1000. CLA-L1 does not match the geochemistry of glass from the most explosive eruption of the Grímsvötn volcano during this period (AD 1783 - Reilly and Mitchell, 2015). The eruptions of AD 1354, 1659 and 1774 are all possible sources for this tephra based on geochemistry despite their relatively low explosivity (1659 and 1774 VEI 2, 1354 VEI unknown) (Global Volcanism Program, 2013).

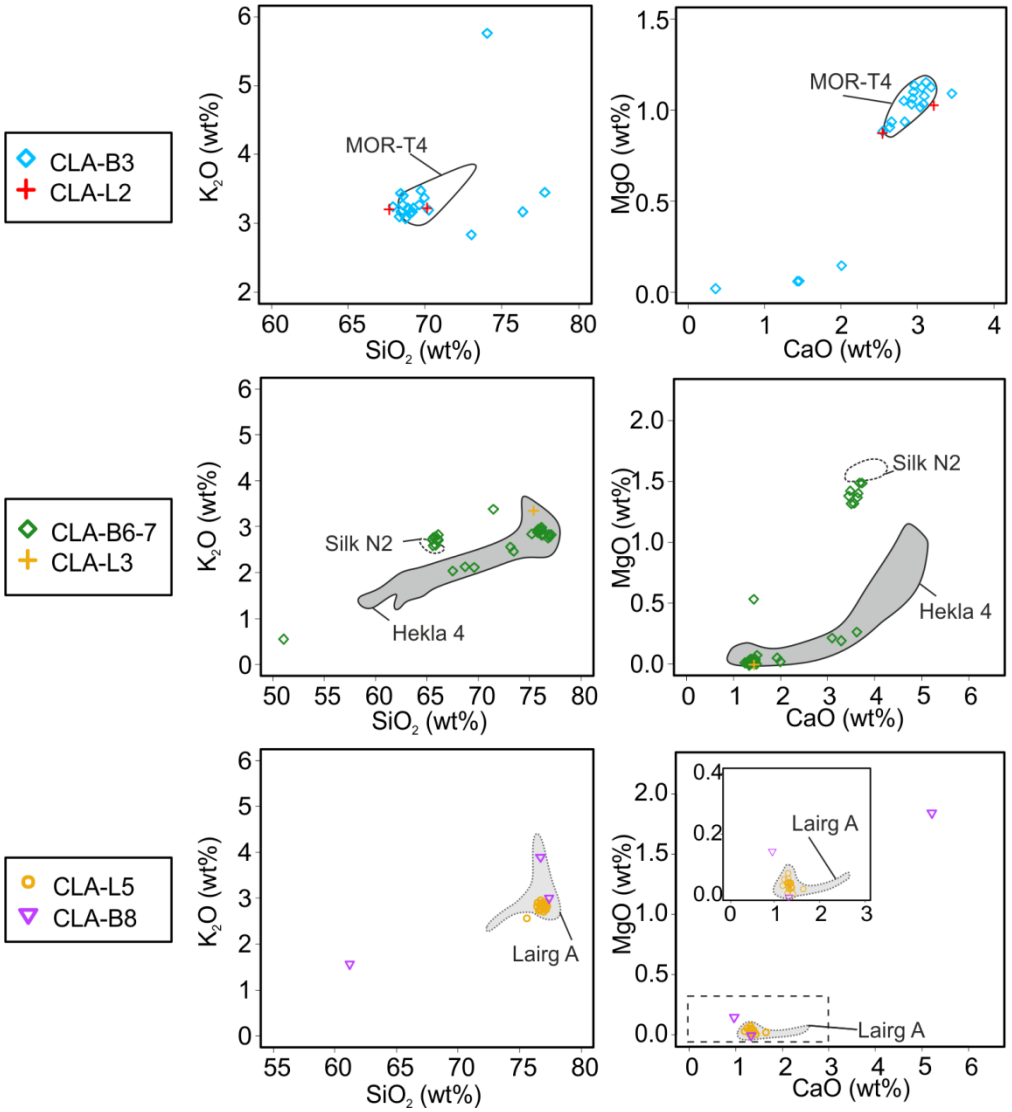

Fig. 5. Geochemical bi-plots of major elements of glass found in both Claraghmore Lake and peatland plotted against envelopes for the glass geochemistry of known tephras based on type data from the Tephrabase database (type data references in Table 2). All data have been normalised. Inset plots show zoomed in view.

	SiO_2	TiO_2	Al_2O_3	FeO	MnO	MgO	CaO	Na_2O	K_2O	P_2O_5	Total
CLA-L1 Claraghmore Lake 110-113 cm *Unknown eruption of Grímsvötn volcano*	67.30	1.30	14.25	5.50	0.18	1.21	3.12	4.99	2.81	0.30	100.96
	63.78	0.92	14.96	7.42	0.18	1.24	4.46	4.53	1.87	0.33	99.70
	50.71	2.34	14.85	11.70	0.19	5.54	10.92	3.02	0.38	0.28	99.92
	50.70	2.54	13.76	11.39	0.19	6.73	11.59	2.51	0.45	0.25	100.10
	50.69	2.52	13.12	12.83	0.20	6.18	10.66	2.68	0.41	0.27	99.56
	50.54	2.65	13.69	13.29	0.22	5.86	10.33	2.81	0.40	0.28	100.08
	50.53	2.53	13.26	13.36	0.19	5.80	10.67	2.66	0.37	0.29	99.67
	50.48	2.52	13.68	12.26	0.21	6.07	10.85	2.68	0.38	0.26	99.41
	50.46	2.56	13.72	13.02	0.20	6.06	10.79	2.60	0.36	0.29	100.06
	50.37	2.49	13.37	12.81	0.19	6.23	10.73	2.73	0.39	0.25	99.56
	50.34	2.58	13.50	11.59	0.18	6.89	11.75	2.65	0.38	0.29	100.15
	50.29	2.49	13.63	13.07	0.20	6.18	10.80	2.57	0.35	0.28	99.87
	50.16	2.63	13.47	13.65	0.24	5.52	10.32	2.72	0.38	0.29	99.37
	49.89	2.57	13.44	11.70	0.20	6.57	11.76	3.10	0.38	0.27	99.88
	49.85	2.87	12.92	13.36	0.20	5.52	10.06	2.70	0.48	0.32	98.29
	49.63	2.52	13.18	12.50	0.19	6.18	10.53	2.57	0.38	0.28	97.96
	49.21	2.50	13.44	13.25	0.21	6.35	10.66	2.55	0.41	0.26	98.83
	49.18	2.55	13.26	12.47	0.17	6.45	10.95	2.76	0.46	0.28	98.52
	49.07	2.53	13.01	12.98	0.21	6.26	10.91	2.90	0.39	0.29	98.55
SB-2 Sammakovuoma peatland 67-70 cm *SN-1*	70.59	0.20	15.20	2.98	0.14	0.11	1.04	5.60	4.86	0.02	100.75
	67.75	0.38	15.75	4.46	0.16	0.27	1.81	6.16	4.19	0.07	100.98
	67.39	0.40	16.60	4.21	0.19	0.33	1.87	6.43	4.18	0.06	101.65
	67.16	0.47	16.04	4.55	0.18	0.41	2.22	6.25	3.90	0.09	101.27
	66.92	0.41	16.03	4.15	0.19	0.35	1.95	5.98	4.04	0.07	100.10
	66.69	0.43	16.74	4.34	0.20	0.33	2.12	6.45	4.00	0.07	101.37
	66.44	0.45	16.46	4.40	0.19	0.34	2.03	6.18	4.08	0.81	100.64
	66.39	0.40	16.44	4.13	0.18	0.33	1.90	5.99	4.06	0.07	99.90
	66.34	0.43	16.81	4.29	0.17	0.34	2.12	6.06	3.98	0.07	100.60
	66.32	0.45	16.66	4.67	0.17	0.34	2.03	6.08	4.06	0.07	100.84
	66.15	0.64	15.85	5.63	0.21	0.57	2.01	5.79	4.41	0.14	101.40
	65.65	0.57	17.25	5.17	0.20	0.55	2.52	6.06	3.73	0.12	101.82
	65.58	0.45	18.12	4.18	0.15	0.36	3.00	6.85	3.19	0.09	101.97
	65.52	0.42	16.02	4.46	0.16	0.28	1.90	6.06	4.04	0.05	98.92
	65.15	0.58	16.46	5.28	0.17	0.51	2.64	6.00	3.63	0.14	100.58
	65.14	0.59	16.68	5.28	0.21	0.58	2.77	6.26	3.63	0.13	101.26
	65.11	0.57	17.10	5.37	0.17	0.53	2.55	6.30	3.72	0.12	101.58
	64.82	0.62	16.17	5.72	0.19	0.61	2.55	5.78	3.83	0.13	100.42
	64.70	0.58	16.57	5.03	0.21	0.61	2.48	6.05	3.73	0.14	100.10
	64.44	0.58	16.52	5.28	0.22	0.55	2.71	5.80	3.63	0.11	99.86
	64.44	0.60	16.10	5.46	0.21	0.52	2.56	6.14	3.72	0.15	99.89
	64.42	0.58	16.44	5.42	0.21	0.55	2.52	6.56	3.92	0.11	100.71
	64.28	0.60	16.62	5.08	0.21	0.63	2.59	6.16	3.66	0.13	99.97
	64.22	0.60	16.56	5.27	0.23	0.56	2.50	6.28	3.74	0.11	100.06
	63.86	0.60	16.64	5.35	0.22	0.61	2.61	5.91	3.79	0.13	99.72
	63.54	0.56	15.98	5.28	0.21	0.60	2.52	6.11	3.80	0.11	98.72
SL-2 Sammakovuoma Lake 39-42 cm *SN-1*	70.21	0.17	14.71	2.85	0.12	0.07	1.19	5.61	4.73	0.01	99.69
	66.44	0.40	15.08	4.26	0.17	0.33	1.88	5.57	4.04	0.06	98.22
	66.31	0.47	15.38	4.55	0.19	0.39	2.15	5.45	3.87	0.09	98.86
	66.12	0.42	15.12	4.53	0.17	0.32	1.99	5.63	4.00	0.06	98.36
	65.87	0.56	15.80	5.12	0.21	0.55	2.49	5.45	3.72	0.12	99.90

65.81	0.57	16.15	5.45	0.21	0.56	2.62	5.67	3.52	0.13	100.69
65.61	0.58	15.69	5.06	0.19	0.58	2.61	5.47	3.97	0.12	99.88
65.54	0.59	15.68	5.54	0.22	0.63	2.48	5.38	3.86	0.14	100.06
65.47	0.57	15.90	5.42	0.20	0.62	2.47	5.64	3.72	0.11	100.13
65.43	0.59	15.77	5.29	0.23	0.61	2.61	5.40	3.68	0.13	99.73
65.25	0.45	15.68	4.61	0.16	0.46	2.80	5.81	3.44	0.11	98.78
65.18	0.54	15.92	5.18	0.21	0.53	2.63	5.47	3.80	0.12	99.57
65.15	0.60	15.33	5.16	0.21	0.62	2.53	5.46	3.86	0.13	99.05
65.10	0.55	15.98	5.35	0.22	0.58	2.62	5.73	3.85	0.12	100.11
64.95	0.57	15.84	5.18	0.20	0.57	2.62	5.65	3.78	0.13	99.49
64.89	0.57	15.78	5.40	0.22	0.52	2.42	5.51	3.89	0.12	99.32
64.24	0.60	15.26	5.22	0.20	0.64	2.58	5.28	3.71	0.14	97.87
63.73	0.50	15.30	4.98	0.19	0.60	2.38	5.49	3.55	0.10	96.83
61.97	0.56	15.20	5.08	0.21	0.57	2.55	5.61	3.61	0.14	95.50

Table 3. Non-normalised major element geochemical analysis data for glass shards from the CLA-L1 and SB-2/SL-2 (=SN-1) cryptotephras identified at Claraghmore Lough (CLA-L1) and Sammakovuoma peatland and lake (SB-2/SL-2).

Site 2: Malham

There is evidence of four silicic tephra fallout events in the core taken from Malham Moss (Figs. 3 and 6). All four tephras, Glen Garry (MM-1), Hekla 4 (MM-2), Lairg B (MM-3) and Lairg A (MM-4), have previously been recorded at sites in Great Britain and Ireland. We identify the Lairg A and Lairg B tephras for the first time in England. Only one cryptotephra layer in Malham Tarn contained sufficient shards for geochemical analysis (MT-1) and was identified as the Glen Garry tephra (1966-2210 yr BP) (Fig. 7).

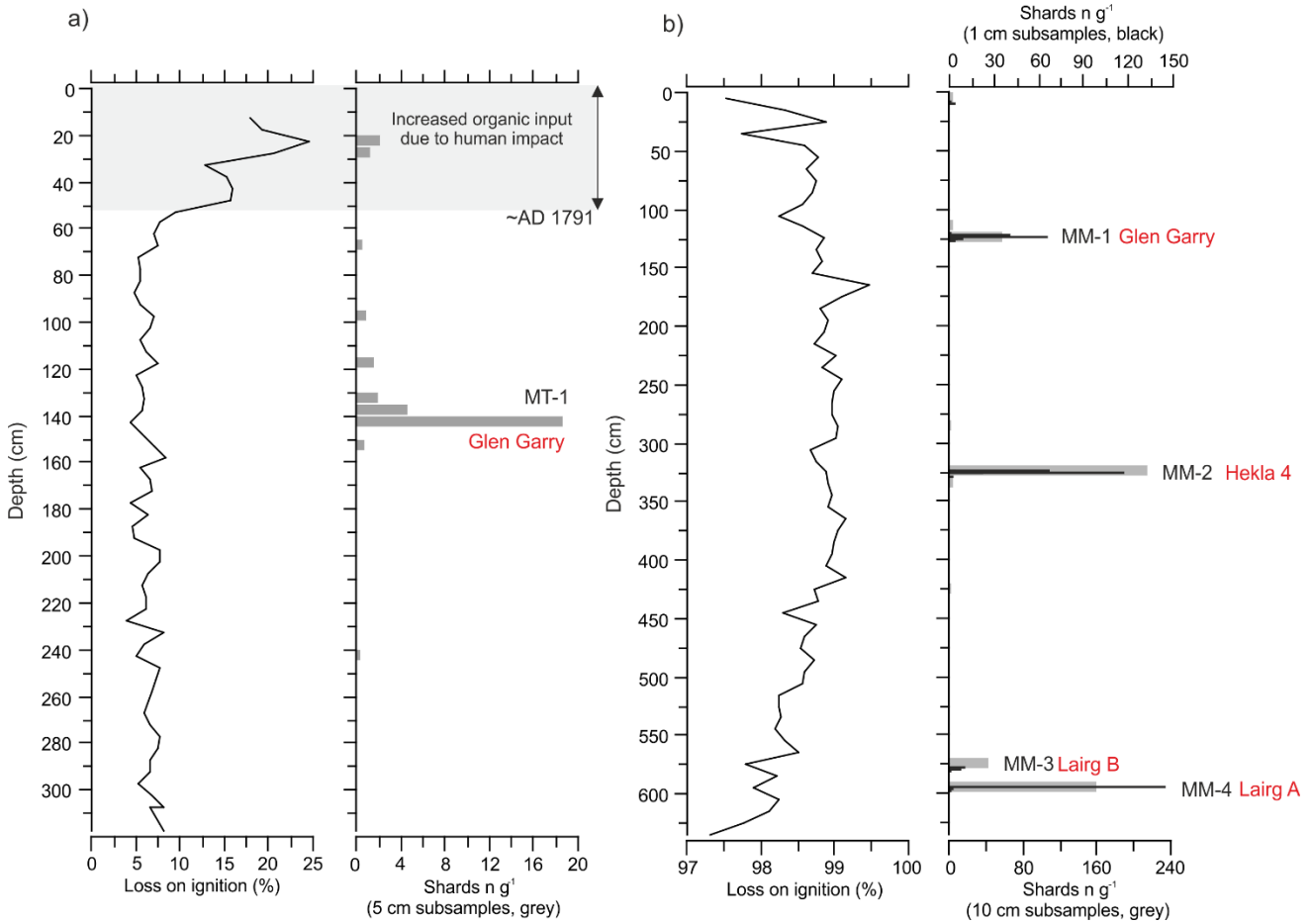

Fig. 6. Diagram showing the tephrostratigraphy and loss-on-ignition values at Malham a) Tarn, b) Moss. Tephra codes are indicated in black. Where assignments to a known tephra isochron have been made based on glass geochemistry and stratigraphy these are indicated in red beside the tephra code. An area of increased organic input has been highlighted at the top of lake profile.

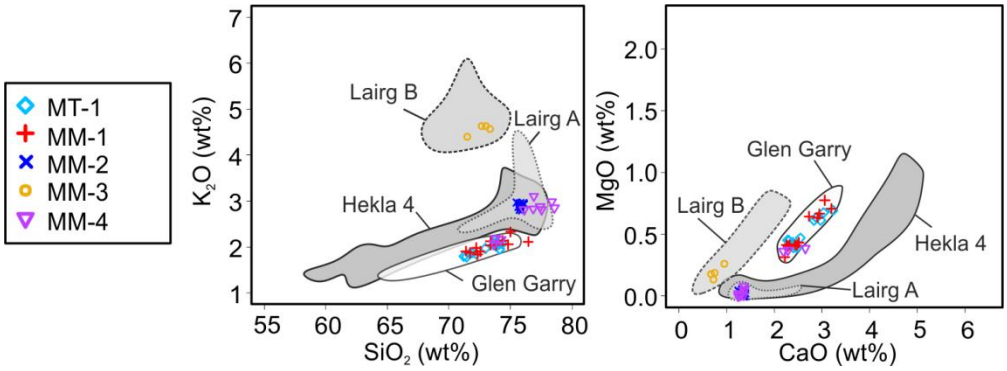

Fig. 7. Geochemical bi-plots of major elements of glass from Malham Tarn and Malham Moss plotted against envelopes for the glass geochemistry of known tephras based on type data from the Tephrabase database (type data references in Table 2). All data have been normalised.

It is likely that the Malham Tarn core does not extend far enough to ascertain whether the Hekla 4 (4345-4229 cal yr BP), Lairg B (6724-6627 cal yr BP) and Lairg A (6947-6852 cal yr BP) cryptotephra layers were also deposited in the lake. Dating of marl sediment is extremely difficult and radiocarbon dating of charcoal and macrofossils from Malham Tarn has proved problematic in the past (Barber *et al*., 2013). Pollen analysis on a basal sample from our core (depth 315-320 cm) is consistent with an age no earlier than the Elm decline 6347-5281 cal yr BP (Parker *et al*., 2002) and perhaps much younger. The absence of the Hekla 4, Lairg A and Lairg B tephras may due to the length of the sediment core which was recovered.

Site 3: Lake Svartkälsjärn and Degerö Stormyr

The tephra record at Degerö Stormyr comprises six silicic cryptotephra layers including tephra from Askja 1875 (SV-B1), Hekla 1104 and Hekla 1158 (SV-B2), Hekla 3 (SV-B3) and Hekla 4 (SV-B5) (Fig. 8). The SV-B4 cryptotephra layer was deposited between SV-B3 (Hekla 3 = 3037-2956 cal yr BP) and SV-B5 (Hekla 4 = 4345-4229 cal yr BP). The geochemical analyses of glass from SV-B4 suggest a match with the Hekla-S/Kebister tephra (3750-3700 cal yr BP) which corresponds to the stratigraphic age interval for the SV-B4 cryptotephra and has been recorded widely across Scandinavia (Wastegård *et al*., 2008). SV-B6 is correlated to Lairg A (6947-6852 cal yr BP) based on glass geochemistry and its stratigraphic position above peat with a radiocarbon age of 7143-6806 cal yr BP.

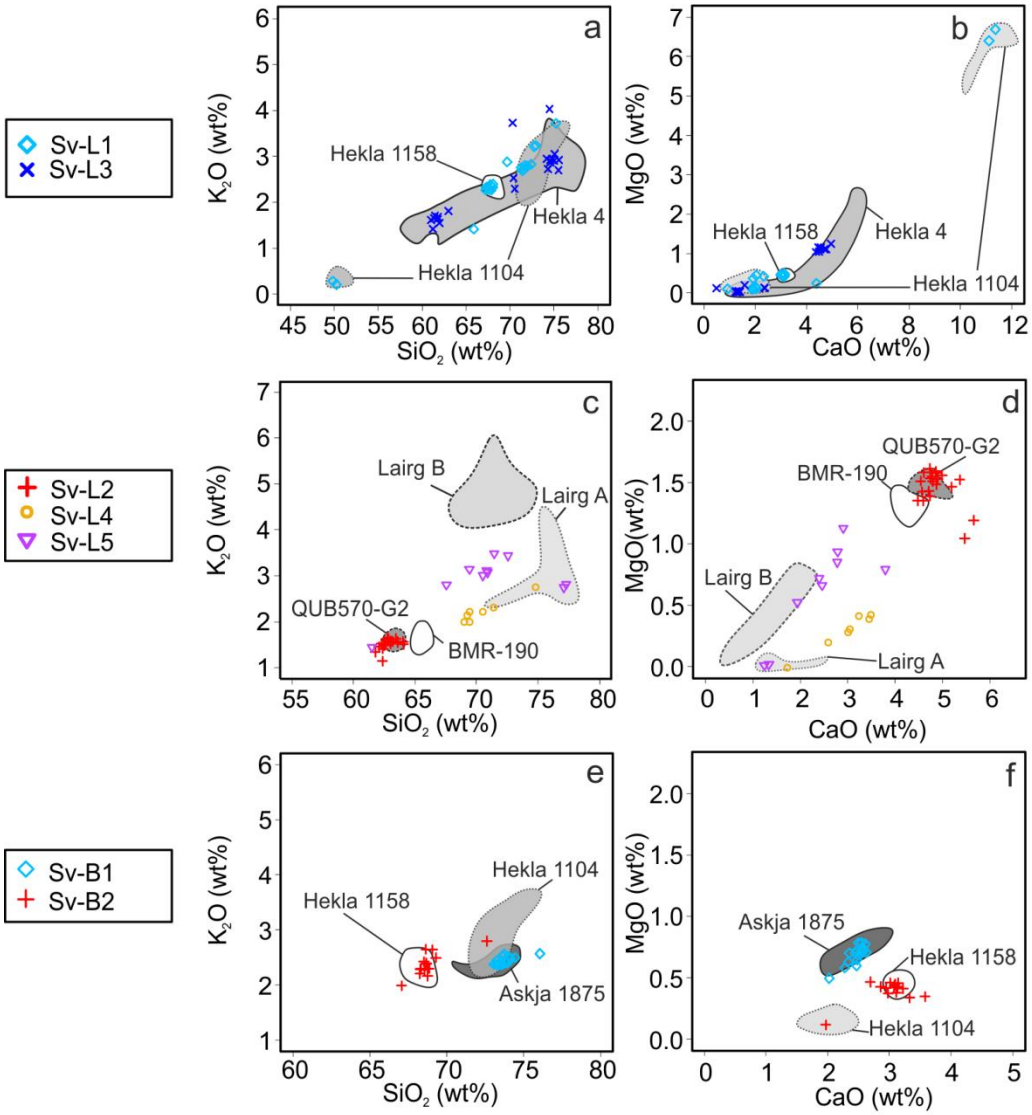

Fig. 8. Geochemical bi-plots of major elements of glass from Lake Svartkälsjärn (a-d) and Degerö Stormyr (e-k) plotted against envelopes for the glass geochemistry of known tephras based on type data from the Tephrabase database (type data references in Table 2). All data have been normalised.

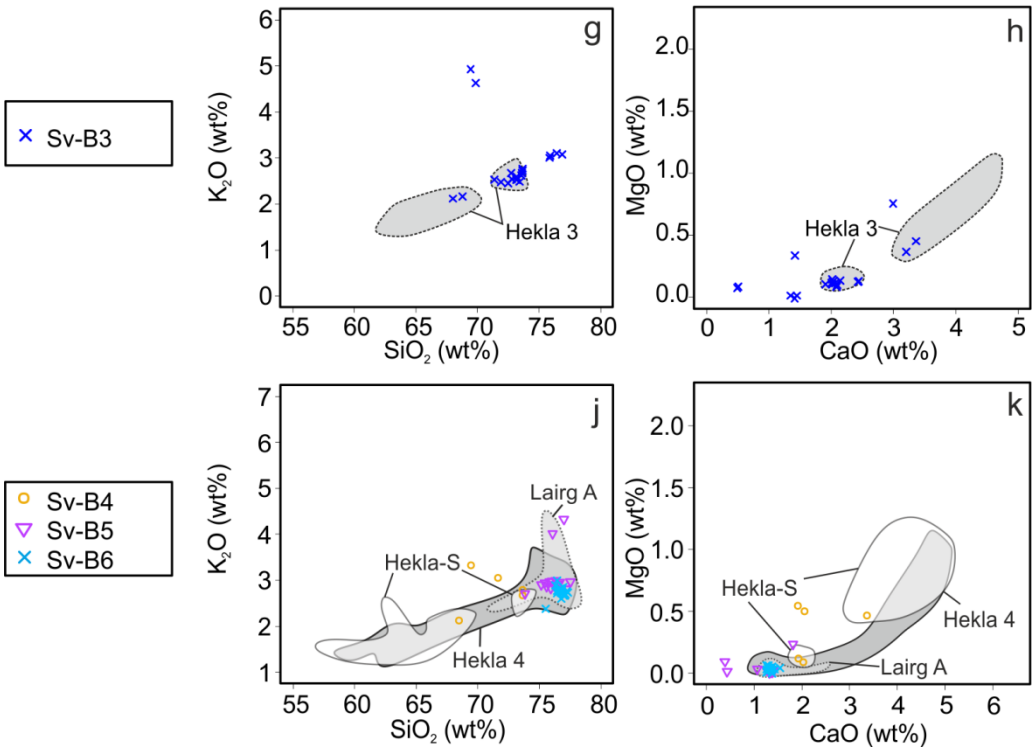

Fig. 8. Cont.

The sediment core recovered from Lake Svartkälsjärn contains five cryptotephra layers from six distinct Icelandic eruptions (Fig. 9). Three of these tephras can be linked based on glass geochemistry and stratigraphy to Hekla 1104/ Hekla 1158 (SV-L1) and Hekla 4 (SV-L3) (Fig. 8). However, the lake core also contains two cryptotephra layers (SV-L2 and SV-L4), the glass analyses from which do not match the glass compositions of established cryptotephras in northern Europe. Approximate ages for these cryptotephras can be ascertained according to their depth and the age-depth model on a core from a different study of the same lake. Although correlations to an existing profile must be made with caution, the core of Barnekow *et al*. (2008) was recovered from a similar location within the basin and the record between surface sediment and basal clay is 1.92 m (similar to that of our core = ~1.9 m). Based on the age-depth model of Barnekow *et al*. (2008), the SV-L2 and SV-L4 tephras have approximate ages of 2500-2000 and 6000-5000 cal yr BP, respectively. SV-L2, which is not present in the Degerö Stormyr peat sequence, is most similar in glass geochemistry to glass shards of the QUB 570 Group 2 (~1300 cal yr BP) tephra, which has been identified at Lofoten, Norway (Pilcher *et al*., 2005). There is also some geochemical similarity with the glass of the BMR-190 tephra (~2595 cal yr BP), although this tephra has not been identified outside

Ireland. Given the uncertainty associated with the dating of SV-L2, we tentatively suggest a correlation with the QUB 570 Group 2 tephra. No geochemical match was identified for shards from SV-L4, which contains glass shards with a range of major element geochemistry and may represent a mixture of tephras deposited onto snow in the lake catchment and then washed into the lake during snowmelt events. Of the ten successful geochemical analyses conducted on glass shards from SV-L5, two indicate geochemical similarity to the glass composition of shards from Lairg A (6947-6852 cal yr BP), which was also identified in the Degerö Stormyr peat sequence. An approximate date of 6500-6000 BP for SV-L5 based on interpolation suggests that at least some of the shards in SV-L5 are from the Lairg A tephra. The eight remaining geochemical analyses do not match the geochemical analyses for any established cryptotephra layers of a similar age.

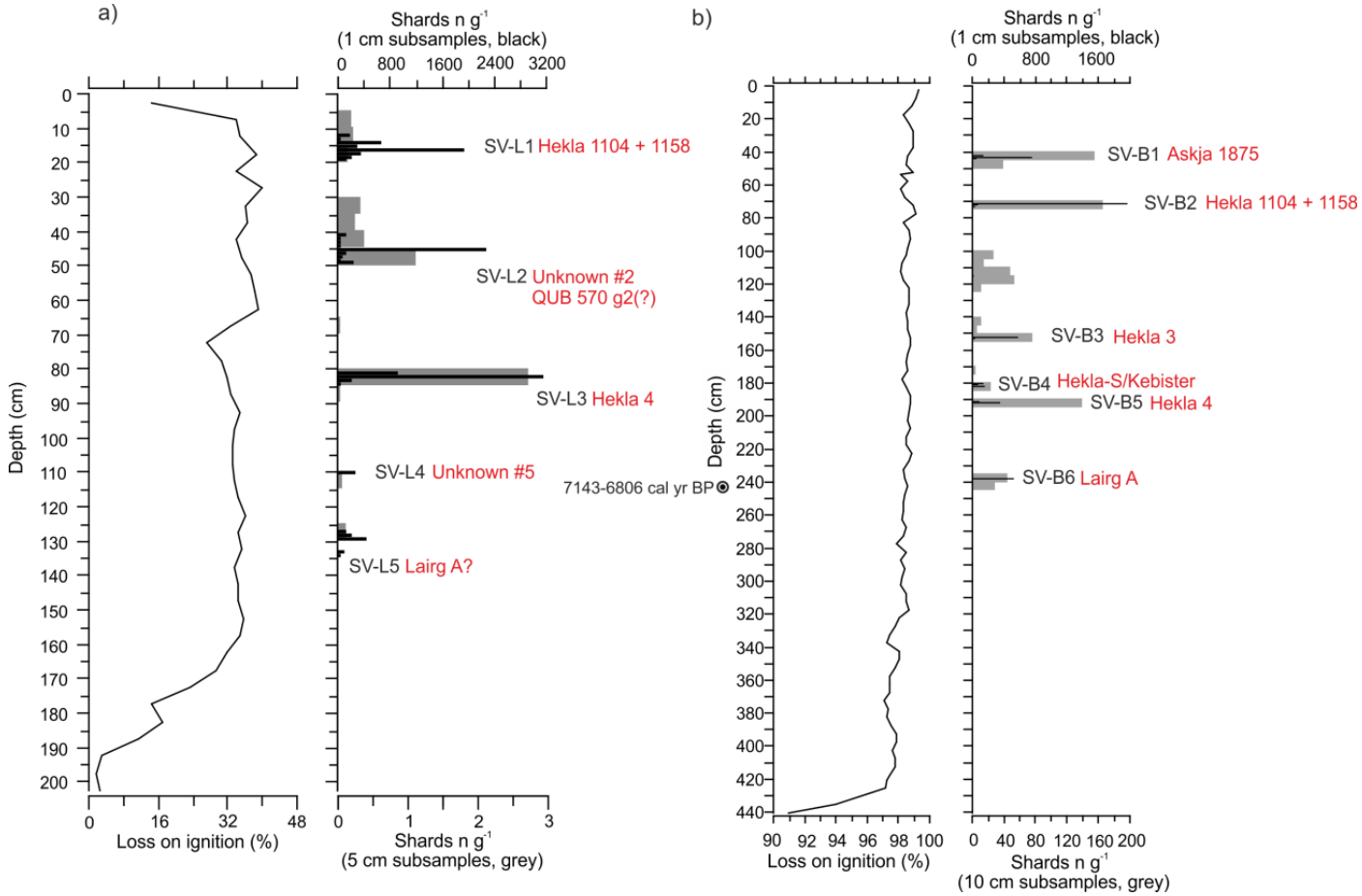

Fig. 9. Diagram showing the tephrostratigraphy and loss-on-ignition values at a) Lake Svartkälsjärn, b) Degerö Stormyr. Tephra codes are indicated in black. Where assignments to a known tephra isochron have been made based on glass geochemistry and stratigraphy these are indicated in red beside the tephra code. Radiocarbon dates shown are the calibrated 2σ range.

Site 4: Sammakovuoma

Cryptotephra layers (SL-1, SB-1) containing glass shards with major elemental geochemistry identical to glass shards from the eruption of Hekla AD 1104 were identified in both Sammakovuoma peatland and lake. A second cryptotephra layer (SL-2, SB-2) containing glass shards of trachydacite geochemistry, was also present in both the peatland and lake at Sammakovuoma (Figs. 10 and 11). Glass geochemistry from the SL-2/SB-2 tephra does not match the geochemistry of glass from any published northern European cryptotephra layer (Fig. 10). However, the glass composition is highly similar to that of the SN-1 tephra from the Icelandic Snæfellsjökull volcano. The age of 'peaty soil' below the SN-1 tephra layer in Iceland indicates a maximum age for the SN-1 tephra of 1860-1520 cal yr BP (Larsen *et al*., 2002). Interpolation between two closely spaced radiocarbon dates in Sammakovuoma peatland suggests SB-2 has an age of between 1183-1147 cal yr BP, more recent than the previous age suggested for the SN-1 tephra (Table 4). However, given that there are no known explosive eruptions of Snæfellsjökull after SN-1, we correlate SL-2/SB-2 to the SN-1 tephra and conclude that a previous age of 1860-1520 cal yr BP for the SN-1 tephra should be considered a maximum age. The SN-1 tephra has been identified on the island of Svalbard (D'Andrea *et al*., 2012), but our identification in Sweden constitutes the first identification of this tephra in continental (northern) Europe. A third cryptotephra layer (SL-3), correlated to the Hekla 4 eruption, was also identified in the lake but was absent from the peatland.

Sample ID	Laboratory ID	Site	Depth (cm)	^{14}C age BP ± 1σ	δ ^{13}C per mil	Calibrated range (2σ)	Material
SBRC1	D-AMS 012524	Sammakovuoma Peatland	64-68	1083 ± 24	-32.2	AD 895-1016	*Sphagnum* leaves/stems
SBRC2	D-AMS 012525	Sammakovuoma Peatland	70-73	1449 ± 29	-27.2	AD 563-651	*Sphagnum* leaves/stems
SBRC3	D-AMS 012526	Sammakovuoma Peatland	352-356	6692 ± 31	-37.6	7614-7505 cal yr BP	*Sphagnum* leaves/stems *Eriophorum* spindles
CLARC1	D-AMS 012527	Claraghmore Bog	855-860	5587 ± 29	-34.1	6432-6303 cal yr BP	*Sphagnum* leaves/stems, seeds
SVRC1	D-AMS 012528	Degerö Stormyr	240-243	6077 ± 29	-31.8	7143-6806 cal yr BP	*Sphagnum* leaves/stems, seeds
CLAL1	*D-AMS 013414*	*Claraghmore Lake*	*113-116*	*2551 ± 22*	*-29.3*	*2517-2750 cal yr BP*	*Bulk sediment*

Table 4. Radiocarbon dates obtained on samples from sites in this study. The CLA-L1 14C date indicated in italics would imply an age reversal with the (MOR-T4, c.AD 1000) cryptotephra from the same core. Given the problems with bulk sediment samples in lakes (carbonate contamination - Barnekow *et al*., 1998), and possible contamination of the lake with older carbon from the neighbouring peatland, we suggest that the 14C date below CLA-L1 is unreliable.

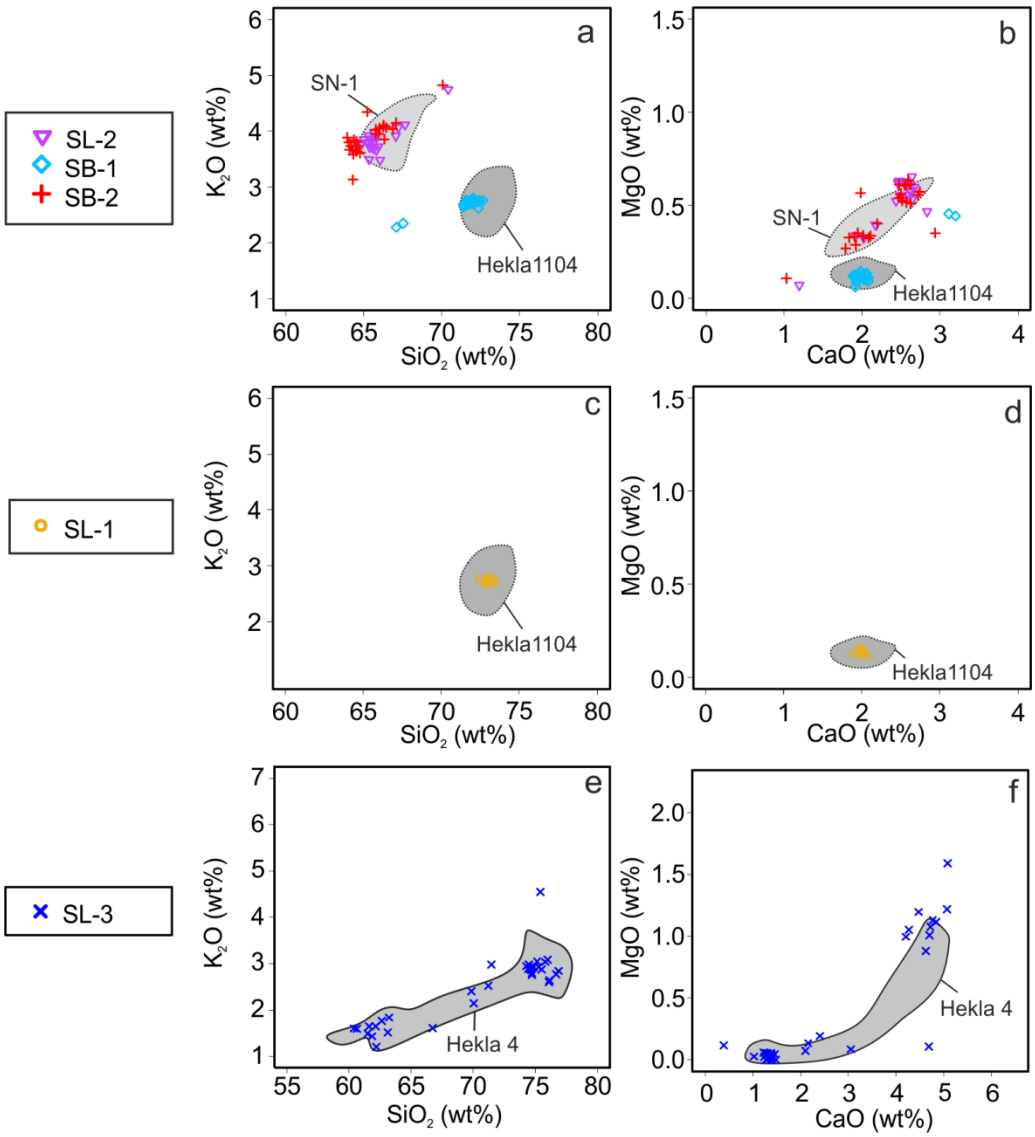

Fig. 10. Geochemical bi-plots of major elements of glass from cryptotephra layers from Sammakovuoma peatland and lake plotted against envelopes for the glass geochemistry of known tephras based on type data from the Tephrabase database (type data references are listed in Table 2). All data have been normalised. (a-d) cryptotephra layers which were found in the lake and the peatland, inset plots show SL-1 tephra which is obscured in the larger plot by SB-1. Both tephras are a geochemical match for the Hekla 1104 tephra, type data for the SN-1 tephra from Larsen *et al*. (2002) and Holmes *et al*. (2016) (e-f) cryptotephra layer found in Sammakovuoma lake and identified as the Hekla 4 tephra.

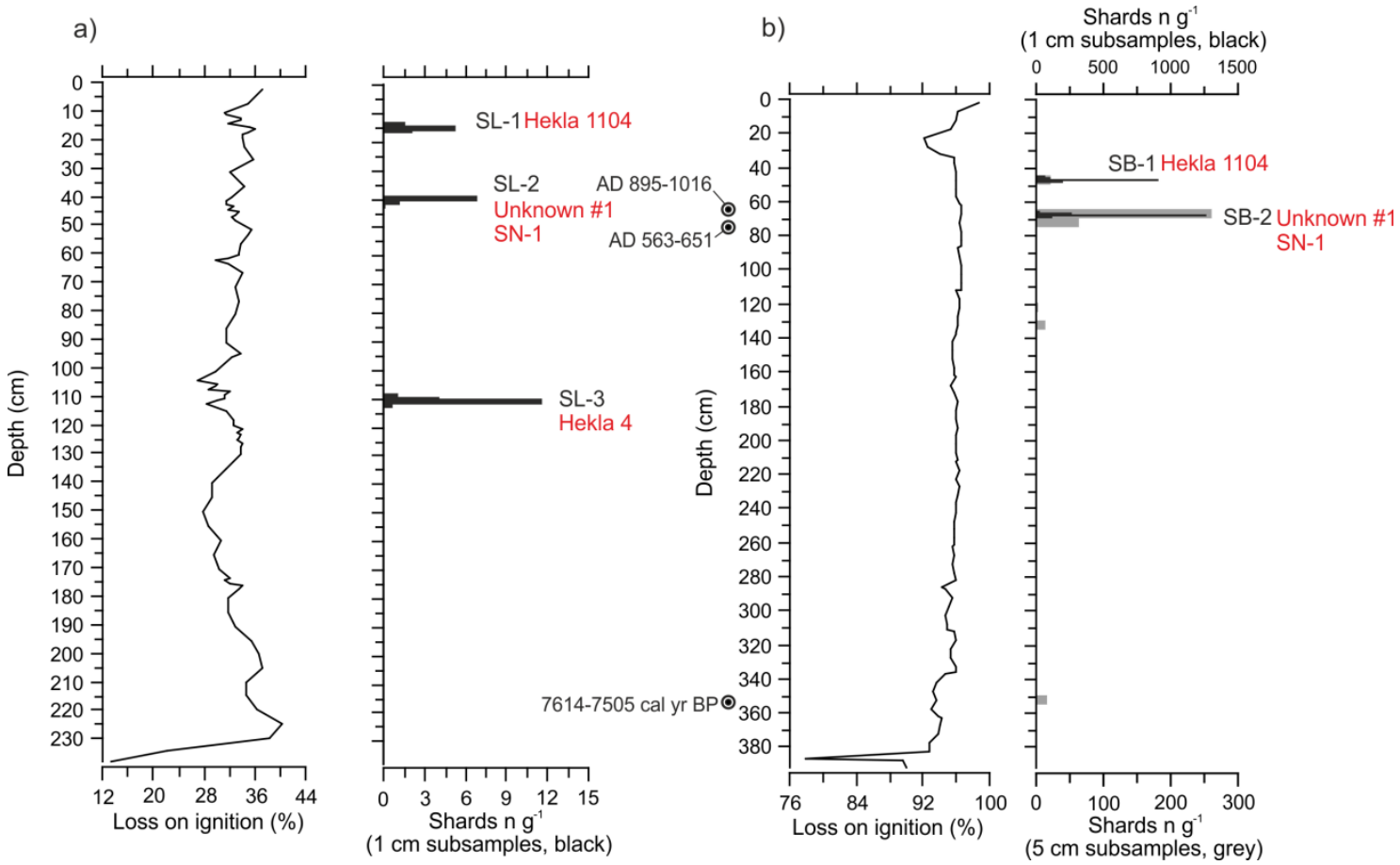

Fig. 11. Diagram showing the tephrostratigraphy and loss-on-ignition values at Sammakovuoma, a) lake and b) peatland. Tephra codes are indicated in black. Where assignments to a known tephra isochron have been made based on glass geochemistry and stratigraphy these are indicated in red beside the tephra code; tephras which could not be assigned to a known tephra isochron are marked as 'unknown', and each unknown tephra is numbered. Radiocarbon dates shown are calibrated 2σ ranges.

5.4.2 Peatland vs. lake archives

Assuming that ash cloud occurrence is homogenous on scales of <10 km and that one core is representative of an entire peatland or lake, we would expect to find the same cryptotephra layers in peat and lake cores from two sites in close proximity. However, despite instances where the same cryptotephra layer was identified in both the peatland and lake records, the overall tephrostratigraphic records in peatlands and lakes differ considerably. There appears to be no consistent difference in the number of cryptotephra layers recorded in lakes and peatlands. In some records localised precipitation patterns or human disturbance (e.g. Claraghmore Lake or Malham Tarn) might account for differences in the tephrostratigraphic records. However, in other instances differences in the number of cryptotephra layers recorded in lakes and peatlands may have been caused by processes of reworking and redistribution (e.g. catchment erosion or intra-lacustrine reworking).

5.4.2.1 Cryptotephra layers absent from peatland records

Loss-on-ignition data can be used to indicate the influence of minerogenic inputs on peatlands. Decreases in loss-on-ignition (% loss) values indicate an increase in minerogenic content. The loss-on-ignition values for all our peatlands exceed 92 % (95 % in 3 out of 4 cases, excluding basal sections where no cryptotephra deposits were identified) (Figs. 2, 6, 9 and 11). Our results indicate that the peatlands in this study have a high organic content and have received very low mineral input. We therefore suggest that all of our peatland sites are ombrotrophic and thus have only received tephra from the air (direct fallout) and that there is no evidence for material being washed into the peatland.

In three of our peatland-lake pairs, at least one of the cryptotephra layers identified in the lake was not present in the peatland. This might be expected as lakes receive tephra in-wash from a wide catchment area, as opposed to ombrotrophic peatlands which record only primary tephra-fall (Bramham-Law *et al*., 2013; Bertrand *et al*., 2014). The core at Sammakovuoma peatland has a basal age predating 7500 cal yr BP and peat would have been present at the site during tephra fallout from the Hekla 4 eruption (4345-4229 cal yr BP). Cryptotephra shards from the Hekla 4 eruption were identified

in Sammakovuoma Lake (SL-3). However, the Hekla 4 tephra was not identified at Sammakovuoma peatland. Cryptotephra layers in northern peatlands and lakes can be affected by tephra fall onto snow cover and subsequent redistribution (Bergman *et al*., 2004; Davies *et al*., 2007). Sammakovuoma peatland and lake are covered in snow and ice for prolonged periods during the winter. It is conceivable that the Hekla 4 tephra might have been deposited onto snow and then reworked from the more exposed peatland by wind and water. Although tephra shards in the lake catchment would have been subject to reworking, they may have been washed into the lake from the wider catchment during snowmelt. In high-latitude regions the impact of tephra fallout onto snow and subsequent redistribution by wind and/or water might explain the absence of some cryptotephra layers from peatlands. However, prolonged snow cover is less likely at Claraghmore bog.

At Claraghmore lake we identified two cryptotephra layers which are absent from the peatland (CLA-L1 = 'Unknown' and CLA-L4 = Lairg B). In this instance we suggest that the peatland has failed to capture sparse cryptotephra layers; glass shards from which have been focussed into the lake from the wider catchment, bringing them above levels of detection in lake sediments. The impact of catchment in-wash on increasing tephra concentrations in lakes is indicated by the total shard counts for some tephras found in both lakes and peatlands in this study. Total shard counts must be interpreted with caution, given the sensitivity to sample volume. However, in some instances total shard counts for the same cryptotephra layer differ greatly in lakes and peatlands. For example, the total shard number for the Lairg A tephra in Claraghmore Lake was 723, an order of magnitude more than identified in the peatland (79 shards). A similar order of magnitude difference was apparent in Hekla 4 shard counts in Degerö Stormyr peatland and Lake Svartkälsjärn (n = 35 and n = 303, respectively). Research on visible tephra layers at lake and bog sites in the Waikato area of North New Zealand identified more visible tephra layers in lakes, perhaps owing to in-wash of tephra from the catchment (Lowe, 1988a, b). Invisible cryptotephra layers containing low concentrations of shards have been identified in subsequent studies of the same bogs (Gehrels *et al*., 2006).

5.4.2.2 Cryptotephra layers absent from lake records

At Malham Moss, Claraghmore and Degerö Stormyr, we identify more cryptotephra layers in the peatland than in the lake. A number of tephras identified toward the top of cores at peatland sites were not identified in nearby lake sites - at Claraghmore Lake and Lake Svartkälsjärn, for example. Possible reasons for the absence of tephras in the top of lake records include: 1) the top of the record was characterised by the soft sediment-water interface and was not recovered in its entire volume during sampling; 2) site specific factors: at Claraghmore and Malham there is sedimentological evidence (LOI) that land management and/or disturbance in the lake catchment (i.e. human factors) may have resulted in a large sediment influx, disturbing the lake sediments and 'diluting' the tephra record in the upper part of these cores; and 3) the cryptotephra layers may have contained insufficient shards to be detected in the lake sediments. Some loss of shards during density separation extraction is inevitable and therefore cryptotephra layers which consist of low concentrations of shards may be under-sampled in lake sediments.

Although care was taken to capture the sediment-water interface at all sites, incomplete recovery of surface sediment cannot be discarded as the reason for missing cryptotephra layers at the top of lake cores. An alternative explanation for the missing cryptotephra layers in the top of Claraghmore Lake is the impact of humans on the recent sediment influx to the lake. LOI data for the lake sediments indicates increased mineral input in the top 50 cm of sediment at Claraghmore Lake. Conversely, there is no sedimentological evidence for human disturbance at Lake Svartkälsjärn. Instead the apparent absence of the Askja 1875 tephra identified in the nearby Degerö peatland (SV-B1) from the tephra record at Lake Svartkälsjärn might be explained by poor recovery of the water-sediment interface.

Recent disturbance and problems with sampling soft sediments at the top of lake profiles cannot account for the missing tephras in the older lake records. Other tephras found in Degerö peatland but not identified in the nearby Lake Svartkälsjärn (SV-B4, SV-B3) lie between tephras which are identified in both lake and peatland records, suggesting that their absence from the lake record is not an artefact of sampling. Similarly, as both the MOR-T4 (CLA-B3/CLA-L2) and Hekla 4 (CLA-B6-B7/CLA-L3)

tephras are identified in Claraghmore lake and peatland, we might expect the Microlite and GB4-150 tephras (2705-2630 cal yr BP and 2750-2708 cal yr BP, respectively) which are present in the peatland between MOR-T4 and Hekla 4 to also to be present in the lake. However, there are no glass shards during this interval in the Claraghmore lake record. One possible explanation is that these tephras were present in lake sediments as very sparse concentrations of shards but were not identified because the shard concentrations were below detection levels. The concentration of shards for the Microlite tephra in Claraghmore bog is lower than the concentrations of glass shards of other tephras also identified in Claraghmore lake (e.g. Hekla 4 and MOR-T4 tephras), and therefore the lake sample may have contained insufficient shards for extraction by density separation.

An alternative reason for the apparent lack of some cryptotephras from lake records is within-basin focussing and redistribution which might reduce shard counts below levels of detection in some areas of the lake. Relatively large with-in basin differences (e.g. 23 cm – 5cm) in the thickness of visible tephra layers provide evidence of the degree to which tephra can be differentially deposited or moved within lake basins (Mangerud *et al*., 1984). In small shallow lakes such as those investigated in this study, small particles can be remobilised by wind-induced currents (Mackay *et al*., 2012). Once tephra has been delivered, within-basin focussing and preferential deposition near stream inlets might result in the concentration of shards from some cryptotephra layers into certain areas of the lake. Conversely, internal redistribution might also result in some tephras being reworked to below detection levels in some parts of the basin. Where shards are present in low concentrations, within-basin focussing in lakes provides a natural means of concentrating a small number of shards. However, this process does not appear to concentrate shards to the same location consistently over time resulting in a patchy distribution of different tephras deposited at different times in different areas of the lake basin. For example, the Lairg A and Hekla 4 tephras have very similar total numbers of shards in Claraghmore bog (79 and 73), but show very different total shard concentrations in the lake (723 and 26 shards). Although the peatland record is not unaffected by redistribution (Watson *et al*., 2015), such a difference in the concentrations of shards for these two cryptotephra layers in the same lake would appear to suggest internal reworking or redistribution. This hypothesis would also

appear to be supported by the range of ash concentrations identified in late glacial micro-tephra layers in Scottish lakes; proximity to catchment inlets was identified as an important factor in determining the concentration of tephra glass shards across the lake basin and spatial ash concentration maxima for different tephra layers varied over time (Pyne-O'Donnell, 2011). The 'patchy' nature of the black basaltic component of the Vedde ash, which varied from visible, to apparently absent (to the naked eye) in different cores from the same Scottish lake also suggests that processes within the catchment and lake can greatly impact on tephra shard concentrations within a lake basin (Davies *et al*., 2001). The consequences of within-basin redistribution are two-fold: firstly the retrieval of one core from the centre of a lake may not result in the recovery of the complete record of tephra which has fallen out over that lake site. Secondly, the re-distribution of shards by within-basin processes might act to favour the detection of ash cloud events depositing only a small number of tephra glass shards by concentrating shards toward one area of the lake thus bringing them above detection levels of current extraction techniques. Our results support the suggestion of previous studies of proximal tephra layers in lakes and catchments (e.g. Boygle, 1999) that a combination of records from both lakes and peatlands must be used to establish the most comprehensive and complete regional (crypto-) tephrostratigraphies.

5.4.3 Preservation of mafic tephras

Prior to this study, tephra from only five basaltic eruptions had been identified in terrestrial Holocene records in northern Europe, the majority in lakes in the Faroe Islands or Ireland (Wastegård *et al*., 2001; Chambers *et al*., 2004). The apparent lack of basaltic tephras in peatlands cannot be easily explained by the different extraction methodologies used to conduct initial scans for tephra on samples from peatlands and lakes. The extraction method commonly applied to lake samples, density separation, can result in the loss of basaltic shards which are not always recovered at a standard float density of 2.5 g cm^{-3} (Davies *et al*., 2001). Conversely, peatland samples are commonly extracted by igniting the surrounding peat (Hall and Pilcher, 2002) a process which involves limited use of chemical treatment or handling and should result in the loss of very few shards of any chemical composition. Three explanations have been proposed

for the dominance of felsic tephras in the distal geological record, and in particular the apparent scarcity of basaltic tephras in peatlands:

1) There is experimental evidence that basaltic glass is more prone than silicic glass to hydration, alteration and even complete dissolution in acidic environments (Pollard *et al*., 2003; Wolff-Boenisch *et al*., 2004);

2) Basaltic glass shards are more dense than silicic shards (2.5-2.9 and 2.3 g cm^{-3}, respectively), and therefore glass shards of basaltic composition are likely to fall out of the atmosphere earlier than silicic shards of the same size (Stevenson *et al*., 2015), and arrive over northern Europe in lower concentrations in the air.

3) Eruptions of basaltic magma are typically less explosive and therefore generally produce less tephra, which is released at a lower height, than eruptions of more silicic magmas. Unlike raised peatlands, lakes concentrate shards from the wider catchment, perhaps increasing the probability of cryptotephra layer detection in lake sediments when fewer glass shards have been deposited at a distal location during an eruption.

Claraghmore lake contains the only basaltic cryptotephra layer identified in this study (CLA-L1) which has a relatively high concentration of shards (n = 141) when compared with those of other cryptotephra layers identified in this lake. No basaltic cryptotephra layers were identified in Claraghmore bog. The presence of large concentrations of basaltic shards in Claraghmore Lake, while the layer was apparently completely absent from the adjacent peatland, suggests that basaltic cryptotephra layers are not recorded representatively when compared to silicic cryptotephra layers in peatlands. Our findings would appear to support the hypothesis that the low numbers of basaltic tephras in the European record may be partly due to the dominance of peatland records, which appear to provide unfavourable conditions for the preservation and/or concentration of basaltic glass shards. There have been many more cryptotephra studies on peatlands in Ireland than have been conducted on lakes. This is not reflected in the number of basaltic cryptotephra layers identified in lakes and peatlands in the region (n = 2 and n = 0, respectively).

As no basaltic cryptotephra layers were identified in both peatland and lake sites it was not possible to compare geochemical data for tephra of mafic composition recovered

from peatlands and lakes. However, Hekla 1104 and SN-1 in Sammakovuoma peatland and lake are geochemically indistinguishable (Figs. 10 and 7) suggesting that rhyolitic (Hekla 1104) and trachydacitic (SN-1) tephras undergo either the same chemical alteration, or a negligible amount of chemical alteration in lake and peatland environments with different pH conditions (lake pH = 7.0, peatland pH = 5.9). Similarly, there is no discernible difference between the major element glass geochemistry of the Glen Garry tephra found in both Malham Tarn and Malham Moss (1966-2210 cal yr BP). This suggests that prolonged exposure to acid (Malham Moss) or alkaline conditions (Malham Tarn, pH = ~8) has not impacted on the tephra geochemistry as determined by EPMA. Samples from both Malham Tarn and Sammakovuoma Lake were extracted for geochemical analysis using density separation, whereas samples from Malham Moss and Sammakovuoma peatland were extracted using acid extraction. In this instance neither the depositional environment nor the method of extraction had a significant impact on the major element geochemistry of glass shards from the Hekla 1104, SN-1 or Glen Garry cryptotephra layers.

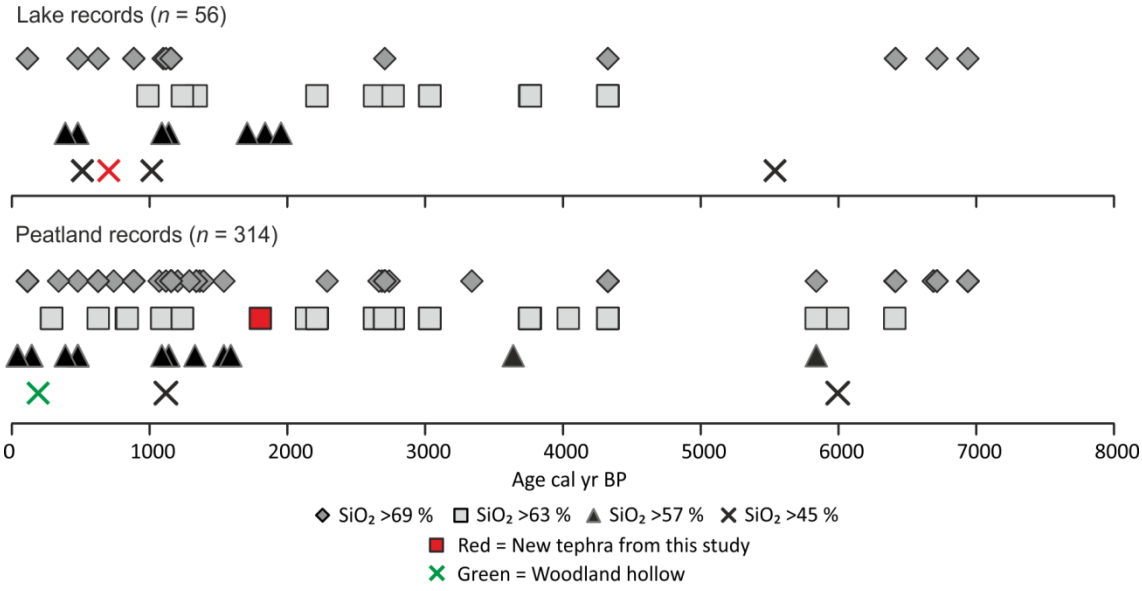

Fig. 12. Diagram indicating the age and geochemistry of glass from cryptotephra layers deposited in peatland and lake sites in northern Europe over the last 7000 years. Silica values (in wt %) are based on the TAS classification system. Age displayed is the mid-age estimate for each tephra. Basaltic tephras have been found in both lakes and peatlands. The two new tephras described in this paper are added in red. Ages of these new tephras are based on interpolation from radiocarbon dates or age depth models and are given in Table 2. The basaltic tephra indicated in green was identified by Reilly and Mitchell, (2015) in a woodland hollow but is included here in the 'peatland' category. References: Swindles *et al.* (2011) database and references therein and Wulf *et al.* (2016).

Given that we only identified one basaltic cryptotephra layer in the lake and peatland sites examined in this study and therefore had only a small sample size, we reviewed tephra records from published literature over the last 7000 years (Fig. 12). There are some examples of basaltic tephras identified in peatlands. The Hov (6190-5720 cal yr BP) and Landnám (AD 871± 2) tephras have been identified in peatland records on the Faroe Islands (Hannon *et al.*, 2001; Wastegård, 2002). Given the close proximity of the Faroe Islands to Iceland, the glass shards at these sites were most likely larger and more numerous than those delivered to peatlands further away from Iceland. Although larger shards have a smaller surface area to volume ratio and are therefore less prone to chemical alteration, we suggest that given the longevity of these shards in peatlands, and given that we identify no evidence of dissolution in tephras of rhyolitic and mixed composition; preservation alone is unlikely to explain the lack of Holocene basaltic tephras in peatlands. Instead, we suggest that, due to differences in eruption style and tephra density, basaltic tephra shards fall out more quickly than rhyolitic tephra shards;

therefore fewer shards reach sites far from the volcano. Raised peatlands record only primary tephra fall material and small concentrations of shards may be below detection levels, whereas lakes focus tephra from across the catchment into a small basin and concentrate the tephra, raising the numbers of shards above detection levels. As previously discussed, this process is complicated because tephras are then subject to additional within-basin redistribution, which can act to bring the number of shards above/below detection levels in areas of the lake basin. This idea is supported by the recent discovery of basaltic tephra from the Laki eruption of 1783 in a small (30 x 15 m) woodland hollow in Ireland. We suggest that similar processes of runoff and the concentration of glass shards might operate in small woodland hollows as operate in small lakes.

5.5 Conclusions

We present evidence that lakes and peatlands provide contrasting records of volcanic ash deposition; the dominance of peatland records of ash fallout in northern Europe may bias our current understanding of ash cloud reoccurrence.

In general, we identify more cryptotephra layers over the same time period in peatlands than lakes. However, there is evidence of incomplete tephra records in both peatlands and lakes. A combination of records from both lakes and peatlands must be used to establish the most comprehensive and complete regional tephrostratigraphies.

We find no evidence for chemical alteration to any of the glass shards which were analysed in this study. We suggest that glass shards do not undergo significant chemical alteration in peatland or lake environments (pH range: 4.3 – 8.2) over the time scale of this study. Instead, we suggest that the low number of basaltic cryptotephra occurrences in peatlands is most likely related to peatlands capturing only primary tephra fall events. This is in contrast to lakes which concentrate tephra fallout from a wider area.

We also find no evidence for the chemical alteration of shards extracted by different extraction processes (density separation vs. acid extraction). We clearly illustrate that acid digestion is a suitable extraction method for glass shards of rhyolitic and trachydacitic composition from ombrotrophic peatlands and does not result in a significant degree of chemical alteration.

We identify a new basaltic tephra at Claraghmore Lake in Ireland (CLA-L1). The geochemistry of glass from this tephra suggests it is derived from an eruption of the Grímsvötn volcano, Iceland, post AD 1000. This basaltic tephra is not present in the adjacent peatland.

We identify a new trachydacitic cryptotephra (SN-1) and extend the existing spatial coverage of cryptotephras in northern Europe to sites in Arctic Sweden. SN-1 is tightly dated to 1183-1147 cal yr BP in one of our peatland sites suggesting an earlier age (1860-1520 cal yr BP: Larsen *et al*., (2002)) on peaty soil underlying SN-1 in Iceland should be considered a maximum estimate. The cryptotephra deposits we describe may provide important marker horizons for palaeoclimatological research in the vulnerable Arctic region.

Acknowledgements

This research was undertaken while Elizabeth Watson held a NERC-funded Doctoral Training Grant (NE/K500847/1). GTS acknowledges support from the Dutch Foundation for the Conservation of Irish Bogs. IS and EJW thank CGS for generous support of the fieldwork in Sweden. We thank Thomas Kelly for help in the field, Chris Hayward for help with tephra geochemical analysis, Matts Nilsson for help with access to Degerö Stormyr and advice on coring Arctic Peatlands, and Stefan Wastegård for help with SN-1 tephra identification. We thank David Lowe and one anonymous reviewer for constructive comments on a previous version of this manuscript.

References

Alexandersson, H., Karlström, C., Larsson-McCann, S., 1991 Temperature and precipitation in Sweden, 1961–90. Reference normals, SMHI report 81, Norrköping.

Barber, K., Brown, A., Langdon, P., Hughes, P., 2013. Comparing and cross-validating lake and bog palaeoclimatic records: a review and a new 5,000 year chironomid-inferred temperature record from northern England. J. Paleolimn. 49, 497-512.

Barnekow, L., Bragée, P., Hammarlund, D., St. Amour, N., 2008. Boreal forest dynamics in north-eastern Sweden during the last 10,000 years based on pollen analysis. Vegetation History and Archaeobotany 17, 687-700.

Barnekow, L., Possnert, G., Sandgren, P., 1998. AMS 14C chronologies of Holocene lake sediments in the Abisko area, northern Sweden – a comparison between dated bulk sediment and macrofossil samples. GFF 120, 59-67.

Bergman, J., Wastegård, S., Hammarlund, D., Wohlfarth, B., Roberts, S.J., 2004. Holocene tephra horizons at Klocka Bog, west-central Sweden: aspects of reproducibility in subarctic peat deposits. Journal of Quaternary Science 19, 241-249.

Bertrand, S., Daga, R., Bedert, R., Fontijn, K., 2014. Deposition of the 2011–2012 Cordón Caulle tephra (Chile, 40°S) in lake sediments: Implications for tephrochronology and volcanology. Journal of Geophysical Research: Earth Surface 119, 2555-2573

Blockley, S.P.E., Pyne-O'Donnell, S.D.F., Lowe, J.J., Matthews, I.P., Stone, A., Pollard, A.M., Turney, C.S.M., Molyneux, E.G., 2005. A new and less destructive laboratory procedure for the physical separation of distal glass tephra shards from sediments. Quaternary Science Reviews 24, 1952-1960.

Boygle, J., 1999. Variability of tephra in lake and catchment sediments, Svínavatn, Iceland. Global and Planetary Change 21, 129-149.

Bramham-Law, C.W.F., Theuerkauf, M., Lane, C.S., Mangerud, J., 2013. New findings regarding the Saksunarvatn Ash in Germany. Journal of Quaternary Science 28, 248-257.

Burt, T.P., Horton, B.P., 2003. The Climate of Malham Tarn. Field Studies 10, 635-652.

Chambers, F.M., Beilman, D.W., Yu, Z., 2010. Methods for determining peat humification and for quanitifying peat bulk density, organic matter and carbon content for palaeostudies of climate and peatland carbon dynamics Mires and Peat 7, 1-10.

Chambers, F.M., Daniell, J.R.G., Hunt, J.B., Molloy, K., O'Connell, M., 2004. Tephrostratigraphy of An Loch Mor, Inis Oirr, western Ireland: implications for Holocene tephrochronology in the northeastern Atlantic region. Holocene 14, 703-720.

D'Andrea, W.J., Vaillencourt, D.A., Balascio, N.L., Werner, A., Roof, S.R., Retelle, M., Bradley, R.S., 2012. Mild Little Ice Age and unprecedented recent warmth in an 1800 year lake sediment record from Svalbard. Geology 40, 1007-1010

Davies, S.M., Abbott, P.M., Pearce, N.J.G., Wastegård, S., Blockley, S.P.E., 2012. Integrating the INTIMATE records using tephrochronology: rising to the challenge. Quaternary Science Reviews 36, 11-27.

Davies, S.M., Elmquist, M., Bergman, J., Wohlfarth, B., Hammarlund, D., 2007. Cryptotephra sedimentation processes within two lacustrine sequences from west central Sweden. Holocene 17, 319-330.

Davies, S.M., Turney, C.S.M., Lowe, J.J., 2001. Identification and significance of a visible, basalt-rich Vedde Ash layer in a Late-glacial sequence on the Isle of Skye, Inner Hebrides, Scotland. Journal of Quaternary Science 16, 99-104.

De Vleeschouwer, F., Chambers, F.M., Swindles, G.T., 2011. Coring and sub-sampling of peatlands for palaeoenvironmental research. Mires and Peat 7, 1-10.

Dugmore, A., Newton, A., 1998. Holocene tephra layers in the Faroe Islands. Frodskaparrit 46, 191-204.

Dugmore, A.J., Larsen, G., Newton, A.J., 1995. 7 Tephra isochrones in Scotland. Holocene 5, 257-266.

Dugmore, A.J., Newton, A.J., Sugden, D.E., Larsen, G., 1992. Geochemical stability of fine-grained silicic Holocene tephra in Iceland and Scotland. Journal of Quaternary Science 7, 173-183.

Dugmore, A.J., Newton, A.J., 1992. Thin tephra layers in peat revealed by X-Radiography. Journal of Archaeological Science 19, 163-170.

Gehrels, M.J., Lowe, D.J., Hazell, Z.J., Newnham, R.M., 2006. A continuous 5300-yr Holocene cryptotephrostratigraphic record from northern New Zealand and implications for tephrochronology and volcanic hazard assessment. The Holocene 16, 173-187.

Global Volcanism Program, 2013. Volcanoes of the World, v. 4.3.4. , In: Venzke, E. (Ed.), Smithsonian Institution.

Gudmundsdóttir, E.R., Eiríksson, J., Larsen, G., 2011. Identification and definition of primary and reworked tephra in Late Glacial and Holocene marine shelf sediments off North Iceland. Journal of Quaternary Science 26, 589-602.

Haflidason, H., Eiriksson, J., Van Kreveld, S., 2000. The tephrochronology of Iceland and the North Atlantic region during the Middle and Late Quaternary: a review. Journal of Quaternary Science 15, 3-22.

Hall, M., Hayward, C., 2014. Preparation of micro- and crypto-tephras for quantitative microbeam analysis. Geological Society, London, Special Publications 398, 21-28.

Hall, V.A., Pilcher, J.R., 2002. Late-Quaternary Icelandic tephras in Ireland and Great Britain: detection, characterization and usefulness. Holocene 12, 223-230.

Hannon, G.E., Wastegård, S., Bradshaw, E., Bradshaw, R.H.W., 2001. Human impact and landscape degradation on the Faroe Islands. Biology and Environment: Proceedings of the Royal Irish Academy. Royal Irish Academy: 129-139.

Hayward, C., 2012. High spatial resolution electron probe microanalysis of tephras and melt inclusions without beam-induced chemical modification. Holocene 22, 119-125.

Holmes, N., Langdon, P.G., Caseldine, C.J., Wastegård, S., Leng, M.J., Croudace, I.W., Davies, S.M., 2016. Climatic variability during the last millennium in Western Iceland from lake sediment records. The Holocene. 0959683615618260.

Jensen, B.J.L., Pyne-O'Donnell, S., Plunkett, G., Froese, D.G., Hughes, P.D.M., Sigl, M., McConnell, J.R., Amesbury, M.J., Blackwell, P.G., van den Bogaard, C., Buck, C.E., Charman, D.J., Clague, J.J., Hall, V.A., Jochum, K.P., Stoll, B., Herwig, K., Willbold, M., Hofmann, A.W., Amini, M., Aarburg, S., Abouchami, W., Hellebrand, E., Mocek, B., Raczek, I., Stracke, A., Alard, O., Bouman, C., Becker, S., Dücking, M., Brätz, H., Klemd, R., de Bruin, D., Canil, D., Cornell, D., de Hoog, C.-J., Dalpé, C., Danyushevsky, L., Eisenhauer, A., Gao, Y., Snow, J.E., Groschopf, N., Günther, D., Latkoczy, C., Guillong, M., Hauri, E.H., Höfer, H.E., Lahaye, Y., Horz, K., Jacob, D.E., Kasemann, S.A., Kent, A.J.R., Ludwig, T., Zack, T., Mason, P.R.D., Meixner, A., Rosner, M., Misawa, K., Nash, B.P., Pfänder, J., Premo, W.R., Sun, W.D., Tiepolo, M., Vannucci, R., Vennemann, T., Wayne, D., Woodhead, J.D., 2006. MPI-DING reference glasses for in situ microanalysis: New reference values for element concentrations and isotope ratios. Geochemistry, Geophysics, Geosystems 7, Q02008.

Jensen, B.J.L., Pyne-O'Donnell, S., Plunkett, G., Froese, D.G., Hughes, P.D.M., Sigl, M., McConnell, J.R., Amesbury, M.J., Blackwell, P.G., van den Bogaard, C., Buck, C.E., Charman, D.J., Clague, J.J., Hall, V.A., Koch, J., Mackay, H., Mallon, G.,

McColl, L., Pilcher, J.R., 2014. Transatlantic distribution of the Alaskan White River Ash. Geology 42, 875-878.

Lane, C.S., Brauer, A., Blockley, S.P.E., Dulski, P., 2013. Volcanic ash reveals time-transgressive abrupt climate change during the Younger Dryas. Geology 41, 1251-1254.

Larsen, G., Dugmore, A., Newton, A., 1999. Geochemistry of historical-age silicic tephras in Iceland. Holocene 9, 463-471.

Larsen, G., Eiríksson, J., Knudsen, K.L., Heinemeier, J., 2002. Correlation of late Holocene terrestrial and marine tephra markers, north Iceland: implications for reservoir age changes. Polar Research 21, 283-290.

Larsen, G., Newton, A.J., Dugmore, A.J., Vilmundardóttir, E.G., 2001. Geochemistry, dispersal, volumes and chronology of Holocene silicic tephra layers from the Katla volcanic system, Iceland. Journal of Quaternary Science 16, 119-132.

Lawson, I.T., Gathorne-Hardy, F.J., Church, M.J., Newton, A.J., Edwards, K.J., Dugmore, A.J., Einarsson, A., 2007. Environmental impacts of the Norse settlement: palaeoenvironmental data from Myvatnssveit, northern Iceland. Boreas 36, 1-19.

Lawson, I.T., Swindles, G.T., Plunkett, G., Greenberg, D., 2012. The spatial distribution of Holocene cryptotephras in north-west Europe since 7 ka: implications for understanding ash fall events from Icelandic eruptions. Quaternary Science Reviews 41, 57-66.

Lowe, D., 1988a. Stratigraphy, age, composition, and correlation of late Quaternary tephras interbedded with organic sediments in Waikato lakes, North Island, New Zealand. New Zealand journal of geology and geophysics 31, 125-165.

Lowe, D.J., 1988b. Late Quaternary volcanism in New Zealand: Towards an integrated record using distal airfall tephras in lakes and bogs. Journal of Quaternary Science 3, 111-120.

Mackay, E.B., Jones, I.D., Folkard, A.M., Barker, P., 2012. Contribution of sediment focussing to heterogeneity of organic carbon and phosphorus burial in small lakes. Freshwater Biology 57, 290-304.

Mangerud, J., Lie, S.E., Furnes, H., Krisiansen, I.L., Lomo, L., 1984. A Younger Dryas ash bed in Western Norway, and its possible correlations with tephra in cores from the Norwegian Sea and the North-Atlantic. Quat. Res. 21, 85-104.

Mangerud, J., Furnes, H., Johansen, J., 1986. A 9000-year-old ash bed on the Faroe Islands. Quat. Res. 26, 262-265.

Newton, A.J., Dugmore, A.J., Gittings, B.M., 2007. Tephrabase: tephrochronology and the development of a centralised European database. Journal of Quaternary Science 22, 737-743.

Nilsson, M., Sagerfors, J., Buffam, I., Laudon, H., Eriksson, T., Grelle, A., Klemedtsson, L., Weslien, P.E.R., Lindroth, A., 2008. Contemporary carbon accumulation in a boreal oligotrophic minerogenic mire – a significant sink after accounting for all C-fluxes. Glob. Change Biol. 14, 2317-2332.

Norwegian Meteorological Institute, 2015. Weather statistics for Gallivare, Norrbotten (Sweden) Online.

http://www.yr.no/place/Sweden/Norrbotten/g%C3%A4llivare/statistics.html [Oct 2015].

Nuñez, R., Spiro, B., Pentecost, A., Kim, A., Coletta, P., 2002. Organo-geochemical and stable isotope indicators ofenvironmental change in a marl lake, Malham Tarn, North Yorkshire,U.K. J. Paleolimn. 28, 403-417.

Oldfield, F., Thompson, R., Crooks, P.R.J., Gedye, S.J., Hall, V.A., Harkness, D.D., Housley, R.A., McCormac, F.G., Newton, A.J., Pilcher, J.R., Renberg, I., Richardson, N., 1997. Radiocarbon dating of a recent high-latitude peat profile: Stor Amyran, northern Sweden. Holocene 7, 283-290.

Parker, A.G., Goudie, A.S., Anderson, D.E., Robinson, M.A., Bonsall, C., 2002. A review of the mid-Holocene elm decline in the British Isles. Prog. Phys. Geogr. 26, 1-45.

Payne, R., Gehrels, M., 2010. The formation of tephra layers in peatlands: An experimental approach. Catena 81, 12-23.

Pentecost, A., 2009. The marl lakes of the British Isles. Freshwater Reviews 2, 167-197.

Persson, C., 1966. 'Forsok till tefrokronologisk datering av nagra Svenska torvmossar'. Geologiska Foreningens i Stockholm Forhandlingar 88, 361-394.

Persson, C., 1968. 'Forsok till tefrokronologisk datering i fyra faroiska myrar'. Geologiska Foreningens i Stockholm Forhandlingar 90, 241-266.

Pigott, C.D., Pigott, M.E., 1963. Late-glacial and post-glacial deposits at Malham, Yorkshire. New Phytologist 62, 317-334.

Pilcher, J., Bradley, R.S., Francus, P., Anderson, L., 2005. A Holocene tephra record from the Lofoten Islands, Arctic Norway. Boreas 34, 136-156.

Pilcher, J.R., Hall, V.A., 1996. Tephrochronological studies in northern England. Holocene 6, 100-105.

Pilcher, J.R., Hall, V.A., McCormac, F.G., 1996. An outline tephrochronology for the Holocene of the north of Ireland. Journal of Quaternary Science 11, 485-494.

Pilcher, J.R., Hall, V.A., McCormac, F.G., 1995. Dates of Holocene Icelandic Volcanic-eruptions from tephra layers in Irish peats. Holocene 5, 103-110.

Plunkett, G., 2006. Tephra-linked peat humification records from Irish ombrotrophic bogs question nature of solar forcing at 850 cal. yr RC. Journal of Quaternary Science 21, 9-16.

Plunkett, G., 2009. Land-use patterns and cultural change in the Middle to Late Bronze Age in Ireland: inferences from pollen records. Vegetation History and Archaeobotany 18, 273-295.

Plunkett, G.M., Pilcher, J.R., McCormac, F.G., Hall, V.A., 2004. New dates for first millennium BC tephra isochrones in Ireland. Holocene 14, 780-786.

Pollard, A.M., Blockley, S.P.E., Ward, K.R., 2003. Chemical alteration of tephra in the depositional environment: theoretical stability modelling. Journal of Quaternary Science 18, 385-394.

Pyne-O'Donnell, S., 2011. The taphonomy of Last Glacial-Interglacial Transition (LGIT) distal volcanic ash in small Scottish lakes. Boreas 40, 131-145.

Rea, H.A., Swindles, G.T., Roe, H.M., 2012. The Hekla 1947 tephra in the north of Ireland: regional distribution, concentration and geochemistry. Journal of Quaternary Science 27, 425-431.

Reilly, E., Mitchell, F.J., 2015. Establishing chronologies for woodland small hollow and mor humus deposits using tephrochronology and radiocarbon dating. The Holocene 25, 241-252.

Reimer, P.J., Bard, E., Bayliss, A., Beck, J.W., Blackwell, P.G., Bronk Ramsey, C., Buck, C.E., Cheng, H., Edwards, R.L., Friedrich, M., Grootes, P.M., Guilderson, T.P., Haflidason, H., Hajdas, I., Hatté, C., Heaton, T.J., Hoffmann, D.L., Hogg, A.G., Hughen, K.A., Kaiser, K.F., Kromer, B., Manning, S.W., Niu, M., Reimer, R.W., Richards, D.A., Scott, E.M., Southon, J.R., Staff, R.A., Turney, C.S.M., van der Plicht, J., 2013. IntCal13 and Marine13 Radiocarbon Age Calibration Curves 0–50,000 Years cal BP. Radiocarbon 55, 1869-1887.

Stevenson, J., Millington, S., Beckett, F., Swindles, G., Thordarson, T., 2015. Big grains go far: reconciling tephrochronology with atmospheric measurements of volcanic ash. Atmos. Meas. Tech. Discuss., 8, 65-120.

Streeter, R., Dugmore, A., 2014. Late-Holocene land surface change in a coupled social–ecological system, southern Iceland: a cross-scale tephrochronology approach. Quaternary Science Reviews 86, 99-114.

Stuiver, M., Reimer, P., 1993. Extended 14C database and revised CALIB radiocarbon calibration program. Radiocarbon 35, 215-230.

Sweeney, J., 1997. Ireland, In: Wheeler, D., Mayes, J. (Eds.), Regional Climates of the British Isles. Routledge, London, pp. 254-275.

Swindles GT. 2006. *Reconstruction of Holocene climate change from peatlands in the north of Ireland.* PhD thesis, Queen's University Belfast

Swindles, G.T., De Vleeschouwer, F., Plunkett, G., 2010. Dating peat profiles using tephra: stratigraphy, geochemistry and chronology Mires and Peat 7, 1-9.

Swindles, G.T., Galloway, J., Outram, Z., Turner, K., Schofield, J.E., Newton, A.J., Dugmore, A.J., Church, M.J., Watson, E.J., Batt, C., Bond, J., Edwards, K.J., Turner, V., Bashford, D., 2013a. Re-deposited cryptotephra layers in Holocene peats linked to anthropogenic activity. The Holocene 23, 1493-1501.

Swindles, G.T., Lawson, I.T., Savov, I.P., Connor, C.B., Plunkett, G., 2011. A 7000 yr perspective on volcanic ash clouds affecting northern Europe. Geology 39, 887-890.

Swindles, G.T., Roe, H.M., 2006. Constraining the age of spheroidal carbonaceous particle (SCP) stratigraphies in peats using tephrochronology. Quaternary Newsletter 110, 2-9.

Swindles, G.T., Savov, I.P., Connor, C.B., Carrivick, J., Watson, E.J., Lawson, I.T., 2013b. Volcanic ash clouds affecting Northern Europe: the long view. Geology Today 29, 215-217.

Swindles, G.T., Watson, E., Turner, T.E., Galloway, J.M., Hadlari, T., Wheeler, J., Bacon, K.L., 2015. Spheroidal carbonaceous particles are a defining stratigraphic marker for the Anthropocene. Sci. Rep. 5. DOI 10.1038/srep10264

Thorarinsson, S., 1944. Tefrokronologiska studier på Island. Pjórsárdalur och Dess Förödelse. Geografiska Annaler 26, 1-217.

Thordarson, T., Self, S., Óskarsson, N., Hulsebosch, T., 1996. Sulfur, chlorine, and fluorine degassing and atmospheric loading by the 1783–1784 AD Laki (Skaftár Fires) eruption in Iceland. Bulletin of Volcanology 58, 205-225.

Tveito, O.E., Førland, E., Heino, R., Hanssen-Bauer, I., Alexandersson, H., Dahlström, B., Drebs, A., Kern-Hansen, C., Jónsson, T., Vaarby Laursen, E., Westman, Y., 2000. Nordic temperature maps. Norwegian Meterological Institute 09/00 KLIMA.

Wastegård, S., 2002. Early to middle Holocene silicic tephra horizons from the Katla volcanic system, Iceland: new results from the Faroe Islands. Journal of Quaternary Science 17, 723-730.

Wastegård, S., Bjorck, S., Grauert, M., Hannon, G.E., 2001. The Mjauvotn tephra and other Holocene tephra horizons from the Faroe Islands: a link between the Icelandic source region, the Nordic Seas, and the European continent. Holocene 11, 101-109.

Wastegård, S., Rundgren, M., Schoning, K., Andersson, S., Bjorck, S., Borgmark, A., Possnert, G., 2008. Age, geochemistry and distribution of the mid-Holocene Hekla-S/Kebister tephra. Holocene 18, 539-549.

Watson, E.J., Swindles, G.T., Lawson, I.T., Savov, I.P., 2015. Spatial variability of tephra and carbon accumulation in a Holocene peatland. Quaternary Science Reviews 124, 248-264.

Wolff-Boenisch, D., Gislason, S.R., Oelkers, E.H., Putnis, C.V., 2004. The dissolution rates of natural glasses as a function of their composition at pH 4 and 10.6, and temperatures from 25 to 74°C. Geochim. Cosmochim. Acta 68, 4843-4858.

Wulf, S., Dräger, N., Ott, F., Serb, J., Appelt, O., Guðmundsdóttir, E., van den Bogaard, C., Słowiński, M., Błaszkiewicz, M., Brauer, A., 2016. Holocene tephrostratigraphy of varved sediment records from Lakes Tiefer See (NE Germany) and Czechowskie (N Poland). Quaternary Science Reviews 132, 1-14.

Zillen, L.M., Wastegård, S., Snowball, I.F., 2002. Calendar year ages of three mid-Holocene tephra layers identified in varved lake sediments in west central Sweden. Quaternary Science Reviews 21, 1583-1591.

Chapter 6: The transport of Icelandic volcanic ash: insights from European tephra records

Watson, E.J.[1]., Swindles, G.T.[1]., Stevenson, J., Savov, I.[2]., Lawson, I.T.[3], Lamentowicz, M.[4]

[1]School of Geography, University of Leeds, Leeds, LS2 9JT, UK
[2]School of Earth and Environment, University of Leeds, Leeds, LS2 9JT, UK
[3]Department of Geography and Sustainable Development, University of St Andrews, St Andrews, KY16 9AL, UK
[4]Department of Biogeography and Paleoecology, Adam Mickiewicz University in Poznan, Dziegielowa 27, 61-680 Poznan, Poland
**Corresponding author: Elizabeth Watson (gy08ejw@leeds.ac.uk)*

Keywords: Shard size, Travel distance, Probabilistic modelling, Iceland, Northern Europe

Abstract

Fine ash produced during explosive volcanic eruptions can remain in the atmosphere for long periods of time (hours to months) and undergo transport over long distances. We analyse the particle size distributions, geochemistry and shard morphology of distal volcanic ash layers distributed across northern Europe. We identify a total of 19 microscopic (crypto-) tephra layers at sites across northern Europe, many geochemically linked to a specific volcanic eruption.

The longest axis (Max A) of the microscopic glass shards in the cryptotephra layers ranges from 10 to 250 µm. Although the 95th percentile values for Max A generally indicate a loss of larger shards from the particle size distribution at sites further from the volcano, we identify no relationship between median Max A and transport distance. Despite their attribution to the same eruption, we find differences in the geochemistry of tephra shards in different regions, indicative of their deposition during different eruptive phases. In some instances the major controls on tephra fallout such as weather conditions, plume height, magma geochemistry and tephra shard morphology vary even during a single eruption. The dynamic nature of the controls on tephra transport, even during the course of one eruption, result in tephra shard size distributions which do not often show a simple relationship between shard size and distance from source.

We develop a probabilistic model of particle fallout and compare it with data from the geological record. However, our simple model, which does not account for transport in the buoyant plume, underestimates the transport distance of the largest shards. We conclude that the shard size information provided by glass shards in distal tephra layers may hold some promise for understanding the eruption parameters of ancient eruptions. However, reworking and redistribution in peatlands and lakes must be considered. The particle size dataset presented provides an important resource for testing more complex models of ash dispersal over northern Europe.

6.1 Introduction

During explosive volcanic eruptions (≥ VEI 3; (Newhall and Self, 1982)) 'extremely fine' ash (<64 μm) can be transported over long distances (Lane *et al*., 2013; Rose and Durant, 2011). In low concentrations volcanic ash poses a small risk to human health, but fine ash can be a hazard for modern aviation (Folch, 2012). Understanding the nature of past volcanic ash clouds can help us to understand more about the risk posed by future events.

Volcanic eruptions which produce a significant amount of fine ash over northern Europe have occurred with a mean return interval of 56 ± 9 years over the last 1000 years (Swindles *et al*., 2011; Swindles *et al*., 2013b). However, there is a lack of data on the particle size distribution of volcanic ash reaching northern Europe. The geological record offers a source of information on distal (> 1000 km) ash fallout. Microscopic (crypto-) tephra layers from past ash clouds are stored in over 120 peatlands and lakes across northern Europe (Dugmore *et al*., 1995; Hall and Pilcher, 2002; Wastegård and Davies, 2009). As cryptotephra form spatially widespread, isochronous horizons they are predominantly used for the correlation of geological records ('tephrochronology') (Lowe, 2011). Cryptotephra layers in the geological record typically span a few centimetres in depth (Davies *et al*., 2007; Payne and Gehrels, 2010). Tephra shards are often counted for the purpose of identifying the depth of the peak shard concentration, which represents the isochron widely used in tephrochronology. However, the size and shape of shards are rarely reported.

Recent work has indicated that the particle size distributions of cryptotephra layers can be used to evaluate the satellite infra-red methods often used to monitor volcanic ash clouds (Stevenson *et al*., 2015). Furthermore, the particle size distributions of distal tephra occurrences can provide more realistic estimates of total erupted tephra volumes (Ponomareva *et al*., 2015) that are currently biased toward tephra which falls out closer to the volcanic source. However, there has been no study into how representative particle size distributions from cryptotephra layers in lakes and peatlands are of the ash cloud fallout over a region. Peatlands are commonly considered to be archives of primary fall out material, whereas tephra in lakes might have fallen elsewhere in the catchment and been subject to a greater amount of reworking (Davies *et al*., 2007). The movement of shards across the terrestrial surface following deposition, and vertical movement in peat and lake sediments might cause the sorting of tephra shards of different sizes, or even lead to the fragmentation of the glass shards before they enter the geological record: resulting in a particle size distribution in the geological record, which does not reflect the particle size distribution of ash fallout over the site. Furthermore, there is no indication as to how many tephra shards must be measured in order to ascertain the particle size distribution for a site. Before cryptotephra particle size distributions can be applied more widely as records of ash clouds, these methodological issues must be understood.

In this paper we analyse the tephra particle size distribution and shard morphology of cryptotephra layers from 14 sites in northern Europe. This study represents the most spatially widespread analysis of cryptotephra particle size distributions across northern Europe. We examine whether cryptotephra particle size distributions in lakes and peatlands are likely to reflect cryptotephra fallout over the region, or whether they are confounded by the sorting of tephra shards in the catchment or across the peatland. The aim of this paper is to understand the extent to which the particle size distribution and shard morphology of cryptotephra layers can be used to provide information about the nature (e.g. plume height, magma geochemistry) of the eruptions which produced them. We also aim to assess whether simple probabilistic modelling can be used to estimate eruption parameters based on cryptotephra particle size distributions in the geological record.

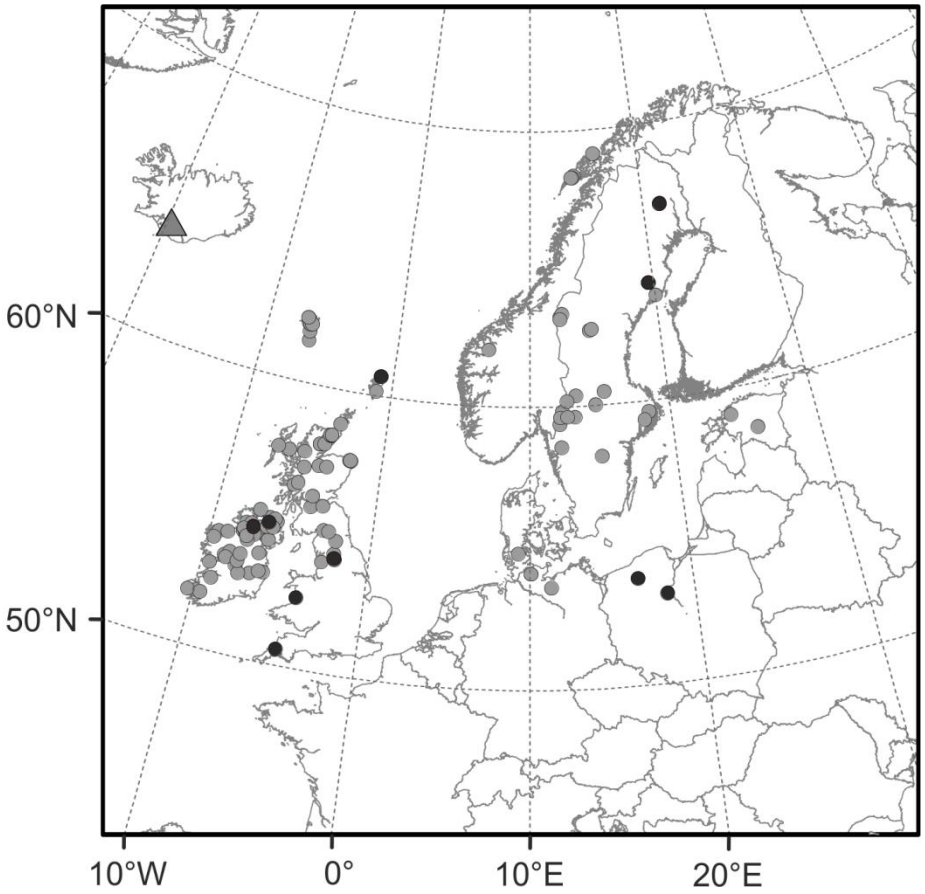

Figure 1. Map showing the distribution of sites where Holocene cryptotephras have been identified. Grey circles indicate lake and peatland sites where cryptotephras have been geochemically analysed. Black circles indicate sites where cryptotephras have been geochemically analysed and where shard size analyses have been conducted. The grey triangle shows the location of the Hekla volcano, the source of the majority of the Holocene tephra layers in Northern Europe.

We test the following hypotheses:

1. The median shard size for the same cryptotephra layer will be significantly different in lakes and peatlands which have received the same primary air fall tephras.
2. Tephra shards will be reworked on the peatland surface according to size, therefore, shard sizes will vary significantly between cores from the same peatland site.
3. The analysis of shard size on just the sample of peak shard concentration might not capture the median shard size for a given cryptotephra because tephra particle size might control the movement of particles vertically through peat and lake sediments (Payne and Gehrels, 2010).
4. The median tephra shard size will decrease with increased distance between the fallout site and the volcanic source.

6.2 Methods

6.2.1The geological record

6.2.1.1 Field sampling

Sites were selected in order to span a range of distances from Iceland, the main source region for tephra layers in northern Europe (Fig. 1). For the purposes of this study the distances from Iceland to each site are the great circle distance between the Hekla volcano, the dominant source of Holocene cryptotephra layers in northern Europe, and the site location (Table 1). To examine possible differences in the particle size distribution of the same tephra in peatlands and lakes, we sampled both a lake and a peatland in close proximity (<10 km apart) at four sites (Sammakovuoma and Degerö Stormyr /Lake Svartkälsjärn in Sweden, Claraghmore in northern Ireland and Malham in England) (c.f. Watson *et al*., 2016).

Cores were extracted using a Russian-type corer (Jowsey, 1966), following the parallel hole method (De Vleeschouwer *et al*., 2011). With the exception of Fallahogy, where multiple cores were retrieved (c.f. Watson *et al*., 2015), one core was extracted from each site. In addition to core samples, surface samples were obtained from the sites identified in Fig. 2. Surface vegetation and the upper ~7cm of peat were sampled, an upturned 2 ltr plastic box was placed onto the surface and with the help of knife the peat was cut around the edges of the box. Samples were subsampled into c. 125 cm^3 blocks.

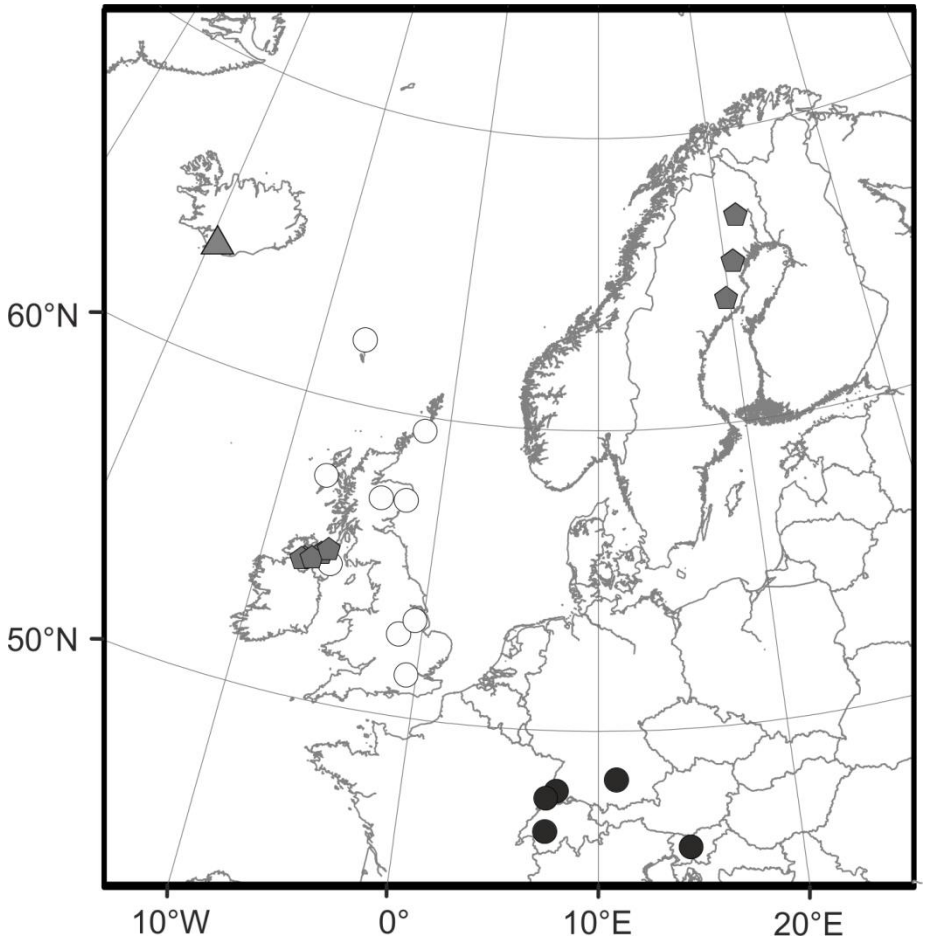

Figure 2. Map showing the distribution of locations where Eyjafjallajökull 2010 tephra was identified in rain gauge (white circles) and air monitoring (black circles) samples (Stevenson *et al.*, 2012). Grey pentagons indicate the locations where moss surface samples were taken and examined for tephra, but none was found. The grey triangle shows the location of the Eyjafjallajökull volcano.

				Tephra																				
Site [Peatland/Lake]	Location		Distance from Hekla (km)	Hekla 4	Hekla 1104	Hekla 1158	**AD 860 B**	SN-1	**Glen Garry**	MOR-T4	Askja 1875	Lairg A	Lairg B	Hekla 1947	Hekla 1845	Hekla 1510	Öræfajökull 1362	Microlite/GB4-150	CLA-L1 Grímsvötn?	Hekla-S/Kebister	Hekla 3	**QUB_384_G3/G4**	AD 860 A	**Unknown Alaska?**
Shetland Underhoull, Unst [P]	60.719°N	0.948°W	1075	1	1	1														1				
Claraghmore bog [P]	54.633°N	7.454°W	1246	1			1			1							1	1						
Claraghmore Lough [L]	54.631°N	7.450°W	1246									1	1						1					
Fallahogy [P]	54.911°N	6.557°W	1247											1	1	1								
Malham Tarn Moss [P]	54.097°N	2.173°W	1478	1					1			1	1											
Malham Tarn [L]	54.096°N	2.165°W	1478						1															
Cors Fochno [P]	52.504°N	4.012°W	1563							1				1	1							1		
Bodmin [P]	50.589°N	4.625°W	1733				1																1	
Degerö Stormyr [P]	64.181°N	19.564°E	1878	1	1	1					1										1			
Lake Svartkälsjärn [L]	64.264°N	19.552°E	1878	1	1	1																		
Sammakovuoma lake [L]	66.992°N	21.500°E	1891	1	1			1																
Sammakovuoma bog [P]	66.995°N	21.457°E	1891		1			1																
Kusowskie Bagno [P]	53.816°N	16.588°E	2326																					1
Linje [P]	53.187°N	18.309°E	2457								1													
			Total sites	6	5	3	3	2	2	2	2	2	2	2	2	1	1	1	1	1	1	1	1	

Table 1. Table indicating the location of each site and the tephras identified. Lake and peatland pairs in close proximity are highlighted in grey. Sites are ordered by distance from the Hekla volcano, the source of the majority of Holocene tephra layers in Northern Europe. Tephras which have not been attributed to an Icelandic source eruption (Glen Garry, QUB 384 G3-4), or which have been attributed to an alternative source region (e.g. Alaska) (AD 860 B) are shown in bold. Data from Shetland from (Stevenson *et al*., 2015; Swindles *et al*., 2013a).

6.2.1.2 Tephra analysis

Cores were initially examined in 5 cm^3 contiguous samples. Where tephra was identified the cores were re-sampled at 1 cm intervals to identify the location of the peak shard concentration. Samples from ombrotrophic peatlands were prepared using the method outlined by Hall and Pilcher (2002); Swindles *et al*. (2010). Samples containing minerogenic material (all lake cores, surface samples and the samples from the Swedish peatlands) were extracted using heavy density liquid flotation (cleaning float 2.25 g cm^{-3}, retaining float 2.5 g cm^{-3}) (Blockley *et al*., 2005). During both methods, sieving of samples through a 10 µm mesh was necessary to remove detrital material. Therefore, excluding the samples from Unst which were sieved at 20 µm, the minimum particle size analysed in this study is that retained by a nominal 10 µm mesh.

Shards were mounted onto slides using Histomount and examined at 200-400 x magnification. Shards from one eruption typically have a vertical span of a few centimetres in lake and peatland records (Davies *et al*., 2007). Therefore all samples within each vertical tephra spread were examined, not only the peak sample. The low shard count totals for each eruption (typically tens to hundreds of shards) in distal records provided insufficient quantities of shards for automated analysis of shard size/shape by Laser granulometer or Coulter counter (<1 g). Therefore, shards were identified and measured using an eye-piece graticule. Shard size was measured in two dimensions, i.) the length of the longest axis (Max A) and, ii.) the maximum width at 90° to the first measurement (Max B). Aspect ratio was calculated as Max A over Max B. Bootstrap re-analysis of Max A measurements from different tephra layers identified at sites in this study suggests that in general < 100 shards must be measured from samples in either lake or peatland sites in order to assess the median shard size (Max A) (± 5 µm) for a sample with in a 95% confidence window (Fig. S1). Therefore a minimum of 100 shards were measured in each sample. Where samples contained <100 shards the maximum number of shards possible was counted.

Tephra shards were extracted for geochemistry using two established methods. In peat with little minerogenic material extraction was through acid digestion (Dugmore and Newton, 1992). Samples were treated with conc. HNO_3 and H_2SO_4 acids before sieving the residue at 10 µm and rinsing thoroughly with distilled water. Samples with larger

amounts of minerogenic material were extracted by density separation as above with the exclusion of the ashing step.

Samples were either mounted onto glass slides (Dugmore and Newton, 1992) or mounted into blocks (Hall and Hayward, 2014). All samples were polished to a 0.25 µm finish. The majority of geochemical data was obtained at the University of Edinburgh Tephra Analytical Unit. A beam size of 5 µm was used throughout and beam current was varied during each analysis to limit volatile losses (Hayward, 2012). All analyses were conducted at 15 kV with beam currents of 2 nÅ (Na, Mg, Al, Si, K, Ca, Fe) or 80 nÅ (P, Ti, Mn). Secondary glass standards were analysed before and after EPMA runs of unknown glass shard analyses. Analyses for Malham Tarn Moss tephra and some of the Unst samples were conducted at the University of Leeds on a JEOL8230 electron microprobe using a 10 µm beam. Assignments to eruptive event were based on stratigraphy and comparison of tephra geochemistry with the European tephra geochemistry database 'Tephrabase' (Newton *et al*., 2007) and our own database constructed from published literature.

6.2.2 Modelling cryptotephra fallout

One of the major challenges in modelling tephra fallout from past volcanic eruptions is uncertainty in model input parameters. Basic model input parameters such as plume height and wind speed are often poorly constrained, or completely unknown for pre-written record eruptions. In these instances a stochastic approach, whereby input parameters are sampled from probability density functions, allows for an assessment of various scenarios (Bonadonna *et al*., 2005). We developed a simple probabilistic model which calculates the terminal velocity and thus the distance travelled and fallout time for tephra shards released during a volcanic eruption. The model consists of two main parts, a physical sub-model which calculates the distance travelled by each particle based on input parameters including plume height, wind speed and particle size; and a stochastic sub-model which is used to sample input parameters for the physical model from probability density functions to forecast a variety of conceivable outcomes, full details of the model are given in supplementary file 1 (Fig. S2).

Probability density functions for plume height, sphericity and wind speed were constructed based on empirical observations and previous published literature (Alfano *et al*., 2011; Bonadonna and Phillips, 2003) (Table 2). Plume height is sampled from a log uniform distribution truncated at 4 km and 35 km. Although there is some evidence for the transport of fine tephra shards from plume heights < 4 km (Stevenson *et al*., 2013b), shards released at such low altitudes are likely to represent a negligible proportion of the shards contained in northern European cryptotephra records. Explosive eruptions associated with plume heights exceeding 30 km do not occur frequently in Iceland. However, to account for eruptions such as that of Askja in 1875 (VEI 5 plume height ~35 km) we set 35 km as the maximum plume height. The log distribution reflects the bias toward a higher frequency of low magnitude eruptions with lower plume heights (Simkin and Siebert, 1994). Wind speed is sampled from a normal distribution based on the average wind speed values between 0-48 km height as reported by Lacasse (2001) and maximum and minimum wind speed values of 10 – 30 ms^{-1}. Examples of values sampled from each of the above PDFs are given in Fig. S3.

Particle aggregation and precipitation can promote the early fallout of atmospheric particles (Durant *et al*., 2009; Mattsson and Vesanen, 1988). However, we do not account for aggregation or the impact of precipitation, as the processes controlling the aggregation of particles are not well parameterised (Brown *et al*., 2012). We also do not take into account the particle size distribution at source (Beckett *et al*., 2015), instead the model is run for a given tephra size. The model also does not include transport while suspended in the turbulent spreading plume.

Model parameter (units)	Input value (or range)	Reference
Atmospheric properties		
Air viscosity *(Pa s)*	1.78×10^{-5}	Stevenson *et al*., (2015)
Air density *(kg m^{-3})*	Varies with height	Connor *et al*., (2013)
Particle properties		
Size/diameter *(µm)*	Specified by user (0-250 µm)	
Density *(kg m^{-3})*	Varies with particle size	Bonadonna and Phillips, (2003)
Shape *(sphericity, dimensionless)*	Sampled from probability density function. Normal distribution: mean = 0.8 Std Dev =0.1	Alfano *et al*., (2011)
Release properties		
Release height *(km)*	Sampled from a probability density function. Log-uniform distribution: max = 35 km, min = 4 km, smaller plume heights more likely.	Connor *et al*., (2009)
Meteorology		
Wind speed *(m s^{-1})*	Sampled from a probability density function. Truncated Normal distribution mean = 17.4, Std Dev = 4, Min = 10, Max = 30	Lacasse, (2001)
Gravity *(m s^{-2})*	9.81	

Table 2. Table outlining the model parameters and input values (or ranges) used in the simple tephra fallout model applied in this paper.

6.3 Results

6.3.1 Maximum shard size

The maximum length of the A and B axes of over 9500 shards from 19 different tephra layers was measured (Supplementary file 2). The geochemistry of the tephra layers ranged from basaltic to andesitic, dacitic, trachydacitic and rhyolitic (Fig. 3). The majority of tephra layers could be geochemically correlated to Icelandic eruptions. However, three tephra layers contain glass shards with a major element geochemistry which does not match the geochemistry of tephra from known Icelandic eruptions, for two of these tephras the source region remains unknown (Glen Garry- Dugmore *et al*. (1995) and QUB 384-G3-G4-Pilcher *et al*. (2005)). Glass shards from the third, match the major element geochemistry of glass shards from the AD 860 B tephra, correlated to the White River Ash (WRAe) from the Bona-Churchill massif, Alaska (Jensen *et al*., 2014). Only the 15 tephras with a known or suggested source eruption in Iceland are included in subsequent analyses.

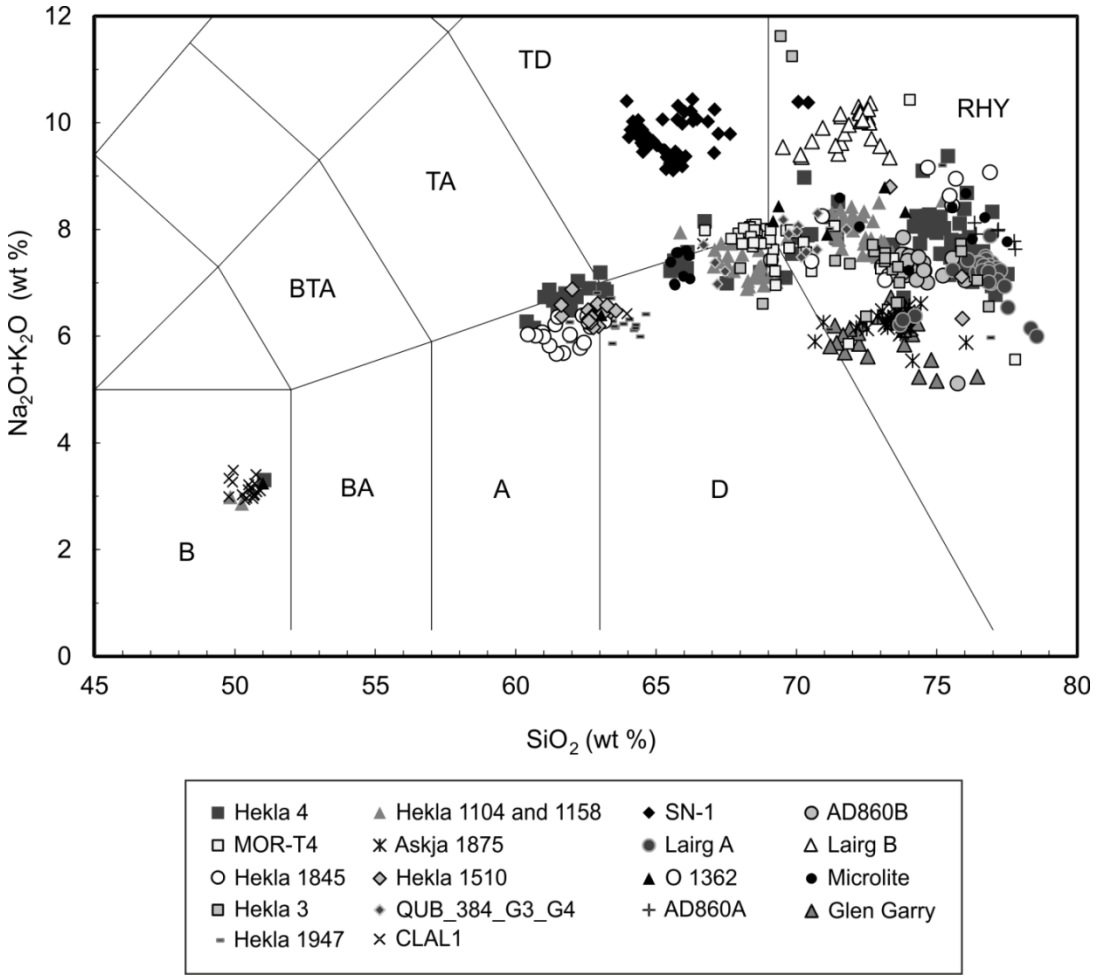

Figure 3. Total Alkali Silica (TAS) Diagram showing the geochemistry of tephras included in this study. Annotations follow standard terminology e.g. RHY = Rhyolite, D = Dacite, A = Andesite (Le Maitre *et al*., 1989). The geochemistry of the tephra layers identified ranged from basaltic to andesitic, dacitic, Trachydacitic and rhyolitic. O 1362 = Öræfajökull 1362.

The median values of Max A for tephras varied between 35 and 75 µm (median = 51 µm) (Fig. 4). The largest tephra shard had a Max A of 250 µm (identified 1878 km from Iceland) indicating that large shards can be transported long distances from their source volcano. However, large shards were relatively rare. Although 90% of particles were 30 µm or larger and 40% were over 50 µm, only 3% of shards were over 100 µm, suggesting that the majority of shards with a Max A >100 µm fall out before reaching our sites (including the Shetland Islands, UK, Ireland and continental Europe). In agreement with Stevenson *et al*. (2015), in both lake and peatland records the majority of particle size distributions exhibit a log normal distribution, with a tail of larger shards. The only basaltic tephra included in this study (CLA-L1) does not display the same log normal shard size (Max A) distribution.

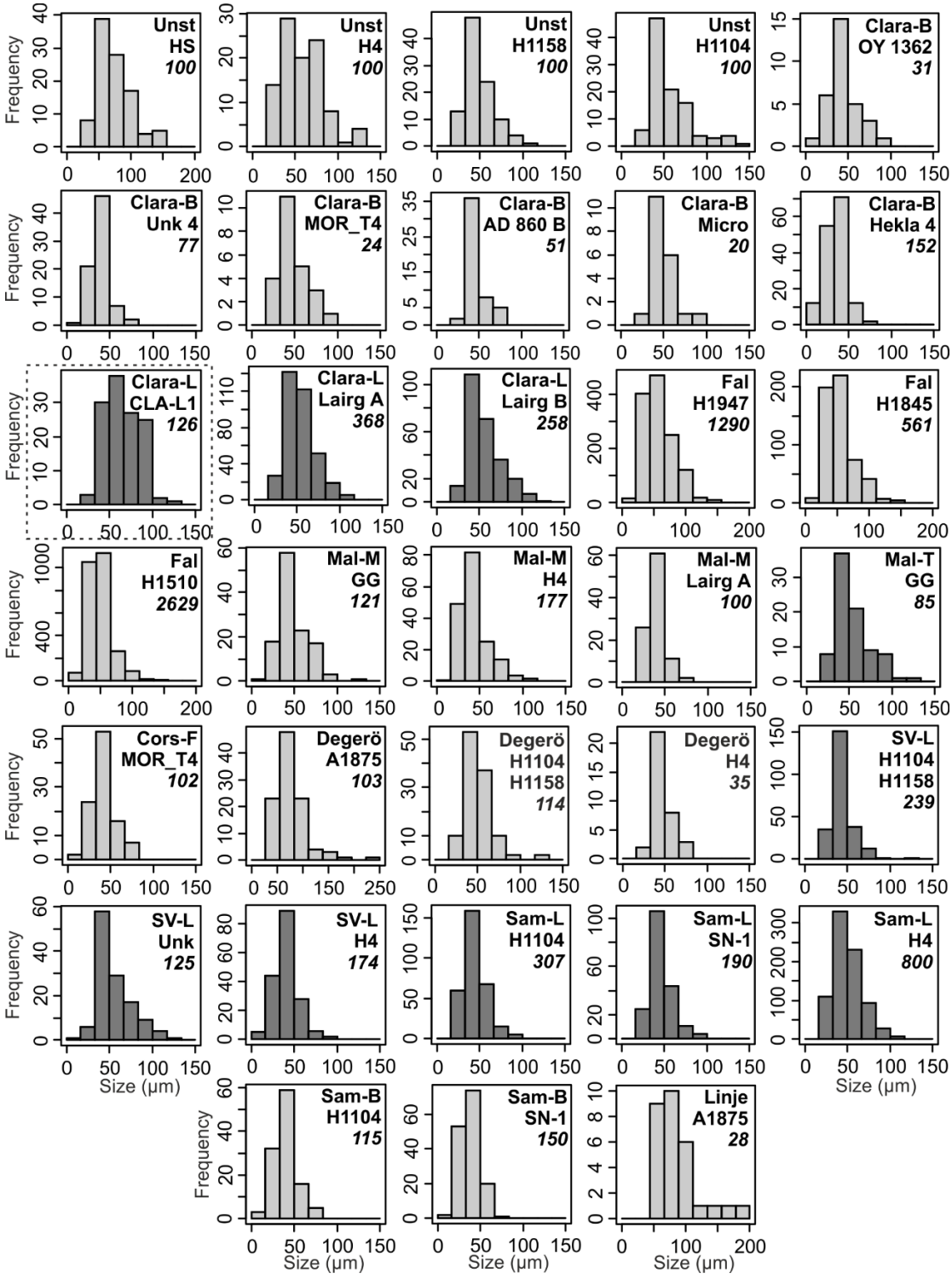

Figure 4. Histograms showing the distributions of shard size for tephras at sites in the study. Lake samples are dark grey, peatland samples are light grey. CLA-L1 is the only tephra of basaltic composition to be included in this study and is highlighted by a dashed box. Abbreviations are as follows, tephras: H = Hekla, HS = Hekla Selsund, OY = Öræfajökull, Unk = Unknown, Micro = Microlite/GB4-150, GG = Glen Garry, A = Askja, SN-1 = Snæfellsjökull SN-1 tephra, CLA-L1 basaltic tephra from an eruption of the Grímsvötn volcano (Watson *et al*., in review). Site names: Clara-B = Claraghmore peatland, Clara-L

= Claraghmore lake, Fal = Fallahogy, Mal-M = Malham Moss, Mal-T = Malham Tarn, Cors-F = Cors Fochno, Degerö = Degerö Stormyr, SV-L = Lake Svartkälsjärn, Sam-L = Lake Sammakovuoma, Sam-B = Sammakovuoma bog. Only tephras with over 20 shards are plotted. The number of shards counted in each sample is shown in italics.

6.3.2 Aspect ratio

Aspect ratio is a simple descriptor for predicting the terminal velocity of volcanic ash (Riley *et al.*, 2003). The cryptotephras in this study were predominantly non-spherical and measured aspect ratio ranged from 1.0 to 10.5 (1.0 being spherical). However, the majority of shards had a measured aspect ratio <3 (Fig. 5). Aspect ratio for all Icelandic eruptions had a mean of 1.5.

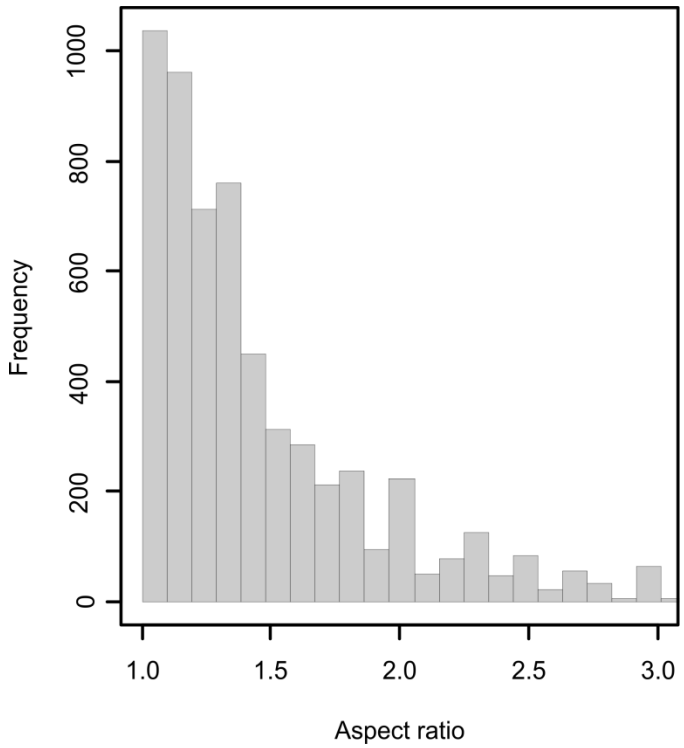

Figure 5. Histogram showing the aspect ratios of the cryptotephras of Icelandic source a selected range of aspect ratio. Full range was 1.0 to 10.5 (1.0 being spherical), the majority of shards had an aspect ratio < 3.

6.3.3 Surface samples

Figure 2 shows the locations where Grímsvötn 2011 and Eyjafjallajökull 2010 tephra were identified in rain gauge samples (Gudmundsson *et al*., 2012; Stevenson *et al*., 2013b), alongside the locations of moss surface samples which were obtained and examined for the presence of Eyjafjallajökull 2010 and/or Grímsvötn 2011 tephra as part of this study. No tephra was identified in any of the moss surface samples. This suggests that events which are large enough to result in ash fallout into rain gauge samples might be missing from the geological record.

6.4 Discussion

6.4.1 Records of tephra shard size distributions in lakes and peatlands

6.4.1.1 Hypothesis 1

In one instance (Malham) the median shard size (Max A) is identical in the lake and peatland (Fig. 6). Where significant differences are identified in Max A between peatlands and lakes, median Max A is generally larger in the lake (Fig. 6, Table S1). The largest shards were always found in lakes, which generally also contain particle size distributions with a higher upper quartile shard size. The trend toward a higher amount of larger shards (Max A) in lakes might be due to the in-wash of shards from across the catchment, or within basin redistribution of glass shards. As lakes generally capture the largest shards to fall out over a region, tephra shard size data from small lakes may be more valuable to modellers, than that from peatlands. There was no significant difference in the aspect ratio for the tephras in lakes and peatlands, suggesting that fragmentation in the catchment has a negligible impact on tephra morphology.

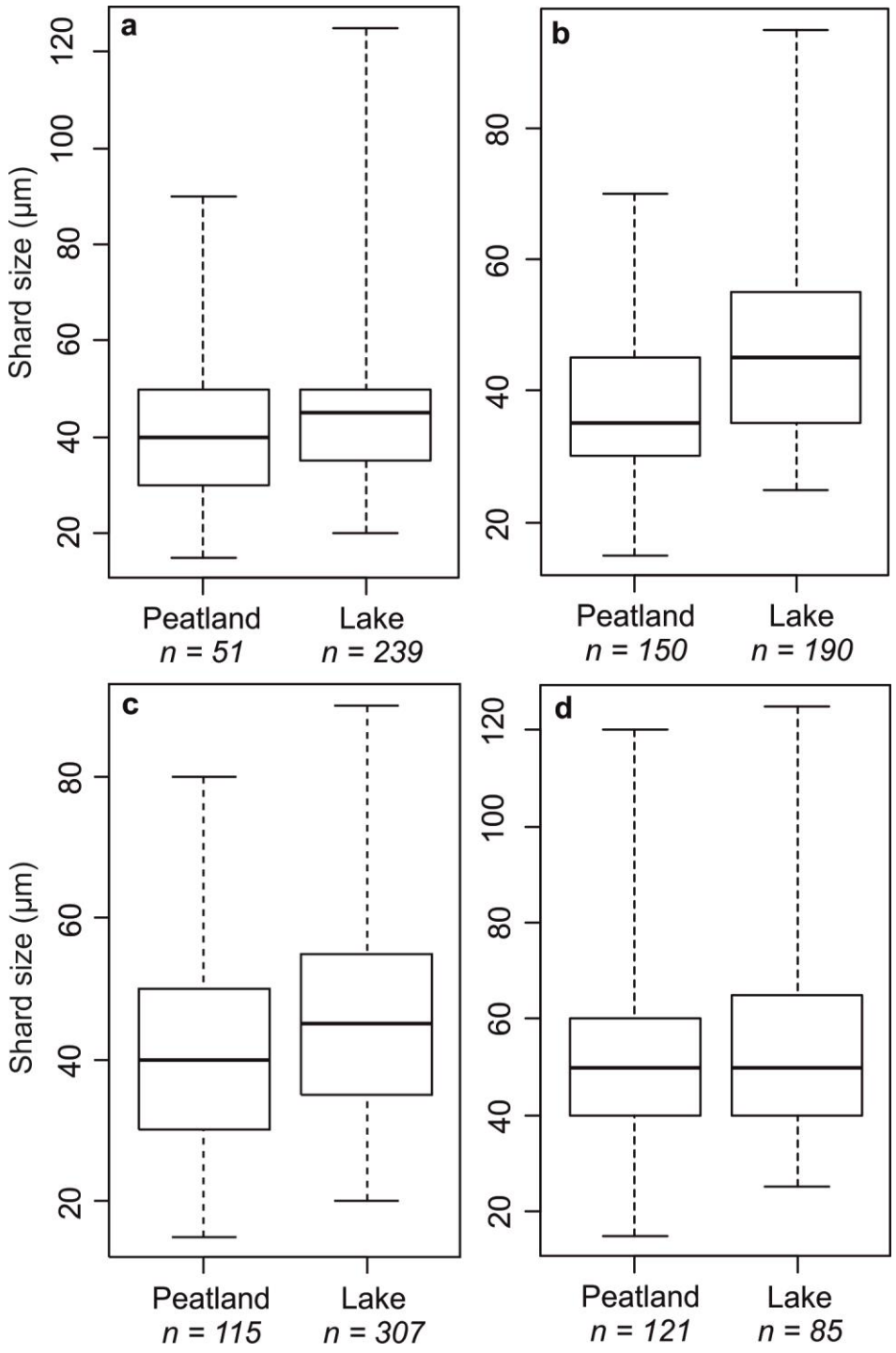

Figure 6. Boxplots indicating shard size for the same tephra in peatland and lake sites which are in close proximity (<10 km apart). a) Hekla 1104 and 1158 tephra layer in Degerö Stormyr (peatland) and Svartkälsjärn lake, b) SN-1 tephra in Sammakovuoma lake and peatland, c) Hekla 1104 tephra layer in Sammakovuoma lake and peatland, d) Glen Garry tephra layer in Malham Moss and Malham Tarn. Boxplot convention is as follows: boxes indicate the interquartile range; the central line through each box indicates the median. The far extents of the upper and lower lines from each quartile indicate the maximum and minimum.

6.4.1.2 Hypothesis 2

We examined the median Max A of shards from the Hekla 1510 tephra which were identified in 14 cores at Fallahogy peatland (Fig. 7). A minimum of 97 shards were examined in each core. There is a significant difference in the median Max A for different cores, with a range of values from 40-50 µm (Kruskal Wallis: H = 138.14, p = 0.0001). Our results suggest that tephra shards are differentially deposited according to size, or reworked differentially according to size. The degree of within site variability in median Max A must be considered when making comparisons between sites (e.g. intra site differences must be smaller than between site differences). There are also differences in the 95th percentile values (Max A) which range from 62-100 µm.

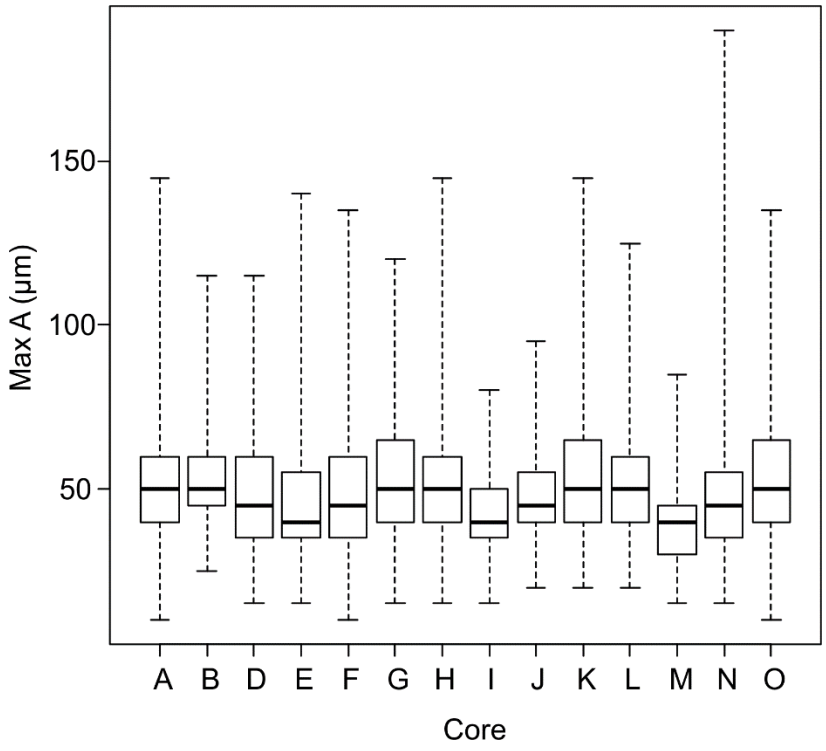

Figure 7. Max A measurements for the Hekla 1510 tephra taken from 14 cores from Fallahogy peatland (Watson *et al*., 2015), *n* as follows: A = 199, B = 101, D = 176, E = 508, F = 163, G = 123, H = 96, I = 147, J = 145, K = 141, L = 119, M = 114, M = 204, O = 393.

6.4.2 Vertical movement of cryptotephra shards

6.4.2.1 Hypothesis 3

It has been suggested, that tephra shards might be subject to differential vertical movement through peat profiles according to size, with smaller shards penetrating further through the peat profile (Payne and Gehrels, 2010). However, we identify no significant difference between the median tephra size (Max A) in the sample of peak tephra concentration, and the overall median tephra size (Max A) of a tephra layer, in either peatlands or lakes, suggesting that substantial vertical sorting of cryptotephra by size in lake sediments or peats is not occurring (Table S2). Therefore conducting shard size analysis on at least 100 shards in the sample of peak shard concentration should be sufficient to identify the median shard size (Max A) for a given location.

6.4.3 Information from particle size analysis

6.4.3.1 Hypothesis 4 Maximum shard size

The intra-site differences in Max A identified at Fallahogy (which ranged from 40-50 µm) (Hypothesis 2) must be considered when using Max A values from multiple sites to examine possible differences in shard size with distance from Iceland. However, the range of median Max A shard size across all tephras at all sites in this study was 35-70 µm, much greater than the intra-site differences identified at Fallahogy. Median shard size (Max A) might be expected to decrease with increased distance from Iceland as larger, heavier, shards reach terminal velocity sooner and fall out closer to the source. However, there was only a weak correlation between median shard size (Max A) and the distance from Iceland (Spearman's rank correlation: $r = -0.127$, $p < 0.0001$) (Fig. 8) over the range of distances covered by our sites (1075 – 2457 km). A trend toward a lower amount of larger shards (lower 95^{th} percentile values) is apparent with increased distance from Iceland. However, there are still outliers, such as the Askja 1875 tephra which was identified in Poland.

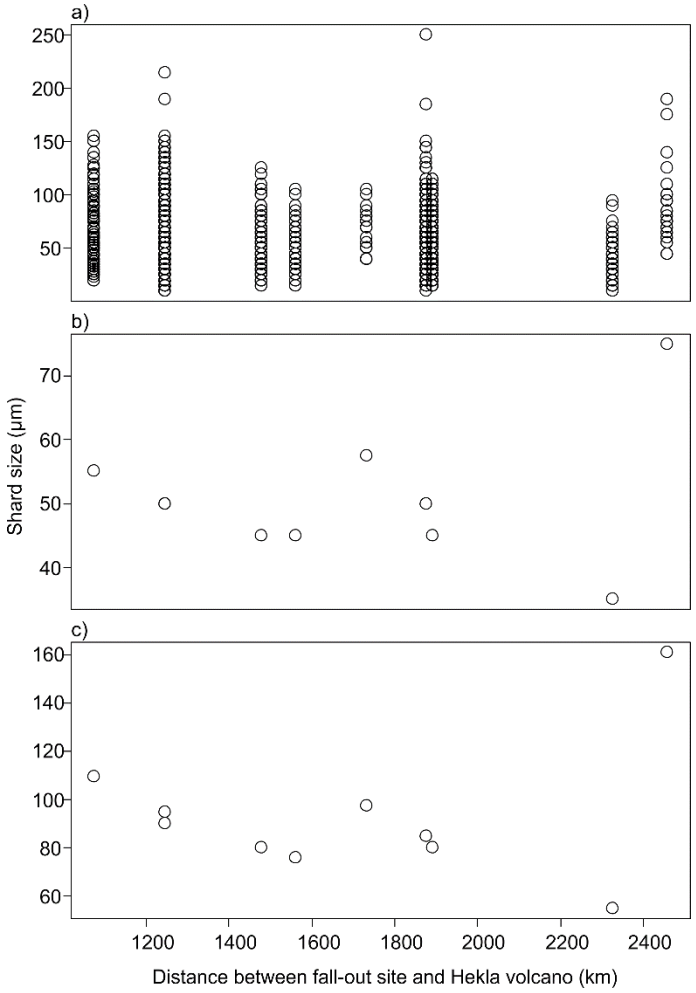

Figure 8. Maximum shard size (Max A) for all tephra layers identified in this study, a) all data, b) median values for each distance, c) 95th percentile values for each distance

Owing to the patchy nature of cryptotephra fallout, even cryptotephras which form the most widespread isochrons, for example the Hekla 4 tephra (2395-2279 BC; (Lawson *et al*., 2012)), are not present at every site. Therefore, sample sizes for analysis of shard size (Max A) with distance are reduced when focussing on tephra produced during one eruption. Two tephras, geochemically and stratigraphically correlated to the Hekla 4 and Hekla 1104 eruptions were identified at six sites and five sites, respectively. Despite the range of distances where Hekla 4 tephra was identified (~1000 – 1900 km) the median shard size (Max A) varied across a relatively small range (35-55 µm) (although still larger than the intra-site differences identified at Fallahogy). There is a significant positive correlation between shard size and distance from Iceland for the Hekla 4 tephra (SRC: $r = 0.189$, $p = <0.0001$). This is contrary to the expectation that shard size would decrease with increasing distance from the volcano. This correlation is weak and is

screwed by the most distal site (Sammakovuoma Lake) which has a relatively large median shard size of 50 µm (Fig. 9). The 95th percentile for the Max A size of the Hekla 4 tephra is considerably higher (99 µm) at the site closest to Iceland (Unst, ~1000 km) than at sites in Ireland (57 µm, ~1200 km), England (75 µm, ~1500 km) and Sweden (70 µm, ~ 1900 km). Although there still appears to be no simple relationship between shard size and distance from source (Fig. 9).

There is a significant difference between shard size values for the Hekla 1104 tephra from a site in Shetland (n = 102) and two sites in Sweden (Sammakovuoma lake and peatland combined (n = 422), Lake Svartkälsjärn and Dëgro Stormyr combined (n = 290)), supporting the hypothesis that shard size decreases with increasing distance (Kruskal Wallis: H = 36.7, p = <0.0001, median Max A for Shetland and Swedish sites = 50 µm and 40 µm, respectively) (Fig. 10). The 95th percentile of Max A for Hekla 1104 is considerably larger (110 µm) in Unst, Shetland (~1000 km from Iceland) than at sites in Sweden, 1900 km from Iceland (60-70 µm). Differences in the 95th percentile shard size with distance for both the Hekla 4 and Hekla 1104 eruptions indicate that larger shards are being lost as distance increases. Although this is not significantly impacting the median Max A size, it is evident when the very largest shards are considered.

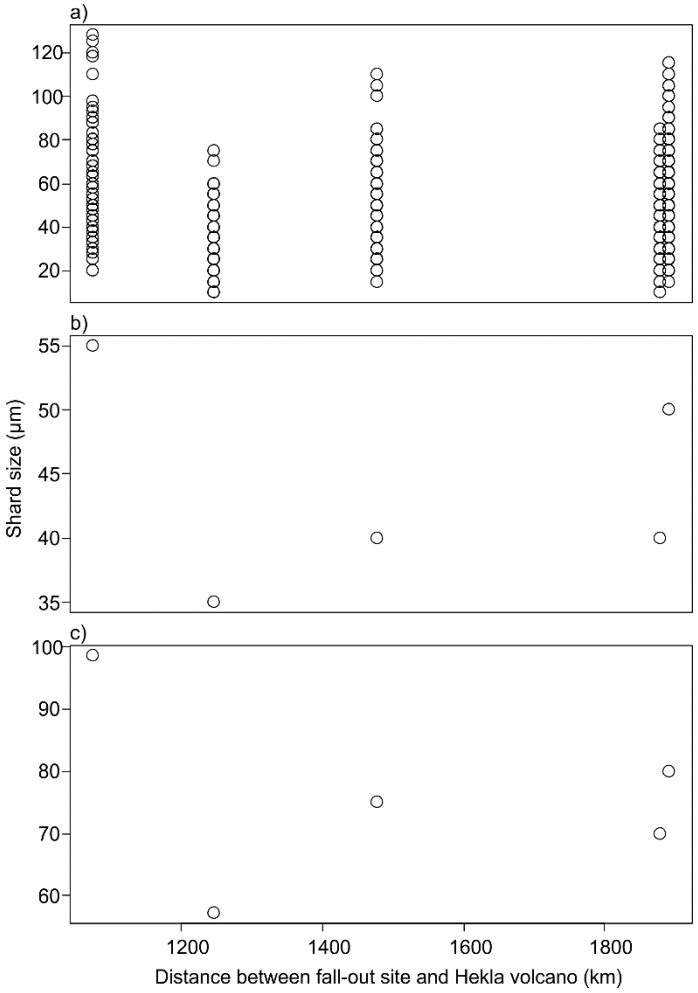

Figure 9. Maximum shard size (Max A) of the Hekla 4 tephra identified at 5 sites across northern Europe, a) all data, b) median values for each distance, c) 95th percentile values for each distance

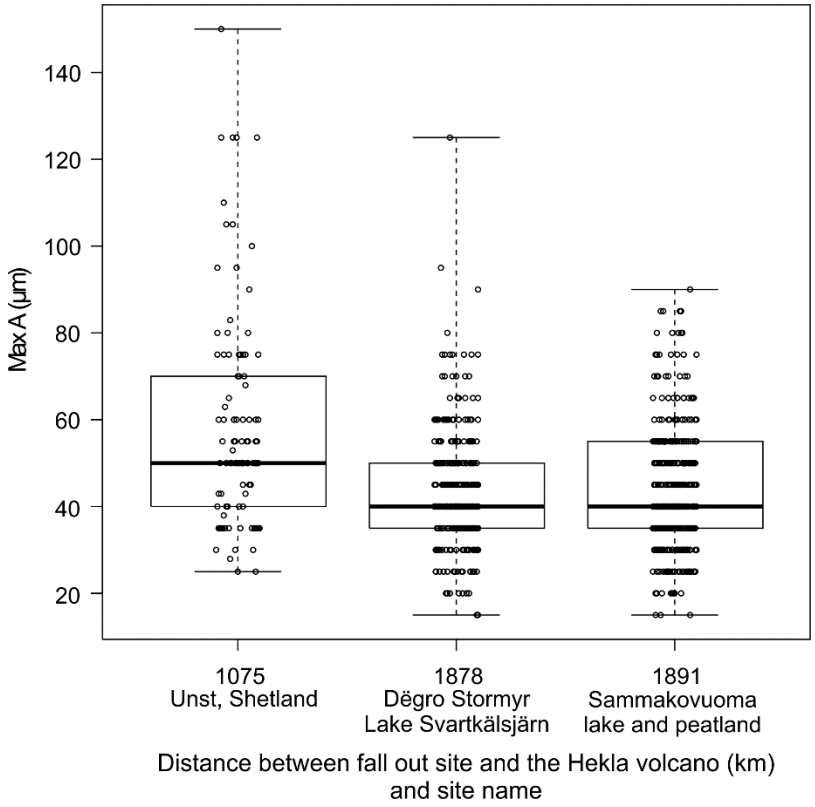

Figure 10. Boxplots (with overlain jitter plot) of Maximum shard size (Max A) of the Hekla 1104 tephra identified at sites in Sweden (1878 and 1891 km from the Hekla volcano) and Shetland (1075 km from the Hekla volcano). Please note: Unst samples were sieved at 20 µm. Boxplot convention is as follows: boxes indicate the interquartile range; the central line through each box indicates the median. The far extent of the upper and lower lines from each quartile indicate the maximum and minimum. Hollow circles indicate raw data values.

There are a number of possible reasons for the strength and variety of correlations of median Max A observed in changes in shard size with distance, even in tephra from a single eruption. Firstly, the major controls on transport distance such as weather conditions, the height of the eruption column, mass eruption rate and degree of tephra fragmentation vary even during a single eruption (Carey *et al*., 2010; Gudmundsson *et al*., 2012), and in this instance the only true comparison would be between tephra shards released during the same phase of an eruption. The hypothesis that tephra at different sites may have been deposited during different phases of an eruption is supported by geochemical data. The geochemistry of the Hekla 4 tephra varies at different sites in this study, reflecting geochemical variation which has been identified in the proximal geological record where products of the Hekla 4 eruption show a range of geochemistry as the eruption progresses with SiO_2 content decreasing from c. 74 % to 57% (Langdon

and Barber, 2004; Larsen and Thorarinsson, 1977) (Fig. S5). Some sites in this study (e.g. Sammakovuoma Lake) show two distinct groups of tephra geochemistry and may have received fallout on more than one occasion during the Hekla 4 eruption.

Another possible reason for the lack of strong correlation between shard size and distance is that tephra shards may have aggregated and fallen out earlier than would be predicted based on their individual size (Durant *et al*., 2009). Aggregate grains close to the volcano can be relatively large and composed of component shards with shard lengths in the range of those examined in this study (63-250 μm) (Taddeucci *et al*., 2011). However, the examination of aggregate grains which travelled further and fell over the UK during the eruption of Eyjafjallajökull 2010 shows they are smaller (mean size 85 μm) and made up predominantly of tephra shards <5 μm in diameter (Stevenson *et al*., 2012). Such aggregate grains would have most likely broken up (upon burial) in the geological record into constituent shards below the minimum sample size examined here (10 μm). Therefore premature fallout of tephra shards by aggregation would appear unlikely to be the primary reason for our observations.

Finally, the 'great circle distance' used in this study represents a minimum travel distance between the source and site where the tephra was deposited. Detailed weather data is not available for many Holocene tephras. However, based on observations of recent Icelandic eruptions, it is likely that tephra was transported over longer distances than the great circle distance between source and fallout site (Cooke *et al*., 2014; Stevenson *et al*., 2013c; Thorarinsson, 1981).

6.4.3.2 Aspect ratio

There is a significant correlation between increasing shard size and increasing aspect ratio (Spearman's rank correlation $p = <0.0001$, $r = 0.293$). This is in agreement with the principle that non-spherical objects travel further in the atmosphere before deposition than spherical objects of the same size (Rose *et al*., 2003).

The distal cryptotephra record is dominated by events of a rhyolitic or intermediate composition (Lawson *et al*., 2012). We grouped tephras according to geochemistry into 3 groups: basaltic (*n shards* = 126), rhyolitic (*n shards* = 2336), and intermediate (dacitic/andesitic *n shards* = 1627). The median aspect ratio of basaltic and rhyolitic

shards (1.22, 1.25 respectively) was slightly lower than that of intermediate shards (1.33). There was a significant difference between the aspect ratios for basaltic and intermediate tephra shards (Mann-Whitney test, $p = 0.02$), but no significant difference in aspect ratios of rhyolitic and basaltic shards (Mann-Whitney test, $p = 0.42$). Intermediate shards in our dataset are dominantly from the Hekla 1510, 1845 and 1947 eruptions, which formed highly vesicular dacitic-andesitic shards (Watson *et al*., 2015).

6.4.4 Comparing modelling output with the geological record

Fig. 11 shows a summary of the model outputs for the set up detailed in Table 2. Data on shard size from geological records lies within the fallout transport range of our modelled eruption parameters for Iceland. As our model does not account for aggregation the fallout of individual small tephra shards could be expected at these sites without the need to invoke aggregation. The majority of the median Max A values from the geological record lie between the upper and lower quartile of the range of possible transport distances based on the range of model parameters outlined in Table 2.

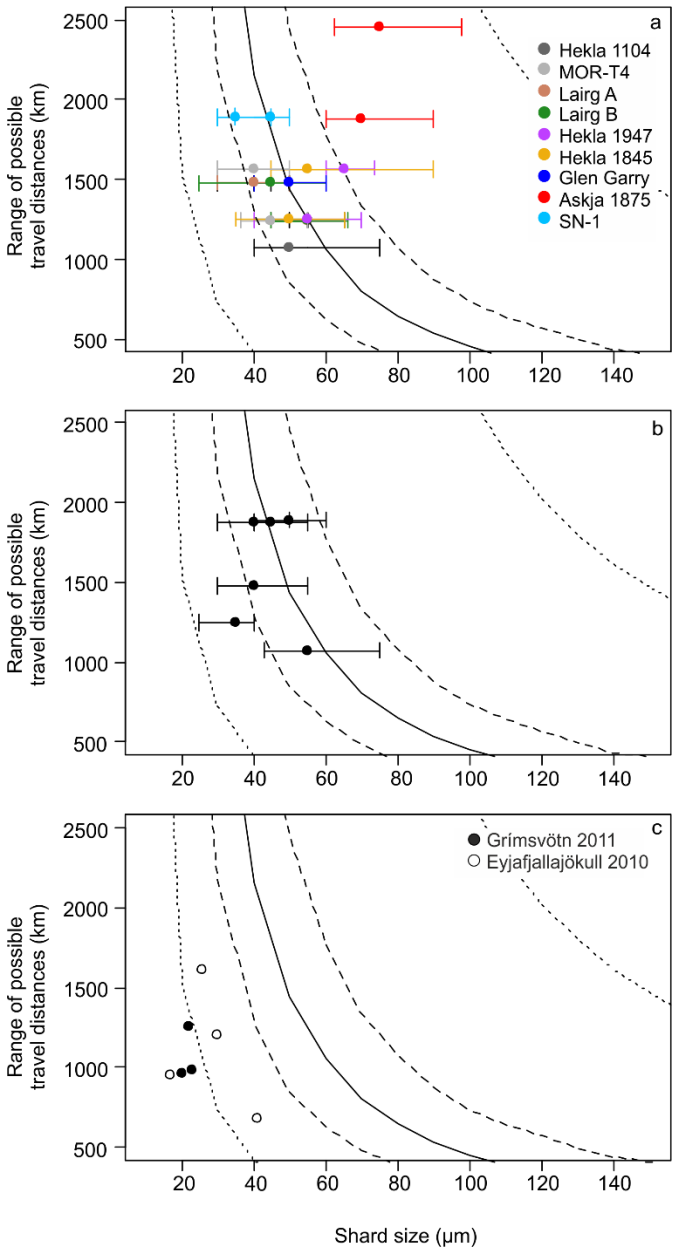

Figure 11. Diagram showing model outputs for the set up detailed in Table 2 in comparison to cryptotephra in the geological record. Curved lines indicate a summary of model output (Dotted lines = minimum and maximum, dashed lines = lower and upper quartiles, solid line = median value). Points show cryptotephra layers (median shard length), horizontal bars on all plots indicate the upper quartile and lower quartile values for shard size at each site. a) range of possible travel distances plotted against those travelled by all cryptotephras identified at ≥2 sites in the geological record at sites in this study (excluding Hekla 4) key indicates tephra layer, b) limited range of possible travel distances plotted against those travelled by cryptotephra from the Hekla 4 eruption which was identified in the geological record at 6 sites in this study, c) limited range of possible travel distances plotted against those travelled by all cryptotephras collected from rain gauge samples by (Stevenson *et al.*, 2013a; Stevenson *et al.*, 2012).

According to our model, the most likely range of wind speeds and plume height combinations which resulted in the deposition of the tephra shards in the geological record is a plume height of c.10 km and a wind speed of c.17 ms^{-1}. However it is also possible (although less likely) that tephras in the geological record were deposited during an eruption with a plume height as low as 4 km but where wind speeds were high (>20 ms^{-1}) (Fig. S6). This combination of input parameters is less likely to occur, as faster wind speeds are less common. Sphericity has less of an impact on modelled transport distance than plume height and wind speed. However, less spherical particles travel further, for example a 30 μm non-spherical particle (sphericity of 0.45) will travel 35% further than a spherical particle of the same size.

Tephra fallout from rain gauge samples (Eyjafjallajökull 2010 and Grímsvötn 2011) display smaller shard sizes than cryptotephras found in geological records (Stevenson *et al*., 2013a; Stevenson *et al*., 2012) (Fig.11). According to the model output, tephra of the shard size identified in rain gauge samples are likely to have come from eruptions with lower plume heights and slower wind speeds when compared to tephras we identify in the geological record. In accordance with our model output, air mass trajectories indicate that although plume heights during Grímsvötn 2011 reached 20 km, only tephra from the lowest 4 km of the plume was transported toward the UK (Stevenson *et al*., 2013b). No tephra was identified in the moss surface samples obtained during this study, suggesting that ash clouds produced during smaller eruptions may be missing from the geological record, suggesting that estimates of volcanic ash cloud reoccurrence based on the geological record e.g. Swindles *et al*. (2011) provide a minimum estimate. However, it cannot be completely disregarded that our failure to identify tephra shards in moss surface samples was due to sampling bias. The addition of more sites would improve spatial coverage and increase the probability of finding evidence for the Eyjafjallajökull 2010 or Grímsvötn 2011 tephras in the geological record.

Although our model can account for the median shard size in geological records, in some instances it cannot account for the transport of the very largest shards over long distances. Below, we examine two examples.

6.4.5.1 Askja 1875 and the AD 860 B tephra

Askja 1875 is of special interest as tephra shards identified in the geological record from this eruption are anomalously large when compared to tephra shards from other eruptions. In Linje mire, northern Poland, 2500 km from the Askja crater, the median Max A for this tephra is 75 µm (maximum 190 µm, n = 28). Under the set of eruption parameters in Table 2, our model does not predict the transport of tephra shards of 190 µm beyond ~1074 km. However, the eruption parameters in Table 2 may not be suitable for the eruption of Askja 1875 which is estimated to have had a combination of high plume heights (26-37 km) and fast wind speeds (up to 43 ms^{-1}) (Carey *et al*., 2010; Carey and Sparks, 1986). Using these input parameters, the maximum predicted travel distance for a shard of 190 µm is 1409 km, still much shorter than the 2500 km distance recorded in the geological record. In order to simulate the transport of particle of 190 µm over 2500 km a plume height of >50 km would need to be combined with a wind speed of 43 ms^{-1}. These eruption parameters would appear to be highly unlikely and are not supported by tephrostratigraphic data in Iceland.

Increasingly cryptotephras are being linked to volcanoes further afield (Ponomareva *et al*., 2015). An example is the 'AD 860 B' tephra correlated to the White River Ash from the Bona-Churchill massif, Alaska (61.38ºN, 141.75ºW) (Jensen *et al*., 2014). The median Max A for 'AD 860 B' at Claraghmore peatland (6500 km distant) is 45 µm, similar to the overall median Max A for all eruptions of an Icelandic source (50 µm), despite the difference in transport distance of 5200 km. The Bona-Churchill massif eruption had a magnitude of VEI 6 based on an estimated eruptive volume of ~50 km^3 (Lerbekmo, 2008). The maximum distance travelled by a 75 µm shard (maximum shard size for AD 860 B, n = 51) based on a plume height of 40 km and a wind speed of 30 ms^{-1} in our simple model is 4600 km. It is possible that tephra shards were transported in the Polar jet stream (10-15 km height) which can reach speeds in excess of 50 ms^{-1} (Ahrens, 2012). However, a particle released from 40 km which travels at a wind speed of 30 ms^{-1} and enters the jet stream from 10-15 km at a wind speed of 50 ms^{-1} is still transported only 5200 km. In these instances our model does not reproduce the evidence (maximum Max A) from the geological record. This is most likely because larger shards are affected greatly by turbulence and buoyancy in the spreading plume, which are not represented in our model.

6.5 Conclusions

We report the geochemistry and examine shard size distributions for distal cryptotephra layers at 14 sites across northern Europe, and confirm the lognormal distribution of particle size identified in a small number of cryptotephra records by Stevenson *et al*. (2015). Surprisingly, there is only a weak, but significant negative correlation between median tephra shard size and distance of the fallout site from Iceland. For the Hekla 4 tephra shard size appears to *increase* with distance from Iceland, most likely due to the deposition of tephra over different regions during different eruptive phases.

We examined the replicability of shard size measurements within one core and within different cores from the same peatland. Our results indicate that median (Max A) shard size can vary within a site. In one instance (Malham) the shard size distributions from peatlands and lakes (in close proximity) displayed identical median sizes. However, lakes generally contained a higher number of larger shards than peatlands.

Given the range of distances between Iceland and our fallout sites, the range of median shard sizes identified in this study is relatively low (35-75 μm). Furthermore, the shard size of tephra layers from eruptions further afield (e.g. Alaska, 45 μm) is not dissimilar to those from Icelandic tephras (50 μm), despite a difference of ~5200 km in transport distance. When combined with uncertainties about wind speed during ancient eruptions, this makes refining possible source regions based on shard size alone challenging.

A lack of evidence of tephra from the eruptions of Eyjafjallajökull 2010 and Grímsvötn 2011 in moss surface samples supports the argument that the calculation of reoccurrence intervals based on geological records provides an underestimate of ash cloud frequency.

The particle size dataset presented here provides an important resource for testing more complex models of ash dispersal over northern Europe. However, detailed analysis of shard size relies on identifying and measuring the same tephra at multiple sites across a range of distances. The current 'database' of shard sizes is limited to a small number of sites, an even smaller number contain the same tephras and therefore it is difficult to form well-founded conclusions on the utility of these records for palaeo-hazard research. Routine analysis of shard sizes is required, certainly for the most widespread tephras.

Acknowledgements

This research was undertaken while Elizabeth Watson held a NERC-funded Doctoral Training Grant (NE/K500847/1).

References

Ahrens, C.D., 2012. Meteorology today: an introduction to weather, climate, and the environment. Cengage Learning.

Alfano, F., Bonadonna, C., Delmelle, P., Costantini, L., 2011. Insights on tephra settling velocity from morphological observations. Journal of Volcanology and Geothermal Research 208, 86-98.

Beckett, F., Witham, C., Hort, M., Stevenson, J., Bonadonna, C., Millington, S., 2015. Sensitivity of dispersion model forecasts of volcanic ash clouds to the physical characteristics of the particles. Journal of Geophysical Research: Atmospheres 120, 11,636–11,652.

Blockley, S.P.E., Pyne-O'Donnell, S.D.F., Lowe, J.J., Matthews, I.P., Stone, A., Pollard, A.M., Turney, C.S.M., Molyneux, E.G., 2005. A new and less destructive laboratory procedure for the physical separation of distal glass tephra shards from sediments. Quaternary Science Reviews 24, 1952-1960.

Bonadonna, C., Connor, C.B., Houghton, B., Connor, L., Byrne, M., Laing, A., Hincks, T., 2005. Probabilistic modeling of tephra dispersal: Hazard assessment of a multiphase rhyolitic eruption at Tarawera, New Zealand. Journal of Geophysical Research: Solid Earth 110.

Bonadonna, C., Phillips, J.C., 2003. Sedimentation from strong volcanic plumes. Journal of Geophysical Research: Solid Earth 108, 2340.

Brown, R.J., Bonadonna, C., Durant, A.J., 2012. A review of volcanic ash aggregation. Physics and Chemistry of the Earth, Parts A/B/C 45–46, 65-78.

Carey, R.J., Houghton, B.F., Thordarson, T., 2010. Tephra dispersal and eruption dynamics of wet and dry phases of the 1875 eruption of Askja Volcano, Iceland. Bulletin of Volcanology 72, 259-278.

Carey, S., Sparks, R.S.J., 1986. Quantitative models of the fallout and dispersal of tephra from volcanic eruption columns. Bulletin of Volcanology 48, 109-125.

Cooke, M.C., Francis, P.N., Millington, S., Saunders, R., Witham, C., 2014. Detection of the Grímsvötn 2011 volcanic eruption plumes using infrared satellite measurements. Atmospheric Science Letters 15, 321-327.

Davies, S.M., Elmquist, M., Bergman, J., Wohlfarth, B., Hammarlund, D., 2007. Cryptotephra sedimentation processes within two lacustrine sequences from west central Sweden. Holocene 17, 319-330.

De Vleeschouwer, F., Chambers, F.M., Swindles, G.T., 2011. Coring and sub-sampling of peatlands for palaeoenvironmental research. Mires and Peat 7, 1-10.

Dugmore, A.J., Larsen, G., Newton, A.J., 1995. 7 Tephra isochrones in Scotland. Holocene 5, 257-266.

Dugmore, A.J., Newton, A.J., 1992. Thin tephra layers in peat revealed by X-Radiography. Journal of Archaeological Science 19, 163-170.

Durant, A.J., Rose, W.I., Sarna-Wojcicki, A.M., Carey, S., Volentik, A.C.M., 2009. Hydrometeor-enhanced tephra sedimentation: Constraints from the 18 May 1980 eruption of Mount St. Helens. Journal of Geophysical Research: Solid Earth 114.

Folch, A., 2012. A review of tephra transport and dispersal models: Evolution, current status, and future perspectives. Journal of Volcanology and Geothermal Research 235, 96-115.

Gudmundsson, M.T., Thordarson, T., Hoskuldsson, A., Larsen, G., Bjornsson, H., Prata, F.J., Oddsson, B., Magnusson, E., Hognadottir, T., Petersen, G.N., Hayward, C.L., Stevenson, J.A., Jonsdottir, I., 2012. Ash generation and distribution from the April-May 2010 eruption of Eyjafjallajokull, Iceland. Sci Rep 2.

Hall, M., Hayward, C., 2014. Preparation of micro- and crypto-tephras for quantitative microbeam analysis. Geological Society, London, Special Publications 398, 21-28.

Hall, V.A., Pilcher, J.R., 2002. Late-Quaternary Icelandic tephras in Ireland and Great Britain: detection, characterization and usefulness. Holocene 12, 223-230.

Hayward, C., 2012. High spatial resolution electron probe microanalysis of tephras and melt inclusions without beam-induced chemical modification. Holocene 22, 119-125.

Jensen, B.J.L., Pyne-O'Donnell, S., Plunkett, G., Froese, D.G., Hughes, P.D.M., Sigl, M., McConnell, J.R., Amesbury, M.J., Blackwell, P.G., van den Bogaard, C., Buck, C.E., Charman, D.J., Clague, J.J., Hall, V.A., Koch, J., Mackay, H., Mallon, G., McColl, L., Pilcher, J.R., 2014. Transatlantic distribution of the Alaskan White River Ash. Geology 42, 875-878.

Jowsey, P., 1966. An improved peat sampler. New Phytologist 65, 245-248.

Lacasse, C., 2001. Influence of climate variability on the atmospheric transport of Icelandic tephra in the subpolar North Atlantic. Global and Planetary Change 29, 31-55.

Lane, C.S., Chorn, B.T., Johnson, T.C., 2013. Ash from the Toba supereruption in Lake Malawi shows no volcanic winter in East Africa at 75 ka. Proceedings of the National Academy of Sciences 110, 8025-8029.

Langdon, P.G., Barber, K.E., 2004. Snapshots in time: precise correlations of peat-based proxy climate records in Scotland using mid-Holocene tephras. Holocene 14, 21-33.

Larsen, G., Thorarinsson, S., 1977. Hekla 4 and other acidic Hekla tephra layers. Jokull 27, 28-46.

Lawson, I.T., Swindles, G.T., Plunkett, G., Greenberg, D., 2012. The spatial distribution of Holocene cryptotephras in north-west Europe since 7 ka: implications for understanding ash fall events from Icelandic eruptions. Quaternary Science Reviews 41, 57-66.

Le Maitre, R.W., Bateman, P., Dudek, A., Keller, J., Lameyre, J., Le Bas, M., Sabine, P., Schmid, R., Sorensen, H., Streckeisen, A., 1989. A classification of igneous rocks

and glossary of terms: Recommendations of the International Union of Geological Sciences Subcommission on the Systematics of Igneous Rocks. Blackwell Oxford.

Lerbekmo, J.F., 2008. The White River Ash: largest Holocene Plinian tephra. Canadian Journal of Earth Sciences 45, 693-700.

Lowe, D.J., 2011. Tephrochronology and its application: A review. Quaternary Geochronology 6, 107-153.

Mattsson, S., Vesanen, R., 1988. Patterns of Chernobyl fallout in relation to local weather conditions. Environment International 14, 177-180.

Newhall, C.G., Self, S., 1982. The volcanic explosivity index/VEI/- An estimate of explosive magnitude for historical volcanism. Journal of Geophysical Research 87, 1231-1238.

Newton, A.J., Dugmore, A.J., Gittings, B.M., 2007. Tephrabase: tephrochronology and the development of a centralised European database. Journal of Quaternary Science 22, 737-743.

Payne, R., Gehrels, M., 2010. The formation of tephra layers in peatlands: An experimental approach. Catena 81, 12-23.

Pilcher, J., Bradley, R.S., Francus, P., Anderson, L., 2005. A Holocene tephra record from the Lofoten Islands, Arctic Norway. Boreas 34, 136-156.

Ponomareva, V., Portnyagin, M., Davies, S.M., 2015. Tephra without borders: Far-reaching clues into past explosive eruptions. Frontiers in Earth Science 3, 83.

Riley, C.M., Rose, W.I., Bluth, G.J.S., 2003. Quantitative shape measurements of distal volcanic ash. Journal of Geophysical Research: Solid Earth 108, 2504.

Rose, W., Riley, C., Dartevelle, S., 2003. Sizes and shapes of 10 - Ma distal fall pyroclasts in the Ogallala Group, Nebraska. The Journal of geology 111, 115-124.

Rose, W.I., Durant, A.J., 2011. Fate of volcanic ash: Aggregation and fallout. Geology 39, 895-896.

Simkin, T., Siebert, L., 1994. Volcanoes of the World: A Regional Directory, Gazetteer, and Chronology of Volcanism During the Last 10,000 Years, 349 pp. Geoscience, Tucson, Ariz.

Stevenson, J., Millington, S., Beckett, F., Swindles, G., Thordarson, T., 2015. Big grains go far: reconciling tephrochronology with atmospheric measurements of volcanic ash. Atmos. Meas. Tech. Discuss., 8, 65-120.

Stevenson, J.A., Loughlin, S., Font, A., Fuller, G.W., MacLeod, A., Oliver, L.W., Jackson, B., Horwell, C.J., Thordarson, T., Dawson, I., 2013a. UK Monitoring and deposition of tephra from the May 2011 eruption of Grimsvotn, Iceland. Journal of Applied Volcanology 2.

Stevenson, J.A., Loughlin, S., Rae, C., Thordarson, T., Milodowski, A.E., Gilbert, J.S., Harangi, S., Lukacs, R., Hojgaard, B., Arting, U., Pyne-O'Donnell, S., MacLeod, A., Whitney, B., Cassidy, M., 2012. Distal deposition of tephra from the Eyjafjallajokull 2010 summit eruption. Journal of Geophysical Research-Solid Earth 117.

Stevenson, J.A., Loughlin, S.C., Font, A., Fuller, G.W., MacLeod, A., Oliver, I.W., Jackson, B., Horwell, C.J., Thordarson, T., Dawson, I., 2013b. UK monitoring and

deposition of tephra from the May 2011 eruption of Grímsvötn, Iceland. Journal of Applied Volcanology 2, 1-17.

Stevenson, J.A., Millington, S., Beckett, F., Thordarson, T., Swindles, G.T., 2013c. Big volcanic ash grains, even from small plumes, travel long distances: implications for satellite remote sensing, EGU, Vienna

Swindles, G.T., De Vleeschouwer, F., Plunkett, G., 2010. Dating peat profiles using tephra: stratigraphy, geochemistry and chronology Mires and Peat 7, 1-9.

Swindles, G.T., Galloway, J., Outram, Z., Turner, K., Schofield, J.E., Newton, A.J., Dugmore, A.J., Church, M.J., Watson, E.J., Batt, C., Bond, J., Edwards, K.J., Turner, V., Bashford, D., 2013a. Re-deposited cryptotephra layers in Holocene peats linked to anthropogenic activity. The Holocene 23, 1493-1501.

Swindles, G.T., Lawson, I.T., Savov, I.P., Connor, C.B., Plunkett, G., 2011. A 7000 yr perspective on volcanic ash clouds affecting northern Europe. Geology 39, 887-890.

Swindles, G.T., Savov, I.P., Connor, C.B., Carrivick, J., Watson, E., Lawson, I.T., 2013b. Volcanic ash clouds affecting Northern Europe: the long view. Geology Today 29, 214-217.

Taddeucci, J., Scarlato, P., Montanaro, C., Cimarelli, C., Del Bello, E., Freda, C., Andronico, D., Gudmundsson, M.T., Dingwell, D.B., 2011. Aggregation-dominated ash settling from the Eyjafjallajökull volcanic cloud illuminated by field and laboratory high-speed imaging. Geology 39, 891-894.

Thorarinsson, S., 1981. Greetings from Iceland. Ash-falls and volcanic aerosols in Scandinavia. Geografiska Annaler. Series A. Physical Geography, 109-118.

Wastegård, S., Davies, S.M., 2009. An overview of distal tephrochronology in northern Europe during the last 1000 years. Journal of Quaternary Science 24, 500-512.

Watson, E.J., Swindles, G.T., Lawson, I.T., Savov, I.P., 2015. Spatial variability of tephra and carbon accumulation in a Holocene peatland. Quaternary Science Reviews 124, 248-264.

Watson, E.J., Swindles, G.T., Lawson, I.T., Savov, I.P., 2016. Do peatlands or lakes provide the most comprehensive distal tephra records? Quaternary Science Reviews 139, 110-128.

Chapter 7: Climatic control on Icelandic volcanic activity during the Holocene

Watson, E.J*[1], Swindles, G.T.[1], Savov, I.P.[2], Lawson, I.T.[3], Schmidt, A.[2], Hooper, A. [2], Carrivick, J.L..[1]

[1]School of Geography, University of Leeds, Leeds, LS2 9JT, UK
[2]School of Earth and Environment, University of Leeds, Leeds, LS2 9JT, UK
[3]Department of Geography and Sustainable Development, University of St Andrews, St Andrews, KY16 9AL, UK
**Corresponding author: Elizabeth Watson (gy08ejw@leeds.ac.uk)*
For submission to: PNAS

Abstract

Glacial unloading can affect volcanic eruption rates on glacial-interglacial timescales[1]. Numerical models suggest that smaller changes in ice volume over shorter timescales may also influence rates of mantle melt generation[2], but this effect has not been empirically demonstrated. Furthermore, the time between climatic forcing and a resulting change in the frequency of volcanic eruptions is unknown. We present the first empirical evidence that the frequency of volcanic eruptions in Iceland was affected by climate, modulated by glacial extent, on ~1000 year timescales during the Holocene. We compare the frequency of Icelandic eruptions with the frequency of volcanic ash clouds over Northern Europe and identify two periods of reduced volcanic activity (5.5-4.5 and 2.6-1.6 ka BP). Both periods are preceded by global changes in circulation patterns and climate, expressed in the North Atlantic as a deepening of the Icelandic Low, favouring glacier advances on Iceland. We identify a significant cross-correlation between ice core proxy data for a deepening of the Icelandic Low and a decreased frequency of Icelandic eruptions. There is a lag of 400-1500 years between a shift in climate and the resulting change in volcanic frequency. We conclude that the advance of glaciers on Iceland has reduced eruption frequency at least twice during the last 7000 years. Given the time lags involved any increase in eruption rate due to ongoing deglaciation since the end of the Little Ice Age may not become apparent for hundreds of years.

Significance statement

Human-induced climate change is causing the melting of ice in many volcanic regions. On glacial-interglacial timescales changes in surface loading exerted by large variations in glacier size affect mantle melt rates and thus the rate of volcanic activity. We provide empirical evidence for variations in the rate of Icelandic eruptions caused by much smaller ice volume changes, over shorter (Holocene) timescales. Reduced volcanic activity is preceded by a deepening of the Icelandic Low (a control on glacier extent). For the first time, we are able to estimate a lag time of 400-1500 years between climate forcing (deeper Icelandic Low) and a change in eruption frequency. The impact of current deglaciation on volcanism may not become apparent for hundreds of years.

7.1 Main text

The link between large-scale glacier ice mass decline and an increase in average volcanic eruption rates at the end of the last glacial period, ~ 12 ka BP, is well established[1]. However, a number of questions remain regarding the sensitivity and response time of volcanoes to smaller changes in ice mass, such as those which occur over shorter timescales (e.g. during the Holocene)[3]. The loading and unloading of glaciers changes surface pressure and stress relationships in the crust and upper mantle. Numerical models suggest that glacial unloading increases mantle melt generation at depth and alters storage capacity in the crust[4]. Even small changes in surface loading can alter the stress field around shallow magma chambers, increasing or decreasing the likelihood of eruptions at ice-covered volcanoes[5].

For the first time we examine records of Icelandic eruptions alongside records of distal ash cloud events from Northern Europe. Examining past trends in the frequency of eruptions using proximal records (e.g. tephra layers and lava flows) is often complicated by reworking or burial of evidence by more recent eruptions. However, evidence of past volcanic eruptions can also be recorded by small, far-travelled ‘cryptotephra’ shards, which eventually fall out from ash clouds, forming invisible layers in peatlands and lakes[6]. Cryptotephra layers provide a record of explosive volcanism unaffected by many of the reworking issues that can confound proximal records of volcanic activity.

Over the last 7000 years, the frequency of Icelandic eruptions and Northern European ash clouds generally display a positive correlation through time (Fig. S1). An apparent increase in the frequency of Icelandic eruptions over the last 1000-1500 years is most likely an artefact of increased observations, and preferential geological preservation of more recent events (Fig.1). Another feature of both proximal and distal records is the apparent decrease in the frequency of volcanic eruptions during the mid-Holocene (~5-2 ka BP). Possible reasons for a low frequency of Icelandic eruptions during the mid-Holocene at some volcanic systems have been discussed elsewhere[7].

We identify two marked ~1000 year periods of volcanic quiescence apparent in records of Icelandic eruptions during the Holocene (Fig. 1). The longest period without any evidence of ash clouds is between 5.5-4.5 ka BP. During this time period, there is a corresponding decrease in the frequency of Icelandic eruptions, in particular explosive eruptions (Volcanic explosivity index (VEI) ≥ 4). The repose interval for eruptions with a VEI ≥ 4 during this period (1800 years: 6.1-4.3 ka BP) represents a significant departure from the average return interval over the last 7000 years (149 years, 507 years if last 1000 years are excluded). Although less pronounced, a second period of quiescence is apparent, particularly in records of explosive ($\geq$ VEI 4) Icelandic eruptions between 2.6-1.6 ka BP. This second time period corresponds with the second longest repose interval for Icelandic eruptions $\geq$ VEI 4 (2.7-1.1 ka BP, a period of 1520 years). There is also a reduction in the volume of lava erupted between 5.5-4.5 and 2.6-1.6 ka BP indicating a change in the rate of effusive volcanism. Identification of corresponding periods of quiescence in both Icelandic and Northern European records suggests that these periods reflect changes in the frequency of eruptions in Iceland rather than periods of poor preservation in the geological record.

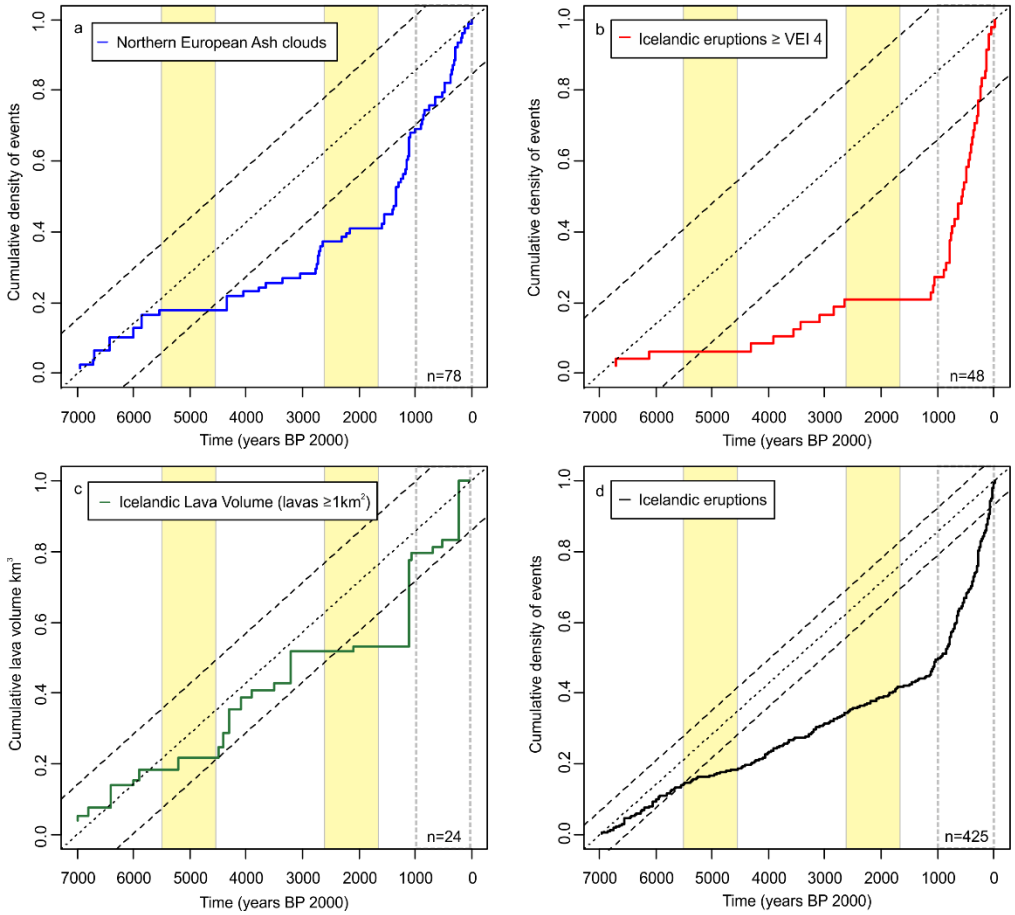

Figure 1. The cumulative frequency of explosive (a, b) and effusive volcanic activity (c), a) Northern European ash clouds, b) Icelandic eruptions with a VEI ≥4[8], c) lava volume (km^3) (lava flows with an area ≥1km^2[29]), d) Icelandic eruptions[8]. The Kolmogorov-Smirnov test indicates that all of these series deviate significantly from the steady state model over the last 7000 years ($p < 0.05$). The dense dashed line indicates a steady state model; loosely dashed lines indicate 95% confidence interval. Shaded areas indicate periods of quiescence (5.5-4.5 ka BP and 2.6-1.6 ka BP). Grey dashed lines indicate improved geological preservation and historical records over the last 1000 years.

Icelandic volcanism is controlled by complex interactions between rifting, mantle plume activity and environmental factors such as ice loading. Plate boundary rifting in Iceland is not constant and previous work has attributed short-term (centennial) changes in eruption frequency to changes in the rate of rifting, although the underlying cause of periodic activity over these timescales remains unknown[10]. Pulses in mantle plume activity may be the cause of longer term (multi-millennial) decreases in eruption frequency at the Grímsvötn, Bárdarbunga and Kverkfjöll subglacial volcanic centres[7]. Although changes in the magma supply rate due to this effect cannot be completely discounted as a reason for the periods of reduced volcanic output we identify, it appears

highly unlikely that such pulses would result in simultaneous periods of quiescence of ~1000 years across multiple volcanic systems in Iceland. A more plausible scenario is that an external driver, for example, changing ice load, might have impacted on eruption frequency during the two periods of quiescence we identify.

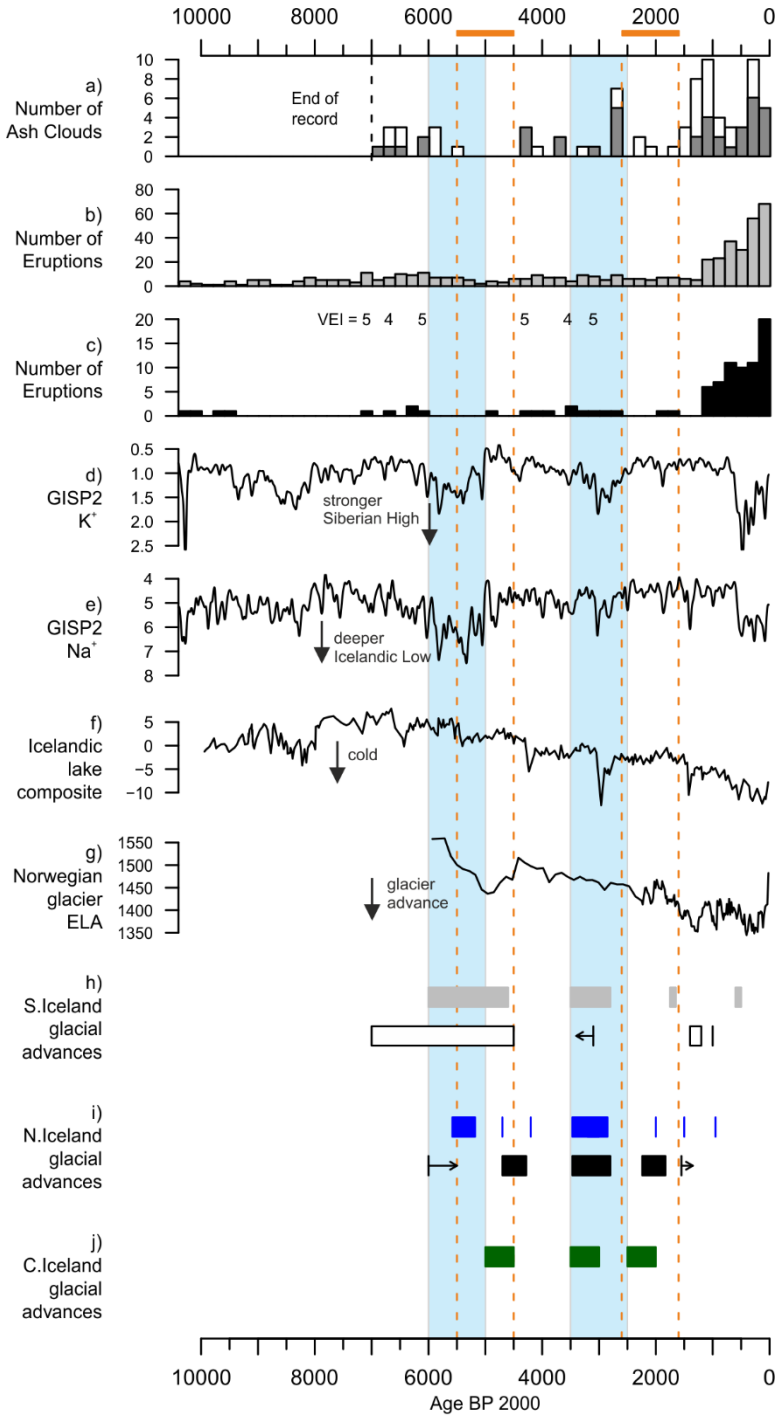

Figure 2. a) Northern European ash clouds, white indicates eruptions where Iceland is the most probable source region; dark grey indicates ash clouds directly assigned to an Icelandic source, b) the frequency

Icelandic eruptions[8], c) the frequency of Icelandic eruptions VEI ≥ 3, eruptions of the Hekla volcano from the time period >1000 BP are highlighted with numbers corresponding to their VEI d) GISP2 (K^+ ppb) 200 year Gaussian smoothed[11], e) GISP2 (Na^+ ppb) 200 year Gaussian smoothed [11], f)) Icelandic lake composite record[12], g) Folgefonna glacier (Norway) reconstructed equilibrium line altitude (ELA)[13], h) Glacial advances in Southern Iceland Kvíárjökull (grey)[14], Sólheimajökull (outline)[15], i) Glacial advances in Northern Iceland Tröllaskagi[16] (blue), Tröllaskagi (black)[17], j) Glacial advances central Iceland[18]. Light blue shading indicates global-scale rapid climate change events[19]. Dashed orange lines indicate periods of quiescence.

Icelandic glaciers are known to respond actively to climatic fluctuations[20,21]. During the Holocene Thermal Maximum (HTM ~ 8 to 5.5 ka BP[12]) Iceland was largely ice free. Although some ice caps may have persisted, albeit greatly reduced in volume when compared to their present state. Multiple paleoclimate records indicate changing conditions in Iceland and in the surrounding oceans prior to both periods of volcanic quiescence. Records from both the Icelandic shelf (c.7.4-6.2 ka BP[22]) and North Atlantic (post 6 ka BP; c. 3 ka BP[23]) indicate oceanic cooling. Furthermore, decreased productivity in lake records from Iceland suggests a cooling event ~6.4 ka BP, with the onset of long-term summer cooling from 5.7-5.5 ka BP[12,24]. Further cold perturbations occurred between 3.1 and 2.8 ka BP[12] and in Northern Iceland at ~3.3 ka BP[25]. The concentration of Sodium (Na^+) in the Greenland ice core, shows a major deviation in the periods 6-5 ka BP and 3.5-2.5 ka BP[11] indicating a deeper Icelandic Low. The Icelandic Low influences both temperature and precipitation in the North Atlantic, two of the dominant controls on the size of glaciers in Iceland[20,21]. These climatic changes in Iceland correspond to the timing of two global-scale rapid climate change events at 6-5 ka BP and 3.5-2.5 ka BP[19].

Coinciding with climatic changes, there is evidence of glacial advances in the south (7-4.5 ka BP), centre (4.5-5 ka BP) and north (before 5 ka BP) of Iceland[14,15,17,18]. Some glaciers may have advanced to their maximum Holocene extent (exceeding LIA limits)[14]. Evidence for substantial expansion of the Langjökull ice cap prior to 5.5 ka is lacking[26]. It is likely that smaller glaciers, which respond rapidly to climate forcing accounted for the majority of glacial expansion following the HTM[18]. There is evidence for subsequent glacial advances c. 3.5-2.5 ka BP in the north (Vatnsdalur II, 3.2-3.0 ka BP); centre (3.5-3.0 ka BP); and south (Hólsárgil >3.1 ka BP) of Iceland[14,16-18]. There are

no estimates for the relative magnitude of glacial advances, but those during the Drangagil/Vatnsdalur I period (6-4.5 ka BP) and Vatnsdalur II/ Hólsárgil period (3.5-2.8 ka BP) are spatially widespread[14].

Although there is evidence for the advance of glaciers in the periods preceding reductions in eruption frequency, there are no quantitative reconstructions of glacier volume that we can compare to volcanic frequency data. Therefore, we conducted cross correlation analysis on the GISP2 Na^+ record (depth of Icelandic Low) and both the European ash cloud record and Icelandic eruption frequency over the last 7000 years. In both instances an increase in Na^+ was followed by a significant ($p < 0.05$) decrease in volcanic eruptions (Icelandic eruptions strongest correlation -0.33 at a lag of 600 years; European ash clouds strongest correlation -0.35 at a lag of 700 years) (Fig. S2). Given the range of response times exhibited by Icelandic glaciers to changing climate (10-1000 years[27]), and uncertainties involved in the time taken for new melt produced in the mantle to reach the surface[1], a lag time of ~600-700 years between climate forcing and a reduction in the frequency of volcanic activity would support the argument for the modulation of climatic forcing by glacial expansion. The range of lag times most likely reflects differences in the magnitude and duration of climatic forcing (deviations the Icelandic Low) and the modulation of climate signal due to the differing response times of mountain glaciers and large ice caps (Fig. 3).

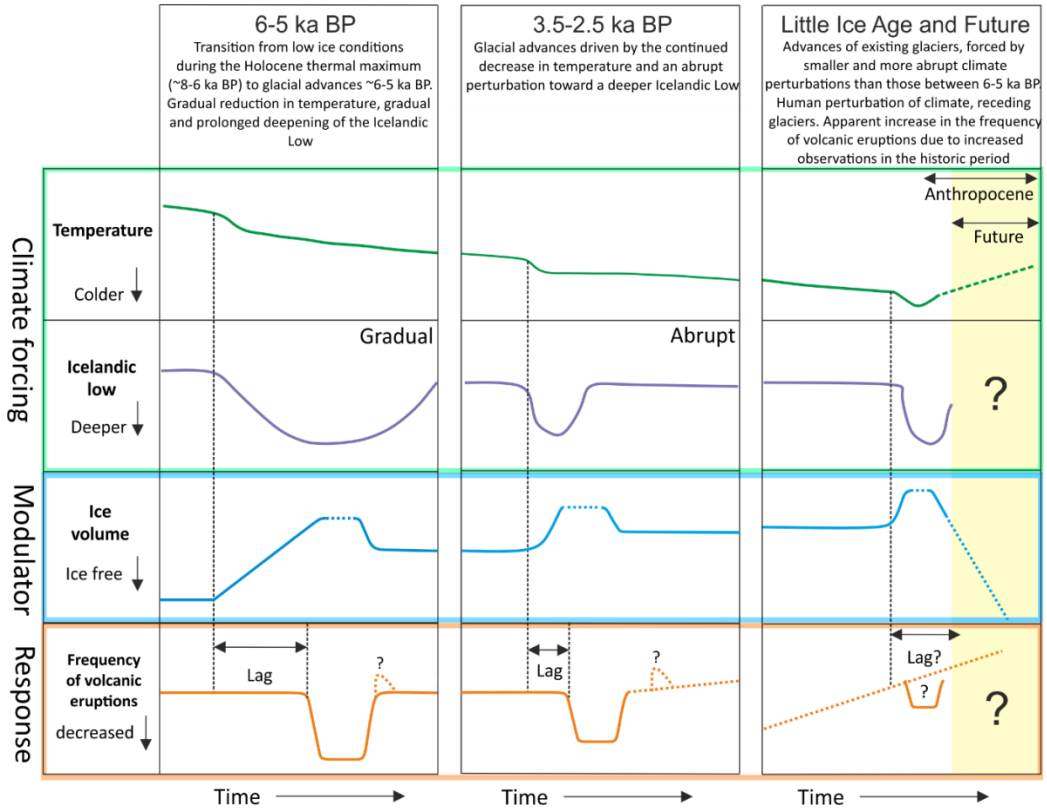

Figure 3. Conceptual diagram showing the impact of climatic forcing on the frequency of volcanic eruptions during interglacial periods and how this is modulated by changes in ice volume. Columns indicate how differences in the magnitude and duration of forcing impact on the lag time between the onset of climatic forcing and a change in the frequency of volcanic eruptions.

Schmidt, *et al*. [2] modelled a significant increase in mantle melt production (100-135 %) due to deglaciation between AD1890 and 2010. It is likely that the rate of ice accumulation between the HTM and 5 ka BP was of a similar magnitude to the current rate of ice loss since the LIA. If this was the case, the same model would predict extremely reduced, or even a complete shutdown of melting between the HTM and 5 ka BP, assuming that the spatial distribution of changes in ice mass between the HTM and 5 ka BP was not significantly different to that between AD1890 and 2010. The reduction in volcanic frequency between 5.5-4.5 ka BP was greater in the geological record when compared to the period 2.6-1.6 ka BP. This is attributed to the larger magnitude of changes in ice volume between 6-5 ka BP when compared to 3.5-2.5 ka BP. The resumption of volcanic activity was most likely driven by a change in climate and subsequent glacier retreat. There is evidence for a weakening of the Icelandic Low and a reduction in ice rafting events in the North Atlantic preceding the resumption of greater volcanic activity following both periods of quiescence[28].

The most recent glacial advances in Iceland occurred during the LIA ~AD 1600 to AD 1880. Although some glaciers reach their maximum Holocene extent during the LIA[21], the magnitude of changes in the Icelandic Low is smaller than at 6-5 ka BP. Climate warming driven by human activity may also have curtailed ice expansion in the 20th century. Given the lag time between climate forcing and changes in eruption frequency (600-700 years) and the short duration of the LIA glacier expansions, any reduction in melt generation may not become apparent for hundreds of years.

We conclude that climate forcing, modulated by the advance of glaciers on Iceland, reduced the frequency of volcanic eruptions at least twice over the last 7000 years. Our results support modelling efforts that suggest that moderate to small changes in ice volume, such as those that have occurred, and continue to occur during the Holocene, can affect the frequency of volcanic eruptions. Given the lag times we identify between climate forcing and changes in eruption frequency, the impact of anthropogenically-induced deglaciation on volcanic eruption frequency may not be felt for hundreds of years.

7.2 Methods

The Northern European ash cloud record originally compiled by Swindles, *et al*. [6] was updated as of autumn 2015. Data are based on historical records of observed ash clouds (which span only the last ~1000 years) and cryptotephra layers from sites in northern Europe, which have been geochemically analysed. Not all tephra layers recorded in Northern Europe are from an Icelandic source. Tephra layers with a known source eruption outside of Iceland such as those from: Alaska (AD 860 B c.f.[29]), potentially the Azores, and Jan Mayen were removed from the database (DCSH-2, MOR-T7, MOR-T8, MOR-T9, PMG-5, MOR-T2[30,31]). The glass major element geochemistry of shards from cryptotephra layers which have not been linked to a known source eruption was plotted against the glass major element geochemistry of shards from other distal tephra layers known to have originated from Icelandic volcanoes. All tephra layers with a major element geochemistry matching the geochemical envelope for tephra produced during eruptions of Icelandic volcanoes were retained. Data for Icelandic eruptions was taken from the Smithsonian Volcanoes of the World Database[8]. The database contains evidence of volcanic eruptions from both the proximal geological record and historical observations. In all instances the age of cryptotephra layers or Icelandic eruptions was the midpoint age. Unless otherwise stated all ages are reported as cal years BP 2000. The Kolmogorov-Smirnov test was used to determine whether the rate of eruptions or lava flows has been steady over the last 7000 years. A two sample test was conducted to compare a cumulative steady state model to the cumulative observed values. 95% confidence bounds were calculated for each series as follows: $\frac{1.36}{\sqrt{N_{S,T}}}$ where S and T were the first and last event in the sequence[32]. Cross correlation analysis was conducted on Na^+ data from the GISP2 ice core, a proxy for the depth of the Icelandic Low[11]. Both eruption frequency data and ash cloud data were split into 100 year bins. Na^+ data was averaged into 100 year bins. Cross correlation was conducted using the 'astsa' package in R version 3.1.1.

Acknowledgements

This research was undertaken while Elizabeth Watson held a NERC-funded Doctoral Training Grant (NE/K500847/1).

References

1 Maclennan, J., Jull, M., McKenzie, D., Slater, L. & Grönvold, K. The link between volcanism and deglaciation in Iceland. *Geochemistry, Geophysics, Geosystems* **3**, 1-25, doi:10.1029/2001GC000282 (2002).

2 Schmidt, P. *et al.* Effects of present-day deglaciation in Iceland on mantle melt production rates. *Journal of Geophysical Research: Solid Earth* **118**, 3366-3379 (2013).

3 Tuffen, H. How will melting of ice affect volcanic hazards in the twenty-first century? *Philosophical Transactions of the Royal Society of London A: Mathematical, Physical and Engineering Sciences* **368**, 2535-2558 (2010).

4 Hooper, A. *et al.* Increased capture of magma in the crust promoted by ice-cap retreat in Iceland. *Nat. Geosci.* **4**, 783-786, doi:10.1038/ngeo1269 (2011).

5 Albino, F., Pinel, V. & Sigmundsson, F. Influence of surface load variations on eruption likelihood: application to two Icelandic subglacial volcanoes, Grímsvötn and Katla. *Geophysical Journal International* **181**, 1510-1524, doi:10.1111/j.1365-246X.2010.04603.x (2010).

6 Swindles, G. T., Lawson, I. T., Savov, I. P., Connor, C. B. & Plunkett, G. A 7000 yr perspective on volcanic ash clouds affecting northern Europe. *Geology* **39**, 887-890, doi:10.1130/g32146.1 (2011).

7 Óladóttir, B., Larsen, G. & Sigmarsson, O. Holocene volcanic activity at Grímsvötn, Bárdarbunga and Kverkfjöll subglacial centres beneath Vatnajökull, Iceland. *Bulletin of Volcanology* **73**, 1187-1208, doi:10.1007/s00445-011-0461-4 (2011).

8 Global Volcanism Program. *Volcanoes of the World, v. 4.3.4.* , <http://dx.doi.org/10.5479/si.GVP.VOTW4-2013> (2013).

9 Hjartarson, Á. *Postglacial lava production in Iceland in The Skagafjörður Unconformity, North Iceland, and its Geological History*, University of Copenhagen, (2003).

10 Larsen, G., Gudmundsson, M. T. & Björnsson, H. Eight centuries of periodic volcanism at the center of the Iceland hotspot revealed by glacier tephrostratigraphy. *Geology* **26**, 943-946, doi:10.1130/0091-7613 (1998).

11 Mayewski, P. A. *et al.* Major features and forcing of high-latitude northern hemisphere atmospheric circulation using a 110,000-year-long glaciochemical series. *Journal of Geophysical Research: Oceans* **102**, 26345-26366, doi:10.1029/96JC03365 (1997).

12 Geirsdóttir, Á., Miller, G. H., Larsen, D. J. & Ólafsdóttir, S. Abrupt Holocene climate transitions in the northern North Atlantic region recorded by synchronized lacustrine records in Iceland. *Quaternary Science Reviews* **70**, 48-62, doi:http://dx.doi.org/10.1016/j.quascirev.2013.03.010 (2013).

13 Bakke, J., Lie, ø., Nesje, A., Dahl, S. O. & Paasche, ø. Utilizing physical sediment variability in glacier-fed lakes for continuous glacier reconstructions during the Holocene, northern Folgefonna, western Norway. *The Holocene* **15**, 161-176, doi:10.1191/0959683605hl797rp (2005).

14 Kirkbride, M. P. & Dugmore, A. J. Timing and significance of mid-Holocene glacier advances in northern and central Iceland. *Journal of Quaternary Science* **16**, 145-153, doi:10.1002/jqs.589 (2001).

15 Dugmore, A. in *Glacier fluctuations and climatic change* 37-55 (Springer, 1989).

16 Stötter, J., Wastl, M., Caseldine, C. & Häberle, T. Holocene palaeoclimatic reconstruction in northern Iceland: approaches and results. *Quaternary Science Reviews* **18**, 457-474, doi:http://dx.doi.org/10.1016/S0277-3791(98)00029-8 (1999).

17 Gudmundsson, H. J. A review of the holocene environmental history of Iceland. *Quaternary Science Reviews* **16**, 81-92, doi:http://dx.doi.org/10.1016/S0277-3791(96)00043-1 (1997).

18 Kirkbride, M. P. & Dugmore, A. J. Responses of mountain ice caps in central Iceland to Holocene climate change. *Quaternary Science Reviews* **25**, 1692-1707, doi:http://dx.doi.org/10.1016/j.quascirev.2005.12.004 (2006).

19 Mayewski, P. A. *et al.* Holocene climate variability. *Quat. Res.* **62**, 243-255, doi:http://dx.doi.org/10.1016/j.yqres.2004.07.001 (2004).

20 Flowers, G. E. *et al.* Holocene climate conditions and glacier variation in central Iceland from physical modelling and empirical evidence. *Quaternary Science Reviews* **27**, 797-813, doi:http://dx.doi.org/10.1016/j.quascirev.2007.12.004 (2008).

21 Caseldine, C. & Stötter, J. 'Little Ice Age' glaciation of Tröllaskagi peninsula, northern Iceland: climatic implications for reconstructed equilibrium line altitudes (ELAS). *The Holocene* **3**, 357-366, doi:10.1177/095968369300300408 (1993).

22 Bendle, J. A. P. & Rosell-Melé, A. High-resolution alkenone sea surface temperature variability on the North Icelandic Shelf: implications for Nordic Seas palaeoclimatic development during the Holocene. *The Holocene* **17**, 9-24, doi:10.1177/0959683607073269 (2007).

23 Giraudeau, J., Cremer, M., Manthé, S., Labeyrie, L. & Bond, G. Coccolith evidence for instabilities in surface circulation south of Iceland during Holocene times. *Earth Planet. Sci. Lett.* **179**, 257-268, doi:http://dx.doi.org/10.1016/S0012-821X(00)00113-8 (2000).

24 Blair, C. L., GeirsdÓTtir, Á. & Miller, G. H. A high-resolution multi-proxy lake record of Holocene environmental change in southern Iceland. *Journal of Quaternary Science* **30**, 281-292, doi:10.1002/jqs.2780 (2015).

25 Wastl, M., Stötter, J. & Caseldine, C. Reconstruction of Holocene Variations of the Upper Limit of Tree or Shrub Birch Growth in Northern Iceland Based on Evidence from Vesturárdalur-Skíðadalur, Tröllaskagi. *Arctic, Antarctic, and Alpine Research* **33**, 191-203, doi:10.2307/1552220 (2001).

26 Larsen, D. J., Miller, G. H., Geirsdottir, A. & Olafsdottir, S. Non-linear Holocene climate evolution in the North Atlantic: a high-resolution, multi-proxy record of glacier activity and environmental change from Hvitarvatn, central Iceland. *Quaternary Science Reviews* **39**, 14-25, doi:10.1016/j.quascirev.2012.02.006 (2012).

27 Jóhannesson, T. The response time of glaciers in Iceland to changes in climate. *Annals of Glaciology* **8**, 100-101 (1985).

28 Bond, G. *et al.* Persistent solar influence on North Atlantic climate during the Holocene. *Science* **294**, 2130-2136 (2001).

29 Jensen, B. J. L. *et al.* Transatlantic distribution of the Alaskan White River Ash. *Geology* **42**, 875-878, doi:10.1130/g35945.1 (2014).

30 Reilly, E. & Mitchell, F. J. Establishing chronologies for woodland small hollow and mor humus deposits using tephrochronology and radiocarbon dating. *The Holocene* **25**, 241-252, doi:10.1177/0959683614557571 (2015).

31 Chambers, F. M., Daniell, J. R. G., Hunt, J. B., Molloy, K. & O'Connell, M. Tephrostratigraphy of An Loch Mor, Inis Oirr, western Ireland: implications for Holocene tephrochronology in the northeastern Atlantic region. *Holocene* **14**, 703-720, doi:10.1191/0959683604hl749rp (2004).

32 Connor, C., Bebbington, M. & Marzocchi, W. in *The Encyclopedia of Volcanoes (Second Edition)* (ed Haraldur Sigurdsson) 897-910 (Academic Press, 2015).

Chapter 8: Estimating the frequency of volcanic ash clouds over northern Europe

Watson, E.J.[1]., Swindles, G.T.[1]., Savov, I.[2]., Lawson, I.T.[3], Connor, C.[4], Wilson, J.[4], Lamentowicz, M.[5]

[1]*School of Geography, University of Leeds, Leeds, LS2 9JT, UK*
[2]*School of Earth and Environment, University of Leeds, Leeds, LS2 9JT, UK*
[3]*Department of Geography and Sustainable Development, University of St Andrews, St Andrews, KY16 9AL, UK*
[4] *School of Geosciences, University of South Florida, Tampa, FL 33620-5550, USA*
[5]*Department of Biogeography and Paleoecology, Adam Mickiewicz University in Poznan, Dziegielowa 27, 61-680 Poznan, Poland*
**Corresponding author: Elizabeth Watson (gy08ejw@leeds.ac.uk)*

Keywords: Cryptotephra, reoccurrence, survival analysis, hazards, tephra, eruptions, Iceland

Abstract

Fine ash produced during explosive volcanic eruptions can be dispersed far from the volcanic source, where it poses a threat to aviation, human health and infrastructure. Here, we focus on northern Europe, which lies in the predominant transport direction for volcanic ash from Iceland, one of the most active volcanic regions in the world. We interrogate existing and newly produced geological and written records of past ash fallout over northern Europe in the last 1000 years and estimate the mean return (repose) interval of a volcanic ash cloud over the region to be 44 ± 7 years. Our results suggest that ash clouds are more common over northern Europe than previously proposed (56 ± 9 years; Swindles *et al*., 2011). We compare northern European tephra records with records of proximal Icelandic volcanism and suggest that an Icelandic eruption with a Volcanic explosivity index rating (VEI; Newhall and Self, 1982) ≥ 4 and a silicic magma composition presents the greatest risk of producing volcanic ash that can reach northern Europe. None of the ash clouds in the European record which have a known source eruption are linked to a source eruption with VEI < 4. Our estimate for the reoccurrence of volcanic ash cloud events from distal tephra records is

concurrent with our understanding of the type of eruptions which have deposited ash over northern Europe in the past as it lies between the of return interval for all VEI ≥ 4 eruptions (25 years) (maximum estimate) and all VEI ≥ 4 eruptions of silicic geochemistry (90 years) (minimum estimate).

8.1 Introduction

Explosive volcanic eruptions can release large volumes of fine ash into the atmosphere. Fine ash particles may be transported long distances (1000s of kilometres) downwind of the volcano. Volcanic ash is a hazard for human health and even in moderate concentrations can cause engine failure in modern jet aircraft (Casadevall, 1994). The impact of volcanic ash clouds on aviation can be geographically extensive and air traffic can be affected even far from the volcano. For example, the eruption of the Cordón Caulle volcano in Chile (2011) led to the disruption of air traffic in Australia (Pistolesi *et al*., 2015). Reliable estimates of the frequency of such events would help society, governments and business to mitigate for the social and economic losses incurred during future ash clouds. One approach to understanding the frequency of future volcanic ash fallout in Europe is to examine the frequency of ash clouds in the past and use this information to forecast future hazard (Connor *et al*., 2015).

Iceland is one of the most volcanically active regions of the planet, and lies in the North Atlantic close to the path of trans-Atlantic air traffic (Thordarson and Hoskuldsson, 2008). The principal transport direction for volcanic ash from Iceland is easterly to south-easterly toward northern Europe, directly towards some of the busiest airports in the world (Wastegård and Davies, 2009). Over the last few centuries a number of ash clouds have been witnessed over northern Europe, such as those during the eruptions of Askja in 1875 and Hekla in 1947 (Mohn, 1878; Thorarinsson, 1954). The eruption of the Icelandic volcano Eyjafjallajökull in 2010 caused widespread disruption to travel and major financial losses. The eruption, which lasted 39 days led to the diversion and grounding of aircraft across northern Europe (Gudmundsson *et al*., 2012). In May 2011, another Icelandic volcano Grímsvötn, erupted and produced an ash cloud which led to minor travel disruption in Scotland (Stevenson *et al*., 2013a). Successful efforts have

been made to monitor ash fallout from these two most recent ash clouds using rain gauge samples and PM_{10} measurements (from air quality sampling equipment) (Stevenson *et al*., 2012; Stevenson *et al*., 2013b).

However, observed events and historical records only extend over a short period of time (none before 1600) (Swindles *et al*., 2013). The only evidence of pre-historic ash clouds are traces of ash ('tephra') which are eventually deposited and incorporated into ice sheets, peatlands, marine and lake sediments (Lowe, 2011; Watson *et al*., 2016). In locations far from the volcano, tephra shards form horizons so sparse in concentration they are not visible to the human eye ('cryptotephra'). The examination of peatlands and lake sediments spanning the last 7000 years across northern Europe has led to the identification of multiple cryptotephra layers, each representing ash fall from a different eruption (Lawson *et al*., 2012). The first estimate for the average return interval of volcanic ash fallout over northern Europe was made by Swindles *et al*. (2011). They combined data on the ages of cryptotephra layers with the ages of observed ash clouds recorded in historical documents and calculated an average return interval for volcanic ash clouds over northern Europe of 56 ± 9 years, which equates to a 16% chance of an ash cloud over northern Europe in any 10 year period.

A forecast of reoccurrence based on geological records, such as cryptotephra layers, will always represent a minimum estimate because there is the possibility that some events have not been preserved (or yet identified) in the geological record. Satellite images of the ash clouds produced during recent Icelandic eruptions indicate that volcanic ash distribution in the atmosphere is patchy, and transport trajectories are dependent on wind direction (Folch *et al*., 2012). Cryptotephra deposits are equally patchy, with different cryptotephra layers displaying different spatial distributions throughout northern Europe (Lawson *et al*., 2012). The cryptotephra data utilised by Swindles *et al*. (2011) was not collected for the purpose of calculating the frequency of past ash clouds and contained temporal, and spatial gaps. Spatial gaps in European cryptotephra distribution may represent the true margins of the distribution of Icelandic tephra, or they may be an artefact of sampling density. Should they be the latter, these 'gap' regions offer the most promise for identifying new, previously undiscovered tephra

layers. As more research is conducted to address spatial and temporal gaps in cryptotephra records, there is a probability that evidence for more volcanic eruptions will be identified, directly affecting the model of Icelandic ash cloud frequency over northern Europe.

The majority of cryptotephra layers in northern Europe are of Icelandic origin. However, there has been no detailed comparison of Icelandic eruption records and cryptotephra records of ash clouds in northern Europe. Understanding the characteristics of the Icelandic eruptions which have resulted in ash fall events over northern Europe during the last 7000 years may allow for the estimation of a range of estimates (minimum and maximum) for the frequency of ash clouds reaching northern Europe.

In this paper we:

- Report new data on tephra layers extending the coverage of cryptotephra layers across northern Europe and utilising these new data to present a new reoccurrence model for volcanic ash clouds over northern Europe.
- Compare data from the European geological record and historical observations with data on Icelandic volcanism in order to refine our understanding of the type of Icelandic eruption which poses the greatest risk of producing an ash cloud reaching northern Europe.
- Model the frequency of Icelandic eruptions with various geochemical compositions and explosivity. Using these models, and information on which Icelandic eruptions are most likely to produce ash clouds over northern Europe, we suggest a range of estimates for the return interval of volcanic ash clouds over northern Europe.

8.2 Methods

8.2.1 Addressing spatial gaps in existing cryptotephra records

We focussed our research on the spatial gaps in northern European tephra records which offered the most promise for identifying previously undiscovered cryptotephras: northern Sweden, Poland, Wales and southern England. These regions are far from existing cryptotephra finds, and contain peatlands and/or lakes with the potential to record cryptotephra fallout over the last 7000 years. We curtail our analysis at 7000 years as there is evidence for an increase in the frequency of Icelandic volcanism following glacial unloading at the end of the last glacial (Jull and McKenzie, 1996). Therefore, records of ash cloud frequency from before 7000 yr BP may not reflect the frequency of ash clouds under current and future conditions.

Details of sampling strategy and tephra identification for sites in northern Sweden have been published in detail elsewhere (Watson *et al*., 2016). Peatland sites in Poland, Wales and Southern England were sampled using a Russian-type peat corer (De Vleeschouwer *et al*., 2011). Samples were combusted to remove organic material and the residue rinsed in 10% HCl before mounting onto slides (Hall and Pilcher, 2002). Tephra shards were identified under a high power microscope. Samples which contained tephra were re-extracted for geochemical analysis following either the acid digestion method of Dugmore and Newton (1992) (excluding NaOH treatment) or, where large quantities of biogenic silica or minerals were present, following the density separation technique of Blockley *et al*. (2005). Tephra shards were mounted onto glass slides (Dugmore *et al*., 1992) or into blocks (Hall and Hayward, 2014). All samples were polished to a 0.25 µm finish. Major element geochemistry was analysed using an electron probe micro analyser (EPMA) at the University of Edinburgh (Hayward, 2012). Analyses were conducted at 15 kV. Secondary glass standards (Lipari obsidian and BCR-2G: Jochum *et al*. (2005)) were analysed before and after EPMA runs of unknown glass shard analyses. Assignments to specific eruptions were based on stratigraphy and

comparison of tephra geochemistry with the Tephrabase database (Newton *et al*., 2007) and published literature.

8.2.2 Calculating reoccurrence rates

The new northern European cryptotephra database includes new tephra layers from geological records and observations. Data on Icelandic eruptions, VEI and geochemistry were drawn from the Smithsonian Holocene Volcano Database (Global Volcanism Program, 2013). Eruptions were grouped according to geochemistry into mafic and silicic eruptions (silicic > 63% SiO_2). Return intervals were calculated using the methods described by Connor *et al*. (2006). The empirical survivor function (in uncensored data as here = Kaplan-Meier estimate (Dzierma and Wehrmann, 2012)) was calculated using the repose intervals (taken as the time between the onset of two successive eruptions). In cases where the start time for an eruption had not been historically recorded, start time was assumed to be the mid-age. In this instance the survivor function S(t) gives the probability that T (repose interval) exceeds a given time interval (t) (Cox and Oakes, 1984):

$$S_T(t) = P[T > t]$$

The Kaplan-Meier survival function for each repose interval was calculated as below (where *ti* is a given repose interval from 1…N and N is the total number of events):

$$S(t_i) = \frac{N-i}{N} \quad i = 1, \ldots., N.$$

In order to forecast survival with precision, a parametric model of survival function was fit to the empirical survival time data. We applied the Kolmogorov-Smirnov (KS) goodness-of-fit test to aid in the selection of the parametric model of best fit. Examples of commonly used parametric models of survival function for natural hazard modelling include the Exponential (Swindles *et al*., 2011); Weibull (Dzierma and Wehrmann, 2012) and Log Logistic distributions (Connor *et al*., 2006). We fitted each of the above parametric models to our dataset using maximum likelihood (using package Flexsurv in

R version 3.1.0). For each dataset, the model which offered the best fit to the Kaplan-Meier estimate was used to forecast the return interval of events.

To examine the reoccurrence rate of both Icelandic eruptions and ash clouds over the last 7000 years, during which time the frequency of volcanic eruptions has not been stationary we apply the Volcanic Event Reoccurence Rate Model (VERRM) (Wilson, 2016). Unlike the methods outlined above (e.g. Poisson distributions), VERRM can estimate the uncertainty in the reoccurrence rate over time.

8.3 Results

8.3.1 The new distal tephra record

We identified evidence for volcanic ash fallout, in the form of at least one cryptotephra layer, at every new site studied, suggesting that spatial gaps in cryptotephra records are an artefact of research intensity and do not represent the margins of volcanic ash distribution in northern Europe (Figure 1). Additional cryptotephra layers and observed eruptions added to the database from this study and other research are listed in Supplementary file 1, and geochemical plots indicating assignments are provided in Supplementary file 2.

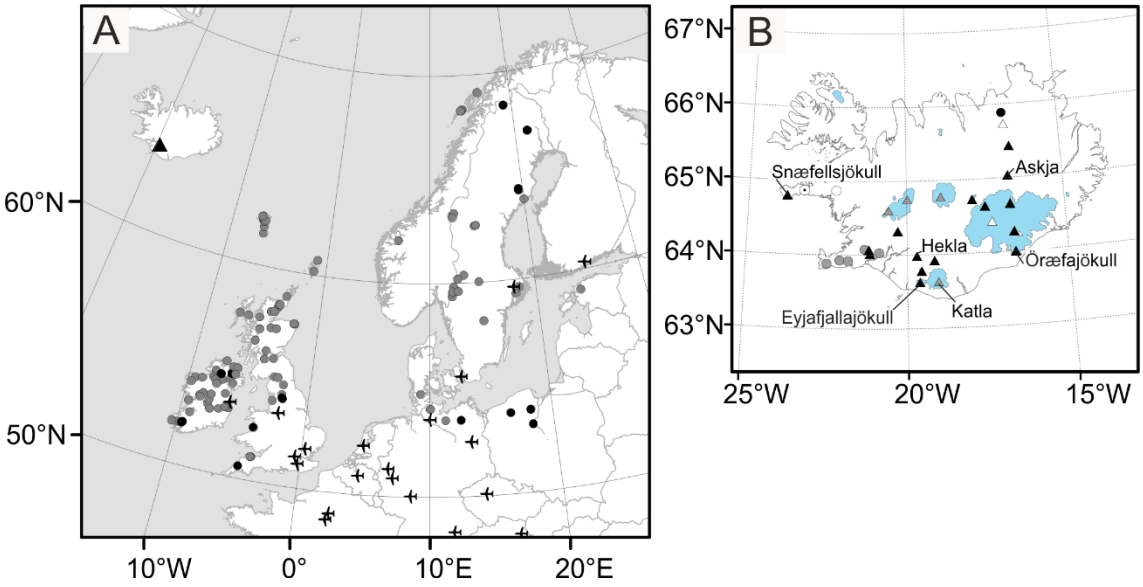

Figure 1. A) map indicating the location of sites in northern Europe where cryptotephra layers have been identified, grey circles indicate sites included in the original database compiled by Swindles *et al.* (2011), black circles indicate new sites added to the database, from this and other studies, see Supplementary Table 1 for references. Aeroplane symbols indicate the locations of airports which are included in a list of the thirty busiest European airports (2006), data from the Eurostat geographic databases GISCO (Eurostat, 2006). B) Map of Iceland indicating Holocene volcanoes and the location of large ice sheets (blue shading). Data on Holocene volcanoes from the Smithsonian Database (Global Volcanism Program, 2013). Volcanoes are indicated as follows: white triangle = caldera, white circle = fissure vent, white circle with point = pyroclastic cone, black circle = shield volcano, black triangle = stratovolcano, grey triangle = sub-glacial, grey circle = crater.

Cryptotephra layers identified at sites in northern Sweden, Poland, southern England and Wales have extended the known spatial distribution patterns of widely dispersed cryptotephra layers such as Hekla 4 and Hekla 1104 and less well established isochrons such as Hekla 1158 (previously identified at only one distal site (Pilcher *et al.*, 2005)). Updated spatial maps of cryptotephra distributions in northern Europe are provided in Supplementary file 3.

Six new cryptotephras, previously not identified in northern Europe, have been added to the database. Two new basaltic cryptotephra layers have been identified in Ireland (Reilly and Mitchell, 2015; Watson, 2016 in Press) and one in Germany (Wulf *et al.*, 2016). Glass tephra shards from all of these basaltic tephra layers show geochemical

similarity to glass from eruptions of the Grímsvötn volcano which is a subglacial volcano and is prone to phreatomagmatic eruptions, such as those during its most recent eruption in 2011. Historically (AD 1200-2004) Grímsvötn has been the most active volcano on Iceland (Thordarson and Hoskuldsson, 2008). The recent identification of more basaltic cryptotephra layers may reflect an increased focus on the analysis of sparse tephra layers (Lake Tiefer See, Unknown Grímsvötn tephra, contained just two shards (Wulf *et al*., 2016)), which has, in part been facilitated by new techniques for the mounting and EPMA analysis of fewer and smaller shards (Hall and Hayward, 2014; Hayward, 2012).

8.3.2 Repose time distribution fits

On the basis of KS tests, log likelihood and Akaike Information Criterion (Akaike, 1998) we conclude that the majority of proximal Icelandic and distal European eruption frequency data over the last 1000 years are best described by Exponential and Weibull distributions (Table 1, Figure 2, Supplementary file 4). The Exponential model describes a simple stochastic point process (Poisson process), suggesting that the rate of eruptions is constant over time. The Weibull model also describes a model of simple failure, but allows for an increase or decrease in hazard over time. In datasets for which the Weibull model was the best fit, the data indicated an increasing hazard rate, perhaps indicating increased volcanic activity in recent times. Future eruption probabilities were calculated using the model of best fit for each dataset (Table 1).

Dataset	Model	Average Repose	% chance of event in any 10 year period	*n* of repose intervals	Range of repose intervals (years)
All Icelandic eruptions	Exponential	4.53	89	213	0-46
European ash clouds	Exponential	43.96	20	23	0-111
All Icelandic Eruptions VEI ≥4	Weibull	25.91	21	35	0-63
Silicic Icelandic Eruptions VEI ≥4	Weibull	90.63	<1	10	54-148
Silicic Icelandic Eruptions VEI ≥3	Weibull	50.33	8	18	9-121

Table 1. Table indicating the model used to predict reoccurrence, average repose interval and % chance of an event in any 10 year period.

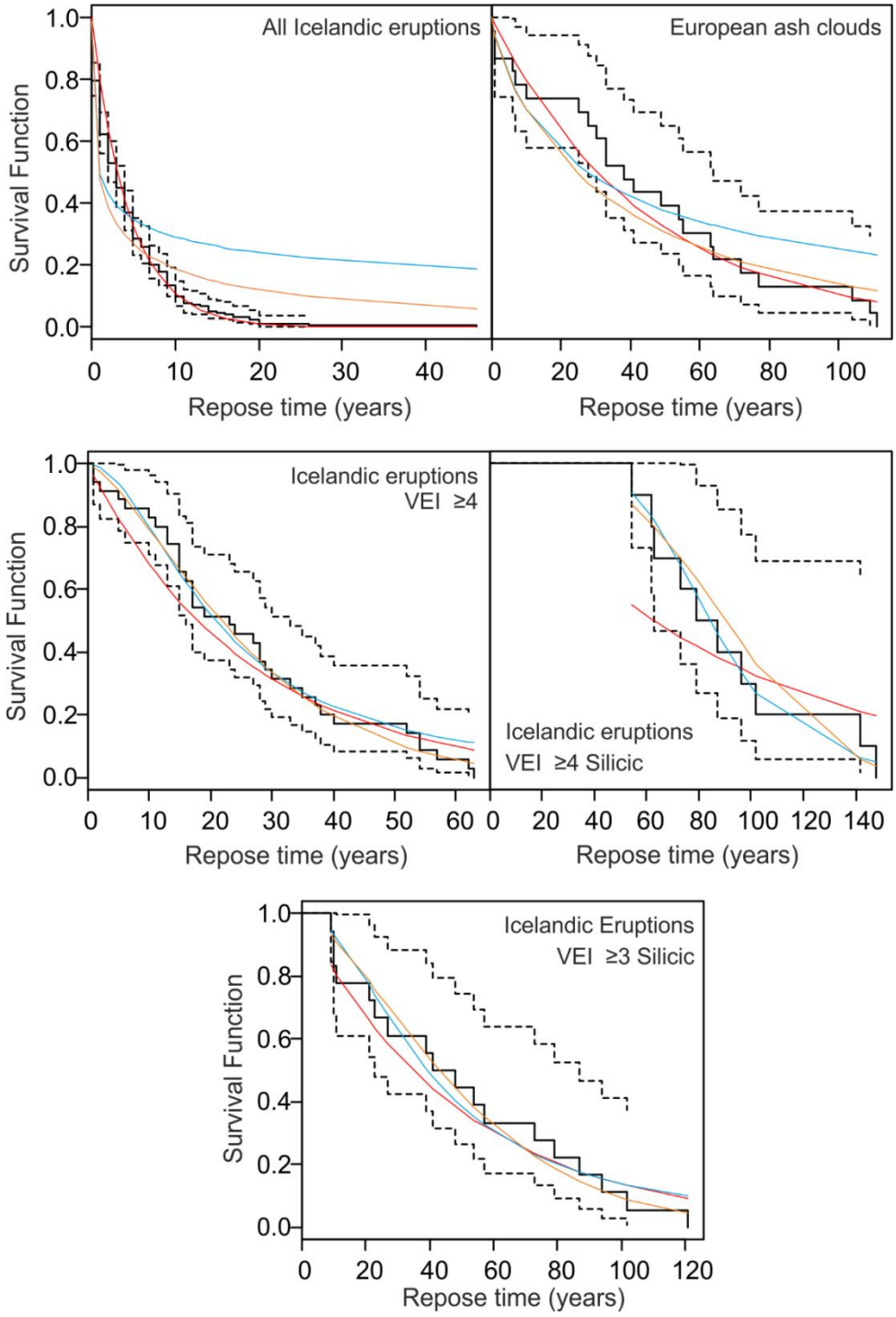

Figure 2. Kaplan-Meier estimate of the survivor function (last 1000 years) with fits for the Exponential (red), Log logistic (blue) and Weibull (orange) distribution functions. Broken lines indicate 95% confidence interval on the Kaplan-Meier estimate.

8.4 Discussion

The recurrence rate of both Icelandic volcanism and European ash clouds has varied over the last 7000 years (Figure 3). Variation in the frequency of Icelandic volcanism over time can be explained by periodic changes in rifting activity in Iceland and the influence of surface loading (glacier extent) on rates of volcanism (Larsen *et al*., 1998; Schmidt *et al*., 2013). The recurrence rate of European ash clouds and all Icelandic eruptions shows a general increase in the last 1500 years. This is due to the preferential preservation of more recent deposits over older deposits in the geological record, and the increased recording of observed historical events.

The recurrence rate of northern European ash clouds is lower than that of Icelandic eruptions as recorded by tephra layers and historical records. A peak in European ash records is evident ~1000 BP, corresponding to a small increase in Icelandic eruption frequency around this time. However, the median recurrence rate for ash fallout does not exceed 0.11 eruptions year^{-1} (1150 BP), much lower than the recurrence rate for Icelandic eruptions (proximal record) which peaks at 2.2 (659 BP). Not every Icelandic eruption will result in an ash cloud over northern Europe. This is partly a reflection of the nature of Icelandic volcanism which is dominated by mafic magma compositions (91% of post-glacial eruptions) associated primarily with effusive eruptions which produce little or no fine ash, although phreatomagmatic mafic eruptions can produce large quantities of fine ash (Thordarson and Hoskuldsson, 2008). In addition to being sensitive to changes in the rate of Icelandic volcanism, the frequency of distal ash clouds reaching northern Europe is affected by wind direction, wind speed and rainfall, all of which affect the probability and trajectory of long range ash transport (Davies *et al*., 2010).

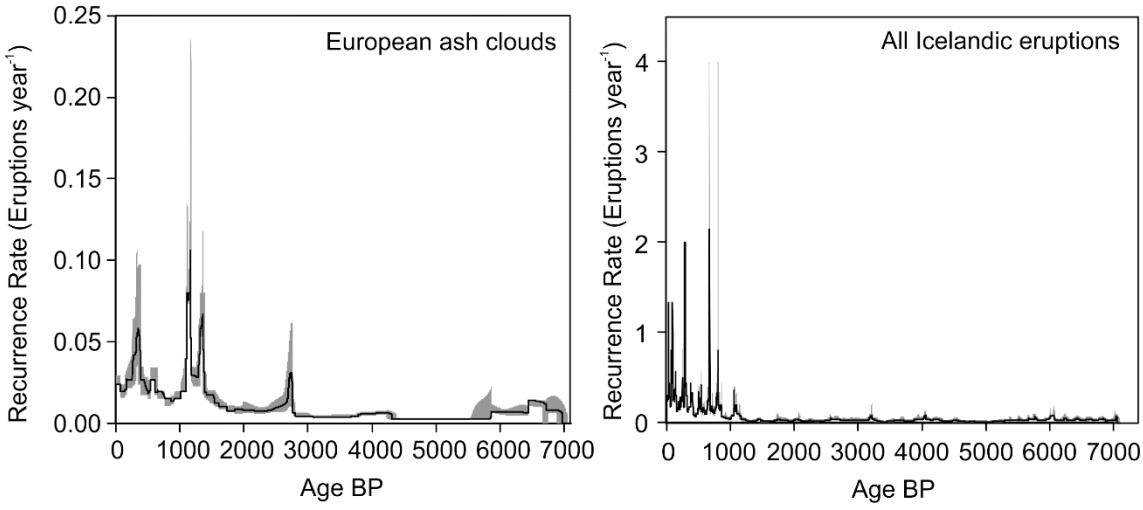

Figure 3. The Recurrence Rate of European ash clouds and all Icelandic eruptions for the last 7000 years. Black line indicates the median recurrence rate calculated using a moving average recurrence rate window size 4 (n = 2). Grey shading indicates 90% confidence interval. Output from the Volcanic Event Recurrence Rate Model (VERRM) (Wilson, 2016 personal comm.).

Figure 4 indicates the volcanic source for ash as recorded in northern Europe over the last 7000 years. A total of 84 ash clouds have been either observed over northern Europe or identified as cryptotephra layers in the last 7000 years. The majority of the ash clouds for which a source volcano or region has been identified (n = 46) have an origin in the Eastern Volcanic Zone of Iceland (n = 35), which is also the source region for the majority of proximal Icelandic tephra deposits (Larsen *et al.*, 1999). The Hekla volcano has been the most prolific volcano for the production of ash fallout over northern Europe during the Holocene (cryptotephra layers and observations, n = 9 and n = 6 respectively). Over half of the cryptotephra layers identified in northern Europe have not been assigned to a source volcano (n = 38), but contain glass shards with a major element geochemistry consistent with an Icelandic origin. A minority of cryptotephra layers (n = 6) contain glass shards which do not have a geochemical composition affinity toward glasses produced by Icelandic volcanoes and have been linked to eruptions of volcanoes further from northern Europe, in: Jan Mayen (71.0°N, 8.5°W, n = 4) (Chambers *et al.*, 2004), Alaska (61.4°N, 141.7°W, n = 1) (Jensen *et al.*, 2014) and perhaps even the Azores (39.0°N, 28.0°W, n = 1) (Reilly and Mitchell, 2015). Although cryptotephra layers demonstrate that ash from distant eruptive centres

such as Alaska can reach northern Europe, based on past records, the greatest future risk of ash clouds is posed by eruptions of Icelandic volcanoes. In particular by eruptions of the volcanoes in the Eastern Volcanic Zone, the source region for >80% of Icelandic eruptions during the Holocene (Thordarson and Hoskuldsson, 2008).

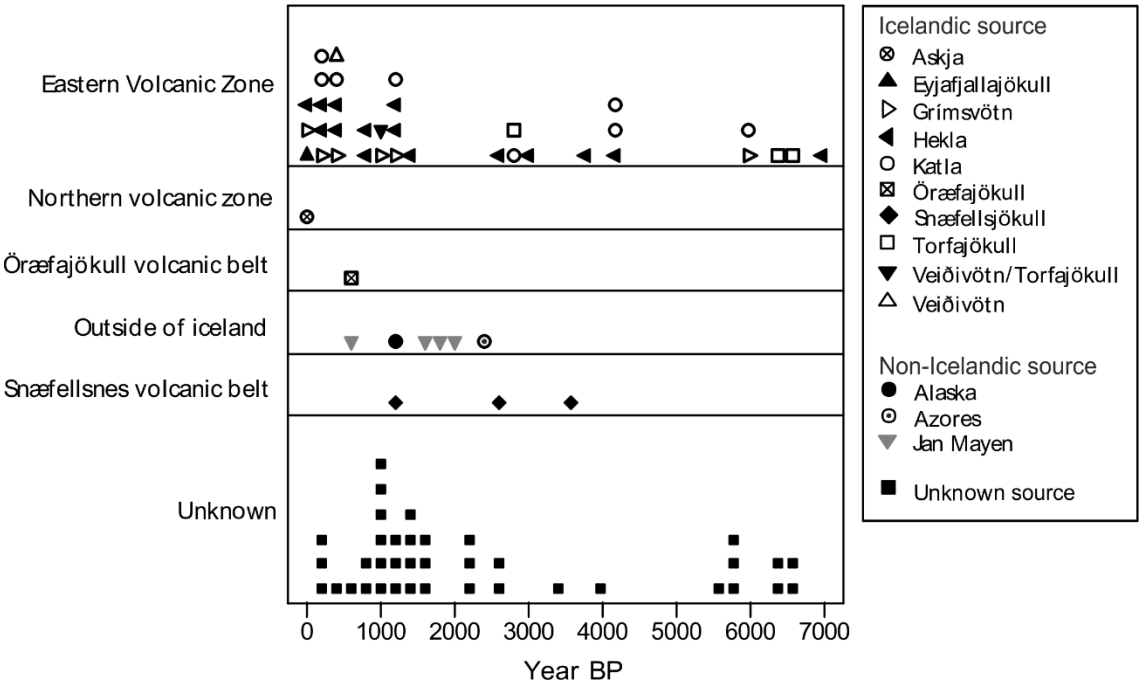

Figure 4. Diagram illustrating the frequency, source region and source volcano of cryptotephra layers identified in northern Europe over the last 7000 years based on the database of Swindles *et al.* (2011) which has been updated to include tephras mentioned in Supplementary file 1. The majority of ash clouds are from volcanoes in the Eastern Volcanic zone of Iceland. A small number of tephra layers have been linked to source regions in Jan Mayen (Chambers *et al.*, 2004), Alaska (Jensen *et al.*, 2014) and tentatively to volcanoes in the Azores (Reilly and Mitchell, 2015).

Given the changes in the frequency of Icelandic volcanism over the last 7000 years, we focus the majority of our analysis on the last 1000 years, the period for which the most complete records of volcanic activity and ash clouds exist and for which the frequency of volcanism and ash clouds are most stationary (Supplementary file 5). All but one of the northern European ash clouds in the last 1000 years can be linked to a source in Iceland, or have a major element glass geochemistry in line with the known major element glass geochemistry of the products of Icelandic volcanoes (n = 22). The exception is the MOR-T2 (=PMG-5 (Hall and Mauquoy, 2005)) tephra identified at

three sites in Ireland and attributed, based on glass geochemistry, to an eruption on Jan Mayen (Chambers *et al*., 2004).

The average repose interval for Icelandic eruptions over the past 1000 years is 4.5 years (Table 1). However, not all Icelandic eruptions result in ash fallout which reaches northern Europe. The magnitude of volcanic eruptions is commonly described according to a rating on the Volcanic Explosivity Index (VEI), a logarithmic scale with a higher rating indicating a more explosive eruption (Newhall and Self, 1982). We aim to identify the minimum VEI of an eruption which has resulted in an ash cloud over northern Europe in the last 1000 years. We identify ten cryptotephra layers and ten observed tephra fall-out events with known source eruptions (some eruptions e.g. Askja 1875 were both observed and identified in the geological record). All of the observed and cryptotephra layers which can be linked to Icelandic eruptions with a known VEI over the last 1000 years have been from eruptions with a VEI ≥ 4 (Figure 5). This corresponds to a Plinian eruption style, with an estimated plume height ≥ 10 km, 'definite' stratospheric injection, and a volume of ejected tephra ≥ 0.1 km^3 (Newhall and Self, 1982). The average repose interval for Icelandic eruptions with a VEI ≥ 4 is 26 $\pm$ 3 years (standard error of the mean, range of repose intervals = 0-63 years) (Table 1, Supplementary File 6). The data best fit a Weibull model, suggesting that the probability of an eruption occurring increases exponentially as the time since the last eruption increases (Connor *et al*., 2003). Applying this model, in any 10 year period we calculate a 23% chance of an eruption VEI ≥ 4 occurring in Iceland.

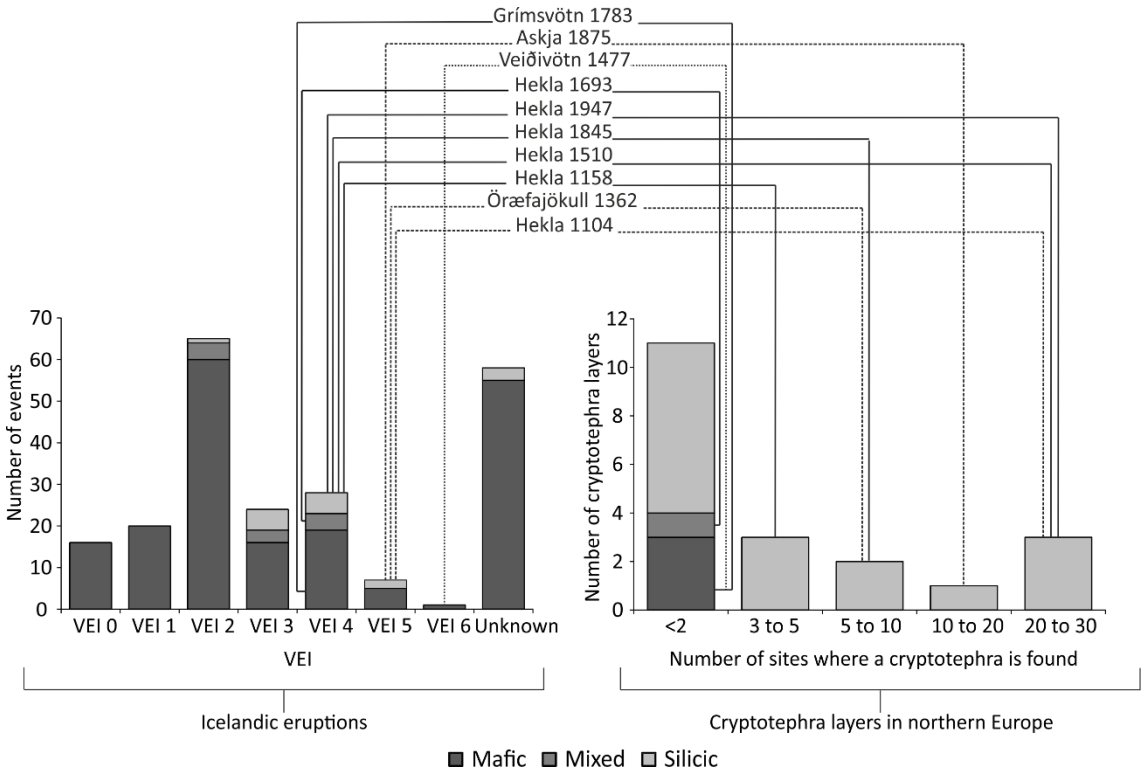

Figure 5. Diagram showing data on Icelandic eruptions and European ash (cryptotephra layers) for the last 1000 years (Global Volcanism Program, 2013) and the European cryptotephra database of Swindles *et al*. (2011) updated as of March 2016. All eruptions and cryptotephra layers are grouped by geochemistry. Icelandic eruption data is grouped by VEI. European cryptotephra records are grouped by the number of sites at which they are found. Cryptotephras which have been linked to a source eruption have been indicated and the connections based on geochemistry, VEI and number of sites where a tephra is identified are highlighted. Pattern of connecting lines reflects VEI of the eruption. Note Y axes are different scales.

The new model for northern European ash clouds indicates an average repose interval of 43.9 years with a standard error of the mean of 7.2 years (range of repose intervals = 0-111 years) (Table 1, Supplementary file 6). Applying an exponential model to ash cloud data results in a 20% chance of an ash cloud in any 10 year period. There have been a total of 36 eruptions with a VEI $\geq$ 4 recorded in Iceland during the last 1000 years, of which 26 have not produced cryptotephra layers which have been identified in the geological record and 21 have been neither observed nor identified in the geological

record. From this we conclude that only ~ 42% of Icelandic eruptions with a VEI ≥ 4 resulted in the transport of ash over northern Europe in the last 1000 years.

The majority (n = 18) of the VEI ≥ 4 eruptions which have not been identified in northern European records have been eruptions of mafic magma (SiO_2 < 63 wt %). Despite the dominance of mafic volcanism on Iceland, the majority of cryptotephras are silicic. The dominance of silicic tephras in distal records in northern Europe has been well documented and possible reasons for the relative lack of mafic cryptotephra layers when compared to silicic cryptotephra layers in northern Europe are still debated (Davies *et al*., 2010; Lawson *et al*., 2012; Wastegård and Davies, 2009). Our analysis suggests that even explosive (VEI ≥ 4) mafic eruptions that are favourable to having developed high plume heights are actually rare in European records. There is no relationship between the eruption VEI and the total number of sites at which a cryptotephra is found in northern Europe (p = 0.965). The eruption with the highest VEI rating in the last 1000 years is the Veiðivötn 1477 eruption which has a VEI = 6, indicating an 'ultra Plinian' type (Newhall and Self, 1982). However, cryptotephra from the basaltic Veiðivötn 1477 eruption has been identified at only two sites in northern Europe, in Ireland (Chambers *et al*., 2004) and in central Sweden (Davies *et al*., 2007). Conversely, silicic cryptotephra from the less explosive Hekla 1104 eruption (VEI = 5) has been recorded at 27 sites. The mafic composition of the Veiðivötn 1477 eruption might explain its identification at only two sites when compared to tephras of less explosive silicic compositions. Tephra shards of mafic composition are generally less vesicular and more dense than tephras of silicic composition, therefore basaltic tephra shards may be transported over shorter distances. However, differences in distribution by wind and spatial sampling bias cannot be discounted as reasons for the small number of distal tephra records identified.

Icelandic eruptions with a silicic geochemistry and a VEI ≥ 4 occur less frequently than all Icelandic eruptions of a mafic geochemistry. However, given an Icelandic eruption VEI ≥ 4 of silicic composition there is a 73% chance that ash will be deposited over northern Europe. In the last 1000 years only three Icelandic eruptions of silicic

composition have not been identified as cryptotephra layers in northern Europe, the eruptions of Hekla in 1766, 1597 and 1300.

There are many reasons for the apparent absence of these events in the European geological record. For instance, the wind direction may have transported volcanic ash away from northern Europe, or toward a part of northern Europe which has not been sampled for cryptotephra layers. Larsen *et al*. (1999) present maps of the main axis of distribution of tephra from historical age silicic eruptions, based on isopach mapping of tephra layers on Iceland. During the eruptions of Hekla 1300 and 1766 the main axis of transport was toward the Northern Iceland, i.e. ash from these eruptions may have been carried away from northern Europe. However, predicting the transport direction of distal ash based on isopach maps can be misleading due to differences in wind direction with height. Wind shear can result in tephra from higher in the plume being transported in a different direction to tephra released lower in the plume. Tephra released higher in the plume is more likely to be transported over long distances and therefore proximal isopachs and distal cryptotephra deposition may appear contradictory.

Another important consideration is erupted volume. There is a significant difference in the median erupted volumes of historical silicic eruptions of Icelandic volcanoes (Larsen *et al*., 1999) which have, and have not reached sites in northern Europe (Mann Whitney test, $p = 0.039$). Median erupted volume values for eruptions which have and have not been identified in northern Europe are 0.33 km^3 and 0.18 km^3 respectively (Figure 6). The eruption of Hekla 1104 had a larger erupted volume (~2.0 km^3) when compared to the events of Hekla 1300 and 1766 (0.5 and 0.4 km^3 respectively). The identification of cryptotephra from the Hekla 1104 eruption in Ireland suggests that, contrary to Icelandic tephra records which suggest a dominant transport direction to the north, southerly transport of ash occurred. The transport of ash toward the south was perhaps favoured by the large volume of tephra erupted increasing the chances of a small amount of tephra being transported toward northern Europe. Conversely, eruptions with low tephra volumes, but favourable wind conditions can also be identified in northern Europe. For example, cryptotephra from the eruption of Hekla in 1947 which had relatively small erupted volume (0.18 km^3), but during which the

dominant transport direction was toward the south, has been identified at 22 sites in northern Europe, albeit in a constrained spatial region (Dugmore *et al*., 1996; Lawson *et al*., 2012).

Indeed, where available, Icelandic isopach maps of the majority of tephra layers identified in northern European records over the last 1000 years suggest a dominant wind direction toward the south or east rather than the north or west (n = 5 and 3 respectively). We suggest that wind direction, combined with a low erupted volume < 1 km^3 (Hekla 1300 = 0.50 km^3, Hekla 1766 = 0.40 km^3: (Larsen *et al*., 1999)) may explain the apparent absence of cryptotephra from the silicic eruptions of Hekla in 1300 and 1766 in northern Europe.

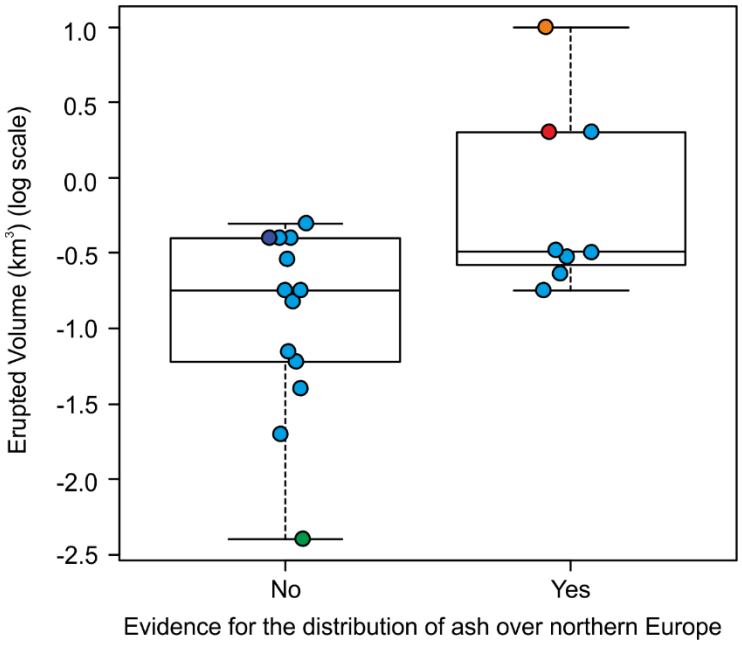

Figure 6. Boxplots (with overlain jitter plot) showing the total erupted volumes (km^3) for the historic silicic eruptions of Icelandic volcanoes (Hekla (light blue), Askja (red), Öræfajökull (orange), Eyjafjallajökull (green) and Torfajökull (dark blue)) n = 21, volume data compiled by Larsen *et al*. (1999). Data are grouped into eruptions which resulted in evidence for the distribution of ash over northern Europe, and those for which there is no evidence of ash distribution over northern Europe. Boxplot convention is as follows: boxes indicate the interquartile range; the central line through each box indicates the median. The far extent of the upper and lower lines from each quartile indicate the maximum and minimum.

However, neither wind direction nor eruptive volume can easily explain the lack of 1597 tephra in northern European records as isopach maps suggest the dominant axis of distribution was South east, toward northern Europe, and the erupted volume (0.3 km^3) exceeded that of the Hekla 1947 eruption, which has been identified in Europe. Despite the (geologically) short interval between the eruptions of Hekla 1510 and 1597 eruption, which resulted in the deposition of tephra at multiple sites in Ireland, it is unlikely that the Hekla 1597 tephra has been miss-correlated to the eruption of Hekla 1510, as the geochemistry of Hekla 1597 is distinct (Dugmore and Newton, 2012). Therefore, it remains unclear why the Hekla 1597 tephra has not been identified in any European sites.

Given that the majority of Icelandic eruptions with a VEI ≥ 4 and a silicic composition have resulted in deposition of ash over northern Europe, we calculated the probability of an eruption satisfying these criteria. According to available data, the average repose interval of a VEI ≥ 4 Icelandic eruption with a silicic composition is 91 years; applying the Weibull model, this equates to <1% chance of this type of eruption in any 10 year interval. Given that the newly computed average return interval for ash clouds in northern Europe is 44 years, it stands to reason that silicic eruptions VEI ≥ 4 have not been the only source of ash clouds over northern Europe. However, from geological and observational records it would appear that the biggest risk of widespread ash clouds over northern Europe is posed by eruptions with a VEI ≥ 4 and a silicic magma composition.

Alongside the distal European tephra layers which have been assigned to a specific Icelandic eruption there are nine cryptotephra layers which contain glass shards with a geochemistry consistent with an Icelandic origin but which have not been assigned to an eruption and therefore could not be traced to an eruptive source and VEI rating (Figure 7). All of these unassigned tephra layers have been identified at fewer than four sites; five have been identified at only one site. By comparison, the majority (seven out of ten) of the tephras which have been assigned to an eruption have been identified at four or more sites. Furthermore, many of the unassigned tephra layers have been identified only in one region; for example the Loch Portain B tephra has not been identified

outside of Scotland and the Outer Hebrides (Dugmore *et al*., 1995), and the MOR-T4 tephra, although identified at four sites, appears to have a fallout region confined to Ireland and Wales (Chambers *et al*., 2004; Watson *et al*., 2016). The limited spatial distribution of many of these unassigned tephra layers, and the lack of assignment to a major eruptive event, might suggest they were deposited during smaller eruptions producing distal ash over a smaller area during short explosive phases. The proximal geochemistry for smaller magnitude, less explosive eruptions may not have been so well characterised, making correlations between European and Icelandic tephra layers more difficult. The geochemistry of eruptives from some rhyolite Icelandic volcanoes, such as Torfajøkull and Snaefellsnes, has not been well characterised and therefore there is lack of proximal Icelandic data for comparison with the geochemistry of European cryptotephra layers (Haflidason *et al*., 2000). Cryptotephra layers in northern Europe may even represent a record of Icelandic volcanism which has been eroded from the Icelandic record by subsequent eruptions. It is possible that some eruptions with a VEI = 3 did produce ash over Europe, with only limited spatial distribution. The average recurrence rate of VEI ≥ 3 eruptions of silicic composition is 50 years, which equates to a chance of 8% of an eruption of this type in a 10 year period (Table 1).

Although stochastic estimates of reoccurence can provide a basis for estimating future hazard posed by volcanoes and volanic ash clouds they must be interpreted with caution. According to the exponential model applied to records of past northern European ash clouds the probability of two ash clouds over northern Europe in a 10 year period is <1%. However, the eruption of Eyjafjallajökull in 2010, was followed the next year, by the eruption of Grímsvötn, both eruptions produced ash clouds over northern Europe, highlighting the fact that statistical models of reoccurrence based on past records must be interpreted with caution.

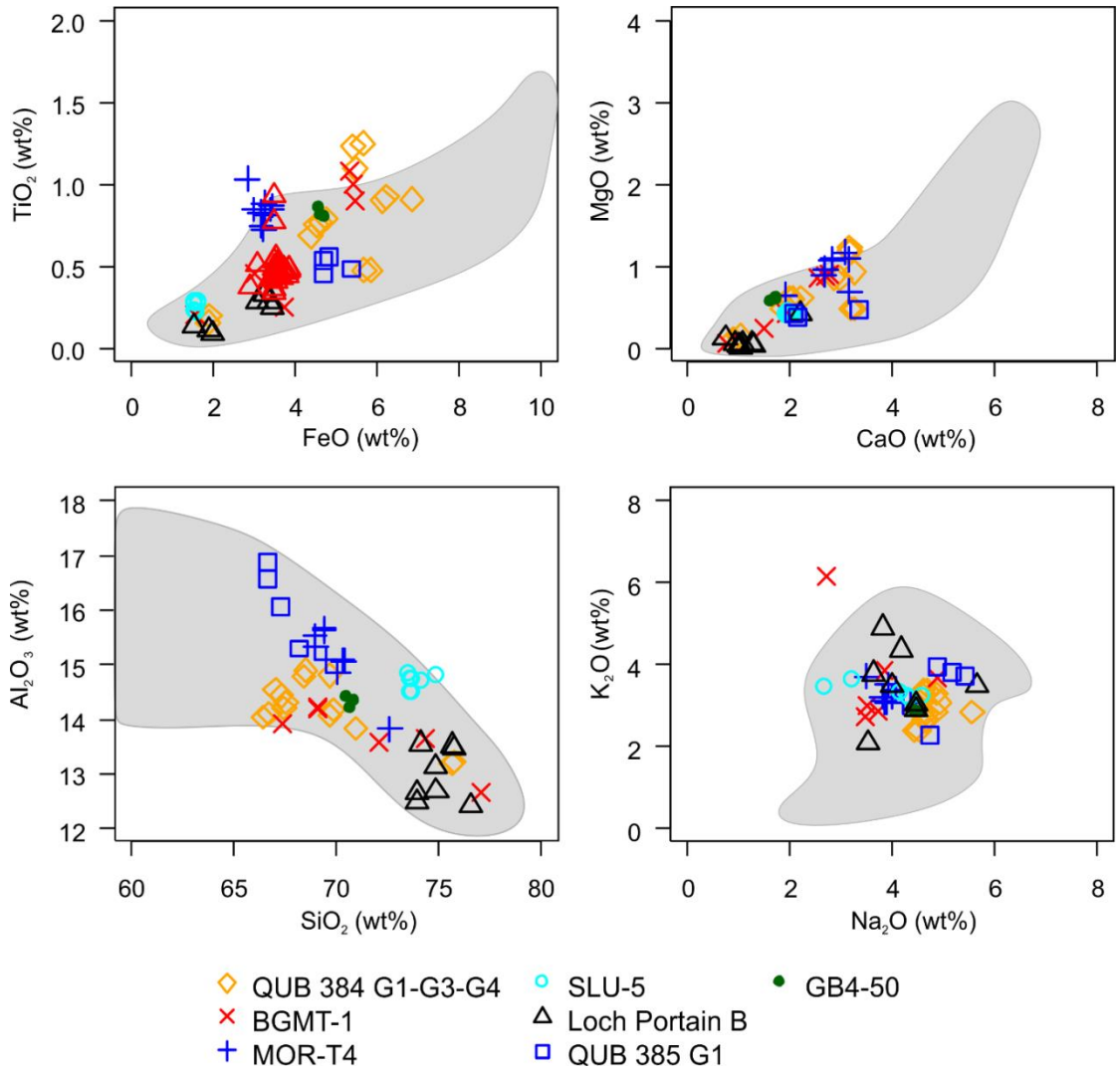

Figure 7. Tephras not linked to a source volcano, but which have a major element glass geochemistry consistent with possible Icelandic origin (grey shaded region). Icelandic geochemical envelope based on tephra data from Tephrabase (Newton *et al*., 2007). The QUB 384 tephra contains glass shards in three distinct geochemical groups (G1, G3 and G4). Tephra data from Chambers *et al*. (2004); Dugmore *et al*. (1995); Hall and Pilcher (2002); Langdon and Barber (2001); Pilcher *et al*. (2005).

8.5 Conclusions

In this paper we have examined spatial gaps identified in cryptotephra records across northern Europe. The discovery of Icelandic cryptotephras in these regions and others with few cryptotephra studies (e.g. Germany), by this study and other recent work (Wulf *et al*., 2016) suggests that spatial gaps in northern European cryptotephra layers

are an artefact of research intensity and do not represent the margins of ash clouds over northern Europe. However, sparse numbers of shards indicate that glass shards from some eruptions are approaching the margins of their detectable range. Future research focused on identifying new cryptotephras in northern Europe should focus on regions which appear to represent gaps in current records.

We have utilised new data, alongside newly published data, to recalculate an up to date version of the return interval for European ash cloud events. Our new estimate decreases the return interval from 56 ± 9 years to 44 ± 7 years, suggesting that ash clouds are indeed more common over northern Europe than previously proposed (Swindles *et al*., 2011). Applying an exponential model, our new database suggests a 20% chance of an ash cloud over northern Europe in a 10 year period. Our model still represents a minimum estimate for the reoccurrence rate of European ash clouds, but increased spatial coverage of sites within Europe means the new estimate is less likely to be confounded by sampling bias than previous modelling efforts.

We conduct a comprehensive examination of the erupted volumes, VEI rating and the dominant tephra transport pathways of Icelandic volcanoes which have resulted in distal ash deposition in northern Europe over the last 1000 years. All cryptotephras and observed tephras which can be linked to a source eruption in Iceland are from eruptions with a VEI ≥ 4, corresponding to Plinian eruptions. A ‘maximum’ estimate for the frequency of recurrence of ash clouds over northern Europe is provided by the average return interval of VEI ≥ 4 events (26 years). However, not all VEI ≥ 4 eruptions result in distal ash deposition and mafic compositions are under-represented in the distal record. 73% of Icelandic eruptions VEI ≥ 4 of silicic composition have deposited ash over northern Europe. The average return interval for eruptions of this type is 91 years. It is possible that some events with a VEI = 3 produced ash fall over Europe, with only limited spatial distribution, perhaps corresponding to tephra layers identified in northern Europe at few sites which are of an “unknown source”, but which contain glass shards which fit well the geochemical envelope for Icelandic volcanoes.

References

Akaike, H., 1998. Information theory and an extension of the maximum likelihood principle, Selected Papers of Hirotugu Akaike. Springer, pp. 199-213.

Blockley, S.P.E., Pyne-O'Donnell, S.D.F., Lowe, J.J., Matthews, I.P., Stone, A., Pollard, A.M., Turney, C.S.M., Molyneux, E.G., 2005. A new and less destructive laboratory procedure for the physical separation of distal glass tephra shards from sediments. Quaternary Science Reviews 24, 1952-1960.

Casadevall, T.J., 1994. Volcanic ash and aviation safety: proceedings of the first international symposium, Seattle, Washington, July 1991. US Geological Survey Bulletin 2047.

Chambers, F.M., Daniell, J.R.G., Hunt, J.B., Molloy, K., O'Connell, M., 2004. Tephrostratigraphy of An Loch Mor, Inis Oirr, western Ireland: implications for Holocene tephrochronology in the northeastern Atlantic region. Holocene 14, 703-720.

Connor, C., Bebbington, M., Marzocchi, W., 2015. Chapter 51 - Probabilistic Volcanic Hazard Assessment, in: Sigurdsson, H. (Ed.), The Encyclopedia of Volcanoes (Second Edition). Academic Press, Amsterdam, pp. 897-910.

Connor, C.B., McBirney, A.R., Furlan, C., 2006. What is the probability of explosive eruption at a long-dormant volcano?, in: Mader, H.M., Coles, S.G., Connor, C.B., Connor, L.J. (Eds.), Statistics in Volcanology The Geological Society London, pp. 39-46.

Connor, C.B., Sparks, R., Mason, R., Bonadonna, C., Young, S., 2003. Exploring links between physical and probabilistic models of volcanic eruptions: The Soufriere Hills Volcano, Montserrat. Geophysical Research Letters 30, 1701.

Cox, D.R., Oakes, D., 1984. Analysis of Survival Data: Monographs on Statistics and Applied Probability Chapman and Hall London.

Davies, S.M., Elmquist, M., Bergman, J., Wohlfarth, B., Hammarlund, D., 2007. Cryptotephra sedimentation processes within two lacustrine sequences from west central Sweden. Holocene 17, 319-330.

Davies, S.M., Larsen, G., Wastegård, S., Turney, C.S.M., Hall, V.A., Coyle, L., Thordarson, T., 2010. Widespread dispersal of Icelandic tephra: how does the Eyjafjöll eruption of 2010 compare to past Icelandic events? Journal of Quaternary Science 25, 605-611.

De Vleeschouwer, F., Chambers, F.M., Swindles, G.T., 2011. Coring and sub-sampling of peatlands for palaeoenvironmental research. Mires and Peat 7, 1-10.

Dugmore, A.J., Larsen, G., Newton, A.J., 1995. 7 Tephra isochrones in Scotland. Holocene 5, 257-266.

Dugmore, A.J., Newton, A.J., 1992. Thin tephra layers in peat revealed by X-Radiography. Journal of Archaeological Science 19, 163-170.

Dugmore, A.J., Newton, A.J., 2012. Isochrons and beyond: maximising the use of tephrochronology in geomorphology. Jökull 62, 39-52.

Dugmore, A.J., Newton, A.J., Edwards, K.J., Larsen, G., Blackford, J.J., Cook, G.T., 1996. Long-distance marker horizons from small-scale eruptions: British tephra deposits from the AD 1510 eruption of Hekla, Iceland. Journal of Quaternary Science 11, 511-516.

Dzierma, Y., Wehrmann, H., 2012. On the likelihood of future eruptions in the Chilean Southern Volcanic Zone: interpreting the past century's eruption record based on statistical analyses. Andean Geology 39, 380-393.

Eurostat, 2006. GISCO Airports 2006, http://ec.europa.eu/eurostat/web/gisco/geodata/reference-data/transport-networks.

Folch, A., Costa, A., Basart, S., 2012. Validation of the FALL3D ash dispersion model using observations of the 2010 Eyjafjallajokull volcanic ash clouds. Atmospheric Environment 48, 165-183.

Global Volcanism Program, 2013. Volcanoes of the World, v. 4.3.4. , in: Venzke, E. (Ed.), Smithsonian Institution.

Gudmundsson, M.T., Thordarson, T., Hoskuldsson, A., Larsen, G., Bjornsson, H., Prata, F.J., Oddsson, B., Magnusson, E., Hognadottir, T., Petersen, G.N., Hayward, C.L., Stevenson, J.A., Jonsdottir, I., 2012. Ash generation and distribution from the April-May 2010 eruption of Eyjafjallajokull, Iceland. Sci Rep 2.

Haflidason, H., Eiriksson, J., Van Kreveld, S., 2000. The tephrochronology of Iceland and the North Atlantic region during the Middle and Late Quaternary: a review. Journal of Quaternary Science 15, 3-22.

Hall, M., Hayward, C., 2014. Preparation of micro- and crypto-tephras for quantitative microbeam analysis. Geological Society, London, Special Publications 398, 21-28.

Hall, V.A., Mauquoy, D., 2005. Tephra-dated climate- and human-impact studies during the last 1500 years from a raised bog in central Ireland. Holocene 15, 1086-1093.

Hall, V.A., Pilcher, J.R., 2002. Late-Quaternary Icelandic tephras in Ireland and Great Britain: detection, characterization and usefulness. Holocene 12, 223-230.

Hayward, C., 2012. High spatial resolution electron probe microanalysis of tephras and melt inclusions without beam-induced chemical modification. Holocene 22, 119-125.

Jensen, B.J.L., Pyne-O'Donnell, S., Plunkett, G., Froese, D.G., Hughes, P.D.M., Sigl, M., McConnell, J.R., Amesbury, M.J., Blackwell, P.G., van den Bogaard, C., Buck, C.E., Charman, D.J., Clague, J.J., Hall, V.A., Koch, J., Mackay, H., Mallon, G., McColl, L., Pilcher, J.R., 2014. Transatlantic distribution of the Alaskan White River Ash. Geology 42, 875-878.

Jull, M., McKenzie, D., 1996. The effect of deglaciation on mantle melting beneath Iceland. Journal of Geophysical Research-Solid Earth 101, 21815-21828.

Langdon, P.G., Barber, K.E., 2001. New Holocene tephras and a proxy climate record from a blanket mire in northern Skye, Scotland. Journal of Quaternary Science 16, 753-759.

Larsen, G., Dugmore, A., Newton, A., 1999. Geochemistry of historical-age silicic tephras in Iceland. Holocene 9, 463-471.

Larsen, G., Gudmundsson, M.T., Björnsson, H., 1998. Eight centuries of periodic volcanism at the center of the Iceland hotspot revealed by glacier tephrostratigraphy. Geology 26, 943-946.

Lawson, I.T., Swindles, G.T., Plunkett, G., Greenberg, D., 2012. The spatial distribution of Holocene cryptotephras in north-west Europe since 7 ka: implications for understanding ash fall events from Icelandic eruptions. Quaternary Science Reviews 41, 57-66.

Lowe, D.J., 2011. Tephrochronology and its application: A review. Quaternary Geochronology 6, 107-153.

Mohn, H., 1878. Askeregnen den 29de-30-teMarts 1875. Forhandlinger I Videnskapsselskabet I Christiania aar 1877 10, 89–92.

Newhall, C.G., Self, S., 1982. The volcanic explosivity index/VEI/- An estimate of explosive magnitude for historical volcanism. Journal of Geophysical Research 87, 1231-1238.

Newton, A.J., Dugmore, A.J., Gittings, B.M., 2007. Tephrabase: tephrochronology and the development of a centralised European database. Journal of Quaternary Science 22, 737-743.

Pilcher, J., Bradley, R.S., Francus, P., Anderson, L., 2005. A Holocene tephra record from the Lofoten Islands, Arctic Norway. Boreas 34, 136-156.

Pistolesi, M., Cioni, R., Bonadonna, C., Elissondo, M., Baumann, V., Bertagnini, A., Chiari, L., Gonzales, R., Rosi, M., Francalanci, L., 2015. Complex dynamics of small-moderate volcanic events: the example of the 2011 rhyolitic Cordón Caulle eruption, Chile. Bulletin of Volcanology 77, 1-24.

Reilly, E., Mitchell, F.J., 2015. Establishing chronologies for woodland small hollow and mor humus deposits using tephrochronology and radiocarbon dating. The Holocene 25, 241-252.

Schmidt, P., Lund, B., Hieronymus, C., Maclennan, J., Árnadóttir, T., Pagli, C., 2013. Effects of present-day deglaciation in Iceland on mantle melt production rates. Journal of Geophysical Research: Solid Earth 118, 3366-3379.

Stevenson, J.A., Loughlin, S., Font, A., Fuller, G.W., MacLeod, A., Oliver, L.W., Jackson, B., Horwell, C.J., Thordarson, T., Dawson, I., 2013a. UK Monitoring and deposition of tephra from the May 2011 eruption of Grimsvotn, Iceland. Journal of Applied Volcanology 2.

Stevenson, J.A., Loughlin, S., Rae, C., Thordarson, T., Milodowski, A.E., Gilbert, J.S., Harangi, S., Lukacs, R., Hojgaard, B., Arting, U., Pyne-O'Donnell, S., MacLeod, A.,

Whitney, B., Cassidy, M., 2012. Distal deposition of tephra from the Eyjafjallajokull 2010 summit eruption. Journal of Geophysical Research-Solid Earth 117.

Stevenson, J.A., Loughlin, S.C., Font, A., Fuller, G.W., MacLeod, A., Oliver, I.W., Jackson, B., Horwell, C.J., Thordarson, T., Dawson, I., 2013b. UK monitoring and deposition of tephra from the May 2011 eruption of Grímsvötn, Iceland. Journal of Applied Volcanology 2, 1-17.

Swindles, G.T., Lawson, I.T., Savov, I.P., Connor, C.B., Plunkett, G., 2011. A 7000 yr perspective on volcanic ash clouds affecting northern Europe. Geology 39, 887-890.

Swindles, G.T., Savov, I.P., Connor, C.B., Carrivick, J., Watson, E.J., Lawson, I.T., 2013. Volcanic ash clouds affecting Northern Europe: the long view. Geology Today 29, 215-217.

Thorarinsson, S., 1954. The tephra-fall from Hekla on March 29th 1947, in: Einarsson T, Kjartansson G, S, T. (Eds.), The eruption of Hekla 1947–48. Societas Scientarum Islandica, Reykjavik, pp. 1–68.

Thordarson, T., Hoskuldsson, A., 2008. Postglacial volcanism in Iceland. Jokull 58, 197-228.

Wastegård, S., Davies, S.M., 2009. An overview of distal tephrochronology in northern Europe during the last 1000 years. Journal of Quaternary Science 24, 500-512.

Watson, E.J., Swindles, G.T., Lawson, I.T., Savov, I.P., 2016. Do peatlands or lakes provide the most comprehensive distal tephra records? Quaternary Science Reviews 139, 110-128.

Wilson, J. "Volcanic Event Recurrence Rate Model (VERRM): Incorporating Radiometric Ages, Volcanic Stratigraphy and Paleomagnetic Data into a Monte Carlo Simulation to Estimate Uncertainty in Recurrence Rate through Time." unpublished MS thesis. University of South Florida.

Wulf, S., Dräger, N., Ott, F., Serb, J., Appelt, O., Guðmundsdóttir, E., van den Bogaard, C., Słowiński, M., Błaszkiewicz, M., Brauer, A., 2016. Holocene tephrostratigraphy of varved sediment records from Lakes Tiefer See (NE Germany) and Czechowskie (N Poland). Quaternary Science Reviews 132, 1-14.

Chapter 9: Discussion and conclusion

In this chapter I aim to summarise and critically examine the results and discussions previously reported in Chapters 3 to 8. I outline the main findings of the research presented in this thesis with reference to the overall aim and objectives outlined in Chapter 1; explain the significance to the wider scientific community; and describe directions for future work. The aim of this thesis was: to evaluate the use of cryptotephra layers for providing information on the timing, characteristics and spatial extent of past volcanic ash clouds. In order to achieve this aim two research compartments were identified, these are briefly discussed in Section 9.1.

In addition to the objectives which fit into the two research compartments, two overarching objectives were outlined. These objectives focussed on conducting new field campaigns in order to fill spatial gaps in existing cryptotephra records through the development of new, high quality tephrostratigraphies (Thesis Objective 8 and Thesis Objective 9). These objectives have been achieved through the addition of new sites to the existing cryptotephra database compiled by Swindles *et al*. (2011). I examined tephra layers from 13 new sites and contributed toward filling spatial gaps in northern European tephra records in northern Sweden, Poland, Wales and Southern England. At least one tephra layer was identified at every site, suggesting that the spatial gaps in the distribution of northern European cryptotephra layers are an artefact of research intensity and do not represent the margins of Icelandic volcanic ash distribution over northern Europe. Future research with a focus on identifying new cryptotephra in northern Europe should concentrate on regions which appear to represent remaining large gaps in current the records.

My research has extended the known spatial distribution patterns of well-established cryptotephra layers such as Hekla 4 and Hekla 1104, which have each been identified at five additional sites. Furthermore, the identification of less well established cryptotephras, such as Hekla 1158 (previously identified at only one distal site (Pilcher *et al*., 2005)), at three new sites, indicates that these cryptotephra layers may form important regional isochrones. Two new northern European tephra layers have been

identified as part of this study: a basaltic tephra, CLA-L1 which, based on geochemistry and stratigraphy, is most likely derived from an eruption of the Iceland's Grímsvötn volcano after AD 1000 and SN-1, a cryptotephra from the Icelandic Snæfellsjökull volcano, which contains glass shards of a trachydacitic composition - identified for the first time in mainland Europe (Chapter 5). The age for SN-1 is further constrained to 1183-1147 cal yr BP based on new radiocarbon dates (Chapter 5). The SN-1 tephra, which is identified at three sites in northern Sweden, may provide an important regional isochron for dating palaeoclimatological research in the Arctic region. Finally, the discovery of the Hekla 1845 tephra in 14 cores from Fallahogy peatland, Northern Ireland (Chapter 3) indicates that even in regions which have previously been subject to intensive cryptotephra research at multiple sites, sparse tephra layers may remain undetected.

Beyond northern Europe, the identification of two tephra layers in Aucayacu peatland, Peru (Chapter 4) indicates that tephra shards can be successfully geochemically analysed by electron microprobe (EPMA), even after being exposed to the aggressive environment of a tropical peatland. The AUC-1 cryptotephra, tentatively attributed to a segment of the Andean volcanic arc chain in Ecuador, is the first cryptotephra to be identified inside the Amazon basin. These exciting results highlight the opportunities for extending tephrochronology into tropical regions elsewhere in the world. However, the sparse number of proximal as well as distal tephra samples which have been analysed by EPMA from volcanic systems in Peru and Ecuador present challenges as well as opportunities for future cryptotephra research in this region.

9.1 Research synthesis

9.1.1 Research compartment 1: The limits of tephrochronology

This research compartment focused on assessing the 'robustness' of tephrochronology, specifically cryptotephra layers in lakes and peatlands and how this might impact on their utility for understanding past volcanic ash distribution. This study critically

examines the influence of deposition, redistribution and reworking processes on tephra records in peatlands and lakes.

A multiple core study was conducted at Fallahogy bog, an ombrotrophic peatland in northern Ireland. Fifteen replicate cores were taken at distances of tens to hundreds of metres from each other across the peatland surface. Contrary to previous research, which has suggested that tephra layers can be discontinuous even within one peatland (Bergman *et al*., 2004), three tephra layers (Hekla 1947, Hekla 1845 and Hekla 1510) were identified in 14 out of 15 cores from Fallahogy peatland (Chapter 3, Thesis Objective 1). Where three district tephra layers were not identified ($n = 1$) there is evidence that the core location had been subject to anthropogenic disturbance. The replicability of the tephrostratigraphy in the top 50 cm of peat across Fallahogy peatland suggests that in mid-latitude peatlands the extraction of one core is sufficient to determine the presence or absence of a given tephra layer. However, differences were identified in tephra shard counts (per unit area) which vary by an order of magnitude between cores. Several cores are required to reliably estimate the median shard concentrations at a given site. The differences in total shard concentrations that were identified within different cores from the same peatland indicate that studies which infer differences in regional ash cloud fallout based on the concentration of shards in one core from a site may be misleading due to the choice of coring location within each site (cf. Rea *et al*., 2012).

A multiple core study of this type is unprecedented in tephrochronological research and the results will have a major impact on future palaeo-environmental studies involving tephra horizons. Variations in the total number of tephra shards and spheroidal carbonaceous particles (SCPs) in different cores from the same peatland provide evidence that particles, in this instance tephra and SCPs, but most likely also other proxies (e.g. pollen) move around on the peatland surface prior to incorporation into the peat profile. Unlike other paleo-environmental proxies, tephra shards are deposited during one event and provide an ideal natural ‘tracer’ with which to conduct research into the impact of microtopography on particle distribution on peatlands. In this project, for the first time, tephra layers are used successfully to provide a robust chronological

framework, within which to evaluate peat accumulation rates at an intra-site (fine/small) scale (Chapter 3).

Tephra deposited on to peatlands and into lakes is subject to different conditions for preservation and processes of reworking. This could result in a bias in European records, which are based predominantly on tephra layers identified in peatlands (Swindles *et al*., 2011). This thesis included the first study of the tephrostratigraphies recorded by peatland and lake sites in close proximity to one another (<10 km distant). Given the results reported in Chapter 3, which indicate that one core from a peatland is sufficient to identify all ash fallout events over that site, this study was based on one core from each peatland and one from each lake. The study, which includes four lake and peatland pairs, indicates that neither lakes nor peatlands provide complete records of volcanic ash deposition (Chapter 5, Thesis Objective 3). Generally more tephra layers were present in peatlands than in lakes, which is contrary to suggestions that lakes would be expected to contain more tephra layers due to the delivery of tephra from the wider catchment (Bertrand *et al*., 2014; Bramham-Law *et al*., 2013). One possible explanation for the absence of some tephra layers which are present in adjacent peatlands, from lake sediment records, is the impact of within-basin redistribution and the preferential deposition of tephra shards near to inlets which can act to concentrate tephra shards into certain areas of the lake basin (Pyne-O'Donnell, 2011). One limitation of this research is the retrieval of only one core from each lake which was necessary due to time constraints and financial restrictions on laboratory analysis and EPMA time. Future studies should examine multiple cores in a lake and compare the tephrostratigraphy to nearby peatland sites.

In addition to examining the number of tephra layers identified in peatland and lake sites in close proximity, this thesis evaluated the hypothesis that tephra layers containing glass shards of different geochemical compositions are preserved differently in lakes and peatlands (Chapter 5, Thesis Objective 3). Basaltic tephra layers are rare in the Holocene cryptotephra record of northern Europe and the majority have been identified in lakes rather than in peatlands, leading to speculations that acidic peatlands provide poor environments for the preservation of glass shards of basaltic composition

(Lawson *et al*., 2012). The results presented in this thesis show no evidence for the chemical alteration of tephra shards which were analysed by EPMA in either lakes or peatlands, over the timescale of this study (mid- to late- Holocene). Instead, the reason for the identification of more basaltic tephra layers in lakes, as opposed to peatlands, is most likely due the concentration of basaltic tephra shards from the catchment and within the lake basin itself. Sparse glass shard concentrations which fell onto the catchment, might be concentrated into the lake and brought above the level of detection in the lake sediments.

Only one basaltic cryptotephra layer (CLA-L1) is identified in this study. CLA-L1 was present in Claraghmore lake, whilst absent from the adjacent peatland. This prevented a comparison of the major element glass chemistry of basaltic tephra shards subject to storage in different environments (e.g. acidic peatlands and neutral lakes). For this reason, in Chapter 5 an examination of wider literature is used to supplement observations from this study. However, the identification of only one basaltic tephra layer is a major limitation of this research. Future work should focus on lakes where a basaltic tephra has already been identified and examine a nearby peatland site to confirm the presence/absence and geochemical deterioration (if any) of basaltic tephra shards subject to storage in different environments.

According to experimental observations the process of chemical attack on glass in acidic (low pH) environments is accelerated by elevated temperatures (Wolff-Boenisch *et al*., 2004). Until recently, the majority of cryptotephra research has been conducted in regions where temperatures are lower than in the tropics. However, to what extent might the deterioration of tephra glass shard chemistry confound efforts to utilise cryptotephras as records of past volcanic activity in regions where tephra has been subject to hostile preservation conditions (low pH, high temperatures). In Chapter 4 I report the tephrostratigraphy of a high acidity (pH ~4) and high temperature (average ~ 26ºC and daytime temperatures reaching 30ºC) peatland site in the Peruvian Amazon (Swindles *et al*., 2014) (Chapter 4, Thesis Objective 2). The sequence, which is only the top 1 m of a 7 m core, contains two cryptotephra layers, one of which contains sufficient shards for geochemical analysis. EPMA analysis of glass shards from the

AUC-1 cryptotephra layer suggest that fine ashes can be preserved in acidic tropical peatlands, with no indication of chemical alteration (visual or evidenced by SEM/EPMA analysis), for at least several hundreds of years. The AUC-1 tephra layer, which is tentatively linked to a series of rhyolite calderas in Ecuador, represents the first discovery of a historic microscopic tephra (cryptotephra) from Amazonia and presents an opportunity for further research into the tephrochronology of this region. Further examination of the Aucayacu core (7 m length, only top 1m examined) may identify the presence of additional cryptotephra layers.

In this research compartment I have critically examined the reworking, redistribution and preservation of cryptotephra layers in a variety of lake and peatland environments. The results suggest that the northern European tephra record is most likely not significantly biased by the inclusion of only one core from each peatland site. In undisturbed, mid-latitude peatlands, the presence or absence of tephra from a given eruption can be determined, with a high degree of certainty, by analysing a single core. The results of the analysis of the tephrostratigraphies of lake and peatland sites in close proximity are less clear. There are differences in the tephrostratigraphy recorded in lakes and peatlands which would have been expected to receive the same primary air fall tephras. Peatlands generally contain more tephra layers than lakes. However, tephras are identified in lakes which are not present in nearby peatlands. This indicates that a bias toward peatland records in the current northern European tephra database (peatland and lakes sites n =100 and 200, respectively) could result in ash clouds not being identified as cryptotephra deposits. There is no evidence for the geochemical alteration of shards in either peatlands (Chapters 4 and 5) or lakes (Chapter 5).

The spatial patchiness of cryptotephra layers on a regional scale is well established (Langdon and Barber, 2004). This study suggests that on one hand, cryptotephras can be less spatially patchy than previously thought, at least in some peatland sites on an intra-site scale. However, differences in the tephrostratigraphies recorded by peatlands and lakes in close proximity to one another, suggests that multiple sites (lakes and peatlands) are required to obtain a representative regional tephrostratigraphy. When using tephra layers as a record of eruption frequency, the more complete the geological

record on which the model is based, the better. The spatial patchiness of cryptotephras even over small scales (<10 km) highlights the need for the examination of as many sites as possible. The current recurrence model may also be biased due to the low number of lake sites, which appear to preserve more tephras of mafic composition when compared with peatlands.

9.1.2 Research compartment 2: The application of tephra layers as records of volcanic ash

This research compartment focussed on identifying opportunities for the application of cryptotephra layers as records of volcanic ash deposition. Having conducted field work to address spatial gaps in the cryptotephra record of northern Europe, I updated the database of Swindles *et al*. (2011) to include new tephra layers identified in this study (Chapter 8, Thesis Objectives 8 and 9), and those from work published since the completion of the Swindles *et al*. (2011) data compilation (Chapter 8, Thesis objective 7). The new database was then utilised, together with new knowledge of the limitations and bias in the datasets from Compartment 1, in order to answer research questions around the frequency and nature of volcanic eruptions.

This study included the first routine analysis of tephra particle size and morphology across multiple sites (n = 13) and the comparison of observations to probabilistic model estimates (Chapter 6, Thesis Objective 4). Large shards (up to 250 µm) were identified at sites 1000s of km from the volcanic source. Surprisingly, there was only a weak correlation between tephra shard size and distance of the fallout site from Iceland. This is most likely to be because the major controls on tephra fallout are weather conditions which vary between and even during eruptions, and the dynamics not only of each eruption, but of individual eruptive phases, during which major controls on tephra production and transport (e.g. plume height, vent diameter, magma volatile composition and the extent of tephra fragmentation) vary. Further evidence for the varying nature of ash shard deposition during different eruptive phases is provided by differences in the chemistry of tephra deposited from a single eruption of Hekla volcano (Hekla 4) in

different regions. This study represents an important ‘first attempt’ at linking the cryptotephra shard size and morphology with the source eruption parameters. However, detailed analysis of shard size relies on identifying and measuring tephra from the same eruption at multiple sites across a range of distances from the source volcano. The current database of shard sizes is limited to a small number of sites, an even smaller number contain tephra from the same eruptions and therefore it is difficult to form well-founded conclusions on the utility of these records for palaeo-hazard research. The range of distances at which sites in northern Europe are located from Iceland will always be restricted by the fallout of a large amount of tephra from Icelandic eruptions into the North Atlantic, Norwegian Sea and North Sea. Routine analysis of shard size is required, certainly for the most widespread tephras

Manual measuring of shard size using an eye piece graticule is time consuming. Particle size analysis conducted during this study provides evidence that the shard size of tephra in the sample of peak tephra concentration is likely to reflect the shard size of the entire vertical spread of tephra, suggesting that laboratory time can be saved by analysing shard size in only a subset of most abundant shards within a given tephra layer. Furthermore, I estimate that assessing the size of 100 shards is sufficient to estimate the median shard size for a tephra layer at a given site (Chapter 6). These methodological alterations are similar to the modern approach used in characterizing proximal tephra deposits using a subset of scoria/pumice size fractions and are important as they reduce the time required to process each shard size sample and may encourage routine reporting of tephra shard size. However, future work should focus on an automated approach to estimating the shard size of cryptotephra samples. Automated imaging (perhaps even in 3 dimensions) of small shards present in only sparse concentrations, would allow for the quantification of morphological characteristics (e.g. vesicularity), which in this thesis were recorded qualitatively. As atmospheric models of volcanic ash increase in complexity, understanding the precise morphology and size characteristics of distal volcanic ash will become increasingly important.

In Chapters 7 and 8, for the first time, proximal records of Icelandic volcanism are compared with the distal cryptotephra record over the last 7000 years (Chapters 7 and 8,

Thesis Objective 6). Examining past trends in the frequency of volcanism using proximal records (e.g. tephra layers and lava flows) is often complicated by issues of reworking or the burial of evidence by younger eruptions. The novel approach of using distal cryptotephra records to compliment the proximal geological record offers an additional line of evidence, supporting the idea that changes in the frequency of volcanism over time are not due to preservation bias in the proximal geological record. The frequency of both Icelandic volcanism and European ash clouds has varied over the last 7000 years. Variation in the frequency of Icelandic volcanism over time can be explained by periodic changes in the spreading rate of the mid ocean rift zone splitting Iceland and the influence of surface loading (glacier extent) on rates of volcanism (Larsen *et al*., 1998; Schmidt *et al*., 2013). In addition to being sensitive to changes in the rate of Icelandic volcanism, the frequency of distal ash accumulations over northern Europe is affected by wind direction, wind speed and rainfall, all of which affect the probability and trajectory of long range ash particle transport (Davies *et al*., 2010) (Chapter 8 Thesis objective 7).

There is a positive correlation between the frequency of Icelandic volcanism and the record of distal ash clouds reaching N. Europe throughout the Holocene. Furthermore, synchronous periods of quiescence occur at least twice during the last 7000 years in records of Icelandic volcanic eruptions and ash clouds over northern Europe (5.5-4.5 and 2.6-1.6 ka BP) (Chapter 7, Thesis objective 6). These periods are not easily explained by changes in the rate of rifting or mantle plume dynamics, as such plate-scale (or large scale) parameter fluctuations necessitate much longer timescales. Instead, following an analysis of global and regional climate data I propose that climate (modulated by glacial loading and unloading) has exerted control on the frequency of volcanism in Iceland over the Holocene. Evidence for this hypothesis is provided in the form of a significant correlation between a deepening of the Icelandic Low (a control on glacier extent), and periods of less frequent volcanic eruptions with a lag of 400-1500 years. This research provides the first empirical evidence to support numerical modelling efforts which suggest that moderately small changes in ice volume, such as those which have occurred during the Holocene in Iceland, can have an impact on the

frequency of volcanism (Schmidt *et al*., 2013). However, more research is required into the magnitude of changes in past glacial extent on Iceland and the impacts of moderate changes in surface loading on melt production rates in the mantle under Iceland. Advancing our understanding of the links between climate, glaciology and the frequency of volcanic activity will become increasingly important as ice caps and glaciers retreat under anthropogenic-driven warming.

In order to estimate the future probability of an ash cloud over northern Europe (Thesis objective 7) I examined both the new European ash cloud database, and Icelandic eruption records. Given the changes in the frequency of Icelandic eruptions evidenced by both proximal records and records of ash deposition over the last 7000 years (Chapters 7 and 8), I examined the period for which the rate of both ash clouds and Icelandic eruptions has been the most stationary (with only minor fluctuation) - the last 1000 years. A comparison of Icelandic and European tephra records over the last 1000 years revealed that all ash clouds in northern European geological record have been produced by highly explosive Plinian eruptions with a VEI ≥ 4 (Chapter 8, Thesis Objectives 6 and 7). According to the geological record, Icelandic eruptions with a VEI ≥ 4 and a silicic magma composition present the most risk of producing an ash cloud over northern Europe. A number of cryptotephra layers in the geological record do not have a known source, and are found in fewer distal sites. These cryptotephra layers might represent ash clouds which were produced by eruptions with a lower VEI. These cryptotephra layers have a major element glass geochemical composition consistent with a source eruption in Iceland, but have not been traced to a specific vent site/volcanic centre. Future research should concentrate on trying to identify a source volcano for these tephra layers. This might involve work on proximal deposits in Iceland, to characterise the geochemistry of tephra derived from eruptions of a smaller magnitude or lesser studied volcanic regions (Haflidason *et al*., 2000). Cryptotephra layers in northern Europe may even represent a record of Icelandic volcanism which has been eroded from the Icelandic record by subsequent eruptions. The average return interval of a volcanic ash cloud over northern Europe based on the new database is 44 ±

7 years, suggesting that ash clouds are more common over northern Europe than previously proposed (56 ± 9 years; Swindles *et al*. (2011)).

During thesis compartment 2 I have explored a range of ways in which cryptotephra layers can be used as a record of past volcanic eruptions. I have studied the use of tephra particle size measurements to examine the fallout of ash across sites in northern Europe, tephra shard size, which is not currently routinely reported, offers some promise for understanding the nature of eruptions (e.g. plume height) from which the shards are derived. However, there are limitations to the application of shard size and morphology data as weather conditions, a major control on tephra dispersal, are often unknown for ancient eruptions. The examination of proximal records of Icelandic eruption frequency and European ash fall records has, for the first time, provided empirical evidence that small changes in ice mass, driven by climate, can impact on the frequency of volcanism. These results add weight to previous studies relying on numerical modelling and have major implications for the frequency of volcanic eruptions under glacial unloading caused by anthropogenic climate change. Comparisons of Icelandic eruption records and cryptotephra records have also indicated the type of volcanic eruption (VEI ≥ 4 and a with silicic magma composition) which are most likely to produce ash clouds over northern Europe. Finally, by combining information on the new tephra layers identified in Chapters (3, 4, 5 and 6) a new estimate for the recurrence of ash clouds over northern Europe has been calculated (44 ± 7 years). Although this still represents a minimum estimate for volcanic ash clouds reaching northern Europe in the past, it is less likely to be confounded by spatial and temporal sampling bias than the previous estimate of Swindles *et al*. (2011).

9.2 Research implications

Cryptotephra layers are widely used in the dating and correlation of paleoenvironmental research. Furthermore, cryptotephras represent the only evidence of pre-historic ash clouds and are an important record of past volcanism. During this research project three new distal tephra layers (AUC-1, CLA-L1 and SN-1) have been identified, geochemically analysed and reported. Furthermore, a large number of high quality

EPMA glass geochemical analyses, conducted with the use of secondary standards, on glass shards from both well-established and less well-established cryptotephra layers have been collected. These data provide an important resource for future studies of northern European and Peruvian tephra layers and will be uploaded onto community databases e.g. Tephrabase (Newton *et al*., 2007) following completion of this project.

Understanding the reworking, redistribution and preservation of cryptotephra layers is crucial both when using them as records of ash clouds and when utilising them as a chronological tool. In this study, a number of methodological advances are presented, which are important for the design of future tephra studies. These advances in methods will be of importance to scientists in the field of tephrochronology, but also to those working in atmospheric science and paleoecology. Beyond methodological advances, this study demonstrates how cryptotephra records can be utilised in new ways to compliment proximal records of volcanism and to present a new recurrence estimate for the frequency of ash cloud events over northern Europe. Our new findings are of direct relevance to insurance and aviation industries, governments and the general public. A number of important methodological advances and novel approaches from this thesis are listed below.

9.2.1 Advances in methods

- Three tephra layers that correlate to the Hekla eruptions of 1510, 1845 and 1947 were detected in 14 cores from the same peatland, suggesting that in small, largely undisturbed, mid-latitude peatlands, the presence or absence of tephra from a given eruption can be determined, with a high degree of certainty, by analysing a single core (Chapter 3).
- There is evidence of incomplete tephra records in both peatlands and lakes. A combination of records from both lakes and peatlands must be used to establish the most comprehensive and complete regional tephrostratigraphies (Chapter 5).
- The analyses of glass shards by EPMA during this study do not indicate any significant chemical alteration of glass shards extracted by different extraction

processes (density separation vs. acid extraction). Acid digestion is a suitable extraction method for glass shards of rhyolitic and trachydacitic composition from ombrotrophic peatlands and does not result in a significant degree of geochemical alteration. (Chapters 4 and 5).

- Shard size does not vary significantly with depth within a cryptotephra layer and therefore the median shard size for a given tephra can be estimated by measuring 100 shards in the vertical sample of peak tephra shard concentration (Chapter 6).

9.2.2 Novel approaches

- Cryptotephra layers can be used to supplement proximal records of volcanism to further understanding of climate volcano interactions (Chapters 7 and 8).
- Tephra shard size and geochemistry can be used to understand more about the eruption from which the tephra is derived, although usefulness is limited by a lack of records of weather conditions during ancient eruptions (Chapter 6).
- A new model of volcanic ash over northern Europe suggests ash clouds occurred more frequently in the last 1000 years than previously thought (Chapter 8).

9.3 Prospects for future research

The results presented in this thesis open up a number of avenues for future work around the themes of tephrochronology and the use of cryptotephra layers as records of past ash clouds. I present evidence that tephra can be preserved in tropical environments. Further research into the tephrochronology of tropical regions may inform our understanding of the volcanic history of these regions, many of which have poorly preserved, or understudied proximal records of volcanic activity.

I have demonstrated how distal cryptotephra records can be used to complement records of volcanic activity from proximal geological records. Expanding on this work, to look in more detail at specific time periods, or into new volcanic regions may offer the opportunity to identify trends which might be missing or unapparent from the analysis of proximal records of volcanic activity alone. The use of European cryptotephra layers

to supplement proximal records of Icelandic volcanism has allowed for the detection of periods of volcanic quiescence which are apparent in both datasets. The periods of volcanic quiescence are connected to periods of ice expansion on Iceland. Understanding the impact of small magnitude changes in surface loading (on interglacial timescales) may have implications for the impact of future climate warming on rates of volcanic activity. However, a number of questions remain, such as, what is the threshold at which ice loading, or unloading results in changes in volcanic eruption frequency?

Finally, more work could be conducted toward assessing the true margins of volcanic ash distribution of detectable shards suitable for geochemical analysis (>30 μm), by seeking sparse concentrations of tephra shards in sites further from their volcanic source. Modelling (Chapter 6) indicates that a 30 μm shard from an Icelandic eruption with a plume height of 35 km can travel up to 23, 000 km. So we may be far from identifying the true margins of ash cloud distribution from Icelandic volcanoes.

Appendix

Supplementary files

Chapter 3: Spatial variability of tephra and carbon accumulation in a Holocene peatland

(Overleaf)

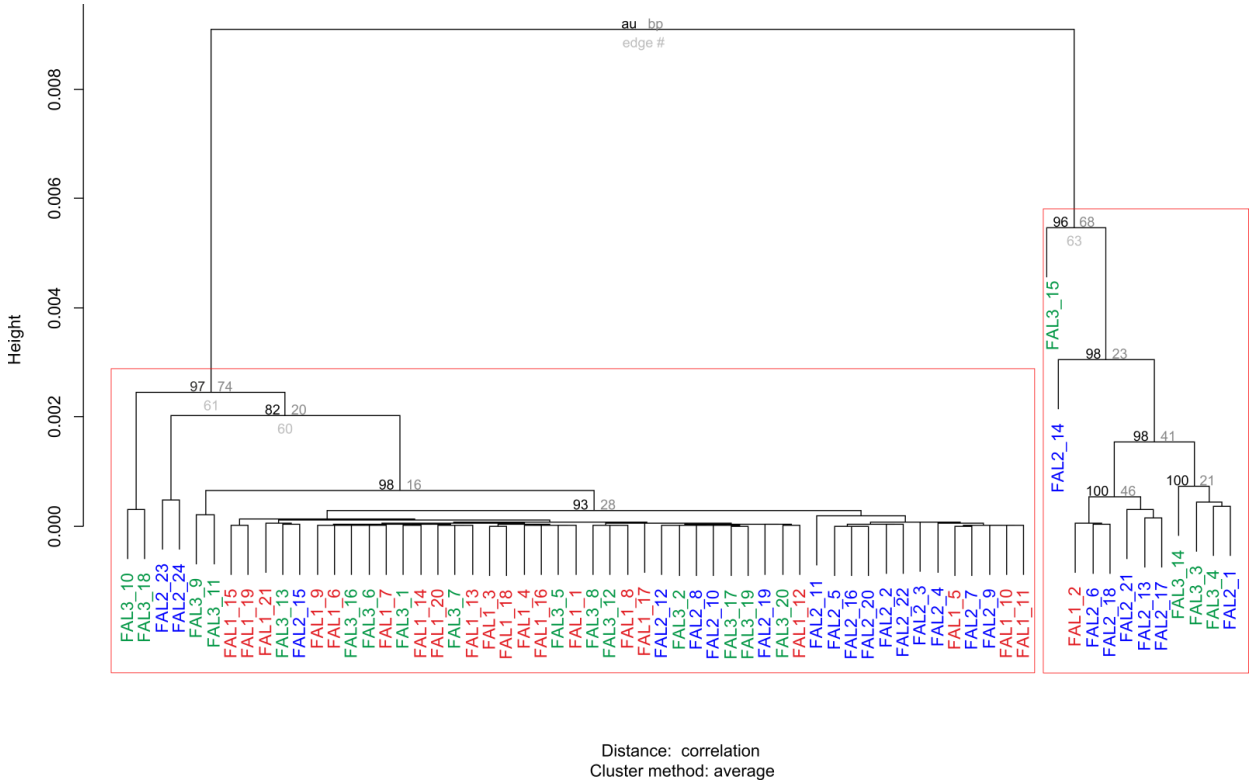

Chapter 3. Fig. S1. Cluster dendrogram based on major element geochemistry of FAL_1 (red), FAL_2 (blue) and FAL_3 (purple) tephras. Approximately Unbiased (AU) and Bootstrap probability (BP) values (%) are illustrated for major clusters. Rectangles highlight clusters with AU values >95%. Analysis conducted in PVCLUST package in R version 3.1.1 (Suzuki and Shimodaira, 2006). Analysis was conducted on raw data (not normalised) with oxide totals >95% (*n*=21, 22 and 20 for FAL_1, FAL_2, FAL_3 respectively).

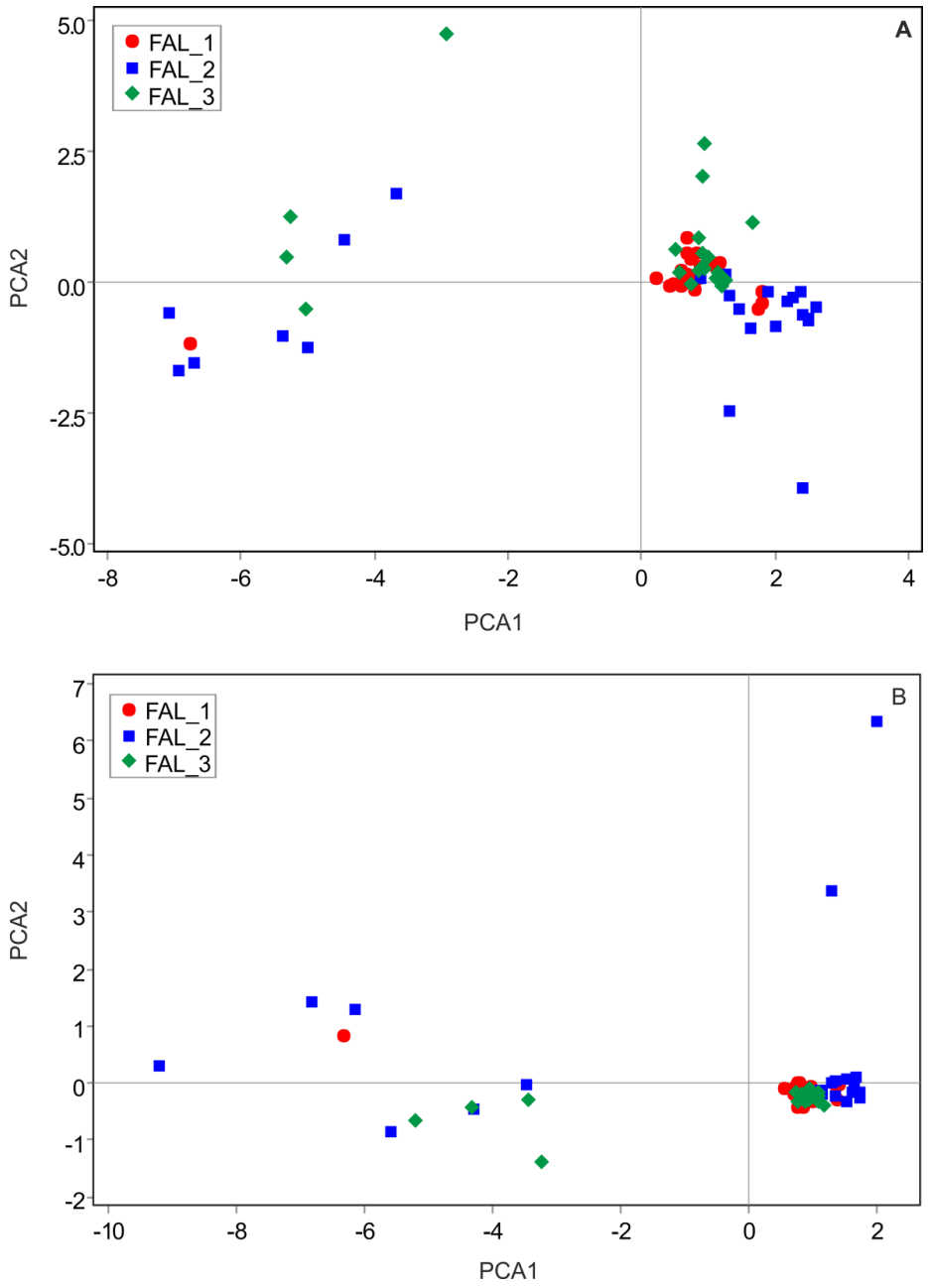

Chapter 3. Fig. S2. Bivariate plot showing principal component scores on component 1 and 2 of (a) raw and (b) additive log ratio transformed data. Analysis was conducted on raw data (not normalised) with oxide totals >95% (*n*=21, 22 and 20 for FAL_1, FAL_2, FAL_3 respectively). One shard was removed following log ratio transformation due to a negative measured value for MgO therefore for (b) *n* = 21, 21, 20 for FAL_1, FAL_2, FAL_3 respectively. Eigenvalues were (a) raw, axis 1 = 7.3086, axis 2 = 1.2560 (b) log ratio transformed, axis 1 = 6.4620, axis 2 = 0.9918.

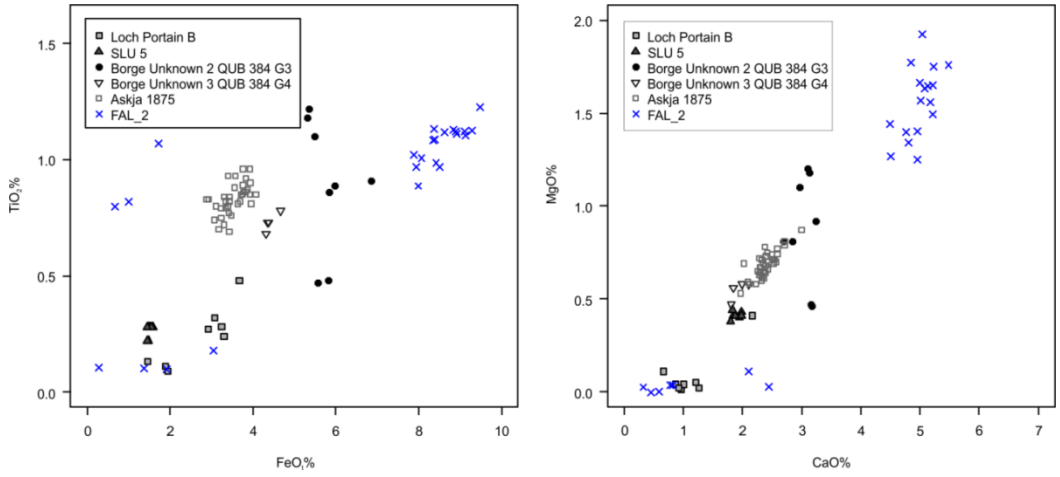

Chapter 3. Fig. S3. Tephra geochemistry bi-plots for FAL_2 (Fallahogy core A) and type data from northern European cryptotephras dated between 1510 and 1947 AD (excluding Hekla 1845). Data from Tephrabase (Newton *et al.*, 2007).

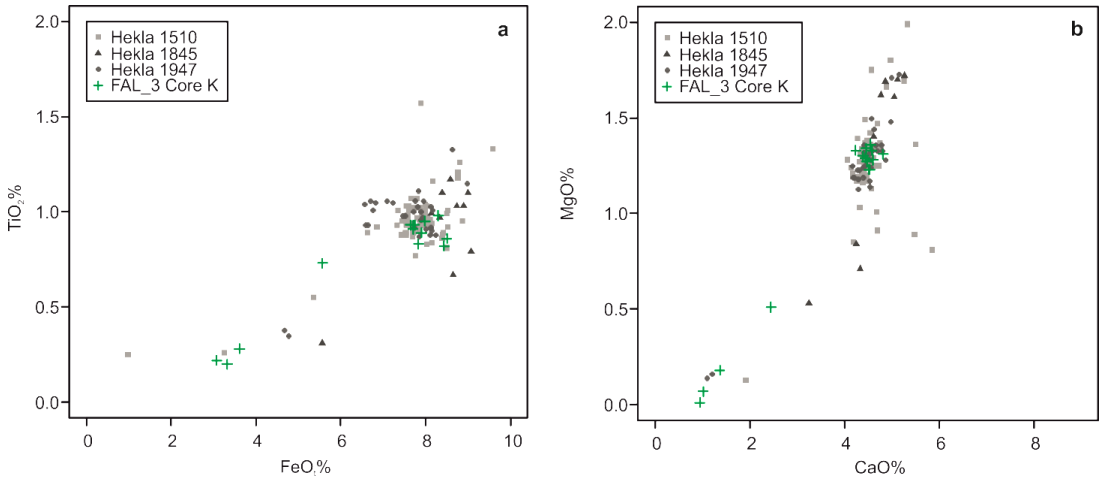

Chapter 3. Fig. S4. Tephra geochemistry bi-plots for (a-b) full range of FeO_t(%), TiO_2(%), CaO(%), MgO(%) values for the FAL_3 tephra from core K plotted against type data for the Hekla eruptions of 1510, 1845 and 1947 from the Tephrabase (Newton *et al.*, 2007).

Chapter 3. Table S1. Major oxide concentration data (wt %) for tephra shards identified in core A and core K at Fallahogy. Core A: FAL_1 = 8-9 cm, FAL_2 = 14-15 cm, FAL_3= 24-25 cm. Core K: FAL_3 = 43-45 cm. Tephra analysis was conducted using a Cameca SX100 electron probe microanalyser at Tephra Analytical Unit (TAU), School of Geosciences, University of Edinburgh. All analyses were conducted with a beam diameter of 5 µm, 15kV and beam currents of 2 nA (Na, Mg, Al, Si, K, Ca, Fe) and 80 nA (P, Ti, Mn) (Hayward, 2012). Analyses with low total oxide values (less than 95%) were excluded. Secondary glass standards (basalt (BCR-2G) and rhyolite (Lipari)), were analysed before and after unknown tephra samples. Analyses on secondary standards are italicised.

	SiO_2	**TiO_2**	**Al_2O_3**	**FeO**	**MnO**	**MgO**	**CaO**	**Na_2O**	**K_2O**	**P_2O_5**	**Total**
Lipari	*74.93*	*0.08*	*13.31*	*1.49*	*0.07*	*0.07*	*0.63*	*4.00*	*5.16*	*0.01*	*99.75*
Lipari	*73.79*	*0.08*	*12.98*	*1.54*	*0.08*	*0.04*	*0.71*	*3.98*	*5.08*	*0.00*	*98.28*
BCR-2G	*54.25*	*2.26*	*13.43*	*12.19*	*0.19*	*3.64*	*7.19*	*3.18*	*1.88*	*0.34*	*98.54*
BCR-2G	*54.71*	*2.25*	*13.43*	*12.55*	*0.20*	*3.80*	*7.15*	*3.21*	*1.85*	*0.37*	*99.52*
	SiO_2	**TiO_2**	**Al_2O_3**	**FeO**	**MnO**	**MgO**	**CaO**	**Na_2O**	**K_2O**	**P_2O_5**	**Total**
FAL_2	73.72	0.10	12.44	0.28	0.02	0.00	0.59	3.74	4.96	0.01	95.88
FAL_2	72.63	1.07	12.00	1.72	0.00	0.02	0.32	4.19	3.94	0.24	96.14
FAL_2	72.62	0.18	14.06	3.04	0.11	0.11	2.10	4.50	2.50	0.04	99.25
FAL_2	72.50	0.10	12.38	1.38	0.05	0.03	0.78	2.67	5.90	0.01	95.80
FAL_2	72.08	0.82	12.73	0.99	0.02	0.00	0.45	3.84	4.40	0.19	95.51
FAL_2	71.64	0.10	12.55	1.92	0.05	0.04	0.82	2.80	5.99	0.03	95.94
FAL_2	67.51	0.80	15.79	0.67	0.01	0.03	2.45	5.05	2.80	0.09	95.19
FAL_2	62.41	0.99	14.69	8.42	0.24	1.40	4.96	4.29	1.85	0.34	99.58
FAL_2	62.03	0.89	14.81	7.99	0.22	1.27	4.51	4.45	1.72	0.31	98.21
FAL_2	61.88	0.97	15.10	7.93	0.21	1.40	4.77	4.57	1.73	0.35	98.91
FAL_2	61.52	0.97	14.76	8.51	0.20	1.49	5.22	4.10	1.61	0.37	98.74
FAL_2	61.20	1.12	15.32	9.11	0.24	1.65	5.22	4.45	1.63	0.45	100.39
FAL_2	61.03	1.02	14.73	7.88	0.21	1.34	4.80	4.34	1.76	0.38	97.50
FAL_2	60.70	1.12	14.79	8.62	0.22	1.64	5.14	4.50	1.65	0.47	98.85
FAL_2	60.64	1.13	15.18	8.37	0.26	1.66	5.00	4.04	1.55	0.47	98.29
FAL_2	60.60	1.08	15.02	8.34	0.22	1.57	5.01	4.47	1.79	0.42	98.53
FAL_2	60.48	1.10	14.77	9.13	0.20	1.63	5.08	4.00	1.58	0.43	98.40
FAL_2	60.41	1.13	14.92	8.83	0.24	1.92	5.03	4.13	1.62	0.47	98.70
FAL_2	60.02	1.09	14.41	8.38	0.22	1.44	4.49	3.96	1.69	0.43	96.13
FAL_2	59.97	1.11	15.04	8.91	0.23	1.56	5.17	4.34	1.55	0.43	98.32
FAL_2	59.58	1.12	14.94	8.89	0.25	1.75	5.23	4.32	1.57	0.47	98.14
FAL_2	58.63	1.23	14.53	9.48	0.22	1.77	4.85	4.30	1.55	0.45	97.00
	SiO_2	**TiO_2**	**Al_2O_3**	**FeO**	**MnO**	**MgO**	**CaO**	**Na_2O**	**K_2O**	**P_2O_5**	**Total**
Lipari	*75.55*	*0.08*	*12.89*	*1.58*	*0.05*	*0.01*	*0.74*	*4.18*	*5.28*	*0.00*	*100.36*
Lipari	*75.06*	*0.08*	*13.04*	*1.61*	*0.07*	*0.02*	*0.74*	*4.15*	*5.13*	*0.00*	*99.91*
Lipari	*74.75*	*0.07*	*13.08*	*1.54*	*0.05*	*0.03*	*0.74*	*4.01*	*5.14*	*0.00*	*99.41*
Lipari	*75.08*	*0.09*	*13.00*	*1.52*	*0.06*	*0.04*	*0.76*	*4.17*	*5.26*	*0.01*	*100.00*
Lipari	*74.00*	*0.08*	*13.00*	*1.55*	*0.07*	*0.05*	*0.76*	*3.98*	*5.22*	*0.00*	*98.71*
Lipari	*73.94*	*0.07*	*12.84*	*1.37*	*0.04*	*0.04*	*0.80*	*3.94*	*5.04*	*0.01*	*98.09*
BCR-2G	*55.17*	*2.25*	*13.86*	*12.45*	*0.17*	*3.75*	*7.20*	*3.20*	*1.81*	*0.32*	*100.18*

BCR-2G	*55.66*	*2.25*	*13.37*	*12.10*	*0.20*	*3.67*	*7.16*	*3.07*	*1.79*	*0.32*	*99.60*
BCR-2G	*55.63*	*2.26*	*13.30*	*12.26*	*0.19*	*3.66*	*7.35*	*3.23*	*1.73*	*0.32*	*99.94*
BCR-2G	*55.63*	*2.26*	*13.29*	*12.43*	*0.18*	*3.61*	*7.43*	*3.12*	*1.85*	*0.32*	*100.13*
BCR-2G	*55.48*	*2.27*	*13.75*	*12.15*	*0.19*	*3.72*	*7.46*	*3.18*	*1.87*	*0.33*	*100.40*
BCR-2G	*55.78*	*2.26*	*13.68*	*12.13*	*0.18*	*3.71*	*7.20*	*3.08*	*1.83*	*0.33*	*100.18*

	SiO_2	**TiO_2**	**Al_2O_3**	**FeO**	**MnO**	**MgO**	**CaO**	**Na_2O**	**K_2O**	**P_2O_5**	**Total**
Lipari	*74.30*	*0.08*	*12.92*	*1.59*	*0.08*	*0.03*	*0.82*	*4.04*	*5.30*	*0.00*	*99.15*
Lipari	*74.23*	*0.08*	*13.07*	*1.66*	*0.05*	*0.04*	*0.78*	*3.85*	*5.25*	*0.01*	*99.02*

	SiO_2	**TiO_2**	**Al_2O_3**	**FeO**	**MnO**	**MgO**	**CaO**	**Na_2O**	**K_2O**	**P_2O_5**	**Total**
FAL_3	76.23	0.32	11.99	3.57	0.12	0.10	1.70	4.09	2.26	0.03	100.42
FAL_3	73.84	0.23	13.39	3.19	0.12	0.01	1.05	5.23	3.61	0.01	100.69
FAL_3	73.65	0.19	13.19	1.30	0.03	0.22	1.50	4.63	2.27	0.06	97.05
FAL_3	63.00	0.83	15.67	8.03	0.20	1.23	4.92	4.85	1.67	0.28	100.67
FAL_3	62.72	0.45	16.37	3.50	0.27	0.26	0.67	7.47	5.46	0.04	97.21
FAL_3	62.71	0.93	15.25	7.72	0.21	1.32	4.70	4.53	1.85	0.32	99.53
FAL_3	62.67	0.92	15.29	7.81	0.21	1.27	4.54	4.76	1.81	0.31	99.60
FAL_3	62.39	0.91	15.16	8.08	0.20	1.22	4.73	4.42	1.70	0.29	99.10
FAL_3	62.35	0.90	15.58	7.84	0.21	1.24	4.64	4.57	1.76	0.32	99.40
FAL_3	62.33	0.94	14.77	7.83	0.21	1.21	4.40	4.39	1.94	0.33	98.34
FAL_3	62.31	0.86	15.56	6.85	0.19	1.02	4.59	4.59	1.76	0.30	98.02
FAL_3	62.31	0.92	15.25	8.05	0.21	1.32	4.75	4.46	1.66	0.34	99.26
FAL_3	62.29	0.92	14.98	7.76	0.21	1.28	4.63	4.61	1.72	0.31	98.70
FAL_3	62.14	0.91	14.78	7.60	0.17	1.27	4.60	4.60	1.85	0.30	98.23
FAL_3	62.08	0.95	14.63	8.44	0.25	1.41	4.64	4.53	1.74	0.31	98.97
FAL_3	61.77	0.98	16.42	6.60	0.22	0.97	5.30	5.12	1.73	0.49	99.59
FAL_3	61.62	0.97	14.87	8.09	0.22	1.35	4.71	4.39	1.75	0.35	98.32
FAL_3	61.53	0.65	17.44	6.65	0.18	1.03	5.75	5.01	1.35	0.23	99.82
FAL_3	61.38	0.65	18.06	5.53	0.16	0.97	6.07	5.39	1.17	0.24	99.60
FAL_3	60.94	0.90	14.68	8.20	0.24	1.32	4.65	4.43	1.68	0.30	97.33

	SiO_2	**TiO_2**	**Al_2O_3**	**FeO**	**MnO**	**MgO**	**CaO**	**Na_2O**	**K_2O**	**P_2O_5**	**Total**
FAL_1	72.40	0.10	12.38	1.60	0.04	0.04	0.97	3.21	5.66	0.02	96.43
FAL_1	64.60	0.91	15.30	7.62	0.22	1.19	4.50	4.32	1.83	0.30	100.80
FAL_1	64.26	0.91	15.21	7.67	0.22	1.22	4.13	4.34	1.88	0.31	100.16
FAL_1	63.62	0.91	14.76	7.88	0.19	1.24	4.34	4.41	1.87	0.30	99.52
FAL_1	63.58	0.89	15.02	7.34	0.18	1.13	4.50	4.21	1.71	0.30	98.86
FAL_1	63.34	0.90	14.86	7.76	0.19	1.20	4.63	4.38	1.81	0.31	99.40
FAL_1	63.14	0.91	15.12	7.90	0.22	1.25	4.49	4.67	1.85	0.27	99.82
FAL_1	63.12	0.88	14.79	7.55	0.23	0.91	3.79	4.30	1.98	0.29	97.84
FAL_1	62.98	0.91	15.44	7.88	0.19	1.15	4.65	4.96	1.87	0.29	100.34
FAL_1	62.97	0.84	15.50	7.86	0.19	1.21	4.88	4.57	1.70	0.26	99.99
FAL_1	62.76	0.94	15.33	7.70	0.22	1.20	4.52	4.46	1.87	0.30	99.31
FAL_1	62.67	0.91	15.53	8.22	0.23	1.26	4.46	4.43	1.79	0.31	99.81
FAL_1	62.64	0.94	14.94	7.71	0.24	1.11	4.47	4.79	1.85	0.30	98.99
FAL_1	62.63	0.91	14.91	7.78	0.23	1.27	4.65	4.38	1.70	0.29	98.75
FAL_1	61.69	0.91	15.06	8.38	0.24	1.31	4.75	4.60	1.65	0.29	98.86
FAL_1	61.59	0.87	14.21	7.80	0.21	1.38	4.81	4.43	1.58	0.29	97.17
FAL_1	61.42	0.90	14.75	7.31	0.20	1.22	4.64	4.52	1.82	0.27	97.05
FAL_1	61.33	1.09	14.83	8.51	0.22	1.54	4.92	4.17	1.70	0.39	98.69

FAL_1	61.31	1.04	14.81	8.64	0.23	1.52	5.02	4.52	1.69	0.42	99.20
FAL_1	61.04	1.07	14.94	8.58	0.22	1.61	5.09	4.19	1.64	0.37	98.74
FAL_1	60.40	0.85	14.65	7.60	0.19	1.20	4.19	4.28	1.71	0.30	95.37

	SiO_2	**TiO_2**	**Al_2O_3**	**FeO**	**MnO**	**MgO**	**CaO**	**Na_2O**	**K_2O**	**P_2O_5**	**Total**
Lipari	*73.04*	*0.07*	*12.84*	*1.51*	*0.06*	*0.00*	*0.71*	*4.04*	*5.06*	*0.01*	*97.34*
Lipari	*73.43*	*0.07*	*12.64*	*1.50*	*0.04*	*0.04*	*0.76*	*4.00*	*5.14*	*0.01*	*97.62*
Lipari	*73.30*	*0.08*	*12.77*	*1.77*	*0.08*	*0.05*	*0.76*	*3.98*	*5.30*	*0.01*	*98.10*
Lipari	*72.86*	*0.08*	*12.80*	*1.25*	*0.06*	*0.00*	*0.73*	*4.12*	*5.30*	*0.01*	*97.20*
Lipari	*72.94*	*0.08*	*12.61*	*1.69*	*0.04*	*0.06*	*0.74*	*3.93*	*5.13*	*0.00*	*97.22*
Lipari	*72.96*	*0.08*	*12.91*	*1.62*	*0.05*	*0.04*	*0.72*	*3.94*	*5.18*	*0.00*	*97.50*
BCR-2G	*54.38*	*2.25*	*13.50*	*11.88*	*0.18*	*3.64*	*7.03*	*3.11*	*1.85*	*0.34*	*98.16*
BCR-2G	*54.61*	*2.25*	*13.14*	*12.46*	*0.16*	*3.68*	*7.07*	*3.29*	*1.90*	*0.35*	*98.91*
BCR-2G	*54.57*	*2.25*	*13.42*	*12.31*	*0.20*	*3.71*	*7.33*	*3.22*	*1.86*	*0.33*	*99.22*
BCR-2G	*54.07*	*2.26*	*13.18*	*12.18*	*0.19*	*3.54*	*7.23*	*3.14*	*1.87*	*0.33*	*97.99*
BCR-2G	*54.24*	*2.26*	*13.19*	*13.06*	*0.19*	*3.60*	*7.33*	*3.16*	*1.89*	*0.32*	*99.23*
BCR-2G	*53.37*	*2.25*	*13.50*	*12.77*	*0.19*	*3.77*	*7.17*	*3.26*	*1.85*	*0.35*	*98.47*

	SiO_2	**TiO_2**	**Al_2O_3**	**FeO**	**MnO**	**MgO**	**CaO**	**Na_2O**	**K_2O**	**P_2O_5**	**Total**
FAL_3_CORE_K	73.19	0.22	12.75	3.07	0.09	0.01	0.95	5.27	3.59	0.00	99.12
FAL_3_CORE_K	71.01	0.20	12.44	3.32	0.13	0.07	1.02	4.67	3.95	0.03	96.83
FAL_3_CORE_K	69.30	0.28	12.87	3.61	0.14	0.18	1.37	5.36	3.40	0.04	96.55
FAL_3_CORE_K	67.97	0.73	13.84	5.57	0.17	0.51	2.45	4.75	2.91	0.14	99.05
FAL_3_CORE_K	63.89	0.93	15.03	7.70	0.22	1.23	4.54	4.73	1.69	0.30	100.27
FAL_3_CORE_K	63.74	0.83	15.19	7.83	0.20	1.36	4.55	4.70	1.77	0.36	100.53
FAL_3_CORE_K	63.72	0.93	15.40	7.65	0.23	1.33	4.58	4.74	1.72	0.30	100.61
FAL_3_CORE_K	63.64	0.82	15.06	8.43	0.20	1.31	4.82	4.64	1.74	0.36	101.03
FAL_3_CORE_K	63.54	0.93	15.15	7.64	0.23	1.29	4.44	4.44	1.69	0.32	99.65
FAL_3_CORE_K	63.51	0.86	14.34	8.50	0.24	1.33	4.24	4.65	1.76	0.30	99.73
FAL_3_CORE_K	63.43	0.98	15.24	8.30	0.20	1.34	4.46	4.76	1.71	0.35	100.77
FAL_3_CORE_K	63.32	0.93	15.18	7.74	0.21	1.23	4.52	4.75	1.73	0.29	99.92
FAL_3_CORE_K	62.97	0.95	14.69	7.98	0.23	1.30	4.39	4.80	1.80	0.31	99.43
FAL_3_CORE_K	60.77	0.89	14.41	7.90	0.22	1.28	4.61	4.41	1.67	0.27	96.45
FAL_3_CORE_K	60.70	0.91	14.36	7.70	0.20	1.27	4.48	4.18	1.75	0.31	95.86

	SiO_2	**TiO_2**	**Al_2O_3**	**FeO**	**MnO**	**MgO**	**CaO**	**Na_2O**	**K_2O**	**P_2O_5**	**Total**
BCR-2G	54.84	2.26	13.48	12.46	0.19	3.67	7.14	3.15	1.77	0.35	99.30
BCR-2G	54.54	2.27	13.38	12.24	0.20	3.80	7.04	3.20	1.79	0.35	98.80
BCR-2G	55.57	2.25	13.57	12.42	0.18	3.74	7.31	3.44	1.78	0.35	100.62
BCR-2G	55.26	2.26	13.59	12.32	0.20	3.81	7.17	3.19	1.85	0.36	100.00
BCR-2G	54.35	2.26	13.37	12.78	0.20	3.74	7.08	3.41	1.81	0.35	99.36
BCR-2G	55.27	2.28	13.31	12.74	0.19	3.79	7.16	3.20	1.76	0.33	100.03
Lipari	73.81	0.08	12.69	1.76	0.05	0.04	0.74	4.20	5.28	0.00	98.66
Lipari	74.29	0.08	12.74	1.60	0.06	0.04	0.76	4.07	5.20	0.01	98.86
Lipari	73.96	0.08	13.03	1.62	0.08	0.03	0.72	4.16	5.35	0.01	99.04
Lipari	74.76	0.08	12.89	1.60	0.06	0.02	0.79	4.15	5.19	0.00	99.55
Lipari	75.23	0.07	13.30	1.63	0.06	0.04	0.66	4.25	5.21	0.01	100.46
Lipari	73.16	0.08	12.51	1.65	0.07	0.06	0.72	4.32	5.43	0.00	98.00

Variable 1	Variable 2	*p* value	Test statistic value
Elevation of core location	Total number of shards 1510	0.887	r = 0.04
	Total number of shards 1845	0.758	r = -0.09
	Total number of shards 1947	0.552	r = 0.18
	Apparent total carbon accumulation	0.108	r = 0.45
Distance from the edge of the peatland	Total number of shards 1510	0.988	r = 0.004
	Total number of shards 1845	0.661	r = -0.13
	Total number of shards 1947	**0.016**	r = 0.65
	Apparent total carbon accumulation	0.358	r = 0.27

Chapter 3. Table S2. *p* values and test statistics for Spearman's Rank Correlation Analysis in sections *4.4.1.* and *4.7.1.* All analysis conducted in Minitab 17. The significant *p* value is highlighted in bold. A normality test was conducted on each variable prior to analysis. The result suggested that the majority of the variables were not normally distributed and therefore a non-parametric test was selected.

Chapter 4: First discovery of Holocene cryptotephra in Amazonia

Chapter 4. Supplementary Table 1: AUC1 Tephra geochemistry and standard data from EPMA

Tephra	SiO_2	TiO_2	Al_2O_3	FeO	MnO	MgO	CaO	Na_2O	K_2O	P_2O_5	Total
AUC10 cm Population 1	76.33	0.12	12.79	0.93	0.03	0.27	1.34	4.23	2.77	0.04	98.86
AUC10 cm Population 1	76.03	0.16	12.38	0.75	0.02	0.18	0.86	3.75	3.97	0.03	98.14
AUC10 cm Population 1	75.29	0.16	11.59	0.74	0.01	0.17	0.89	3.85	3.30	0.02	96.02
AUC10 cm Population 1	74.59	0.07	12.69	0.83	0.07	0.14	0.98	4.11	3.08	0.05	96.61
AUC10 cm Population 1	74.73	0.10	12.27	0.78	0.02	0.25	1.18	4.24	2.71	0.04	96.32
AUC10 cm Population 1	74.15	0.05	12.66	0.81	0.06	0.19	1.09	4.09	3.18	0.06	96.35
AUC10 cm Population 1	75.71	0.15	11.56	0.73	0.03	0.17	0.83	3.56	3.53	0.03	96.32
AUC10 cm Population 1	78.78	0.18	11.70	0.66	0.02	0.11	0.64	3.50	4.02	0.03	99.64
AUC10 cm Population 1	77.00	0.10	12.49	0.82	0.03	0.24	1.02	4.27	2.81	0.04	98.83
AUC10 cm Population 1	75.99	0.16	11.85	0.93	0.03	0.18	0.99	3.90	3.34	0.02	97.40
AUC10 cm Population 1	73.41	0.06	12.98	0.79	0.07	0.16	1.04	4.13	3.18	0.05	95.87
AUC10 cm Population 1	75.10	0.16	11.21	0.79	0.03	0.19	0.87	3.76	3.59	0.03	95.74
AUC10 cm Population 1	73.73	0.06	12.52	0.65	0.06	0.16	0.94	4.10	3.12	0.05	95.40
AUC10 cm Population 1	74.29	0.06	12.80	0.79	0.06	0.15	0.94	4.04	3.08	0.05	96.26
AUC10 cm Population 1	77.14	0.17	12.32	1.00	0.03	0.22	0.99	3.87	3.99	0.04	99.76
AUC10 cm Population 1	77.43	0.16	12.59	0.72	0.03	0.18	0.89	3.64	4.29	0.03	99.96
AUC10 cm Population 1	74.79	0.35	12.77	1.82	0.06	0.40	1.47	4.16	3.17	0.06	99.05
AUC10 cm Population 1	73.46	0.06	12.58	0.80	0.06	0.17	1.06	4.09	3.20	0.05	95.53
AUC10 cm Population 1	75.31	0.24	12.97	1.03	0.02	0.26	1.42	4.09	3.33	0.04	98.71
AUC10 cm Population 1	75.64	0.17	12.55	0.95	0.03	0.18	0.89	3.69	3.86	0.03	97.98
AUC10 cm Population 1	76.56	0.17	12.00	0.84	0.02	0.15	0.96	3.66	3.81	0.04	98.21

AUC10 cm Population 1	73.54	0.12	12.34	0.91	0.03	0.31	1.40	4.36	2.60	0.04	95.66
Min	73.41	0.05	11.21	0.65	0.01	0.11	0.64	3.50	2.60	0.02	95.40
Max	78.78	0.35	12.98	1.82	0.07	0.40	1.47	4.36	4.29	0.06	99.96
Mean	75.41	0.14	12.35	0.87	0.04	0.20	1.03	3.96	3.36	0.04	97.39
Stdev	1.42	0.07	0.49	0.24	0.02	0.07	0.21	0.25	0.47	0.01	1.55

Standard	SiO_2	TiO_2	Al_2O_3	FeO	MnO	MgO	CaO	Na_2O	K_2O	P_2O_5	Total
BCR2g (before unknowns)	54.72	2.25	13.29	12.26	0.20	3.66	7.15	3.11	1.76	0.36	98.76
BCR2g (before unknowns)	55.57	2.28	13.55	12.72	0.21	3.65	6.98	3.31	1.84	0.35	100.47
BCR2g (before unknowns)	54.63	2.27	13.71	12.43	0.20	3.81	7.19	3.23	1.83	0.35	99.65
Lipari (before unknowns)	74.60	0.07	13.27	1.58	0.06	0.06	0.75	4.24	5.22	0.01	99.86
Lipari (before unknowns)	73.69	0.08	12.80	1.51	0.07	0.03	0.74	4.08	5.13	0.00	98.14
Lipari (before unknowns)	75.67	0.08	12.86	1.50	0.08	0.05	0.74	4.45	5.27	0.00	100.70
BCR2g (after unknowns)	53.76	2.24	13.29	12.43	0.20	3.69	7.24	3.24	1.80	0.36	98.27
BCR2g (after unknowns)	53.77	2.23	13.07	12.33	0.19	3.75	7.28	3.38	1.78	0.36	98.15
BCR2g (after unknowns)	53.96	2.27	13.41	12.45	0.20	3.72	7.15	3.40	1.76	0.39	98.71
BCR2g (after unknowns)	53.52	2.23	13.56	12.27	0.19	3.73	7.25	3.31	1.75	0.36	98.16
BCR2g (after unknowns)	54.04	2.24	13.47	12.89	0.21	3.64	7.29	3.22	1.76	0.35	99.11
BCR2g (after unknowns)	54.15	2.24	13.08	12.39	0.20	3.70	7.31	3.31	1.87	0.35	98.60
Lipari (after unknowns)	74.90	0.09	12.79	1.67	0.06	0.03	0.75	4.32	5.25	0.00	99.87
Lipari (after unknowns)	74.42	0.07	13.01	1.51	0.06	0.05	0.77	4.20	5.23	0.01	99.34
Lipari (after unknowns)	73.94	0.08	12.83	1.41	0.06	0.06	0.74	4.11	5.27	0.01	98.50
Lipari (after unknowns)	74.14	0.07	12.91	1.59	0.06	0.05	0.74	4.25	5.17	0.00	98.99
Lipari (after unknowns)	74.44	0.07	12.85	1.55	0.07	0.05	0.77	4.35	5.11	0.01	99.27
Lipari (after unknowns)	74.82	0.07	13.02	1.71	0.07	0.05	0.69	4.22	4.99	0.00	99.64

Chapter 5: Do peatlands or lakes provide the most comprehensive distal tephra records?

Chapter 5. Supplementary file 1: Photographs of lakes and peatlands mentioned in the text. Photos courtesy of authors: EJW, ITL, GTS

Site	**Photographs**
Lake Svartkälsjärn	
Degerö Stormyr	
Malham Tarn Malham Moss	

Claraghmore Lake

Claraghmore Bog

Sammakovuoma Lake

Sammakovuoma Peatland

Chapter 5. Supplementary Table 1. Raw geochemical data. The majority of tephra geochemical analysis was conducted using a Cameca SX100 electron probe microanalyser at Tephra Analytical Unit (TAU), School of Geosciences, University of Edinburgh. All analyses were conducted with a beam diameter of 5 µm, 15kV and beam currents of 2 nA (Na, Mg, Al, Si, K, Ca, Fe) and 80 nA (P, Ti, Mn) (Hayward, 2012). Secondary glass standards (basalt (BCR-2G) and rhyolite (Lipari)), were analysed before and after unknown tephra samples. Samples marked with a (*) were analysed at the University of Leeds using 15 kV, 10µm beam diameter and a beam current of 10 nA. Analyses with low total oxide values (less than 95%) were excluded.

CLA-B1 = Öræfajökull 1362, Hekla 1510? Standard data = Group 1

	SiO_2	TiO_2	Al_2O_3	FeO	MnO	MgO	CaO	Na_2O	K_2O	P_2O_5	Total
CLA-B1	72.24	0.21	13.08	2.93	0.09	0.02	1.05	4.42	3.72	0.02	97.77
CLA-B1	72.14	0.22	13.10	3.31	0.10	0.02	1.03	5.05	3.62	0.02	98.62
CLA-B1	71.41	0.14	16.16	1.64	0.05	0.02	3.01	5.86	2.08	0.06	100.44
CLA-B1	68.61	0.89	14.10	4.58	0.11	0.35	2.29	4.74	3.35	0.17	99.18
CLA-B1	68.24	0.82	13.51	4.21	0.16	0.73	2.21	5.01	3.29	0.18	98.37
CLA-B1	63.49	0.84	15.50	7.80	0.22	1.31	4.75	4.68	1.76	0.33	100.69
CLA-B1	50.06	2.62	13.54	12.52	0.20	5.73	10.02	2.70	0.48	0.29	98.15

CLA-B2 = Unknown #4, mix? Standard data = Group 2

	SiO_2	TiO_2	Al_2O_3	FeO	MnO	MgO	CaO	Na_2O	K_2O	P_2O_5	Total
CLA-B2	74.97	0.34	12.71	2.23	0.12	0.12	0.50	4.69	4.14	0.02	99.83
CLA-B2	74.16	0.34	12.60	2.48	0.09	0.11	0.44	5.48	4.06	0.02	99.78
CLA-B2	73.39	0.29	11.59	2.74	0.08	0.03	0.48	4.06	4.61	0.05	97.33
CLA-B2	72.11	0.34	12.66	3.04	0.16	0.23	1.17	4.94	3.97	0.07	98.69
CLA-B2	70.82	0.25	14.02	2.23	0.08	0.23	0.91	5.03	4.79	0.04	98.40
CLA-B2	70.76	0.42	13.50	5.09	0.12	0.28	2.48	4.60	2.75	0.08	100.06
CLA-B2	69.35	0.28	12.77	3.62	0.14	0.16	1.34	4.17	3.46	0.04	95.33
CLA-B2	69.05	0.26	13.87	2.31	0.06	0.20	0.93	4.77	4.35	0.03	95.83
CLA-B2	68.77	0.57	15.55	5.56	0.17	0.52	3.93	1.56	2.16	0.33	99.12
CLA-B2	68.54	0.26	12.56	3.33	0.12	0.20	1.35	5.00	3.50	0.05	94.90
CLA-B2	68.12	0.25	12.26	3.61	0.14	0.22	1.41	5.05	3.45	0.06	94.57
CLA-B2	67.83	0.57	12.76	5.93	0.20	0.51	2.64	4.53	2.55	0.12	97.63
CLA-B2	67.76	0.72	13.40	4.86	0.13	0.55	2.07	5.18	3.09	0.13	97.90
CLA-B2	67.66	0.48	13.79	5.61	0.16	0.46	3.22	4.31	2.29	0.09	98.07
CLA-B2	66.95	0.80	15.46	4.12	0.06	1.43	3.56	5.06	2.08	0.27	99.78
CLA-B2	66.54	0.59	12.68	6.77	0.20	0.62	4.01	4.47	2.54	0.49	98.90
CLA-B2	61.83	1.17	14.31	8.74	0.23	1.20	4.84	4.32	1.75	0.50	98.90
CLA-B2	61.52	0.85	14.51	6.60	0.21	0.65	4.79	4.57	2.08	0.56	96.34
CLA-B2	60.97	1.12	14.65	7.88	0.23	1.23	4.96	4.41	1.69	0.48	97.63
CLA-B2	60.68	1.19	14.55	8.56	0.19	1.27	4.97	4.48	1.61	0.54	98.04

CLA-B2A = Hekla 1104 Standard data = Group 3

	SiO_2	TiO_2	Al_2O_3	FeO	MnO	MgO	CaO	Na_2O	K_2O	P_2O_5	Total
CLA-B2A	72.14	0.21	13.79	2.88	0.10	0.12	1.87	4.17	2.76	0.02	98.00
CLA-B2A	71.19	0.20	12.96	3.27	0.13	0.09	1.94	1.86	2.56	0.03	94.00
CLA-B2A	70.55	0.19	12.36	3.08	0.12	0.12	1.92	4.52	2.74	0.02	96.00
CLA-B2A	69.33	0.36	13.14	2.05	0.04	0.39	1.59	2.50	4.21	0.08	94.00

CLA-B3 = MOR-T4 Standard data = Group 4

	SiO_2	TiO_2	Al_2O_3	FeO	MnO	MgO	CaO	Na_2O	K_2O	P_2O_5	Total
CLA-B3	75.98	0.07	12.87	1.77	0.04	0.06	1.42	2.06	3.37	0.03	97.67
CLA-B3	75.23	0.09	12.80	1.84	0.08	0.06	1.41	3.89	3.12	0.01	98.52
CLA-B3	71.86	0.18	11.82	2.61	0.08	0.02	0.35	4.53	5.59	0.01	97.05
CLA-B3	70.72	0.79	14.64	3.22	0.06	0.95	2.88	4.78	3.32	0.19	101.55
CLA-B3	69.98	0.74	14.20	3.15	0.04	0.93	2.65	4.55	3.18	0.18	99.61
CLA-B3	69.78	0.18	13.65	2.83	0.10	0.14	1.92	4.23	2.71	0.03	95.57
CLA-B3	69.77	0.70	14.70	3.00	0.04	0.88	2.54	4.56	3.36	0.17	99.72
CLA-B3	69.64	0.81	14.78	3.38	0.06	1.04	3.10	4.48	3.19	0.19	100.66
CLA-B3	68.83	0.77	14.95	3.12	0.05	1.03	2.92	4.78	3.22	0.20	99.88
CLA-B3	68.83	0.76	15.52	3.21	0.06	1.07	2.96	4.98	3.12	0.20	100.70
CLA-B3	68.65	0.69	14.83	2.98	0.06	0.89	2.60	4.11	3.42	0.18	98.42
CLA-B3	68.53	0.81	14.97	3.18	0.05	1.13	2.95	4.78	3.06	0.21	99.67
CLA-B3	68.20	0.72	14.85	3.06	0.04	1.14	3.08	4.50	3.17	0.20	98.95
CLA-B3	68.09	0.79	15.09	3.25	0.05	1.08	2.90	3.67	3.17	0.20	98.31
CLA-B3	67.72	0.74	14.73	3.24	0.06	1.11	3.02	4.76	3.23	0.19	98.78
CLA-B3	67.31	0.78	14.48	3.08	0.05	0.99	2.96	4.55	3.07	0.20	97.46
CLA-B3	67.21	0.65	14.90	3.21	0.05	1.07	3.39	4.43	3.11	0.17	98.19
CLA-B3	67.06	0.80	15.18	3.32	0.05	1.11	3.14	4.62	3.20	0.22	98.70
CLA-B3	65.55	0.79	14.33	3.15	0.04	1.03	2.96	4.45	3.29	0.20	95.79
CLA-B3	65.38	0.72	14.52	3.25	0.03	1.00	2.69	4.29	3.24	0.19	95.31

CLA-B4 = AD 860 B Standard data = Group 2

	SiO_2	TiO_2	Al_2O_3	FeO	MnO	MgO	CaO	Na_2O	K_2O	P_2O_5	Total
CLA-B4	73.98	0.22	14.43	1.62	0.05	0.39	1.93	2.05	2.94	0.05	97.67
CLA-B4	73.70	0.20	14.72	1.47	0.05	0.41	1.99	4.07	3.04	0.06	99.71
CLA-B4	73.11	0.21	14.21	1.49	0.03	0.42	2.09	4.14	3.13	0.05	98.88
CLA-B4	73.08	0.20	14.22	1.65	0.03	0.41	1.96	4.28	3.14	0.06	99.03
CLA-B4	72.88	0.20	14.17	1.55	0.04	0.39	2.10	4.25	3.19	0.06	98.82
CLA-B4	72.83	0.21	14.10	1.44	0.05	0.42	1.93	4.34	3.04	0.05	98.40
CLA-B4	72.63	0.21	14.33	1.58	0.04	0.34	1.96	4.27	3.01	0.05	98.41
CLA-B4	72.55	0.19	14.14	1.58	0.04	0.39	1.90	4.24	3.15	0.07	98.23
CLA-B4	72.47	0.20	13.87	1.60	0.04	0.41	1.93	4.08	2.99	0.05	97.65
CLA-B4	72.40	0.21	13.76	1.39	0.05	0.39	1.92	3.74	3.04	0.06	96.97
CLA-B4	72.00	0.20	13.35	1.54	0.05	0.41	1.98	3.90	3.08	0.06	96.56
CLA-B4	71.03	0.16	15.00	1.21	0.04	0.28	2.35	4.52	2.59	0.05	97.23

CLA-B5 = Microlite GB4-150 Standard data = Group 4

	SiO_2	TiO_2	Al_2O_3	FeO	MnO	MgO	CaO	Na_2O	K_2O	P_2O_5	Total
CLA-B5	74.95	0.12	12.39	1.26	0.03	0.08	0.83	4.29	3.74	0.01	97.70
CLA-B5	74.93	0.12	12.11	1.20	0.03	0.07	0.67	3.07	4.44	0.02	96.67
CLA-B5	74.43	0.16	12.45	1.38	0.04	0.09	0.83	4.20	4.29	0.02	97.88
CLA-B5	74.14	0.16	12.57	1.55	0.04	0.12	1.00	3.33	4.27	0.02	97.21
CLA-B5	72.82	0.15	12.50	1.72	0.05	0.10	0.90	3.90	4.21	0.02	96.38
CLA-B5	72.05	0.69	12.74	3.43	0.12	0.42	0.77	3.68	3.36	0.09	97.36
CLA-B5	70.55	0.75	12.80	3.44	0.13	0.44	1.55	4.57	3.29	0.11	97.64
CLA-B5	68.31	0.74	12.60	3.29	0.14	0.53	1.56	4.32	3.88	0.11	95.48
CLA-B5	65.99	1.36	13.98	5.60	0.19	1.34	3.80	4.58	2.47	0.34	99.67
CLA-B5	65.93	1.36	14.03	5.66	0.19	1.27	3.43	4.79	2.80	0.34	99.78
CLA-B5	65.86	1.35	13.69	6.24	0.19	1.47	3.94	4.94	2.48	0.34	100.50
CLA-B5	65.54	1.32	13.57	6.30	0.21	1.34	3.63	4.52	2.55	0.35	99.33
CLA-B5	65.44	1.35	13.89	5.98	0.19	1.38	3.47	4.93	2.60	0.33	99.55
CLA-B5	65.30	1.35	13.61	6.09	0.19	1.39	3.47	4.94	2.57	0.35	99.26
CLA-B5	65.12	1.27	13.80	6.16	0.19	1.52	3.87	4.47	2.45	0.31	99.17
CLA-B5	65.06	1.35	13.53	5.63	0.20	1.36	3.44	4.85	2.53	0.34	98.30
CLA-B5	65.04	1.32	13.56	6.48	0.21	1.54	3.62	4.37	2.52	0.36	99.02

CLA-B6-B7 Hekla 4 + SILK N2 Standard data = Group 2

	SiO_2	TiO_2	Al_2O_3	FeO	MnO	MgO	CaO	Na_2O	K_2O	P_2O_5	Total
CLA-B6-7	74.56	0.09	12.69	1.81	0.08	0.03	1.30	4.58	2.76	0.02	97.91
CLA-B6-7	74.00	0.09	12.40	1.67	0.08	0.00	1.30	4.74	2.89	0.01	97.17
CLA-B6-7	73.68	0.07	12.23	1.78	0.07	0.01	1.24	3.98	2.66	0.01	95.73
CLA-B6-7	73.65	0.07	12.34	1.70	0.07	0.01	1.19	3.77	2.70	0.01	95.53
CLA-B6-7	73.63	0.09	12.60	2.00	0.08	0.03	1.34	4.57	2.79	0.02	97.14
CLA-B6-7	73.58	0.07	12.09	1.81	0.06	0.04	1.31	4.04	2.70	0.01	95.71
CLA-B6-7	73.50	0.08	12.08	1.81	0.07	0.03	1.36	4.68	2.82	0.07	96.50
CLA-B6-7	73.35	0.09	12.07	1.87	0.08	0.00	1.43	4.56	2.87	0.01	96.32
CLA-B6-7	73.34	0.09	12.54	1.77	0.06	0.01	1.25	4.34	2.73	0.01	96.13
CLA-B6-7	73.15	0.08	12.59	1.83	0.07	0.02	1.41	4.03	2.70	0.01	95.91
CLA-B6-7	73.15	0.07	11.66	1.87	0.07	0.04	1.39	4.35	2.62	0.02	95.24
CLA-B6-7	72.75	0.17	13.37	3.00	0.11	0.02	1.98	5.20	2.44	0.03	99.06
CLA-B6-7	72.75	0.09	12.67	1.99	0.07	0.00	1.27	4.30	2.77	0.03	95.94
CLA-B6-7	72.65	0.09	12.58	1.83	0.08	0.01	1.34	4.37	2.82	0.02	95.78
CLA-B6-7	71.53	0.14	12.61	2.04	0.09	0.07	1.43	4.47	2.70	0.02	95.08
CLA-B6-7	71.02	0.68	13.70	3.29	0.14	0.53	1.42	5.10	3.36	0.09	99.35
CLA-B6-7	70.11	0.16	13.20	3.02	0.13	0.05	1.85	4.84	2.45	0.02	95.85
CLA-B6-7	68.14	0.32	13.89	5.96	0.19	0.19	3.26	5.03	2.11	0.08	99.17
CLA-B6-7	67.80	0.34	13.55	5.31	0.19	0.21	3.01	4.85	2.06	0.08	97.40
CLA-B6-7	66.76	0.44	13.95	6.63	0.24	0.26	3.58	4.90	2.01	0.10	98.87
CLA-B6-7	65.96	1.44	14.03	6.10	0.18	1.41	3.67	4.74	2.60	0.42	100.57
CLA-B6-7	64.92	1.43	13.47	6.23	0.18	1.36	3.40	4.66	2.56	0.37	98.56
CLA-B6-7	64.76	1.43	13.60	5.81	0.18	1.29	3.43	4.47	2.65	0.35	97.98
CLA-B6-7	64.75	1.44	13.83	5.87	0.17	1.35	3.58	4.58	2.73	0.34	98.63
CLA-B6-7	64.63	1.43	13.14	5.86	0.17	1.29	3.48	4.64	2.76	0.33	97.74

CLA-B6-7	64.57	1.43	13.66	5.70	0.18	1.39	3.40	4.43	2.67	0.34	97.77
CLA-B6-7	64.25	1.50	13.37	5.65	0.20	1.45	3.64	4.39	2.72	0.37	97.56
CLA-B6-7	63.41	1.41	13.46	6.02	0.14	1.44	3.56	4.36	2.63	0.34	96.78
CLA-B6-7	49.96	3.24	12.32	14.43	0.22	4.81	9.32	2.69	0.54	0.36	97.88

CLA-B8 = Lairg A Standard data = Group 3

	SiO_2	TiO_2	Al_2O_3	FeO	MnO	MgO	CaO	Na_2O	K_2O	P_2O_5	Total
CLA-B8	73.13	0.17	11.76	1.56	0.03	0.14	0.93	3.90	3.71	0.04	95.37
CLA-B8	*73.04*	*0.08*	*12.02*	*1.57*	*0.07*	*0.00*	*1.26*	*3.50*	*2.83*	*0.02*	*94.38*
CLA-B8	60.60	1.16	14.81	8.94	0.27	1.82	5.16	4.30	1.55	0.43	99.03
CLA-B8	50.46	2.67	13.15	12.20	0.20	5.80	10.11	2.84	0.48	0.31	98.22

CLA-L1 = Unknown #3 Grímsvötn basaltic tephra Standard data = Group 5

	SiO_2	TiO_2	Al_2O_3	FeO	MnO	MgO	CaO	Na_2O	K_2O	P_2O_5	Total
CLA-L1	67.30	1.30	14.25	5.50	0.18	1.21	3.12	4.99	2.81	0.30	100.96
CLA-L1	63.78	0.92	14.96	7.42	0.18	1.24	4.46	4.53	1.87	0.33	99.70
CLA-L1	50.71	2.34	14.85	11.70	0.19	5.54	10.92	3.02	0.38	0.28	99.92
CLA-L1	50.70	2.54	13.76	11.39	0.19	6.73	11.59	2.51	0.45	0.25	100.10
CLA-L1	50.69	2.52	13.12	12.83	0.20	6.18	10.66	2.68	0.41	0.27	99.56
CLA-L1	50.54	2.65	13.69	13.29	0.22	5.86	10.33	2.81	0.40	0.28	100.08
CLA-L1	50.53	2.53	13.26	13.36	0.19	5.80	10.67	2.66	0.37	0.29	99.67
CLA-L1	50.48	2.52	13.68	12.26	0.21	6.07	10.85	2.68	0.38	0.26	99.41
CLA-L1	50.46	2.56	13.72	13.02	0.20	6.06	10.79	2.60	0.36	0.29	100.06
CLA-L1	50.37	2.49	13.37	12.81	0.19	6.23	10.73	2.73	0.39	0.25	99.56
CLA-L1	50.34	2.58	13.50	11.59	0.18	6.89	11.75	2.65	0.38	0.29	100.15
CLA-L1	50.29	2.49	13.63	13.07	0.20	6.18	10.80	2.57	0.35	0.28	99.87
CLA-L1	50.16	2.63	13.47	13.65	0.24	5.52	10.32	2.72	0.38	0.29	99.37
CLA-L1	49.89	2.57	13.44	11.70	0.20	6.57	11.76	3.10	0.38	0.27	99.88
CLA-L1	49.85	2.87	12.92	13.36	0.20	5.52	10.06	2.70	0.48	0.32	98.29
CLA-L1	49.63	2.52	13.18	12.50	0.19	6.18	10.53	2.57	0.38	0.28	97.96
CLA-L1	49.21	2.50	13.44	13.25	0.21	6.35	10.66	2.55	0.41	0.26	98.83
CLA-L1	49.18	2.55	13.26	12.47	0.17	6.45	10.95	2.76	0.46	0.28	98.52
CLA-L1	49.07	2.53	13.01	12.98	0.21	6.26	10.91	2.90	0.39	0.29	98.55

CLA-L2 = MOR T4 Standard data = Group 6

	SiO_2	TiO_2	Al_2O_3	FeO	MnO	MgO	CaO	Na_2O	K_2O	P_2O_5	Total
CLA-L2	70.38	0.79	14.87	3.12	0.05	0.87	2.55	4.28	3.23	0.19	100.34
CLA-L2	68.33	0.78	16.06	3.55	0.05	1.03	3.24	4.48	3.23	0.21	100.96

CLA-L3 = Hekla 4 Standard data = Group 6

	SiO_2	TiO_2	Al_2O_3	FeO	MnO	MgO	CaO	Na_2O	K_2O	P_2O_5	Total
CLA-L3	72.77	0.20	11.47	3.57	0.10	-0.01	1.38	3.77	3.23	0.02	96.52

CLA-L4 = Lairg B Standard data = Group 5

	SiO_2	TiO_2	Al_2O_3	FeO	MnO	MgO	CaO	Na_2O	K_2O	P_2O_5	Total
CLA-L4	71.56	0.29	14.61	2.18	0.06	0.24	1.04	5.15	4.62	0.04	99.78
CLA-L4	71.13	0.24	14.25	2.32	0.05	0.17	0.91	5.07	4.77	0.04	98.97
CLA-L4	71.04	0.19	13.90	2.22	0.04	0.14	0.73	5.27	4.73	0.03	98.29
CLA-L4	70.30	0.19	13.38	2.27	0.05	0.15	0.74	5.27	4.51	0.03	96.90
CLA-L4	70.27	0.20	13.68	2.23	0.06	0.14	0.76	5.20	4.56	0.02	97.10
CLA-L4	70.07	0.20	13.80	2.25	0.06	0.11	0.71	5.06	4.65	0.02	96.93
CLA-L4	69.99	0.39	13.85	2.86	0.07	0.29	1.15	5.07	4.30	0.05	98.02
CLA-L4	69.91	0.26	13.92	2.70	0.08	0.26	1.09	5.21	4.17	0.03	97.64
CLA-L4	69.89	0.20	13.65	2.19	0.08	0.18	0.65	5.40	4.47	0.02	96.73
CLA-L4	69.87	0.19	13.00	2.24	0.06	0.14	0.72	5.38	4.58	0.02	96.19
CLA-L4	69.86	0.21	13.55	1.99	0.04	0.15	0.78	5.10	4.51	0.02	96.22
CLA-L4	69.66	0.19	13.53	2.18	0.08	0.13	0.74	5.35	4.57	0.02	96.46
CLA-L4	69.64	0.21	13.73	1.97	0.08	0.17	0.70	5.23	4.58	0.01	96.31
CLA-L4	69.56	0.19	13.39	2.04	0.05	0.12	0.66	5.22	4.60	0.03	95.86
CLA-L4	69.52	0.31	14.23	2.67	0.05	0.27	1.21	5.15	4.55	0.04	97.99
CLA-L4	69.49	0.34	14.36	2.95	0.09	0.37	1.35	5.24	4.26	0.05	98.49
CLA-L4	69.30	0.50	14.32	3.43	0.09	0.43	1.34	5.01	4.27	0.10	98.79
CLA-L4	69.03	0.22	13.94	2.26	0.07	0.19	0.92	5.27	4.48	0.03	96.42
CLA-L4	68.98	0.32	14.10	3.27	0.09	0.65	1.61	4.96	4.23	0.07	98.28
CLA-L4	68.84	0.42	14.86	3.44	0.05	0.45	1.45	5.24	4.20	0.08	99.01
CLA-L4	68.04	0.23	13.64	2.40	0.06	0.18	0.84	5.25	4.41	0.03	95.08

CLA-L5 = Lairg A Standard data = Group 5

	SiO_2	TiO_2	Al_2O_3	FeO	MnO	MgO	CaO	Na_2O	K_2O	P_2O_5	Total
CLA-L5	75.97	0.09	12.69	1.82	0.06	0.05	1.23	4.60	2.71	0.03	99.24
CLA-L5	75.71	0.08	12.64	1.59	0.08	0.04	1.37	4.43	2.80	0.01	98.74
CLA-L5	75.35	0.07	12.04	1.70	0.03	0.04	1.32	4.26	2.85	0.01	97.68
CLA-L5	74.94	0.08	12.06	1.65	0.07	0.04	1.34	4.49	2.68	0.01	97.38
CLA-L5	74.74	0.07	12.10	1.78	0.06	0.02	1.31	4.11	2.81	0.01	97.01
CLA-L5	74.53	0.08	12.08	1.74	0.07	0.01	1.27	4.14	2.67	0.01	96.59
CLA-L5	74.53	0.07	11.87	1.61	0.05	0.07	1.28	4.25	2.72	0.01	96.47
CLA-L5	74.47	0.09	12.36	1.71	0.07	0.03	1.36	4.24	2.68	0.02	97.02
CLA-L5	74.38	0.06	13.60	1.53	0.06	0.02	1.63	4.61	2.52	0.01	98.43
CLA-L5	74.35	0.07	12.19	1.51	0.08	0.04	1.32	4.07	2.76	0.01	96.40
CLA-L5	74.09	0.08	12.59	1.74	0.07	0.01	1.39	4.24	2.74	0.01	96.94
CLA-L5	74.02	0.08	12.24	1.64	0.06	0.03	1.16	4.44	2.78	0.01	96.47
CLA-L5	73.83	0.07	12.46	1.62	0.04	0.04	1.27	4.05	2.84	0.03	96.24
CLA-L5	73.65	0.08	12.32	1.73	0.07	0.03	1.27	4.31	2.63	0.01	96.11
CLA-L5	73.56	0.08	12.43	1.63	0.05	0.05	1.27	4.31	2.79	0.02	96.19
CLA-L5	73.47	0.09	12.29	1.51	0.05	0.04	1.24	4.19	2.70	0.02	95.61
CLA-L5	73.45	0.08	12.13	1.46	0.05	0.02	1.34	4.40	2.72	0.04	95.69
CLA-L5	73.44	0.07	12.25	1.61	0.07	0.03	1.27	4.09	2.58	0.03	95.45
CLA-L5	73.18	0.08	12.20	1.46	0.05	0.04	1.28	4.20	2.72	0.01	95.22
CLA-L5	73.14	0.09	11.99	1.54	0.05	0.03	1.32	4.21	2.76	0.02	95.14

SV-B1 = Askja 1875 Standard data = Group 4

	SiO_2	TiO_2	Al_2O_3	FeO	MnO	MgO	CaO	Na_2O	K_2O	P_2O_5	Total
SV-B1	75.20	0.68	11.52	2.99	0.08	0.49	2.00	3.27	2.54	0.10	98.89
SV-B1	74.49	0.75	12.03	3.11	0.10	0.58	2.28	4.11	2.50	0.13	100.08
SV-B1	74.32	0.80	12.53	3.37	0.11	0.65	2.49	3.77	2.44	0.15	100.62
SV-B1	74.15	0.76	12.38	3.13	0.09	0.63	2.34	4.06	2.52	0.13	100.17
SV-B1	74.12	0.79	12.52	3.59	0.10	0.69	2.51	3.97	2.39	0.15	100.82
SV-B1	73.94	0.82	12.26	3.44	0.10	0.71	2.64	4.14	2.42	0.16	100.63
SV-B1	73.71	0.80	12.07	3.57	0.10	0.72	2.57	3.77	2.41	0.14	99.88
SV-B1	73.58	0.80	12.55	3.56	0.10	0.79	2.51	3.99	2.38	0.17	100.43
SV-B1	73.53	0.79	12.30	3.52	0.11	0.70	2.35	3.90	2.52	0.14	99.88
SV-B1	73.46	0.81	12.27	3.33	0.09	0.72	2.46	4.06	2.37	0.16	99.75
SV-B1	72.92	0.81	12.27	3.65	0.10	0.70	2.54	3.84	2.35	0.18	99.37
SV-B1	72.78	0.82	12.15	3.39	0.10	0.76	2.56	2.99	2.44	0.17	98.17
SV-B1	72.51	0.80	12.52	3.47	0.11	0.78	2.52	3.67	2.42	0.19	98.98
SV-B1	72.38	0.80	12.17	3.27	0.10	0.69	2.40	3.70	2.51	0.16	98.17
SV-B1	72.26	0.80	12.25	3.60	0.11	0.73	2.54	4.05	2.35	0.18	98.89
SV-B1	71.65	0.67	12.07	3.31	0.10	0.58	2.39	3.66	2.33	0.15	96.91

SV-B2 = Hekla1158 + Hekla 1104 Standard data = Group 3

	SiO_2	TiO_2	Al_2O_3	FeO	MnO	MgO	CaO	Na_2O	K_2O	P_2O_5	Total
SV-B2	71.11	0.20	13.75	3.35	0.10	0.11	1.93	4.62	2.74	0.03	97.94
SV-B2	68.20	0.47	14.16	5.53	0.18	0.46	2.99	4.79	2.28	0.11	99.16
SV-B2	68.15	0.51	12.79	6.80	0.22	0.46	2.66	4.41	2.61	0.10	98.69
SV-B2	67.93	0.48	14.06	5.58	0.19	0.43	3.04	4.58	2.27	0.11	98.67
SV-B2	67.90	0.44	14.37	4.95	0.16	0.33	3.29	5.09	2.13	0.11	98.77
SV-B2	67.70	0.47	13.98	5.53	0.18	0.37	3.07	4.83	2.35	0.09	98.59
SV-B2	67.57	0.46	14.46	5.71	0.17	0.42	3.10	4.70	2.26	0.11	98.97
SV-B2	67.39	0.47	13.88	5.11	0.18	0.45	3.09	5.12	2.35	0.10	98.15
SV-B2	67.38	0.43	14.93	5.36	0.15	0.41	3.18	4.62	2.18	0.09	98.73
SV-B2	67.34	0.47	13.65	5.37	0.18	0.36	2.89	4.39	2.43	0.10	97.19
SV-B2	67.34	0.46	14.23	5.58	0.17	0.41	3.02	4.59	2.38	0.10	98.28
SV-B2	67.14	0.47	13.88	5.90	0.18	0.42	2.79	4.36	2.59	0.10	97.82
SV-B2	67.10	0.47	14.71	5.56	0.19	0.41	2.90	4.55	2.25	0.10	98.22
SV-B2	67.02	0.46	13.83	5.76	0.19	0.44	3.02	4.76	2.22	0.10	97.80
SV-B2	66.74	0.44	16.14	4.77	0.17	0.34	3.56	5.29	1.98	0.09	99.53

SV-B3 = Hekla 3 Standard data = Group 1

	SiO_2	TiO_2	Al_2O_3	FeO	MnO	MgO	CaO	Na_2O	K_2O	P_2O_5	Total
SV-B3	74.59	0.09	12.77	1.94	0.08	0.02	1.33	4.46	3.00	0.02	98.30
SV-B3	74.55	0.22	12.94	1.15	0.05	0.33	1.38	3.38	2.98	0.04	97.00
SV-B3	73.69	0.09	12.51	1.78	0.08	0.02	1.40	3.80	2.99	0.03	96.39
SV-B3	73.62	0.18	14.18	3.16	0.09	0.13	2.03	4.01	2.62	0.04	100.06
SV-B3	73.43	0.09	12.43	1.92	0.08	0.00	1.37	4.57	2.91	0.01	96.80

SV-B3	72.84	0.18	13.83	2.96	0.10	0.12	2.00	5.00	2.52	0.02	99.56
SV-B3	72.77	0.19	13.92	3.10	0.10	0.11	1.90	4.84	2.52	0.02	99.48
SV-B3	72.67	0.18	13.98	3.02	0.10	0.14	2.14	5.04	2.54	0.03	99.85
SV-B3	72.46	0.18	13.72	2.91	0.10	0.09	2.06	4.70	2.45	0.02	98.69
SV-B3	72.17	0.18	13.45	3.20	0.11	0.12	2.04	4.80	2.56	0.03	98.65
SV-B3	72.15	0.18	14.16	2.79	0.10	0.15	2.00	5.00	2.65	0.04	99.22
SV-B3	71.94	0.18	13.47	2.80	0.09	0.11	1.97	4.52	2.61	0.03	97.72
SV-B3	71.61	0.87	12.15	3.83	0.12	0.75	2.95	3.87	2.42	0.21	98.80
SV-B3	71.13	0.18	13.63	3.01	0.10	0.09	2.01	3.77	2.63	0.03	96.57
SV-B3	70.66	0.23	13.96	3.51	0.12	0.13	2.38	4.80	2.43	0.04	98.27
SV-B3	69.96	0.14	13.27	2.71	0.09	0.10	1.99	4.02	2.63	0.05	94.96
SV-B3	69.48	0.35	13.00	4.77	0.22	0.08	0.50	6.70	4.93	0.04	100.06
SV-B3	69.32	0.23	14.01	3.65	0.14	0.13	2.37	4.74	2.46	0.05	97.11
SV-B3	68.59	0.35	12.54	4.84	0.21	0.09	0.51	6.49	4.55	0.03	98.20
SV-B3	68.42	0.37	14.92	5.34	0.17	0.37	3.18	4.42	2.15	0.10	99.45
SV-B3	67.13	0.42	14.28	5.65	0.19	0.45	3.31	5.09	2.09	0.11	98.72

SV-B4 = Hekla-S/Kebister Standard data = Group 6

	SiO_2	TiO_2	Al_2O_3	FeO	MnO	MgO	CaO	Na_2O	K_2O	P_2O_5	Total
SV-B4	70.72	0.47	14.59	2.28	0.15	0.54	1.89	5.00	3.01	0.09	98.74
SV-B4	70.54	0.17	12.96	3.01	0.09	0.11	1.85	4.38	2.67	0.04	95.83
SV-B4	70.50	0.18	13.25	3.04	0.09	0.09	1.94	4.03	2.56	0.04	95.73
SV-B4	68.35	0.74	14.18	4.52	0.15	0.49	2.03	4.52	3.27	0.14	98.40
SV-B4	66.66	0.42	14.32	5.56	0.15	0.45	3.28	4.29	2.07	0.16	97.37

SV-B5 = Hekla 4 Standard data = Group 6

	SiO_2	TiO_2	Al_2O_3	FeO	MnO	MgO	CaO	Na_2O	K_2O	P_2O_5	Total
SV-B5	76.70	0.09	12.62	1.28	0.06	0.03	1.05	4.15	2.94	0.02	98.94
SV-B5	75.28	0.36	11.09	2.33	0.10	0.09	0.38	3.92	4.23	0.01	97.79
SV-B5	75.10	0.07	12.21	1.73	0.07	0.02	1.37	3.99	2.74	0.00	97.30
SV-B5	75.08	0.10	12.28	1.68	0.09	0.03	1.24	4.53	2.90	0.01	97.94
SV-B5	74.47	0.09	12.96	2.06	0.08	0.01	1.33	4.69	2.82	0.01	98.54
SV-B5	74.38	0.20	11.81	2.37	0.08	0.01	0.43	4.57	3.93	0.01	97.77
SV-B5	73.88	0.10	13.53	1.90	0.08	0.02	1.36	4.11	2.89	0.06	97.93
SV-B5	73.70	0.09	12.63	1.82	0.09	0.01	1.27	4.25	2.81	0.01	96.69
SV-B5	73.60	0.10	12.71	1.96	0.08	0.03	1.28	4.45	2.74	0.01	96.95
SV-B5	73.41	0.09	12.39	1.90	0.08	0.01	1.33	4.08	2.89	0.01	96.19
SV-B5	73.33	0.10	12.38	1.99	0.06	0.00	1.28	4.65	2.88	0.03	96.70
SV-B5	73.29	0.09	12.71	1.81	0.09	0.02	1.34	4.07	2.77	0.01	96.19
SV-B5	73.28	0.08	12.53	1.84	0.07	0.02	1.33	4.29	2.88	0.06	96.39
SV-B5	73.24	0.09	13.21	2.12	0.08	0.02	1.35	4.52	2.83	0.01	97.48
SV-B5	72.86	0.10	12.12	1.79	0.09	0.03	1.25	4.22	2.78	0.02	95.25
SV-B5	*69.74*	*0.33*	*12.08*	*3.66*	*0.13*	*0.22*	*1.71*	*3.78*	*2.56*	*0.26*	*94.47*

SV-B6 = Lairg A Standard data = Group 1

	SiO_2	TiO_2	Al_2O_3	FeO	MnO	MgO	CaO	Na_2O	K_2O	P_2O_5	Total
SV-B6	76.08	0.07	12.37	1.75	0.06	0.01	1.25	4.39	2.66	0.00	98.64

SV-B6	75.78	0.07	12.10	1.73	0.05	0.03	1.24	4.38	2.71	0.01	98.12
SV-B6	75.69	0.07	12.67	1.65	0.07	0.06	1.29	4.58	2.76	0.01	98.85
SV-B6	75.66	0.07	12.36	1.81	0.06	0.04	1.34	4.55	2.69	0.01	98.59
SV-B6	75.45	0.07	12.58	1.46	0.06	0.03	1.30	4.31	2.61	0.03	97.90
SV-B6	75.45	0.07	12.55	1.63	0.07	0.04	1.28	4.62	2.55	0.01	98.27
SV-B6	75.40	0.07	12.33	1.51	0.06	0.02	1.34	4.53	2.65	0.02	97.92
SV-B6	75.39	0.08	12.09	1.70	0.06	0.01	1.25	4.28	2.66	0.02	97.53
SV-B6	75.36	0.08	12.42	1.68	0.07	0.04	1.31	4.42	2.73	0.01	98.11
SV-B6	75.35	0.08	12.81	1.55	0.06	0.03	1.36	4.31	2.74	0.01	98.29
SV-B6	75.34	0.09	12.31	1.67	0.06	0.04	1.27	4.48	2.61	0.01	97.88
SV-B6	75.32	0.07	12.39	1.82	0.06	0.04	1.29	4.57	2.95	0.02	98.54
SV-B6	75.30	0.08	12.46	1.67	0.06	0.02	1.34	4.32	2.73	0.02	97.98
SV-B6	75.12	0.09	12.41	1.57	0.06	0.06	1.24	4.56	2.66	0.01	97.78
SV-B6	74.90	0.08	12.57	1.63	0.06	0.04	1.33	4.46	2.70	0.01	97.78
SV-B6	74.88	0.08	12.34	1.66	0.07	0.00	1.34	4.35	2.66	0.01	97.38
SV-B6	74.86	0.08	12.64	1.62	0.07	0.05	1.35	4.59	2.84	0.02	98.13
SV-B6	74.85	0.08	12.30	1.64	0.07	0.04	1.28	4.37	2.60	0.00	97.22
SV-B6	74.84	0.07	12.38	1.62	0.07	0.04	1.25	4.23	2.78	0.02	97.30
SV-B6	74.73	0.08	12.16	1.76	0.06	0.04	1.32	4.48	2.75	0.02	97.40
SV-B6	74.68	0.07	12.52	1.62	0.07	0.04	1.30	4.66	2.70	0.02	97.69
SV-B6	74.23	0.07	12.27	1.69	0.06	0.03	1.39	4.73	2.64	0.02	97.11
SV-B6	73.92	0.07	13.47	1.47	0.06	0.04	1.51	5.04	2.33	0.01	97.92

SV-L1 = Hekla 1104 + Hekla 1158 Standard data = Group 7

	SiO_2	TiO_2	Al_2O_3	FeO	MnO	MgO	CaO	Na_2O	K_2O	P_2O_5	Total
SV-L1	74.69	0.16	13.09	1.83	0.04	0.10	0.92	4.78	3.70	0.01	99.30
SV-L1	73.62	0.21	15.26	1.47	0.04	0.37	1.94	4.99	3.25	0.06	101.21
SV-L1	73.02	0.20	14.17	1.64	0.02	0.44	2.04	5.27	3.24	0.05	100.10
SV-L1	72.55	0.20	13.65	3.16	0.12	0.14	2.01	5.51	2.83	0.02	100.18
SV-L1	72.45	0.20	14.98	3.41	0.10	0.13	1.92	5.65	2.80	0.02	101.66
SV-L1	72.34	0.22	14.72	3.17	0.11	0.11	2.07	5.34	2.82	0.02	100.93
SV-L1	71.91	0.20	14.07	3.28	0.12	0.16	2.00	5.33	2.79	0.03	99.89
SV-L1	71.75	0.20	14.59	3.12	0.11	0.13	2.02	5.49	2.73	0.03	100.15
SV-L1	70.07	0.56	12.74	6.24	0.22	0.42	2.34	4.97	2.90	0.11	100.58
SV-L1	69.90	0.20	14.71	3.19	0.10	0.08	1.85	5.18	2.63	0.02	97.87
SV-L1	68.91	0.47	14.51	5.83	0.15	0.46	3.04	5.48	2.36	0.09	101.29
SV-L1	68.67	0.46	15.22	5.79	0.16	0.47	3.15	5.26	2.36	0.08	101.64
SV-L1	68.50	0.48	14.77	5.49	0.16	0.46	3.17	5.54	2.29	0.10	100.95
SV-L1	68.28	0.48	15.33	5.67	0.18	0.42	3.12	5.48	2.36	0.10	101.42
SV-L1	67.91	0.46	14.26	5.74	0.18	0.49	3.12	5.12	2.39	0.09	99.77
SV-L1	67.77	0.47	14.95	5.80	0.18	0.44	3.08	4.83	2.38	0.08	99.99
SV-L1	67.62	0.47	15.79	5.43	0.15	0.42	3.14	5.15	2.28	0.09	100.54
SV-L1	67.48	0.47	14.71	5.62	0.18	0.46	3.00	5.43	2.28	0.10	99.72
SV-L1	66.94	0.29	18.25	3.22	0.09	0.24	4.46	6.63	1.44	0.06	101.63
SV-L1	50.48	1.93	14.12	13.07	0.21	6.43	11.17	2.66	0.21	0.17	100.47
SV-L1	49.94	1.90	14.09	12.79	0.22	6.70	11.39	2.70	0.29	0.19	100.22

SV-L2 = QUB 570 Group 2 (c. AD 650)?(Unknown #2) Standard data = Group 8

	SiO_2	TiO_2	Al_2O_3	FeO	MnO	MgO	CaO	Na_2O	K_2O	P_2O_5	Total
SV-L2	64.66	0.95	16.50	6.54	0.18	1.45	4.65	4.83	1.59	0.33	101.68
SV-L2	64.43	0.93	16.39	6.33	0.14	1.36	4.50	4.67	1.52	0.30	100.58
SV-L2	64.15	0.95	15.54	6.82	0.14	1.35	4.60	4.68	1.57	0.35	100.15
SV-L2	63.93	0.99	15.27	7.06	0.19	1.56	5.01	4.59	1.56	0.34	100.50
SV-L2	63.85	0.94	16.19	6.79	0.17	1.44	4.76	4.97	1.59	0.31	101.00
SV-L2	63.76	0.96	15.59	6.92	0.16	1.40	4.75	5.02	1.64	0.31	100.49
SV-L2	63.49	0.89	18.66	5.05	0.18	1.06	5.57	5.45	1.16	0.31	101.83
SV-L2	63.41	1.03	15.97	7.58	0.18	1.53	4.58	4.71	1.68	0.34	101.01
SV-L2	63.33	1.00	15.92	7.07	0.19	1.52	4.85	5.32	1.56	0.34	101.11
SV-L2	63.13	0.96	15.98	7.26	0.21	1.54	4.94	5.11	1.50	0.33	100.97
SV-L2	63.06	0.99	16.06	7.17	0.17	1.48	5.25	5.19	1.54	0.36	101.27
SV-L2	62.96	1.00	15.52	7.54	0.18	1.49	4.90	5.28	1.53	0.35	100.76
SV-L2	62.72	0.98	15.95	7.23	0.16	1.58	4.87	4.94	1.53	0.34	100.31
SV-L2	62.67	0.98	15.93	6.73	0.19	1.57	4.57	4.83	1.57	0.33	99.36
SV-L2	62.51	0.91	15.42	7.26	0.17	1.52	5.37	5.27	1.41	0.34	100.20
SV-L2	62.34	1.00	16.08	6.98	0.19	1.59	4.84	4.90	1.48	0.35	99.75
SV-L2	62.23	0.83	18.18	5.98	0.17	1.20	5.70	4.81	1.35	0.29	100.74
SV-L2	62.14	0.98	15.40	6.82	0.17	1.59	4.67	5.00	1.50	0.37	98.64
SV-L2	62.06	1.00	16.30	7.10	0.17	1.55	4.78	5.18	1.46	0.38	99.96
SV-L2	60.96	0.98	15.21	6.68	0.18	1.49	4.60	4.91	1.58	0.37	96.95

SV-L3 = Hekla 4 Standard data = Group 7

	SiO_2	TiO_2	Al_2O_3	FeO	MnO	MgO	CaO	Na_2O	K_2O	P_2O_5	Total
SV-L3	76.25	0.08	13.55	1.79	0.09	0.02	1.38	4.78	2.95	0.02	100.92
SV-L3	75.52	0.10	14.18	2.09	0.08	0.04	1.38	5.43	2.77	0.02	101.59
SV-L3	73.96	0.35	12.96	2.24	0.10	0.12	0.48	5.03	4.00	0.03	99.28
SV-L3	73.94	0.07	13.38	1.55	0.04	0.05	1.23	4.99	2.64	0.01	97.90
SV-L3	73.85	0.10	13.17	1.85	0.08	0.03	1.21	5.10	3.00	0.02	98.40
SV-L3	73.61	0.10	13.32	1.75	0.08	0.03	1.38	5.20	2.90	0.01	98.38
SV-L3	72.99	0.09	13.40	2.04	0.10	0.02	1.34	5.07	2.80	0.01	97.87
SV-L3	72.73	0.10	13.99	1.96	0.09	0.01	1.26	5.01	2.88	0.00	98.03
SV-L3	72.73	0.10	13.03	1.95	0.10	0.04	1.31	4.87	2.82	0.02	96.98
SV-L3	72.72	0.09	13.66	1.82	0.05	0.02	1.37	4.93	2.84	0.01	97.50
SV-L3	72.37	0.25	15.78	3.40	0.09	0.14	2.42	5.76	2.35	0.03	102.60
SV-L3	69.99	0.36	14.00	4.33	0.13	0.19	1.58	5.23	3.71	0.08	99.58
SV-L3	67.88	0.23	14.30	3.85	0.13	0.11	2.28	5.17	2.44	0.03	96.43
SV-L3	63.77	0.83	14.91	8.40	0.26	1.05	4.43	5.44	1.83	0.27	101.19
SV-L3	62.62	0.86	16.27	8.57	0.23	1.06	4.54	5.23	1.66	0.32	101.37
SV-L3	62.20	0.90	16.13	8.88	0.27	1.17	4.50	5.05	1.73	0.37	101.19
SV-L3	62.18	0.90	16.42	8.10	0.24	1.12	4.56	4.94	1.56	0.34	100.35
SV-L3	61.58	0.88	15.91	8.56	0.26	1.25	4.98	5.48	1.43	0.29	100.62
SV-L3	61.53	0.91	15.22	8.94	0.28	1.11	4.74	4.82	1.67	0.34	99.56
SV-L3	61.46	0.93	15.29	9.37	0.28	1.10	4.71	5.02	1.66	0.37	100.19
SV-L3	59.68	0.90	15.25	9.19	0.27	1.13	4.46	5.00	1.58	0.33	97.79

SV-L4 = Unknown #5 Standard data = Group 3

	SiO_2	TiO_2	Al_2O_3	FeO	MnO	MgO	CaO	Na_2O	K_2O	P_2O_5	Total
SV-L4	72.05	0.10	13.00	1.73	0.05	-0.01	1.67	5.08	2.65	0.02	96.00
SV-L4	69.58	0.29	13.06	4.67	0.16	0.19	2.53	4.64	2.25	0.07	97.00
SV-L4	68.72	0.32	13.48	5.02	0.19	0.27	2.93	4.24	2.17	0.08	97.00
SV-L4	68.54	0.40	13.36	6.29	0.22	0.38	3.40	4.03	1.98	0.13	99.00
SV-L4	68.43	0.34	14.54	5.13	0.19	0.30	3.00	4.32	2.19	0.09	99.00
SV-L4	68.32	0.40	13.62	6.04	0.20	0.41	3.19	4.25	2.11	0.12	99.00
SV-L4	66.83	0.43	13.28	6.18	0.22	0.41	3.37	4.05	1.93	0.13	97.00

SV-L5 = Lairg A? Standard data = Group 3

	SiO_2	TiO_2	Al_2O_3	FeO	MnO	MgO	CaO	Na_2O	K_2O	P_2O_5	Total
SV-L5	73.47	0.08	12.09	1.50	0.07	0.02	1.28	4.18	2.61	0.01	95.00
SV-L5	73.04	0.08	11.92	1.61	0.06	0.01	1.17	3.94	2.66	0.01	95.00
SV-L5	71.67	0.86	13.08	2.87	0.05	0.52	1.91	4.00	3.40	0.43	98.79
SV-L5	70.87	1.04	13.52	3.86	0.06	0.72	2.40	4.27	3.12	0.21	100.00
SV-L5	70.01	0.73	12.78	3.62	0.06	0.65	2.41	4.19	3.41	0.14	98.01
SV-L5	69.13	1.09	12.68	3.66	0.07	0.83	2.71	4.10	3.00	0.22	97.00
SV-L5	68.52	1.11	13.09	4.44	0.08	1.11	2.87	4.12	3.11	0.26	98.70
SV-L5	67.77	0.92	12.47	3.96	0.06	0.90	2.68	4.24	2.89	0.20	96.00
SV-L5	65.63	0.85	15.75	3.07	0.05	0.77	3.68	4.43	2.73	0.18	97.16
SV-L5	60.40	0.75	19.53	2.16	0.04	0.45	7.50	5.10	1.42	0.87	98.00

MT-1 Glen Garry Standard data = Group 9

	SiO_2	TiO_2	Al_2O_3	FeO	MnO	MgO	CaO	Na_2O	K_2O	P_2O_5	Total
MT-1	73.97	0.51	12.22	3.75	0.09	0.45	2.27	4.14	2.06	0.08	99.53
MT-1	73.68	0.51	12.58	3.91	0.09	0.42	2.36	4.13	2.15	0.09	99.92
MT-1	73.60	0.51	12.58	4.02	0.09	0.41	2.29	4.08	2.01	0.10	99.69
MT-1	73.55	0.51	12.61	3.65	0.08	0.41	2.33	4.04	1.94	0.09	99.21
MT-1	73.43	0.51	12.40	3.91	0.07	0.43	2.37	4.19	2.06	0.07	99.44
MT-1	73.02	0.58	12.55	4.35	0.10	0.47	2.55	4.39	1.97	0.10	100.08
MT-1	72.66	0.51	12.21	3.64	0.09	0.44	2.27	4.36	2.08	0.09	98.36
MT-1	72.30	0.52	12.22	3.74	0.07	0.41	2.31	3.97	2.01	0.08	97.63
MT-1	72.03	0.51	12.04	3.79	0.09	0.38	2.34	4.15	2.03	0.09	97.47
MT-1	71.76	0.51	12.20	3.99	0.07	0.38	2.41	4.10	1.99	0.08	97.49
MT-1	71.71	0.67	12.85	4.33	0.10	0.63	2.86	4.17	1.84	0.14	99.31
MT-1	71.57	0.66	12.75	4.81	0.09	0.61	2.82	4.24	1.86	0.14	99.55
MT-1	71.37	0.66	13.17	4.59	0.11	0.61	2.96	4.14	1.85	0.14	99.59
MT-1	70.94	0.77	12.80	5.16	0.10	0.69	3.22	3.99	1.79	0.16	99.62
MT-1	70.84	0.72	12.94	4.90	0.13	0.67	3.01	4.05	1.77	0.15	99.17

MM-1 = Glen Garry *

	SiO_2	TiO_2	Al_2O_3	FeO	MnO	MgO	CaO	Na_2O	K_2O	P_2O_5	Total
MM-1	69.98	0.76	12.36	4.95	0.14	0.69	3.12	3.72	1.83	-	97.56
MM-1	70.64	0.69	12.48	4.65	0.08	0.65	2.88	3.78	1.94	-	97.79
MM-1	73.76	0.50	10.42	3.90	0.11	0.40	2.35	3.01	2.04	-	96.49

MM-1	73.10	0.53	11.91	3.80	0.14	0.40	2.42	3.41	2.01	-	97.72
MM-1	71.89	0.61	12.21	3.99	0.09	0.42	2.45	3.69	1.99	-	97.35
MM-1	71.02	0.67	13.48	4.64	0.18	0.64	2.72	4.26	1.90	-	99.51
MM-1	71.75	0.59	12.31	3.54	0.13	0.30	2.12	2.70	2.23	-	95.66
MM-1	70.85	0.71	12.72	4.38	0.06	0.62	2.84	3.62	1.86	-	97.66
MM-1	74.07	0.45	13.06	4.00	0.15	0.41	2.25	3.08	2.13	-	99.60
MM-1	73.16	0.48	12.93	4.14	0.07	0.40	2.28	4.21	2.03	-	99.70
MM-1	72.28	0.58	12.71	3.52	0.11	0.41	2.29	4.52	2.10	-	98.52
MM-1	70.96	0.78	11.34	4.96	0.21	0.76	3.00	4.31	1.80	-	98.11

MM-2 = Hekla 4 *

	SiO_2	TiO_2	Al_2O_3	FeO	MnO	MgO	CaO	Na_2O	K_2O	P_2O_5	Total
MM-2	72.38	0.10	12.62	1.87	0.07	0.04	1.19	4.40	2.67	-	95.34
MM-2	72.58	0.14	12.54	1.75	0.10	0.02	1.30	4.18	2.79	-	95.39
MM-2	72.41	0.12	12.57	1.97	0.05	0.03	1.26	4.38	2.75	-	95.53
MM-2	72.86	0.13	12.46	1.93	0.09	0.02	1.30	4.17	2.83	-	95.79
MM-2	72.81	0.10	12.56	1.95	0.05	0.00	1.33	4.64	2.70	-	96.15
MM-2	73.23	0.09	12.57	1.99	0.03	0.02	1.34	4.56	2.84	-	96.68
MM-2	73.11	0.07	12.95	2.09	0.07	0.04	1.28	4.37	2.87	-	96.85
MM-2	72.53	0.15	12.38	1.97	0.13	0.00	1.28	4.40	2.83	-	95.67
MM-2	72.01	0.10	12.57	1.87	0.05	0.05	1.26	4.38	2.75	-	95.03
MM-2	72.76	0.12	12.64	1.90	0.08	0.05	1.34	4.53	2.76	-	96.17

MM-3 = Lairg B *

	SiO_2	TiO_2	Al_2O_3	FeO	MnO	MgO	CaO	Na_2O	K_2O	P_2O_5	Total
MM-3	70.77	0.19	13.87	2.15	0.12	0.13	0.71	4.93	4.51	-	97.38
MM-3	69.43	0.17	13.45	2.14	0.03	0.17	0.64	4.68	4.41	-	95.13
MM-3	68.84	0.24	14.53	2.39	0.05	0.25	0.92	4.83	4.23	-	96.28
MM-3	70.72	0.20	13.45	2.14	0.04	0.18	0.72	4.61	4.40	-	96.45

MM-4 = Lairg A *

	SiO_2	TiO_2	Al_2O_3	FeO	MnO	MgO	CaO	Na_2O	K_2O	P_2O_5	Total
MM-4	73.58	0.12	11.77	1.57	0.07	0.04	1.30	3.85	2.74	-	95.04
MM-4	74.71	0.11	11.68	1.67	0.02	0.01	1.29	3.01	2.85	-	95.35
MM-4	74.85	0.49	12.55	3.74	0.20	0.37	2.21	4.25	2.18	-	100.84
MM-4	73.16	0.59	12.78	3.33	0.23	0.38	2.63	4.12	2.05	-	99.28
MM-4	72.84	0.51	12.69	3.71	0.11	0.37	2.26	4.06	2.16	-	98.71
MM-4	74.84	0.00	11.86	1.56	0.11	0.01	1.27	4.65	3.02	-	97.31
MM-4	73.81	0.09	11.97	1.67	0.06	0.08	1.29	3.54	2.68	-	95.19
MM-4	74.69	0.20	12.48	1.78	0.00	0.02	1.21	4.06	2.75	-	97.19
MM-4	75.51	0.08	11.90	1.57	0.09	0.00	1.20	3.02	2.74	-	96.11
MM-4	73.07	0.10	12.74	1.54	0.06	0.05	1.32	4.43	2.70	-	96.01

SB-1 = Hekla 1104 Standard data = Group 7

	SiO_2	TiO_2	Al_2O_3	FeO	MnO	MgO	CaO	Na_2O	K_2O	P_2O_5	Total
SB-1	73.00	0.21	14.22	3.37	0.10	0.11	1.99	5.01	2.78	0.02	100.81

SB-1	72.72	0.21	14.32	3.13	0.10	0.14	2.08	5.54	2.78	0.03	101.04
SB-1	72.43	0.21	14.80	3.12	0.12	0.13	1.91	5.57	2.73	0.03	101.04
SB-1	72.30	0.19	14.56	3.80	0.09	0.12	1.94	4.90	2.62	0.04	99.93
SB-1	72.16	0.21	14.40	2.94	0.09	0.12	1.95	5.48	2.73	0.02	100.11
SB-1	71.99	0.21	15.09	3.27	0.10	0.14	1.99	5.13	2.73	0.03	100.67
SB-1	71.98	0.20	15.40	3.15	0.12	0.09	1.94	5.22	2.71	0.02	100.84
SB-1	71.97	0.20	13.91	3.10	0.09	0.11	1.89	5.48	2.72	0.03	99.51
SB-1	71.71	0.21	14.82	3.00	0.08	0.06	1.92	5.61	2.78	0.02	100.20
SB-1	71.71	0.20	14.42	3.05	0.09	0.11	2.01	5.15	2.79	0.04	99.56
SB-1	71.70	0.19	15.13	3.15	0.10	0.09	2.08	4.95	2.69	0.03	100.10
SB-1	71.63	0.20	14.58	3.04	0.11	0.11	2.08	5.36	2.74	0.01	99.85
SB-1	71.51	0.21	14.14	3.16	0.11	0.12	1.97	5.26	2.73	0.02	99.22
SB-1	71.10	0.21	14.10	2.83	0.11	0.10	2.00	5.58	2.74	0.02	98.79
SB-1	70.76	0.20	15.03	2.88	0.10	0.11	2.00	5.37	2.62	0.02	99.09
SB-1	70.19	0.19	14.77	3.11	0.12	0.14	1.94	4.98	2.68	0.01	98.15
SB-1	69.50	0.19	13.15	3.12	0.11	0.12	1.97	4.84	2.64	0.02	95.66
SB-1	69.43	0.19	13.93	3.08	0.11	0.12	1.84	5.19	2.60	0.03	96.52
SB-1	67.58	0.47	15.17	5.65	0.18	0.45	3.11	4.99	2.35	0.10	100.07
SB-1	67.45	0.47	15.39	5.64	0.18	0.44	3.21	5.36	2.29	0.10	100.54

SB-2 = SN-1 Standard data = Group 10

	SiO_2	TiO_2	Al_2O_3	FeO	MnO	MgO	CaO	Na_2O	K_2O	P_2O_5	Total
SB-2	70.59	0.20	15.20	2.98	0.14	0.11	1.04	5.60	4.86	0.02	100.75
SB-2	67.75	0.38	15.75	4.46	0.16	0.27	1.81	6.16	4.19	0.07	100.98
SB-2	67.39	0.40	16.60	4.21	0.19	0.33	1.87	6.43	4.18	0.06	101.65
SB-2	67.16	0.47	16.04	4.55	0.18	0.41	2.22	6.25	3.90	0.09	101.27
SB-2	66.92	0.41	16.03	4.15	0.19	0.35	1.95	5.98	4.04	0.07	100.10
SB-2	66.69	0.43	16.74	4.34	0.20	0.33	2.12	6.45	4.00	0.07	101.37
SB-2	66.44	0.45	16.46	4.40	0.19	0.34	2.03	6.18	4.08	0.81	100.64
SB-2	66.39	0.40	16.44	4.13	0.18	0.33	1.90	5.99	4.06	0.07	99.90
SB-2	66.34	0.43	16.81	4.29	0.17	0.34	2.12	6.06	3.98	0.07	100.60
SB-2	66.32	0.45	16.66	4.67	0.17	0.34	2.03	6.08	4.06	0.07	100.84
SB-2	66.15	0.64	15.85	5.63	0.21	0.57	2.01	5.79	4.41	0.14	101.40
SB-2	65.65	0.57	17.25	5.17	0.20	0.55	2.52	6.06	3.73	0.12	101.82
SB-2	65.58	0.45	18.12	4.18	0.15	0.36	3.00	6.85	3.19	0.09	101.97
SB-2	65.52	0.42	16.02	4.46	0.16	0.28	1.90	6.06	4.04	0.05	98.92
SB-2	65.15	0.58	16.46	5.28	0.17	0.51	2.64	6.00	3.63	0.14	100.58
SB-2	65.14	0.59	16.68	5.28	0.21	0.58	2.77	6.26	3.63	0.13	101.26
SB-2	65.11	0.57	17.10	5.37	0.17	0.53	2.55	6.30	3.72	0.12	101.58
SB-2	64.82	0.62	16.17	5.72	0.19	0.61	2.55	5.78	3.83	0.13	100.42
SB-2	64.70	0.58	16.57	5.03	0.21	0.61	2.48	6.05	3.73	0.14	100.10
SB-2	64.44	0.58	16.52	5.28	0.22	0.55	2.71	5.80	3.63	0.11	99.86
SB-2	64.44	0.60	16.10	5.46	0.21	0.52	2.56	6.14	3.72	0.15	99.89
SB-2	64.42	0.58	16.44	5.42	0.21	0.55	2.52	6.56	3.92	0.11	100.71
SB-2	64.28	0.60	16.62	5.08	0.21	0.63	2.59	6.16	3.66	0.13	99.97
SB-2	64.22	0.60	16.56	5.27	0.23	0.56	2.50	6.28	3.74	0.11	100.06
SB-2	63.86	0.60	16.64	5.35	0.22	0.61	2.61	5.91	3.79	0.13	99.72
SB-2	63.54	0.56	15.98	5.28	0.21	0.60	2.52	6.11	3.80	0.11	98.72

SL-1 = Hekla 1104 Standard data = Group 11

	SiO_2	TiO_2	Al_2O_3	FeO	MnO	MgO	CaO	Na_2O	K_2O	P_2O_5	Total
SL-1	72.91	0.19	13.68	2.91	0.09	0.12	1.87	4.84	2.68	0.02	99.31
SL-1	72.16	0.20	13.55	3.27	0.11	0.14	2.00	4.80	2.73	0.02	98.97
SL-1	72.15	0.20	13.50	2.93	0.11	0.15	1.95	4.88	2.78	0.02	98.66
SL-1	72.08	0.20	13.85	3.11	0.11	0.12	2.00	4.71	2.69	0.02	98.89
SL-1	71.75	0.19	13.86	3.08	0.11	0.11	1.94	4.74	2.64	0.02	98.45
SL-1	71.68	0.20	13.44	3.00	0.10	0.15	1.94	4.94	2.70	0.02	98.16
SL-1	71.52	0.18	13.43	2.84	0.10	0.12	1.95	4.57	2.67	0.03	97.40
SL-1	70.56	0.19	13.71	3.03	0.09	0.10	2.03	4.93	2.70	0.03	97.37

SL-2 = SN-1 Standard data = Group 11

	SiO_2	TiO_2	Al_2O_3	FeO	MnO	MgO	CaO	Na_2O	K_2O	P_2O_5	Total
SL-2	70.21	0.17	14.71	2.85	0.12	0.07	1.19	5.61	4.73	0.01	99.69
SL-2	66.44	0.40	15.08	4.26	0.17	0.33	1.88	5.57	4.04	0.06	98.22
SL-2	66.31	0.47	15.38	4.55	0.19	0.39	2.15	5.45	3.87	0.09	98.86
SL-2	66.12	0.42	15.12	4.53	0.17	0.32	1.99	5.63	4.00	0.06	98.36
SL-2	65.87	0.56	15.80	5.12	0.21	0.55	2.49	5.45	3.72	0.12	99.90
SL-2	65.81	0.57	16.15	5.45	0.21	0.56	2.62	5.67	3.52	0.13	100.69
SL-2	65.61	0.58	15.69	5.06	0.19	0.58	2.61	5.47	3.97	0.12	99.88
SL-2	65.54	0.59	15.68	5.54	0.22	0.63	2.48	5.38	3.86	0.14	100.06
SL-2	65.47	0.57	15.90	5.42	0.20	0.62	2.47	5.64	3.72	0.11	100.13
SL-2	65.43	0.59	15.77	5.29	0.23	0.61	2.61	5.40	3.68	0.13	99.73
SL-2	65.25	0.45	15.68	4.61	0.16	0.46	2.80	5.81	3.44	0.11	98.78
SL-2	65.18	0.54	15.92	5.18	0.21	0.53	2.63	5.47	3.80	0.12	99.57
SL-2	65.15	0.60	15.33	5.16	0.21	0.62	2.53	5.46	3.86	0.13	99.05
SL-2	65.10	0.55	15.98	5.35	0.22	0.58	2.62	5.73	3.85	0.12	100.11
SL-2	64.95	0.57	15.84	5.18	0.20	0.57	2.62	5.65	3.78	0.13	99.49
SL-2	64.89	0.57	15.78	5.40	0.22	0.52	2.42	5.51	3.89	0.12	99.32
SL-2	64.24	0.60	15.26	5.22	0.20	0.64	2.58	5.28	3.71	0.14	97.87
SL-2	63.73	0.50	15.30	4.98	0.19	0.60	2.38	5.49	3.55	0.10	96.83
SL-2	61.97	0.56	15.20	5.08	0.21	0.57	2.55	5.61	3.61	0.14	95.50

SL-3 = Hekla 4 Standard data = Group 10

	SiO_2	TiO_2	Al_2O_3	FeO	MnO	MgO	CaO	Na_2O	K_2O	P_2O_5	Total
SL-3	77.14	0.07	13.36	1.45	0.08	0.03	1.03	4.63	2.79	0.01	100.58
SL-3	76.89	0.08	12.58	1.80	0.05	0.04	1.46	4.31	2.84	0.02	100.02
SL-3	75.80	0.08	12.77	1.80	0.08	0.05	1.28	5.07	3.04	0.02	99.97
SL-3	74.85	0.10	13.58	1.97	0.09	0.00	1.27	5.52	2.77	0.01	100.14
SL-3	74.55	0.09	12.88	1.60	0.05	0.05	1.27	4.85	2.58	0.01	97.93
SL-3	74.17	0.06	12.14	1.71	0.08	0.05	1.20	5.17	3.01	0.01	97.61
SL-3	74.17	0.08	12.88	1.83	0.07	0.03	1.30	4.57	2.54	0.02	97.49
SL-3	73.56	0.09	12.91	1.96	0.08	0.01	1.29	4.97	2.87	0.01	97.75
SL-3	73.53	0.10	13.59	1.86	0.05	0.04	1.33	5.25	2.85	0.02	98.63
SL-3	73.32	0.08	12.92	1.76	0.09	0.00	1.36	4.76	2.79	0.01	97.08
SL-3	72.91	0.36	11.67	2.05	0.11	0.11	0.38	4.67	4.40	0.03	96.69
SL-3	72.63	0.09	12.79	1.75	0.08	0.02	1.32	5.01	2.95	0.02	96.66

SL-3	72.59	0.10	13.48	1.76	0.08	0.04	1.35	5.01	2.85	0.02	97.27
SL-3	72.56	0.10	13.13	1.92	0.08	0.00	1.36	5.24	2.78	0.02	97.19
SL-3	72.49	0.09	13.61	1.90	0.09	0.02	1.21	5.03	2.90	0.01	97.35
SL-3	72.32	0.09	13.00	1.86	0.08	0.00	1.43	5.26	2.71	0.01	96.77
SL-3	72.24	0.19	14.36	3.90	0.13	0.14	2.18	4.91	3.02	0.04	101.11
SL-3	72.22	0.09	13.10	1.76	0.07	0.05	1.33	5.19	2.81	0.01	96.64
SL-3	71.72	0.11	13.80	1.88	0.07	0.04	1.31	4.68	2.78	0.01	96.39
SL-3	71.50	0.09	12.99	1.85	0.06	0.02	1.29	4.87	2.80	0.02	95.48
SL-3	71.12	0.10	13.51	1.78	0.07	0.01	1.25	5.08	2.82	0.01	95.75
SL-3	70.56	0.26	14.87	4.86	0.17	0.19	2.43	5.20	2.43	0.06	101.03
SL-3	70.28	0.15	16.37	1.52	0.05	0.07	2.07	5.63	2.49	0.03	98.66
SL-3	68.04	0.20	16.27	1.85	0.07	0.08	2.96	5.54	2.08	0.04	97.13
SL-3	66.23	0.14	18.53	1.30	0.05	0.11	4.65	6.49	1.60	0.16	99.25
SL-3	63.57	0.80	16.41	7.83	0.25	1.07	4.34	5.20	1.80	0.25	101.51
SL-3	63.31	0.89	14.59	8.71	0.24	1.00	4.21	5.00	1.84	0.32	100.11
SL-3	62.59	0.83	15.65	8.22	0.20	1.01	4.73	5.86	1.21	0.30	100.59
SL-3	62.13	0.89	14.85	9.12	0.22	1.19	4.47	5.08	1.65	0.34	99.94
SL-3	61.92	0.82	14.78	7.85	0.24	0.86	4.53	5.26	1.49	0.31	98.06
SL-3	61.74	0.89	15.56	8.88	0.24	1.13	4.78	4.97	1.65	0.36	100.19
SL-3	61.19	0.88	15.67	8.76	0.23	1.11	4.81	5.02	1.49	0.33	99.50
SL-3	60.81	0.92	15.03	8.76	0.24	1.06	4.64	5.10	1.41	0.36	98.33
SL-3	60.03	0.88	15.47	9.57	0.27	1.58	5.05	4.64	1.59	0.33	99.40
SL-3	57.91	0.89	14.59	9.51	0.27	1.16	4.84	4.35	1.53	0.44	95.49

Group 1

Standard	SiO_2	TiO_2	Al_2O_3	FeO	MnO	MgO	CaO	Na_2O	K_2O	P_2O_5	Total
BCR2g	54.99	2.27	13.09	12.27	0.19	3.85	7.00	3.48	1.86	0.37	99.36
BCR2g	54.01	2.29	13.43	12.32	0.19	3.68	7.07	3.30	1.76	0.37	98.41
BCR2g	54.69	2.27	13.44	12.40	0.20	3.60	7.19	3.22	1.76	0.35	99.14
BCR2g	53.99	2.26	13.65	12.09	0.20	3.66	7.21	3.37	1.82	0.36	98.61
BCR2g	53.59	2.27	13.39	12.16	0.20	3.67	7.16	3.42	1.83	0.36	98.03
BCR2g	54.49	2.26	13.53	12.30	0.20	3.59	7.18	3.38	1.74	0.35	99.01
BCR2g	54.31	2.26	13.31	12.11	0.21	3.56	7.11	3.26	1.80	0.36	98.29
BCR2g	54.39	2.26	13.57	12.57	0.19	3.60	7.09	3.19	1.79	0.37	99.03
BCR2g	54.84	2.26	13.48	12.46	0.19	3.67	7.14	3.15	1.77	0.35	99.30
BCR2g	54.54	2.27	13.38	12.24	0.20	3.80	7.04	3.20	1.79	0.35	98.80
BCR2g	55.57	2.25	13.57	12.42	0.18	3.74	7.31	3.44	1.78	0.35	100.62
BCR2g	55.26	2.26	13.59	12.32	0.20	3.81	7.17	3.19	1.85	0.36	100.00
BCR2g	54.35	2.26	13.37	12.78	0.20	3.74	7.08	3.41	1.81	0.35	99.36
BCR2g	55.27	2.28	13.31	12.74	0.19	3.79	7.16	3.20	1.76	0.33	100.03
Lipari	73.81	0.08	12.69	1.76	0.05	0.04	0.74	4.20	5.28	0.00	98.66
Lipari	74.29	0.08	12.74	1.60	0.06	0.04	0.76	4.07	5.20	0.01	98.86
Lipari	73.96	0.08	13.03	1.62	0.08	0.03	0.72	4.16	5.35	0.01	99.04
Lipari	74.76	0.08	12.89	1.60	0.06	0.02	0.79	4.15	5.19	0.00	99.55
Lipari	75.23	0.07	13.30	1.63	0.06	0.04	0.66	4.25	5.21	0.01	100.46
Lipari	73.16	0.08	12.51	1.65	0.07	0.06	0.72	4.32	5.43	0.00	98.00
Lipari	74.00	0.08	12.58	1.57	0.06	0.07	0.79	4.31	5.23	0.00	98.70
Lipari	74.50	0.08	12.73	1.62	0.07	0.05	0.80	4.27	5.24	0.00	99.36

Lipari	75.00	0.08	12.94	1.55	0.06	0.05	0.73	4.23	5.14	0.01	99.78
Lipari	74.43	0.07	12.66	1.46	0.07	0.02	0.81	4.18	5.34	0.01	99.05

Group 2

Standard	SiO_2	TiO_2	Al_2O_3	FeO	MnO	MgO	CaO	Na_2O	K_2O	P_2O_5	Total
BCR2g	54.25	2.26	13.43	12.19	0.19	3.64	7.19	3.18	1.88	0.34	98.54
BCR2g	54.71	2.25	13.43	12.55	0.20	3.80	7.15	3.21	1.85	0.37	99.52
BCR2g	55.17	2.25	13.86	12.45	0.17	3.75	7.20	3.20	1.81	0.32	100.18
BCR2g	55.66	2.25	13.37	12.10	0.20	3.67	7.16	3.07	1.79	0.32	99.60
BCR2g	55.63	2.26	13.30	12.26	0.19	3.66	7.35	3.23	1.73	0.32	99.94
BCR2g	55.63	2.26	13.29	12.43	0.18	3.61	7.43	3.12	1.85	0.32	100.13
BCR2g	55.48	2.27	13.75	12.15	0.19	3.72	7.46	3.18	1.87	0.33	100.40
BCR2g	55.78	2.26	13.68	12.13	0.18	3.71	7.20	3.08	1.83	0.33	100.18
Lipari	75.55	0.08	12.89	1.58	0.05	0.01	0.74	4.18	5.28	0.00	100.36
Lipari	75.06	0.08	13.04	1.61	0.07	0.02	0.74	4.15	5.13	0.00	99.91
Lipari	74.75	0.07	13.08	1.54	0.05	0.03	0.74	4.01	5.14	0.00	99.41
Lipari	75.08	0.09	13.00	1.52	0.06	0.04	0.76	4.17	5.26	0.01	100.00
Lipari	74.00	0.08	13.00	1.55	0.07	0.05	0.76	3.98	5.22	0.00	98.71
Lipari	73.94	0.07	12.84	1.37	0.04	0.04	0.80	3.94	5.04	0.01	98.09
Lipari	74.93	0.08	13.31	1.49	0.07	0.07	0.63	4.00	5.16	0.01	99.75
Lipari	73.79	0.08	12.98	1.54	0.08	0.04	0.71	3.98	5.08	0.00	98.28

Group 3

Standard	SiO_2	TiO_2	Al_2O_3	FeO	MnO	MgO	CaO	Na_2O	K_2O	P_2O_5	Total
BCR2g	54.49	2.28	13.62	12.16	0.20	3.61	7.09	3.32	1.77	0.36	98.89
BCR2g	53.91	2.28	13.33	12.70	0.19	3.58	7.06	3.17	1.81	0.36	98.40
BCR2g	54.72	2.27	13.37	12.33	0.21	3.71	7.23	3.18	1.86	0.36	99.23
BCR2g	54.73	2.26	13.45	12.79	0.19	3.68	7.00	3.09	1.81	0.37	99.36
BCR2g	54.33	2.28	13.09	12.91	0.20	3.67	7.18	3.18	1.87	0.36	99.09
Lipari	73.96	0.08	12.69	1.52	0.07	0.00	0.69	4.06	5.11	0.00	98.18
Lipari	74.17	0.08	13.17	1.56	0.07	0.03	0.76	3.94	5.10	0.00	98.88
Lipari	73.74	0.08	13.09	1.69	0.07	0.01	0.76	4.13	5.19	0.01	98.77
Lipari	73.83	0.07	12.99	1.56	0.07	0.06	0.76	4.16	5.09	0.01	98.62
Lipari	74.29	0.08	12.57	1.48	0.07	0.04	0.73	4.01	5.34	0.01	98.62
Lipari	75.10	0.07	12.91	1.44	0.06	0.04	0.72	4.09	5.06	0.00	99.50
Lipari	75.16	0.07	12.63	1.47	0.06	0.04	0.81	4.06	5.09	0.00	99.39
Lipari	75.06	0.07	12.96	1.47	0.07	0.04	0.74	3.88	5.10	0.02	99.41
Lipari	74.15	0.07	12.48	1.69	0.07	0.04	0.77	3.77	5.26	0.00	98.29
Lipari	73.76	0.08	13.16	1.56	0.07	0.04	0.74	4.01	5.25	0.00	98.68

Group 4

Standard	SiO_2	TiO_2	Al_2O_3	FeO	MnO	MgO	CaO	Na_2O	K_2O	P_2O_5	Total
BCR2g	54.72	2.25	13.29	12.26	0.20	3.66	7.15	3.11	1.76	0.36	98.76
BCR2g	55.57	2.28	13.55	12.72	0.21	3.65	6.98	3.31	1.84	0.35	100.47
BCR2g	54.63	2.27	13.71	12.43	0.20	3.81	7.19	3.23	1.83	0.35	99.65
BCR2g	53.76	2.24	13.29	12.43	0.20	3.69	7.24	3.24	1.80	0.36	98.27
BCR2g	53.77	2.23	13.07	12.33	0.19	3.75	7.28	3.38	1.78	0.36	98.15
BCR2g	53.96	2.27	13.41	12.45	0.20	3.72	7.15	3.40	1.76	0.39	98.71
BCR2g	53.52	2.23	13.56	12.27	0.19	3.73	7.25	3.31	1.75	0.36	98.16
BCR2g	54.04	2.24	13.47	12.89	0.21	3.64	7.29	3.22	1.76	0.35	99.11

BCR2g	54.15	2.24	13.08	12.39	0.20	3.70	7.31	3.31	1.87	0.35	98.60
Lipari	74.60	0.07	13.27	1.58	0.06	0.06	0.75	4.24	5.22	0.01	99.86
Lipari	73.69	0.08	12.80	1.51	0.07	0.03	0.74	4.08	5.13	0.00	98.14
Lipari	75.67	0.08	12.86	1.50	0.08	0.05	0.74	4.45	5.27	0.00	100.70
Lipari	74.90	0.09	12.79	1.67	0.06	0.03	0.75	4.32	5.25	0.00	99.87
Lipari	74.42	0.07	13.01	1.51	0.06	0.05	0.77	4.20	5.23	0.01	99.34
Lipari	73.94	0.08	12.83	1.41	0.06	0.06	0.74	4.11	5.27	0.01	98.50
Lipari	74.14	0.07	12.91	1.59	0.06	0.05	0.74	4.25	5.17	0.00	98.99
Lipari	74.44	0.07	12.85	1.55	0.07	0.05	0.77	4.35	5.11	0.01	99.27
Lipari	74.82	0.07	13.02	1.71	0.07	0.05	0.69	4.22	4.99	0.00	99.64

Group 5

Standard	SiO_2	TiO_2	Al_2O_3	FeO	MnO	MgO	CaO	Na_2O	K_2O	P_2O_5	Total
BCR2g	55.16	2.23	13.17	12.69	0.17	3.58	7.24	3.20	1.79	0.33	99.58
BCR2g	53.15	2.22	13.34	12.05	0.20	3.60	7.24	3.16	1.83	0.35	97.15
BCR2g	53.91	2.22	13.09	12.17	0.19	3.81	7.07	3.18	1.79	0.33	97.75
BCR2g	54.11	2.21	13.25	12.19	0.17	3.76	7.40	3.18	1.79	0.34	98.40
BCR2g	55.03	2.26	13.51	12.26	0.19	3.67	7.36	3.13	1.80	0.35	99.55
BCR2g	54.76	2.28	13.14	12.34	0.21	3.65	7.31	3.07	1.85	0.36	98.97
BCR2g	55.13	2.26	13.47	12.85	0.20	3.68	7.19	3.22	1.79	0.36	100.15
BCR2g	54.57	2.23	13.66	12.83	0.19	3.72	7.10	3.13	1.73	0.35	99.51
BCR2g	54.48	2.26	13.23	12.43	0.18	3.59	7.26	3.03	1.85	0.36	98.67
BCR2g	54.91	2.28	13.46	12.27	0.18	3.66	7.19	3.14	1.75	0.37	99.21
BCR2g	55.14	2.26	13.59	12.33	0.17	3.70	7.14	3.08	1.72	0.37	99.50
BCR2g	54.82	2.22	13.48	12.55	0.17	3.80	7.26	3.13	1.72	0.35	99.49
BCR2g	54.83	2.22	13.46	12.26	0.15	3.75	7.24	3.25	1.79	0.36	99.30
BCR2g	54.63	2.25	13.77	12.65	0.18	3.69	7.25	3.24	1.73	0.36	99.76
Lipari	74.03	0.08	12.78	1.46	0.06	0.04	0.77	3.79	5.07	0.00	98.09
Lipari	74.30	0.07	13.00	1.38	0.08	0.05	0.75	4.23	5.37	0.01	99.22
Lipari	74.63	0.09	13.23	1.53	0.05	0.04	0.70	3.87	5.19	0.01	99.35
Lipari	74.22	0.08	12.88	1.47	0.05	0.05	0.76	3.87	5.32	0.00	98.71
Lipari	75.35	0.07	13.10	1.36	0.07	0.02	0.76	4.05	5.22	0.00	100.01
Lipari	74.89	0.08	12.98	1.65	0.06	0.03	0.69	3.97	5.18	0.00	99.53
Lipari	75.13	0.08	12.88	1.66	0.08	0.05	0.75	3.95	5.30	0.00	99.87
Lipari	74.18	0.08	13.04	1.60	0.04	0.02	0.69	4.10	5.37	0.01	99.12
Lipari	74.23	0.08	12.83	1.74	0.06	0.02	0.77	3.97	5.30	0.00	99.01
Lipari	73.43	0.08	12.65	1.59	0.07	0.05	0.76	4.04	5.29	0.01	97.96
Lipari	74.17	0.07	12.75	1.61	0.06	0.04	0.73	3.85	5.30	0.00	98.59
Lipari	74.78	0.08	12.89	1.66	0.06	0.05	0.75	4.15	5.40	0.00	99.83
Lipari	73.39	0.08	12.91	1.50	0.08	0.05	0.79	3.95	5.30	0.01	98.06
Lipari	73.78	0.07	12.80	1.40	0.07	0.00	0.81	3.97	5.23	0.01	98.14
Lipari	74.83	0.08	13.02	1.51	0.05	0.03	0.81	4.18	5.12	0.01	99.64
Lipari	73.14	0.08	13.09	1.63	0.06	0.03	0.77	3.88	5.19	0.00	97.88
Lipari	73.85	0.07	12.96	1.55	0.05	0.07	0.76	3.96	5.27	0.01	98.56

Group 6

Standard	SiO_2	TiO_2	Al_2O_3	FeO	MnO	MgO	CaO	Na_2O	K_2O	P_2O_5	Total
BCR2g	54.73	2.26	13.45	12.79	0.19	3.68	7.00	3.09	1.81	0.37	99.36
BCR2g	54.33	2.28	13.09	12.91	0.20	3.67	7.18	3.18	1.87	0.36	99.09
BCR2g	54.46	2.27	13.40	12.44	0.20	3.65	7.31	2.60	1.66	0.36	98.36

BCR2g	54.82	2.23	13.54	12.35	0.20	3.68	7.11	2.83	1.87	0.35	98.99
BCR2g	54.87	2.26	13.45	12.29	0.19	3.73	7.12	2.26	1.77	0.36	98.30
BCR2g	54.68	2.26	13.23	12.93	0.19	3.62	7.04	3.01	1.81	0.38	99.13
BCR2g	54.49	2.24	13.44	12.47	0.21	3.70	7.18	2.04	1.92	0.38	98.08
BCR2g	54.49	2.26	13.50	12.39	0.21	3.64	7.03	3.13	1.83	0.38	98.86
Lipari	74.71	0.07	12.76	1.60	0.07	0.04	0.67	3.75	5.17	0.00	98.84
Lipari	74.89	0.07	12.75	1.43	0.06	0.04	0.75	3.78	5.22	0.01	99.00
Lipari	74.82	0.07	13.07	1.49	0.06	0.03	0.77	3.94	5.29	0.00	99.53
Lipari	74.21	0.08	12.82	1.84	0.06	0.01	0.66	3.94	5.27	0.01	98.90
Lipari	74.96	0.07	12.68	1.57	0.08	0.04	0.75	3.83	5.17	0.01	99.16
Lipari	74.31	0.08	13.29	1.47	0.06	0.03	0.81	3.79	5.22	0.00	99.06
Lipari	75.16	0.07	12.63	1.47	0.06	0.04	0.81	4.06	5.09	0.00	99.39
Lipari	75.06	0.07	12.96	1.47	0.07	0.04	0.74	3.88	5.10	0.02	99.41
Lipari	74.15	0.07	12.48	1.69	0.07	0.04	0.77	3.77	5.26	0.00	98.29
Lipari	73.76	0.08	13.16	1.56	0.07	0.04	0.74	4.01	5.25	0.00	98.68

Group 7

Standard	SiO_2	TiO_2	Al_2O_3	FeO	MnO	MgO	CaO	Na_2O	K_2O	P_2O_5	Total
BCR2g	53.91	2.26	13.70	12.56	0.19	3.82	7.26	3.20	1.79	0.34	99.03
BCR2g	54.59	2.28	13.63	12.29	0.19	3.65	7.06	3.48	1.84	0.35	99.35
BCR2g	54.83	2.27	13.42	11.95	0.20	3.71	7.04	3.49	1.79	0.35	99.04
BCR2g	54.19	2.27	14.20	12.76	0.19	3.76	6.95	3.45	1.77	0.30	99.83
BCR2g	54.34	2.26	14.77	12.82	0.20	3.74	7.07	3.81	1.82	0.34	101.16
BCR2g	54.90	2.28	13.60	12.46	0.19	3.77	7.25	3.20	1.84	0.32	99.81
BCR2g	54.93	2.28	13.75	12.93	0.20	3.65	7.10	3.45	2.00	0.33	100.60
BCR2g	55.03	2.28	13.35	12.50	0.18	3.83	7.03	3.60	1.80	0.33	99.92
BCR2g	55.18	2.28	14.59	12.69	0.22	3.69	7.17	3.59	1.90	0.35	101.65
Lipari	73.83	0.08	12.99	1.62	0.06	0.04	0.65	3.98	5.02	0.01	98.29
Lipari	74.44	0.08	12.98	1.62	0.07	0.04	0.66	4.12	5.29	0.01	99.31
Lipari	74.61	0.07	12.95	1.54	0.09	0.05	0.67	4.16	5.19	0.01	99.33
Lipari	75.02	0.07	13.30	1.65	0.09	0.04	0.76	4.24	5.22	0.01	100.39
Lipari	74.80	0.08	13.82	1.69	0.09	0.06	0.70	4.63	5.09	0.01	100.97
Lipari	74.76	0.08	13.40	1.63	0.07	0.05	0.76	4.49	5.17	0.01	100.40
Lipari	74.94	0.07	13.15	1.57	0.06	0.04	0.79	4.55	5.27	0.00	100.44
Lipari	75.09	0.08	13.81	1.52	0.06	0.04	0.77	4.45	5.25	0.01	101.08
Lipari	74.66	0.07	13.44	1.61	0.08	0.05	0.68	4.20	5.04	0.02	99.86
Lipari	75.19	0.09	12.79	1.75	0.08	0.02	0.73	4.48	5.13	0.00	100.27

Group 8

Standard	SiO_2	TiO_2	Al_2O_3	FeO	MnO	MgO	CaO	Na_2O	K_2O	P_2O_5	Total
BCR2g	55.20	2.30	13.56	12.15	0.20	3.60	6.93	3.21	1.79	0.36	99.29
BCR2g	54.41	2.26	13.38	12.48	0.17	3.72	7.13	3.28	1.74	0.38	98.96
BCR2g	54.54	2.26	13.16	12.58	0.21	3.75	6.91	3.32	1.88	0.39	99.00
BCR2g	53.96	2.26	13.23	12.38	0.20	3.77	7.03	3.52	1.79	0.38	98.51
BCR2g	54.11	2.26	13.23	12.50	0.18	3.69	6.99	3.21	1.86	0.36	98.40
BCR2g	54.70	2.27	13.33	12.72	0.20	3.76	7.09	3.42	1.76	0.36	99.60
BCR2g	54.92	2.26	13.41	12.62	0.19	3.66	7.11	3.42	1.81	0.38	99.77
BCR2g	54.22	2.28	13.08	11.70	0.20	3.80	7.00	3.25	1.86	0.35	97.74
BCR2g	54.50	2.27	13.13	12.34	0.20	3.85	7.31	3.41	1.74	0.34	99.08
BCR2g	54.24	2.28	13.50	12.54	0.20	3.70	7.00	3.30	1.78	0.36	98.89

BCR2g	54.57	2.25	13.56	12.45	0.19	3.72	7.19	3.31	1.80	0.36	99.40
Lipari	74.43	0.07	12.70	1.76	0.07	0.04	0.81	4.18	5.23	0.00	99.30
Lipari	74.04	0.08	12.68	1.63	0.07	0.04	0.71	4.16	4.96	0.01	98.36
Lipari	74.78	0.07	12.99	1.59	0.07	0.06	0.72	4.27	5.21	0.00	99.76
Lipari	74.50	0.07	12.80	1.65	0.07	0.02	0.79	4.01	5.24	0.00	99.15

Group 9

Standard	SiO_2	TiO_2	Al_2O_3	FeO	MnO	MgO	CaO	Na_2O	K_2O	P_2O_5	Total
BCR2g	54.38	2.25	13.50	11.88	0.18	3.64	7.03	3.11	1.85	0.34	98.16
BCR2g	54.61	2.25	13.14	12.46	0.16	3.68	7.07	3.29	1.90	0.35	98.91
BCR2g	54.57	2.25	13.42	12.31	0.20	3.71	7.33	3.22	1.86	0.33	99.22
BCR2g	54.07	2.26	13.18	12.18	0.19	3.54	7.23	3.14	1.87	0.33	97.99
BCR2g	54.24	2.26	13.19	13.06	0.19	3.60	7.33	3.16	1.89	0.32	99.23
BCR2g	53.37	2.25	13.50	12.77	0.19	3.77	7.17	3.26	1.85	0.35	98.47
Lipari	74.30	0.08	12.92	1.59	0.08	0.03	0.82	4.04	5.30	0.00	99.15
Lipari	74.23	0.08	13.07	1.66	0.05	0.04	0.78	3.85	5.25	0.01	99.02
Lipari	73.04	0.07	12.84	1.51	0.06	0.00	0.71	4.04	5.06	0.01	97.34
Lipari	73.43	0.07	12.64	1.50	0.04	0.04	0.76	4.00	5.14	0.01	97.62
Lipari	73.30	0.08	12.77	1.77	0.08	0.05	0.76	3.98	5.30	0.01	98.10
Lipari	72.86	0.08	12.80	1.25	0.06	0.00	0.73	4.12	5.30	0.01	97.20
Lipari	72.94	0.08	12.61	1.69	0.04	0.06	0.74	3.93	5.13	0.00	97.22
Lipari	72.96	0.08	12.91	1.62	0.05	0.04	0.72	3.94	5.18	0.00	97.50

Group 10

Standard	SiO_2	TiO_2	Al_2O_3	FeO	MnO	MgO	CaO	Na_2O	K_2O	P_2O_5	Total
BCR2g	54.50	2.27	13.13	12.34	0.20	3.85	7.31	3.41	1.74	0.34	99.08
BCR2g	54.24	2.28	13.50	12.54	0.20	3.70	7.00	3.30	1.78	0.36	98.89
BCR2g	54.57	2.25	13.56	12.45	0.19	3.72	7.19	3.31	1.80	0.36	99.40
BCR2g	53.91	2.26	13.70	12.56	0.19	3.82	7.26	3.20	1.79	0.34	99.03
BCR2g	54.59	2.28	13.63	12.29	0.19	3.65	7.06	3.48	1.84	0.35	99.35
BCR2g	54.83	2.27	13.42	11.95	0.20	3.71	7.04	3.49	1.79	0.35	99.04
Lipari	73.83	0.08	12.99	1.62	0.06	0.04	0.65	3.98	5.02	0.01	98.29
Lipari	74.44	0.08	12.98	1.62	0.07	0.04	0.66	4.12	5.29	0.01	99.31
Lipari	74.61	0.07	12.95	1.54	0.09	0.05	0.67	4.16	5.19	0.01	99.33
Lipari	75.02	0.07	13.30	1.65	0.09	0.04	0.76	4.24	5.22	0.01	100.39

Group 11

Standard	SiO_2	TiO_2	Al_2O_3	FeO	MnO	MgO	CaO	Na_2O	K_2O	P_2O_5	Total
BCR2g	54.79	2.25	13.49	12.64	0.19	3.78	7.18	3.24	1.74	0.36	99.66
BCR2g	55.21	2.28	13.39	12.08	0.21	3.63	7.11	3.24	1.90	0.35	99.39
BCR2g	55.23	2.26	13.51	12.95	0.22	3.68	7.14	2.27	1.83	0.38	99.48
BCR2g	54.69	2.26	13.27	12.65	0.19	3.68	6.89	3.45	1.82	0.37	99.25
BCR2g	54.71	2.26	13.81	12.38	0.20	3.64	7.11	3.19	1.70	0.38	99.38
BCR2g	54.43	2.26	13.44	12.39	0.21	3.82	7.12	3.35	1.88	0.36	99.26
BCR2g	54.72	2.26	13.77	12.85	0.18	3.76	7.23	3.29	1.78	0.38	100.22
BCR2g	54.12	2.25	13.50	12.71	0.20	3.74	7.20	3.40	1.84	0.37	99.31
Lipari	74.79	0.08	13.05	1.54	0.06	0.04	0.70	4.27	5.22	0.01	99.76
Lipari	75.18	0.08	13.23	1.45	0.06	0.03	0.82	4.02	5.25	0.00	100.13
Lipari	74.45	0.08	13.12	1.70	0.07	0.03	0.72	4.43	5.08	0.00	99.68
Lipari	74.72	0.08	13.12	1.44	0.07	0.06	0.81	4.42	5.20	0.00	99.91

Chapter 6: The transport of Icelandic volcanic ash: insights from European tephra records

Model description and testing

The physical model calculates the terminal fall velocity of a particle using the 'Ganser scheme' described by (Stevenson *et al*., 2015), which accounts for the non-spherical shape of particles (Ganser, 1993). Particle density varies exponentially with particle size; larger particles (2000 μm, 440 kg m^{-3}) being less dense than smaller particles (8 μm, 2300 kg m^{-3}) (due to a larger proportion of vesicles (Bonadonna and Phillips, 2003; Connor *et al*., 2013). The tephra glass density for calculations is based on the density of rhyolitic (SiO_2>69 wt %) glass (2.3 g cm^{-2}), the most commonly identified cryptotephra composition. Particles fall through an atmosphere with layers of 100 m vertical thickness. Wind speed and air viscosity are constant with height, however atmospheric density decreases with height (Connor *et al*., 2013).

In order to assess our model, we compare the model output to geological distal tephra dispersion for an eruption which has relatively well described input parameters (plume height and wind speed) and well mapped distal tephra deposits: the May 1980 eruption of Mount St Helens. Wind speed for the event is estimated at an average of 28 ms^{-1} and plume height between 15-20 km (Carey and Sigurdsson, 1982). As sphericity is not well defined for tephra from this eruption, values are sampled from the standard input probability density function.

Our results are generally in good agreement with the empirical observations (Carey and Sigurdsson, 1982) especially for shards ≥ 200 μm (Max A) (Fig. S4). However, our model overestimates the transport distance of smaller shards (100 μm). There is evidence that aggregation resulted in the early fallout of small shards (<100 μm) (Durant *et al*., 2009). As our model does not account for aggregation, small shards do not fall as early as the denser aggregates and travel further. This is most likely the

reason that the empirical data and our model output do not show complete alignment for shards of ~100 µm size. There is no empirical data for shard sizes (Max A) <100 µm.

Bonadonna, C., Phillips, J.C., 2003. Sedimentation from strong volcanic plumes. Journal of Geophysical Research: Solid Earth 108, 2340.

Carey, S.N., Sigurdsson, H., 1982. Influence of particle aggregation on deposition of distal tephra from the MAy 18, 1980, eruption of Mount St. Helens volcano. Journal of Geophysical Research: Solid Earth 87, 7061-7072.

Connor, C.B., Connor, L.J., Bonadonna, C., Luhr, J., Savov, I.P., Navarro-Ochoa, C., 2013. Modeling tephra thickness and particle size distribution of the 1913 eruption of Volcán de Colima, Mexico., in: Varley, N. (Ed.), Volcan de Colima, Special Publications. Geological Society of America, p. in press.

Durant, A.J., Rose, W.I., Sarna-Wojcicki, A.M., Carey, S., Volentik, A.C.M., 2009. Hydrometeor-enhanced tephra sedimentation: Constraints from the 18 May 1980 eruption of Mount St. Helens. Journal of Geophysical Research: Solid Earth 114, n/a-n/a.

Ganser, G.H., 1993. A rational approach to drag prediction of spherical and nonspherical particles. Powder Technology 77, 143-152.

Stevenson, J., Millington, S., Beckett, F., Swindles, G., Thordarson, T., 2015. Big grains go far: reconciling tephrochronology with atmospheric measurements of volcanic ash. Atmos. Meas. Tech. Discuss., 8, 65-120.

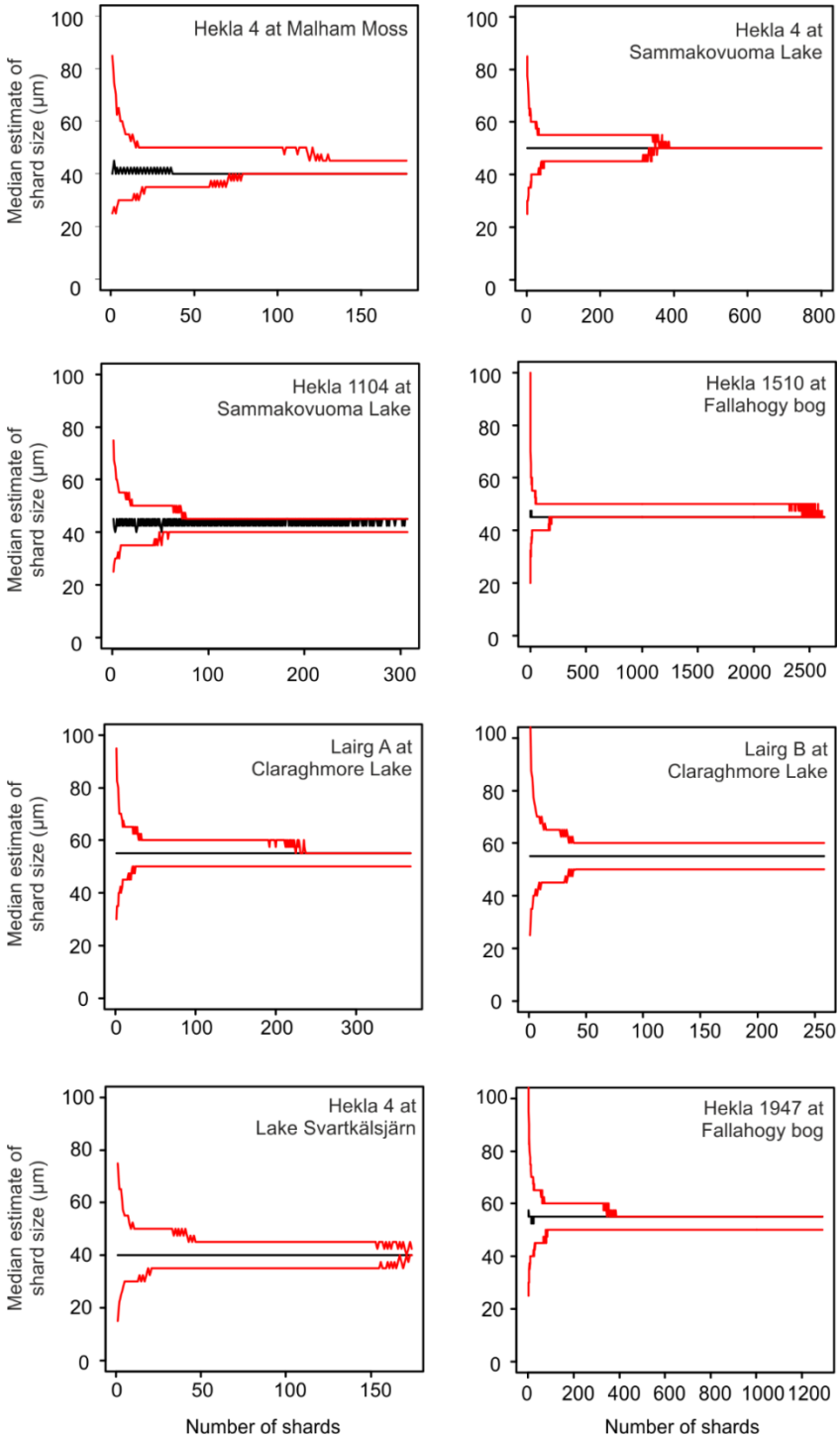

Chapter 6. Figure S1. The results of bootstrap resampling on a selection of the tephra layers identified in this study. Red lines indicate 0.025 and 0.975 error bounds.

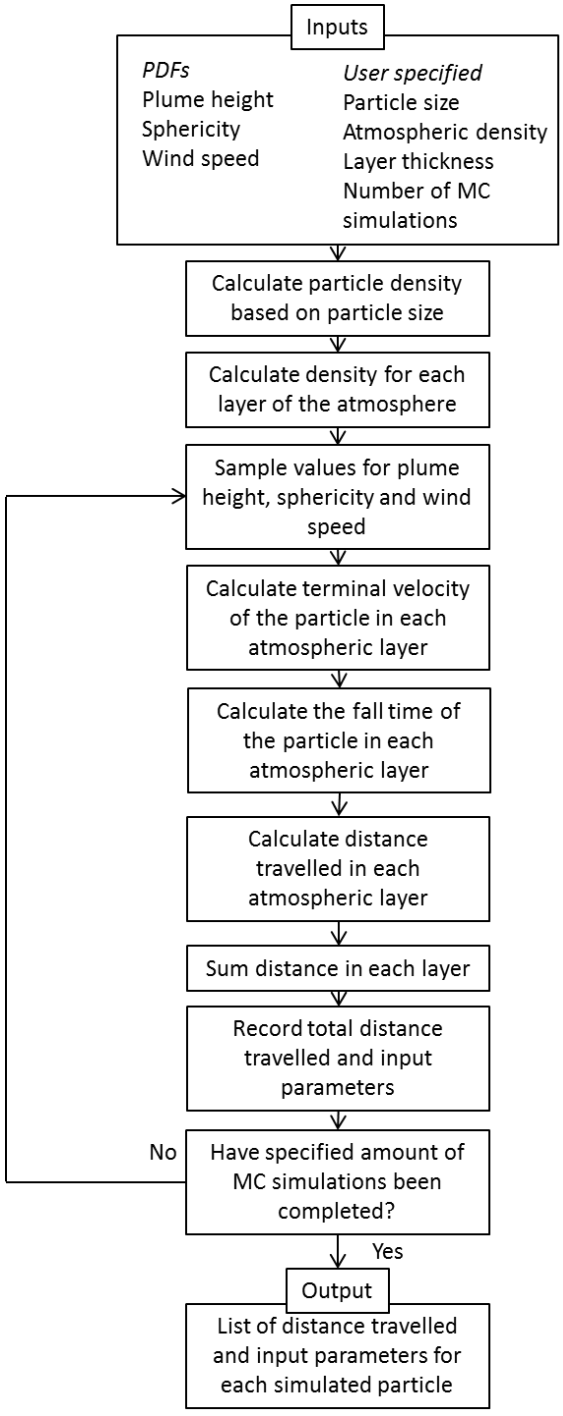

Chapter 6. Figure S2. Flowchart outline of the tephra fallout model applied in this paper.

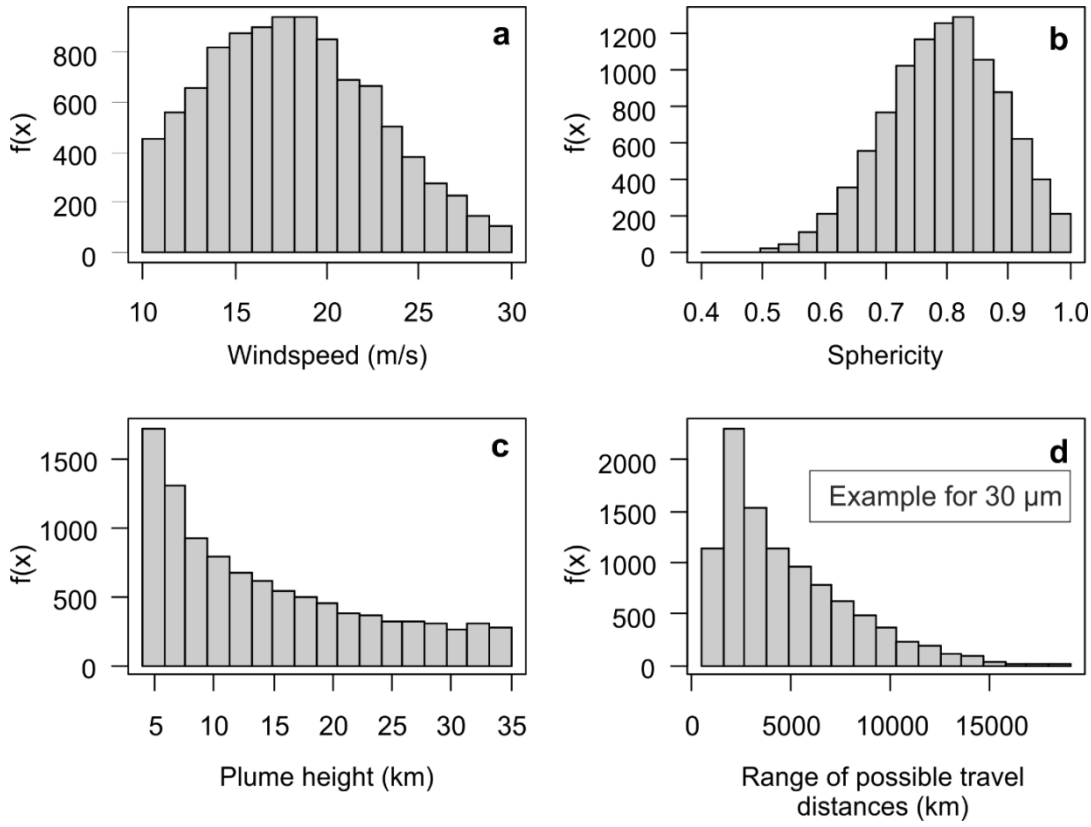

Chapter 6. Figure S3. Plots showing the values sampled from probability distribution functions for a) wind speed, b) sphericity c) plume height and d) an example of the range of output distances during a model run with a particle diameter of 30 µm.

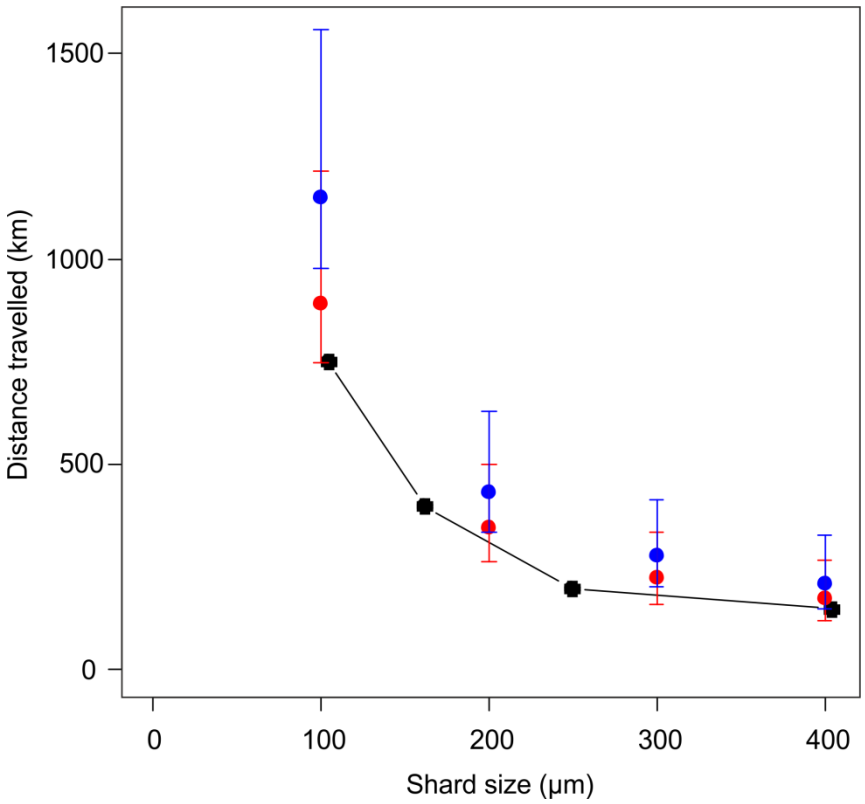

Chapter 6. Figure S4. Model fallout distances plotted against empirical data for the Mount St Helens 1980 eruption. Tephra data and eruption input parameters all from Carey and Sigurdsson (1982) plotted in black. No observed data is available for shard sizes <100 μm. Data from model outputs: point = median output value; horizontal bars indicate maximum and minimum values from model outputs. Plume height estimates for the eruption vary between 15km and 20km therefore two separate model simulations were run (red and blue lines respectively).

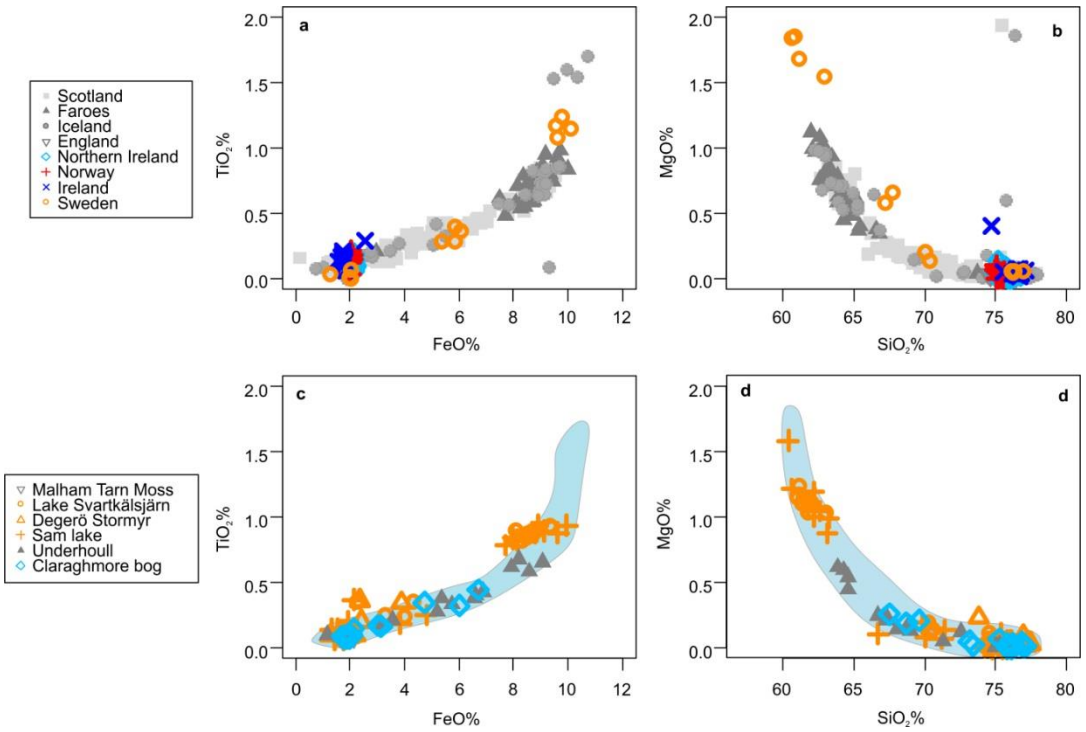

Chapter 6. Figure S5. Geochemical data for the Hekla 4 tephra plotted by region, including data from sites in this study. All data has been normalised to 100% for comparison. Colours correspond to regions as follows: Sweden (Orange); N. Ireland (Sky blue); Faroes/Shetland (Dark grey); Scotland (light grey); Ireland (Dark Blue); Norway (Red). A-B) Data from Tephrabase: England (Pilcher *et al*., 1996); Faroe Islands (Dugmore *et al*., 1996, Wastegård *et al*., 2001); Iceland (Dugmore *et al*., 1992, Boygle, 1995); Ireland (Pilcher *et al*., 1996); Northern Ireland (Pilcher *et al*., 1996, Pilcher *et al*., 1995, Swindles, 2006); Norway (North)(Pilcher *et al*., 2005); Scotland (Dugmore *et al*., 1992, Dugmore and Newton, 1992, Dugmore *et al*., 1995); Central Sweden (Zillen *et al*., 2002). C-D) Hekla 4 type data (blue shaded region) plotted against Hekla 4 tephra layers from sites in this study. A small number of shards at Claraghmore bog with a TiO2 content of ~1.5% are from an eruption of Katla which occurred at approximately the same time as the Hekla 4 eruption and have been removed from these plots for clarity (Silk N2 (Plunkett *et al*., 2004)) . The errors associated with the analytical work (EPMA) are smaller than the size of the symbols used.

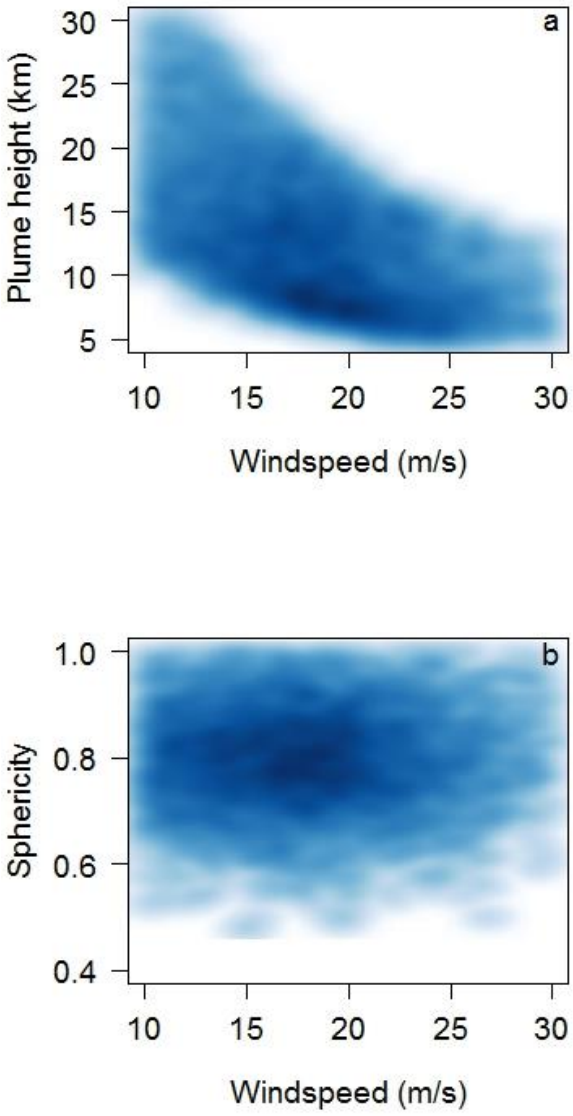

Chapter 6. Figure S6. Combinations of sampled input parameters which result in transport distances which lie between the UQ and LQ range (the range which appears to match our geological samples). Darker colours represent input parameter combinations which were stochastically sampled more often.

Tephra layer	Lake (median shard size)	Peatland (median shard size)	*p* value
Glen Garry	Malham tarn (50 µm)	Malham tarn moss (50 µm)	0.07
Hekla 1104	Sammakovuoma lake (45 µm)	Sammakovuoma peatland (40 µm)	**0.03**
SN-1	Sammakovuoma lake (45 µm)	Sammakovuoma peatland (35 µm)	**0.00**
Hekla 1104, Hekla 1158 (one mixed layer)	Lake Svartkälsjärn (45 µm)	Degerö Stormyr (40 µm)	**0.05**
Hekla 4	Lake Svartkälsjärn (40 µm)	Degerö Stormyr (45 µm)	**0.04**

Chapter 6. Table S1. Table indicating the outcome of Mann Whitney statistical tests comparing the maximum tephra grain length of tephra layers recorded in peatlands and lakes in close proximity. Statistically significant p values (indicating a significant difference in the median shard size in the lake and peatland at 95% confidence interval) are highlighted in bold.

Tephra layer	Site type	Site (and core if applicable)	Median tephra size in sample of peak tephra concentration (Max A)	Overall median tephra size (Max A)	*p* value
Hekla 1510	Peatland	Fallahogy (1)	40	40	0.85
Hekla 1510	Peatland	Fallahogy (2)	50	60	0.14
Hekla 1510	Peatland	Fallahogy (3)	50	50	0.73
Hekla 1510	Peatland	Fallahogy (4)	50	50	0.61
Hekla 1510	Peatland	Fallahogy (6)	40	40	0.39
Hekla 1510	Peatland	Fallahogy (7)	50	50	0.91
Hekla 1510	Peatland	Fallahogy (8)	40	45	0.09
Hekla 1510	Peatland	Fallahogy (9)	50	45	0.94
Hekla 1510	Peatland	Fallahogy (10)	45	45	0.82
Hekla 1510	Peatland	Fallahogy (11)	50	50	0.32
Hekla 4	Peatland	Claraghmore peatland	30	35	0.48
Hekla 4	Peatland	Malham Moss	45	40	0.45
Hekla 4	Peatland	Dëgro Stormyr	45	45	0.95
CLA-L1	Lake	Claraghmore Lake	65	65	0.65
Hekla 1104	Lake	Sammakovuoma lake	40	45	0.62
SN-1	Lake	Sammakovuoma lake	45	45	0.32
Glen Garry	Lake	Malham Tarn	50	50	0.56
Hekla 4	Lake	Lake Svartkälsjärn	40	40	0.17

Chapter 6. Table S2. Table indicating the outcome of Mann Whitney statistical tests comparing the median tephra shard size (Max A) in the sample of peak concentration with the overall median tephra shard size (Max A) for a tephra layer. There are no statistically significant p values (indicating a significant difference in the median shard size in the lake and peatland at 95% confidence interval) suggesting that shards of different sizes (Max A) are not being reworked vertically through peatlands or lakes significantly differently.

Chapter 6 Supplementary file 2. A spreadsheet containing raw data on shard size, morphology and colour for each shard in this study. Due to space constraints in this thesis and the large number of rows in this table (9500) this file is not included in the thesis.

Chapter 7: Climatic control on Icelandic volcanic activity during the Holocene

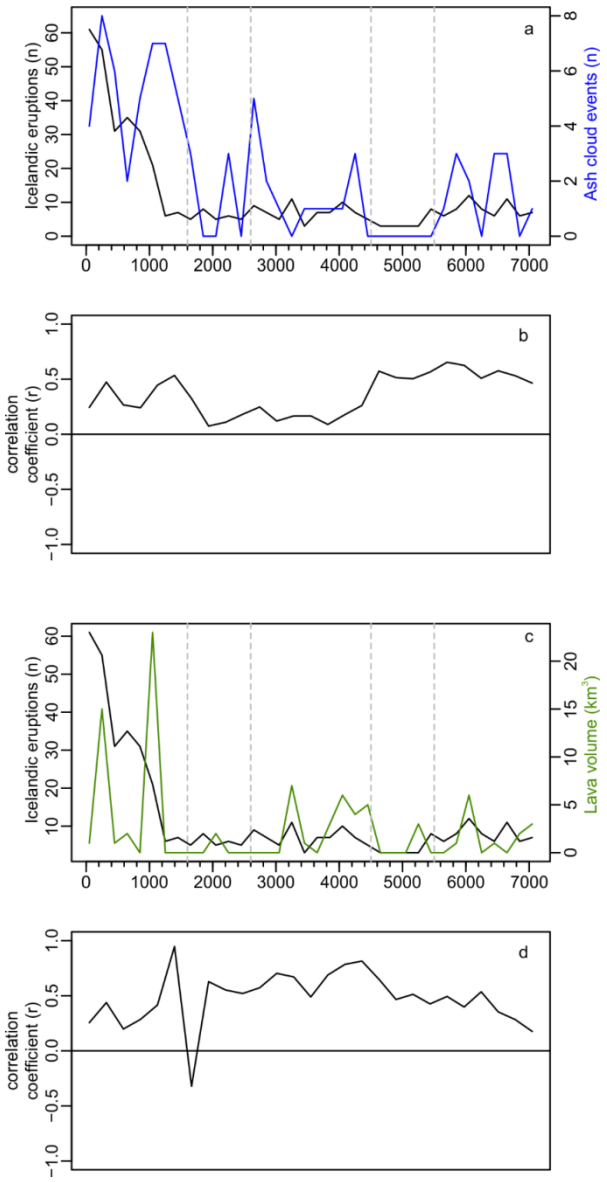

Figure S1. Plots indicating a) the frequency of Icelandic eruptions (explosive and effusive) and ash cloud events, b) the results of running correlation analysis on Icelandic eruption and ash cloud event data (width 10), c) the frequency of Icelandic eruptions and volume of lava erupted from Iceland, d) the results of running correlation analysis on Icelandic eruption frequency and lava volume (width 10). Owing to dating uncertainties on data all data are binned into 200 year bins. Dashed vertical grey lines indicate periods of reduced frequency of explosive volcanic eruptions and ash clouds in the periods between 5.5-4.5 ka BP and 2.6-1.6 ka BP

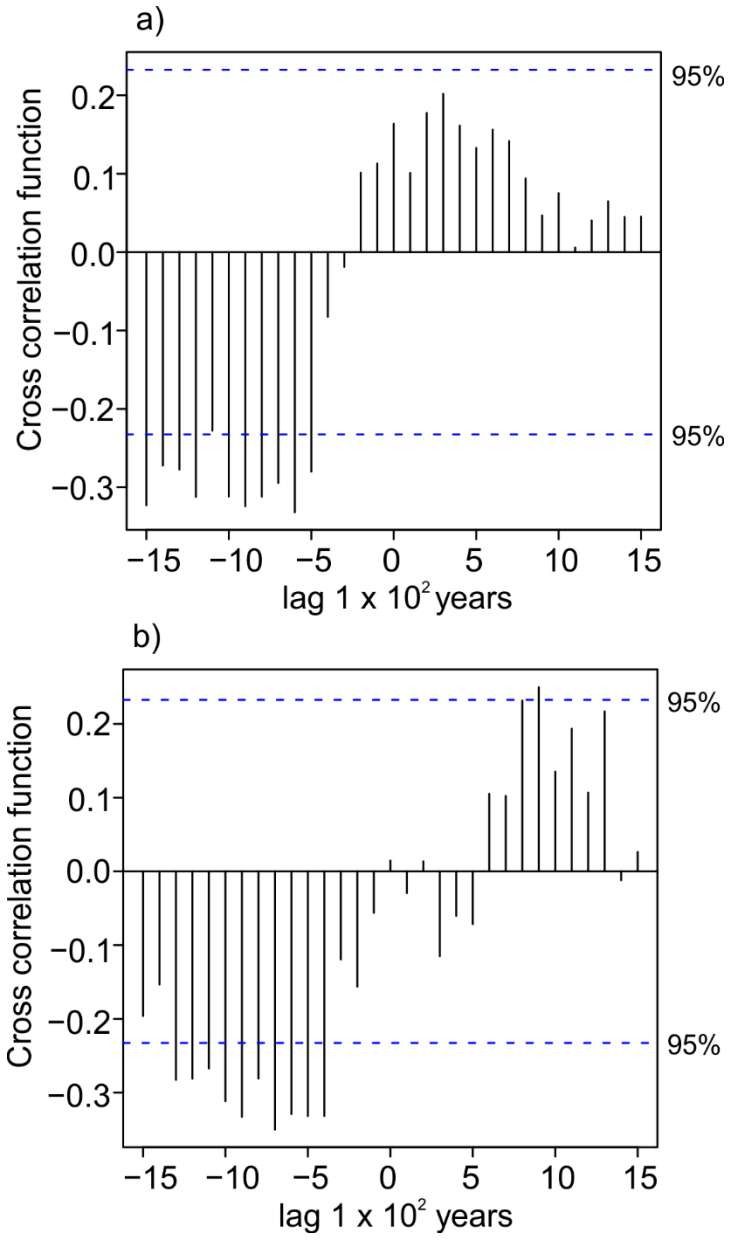

Figure S2. Plots showing the results of cross correlation analysis between a) GISP2 Na+ and Icelandic eruption frequency, b) GISP2 Na+ and ash cloud frequency over the last 7000 years. Icelandic eruption frequency and ash cloud frequency in 100 year bins, GISP2 Na+ values averaged across 100 years. Blue lines indicate 95% confidence intervals. Strongest correlations: Icelandic eruptions -0.33 at a lag of 600 years; European ash clouds -0.35 at a lag of 700 years.

Chapter 8: Estimating the frequency of volcanic ash clouds over northern Europe

Chapter 8. Supplementary File 1 Table indicating the new tephra layers identified in northern Europe since the original database by Swindles 2011 was compiled. Maps showing the new tephra layers in reference to the spatial gaps identified by Lawson *et al*., 2012 are provided in Supplementary File 3. New sites extend the existing distribution of some previously identified tephra layers such as Hekla 1158. New, additional tephra layers which do not match the geochemistry or timing of previously identified tephra layers in northern Europe have also been discovered (highlighted in bold). Tephra layers which may represent new previously unrecognised horizons, but which have too few geochemical analyses or show a large range of different geochemistry and therefore are not completely confirmed as new tephra layers are highlighted in bold italics.

Tephra	Type of record	Age/ mid-age Estimate	Source region	Source volcano	Geochemical composition	Site, Region	Location (decimal degrees)	Reference
Grímsvötn 2011	Observed	AD 2011	Iceland	Grímsvötn	Basaltic	Multiple	n/a	Stevenson *et al.*, (2013)
Hekla 1947	Cryptotephra	3 BP	Iceland	Hekla	Dacitic-Andesitic	Cors Fochno, Wales	52.504°N, 4.012°W	This study
						Roman Lode, England	51.129°N, 3.783°W	Matthews *et al.* (2008)
Askja 1875	Cryptotephra	75 BP	Iceland	Askja	Rhyolitic	Degerö Stormyr, Sweden	64.181°N, 19.564°E	Watson *et al.*, (in press)
						Linje, Poland	53.187°N, 18.309°E	This Study
						Lake Czechowskie, Poland	53.874°N, 18.238°E	Wulf *et al*, (2016)
						Lake Tiefer See, Germany	53.593°N, 12.529°E	
Hekla 1845	Cryptotephra	105 BP	Iceland	Hekla	Dacitic-Andesitic	Cors Fochno, Wales	52.504°N, 4.012°W	This study
						Fallahogy, N. Ireland	54.911°N, 6.557°W	Watson *et al.*, (2015)
BRACSH-1	**Cryptotephra**	**146 BP**	**Iceland**	**Grímsvötn?**	**Basaltic**	**Brackloon, Ireland**	**53.753°N, 9.560°W**	**Reilly *et al.*, (2015)**
QUB 384_G3_G4	Cryptotephra	250 BP	Unknown	Unknown	Dacitic	Cors Fochno, Wales	52.504°N, 4.012°W	This study
Hekla 1693	**Cryptotephra**	**257 BP**	**Iceland**	**Hekla**	**Intermediate**	**Lough Naman, N. Ireland**	**54.439°N, 7.885°W**	**Rea *et al.*, (2011)**
	Cryptotephra					**Moneygal, N. Ireland**	**54.742°N, 7.631°W**	
	Observed					**n/a**	**n/a**	**Thorarinsson, (1981)**
Hekla 1510	Cryptotephra	440 BP	Iceland	Hekla	Dacitic-Andesitic	Camillan, Ireland	52.017°N, 9.533°W	Reilly *et al.*, (2015)
						Ricksy Ball, England	51.128°N, 3.843°W	Fyfe *et al.*, (2014)
						Roman Lode, England	51.129°N, 3.783°W	Matthews *et al.*, (2008)
Öræfajökull 1362	Cryptotephra	588 BP	Iceland	Öræfajökull	Rhyolitic	Claraghmore Bog, N. Ireland	54.633°N, 7.454°W	Watson *et al.*, (in press)
Unknown	***Cryptotephra***	***778 BP***	***Unknown***	***Unknown***	**Andesitic-Dacitic**	***Cors Fochno, Wales***	***52.504°N, 4.012°W***	***This study***
Hekla 1158	Cryptotephra	792 BP	Iceland	Hekla	Dacitic	Degerö Stormyr, Sweden	64.181°N, 19.564°E	Watson *et al.*, (in press)
						Lake Svartkälsjärn, Sweden	64.264°N, 19.552°E	
						Stordalen, Sweden	68.356°N, 19.044°E	Swindles *et al.*, (2015)
Hekla 1104	Cryptotephra	846 BP	Iceland	Hekla	Rhyolitic	Camillan, Ireland	52.017°N, 9.533°W	Reilly *et al.*, (2015)
						Claraghmore Bog, N. Ireland	54.633°N, 7.454°W	Watson *et al.*, 2016 in press
						Degerö Stormyr, Sweden	64.181°N, 19.564°E	
						Lake Svartkälsjärn, Sweden	64.264°N, 19.552°E	
						Sammakovuoma bog, Sweden	66.995°N, 21.457°E	
						Lake Sammakovuoma, Sweden	66.992°N, 21.500°E	
CLA-L1	***Cryptotephra***	***Younger then MOR-T4 = 950 BP***	**Iceland**	**Grímsvötn**	**Basaltic**	**Claraghmore lake , N. Ireland**	**54.631°N, 7.450°W**	**Watson *et al.*, (in press)**
MOR-T4	Cryptotephra	950 BP	Iceland	Unknown	Rhyolitic-Dacitic	Cors Fochno, Wales	52.504°N, 4.012°W	This study
						Claraghmore Bog, N. Ireland	54.633°N, 7.454°W	Watson *et al.*, (2016)
						Claraghmore lake , N. Ireland	54.631°N, 7.450°W	

Unknown Grímsvötn	**Cryptotephra**	**1077 BP**	**Iceland**	**Grímsvötn**	**Basaltic**	Lake Tiefer See, Germany	53.593°N, 12.529°E	Wulf *et al*., (2016)
AD 860 B	Cryptotephra	1103 BP	Alaska	Bona-Churchill massif	Rhyolitic	Rough Tor, England?	50.589°N, 4.625°W	This study
AD 860 A	Cryptotephra	1117 BP	Iceland?	Grímsvötn?	Rhyolitic	Rough Tor, England?	50.589°N, 4.625°W	This study
						Ricksy Ball, England	51.128°N, 3.843°W	Fyfe *et al*., (2014)
SN-1	**Cryptotephra**	**1165 BP**	**Iceland**	**Snæfellsjökull**	**Trachydacite**	**Sammakovuoma bog, Sweden**	**66.995°N, 21.457°E**	**Watson *et al*., (in press)**
						Lake Sammakovuoma, Sweden	**66.992°N, 21.500°E**	
Unknown Icelandic = DOM 4?	**Cryptotephra**	**1890 BP and 1960 BP**	**Iceland?**	**Unknown**	**Rhyolitic**	**Lake Czechowskie, Poland**	**53.874°N, 18.238°E**	**Wulf *et al*., (2016)**
Glen Garry	Cryptotephra	2176 BP	Iceland?	Unknown	Dacitic-Rhyolitic	Malham Tarn Moss, England	54.097°N, 2.173°W	Watson *et al*., (in press)
						Malham Tarn, England	54.096°N, 2.165°W	
						Lake Tiefer See, Germany	53.593°N, 12.529°E	Wulf *et al*., (2016)
SV-L2 - QUB 570 Group 2 (c. AD 650)?	***Cryptotephra***	***2250 BP***	***?***	***Unknown***	***Dacitic-Andesitic***	***Lake Svartkälsjärn, Sweden***	***64.264°N, 19.552°E***	***Watson et al., (in press)***
DCSH-2	**Cryptotephra**	**2365 BP**	**Azores?**	**Furnas volcano?**	**Trachydacite**	**Derrycunihy, Ireland**	**51.970°N, 9.600°W**	**Reilly *et al*., (2015)**
BMR-190	Cryptotephra	2595 BP	Iceland	Hekla	Dacitic	Camillan, Ireland	52.017°N, 9.533°W	Reilly *et al*., (2015)
OMH-185 Population 2	Cryptotephra	2668 BP	?	Unknown	Rhyolitic-Dacitic	Ricksy Ball, England	51.128°N, 3.843°W	Fyfe *et al*., (2014)
Microlite	Cryptotephra	2668 BP	Iceland	Snaefellsjökull	Rhyolitic	Roman Lode, England	51.129°N, 3.783°W	Matthews *et al.* (2008)
Hekla 3	Cryptotephra	2996 BP	Iceland	Hekla	Dacitic-Rhyolitic	Degerö Stormyr, Sweden	64.181°N, 19.564°E	Watson *et al*., (in press)
Hekla-S/Kebister	Cryptotephra	3725 BP	Iceland	Hekla	Dacitic-Rhyolitic	Degerö Stormyr, Sweden	64.181°N, 19.564°E	Watson *et al*., (in press)
Silk-N2	Cryptotephra	4287 BP	Iceland	Katla	Dacitic-Trachydacitic	Claraghmore Bog, N. Ireland	54.633°N, 7.454°W	Watson *et al*., (in press)
Hekla 4	Cryptotephra	4287 BP	Iceland	Hekla	Rhyolitic-Dacitic	Degerö Stormyr, Sweden	64.181°N, 19.564°E	Watson *et al*., (in press)
						Lake Svartkälsjärn, Sweden	64.264°N, 19.552°E	
						Lake Sammakovuoma, Sweden	66.992°N, 21.500°E	
						Malham Tarn Moss, England	54.097°N, 2.173°W	
						Claraghmore lake , N. Ireland	54.631°N, 7.450°W	
						Fallahogy, N. Ireland	54.911°N, 6.557°W	Roland *et al*., (2014)
						Lake Tiefer See, Germany	53.593°N, 12.529°E	Wulf *et al*., (2016)
Unknown #5	***Cryptotephra***	***5500 BP***	***?***	***?***	***Rhyolitic-Dacitic***	***Lake Svartkälsjärn, Sweden***	***64.264°N, 19.552°E***	***Watson et al., (in press)***
Lairg B	Cryptotephra	6676 BP	Iceland	Torfajökull	Rhyolitic	Claraghmore lake , N. Ireland	54.631°N, 7.450°W	Watson *et al*., (in press)
						Malham Tarn Moss, England	54.097°N, 2.173°W	
						Ricksy Ball, England	51.128°N, 3.843°W	Fyfe *et al*., (2014)

						Lake Tiefer See, Germany	53.593°N, 12.529°E	Wulf *et al.*, (2016)
Lairg A	Cryptotephra	6900 BP	Iceland	Hekla	Rhyolitic	Claraghmore lake, N. Ireland	54.631°N, 7.450°W	Watson *et al.*, (in press)
						Claraghmore Bog, N. Ireland	54.633°N, 7.454°W	
						Malham Tarn Moss, England	54.097°N, 2.173°W	
						Degerö Stormyr, Sweden	64.181°N, 19.564°E	
						Ricksy Ball, England	51.128°N, 3.843°W	Fyfe *et al.*, (2014)

Chapter 8. Supplementary File 2. New tephras in Southern England, Wales and Poland.

Bodmin Moor (Rough Tor South)

Bodmin Moor is an area of moorland in the South of England. Rough Tor South is a topogenous valley mire located to the northwest of Bodmin Moor (50.59°N, 4.63°W), the mire has accumulated around a spring and has been subject to previous stratigraphic and paleoecological study (Gearey *et al*., 2000; Hopla and Gearey, 2009). Previous research has identified a record spanning ~3 meters of peat at Rough Tor South (Gearey and Charman, 1996).

Despite extensive investigation of the area, the deepest peat identified during this study was 140 cm in depth. The bottom of the core contains increasing amounts of mineral material, as evidenced by loss-on-ignition values (% loss-on-ignition < 5%), suggesting that the peat-mineral soil interface was sampled. We identified two tephra layers in the Rough Tor South core at depths of 30-31 cm (BD 30) and 36-37 cm (BD 36). The major element glass geochemistry of shards from these two tephra layers suggests a correlation to the AD 860 layers (B and A respectively). Radiocarbon dates from previous paleoenvironmental studies at Rough Tor South indicate an age of 1675 cal yr BP for peat at a depth of 115 cm (Gearey *et al*., 2000). Based on linear interpolation, peat at ~30cm depth would have an age of 395 cal yr BP, much more recent than the age of the AD 860 tephra layers (1090 cal yr BP). However, areas of peat on Bodmin Moor have been subject to anthropogenic disturbance, through peat cutting, artificial drainage and tin steaming (Gearey *et al*., 2000). Rough Tor has a high density of archaeological remains and paleoenvironmental investigations indicate that humans have been in the area since the Neolithic (Hopla and Gearey, 2009). We therefore suggest that the top of the core obtained from Rough Tor South for this study was lost due to peat cutting or anthropogenic disturbance in the past. Our conclusion is supported by the short length of the core recovered when compared to those retrieved by previous studies; our core of 1.4 m was shorter than the 2.8 m cores retrieved by (Gearey *et al*., 2000; Hopla and Gearey, 2009). Secondly, we conducted a scan in the top section of the core for spheroidal carbonaceous particles (SCPs); microscopic soot

particles which are indicators of post industrial revolution air pollution (Rose and Harlock, 1998). SCPs have been identified in the surface sediments of lakes in Cornwall (Rose and Harlock, 1998). However, no SCPs were identified in the top of the core from Rough Tor South, adding weight to our hypothesis that the top of the core at Rough Tor South was lost due to anthropogenic disturbance and supporting our correlation of the tephras identified to the AD 860 A (BD 36) and AD 860 B (BD 30) tephra layers.

The AD 860 layers (1090 cal yr BP) were originally discovered in Sluggan bog, Ireland, apparent in the peat as one tephra layer but containing glass shards of two different geochemical compositions (Pilcher *et al*., 1995). The AD 860 B tephra has been identified at 20 sites in Ireland, Great Britain, Scandinavia and Germany (Langdon and Barber, 2004; Pilcher *et al*., 2005; Pilcher *et al*., 1995; Van Den Bogaard and Schmincke, 2002) The BD 30 tephra at Rough Tor South represents the first identification of the AD 860 B in the south of England, despite other tephrochronological studies in the region (Fyfe *et al*., 2014; Matthews, 2008). The AD 860 B tephra was recently linked to a source eruption in Alaska (Jensen *et al*., 2014) and has been precisely dated in the NGRIP ice core to AD 846-848 (1103 cal yr BP) (Coulter *et al*., 2012). The AD 860 A tephra has been tentatively linked to an eruption of the Grímsvötn volcanic system, Iceland (Wastegård *et al*., 2003). AD 860 A has a more confined spatial distribution when compared to the AD 860 B tephra layer and has been identified at 7 sites, the majority (n = 6) in Great Britain and Ireland (Chambers *et al*., 2004; Langdon and Barber, 2004; Swindles, 2006). BD 36 represents the second finding of the AD 860 A tephra in Southern England, where it has recently been identified on Exmoor (Fyfe *et al*., 2014).

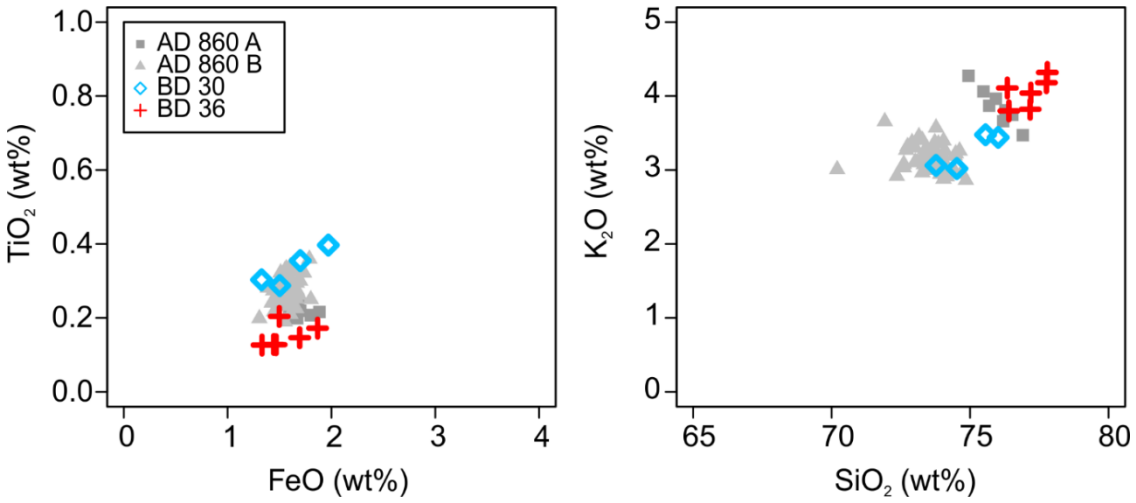

Chapter 8. Supplementary file 2. Figure 1- Geochemical bi-plots of major elements of glass from the two tephra layers detected at Bodmin moor (Rough Tor South) plotted against the glass geochemistry of known tephras based on type data from Hall and Pilcher (2002); Pilcher *et al*. (1995); Swindles (2006)

Wales (Cors Fochno)

Cors Fochno (Borth Bog) is a raised bog in Ceredigion, West Wales (52.50°N, 4.01°W). Previous paleoenvironmental research on the site indicates a peat age of 6910–7170 cal yr BP at a depth of ~6.9 meters (Hughes and Schulz, 2001). A core of 7.2 meters of well humified peat was sampled from the peatland for this study. Continuous analysis of the core identified five cryptotephra layers, all found in the top 130 cm of peat. Samples of the core below 130 cm occasionally contain one or two glass shards resembling cryptotephra, but glass shard concentrations are too sparse to be suitable for geochemical analysis.

The top 24 cm of peat at Cors Fochno contains two cryptotephra layers of similar major element glass geochemistry, CF-1 (13-15 cm) and CF-2 (23-24 cm). Both CF-1 and CF-2 are comprised of a sparse concentration of small brown glass shards. Geochemical analysis suggests that both tephra layers have a dacitic-andesitic glass shard geochemistry similar to the composition of glass shards from historic eruptions of the Hekla volcano (Figure 2a-b). Over the last 500 years multiple tephra layers with highly similar major element geochemistry have been deposited over northern Europe during

eruptions of the Hekla volcano in: AD 1510, 1845 and 1947 (Dugmore *et al*., 1996; Rea *et al*., 2012; Watson *et al*., 2015).

Spheroidal carbonaceous particles (SCPs) are a marker produced by the burning of fossil fuels, SCPs first appear in records during the industrial revolution and gradually increase in abundance before reaching a peak in concentration in samples dating to c. 1970 in the UK (Rose and Harlock, 1998). SCPs were detected in large numbers in samples containing the CF-1 tephra, whereas, only a small number of SCPs were present in samples containing the CF-2 tephra. The presence of SCPS alongside glass shards from both the CF-1 and CF-2 tephras layers suggests that these tephras were deposited too recently to be from the Hekla eruption of AD 1510 because this eruption predates the industrial revolution, the point at which SCPs appear in the geological record (Swindles and Roe, 2006). Given the overall stratigraphy and SCP concentrations we assign CF-1 and CF-2 to the eruptions of Hekla in 1947 and 1845, respectively. The Hekla 1947 tephra has been identified at 21 sites, the majority (n = 19) in Ireland. The Hekla 1947 tephra has also recently been identified at sites in Scotland (Housley *et al*., 2010) and southern England (Matthews, 2008). The Hekla 1845 tephra has only recently been identified at sites in Ireland (Rea, 2011; Watson *et al*., 2015). Our discovery represents the first record of these cryptotephra layers in Wales, and the first of the Hekla 1845 tephra outside of Ireland.

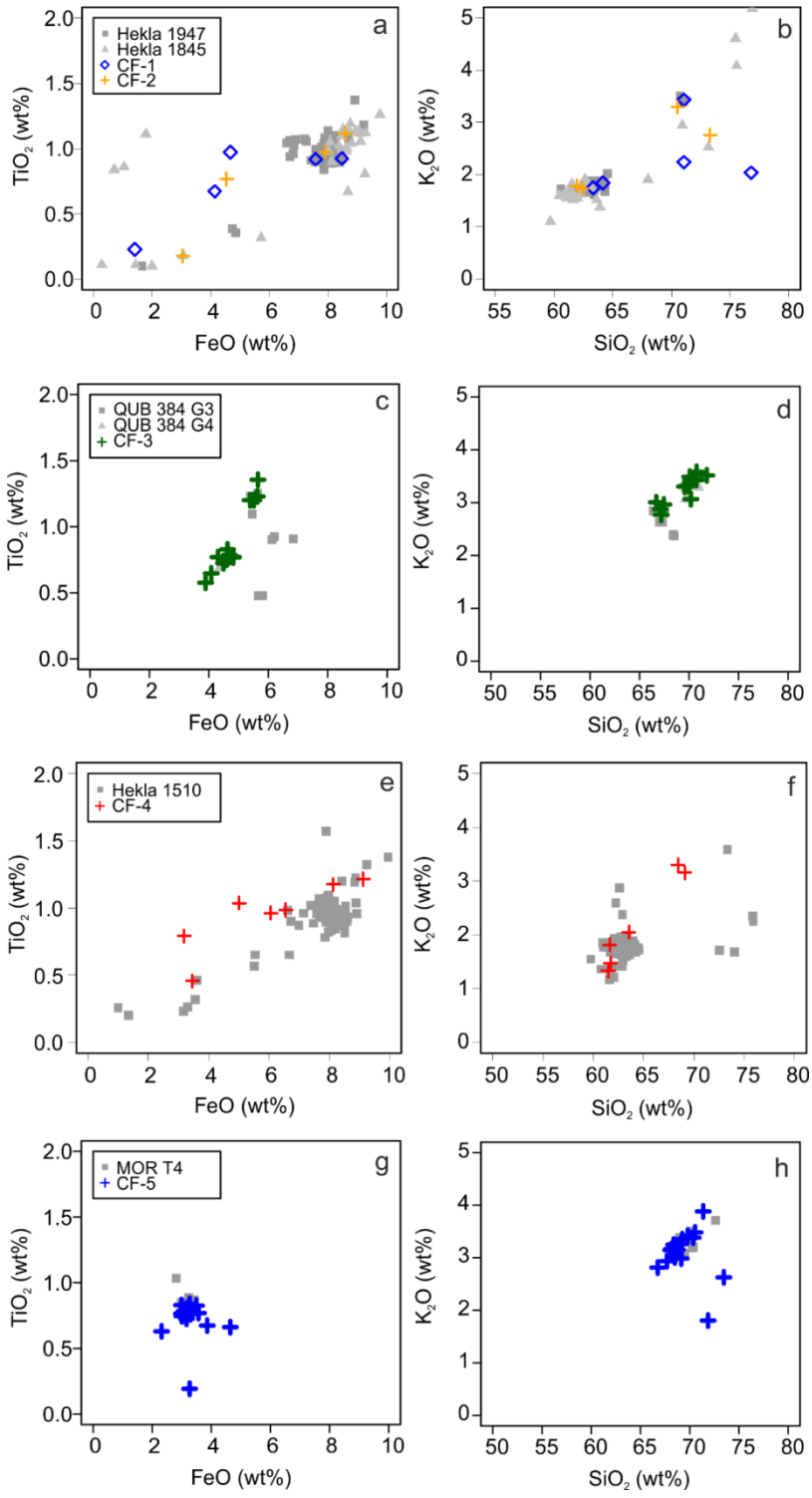

Chapter 8. Supplementary file 2. Figure 2- Geochemical bi-plots of major elements of glass from the five tephra layers detected at Cors Fochno, Wales, plotted against the glass geochemistry of known tephras based on type data from Dugmore *et al*. (1995); Hall and Pilcher (2002); Larsen *et al*. (1999); Pilcher *et al*. (2005); Pilcher *et al*. (1996); Swindles (2006); Wastegård (2002); Watson *et al*. (2015).

A third tephra layer, CF-3 (31-34 cm) contains clear glass shards with a pink tinge. The major element geochemistry of glass shards from this tephra layer suggests CF-3 contains shards from two geochemical compositions (Figure 2c-d). The best geochemical match for this tephra appears to be with glass shards from the QUB 384 tephra population groups 3 and 4. The QUB 384 tephra groups 3 and 4 were also identified as a single peak in tephra shard concentration on the Lofoten Islands, northern Norway (Pilcher *et al*., 2005). Assignment to the QUB 384 group 3 and 4 tephras (200-300 cal yr BP) is supported by the age of the CF-3 tephra layer, which is bracketed by the tephra layers of CF-2 (=Hekla 1845, 23 cm) and CF-5 (=MOR-T4, 96 cm) to an age of between 105-950 cal yr BP. CF-3 represents the second discovery of the QUB 384 group 3 and 4 tephra layers and greatly extends the known fallout region of these tephra layers.

The tephra layer CF-4 (95-97 cm) consists mainly of brown glass shards. We were able to obtain only 7 successful geochemical analyses on glass shards from the CF-4 tephra layer (Figure 4e-f). These analyses indicate a wide range of geochemistry and very little similarity between the geochemistry of tephra shards from this layer. CF-4 is above CF-5 which is geochemically correlated to the MOR-T4 tephra and gives a maximum age for CF-4 of after ~1000 AD. We could not identify a geochemical match between the geochemistry of glass shards from CF-4 and the geochemistry of any cryptotephra layers identified in northern Europe which are younger than CF-5 (= MOR-T4 ~AD 1000). Some of the analyses indicate a geochemical match to the Hekla 1510 tephra, which has previously been identified at sites in the South of England (Fyfe *et al*., 2014; Matthews, 2008). CF-4 may represent a new tephra layer, however due to a lack of successful geochemical analyses and the range of geochemistry in analyses of different glass shards more information is required before CF-4 is described as a new tephra rather than a mix of tephras from previously identified cryptotephras.

CF-5 (115-118 cm) is correlated based on analyses of glass shard geochemistry to the MOR-T4 tephra previously identified in Ireland (Chambers *et al*., 2004; Watson, 2016 in Press) (Figure 4g-h). The discovery of the MOR-T4 tephra at Cors Fochno is the first identification of this tephra outside of Ireland. The source eruption for the MOR-T4

tephra is unknown but the tephra is thought to be of Icelandic origin (Chambers *et al*., 2004).

Poland (Linje)

Linje mire is located in northern Poland (53.18°N, 18.30°E) the peatland vegetation is indicative of a poor fen, but areas of ombrotrophic vegetation are present (Słowińska *et al*., 2010). A 70 cm long core was extracted from Linje mire. The core contained only one tephra layer (Linje-1) at a depth of 56-60 cm. The Linje-1 tephra layer consists of large clear glass shards of vesicular morphology. The major element geochemistry of glass shards from Linje-1 is a match to glass shards from the Askja 1875 tephra (Figure 3). The assignment of Linje-1 to the eruption of Askja 1875 is further supported by a ^{14}C age-depth model from another core from the same peatland, which suggests that the age of peat at the depth of the Linje-1 tephra (56-60 cm) is ~1800-1900 AD (Lamentowicz, personal comm.). Tephra from the eruption of Askja 1875 was dispersed widely over Scandinavia (Wastegård, 2005), is found at two sites in Germany, (Van Den Bogaard and Schmincke, 2002; Wulf *et al*., 2016) and has recently been identified in the sediment of Lake Czechowskie in Poland (Wulf *et al*., 2016).

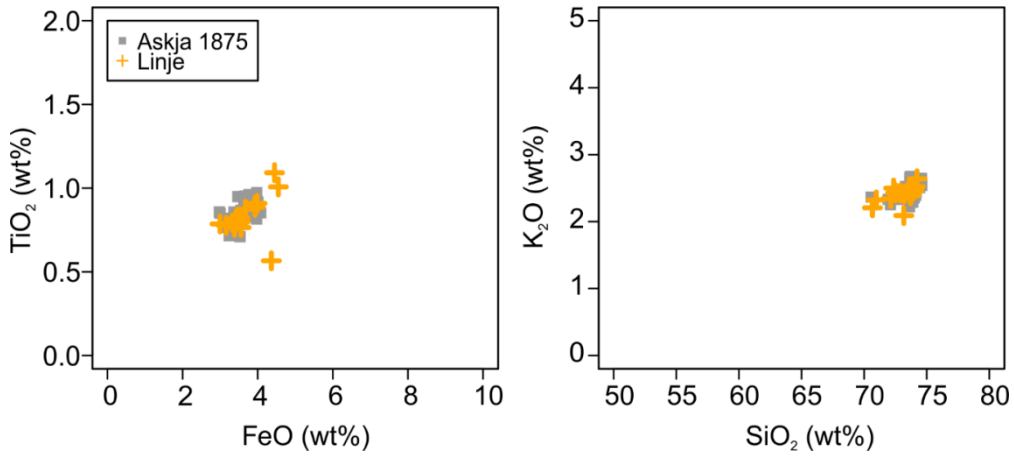

Chapter 8. Supplementary file 2. Figure 3- Geochemical bi-plots of major elements of glass from the tephra layer detected at Linje Mire, Poland, plotted against the glass geochemistry of the Askja 1875 tephra layer based on type data from Larsen *et al*. (1999); Oldfield *et al*. (1997); Pilcher *et al*. (2005).

Poland (Kusowskie Bagno)

Kusowskie Bagno is a Baltic bog in northern Poland (53.82°N, 16.59°E). A core of 8 meters, spanning the entire depth of peat at the site was extracted (Lamentowicz *et al*., 2008). Only one tephra layer was identified (Kusowskie-1). Glass shards were detected at a depth of 4-4.5 meters and the analysis of major elements of these shards indicate geochemical similarity to glass shards from the AD 860 B tephra (Figure 4), recently correlated to an eruption in Alaska (Jensen *et al*., 2014). However, the depth at which the Kusowskie Bagno tephra was identified would require an exceptional rate of peat accumulation since AD 860. We therefore suggest that the tephra identified at Kusowskie Bagno is derived from an unknown eruption, most likely in Alaska.

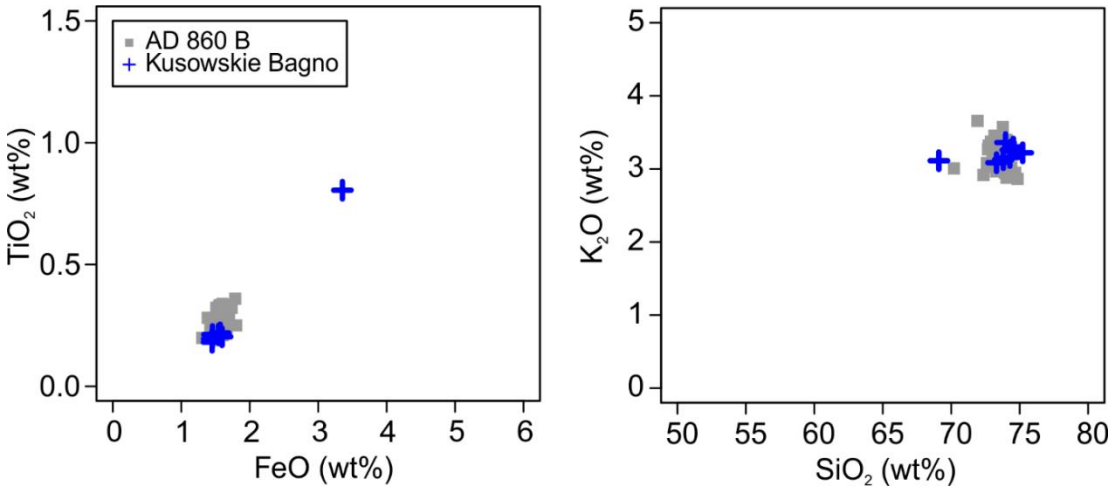

Chapter 8. Supplementary file 2. Figure 4- Geochemical bi-plots of major elements of glass from the tephra layer detected at Kusowskie Bagno Peatland, Poland, plotted against the glass geochemistry of the AD 860 B tephra layer based on type data from Hall and Pilcher (2002); Pilcher *et al*. (2005); Swindles (2006)

Arctic Sweden (Stordalen)

Stordalen peatland is located near to Abisko, northern Sweden (68.36°N, 19.04°E). Two tephra layers have been identified in the peatland at Storadalen, a tephra layer at 22-24 cm (SD4) was identified and correlated to the Hekla 1158 eruption by Swindles *et al*.

(2015). A second tephra layer in the same core at 36-38 cm (SD5) contains glass shards of a similar geochemistry to those from the SN-1 tephra (1183-1147 cal yr BP) which has recently been identified in two other sites in Northern Sweden (Watson, 2016 in Press) (Figure 5).

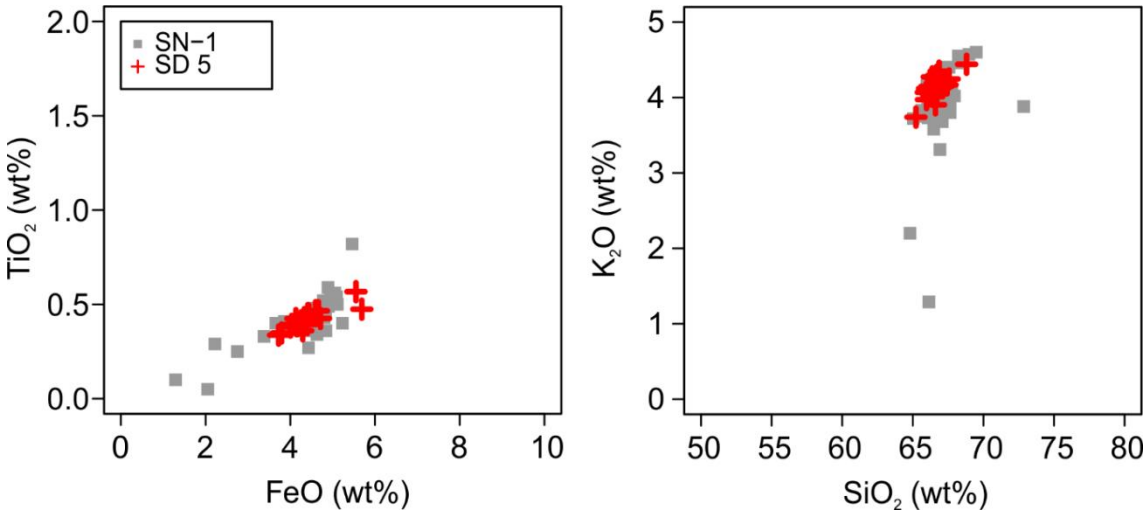

Chapter 8. Supplementary file 2. Figure 5- Geochemical bi-plots of major elements of glass from the tephra layer detected at Stordalen peatland, Sweden, plotted against the glass geochemistry of the SN-1 tephra layer based on type data from Holmes *et al*. (2016); Larsen *et al*. (2002).

References

Chambers, F.M., Daniell, J.R.G., Hunt, J.B., Molloy, K., O'Connell, M., 2004. Tephrostratigraphy of An Loch Mor, Inis Oirr, western Ireland: implications for Holocene tephrochronology in the northeastern Atlantic region. Holocene 14, 703-720.

Coulter, S.E., Pilcher, J.R., Plunkett, G., Baillie, M., Hall, V.A., Steffensen, J.P., Vinther, B.M., Clausen, H.B., Johnsen, S.J., 2012. Holocene tephras highlight complexity of volcanic signals in Greenland ice cores. Journal of Geophysical Research-Atmospheres 117.

Dugmore, A.J., Larsen, G., Newton, A.J., 1995. 7 Tephra isochrones in Scotland. Holocene 5, 257-266.

Dugmore, A.J., Newton, A.J., Edwards, K.J., Larsen, G., Blackford, J.J., Cook, G.T., 1996. Long-distance marker horizons from small-scale eruptions: British tephra deposits from the AD 1510 eruption of Hekla, Iceland. Journal of Quaternary Science 11, 511-516.

Fyfe, R., Anderson, P., Barnett, R., Blake, W., Daley, T., Head, K., MacLeod, A., Matthews, I., Smith, D., 2014. Vegetation and climate change on Exmoor over the last

millennium: detailed analysis of Ricksy Ball. http://www.southwestwater.co.uk/media/pdf/5/5/Vegetation_and_climate_change_on_Exmoor_Fyfe_et_al_2014.pdf

Gearey, B., Charman, D., 1996. Rough Tor, Bodmin Moor: testing some archaeological hypotheses with landscape palaeoecology. Devon and East Cornwall field guide, Quaternary Research Association, London, 101-119.

Gearey, B., Charman, D., Kent, M., 2000. Palaeoecological evidence for the prehistoric settlement of Bodmin Moor, Cornwall, Southwest England. Part I: the status of woodland and early human impacts. Journal of archaeological science 27, 423-438.

Hall, V.A., Pilcher, J.R., 2002. Late-Quaternary Icelandic tephras in Ireland and Great Britain: detection, characterization and usefulness. Holocene 12, 223-230.

Holmes, N., Langdon, P.G., Caseldine, C.J., Wastegård, S., Leng, M.J., Croudace, I.W., Davies, S.M., 2016. Climatic variability during the last millennium in Western Iceland from lake sediment records. The Holocene, doi:10.1177/0959683615618260.

Hopla, E., Gearey, B., 2009. Mesolithic-Neolithic anthropogenic impacts on the upland environment of Bodmin Moor, south-west England: a re-investigation of the pollen record from Rough Tor South. Cornish Archaeology 48-49, 253-264.

Housley, R.A., Blockley, S.P.E., Matthews, I.P., MacLeod, A., Lowe, J.J., Ramsay, S., Miller, J.J., Campbell, E.N., 2010. Late Holocene vegetation and palaeoenvironmental history of the Dunadd area, Argyll, Scotland: chronology of events. Journal of Archaeological Science 37, 577-593.

Hughes, P.D.M., Schulz, J., 2001. The development of the Borth Bog (Cors Fochno) mire system and the submerged forst beds at Ynyslas, in: Walker, M.J.C.a.M., D. (Ed.), The Quaternary of West Wales field guide. Quaternary Research Association, pp. 104-112.

Jensen, B.J.L., Pyne-O'Donnell, S., Plunkett, G., Froese, D.G., Hughes, P.D.M., Sigl, M., McConnell, J.R., Amesbury, M.J., Blackwell, P.G., van den Bogaard, C., Buck, C.E., Charman, D.J., Clague, J.J., Hall, V.A., Koch, J., Mackay, H., Mallon, G., McColl, L., Pilcher, J.R., 2014. Transatlantic distribution of the Alaskan White River Ash. Geology 42, 875-878.

Lamentowicz, M., Cedro, A., Gałka, M., Goslar, T., Miotk-Szpiganowicz, G., Mitchell, E.A.D., Pawlyta, J., 2008. Last millennium palaeoenvironmental changes from a Baltic bog (Poland) inferred from stable isotopes, pollen, plant macrofossils and testate amoebae. Palaeogeography, Palaeoclimatology, Palaeoecology 265, 93-106.

Langdon, P.G., Barber, K.E., 2004. Snapshots in time: precise correlations of peat-based proxy climate records in Scotland using mid-Holocene tephras. Holocene 14, 21-33.

Larsen, G., Dugmore, A., Newton, A., 1999. Geochemistry of historical-age silicic tephras in Iceland. Holocene 9, 463-471.

Larsen, G., Eiríksson, J., Knudsen, K.L., Heinemeier, J., 2002. Correlation of late Holocene terrestrial and marine tephra markers, north Iceland: implications for reservoir age changes. Polar Research 21, 283-290.

Matthews, I.P., 2008. Roman Lode, Exmoor, Devon: Tephrochronology, Research Department Report Series. English Heritage.

Oldfield, F., Thompson, R., Crooks, P.R.J., Gedye, S.J., Hall, V.A., Harkness, D.D., Housley, R.A., McCormac, F.G., Newton, A.J., Pilcher, J.R., Renberg, I., Richardson, N., 1997. Radiocarbon dating of a recent high-latitude peat profile: Stor Amyran, northern Sweden. Holocene 7, 283-290.

Pilcher, J., Bradley, R.S., Francus, P., Anderson, L., 2005. A Holocene tephra record from the Lofoten Islands, Arctic Norway. Boreas 34, 136-156.

Pilcher, J.R., Hall, V.A., McCormac, F.G., 1995. Dates of Holocene Icelandic volcanic eruptions from tephra layers in Irish peats. Holocene 5, 103-110.

Pilcher, J.R., Hall, V.A., McCormac, F.G., 1996. An outline tephrochronology for the Holocene of the north of Ireland. Journal of Quaternary Science 11, 485-494.

Rea, H.A., 2011. Peatland records of recent (last c.250 years) climate change in the North of Ireland, Faculty of Engineering and Physical Sciences. Queens University Belfast

Rea, H.A., Swindles, G.T., Roe, H.M., 2012. The Hekla 1947 tephra in the north of Ireland: regional distribution, concentration and geochemistry. Journal of Quaternary Science 27, 425-431.

Rose, N.L., Harlock, S., 1998. The Spatial Distribution of Characterised Fly-Ash Particles and Trace Metals in Lake Sediments and Catchment Mosses in the United Kingdom. Water, Air, and Soil Pollution 106, 287-308.

Słowińska, S., Słowiński, M., Lamentowicz, M., 2010. Relationships between local climate and hydrology in Sphagnum mire: Implications for palaeohydrological studies and ecosystem management. Polish Journal of Environmental Studies 19, 779-787.

Swindles, G.T., 2006. Reconstruction of Holocene climate change from peatlands in the north of Ireland. PhD Thesis. Queens University Belfast.

Swindles, G.T., Morris, P.J., Mullan, D., Watson, E.J., Turner, T.E., Roland, T.P., Amesbury, M.J., Kokfelt, U., Schoning, K., Pratte, S., Gallego-Sala, A., Charman, D.J., Sanderson, N., Garneau, M., Carrivick, J.L., Woulds, C., Holden, J., Parry, L., Galloway, J.M., 2015. The long-term fate of permafrost peatlands under rapid climate warming. Sci Rep 5, 17951.

Swindles, G.T., Roe, H.M., 2006. Constraining the age of spheroidal carbonaceous particle (SCP) stratigraphies in peats using tephrochronology. Quaternary Newsletter 110, 2-9.

Van Den Bogaard, C., Schmincke, H.U., 2002. Linking the North Atlantic to central Europe: a high-resolution Holocene tephrochronological record from northern Germany. Journal of Quaternary Science 17, 3-20.

Wastegård, S., 2002. Early to middle Holocene silicic tephra horizons from the Katla volcanic system, Iceland: new results from the Faroe Islands. Journal of Quaternary Science 17, 723-730.

Wastegård, S., 2005. Late Quaternary tephrochronology of Sweden: a review. Quaternary International 130, 49-62.

Wastegård, S., Hall, V.A., Hannon, G.E., van den Bogaard, C., Pilcher, J.R., Sigurgeirsson, M.Á., Hermanns-Auoardóttir, M., 2003. Rhyolitic tephra horizons in northwestern Europe and Iceland from the AD 700s–800s: a potential alternative for dating first human impact. The Holocene 13, 277-283.

Watson, E.J., Swindles, G.T., Lawson, I.T., Savov, I.P., 2016. Do peatlands or lakes provide the most comprehensive distal tephra records? Quaternary Science Reviews 139, 110-128.

Watson, E.J., Swindles, G.T., Lawson, I.T., Savov, I.P., 2015. Spatial variability of tephra and carbon accumulation in a Holocene peatland. Quaternary Science Reviews 124, 248-264.

Wulf, S., Dräger, N., Ott, F., Serb, J., Appelt, O., Guðmundsdóttir, E., van den Bogaard, C., Słowiński, M., Błaszkiewicz, M., Brauer, A., 2016. Holocene tephrostratigraphy of varved sediment records from Lakes Tiefer See (NE Germany) and Czechowskie (N Poland). Quaternary Science Reviews 132, 1-14.

Chapter 8. Supplementary File 3. Maps indicating new sites at which cryptotephras have been identified. Black circles indicate sites in the database complied by Swindles et al., (2011). Grey circle indicate new sites from published literature (references in supplementary file 2). White stars indicate new sites from this project.

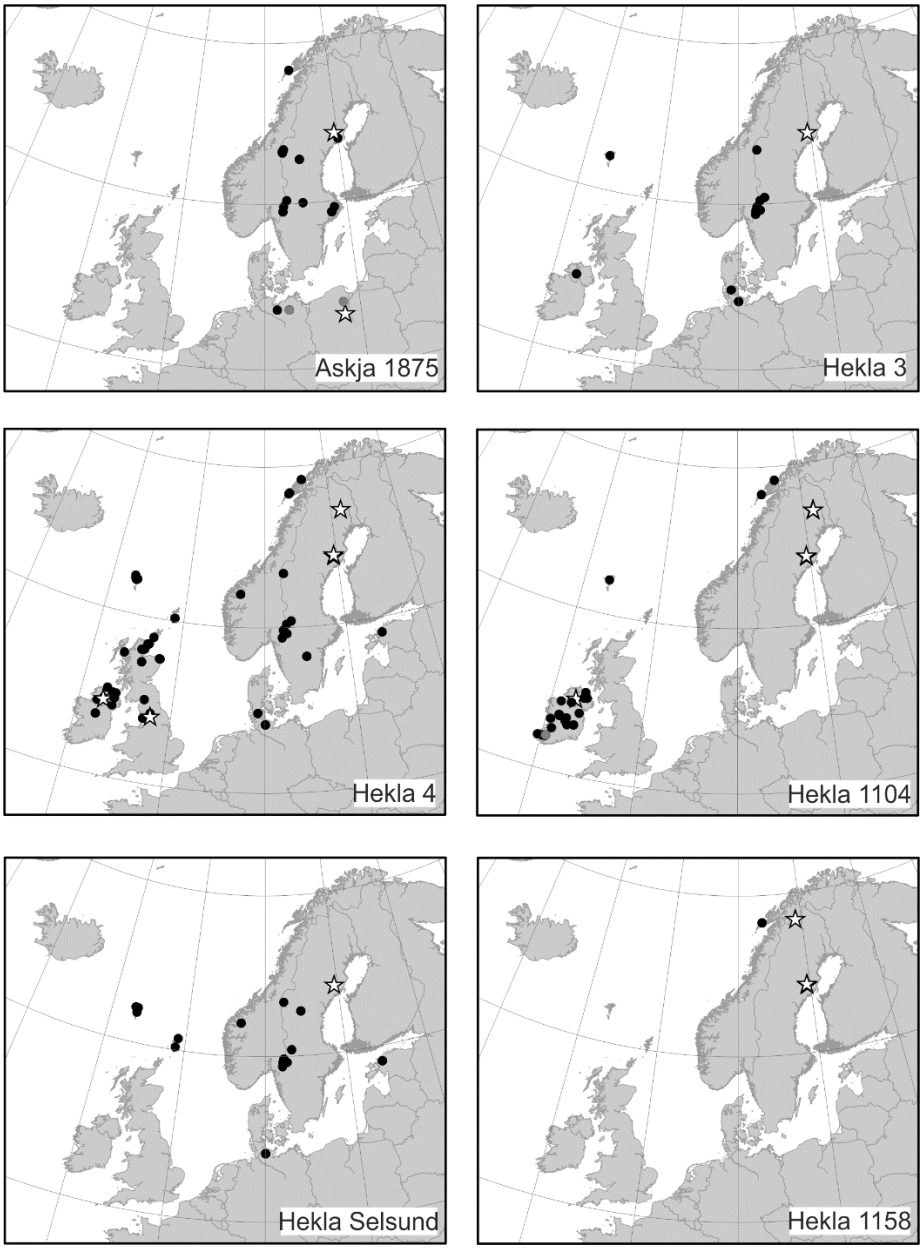

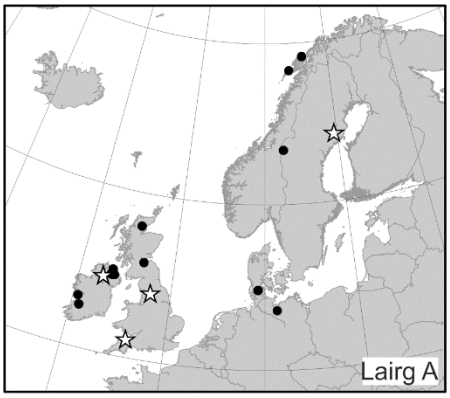
Lairg A


Lairg B


MOR-T4

	Shape parameter		Scale parameter		log (likelihood)	KS-Test *p* value	AIC
	Value	Std.err.	Value	Std.err.			
All Icelandic eruptions	n = 213						
Exponential	0.221	0.015	0.000	0.000	-534.6	0.000	1071.2
Weibull	0.351	0.022	2.319	0.466	-324.2	0.000	652.5
Log-logistic	0.378	0.024	0.960	0.294	-377.3	0.000	758.6
European ash clouds	n = 23						
Exponential	0.023	0.005	0.000	0.000	-110.0	0.913	222.0
Weibull	0.750	0.140	39.996	11.384	-108.7	0.473	221.3
Log-logistic	0.855	0.160	27.716	10.894	-114.4	0.350	232.7
Icelandic Eruptions VEI ≥4	n = 35						
Exponential	0.039	0.007	0.000	0.000	-148.9	0.698	299.8
Weibull	1.404	0.193	28.265	3.564	-146.3	0.957	296.6
Log-logistic	1.887	0.273	20.875	3.183	-150.4	0.895	304.7
Icelandic Eruptions VEI ≥4 Silicic	n = 10						
Exponential	0.011	0.003	0.000	0.000	-55.1	0.418	112.1
Weibull	3.129	0.741	101.430	10.888	-48.3	0.995	100.7
Log-logistic	5.220	1.360	84.250	9.030	-47.7	0.995	99.5
Icelandic Eruptions VEI ≥3 Silicic	n = 18						
Exponential	0.020	0.005	0.000	0.000	-88.5	0.943	179.1
Weibull	1.459	0.279	55.597	9.463	-86.9	0.996	177.7
Log-logistic	1.950	0.374	39.376	8.497	-88.4	0.996	180.9

Supplementary File 4 – Table summarising the goodness of fit of Exponential, Weibull and Log-Logistic distribution to datasets described in the text. The selected distribution of best fit is highlighted in green.

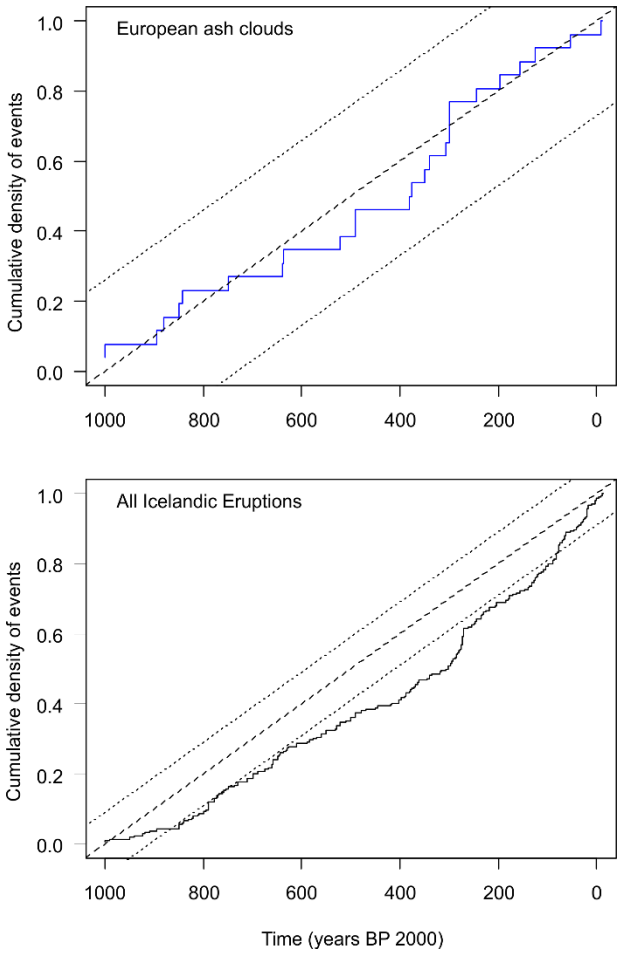

Supplementary file 5 – The cumulative frequency of European ash clouds and Icelandic Eruptions over the last 1000 years. The Kolmogorov-Smirnov test indicates that European ash clouds have not been significantly different from the steady state model over the last 1000 years ($p < 0.05$); Icelandic eruptions show some minor deviations from a steady state. The dense dashed line indicates the steady state model; finely dashed lines indicate 95% confidence interval.

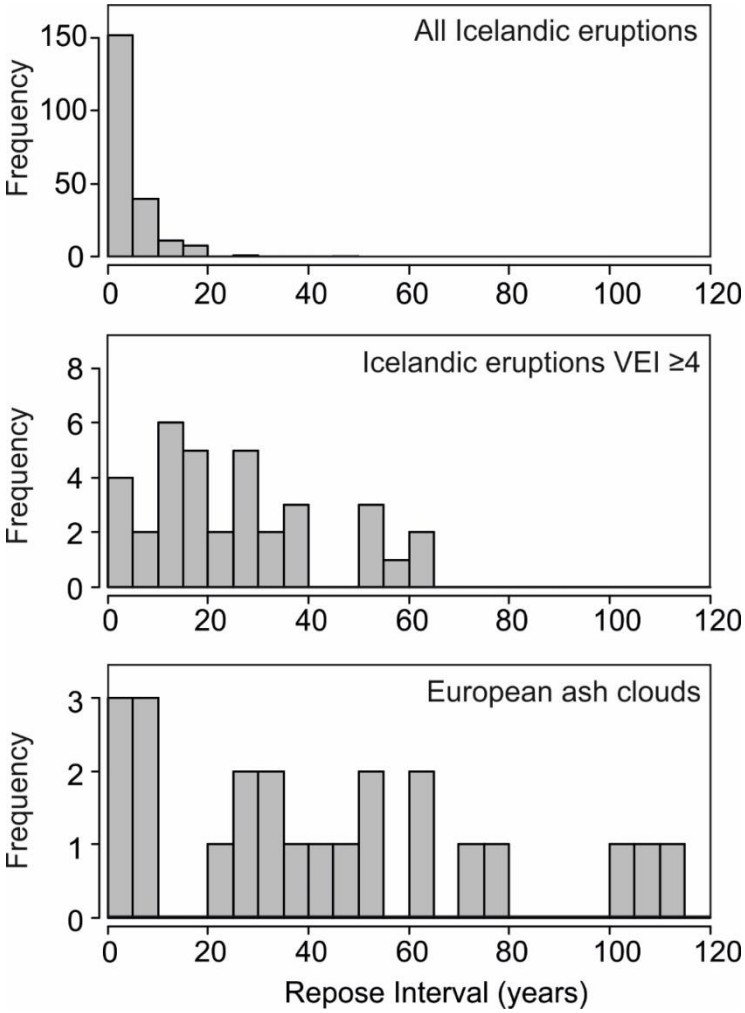

Supplementary file 6 – Histograms showing the range of repose intervals for all Icelandic eruptions, Icelandic eruptions VEI ≥4 and European ash clouds

References

Albino, F., Pinel, V., Sigmundsson, F., 2010. Influence of surface load variations on eruption likelihood: application to two Icelandic subglacial volcanoes, Grímsvötn and Katla. Geophysical Journal International 181, 1510-1524.

Allan, A.S.R., Baker, J.A., Carter, L., Wysoczanksi, R.J., 2008. Reconstructing the Quaternary evolution of the world's most active silicic volcanic system: insights from an ~1.65 Ma deep ocean tephra record sourced from Taupo Volcanic Zone, New Zealand. Quaternary Science Reviews 27, 2341-2360.

Andrews, J.T., Eberl, D., Kristjansdottir, G.B., 2006. An exploratory method to detect tephras from quantitative XRD scans: examples from Iceland and east Greenland marine sediments. The Holocene 16, 1035-1042.

Austin, W.E.N., Wilson, L.J., Hunt, J.B., 2004. The age and chronostratigraphical significance of North Atlantic Ash zone II. Journal of Quaternary Science 19, 137-146.

Aymerich, I.F., Oliva, M., Giralt, S., Martín-Herrero, J., 2016. Detection of Tephra Layers in Antarctic Sediment Cores with Hyperspectral Imaging. PLoS ONE 11.

Baker, D.S., 1983. Igneous rocks. Prentice-Hall New Jersey

Banerjee, A., 2003. Medical Statistics made clear: an introduction to basic concepts. Royal Society of Medicine Press Ltd, London.

Barber, K., Langdon, P., Blundell, A., 2008. Dating the Glen Garry tephra: a widespread late-Holocene marker horizon in the peatlands of northern Britain. Holocene 18, 31-43.

Beckett, F., Witham, C., Hort, M., Stevenson, J., Bonadonna, C., Millington, S., 2015. Sensitivity of dispersion model forecasts of volcanic ash clouds to the physical characteristics of the particles. Journal of Geophysical Research: Atmospheres 120, 11,636–611,652

Bennett, K.D., 1994. Confidence intervals for age estimates and deposition times in late-Quaternary sediment sequences. Holocene 4, 337-348.

Bergman, J., Wastegård, S., Hammarlund, D., Wohlfarth, B., Roberts, S.J., 2004. Holocene tephra horizons at Klocka Bog, west-central Sweden: aspects of reproducibility in subarctic peat deposits. Journal of Quaternary Science 19, 241-249.

Bertrand, S., Daga, R., Bedert, R., Fontijn, K., 2014. Deposition of the 2011–2012 Cordón Caulle tephra (Chile, 40°S) in lake sediments: Implications for tephrochronology and volcanology. Journal of Geophysical Research: Earth Surface 119, 2555-2573.

Bescoby, D., Barclay, J., Andrews, J., 2008. Saints and Sinners: a tephrochronology for Late Antique landscape change in Epirus from the eruptive history of Lipari, Aeolian Islands. Journal of Archaeological Science 35, 2574-2579.

Blaauw, M., Christen, A., J., 2011. Flexible Paleoclimate Age-Depth Models Using an Autoregressive Gamma Process. Bayesian Analysis 6, 457-474.

Blaauw, M., Christen, J.A., 2005. Radiocarbon peat chronologies and environmental change. Journal of the Royal Statistical Society Series C-Applied Statistics 54, 805-816.

Blaauw, M., Heuvelink, G.B.M., Mauquoy, D., van der Plicht, J., van Geel, B., 2003. A numerical approach to C-14 wiggle-match dating of organic deposits: best fits and confidence intervals. Quaternary Science Reviews 22, 1485-1500.

Blaauw, M., Van Geel, B., Mauquoy, D., Van der Plicht, J., 2004. Carbon-14 wiggle-match dating of peat deposits: advantages and limitations. Journal of Quaternary Science 19, 177-181.

Blockley, S.P.E., Lane, C.S., Lotter, A.F., Pollard, A.M., 2007. Evidence for the presence of the Vedde Ash in Central Europe. Quaternary Science Reviews 26, 3030-3036.

Blockley, S.P.E., Pyne-O'Donnell, S.D.F., Lowe, J.J., Matthews, I.P., Stone, A., Pollard, A.M., Turney, C.S.M., Molyneux, E.G., 2005. A new and less destructive laboratory procedure for the physical separation of distal glass tephra shards from sediments. Quaternary Science Reviews 24, 1952-1960.

Bond, G.C., Mandeville, C., Hoffmann, S., 2001. Were rhyolitic glasses in the Vedde Ash and in the North Atlantic's Ash Zone 1 produced by the same volcanic eruption? Quaternary Science Reviews 20, 1189-1199.

Boygle, J., 1999. Variability of tephra in lake and catchment sediments, Svínavatn, Iceland. Global and Planetary Change 21, 129-149.

Boygle, J., 2004. Towards a Holocene tephrochronology for Sweden: geochemistry and correlation with the North Atlantic tephra stratigraphy. Journal of Quaternary Science 19, 103-109.

Bramham-Law, C.W.F., Theuerkauf, M., Lane, C.S., Mangerud, J., 2013. New findings regarding the Saksunarvatn Ash in Germany. Journal of Quaternary Science 28, 248-257.

Buckley, S., Walker, M.J.C., 2002. A mid-Flandrian tephra horizon, Cambrian Mountains, West Wales. Quaternary Newsletter 96, 5-11.

Cage, A.G., Davies, S.M., Wastegård, S., Austin, W.E.N., 2011. Identification of the Icelandic Landnam tephra (AD 871 +/- 2) in Scottish fjordic sediment. Quaternary International 246, 168-176.

Calanchi, N., Dinelli, E., 2008. Tephrostratigraphy of the last 170 ka in sedimentary successions from the Adriatic Sea. Journal of Volcanology and Geothermal Research 177, 81-95.

Carey, S., Sparks, R.S.J., 1986. Quantitative models of the fallout and dispersal of tephra from volcanic eruption columns. Bulletin of Volcanology 48, 109-125.

Carey, S.N., Sigurdsson, H., 1982. Influence of particle aggregation on deposition of distal tephra from the MAy 18, 1980, eruption of Mount St. Helens volcano. Journal of Geophysical Research: Solid Earth 87, 7061-7072.

Caseldine, C., Baker, A., Barnes, W.L., 1999. A rapid, non-destructive scanning method for detecting distal tephra layers in peats. The Holocene 9, 635-638.

Cashman, K.V., 2000. Magmatic fragmentation, In: Sigurdsson, H., Houghton, B., McNutt, S., Rymer, H., Stix, J. (Eds.), Encyclopaedia of Volcanoes. Academic, San Diego, pp. 421-430.

Chambers, F.M., Daniell, J.R.G., Hunt, J.B., Molloy, K., O'Connell, M., 2004. Tephrostratigraphy of An Loch Mor, Inis Oirr, western Ireland: implications for Holocene tephrochronology in the northeastern Atlantic region. Holocene 14, 703-720.

Charman, D.J., Grattan, J., 1999. An assessment of discriminant function analysis in the identification and correlation of distal Icelandic tephras in the British Isles Geological Society (London) Special publications 161, 147-160.

Cole, E.E., Mitchell, F.J.G., 2003. Human impact on the Irish landscape during the late Holocene inferred from palynological studies at three peatland sites. Holocene 13, 507-515.

Connor, C., Bebbington, M., Marzocchi, W., 2015. Chapter 51 - Probabilistic Volcanic Hazard Assessment, In: Sigurdsson, H. (Ed.), The Encyclopedia of Volcanoes (Second Edition). Academic Press, Amsterdam, pp. 897-910.

Connor, C.B., McBirney, A.R., Furlan, C., 2006. What is the probability of explosive eruption at a long-dormant volcano?, In: Mader, H.M., Coles, S.G., Connor, C.B., Connor, L.J. (Eds.), Statistics in Volcanology The Geological Society London, pp. 39-46.

Cooke, M.C., Francis, P.N., Millington, S., Saunders, R., Witham, C., 2014. Detection of the Grímsvötn 2011 volcanic eruption plumes using infrared satellite measurements. Atmospheric Science Letters 15, 321-327.

Coulter, S.E., Pilcher, J.R., Hall, V.A., Plunkett, G., Davies, S.M., 2010. Testing the reliability of the JEOL FEGSEM 6500F electron microprobe for quantitative major element analysis of glass shards from rhyolitic tephra. Boreas 39, 163-169.

Coulter, S.E., Pilcher, J.R., Plunkett, G., Baillie, M., Hall, V.A., Steffensen, J.P., Vinther, B.M., Clausen, H.B., Johnsen, S.J., 2012. Holocene tephras highlight complexity of volcanic signals in Greenland ice cores. Journal of Geophysical Research-Atmospheres 117.

Cox, D.R., Oakes, D., 1984. Analysis of Survival Data: Monographs on Statistics and Applied Probability Chapman and Hall London.

Davies, S.M., 2015. Cryptotephras: the revolution in correlation and precision dating. Journal of Quaternary Science 30, 114-130.

Davies, S.M., Branch, N.P., Lowe, J.J., Turney, C.S., 2002. Towards a European tephrochronological framework for Termination 1 and the Early Holocene. Philosophical Transactions of the Royal Society of London A: Mathematical, Physical and Engineering Sciences 360, 767-802.

Davies, S.M., Elmquist, M., Bergman, J., Wohlfarth, B., Hammarlund, D., 2007. Cryptotephra sedimentation processes within two lacustrine sequences from west central Sweden. Holocene 17, 319-330.

Davies, S.M., Hoek, W.Z., Bohncke, S.J.P., Lowe, J.J., O'Donnell, S.P., Turney, C.S.M., 2005. Detection of Lateglacial distal tephra layers in the Netherlands. Boreas 34, 123-135.

Davies, S.M., Larsen, G., Wastegård, S., Turney, C.S.M., Hall, V.A., Coyle, L., Thordarson, T., 2010. Widespread dispersal of Icelandic tephra: how does the Eyjafjöll eruption of 2010 compare to past Icelandic events? Journal of Quaternary Science 25, 605-611.

Davies, S.M., Turney, C.S.M., Lowe, J.J., 2001. Identification and significance of a visible, basalt-rich Vedde Ash layer in a Late-glacial sequence on the Isle of Skye, Inner Hebrides, Scotland. Journal of Quaternary Science 16, 99-104.

Davies, S.M., Wohlfarth, B., Wastegard, S., Andersson, M., Blockley, S., Possnert, G., 2004. Were there two Borrobol Tephras during the early Lateglacial period: implications for tephrochronology? Quaternary Science Reviews 23, 581-589.

de Angelis, M., Fehrenbach, L., Jehanno, C., Maurette, M., 1985. Micrometre-sized volcanic glasses in polar ices and snows. Nature 317, 52-54.

De Vleeschouwer, F., Chambers, F.M., Swindles, G.T., 2011. Coring and sub-sampling of peatlands for palaeoenvironmental research. Mires and Peat 7, 1-10.

Dellino, P., Gudmundsson, M.T., Larsen, G., Mele, D., Stevenson, J.A., Thordarson, T., Zimanowski, B., 2012. Ash from the Eyjafjallajokull eruption (Iceland): Fragmentation processes and aerodynamic behavior. Journal of Geophysical Research-Solid Earth 117.

Dugmore, A., 1989. Icelandic volcanic ash in Scotland. Scottish Geographical Magazine 105, 168-172.

Dugmore, A., Newton, A., 1998. Holocene tephra layers in the Faroe Islands. Frodskaparrit 46, 191-204.

Dugmore, A.J., Larsen, G., Newton, A.J., 1995. 7 Tephra isochrones in Scotland. Holocene 5, 257-266.

Dugmore, A.J., Newton, A.J., Edwards, K.J., Larsen, G., Blackford, J.J., Cook, G.T., 1996. Long-distance marker horizons from small-scale eruptions: British tephra deposits from the AD 1510 eruption of Hekla, Iceland. Journal of Quaternary Science 11, 511-516.

Dugmore, A.J., Newton, A.J., Smith, K.T., 2011. Workshop on the Eyjafjallajökull eruptions of 2010 and implications for tephrochronology, volcanology and Quaternary studies. Institute of Geography, University of Edinburgh.

Dugmore, A.J., Newton, A.J., Sugden, D.E., Larsen, G., 1992. Geochemical stability of fine-grained silicic Holocene tephra in Iceland and Scotland. Journal of Quaternary Science 7, 173-183.

Dunbar, N.W., 2005. Tephrochronology of the Siple Dome, Antarctica, ice core: analytical challenges and results, 2005 Salt Lake City Annual Meeting.

Dzierma, Y., Wehrmann, H., 2012. On the likelihood of future eruptions in the Chilean Southern Volcanic Zone: interpreting the past century's eruption record based on statistical analyses. Andean Geology 39, 380-393.

Eden, D.N., Froggatt, P.C., Zheng, H., Machida, H., 1996. Volcanic glass found in Late Quaternary Chinese loess: A pointer for future studies? Quaternary International 34, 107-111.

Fiacco, R.J., Palais, J.M., Germani, M.S., Zielinski, G.A., Mayewski, P.A., 1993. Characteristics and possible source of a 1479 AD volcanic ash layer in a Greenland ice core. Quat. Res. 39, 267-273.

Folch, A., 2012. A review of tephra transport and dispersal models: Evolution, current status, and future perspectives. Journal of Volcanology and Geothermal Research 235, 96-115.

Folch, A., Costa, A., Basart, S., 2012. Validation of the FALL3D ash dispersion model using observations of the 2010 Eyjafjallajokull volcanic ash clouds. Atmospheric Environment 48, 165-183.

Froggatt, P.C., 1992. Standardization of the chemical analysis of tephra deposits. Report of the ICCT Working Group. Quaternary International 13–14, 93-96.

Gehrels, M.J., Lowe, D.J., Hazell, Z.J., Newnham, R.M., 2006a. A continuous 5300-yr Holocene cryptotephrostratigraphic record from northern New Zealand and implications for tephrochronology and volcanic hazard assessment. The Holocene 16, 173-187.

Gehrels, M.J., Newnham, R.M., Lowe, D.J., Wynne, S., Hazell, Z.J., Caseldine, C., 2008. Towards rapid assay of cryptotephra in peat cores: Review and evaluation of various methods. Quaternary International 178, 68-84.

Gehrels, W.R., Marshall, W.A., Gehrels, M.J., Larsen, G., Kirby, J.R., Eiríksson, J., Heinemeier, J., Shimmield, T., 2006b. Rapid sea-level rise in the North Atlantic Ocean since the first half of the nineteenth century. The Holocene 16, 949-965.

Global Volcanism Program, 2013. Volcanoes of the World, v. 4.3.4. , In: Venzke, E. (Ed.), Smithsonian Institution.

Gronvold, K., Oskarsson, N., Johnsen, S.J., Clausen, H.B., Hammer, C.U., Bond, G., Bard, E., 1995. Ash layers from Iceland in the Greenland GRIP Ice core correlated with oceanic and land sediments. Earth Planet. Sci. Lett. 135, 149-155.

Gudmundsdóttir, E.R., Eiríksson, J., Larsen, G., 2011. Identification and definition of primary and reworked tephra in Late Glacial and Holocene marine shelf sediments off North Iceland. Journal of Quaternary Science 26, 589-602.

Gudmundsson, A., 2000. Dynamics of volcanic systems in Iceland: example of tectonism and volcanism at juxtaposed hot spot and mid-ocean ridge systems. Annual Review of Earth and Planetary Sciences 28, 107-140.

Gudmundsson, M.T., Larsen, G., Hoskuldsson, A., Gylfason, A.G., 2008. Volcanic hazards in Iceland. Jokull 58, 251-268.

Gudmundsson, M.T., Thordarson, T., Hoskuldsson, A., Larsen, G., Bjornsson, H., Prata, F.J., Oddsson, B., Magnusson, E., Hognadottir, T., Petersen, G.N., Hayward, C.L., Stevenson, J.A., Jonsdottir, I., 2012. Ash generation and distribution from the April-May 2010 eruption of Eyjafjallajokull, Iceland. Sci Rep 2.

Haberle, S.G., Lumley, S.H., 1998. Age and origin of tephras recorded in postglacial lake sediments to the west of the southern Andes, 44 S to 47 S. Journal of Volcanology and Geothermal Research 84, 239-256.

Haflidason, H., Eiriksson, J., Van Kreveld, S., 2000. The tephrochronology of Iceland and the North Atlantic region during the Middle and Late Quaternary: a review. Journal of Quaternary Science 15, 3-22.

Hall, M., Hayward, C., 2014. Preparation of micro- and crypto-tephras for quantitative microbeam analysis. Geological Society, London, Special Publications 398, 21-28.

Hall, V.A., Pilcher, J.R., 2002. Late-Quaternary Icelandic tephras in Ireland and Great Britain: detection, characterization and usefulness. Holocene 12, 223-230.

Hang, T., Wastegård, S., Veski, S., Heinsalu, A., 2006. First discovery of cryptotephra in Holocene peat deposits of Estonia, eastern Baltic. Boreas 35, 644-649.

Hannon, G.E., Wastegård, S., Bradshaw, E., Bradshaw, R.H.W., 2001. Human impact and landscape degradation on the Faroe Islands. Biology and Environment 101B, 129-139.

Hayward, C., 2012. High spatial resolution electron probe microanalysis of tephras and melt inclusions without beam-induced chemical modification. Holocene 22, 119-125.

Heiken, G., 1972. Morphology and petrography of volcanic ashes Geological Society of America Bulletin 83, 1961.

Hodder, A.P.W., De Lange, P.J., Lowe, D.J., 1991. Dissolution and depletion of ferromagnesian minerals from Holocene tephra layers in an acid bog, New Zealand, and implications for tephra correlation. Journal of Quaternary Science 6, 195-208.

Holden, J., Chapman, P.J., Labadz, J.C., 2004. Artificial drainage of peatlands: hydrological and hydrochemical process and wetland restoration. Prog. Phys. Geogr. 28, 95-123.

Holmes, J., Hall, V., Wilson, P., 1999. Volcanoes and peat bogs. Geology Today 15, 60-63.

Hooper, A., 2012. Iceland volcano: and you thought the last eruption was bad... The Telegraph, http://www.telegraph.co.uk/science/9195178/Iceland-volcano-and-you-thought-the-last-eruption-was-bad....html.

Hooper, A., Ofeigsson, B., Sigmundsson, F., Lund, B., Einarsson, P., Geirsson, H., Sturkell, E., 2011. Increased capture of magma in the crust promoted by ice-cap retreat in Iceland. Nature Geosci 4, 783-786.

Housley, R.A., MacLeod, A., Nalepka, D., Jurochnik, A., Masojć, M., Davies, L., Lincoln, P.C., Bronk Ramsey, C., Gamble, C.S., Lowe, J.J., 2013. Tephrostratigraphy of a Lateglacial lake sediment sequence at Węgliny, southwest Poland. Quaternary Science Reviews 77, 4-18.

Hunt, J.B., Hill, P.G., 1993. Tephra geochemistry: a discussion of some persistent analytical problems The Holocene 3, 271-278.

Hunt, J.B., Hill, P.G., 1996. An inter-laboratory comparison of the electron probe microanalysis of glass geochemistry. Quaternary International 34-6, 229-241.

Hunt, J.B., Hill, P.G., 2001. Tephrological implications of beam size-sample-size effects in electron microprobe analysis of glass shards. Journal of Quaternary Science 16, 105-117.

Jennings, A.E., Grönvold, K., Hilberman, R., Smith, M., Hald, M., 2002. High-resolution study of Icelandic tephras in the Kangerlussuaq Trough, southeast Greenland, during the last deglaciation. Journal of Quaternary Science 17, 747-757.

Jensen, B.J.L., Pyne-O'Donnell, S., Plunkett, G., Froese, D.G., Hughes, P.D.M., Sigl, M., McConnell, J.R., Amesbury, M.J., Blackwell, P.G., van den Bogaard, C., Buck, C.E., Charman, D.J., Clague, J.J., Hall, V.A., Koch, J., Mackay, H., Mallon, G., McColl, L., Pilcher, J.R., 2014. Transatlantic distribution of the Alaskan White River Ash. Geology 42, 875-878.

Jull, M., McKenzie, D., 1996. The effect of deglaciation on mantle melting beneath Iceland. Journal of Geophysical Research-Solid Earth 101, 21815-21828.

Juvigne, E., Kozarski, S., Nowaczyk, B., 1995. The occurrence of Laacher-See tephra in Pomerania, NW Poland. Boreas 24, 225-231.

Kilian, M.R., VanDerPlicht, J., VanGeel, B., 1995. Dating raised bogs: New aspects of AMS C-14 wiggle matching, a reservoir effect and climatic change. Quaternary Science Reviews 14, 959-966.

Kiyosugi, K., 2012. Temporal and Spatial Analysis of Monogenetic Volcanic Fields. University of South Florida.

Kurbatov, A.V., Zielinski, G.A., Dunbar, N.W., Mayewski, P.A., Meyerson, E.A., Sneed, S.B., Taylor, K.C., 2006. A 12,000 year record of explosive volcanism in the Siple Dome Ice Core, West Antarctica. Journal of Geophysical Research: Atmospheres 111.

Kylander, M.E., Lind, E.M., Wastegård, S., Lowemark, L., 2012. Recommendations for using XRF core scanning as a tool in tephrochronology. Holocene 22, 371-375.

Lacasse, C., Werner, R., Paterne, M., Sigurdsson, H., Carey, S., Pinte, G., 1998. Long-range transport of Icelandic tephra to the Irminger Basin Site 919, Proceedings of ocean drilling program scientific results. National Science Foundations, pp. 51-66.

Lane, C.S., Blockley, S.P.E., Mangerud, J., Smith, V.C., Lohne, O.S., Tomlinson, E.L., Matthews, I.P., Lotter, A.F., 2012. Was the 12.1 ka Icelandic Vedde Ash one of a kind? Quaternary Science Reviews 33, 87-99.

Lane, C.S., Brauer, A., Blockley, S.P.E., Dulski, P., 2013a. Volcanic ash reveals time-transgressive abrupt climate change during the Younger Dryas. Geology 41, 1251-1254.

Lane, C.S., Chorn, B.T., Johnson, T.C., 2013b. Ash from the Toba supereruption in Lake Malawi shows no volcanic winter in East Africa at 75 ka. Proceedings of the National Academy of Sciences 110, 8025-8029.

Langdon, P.G., Barber, K.E., 2001. New Holocene tephras and a proxy climate record from a blanket mire in northern Skye, Scotland. Journal of Quaternary Science 16, 753-759.

Langdon, P.G., Barber, K.E., 2004. Snapshots in time: precise correlations of peat-based proxy climate records in Scotland using mid-Holocene tephras. Holocene 14, 21-33.

Larsen, G., Eiriksson, J., 2008a. Holocene tephra archives and tephrochronology in Iceland - a brief overview. Jokull 58, 229-250.

Larsen, G., Eiriksson, J., 2008b. Late Quaternary terrestrial tephrochronology of Iceland - frequency of explosive eruptions, type and volume of tephra deposits. Journal of Quaternary Science 23, 109-120.

Larsen, G., Gudmundsson, M.T., Björnsson, H., 1998. Eight centuries of periodic volcanism at the center of the Iceland hotspot revealed by glacier tephrostratigraphy. Geology 26, 943-946.

Larsen, G., Newton, A.J., Dugmore, A.J., Vilmundardóttir, E.G., 2001. Geochemistry, dispersal, volumes and chronology of Holocene silicic tephra layers from the Katla volcanic system, Iceland. Journal of Quaternary Science 16, 119-132.

Lawson, I.T., Edwards, K.J., Church, M.J., Newton, A.J., Cook, G.T., Gathorne-Hardy, F.J., Dugmore, A.J., 2008. Human impact on an island ecosystem: pollen data from Sandoy, Faroe Islands. J. Biogeogr. 35, 1130-1152.

Lawson, I.T., Swindles, G.T., Plunkett, G., Greenberg, D., 2012. The spatial distribution of Holocene cryptotephras in north-west Europe since 7 ka: implications for understanding ash fall events from Icelandic eruptions. Quaternary Science Reviews 41, 57-66.

Lee, E.T., 1992. Statistical Methods for survival data analysis. Wiley USA.

Lim, C., Ikehara, K., Toyoda, K., 2008. Cryptotephra detection using high-resolution trace-element analysis of Holocene marine sediments, southwest Japan. Geochim. Cosmochim. Acta 72, 5022-5036.

Liu, E.J., Cashman, K.V., Rust, A.C., 2015. Optimising shape analysis to quantify volcanic ash morphology. GeoResJ 8, 14-30.

Lowe, D.J., 2011. Tephrochronology and its application: A review. Quaternary Geochronology 6, 107-153.

Lowe, J.J., Blockley, S., Trincardi, F., Asioli, A., Cattaneo, A., Matthews, I.P., Pollard, M., Wulf, S., 2007. Age modelling of late Quaternary marine sequences in the Adriatic:

Towards improved precision and accuracy using volcanic event stratigraphy. Continental Shelf Research 27, 560-582.

Lowe, J.J., Turney, C.S.M., 1997. Vedde ash layer discovered in a small lake basin on the Scottish mainland. J. Geol. Soc. 154, 605-612.

Luhr, J.F., Navarro-Ochoa, C., Savov, I.P., 2010. Tephrochronology, petrology and geochemistry of Late-Holocene pyroclastic deposits from Volcan de Colima, Mexico. Journal of Volcanology and Geothermal Research 197, 1-32.

Mackie, E.A.V., Davies, S.M., Turney, C.S.M., Dobbyn, K., Lowe, J.J., Hill, P.G., 2002. The use of magnetic separation techniques to detect basaltic microtephra in last glacial-interglacial transition (LGIT; 15-10 ka cal. BP) sediment sequences in Scotland. Scottish Journal of Geology 38, 21-30.

Maclennan, J., Jull, M., McKenzie, D., Slater, L., Grönvold, K., 2002. The link between volcanism and deglaciation in Iceland. Geochemistry, Geophysics, Geosystems 3, 1-25.

MacLeod, A., Matthews, I.P., Lowe, J.J., Palmer, A.P., Albert, P.G., 2015. A second tephra isochron for the Younger Dryas period in northern Europe: The Abernethy Tephra. Quaternary Geochronology 28, 1-11.

Mader, H.M., 2006. Volcanic processes as a source of statistical data, In: Mader, H.M., Coles, S.G., Connor, C.B., Connor, L.J. (Ed.), Statistics in Volcanology. The Geological Society London, pp. 1-14.

Marks, P., 2010. Engine strip-downs establish safe volcanic ash levels, New Scientist.

Matthews, I., 2008. Roman Lode, Exmoor, Devon: Tephrochronology Scientific Dating Report, Research Department Report Series English Heritage

Mattsson, S., Vesanen, R., 1988. Patterns of Chernobyl fallout in relation to local weather conditions Environment International 14, 177-180.

McCanta, M.C., Hatfield, R.G., Thomson, B.J., Hook, S.J., Fisher, E., 2015. Identifying cryptotephra units using correlated rapid, nondestructive methods: VSWIR spectroscopy, X-ray fluorescence, and magnetic susceptibility. Geochemistry, Geophysics, Geosystems 16, 4029-4056.

Merkt, J., Müller, H., Knabe, W., Müller, P., Weiser, T., 1993. The early Holocene Saksunarvatn tephra found in lake sediments in NW Germany. Boreas 22, 93-100.

Merlet, C., 1994. An accurate computer correction program for quantitative electron probe microanalysis. Microchimica Acta 114, 363-376.

Miller, T.P., Casadevall, T.J., 2000. Volcanic ash hazards to aviation, In: Sigurdsson, H., Houghton, B., McNutt, S., Rymer, H., Stix, J. (Eds.), Encyclopaedia of Volcanoes Academic, San Diego.

Mortensen, A.K., Bigler, M., Gronvold, K., Steffensen, J.P., Johnsen, S.J., 2005. Volcanic ash layers from the Last Glacial Termination in the NGRIP ice core. Journal of Quaternary Science 20, 209-219.

Newton, A.J., Dugmore, A.J., Gittings, B.M., 2007. Tephrabase: tephrochronology and the development of a centralised European database. Journal of Quaternary Science 22, 737-743.

Nielsen, C.H., Sigurdsson, H., 1981. Quantitative methods for Electron Micro-probe analysis of Sodium in Natural and Synthetic glasses. American Mineralogist 66, 547-552.

Oldfield, F., Thompson, R., Crooks, P.R.J., Gedye, S.J., Hall, V.A., Harkness, D.D., Housley, R.A., McCormac, F.G., Newton, A.J., Pilcher, J.R., Renberg, I., Richardson, N., 1997. Radiocarbon dating of a recent high-latitude peat profile: Stor Amyran, northern Sweden. Holocene 7, 283-290.

Olsen, J., Gudmundsdottir, E.R., Bjorck, S., Odgaard, B.V., Heinemeier, J., 2010. Revised age estimate of the Mjauvotn tephra A on the Faroe Islands based on Bayesian modelling of C-14 dates from two lake sequences. Journal of Quaternary Science 25, 612-616.

Pagli, C., Sigmundsson, F., 2008. Will present day glacier retreat increase volcanic activity? Stress induced by recent glacier retreat and its effect on magmatism at the Vatnajokull ice cap, Iceland. Geophysical Research Letters 35.

Payne, R., Blackford, J., 2008. Distal volcanic impacts on peatlands: palaeoecological evidence from Alaska. Quaternary Science Reviews 27, 2012-2030.

Payne, R., Gehrels, M., 2010. The formation of tephra layers in peatlands: An experimental approach. Catena 81, 12-23.

Pearce, N.J.G., Bendall, C.A., Westgate, J.A., 2008. Comment on "Some numerical considerations in the geochemical analysis of distal microtephra" by A.M. Pollard, S.P.E. Blockley and C.S. Lane. Applied Geochemistry 23, 1353-1364.

Pearce, N.J.G., Denton, J.S., Perkins, W.T., Westgate, J.A., Alloway, B.V., 2007. Correlation and characterisation of individual glass shards from tephra deposits using trace element laser ablation ICP-MS analyses: current status and future potential. Journal of Quaternary Science 22, 721-736.

Pearce, N.J.G., Perkins, W.T., Westgate, J.A., Wade, S.C., 2011. Trace-element microanalysis by LA-ICP-MS: The quest for comprehensive chemical characterisation of single, sub-10 mu m volcanic glass shards. Quaternary International 246, 57-81.

Pearce, N.J.G., Westgate, J.A., Perkins, W.T., Preece, S.J., 2004. The application of ICP-MS methods to tephrochronological problems. Applied Geochemistry 19, 289-322.

Persson, C., 1966. 'Forsok till tefrokronologisk datering av nagra Svenska torvmossar'. Geologiska Foreningens i Stockholm Forhandlingar 88, 361-394.

Persson, C., 1968. 'Forsok till tefrokronologisk datering i fyra faroiska myrar'. Geologiska Foreningens i Stockholm Forhandlingar 90, 241-266.

Persson, C., 1971. 'Tephrochronological investigations of peat deposits in Scandinavia and on the Faroe Islands'. Sveriges Geologiska Undersokning 65, 3-34.

Pilcher, J., Bradley, R.S., Francus, P., Anderson, L., 2005. A Holocene tephra record from the Lofoten Islands, Arctic Norway. Boreas 34, 136-156.

Pilcher, J.R., Hall, V.A., 1992. Towards a tephrochronology for the Holocene in the north of Ireland The Holocene 2 255-259

Pilcher, J.R., Hall, V.A., 1996. Tephrochronological studies in northern England. Holocene 6, 100-105.

Pilcher, J.R., Hall, V.A., McCormac, F.G., 1995. Dates of Holocene Icelandic volcanic eruptions from tephra layers in Irish peats. Holocene 5, 103-110.

Pistolesi, M., Cioni, R., Bonadonna, C., Elissondo, M., Baumann, V., Bertagnini, A., Chiari, L., Gonzales, R., Rosi, M., Francalanci, L., 2015. Complex dynamics of small-moderate volcanic events: the example of the 2011 rhyolitic Cordón Caulle eruption, Chile. Bulletin of Volcanology 77, 1-24.

Plunkett, G., 2006. Tephra-linked peat humification records from Irish ombrotrophic bogs question nature of solar forcing at 850 cal. yr RC. Journal of Quaternary Science 21, 9-16.

Plunkett, G.M., Pilcher, J.R., McCormac, F.G., Hall, V.A., 2004. New dates for first millennium BC tephra isochrones in Ireland. Holocene 14, 780-786.

Pollard, A.M., Blockley, S.P.E., Lane, C.S., 2006. Some numerical considerations in the geochemical analysis of distal microtephra. Applied Geochemistry 21, 1692-1714.

Pollard, A.M., Blockley, S.P.E., Ward, K.R., 2003. Chemical alteration of tephra in the depositional environment: theoretical stability modelling. Journal of Quaternary Science 18, 385-394.

Ponomareva, V., Portnyagin, M., Davies, S.M., 2015. Tephra without borders: Far-reaching clues into past explosive eruptions. Frontiers in Earth Science 3, 83.

Ponomareva, V., Portnyagin, M., Derkachev, A., Juschus, O., Garbe-Schönberg, D., Nürnberg, D., 2013. Identification of a widespread Kamchatkan tephra: A middle Pleistocene tie-point between Arctic and Pacific paleoclimatic records. Geophysical Research Letters 40, 3538-3543.

Pouget, S., Bursik, M., Cortés, J.A., Hayward, C., 2014a. Use of principal component analysis for identification of Rockland and Trego Hot Springs tephras in the Hat Creek Graben, northeastern California, USA. Quat. Res. 81, 125-137.

Pouget, S., Bursik, M., Rogova, G., 2014b. Tephra redeposition and mixing in a Late-glacial hillside basin determined by fusion of clustering analyses of glass-shard geochemistry. Journal of Quaternary Science 29, 789-802.

Pyne-O'Donnell, S., 2011. The taphonomy of Last Glacial-Interglacial Transition (LGIT) distal volcanic ash in small Scottish lakes. Boreas 40, 131-145.

Pyne-O'Donnell, S.D.F., Hughes, P.D.M., Froese, D.G., Jensen, B.J.L., Kuehn, S.C., Mallon, G., Amesbury, M.J., Charman, D.J., Daley, T.J., Loader, N.J., Mauquoy, D., Street-Perrott, F.A., Woodman-Ralph, J., 2012. High-precision ultra-distal Holocene tephrochronology in North America. Quaternary Science Reviews 52, 6-11.

Pyne-O'Donnell, S.D.F., Blockley, S.P.E., Turney, C.S.M., Lowe, J.J., 2008. Distal volcanic ash layers in the Lateglacial Interstadial (GI-1): problems of stratigraphic discrimination. Quaternary Science Reviews 27, 72-84.

Ramsey, C.B., 2009. Bayesian analysis of Radiocarbon dates. Radiocarbon 51, 337-360.

Rasmussen, T., Wastegård, S., Kuijpers, A., Van Weering, T., Heinemeier, J., Thomsen, E., 2003. Stratigraphy and distribution of tephra layers in marine sediment cores from the Faeroe Islands, North Atlantic. Marine Geology 199, 263-277.

Rea, H.A., Swindles, G.T., Roe, H.M., 2012. The Hekla 1947 tephra in the north of Ireland: regional distribution, concentration and geochemistry. Journal of Quaternary Science 27, 425-431.

Reilly, E., Mitchell, F.J., 2015. Establishing chronologies for woodland small hollow and mor humus deposits using tephrochronology and radiocarbon dating. The Holocene 25, 241-252.

Roland, T., Mackay, H., Hughes, P., 2015. Tephra analysis in ombrotrophic peatlands: A geochemical comparison of acid digestion and density separation techniques. Journal of Quaternary Science 30, 3-8.

Rose, N.L., Golding, P.N.E., Battarbee, R.W., 1996. Selective concentration and enumeration of tephra shards from lake sediment cores. Holocene 6, 243-246.

Rose, N.L., Harlock, S., 1998. The Spatial Distribution of Characterised Fly-Ash Particles and Trace Metals in Lake Sediments and Catchment Mosses in the United Kingdom. Water, Air, and Soil Pollution 106, 287-308.

Rose, N.L., Harlock, S., Appleby, P.G., 1999. The Spatial and Temporal Distributions of Spheroidal Carbonaceous Fly-Ash Particles (SCP) in the Sediment Records of European Mountain Lakes. Water, Air, and Soil Pollution 113, 1-32.

Rymer, H., Locke, C.A., Borgia, A., Martinez, M., Brenes, J., Van der Laat, R., Williams-Jones, G., 2009. Long-term fluctuations in volcanic activity: implications for future environmental impact. Terra Nova 21, 304-309.

Sandri, L., Jolly, G., Lindsay, J., Howe, T., Marzocchi, W., 2012. Combining long-and short-term probabilistic volcanic hazard assessment with cost-benefit analysis to support decision making in a volcanic crisis from the Auckland Volcanic Field, New Zealand. Bulletin of Volcanology 74, 705-723.

Schmid, R., 1981. Descriptive nomenclature and classification of pyroclastic deposits and fragments - recommendations of the IUGS subcommission on the systematics of igneous rocks Geology 9, 41-43.

Schmidt, A., Leadbetter, S., Theys, N., Carboni, E., Witham, C.S., Stevenson, J.A., Birch, C.E., Thordarson, T., Turnock, S., Barsotti, S., Delaney, L., Feng, W., Grainger, R.G., Hort, M.C., Höskuldsson, Á., Ialongo, I., Ilyinskaya, E., Jóhannsson, T., Kenny, P., Mather, T.A., Richards, N.A.D., Shepherd, J., 2015. Satellite detection, long-range transport, and air quality impacts of volcanic sulfur dioxide from the 2014–2015 flood lava eruption at Bárðarbunga (Iceland). Journal of Geophysical Research: Atmospheres.

Schmidt, P., Lund, B., Hieronymus, C., Maclennan, J., Árnadóttir, T., Pagli, C., 2013. Effects of present-day deglaciation in Iceland on mantle melt production rates. Journal of Geophysical Research: Solid Earth 118, 3366-3379.

Schmidt, R., van den Bogaard, C., Merkt, J., Müller, J., 2002. A new Lateglacial chronostratigraphic tephra marker for the south-eastern Alps: The Neapolitan Yellow Tuff (NYT) in Längsee (Austria) in the context of a regional biostratigraphy and palaeoclimate. Quaternary International 88, 45-56.

Schön, J., 2011. Physical Properties of Rocks: A Workbook. Elsevier, Oxford.

Shane, P., 2000. Tephrochronology: a new Zealand case study. Earth-Science Reviews 49, 223-259.

Siani, G., Sulpizio, R., Paterne, M., Sbrana, A., 2004. Tephrostratigraphy study for the last 18,000 14 C years in a deep-sea sediment sequence for the South Adriatic. Quaternary Science Reviews 23, 2485-2500.

Sigvaldason, G.E., Annertz, K., Nilsson, M., 1992. Effect of glacier loading deloading on volcanism - postglacial volcanic production-rate of the Dyngjufjoll area, Central Iceland Bulletin of Volcanology 54, 385-392.

Sjøholm, J., Sejrup, H.P., Furnes, H., 1991. Quaternary volcanic ash zones on the Iceland Plateau, southern Norwegian Sea. Journal of Quaternary Science 6, 159-173.

Sparks, R.S.J., Bursik, M.I., Ablay, G.J., Thomas, R.M.E., Carey, S.N., 1992. Sedimentation of tephra by volcanic plumes. Part 2: controls on thickness and grain-size variations of tephra fall deposits. Bulletin of Volcanology 54, 685-695.

Stanton, T., Snowball, I., Zillen, L., Wastegård, S., 2010. Validating a Swedish varve chronology using radiocarbon, palaeomagnetic secular variation, lead pollution history and statistical correlation. Quaternary Geochronology 5, 611-624.

Stevenson, J., Millington, S., Beckett, F., Swindles, G., Thordarson, T., 2015. Big grains go far: reconciling tephrochronology with atmospheric measurements of volcanic ash. Atmos. Meas. Tech. Discuss., 8, 65-120.

Stevenson, J.A., Loughlin, S., Font, A., Fuller, G.W., MacLeod, A., Oliver, L.W., Jackson, B., Horwell, C.J., Thordarson, T., Dawson, I., 2013. UK Monitoring and deposition of tephra from the May 2011 eruption of Grimsvotn, Iceland. Journal of Applied Volcanology 2.

Stevenson, J.A., Loughlin, S., Rae, C., Thordarson, T., Milodowski, A.E., Gilbert, J.S., Harangi, S., Lukacs, R., Hojgaard, B., Arting, U., Pyne-O'Donnell, S., MacLeod, A., Whitney, B., Cassidy, M., 2012. Distal deposition of tephra from the Eyjafjallajokull 2010 summit eruption. Journal of Geophysical Research-Solid Earth 117.

Stokes, S., Lowe, D.J., Froggatt, P.C., 1992. Discriminant function analysis and correlation of Late Quaternary rhyolitic tephra deposits from Taupo and Okataina volcanoes, New Zealand, using glass shard major element composition. Quaternary International 13–14, 103-117.

Surtees, A.P.H., Swindles, G.T., Munshi, T., Savov, I.P., Scowen, I.J., Edwards, H.G.M., 2016. Raman Spectroscopy for the discrimination of tephras from the Hekla eruptions of 1510 and 1947. The Holocene 26, 432–438.

Suzuki, R., Shimodaira, H., 2006. Pvclust: an R package for assessing the uncertainty in hierarchical clustering. Bioinformatics 22, 1540-1542.

Suzuki, T., Eden, D., Danhara, T., Fujiwara, O., 2005. Correlation of the Hakkoda–Kokumoto Tephra, a widespread Middle Pleistocene tephra erupted from the Hakkoda Caldera, northeast Japan. Island Arc 14, 666-678.

Swindles, G.T., De Vleeschouwer, F., Plunkett, G., 2010. Dating peat profiles using tephra: stratigraphy, geochemistry and chronology Mires and Peat 7, 1-9.

Swindles, G.T., Galloway, J., Outram, Z., Turner, K., Schofield, J.E., Newton, A.J., Dugmore, A.J., Church, M.J., Watson, E.J., Batt, C., Bond, J., Edwards, K.J., Turner, V., Bashford, D., 2013. Re-deposited cryptotephra layers in Holocene peats linked to anthropogenic activity. The Holocene 23, 1493-1501.

Swindles, G.T., Lawson, I.T., Savov, I.P., Connor, C.B., Plunkett, G., 2011. A 7000 yr perspective on volcanic ash clouds affecting northern Europe. Geology 39, 887-890.

Swindles, G.T., Reczuga, M., Lamentowicz, M., Raby, C.L., Turner, T.E., Charman, D.J., Gallego-Sala, A., Valderrama, E., Williams, C., Draper, F., 2014. Ecology of testate amoebae in an Amazonian peatland and development of a transfer function for palaeohydrological reconstruction. Microbial ecology 68, 284-298.

Swindles, G.T., Roe, H.M., 2006. Constraining the age of spheroidal carbonaceous particle (SCP) stratigraphies in peats using tephrochronology. Quaternary Newsletter 110, 2-9.

Takemura, K., Danhara, T., 1994. A method for determination of volcanic glass concentrations in sedimentary sequences and its application to Quaternary studies. Geoarchaeology 9, 301-316.

Techer, I., Advocat, T., Lancelot, J., Liotard, J.M., 2001. Dissolution kinetics of basaltic glasses: control by solution chemistry and protective effect of the alteration film. Chemical Geology 176, 235-263.

Thorarinsson, S., 1944. Tefrokronologiska studier på Island. Pjórsárdalur och Dess Förödelse. Geografiska Annaler 26, 1-217.

Thórarinsson, S., 1981. Tephra studies and tephrochronology: a historical review with special reference to Iceland, In: Self, S., Sparks, R.S.J. (Eds.), Tephra Studies. Reidel, Dordrecht, pp. 1-12.

Thordarson, T., Hoskuldsson, A., 2008. Postglacial volcanism in Iceland. Jokull 58, 197-228.

Thorseth, I.H., Fumes, H., Tumyr, O., 1995. Textural and chemical effects of bacterial activity on basaltic glass - an experimental approach. Chemical Geology 119, 139-160.

Tomlinson, E.L., Kinvig, H.S., Smith, V.C., Blundy, J.D., Gottsmann, J., Mueller, W., Menzies, M.A., 2012. The Upper and Lower Nisyros Pumices: Revisions to the

Mediterranean tephrostratigraphic record based on micron-beam glass geochemistry. Journal of Volcanology and Geothermal Research 243, 69-80.

Tomlinson, E.L., Thordarson, T., Müller, W., Thirlwall, M., Menzies, M.A., 2010. Microanalysis of tephra by LA-ICP-MS — Strategies, advantages and limitations assessed using the Thorsmörk ignimbrite (Southern Iceland). Chemical Geology 279, 73-89.

Tryon, C.A., Faith, J.T., Peppe, D.J., Fox, D.L., McNulty, K.P., Jenkins, K., Dunsworth, H., Harcourt-Smith, W., 2010. The Pleistocene archaeology and environments of the Wasiriya Beds, Rusinga Island, Kenya. Journal of Human Evolution 59, 657-671.

Turney, C., Burg, D., Van, K., Wastegård, S., Davies, S., Whitehouse, N., Pilcher, J., Callaghan, C., 2006. North European last glacial–interglacial transition (LGIT; 15–9 ka) tephrochronology: extended limits and new events. Journal of Quaternary Science 21, 335-345.

Turney, C.S.M., 1998. Extraction of rhyolitic component of Vedde microtephra from minerogenic lake sediments. J. Paleolimn. 19, 199-206.

Van Den Bogaard, C., Schmincke, H.U., 2002. Linking the North Atlantic to central Europe: a high-resolution Holocene tephrochronological record from northern Germany. Journal of Quaternary Science 17, 3-20.

Vorren, K.-D., Blaauw, M., Wastegård, S., Van Der Plicht, J., Jensen, C., 2007. High-resolution stratigraphy of the northernmost concentric raised bog in Europe: Sellevollmyra, Andoya, northern Norway. Boreas 36, 253-277.

Wagner, B., Sulpizio, R., Zanchetta, G., Wulf, S., Wessels, M., Daut, G., Nowaczyk, N., 2008. The last 40 ka tephrostratigraphic record of Lake Ohrid, Albania and Macedonia: a very distal archive for ash dispersal from Italian volcanoes. Journal of Volcanology and Geothermal Research 177, 71-80.

Wallace, P.J., 2005. Volatiles in subduction zone magmas: concentrations and fluxes based on melt inclusion and volcanic gas data. Journal of Volcanology and Geothermal Research 140, 217-240.

Wastegård, S., 2002. Early to middle Holocene silicic tephra horizons from the Katla volcanic system, Iceland: new results from the Faroe Islands. Journal of Quaternary Science 17, 723-730.

Wastegård, S., 2005. Late Quaternary tephrochronology of Sweden: a review. Quaternary International 130, 49-62.

Wastegård, S., Bjorck, S., Grauert, M., Hannon, G.E., 2001. The Mjauvotn tephra and other Holocene tephra horizons from the Faroe Islands: a link between the Icelandic source region, the Nordic Seas, and the European continent. Holocene 11, 101-109.

Wastegard, S., Turney, C.S.M., Lowe, D.J., Roberts, S.J., 2000. New discoveries of the Vedde Ash in southern Sweden and Scotland. Boreas 29, 72-78.

Wastegård, S., Veres, D., Kliem, P., Hahn, A., Ohlendorf, C., Zolitschka, B., 2013. Towards a late Quaternary tephrochronological framework for the southernmost part of

South America – the Laguna Potrok Aike tephra record. Quaternary Science Reviews 71, 81-90.

Wastegård, S., Wohlfarth, B., Subetto, D.A., Sapelko, T.V., 2000. Extending the known distribution of the Younger Dryas Vedde Ash into northwestern Russia. Journal of Quaternary Science 15, 581-586.

Watson, E.J., Swindles, G.T., Savov, I.P., Bacon, K.L., 2015. First discovery of Holocene cryptotephra in Amazonia. Sci Rep 5, doi: 10.1038/srep15579.

Wilson, L., Sparks, R.S.J., Huang, T.C., Watkins, N.D., 1978. The Control of Volcanic Column Heights by Eruption Energetics and Dynamics. Journal of Geophysical Research 83, 1829-1836.

Wolfe, C.J., Bjarnason, I.T., VanDecar, J.C., Solomon, S.C., 1997. Seismic structure of the Iceland mantle plume. Nature 385, 245-247.

Wolff-Boenisch, D., Gislason, S.R., Oelkers, E.H., Putnis, C.V., 2004. The dissolution rates of natural glasses as a function of their composition at pH 4 and 10.6, and temperatures from 25 to 74°C. Geochim. Cosmochim. Acta 68, 4843-4858.

Wulf, S., Dräger, N., Ott, F., Serb, J., Appelt, O., Guðmundsdóttir, E., van den Bogaard, C., Słowiński, M., Błaszkiewicz, M., Brauer, A., 2016. Holocene tephrostratigraphy of varved sediment records from Lakes Tiefer See (NE Germany) and Czechowskie (N Poland). Quaternary Science Reviews 132, 1-14.

Zhao, H., Hall, V.A., 2015. Assessing the potential for cryptotephra studies in Northeastern China. The Holocene doi:10.1177/0959683615569320.

Zielinski, G.A., Germani, M.S., Larsen, G., Baillie, M.G., Whitlow, S., Twickler, M.S., Taylor, K., 1995. Evidence of the Eldgjá (Iceland) eruption in the GISP2 Greenland ice core: relationship to eruption processes and climatic conditions in the tenth century. The Holocene 5, 129-140.

Zolitschka, B., Francus, P., Ojala, A.E., Schimmelmann, A., 2015. Varves in lake sediments–a review. Quaternary Science Reviews 117, 1-41.